

**„Dual inhibitors of microsomal prostaglandin E₂
synthase-1 and 5-lipoxygenase as anti-inflammatory
payloads in polymer-based nanoparticles”**

Dissertation

zur Erlangung des akademischen Grades eines

„doctor rerum naturalium“ (Dr. rer. nat.)

vorgelegt dem Rat der Fakultät für Biowissenschaften

der Friedrich-Schiller-Universität Jena

von Dipl.-Pharm. Christian Kretzer

geboren am 27.08.1992 in Weimar

1. Gutachter: Prof. Dr. Oliver Werz, Friedrich-Schiller-Universität Jena
2. Gutachter: Prof. Dr. Ulrich S. Schubert, Friedrich-Schiller-Universität Jena
3. Gutachter: Prof. Dr. Ernst Wagner, Ludwig-Maximilians-Universität München

Einreichung der Dissertation: 15.08.2022

Disputation: 23.02.2023

Table of Contents

I	Abbreviations.....	III
II	Summary.....	VI
III	Zusammenfassung.....	VIII
1.	Introduction	1
1.1	Inflammation and Resolution.....	1
1.2	Chronic inflammation	2
1.3	Lipid mediator biosynthesis.....	3
1.3.1	5-Lipoxygenase and Leukotrienes.....	4
1.3.2	5-Lipoxygenase-activating protein (FLAP).....	7
1.3.3	Cyclooxygenase 1/2 and prostaglandins	7
1.3.4	Microsomal prostaglandin E ₂ synthase-1 (mPGES-1)	9
1.3.5.	15-Lipoxygenase and specialized pro-resolving mediators.....	9
1.4.	Eicosanoid pathway Inhibitors.....	12
1.4.1.	Dual inhibitors of the eicosanoid pathway.....	13
1.4.2.	BRP-187 as dual inhibitor of mPGES-1/FLAP	13
1.4.3.	BRP-201 as new dual mPGES-1/FLAP inhibitor.....	14
1.4.4.	Semisynthetic chalcone-based compounds as potential multitarget inhibitors .	15
1.5.	Polymer-based nanoparticles.....	16
2.	Aim of the thesis.....	18
3.	Manuscripts	20
	Manuscript I.....	23
	Manuscript II.....	45
	Manuscript III.....	60
	Manuscript IV	91
	Manuscript V	112
	Manuscript VI	128
4.	Discussion.....	142
4.1.	The influence of approved therapeutics on LM networks	142
4.2.	LM profiling of new multitarget inhibitors	143
4.3.	mPGES-1/FLAP inhibitors as anti-inflammatory payloads in polymeric NPs	146
4.4.	Promotion of SPM biosynthesis as new pharmacological approach.....	152
4.5.	Conclusion.....	156
5.	References.....	157
IV	Acknowledgements.....	XI
V	Appendix.....	XIII
	Appendix 1 – Contribution to figures in the manuscripts	XIII
	Manuskript Nr. I	XIII
	Manuskript Nr. II	XV
	Manuskript Nr. III	XVII

Manuskript Nr. IV.....	XIX
Manuskript Nr. V.....	XXI
Manuskript Nr. VI.....	XXIII
Appendix 2 – List of Publications and conference contributions	XXV
Appendix 3 – Eigenständigkeitserklärung	XXVIII
Appendix 4 – Curriculum Vitae	Fehler! Textmarke nicht definiert.
Appendix 5 – Supportive information.....	XXIX

I Abbreviations

The following abbreviations are indicated once and consistently utilized in the text, except for the chapters *Summary* and *Zusammenfassung*

5-LOX	5-lipoxygenase
AA	arachidonic acid
Ac-COX-2	acetylated cyclooxygenase-2
AcDex	acetalated dextran
AceDex	ethoxy-acetalated dextran
ADAM-10	a disintegrin and metalloproteinase domain-containing protein 10
APC	antigen presenting cell
API	active pharmaceutical ingredient
BLT	LTB ₄ receptor
cAMP	cyclic adenosine monophosphate
ChemR23	chemerin receptor
COX	cyclooxygenase
cPLA ₂	cytosolic Phospholipase A ₂
CYP	cytochrome P450
cysLT	cysteinyl leukotriene
DAMP	damage-associated molecular pattern
DAPI	4',6-diamidino-2-phenylindole
DHA	docosahexaenoic acid
DiHETE	dihydroxyeicosatetraenoic acid
DMARD	disease modifying anti-rheumatic drug
DP	PGD ₂ receptor
<i>E.coli</i>	<i>escherichia coli</i>
ET	extracellular traps
EET	epoxyeicosatrienoic acid
e.g.	for example
EMA	European Medicines Agency
EP	PGE ₂ receptor
EPA	eicosapentaenoic acid
ERK	extracellular signal-regulated kinase
FA	fatty acid
FDA	U.S. Food and Drug Administration
FLAP	5-lipoxygenase-activating protein

FP	PGF _{2α} receptor
FPR2	formyl peptide receptor 2
GM-CSF	granulocyte-macrophage colony-stimulating factor
GPCR	G protein-coupled receptor
GSH	glutathion
HEK	human embryonic kidney
hERG	human ether-a-go-go related gene
HDHA	hydroxydocosaehaenoic acid
HEPE	hydroxyeicosapentaenoic acid
HETE	hydroxyeicosatetraenoic acid
HpETE	hydroxyperoxy-eicosatetraenoic acid
ICAM-1	intercellular adhesion molecule-1
IF	immunofluorescence
IL	interleukin
IP	PGI ₂ receptor
i.p.	intra peritoneal
i.v.	intra venous
LDH	lactate dehydrogenase
LM	lipid mediator
LOX	lipoxygenase
LPS	lipopolysaccharide
LT	leukotriene
LTA ₄ H	ITA ₄ hydrolase
LTC ₄ S	ITC ₄ synthase
LX	lipoxin
MAPEG	membrane-associated proteins in eicosanoid and glutathione metabolism
MAPK	mitogen-activated protein kinase
MAPKAPK	mitogen-activated protein kinase-activated protein kinase
Mar	maresin
MD	molecular dynamics
MDM	monocyte-derived macrophages
mPGES-1	microsomal prostaglandin E ₂ synthase-1
NET	neutrophil extracellular trap
NFκB	nuclear factor κ-light-chain-enhancer of activated B cells
NSAID	nonsteroidal anti-inflammatory drug
PAMP	pathogen-associated molecular pattern

PC	phosphatidylcholine
PD	protectin
PG	prostaglandin
PGDS	PGD ₂ synthase
PGES	PGE ₂ synthase
PGFS	PGF _{2α} synthase
PGIS	PGI ₂ synthase
PKA	protein kinase A
PLGA	poly(lactide-co-glycolic acid)
PMNL	polymorphonuclear leukocytes
PPARα	peroxisome proliferator-activated receptor-α
PPR	pattern recognition receptor
PSM	phenol-soluble modulin
PUFA	poly unsaturated fatty acid
ROS	reactive oxygen species
RT	room temperature
SACM	<i>staphylococcus aureus</i> conditioned medium
<i>S.aureus</i>	<i>staphylococcus aureus</i>
sEH	soluble epoxide hydrolase
SPM	specialized pro-resolving mediator
TLR	toll-like receptor
TNFα	tumor necrosis factor α
TP	thromboxane receptor
TX	thromboxane
unstim	unstimulated
VCAM-1	vascular cell adhesion protein-1
w/o	without

II Summary

Originated from the enzymatic oxygenation of polyunsaturated fatty acids, lipid mediators (LM) conduct inflammatory and resolving responses of the innate immune system to restore homeostasis after infections or injuries¹. In current pharmacotherapy the production of pro-inflammatory prostaglandins (PG) and leukotrienes (LT) is reduced by inhibition of cyclooxygenase (COX)-1 and -2 or 5-lipoxygenase (LOX), which ameliorates inflammation but also exerts severe side effects upon long-term therapy, because the mediators that are crucial for homeostasis are influenced or substrates are redirected to other metabolic pathways, resulting in dysregulation of the lipid mediator network². Therefore, new pharmacological strategies to specifically modify the production of different lipid mediators are under constant development and the impact of drugs interfering with these metabolic pathways needs to be better understood.

The monitoring of the effects on the metabololipidomic spectrum of clinically relevant drugs like nonsteroidal anti-inflammatory drugs (NSAIDs) and common LM biosynthesis inhibitors in M1 and M2 macrophages, conducted in the first manuscript of this study, is an important step for further development. The treatment of cells with ibuprofen (COX-1/2 inhibitor) and celecoxib (selective COX-2 inhibitor) showed strong elevation of LT levels via a shunting effect due to the strong inhibition of all PGs. The 5-LOX inhibitor zileuton and the 5-lipoxygenase-activating protein (FLAP) inhibitor MK-886 potently reduced LT levels. The most important aspect of the study was to determine the effects of the drugs on the production of specialized pro-resolving mediators (SPM), which actively promote the resolution of inflammation. Here, only MK-886 (FLAP inhibitor) showed a favorably modulated LM profile by reducing pro-inflammatory LTB₄ and PGE₂ in M1 while evoking SPM biosynthesis in M2 macrophages. The findings indicated disadvantages of common therapeutics with respect to the overall LM profiles on the cellular level and pointed out their potential side effects upon long-term therapy. Optimal lipid mediator profiles were only obtained by usage of FLAP/mPGES-1 inhibitors, which are therefore the main target in focus for development of new pharmacological strategies throughout this thesis.

Over the recent years, the structure-activity relationships of dual FLAP/mPGES-1 inhibitors were investigated and as a result of consecutive studies, BRP-187 and BRP-201 were identified as promising drug candidates for anti-inflammatory therapy³⁻⁵. Despite their strong potency these compounds share unfavorable pharmacokinetic properties due to their lipophilic structure, which is required to target FLAP and mPGES-1 as membrane bound proteins. Therefore, new pharmacological strategies involving polymer-based nanocarriers were investigated as part of the project A04 in the SFB 1278 PolyTarget. Here, we formulated stable poly(lactic-co-glycolic acid) (PLGA), acetalated dextran (Ac-Dex) and ethoxy-acetalated

dextran (Ace-Dex) nanoparticles (NP) with BRP-187 and BRP-201 as anti-inflammatory payloads and studied their effectiveness in different *in vitro* and *in vivo* models. Each formulation displayed potent inhibition of LT formation on isolated leukocytes. BRP-187 incorporated into PLGA and Ac-Dex displayed prolonged effectiveness compared to the free drug. At the same time, BRP-187 in PLGA significantly increased the efficacy to reduce PGE₂ production of M1 macrophages, highlighting the favorable potential of the encapsulation. BRP-201 encapsulated in Ace-Dex NPs were tested in bacteria-stimulated human whole blood where it potently reduced LT formation, while free BRP-201 failed in this respect. This effect was confirmed *in vivo* using a zymosan induced peritonitis mouse model with *i.v.* injection of the BRP-201 Ace-Dex NP formulation.

Additionally, new polycaprolactone polymers with different monomeric composition from ϵ -caprolactone (ϵ -CL) and δ -caprolactone (δ -CL) isomers were studied to form the basis of a polymer library. In this study the varying crystallinity of the NPs resulted in differential enzymatic degradation pattern. Tested in ionophore stimulated leukocytes, the NPs with encapsulated BRP-187 showed different potential to reduce LT formation with respect to their crystallinity, implying a potential use for formulations with rapid or delayed drug release properties.

To resolve inflammation and actively regain homeostasis the production of SPMs is crucial⁶. While current anti-inflammatory therapy with NSAIDs or glucocorticoids focusses on the reduction of pro-inflammatory mediators⁷, new approaches to support resolution of inflammation are under development. For this reason, the influence of various compounds that interfere with the metabolism of polyunsaturated fatty acids (PUFAs) was examined in detail. In macrophages BRP-201 displayed not only potent reduction of PGs and LTs, but also upregulated 12/15-LOX products in exotoxin-stimulated M1 and M2 macrophages. Immunofluorescence microscopy confirmed a direct activation of 15-LOX-1 by BRP-201 reflected by subcellular redistribution of the enzyme. These findings were further verified in transfected HEK293 cells with different LOXs and co-expression of FLAP. Here, BRP-201 was able to induce 12/15-LOX product formation in HEK cells expressing 15-LOX-1 and 5-LOX/FLAP but not in 5-LOX-containing HEK cells devoid of FLAP, indicating a potential allosteric modulation of FLAP-bound 5-LOX by BRP-201, which may change the regiospecific oxygenation. In a zymosan-induced peritonitis mouse model BRP-201 showed similar results *in vivo*, suppressing pro-inflammatory LTs and inducing the production of SPMs.

In the consecutive screening of compounds, the dihydrochalcone derivatives MF-14 and MF-15 known to inhibit 5-LOX showed tremendous activation of 12/15-LOX product formation in M1 and M2 macrophages, comparable with activation of lipid mediator biosynthesis by bacterial exotoxins⁸. The activation of 15-LOX-1 was proven via immunofluorescence and is not caused by enhance release of PUFAs, which was confirmed by exogenous supply of fatty

acids. These results demonstrate the potential of these dihydrochalcones to act as a non-immunosuppressant, anti-inflammatory lipid mediator class switch inducers, which could have potential use in inflammatory therapy.

Taken together this thesis revealed the necessity for new pharmacological options for intervention in inflammatory diseases and disclosed a promising new approach to effectively deliver potent dual inhibitors to the site of action via NPs that would otherwise fail to act due to high lipophilicity and overall poor bioavailability. The sophisticated mode of action of these dual inhibitors not only reduces pro-inflammatory mediators but can actively induce the resolution phase by promoting SPM formation. These findings could contribute to a paradigm shift in inflammatory therapy via the combination of novel smart molecules and nanomedicine.

III Zusammenfassung

Lipidmediatoren (LM), die aus der enzymatischen Oxygenierung mehrfach ungesättigter Fettsäuren synthetisiert werden, leiten entzündliche und entzündungsauflösende Reaktionen des angeborenen Immunsystems ein, um die Homöostase nach Infektionen oder Verletzungen wiederherzustellen¹. In der derzeitigen Entzündungstherapie wird die Produktion von entzündungsfördernden Prostaglandinen (PG) und Leukotrienen (LT) durch Hemmung der Cyclooxygenase (COX)-1 und -2 oder 5-Lipoxygenase (LOX) reduziert, was die Entzündung lindert. Hierbei kann es in der Langzeittherapie zu schweren Nebenwirkungen kommen, da für die Homöostase entscheidende Mediatoren beeinflusst oder Substrate auf andere Stoffwechselwege umgeleitet werden, was zu einer Dysbalance des Lipidmediatornetzwerks führt². Die Untersuchung der genauen Auswirkungen von bestehenden Arzneimitteln auf die Lipidmediatorbiosynthese sowie die Erforschung neuer Therapieansätze zur gezielten Modifizierung des Netzwerkes ist ein wichtiger Schritt in der Therapie von entzündlichen Krankheiten.

Die im ersten Manuskript dieser Doktorarbeit durchgeführte Studie zu den Auswirkungen klinisch relevanter Medikamente wie nichtsteroidaler Antiphlogistika (NSAIDs) und gängiger LM-biosynthesehemmer auf das metabololipidomische Spektrum ist ein wichtiger Schritt für die weitere Arzneistoffentwicklung. Die Behandlung von M1- und M2-Makrophagen mit Ibuprofen (COX-1/2-Hemmer) und Celecoxib (selektiver COX-2-Hemmer) zeigte eine starke Erhöhung der LT-Spiegel über einen Shunting-Effekt aufgrund der starken Hemmung der Bildung aller PGs. Der 5-LOX-Inhibitor Zileuton und der 5-Lipoxygenase-Aktivierungsprotein (FLAP)-Inhibitor MK-886 reduzierten die LT-Spiegel deutlich. Der wichtigste Aspekt der Studie war die Bestimmung der Wirkungen der Arzneistoffe auf die Produktion von specialized-pro-resolving mediators (SPMs), die aktiv die Auflösung von Entzündungen fördern. Hierbei zeigte

lediglich MK-886 (FLAP-Inhibitor) ein günstig moduliertes LM-Profil, indem es das entzündungsfördernde LTB₄ und PGE₂ in M1 reduzierte, während es die SPM-Biosynthese in M2-Makrophagen erhöhte. Die Ergebnisse zeigen klare Nachteile gängiger Therapeutika in Bezug auf das Gesamtprofil der LM auf zellulärer Ebene und legen Gründe für potenzielle Nebenwirkungen bei einer Langzeittherapie nahe. Optimale Lipidmediatorprofile wurden nur durch die Verwendung von FLAP/mikrosomalen Prostaglandin-E2-Synthase (mPGES)-1-Inhibitoren erhalten, die daher das Hauptaugenmerk für die Entwicklung neuer pharmakologischer Strategien im Rahmen der Dissertation sind.

Die Struktur-Wirkungs-Beziehungen von dualen mPGES-1/FLAP Inhibitoren wurden in den letzten Jahren intensiv untersucht. Dabei identifizierte man BRP-187 und BRP-201 als vielversprechende Wirkstoffkandidaten für die entzündungshemmende Therapie³⁻⁵. Trotz ihrer hohen Wirksamkeit teilen diese Verbindungen aufgrund ihrer lipophilen Struktur ungünstige pharmakokinetische Eigenschaften, die erforderlich sind, um FLAP und mPGES-1 als membrangebundene Proteine zu inhibieren. Daher wurden im Rahmen eines innovativen Projekts A04 innerhalb des SFB 1278 PolyTarget polymerbasierte Nanopartikel als Wirkstoffträger eingesetzt. Hierbei wurden stabile Nanopartikel (NP) aus Poly(lactid-co-glycolid) (PLGA), acetalisiertem Dextran (Ac-Dex) und ethoxy-acetalisiertem Dextran (Ace-Dex) mit BRP-187 und BRP-201 als entzündungshemmende Wirkstoffe formuliert und ihre Wirksamkeit in verschiedenen In-vitro- und In-vivo-Modellen untersucht. Jede der untersuchten Formulierungen zeigte eine starke Hemmung der LT-Bildung in isolierten Leukozyten. In PLGA und Ac-Dex verkapseltes BRP-187 zeigte eine verlängerte Aktivität im Vergleich zum freien Molekül. Gleichzeitig erhöhte BRP-187 in PLGA die Wirksamkeit zur Verringerung der PGE₂-Produktion von M1-Makrophagen signifikant, was das Potenzial der Verkapselung unterstreicht. Im menschlichen Vollblut hemmen Ace-Dex-NPs mit BRP-201 im Vergleich zum freien Wirkstoff die LT-Bildung stark. Diese Wirkung wurde in einem Zymosan-induzierten Peritonitis-Mausmodell in vivo bestätigt, bei dem die Injektion der BRP-201 Ace-Dex NP-Formulierung i.v. erfolgte.

Zusätzlich wurden neue Polycaprolacton-Polymere mit unterschiedlicher monomerer Zusammensetzung von ε-Caprolacton (ε-CL)- und δ-Caprolacton (δ-CL)-Isomeren untersucht, um die Grundlagen einer Polymerbibliothek zu bilden. In dieser Studie führte die unterschiedliche Kristallinität der NPs zu einem unterschiedlichen enzymatischen Abbau. In Ionophor-stimulierten Leukozyten zeigten die NPs mit eingekapseltem BRP-187 aufgrund ihrer Kristallinität ein unterschiedliches Potenzial zur Verringerung der LT-Bildung, was eine potenzielle Verwendung der Polymere für Formulierungen mit schnellen oder verzögerten Wirkstofffreisetzungseigenschaften impliziert.

Um Entzündungen aufzulösen und die Homöostase aktiv wiederzuerlangen, ist die Produktion von SPMs von entscheidender Bedeutung⁶. Während sich die aktuelle Entzündungstherapie

mit NSAIDs oder Glukokortikoiden auf die Reduktion entzündungsfördernder Mediatoren konzentriert⁷, werden neue Ansätze zur Unterstützung der Auflösung statt der Einleitung von Entzündungen entwickelt. Aus diesem Grund wurde der Einfluss verschiedener Verbindungen, die in den Stoffwechsel mehrfach ungesättigter Fettsäuren (PUFAs) eingreifen, eingehend untersucht. In Makrophagen zeigte BRP-201 nicht nur eine starke Reduktion von PGs und LTs, sondern auch erhöhte 12/15-LOX-Produkte in Exotoxin-stimulierten M1- und M2-Makrophagen. Immunfluoreszenzmikroskopie bestätigte eine direkte Aktivierung der 15-LOX-1 durch BRP-201, sichtbar durch subzelluläre Umverteilung des Enzyms. Diese Ergebnisse wurden in transfizierten HEK293 Zellen mit verschiedenen LOXs mit Koexpression von FLAP verifiziert. Hier war BRP-201 in der Lage, die Bildung von 12/15-LOX-Produkten in HEK Zellen zu induzieren, die 15-LOX-1 und 5-LOX/FLAP exprimieren, jedoch nicht in 5-LOX-HEK Zellen ohne FLAP. Diese Beobachtung lässt auf eine mögliche allosterische Modulation von FLAP-gebundener 5-LOX durch BRP-201 schließen, was die regiospezifische Oxygenierung der LOX verändern könnte. In einem Zymosan-induzierten Peritonitis-Mausmodell zeigte BRP-201 ähnliche Ergebnisse, indem es entzündungsfördernde LTs unterdrückte und die Produktion von SPMs induzierte.

In einem intensiven Screening von Verbindungen, die einen Einfluss auf die LM-Biosynthese haben könnten, zeigten die Dihydrochalcon-Derivate MF-14 und MF-15, von denen bekannt ist, dass sie 5-LOX hemmen, eine enorme Aktivierung der 12/15-LOX-Produktbildung in M1- und M2-Makrophagen. Der Aktivierungsgrad der Lipidmediator-Biosynthese ist mit dem bakterieller Exotoxine vergleichbar⁸. Die Aktivierung der 15-LOX-1 wurde durch Immunfluoreszenzmikroskopie nachgewiesen und wird nicht durch eine verstärkte Freisetzung von PUFAs verursacht, wie durch die exogene Zufuhr von Fettsäuren bestätigt wurde. Diese Daten zeigen das Potenzial von Dihydrochalconen, die als nicht immunsuppressive, entzündungshemmende Lipidmediator-Klassenwechselinduktoren wirken und somit potenziell für die Entzündungstherapie eingesetzt werden könnten.

Zusammenfassend hat diese Dissertation die Notwendigkeit neuer pharmakologischer Optionen für die Intervention bei entzündlichen Erkrankungen klar aufgezeigt und einen vielversprechenden neuen Ansatz untersucht, um potente duale Inhibitoren über NPs effektiv an den zellulären Wirkort zu bringen, die sonst aufgrund hoher Lipophilie und insgesamt schlechter Bioverfügbarkeit nicht wirken würden. Die ausgeklügelte Wirkungsweise dieser dualen Inhibitoren reduziert nicht nur entzündungsfördernde Mediatoren, sondern leitet aktiv die Auflösungsphase von Entzündungen durch Förderung der SPM-Bildung ein. Diese Erkenntnisse könnten durch die Kombination von intelligenten neuen Wirkstoffen und Nanomedizin zu einem Paradigmenwechsel in der Entzündungstherapie beitragen.

1. Introduction

1.1 Inflammation and Resolution

The immune system of mammals is daily triggered by infectious invaders, tissue injuries or other severe disturbances of homeostasis⁹. To eliminate the potentially dangerous stimulus, a local inflammation is displayed by five cardinal signs “dolor” (pain), “calor” (heat), “rubor” (redness), “tumor” (swelling) and in the worst cases “function laesa” (loss of function)¹⁰ first described by the ancient encyclopaedist C. Celsus. Activated through pattern recognition receptors (PRR), Toll-like receptors (TLR) or nucleotide-binding oligomerization domain protein-like receptors (NLRs) on tissue resident macrophages and mast cells the inflammatory cascade is set in motion¹¹. This process is initiated and maintained by pro-inflammatory cytokines, chemokines, vasoactive amines and eicosanoids, which initiate the expression of adhesion proteins (selectin-P, selectin-E) and integrins (ICAM-1, VCAM-1), cause vasodilatation, increase blood vessel permeability and recruit leukocytes from the blood stream (leukodiapedesis)¹². The extravasated leukocytes, mostly neutrophils, now react to the damage- or pathogen associated patterns (DAMPs, PAMPs) and try to eliminate the noxious stimuli by an oxidative burst, different proteinases, hydrolases, antibiotic proteins and by forming of extracellular traps (ETosis) to avoid further contamination in surrounded tissues^{13,14}. Beside the activation of the innate immune response, tissue resident macrophages and dendritic cells as antigen presenting cells (APCs) activate the adaptive immune system, which lead to specific elimination of antigens^{15,16}. This inflammatory cascade is well orchestrated and very important to protect the body from external threats (Figure 1) and remain functional, but if the innate immune system is not able to limit itself, inflammation cannot be resolved, which can lead to chronic inflammatory diseases like asthma, rheumatoid arthritis, Alzheimer disease, autoimmunity, arteriosclerosis, diabetes and even cancer¹⁷. Historically, it was thought that resolution of inflammation is a passive process caused by the dilution of the chemokine gradient resulting in lower leukocyte recruitment¹⁸, but extensive work over the past decades revealed that resolution of inflammation is like the initiation an active process induced by several different mediators. In a normally regulated resolution phase prostaglandin (PG)E₂ and PGD₂ induce a class switch after several hours, where lipoxins (LXs) are produced that inhibit neutrophil migration by induction of cytokine and chemokine scavenging^{19,20}. Additionally, LXs prevent translocation of nuclear factor kappa-light-chain-enhancer of activated B cells (NF-κB), the expression of chemokine receptors, adhesion molecules and further stimulate macrophage polarization to an anti-inflammatory phenotype^{21,22}. Hence, the lipid mediator (LM) spectrum changes from proinflammatory eicosanoids to specialized pro-resolving mediators (SPMs), that enhance phagocytosis and induce efferocytosis of apoptotic

neutrophils^{23,24}. In the end the tissue function is restored, and myeloid cells are incorporated into the tissue or carried away by the lymphatic system, so when leukocyte population is returned to the initial amount in the tissue the inflammation is terminated and homeostasis should be restored²⁵.

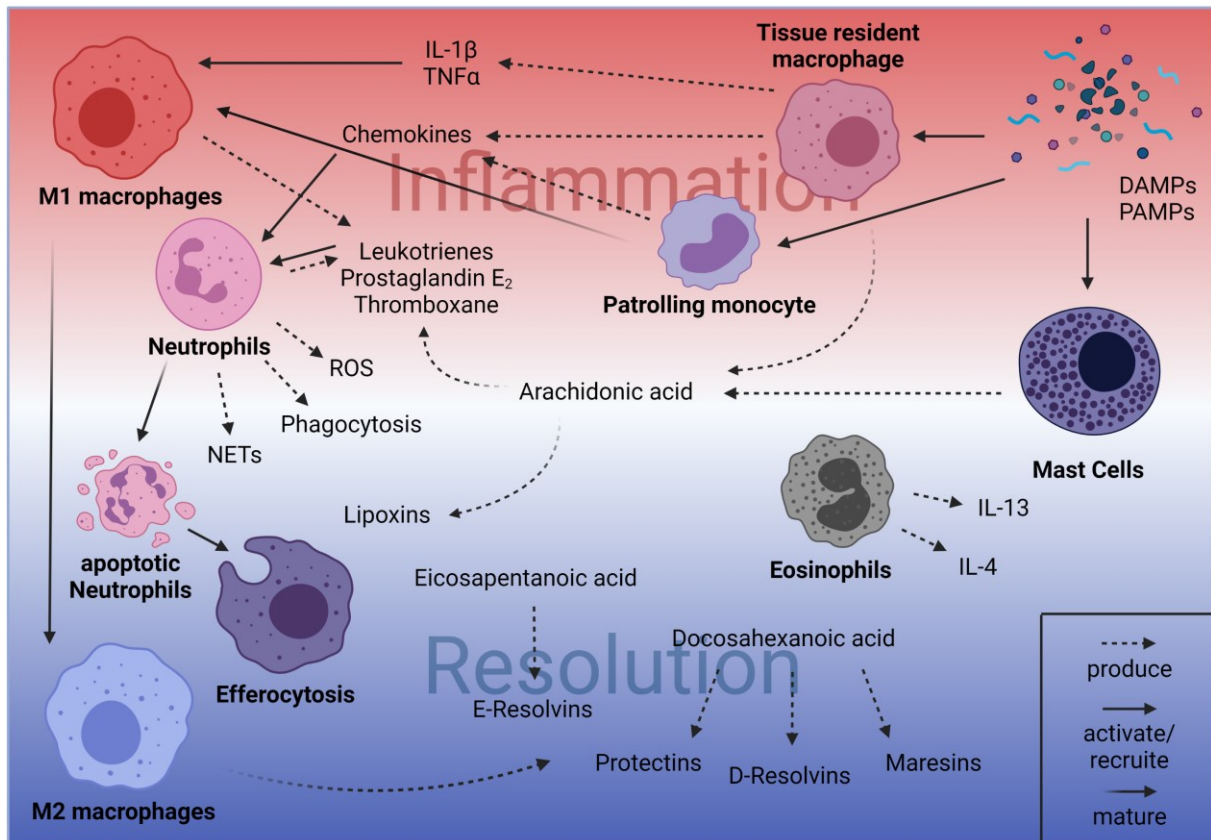


Figure 1 Essential cellular components and mediators that govern inflammation and resolution. Adapted from S.E. Headland et al.¹⁸. PAMPs and DAMPs activate tissue resident macrophages, mast cells and patrolling monocytes that produce IL-1 β , TNF α , different chemokines and proinflammatory lipid mediators (LTB₄, PGE₂ and TXA₂) to recruit neutrophils. The infiltrated neutrophils release ROS, do phagocytosis and NETosis to clear the harmful stimulus. After neutrophil activity apoptosis is induced and the apoptotic cells are cleared by macrophages via efferocytosis. Monocytes and macrophages mature to M2 macrophages which produce SPMs and induce the reinforcement of homeostasis.

1.2 Chronic inflammation

If inflammation fails to subside, an inflammatory state can become chronic. Unresolved inflammation contributes significantly to the pathogenesis of many chronic inflammatory diseases like arteriosclerosis, asthma, rheumatoid arthritis, Alzheimer disease, multiple sclerosis and even cancer²⁶. The main threat of chronic inflammation is not the stimulus itself, but the exaggerated reaction and the dysregulation of pro-inflammatory and anti-inflammatory signals that eventually destroy cells and tissue function^{10,26}. Many of the important inflammatory mechanisms like cytokine release, cell death signals and reactive oxygen species (ROS) formation are not counter-regulated and the resulting tissue damage arouses

further inflammatory responses. For example, in rheumatoid arthritis billions of neutrophils with short half-life (4 h) infiltrate the joint daily. If the neutrophils die, they may release cytosolic peptidyl arginine deiminase type 4, which is activated by the escaping intracellular Ca^{2+} and convert guanidino side chains of L-arginine to citrulline. The antibodies associated with rheumatoid arthritis react to citrulline and as a result more neutrophils are recruited which further secrete inflammatory, destructive cytokines and oxidants leading to further harm^{27,28}. To limit the consequences of this negative feedback loop it is highly important to intervene before irreparable impairments of the body occur. Common therapy to prevent inflammation implies the usage of nonsteroidal anti-inflammatory drugs (NSAIDs), glucocorticoids and disease-modifying agents of rheumatoid diseases (DMARDs) as well as some recombinant biologicals like tumor necrosis factor α (TNF α) and interleukin (IL)-1 β antagonists²⁹. The long-term treatment with these drugs often has serious side effects. Many DMARDs like methotrexate and ciclosporine have a small therapeutic window, where meticulous monitoring is necessary to guarantee therapeutic success³⁰. In addition, the treatment of drugs, that modify the immune response often correlates with high risk of infections with certain bacteria, fungi and virus. Also, persisting infections that normally remain inactive, can be reinforced, which is a significant risk for patients suffering from heavy chronic inflammation³¹. Therefore, long-term anti-inflammatory therapy needs to be calculated by risk:benefit ratio that often not favors a drug treatment²⁹. Because unresolved and chronic inflammation is a major threat for human health and trigger for inflammation-related diseases the necessity of new pharmacological strategies to modulate immune response is of great interest for research and drug development^{1,32,33}.

1.3 Lipid mediator biosynthesis

Lipid mediators are oxidized poly unsaturated fatty acids (PUFAs) being indispensable for the process of inflammation and resolution with a variety of different bioactivities¹. Upon activation of the immune system PUFAs are cleaved by phospholipase A₂ (PLA₂) as a hydrolysis product of the ester-bond in *sn*-2 position from phospholipids of cellular membranes³⁴. Mainly arachidonic acid (AA, 20:4, ω 6), eicosapentaenoic acid (EPA, 20:5, ω 3) and docosahexaenoic acid (DHA, 22:6, ω 3) are used as substrates for cyclooxygenases (COX), lipoxygenases (LOX) or cytochrome P450 (CYP) enzymes, which have different oxidizing functions (Figure 2)^{2,35,36}.

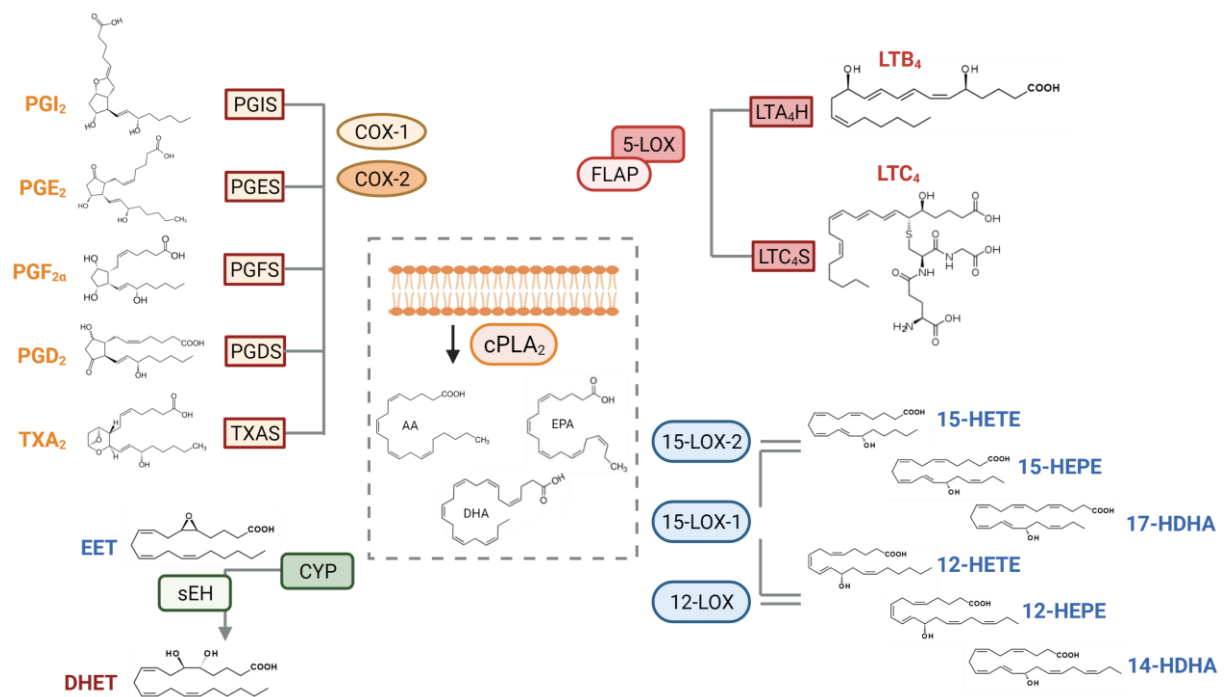


Figure 2 Lipid mediator biosynthesis adapted from E.A. Dennis et al.³⁵. Biosynthesis of LM derived from AA, EPA and DHA which are released by cPLA₂. The different metabolization pathways are indicated with their downstream proteins that produce different LM of one class. Potentially pro-inflammatory LM are written in red, immune modulating LM in yellow and pro-resolving LM and their precursors in blue.

1.3.1 5-Lipoxygenase and Leukotrienes

LTs, which got their name from their origin (leukocytes) and their structural composition (three conjugated double bonds), are pro-inflammatory lipid mediators first discovered in 1976 by Bengt Samuelsson^{37,38}. Since then, LTs and their role in inflammation were extensively studied. The first step of AA metabolization down the LT biosynthetic pathway is executed by 5-LOX. Human 5-LOX is a non-heme iron containing dioxygenase encoded by ALOX5 gene on chromosome 10 with a molecular mass of 77.9 kDa^{39,40}. It consists of a N-terminal regulatory C2 like domain (~120 amino acids) and a C-terminal catalytic domain (~550 amino acids)⁴¹. The catalytic iron is bound in the C-terminal catalytic domain by His367, His372 and His550 as well as the carboxyl moiety of Ile673. In contrast to other lipoxygenases, the active center of the 5-LOX is blocked through a shortened α -2 helix by Phe177 and Tyr181, which prevents the access of fatty acids (FY cork)⁴¹. A mutation at this point to alanine causes a loss of activity in cell-free assays and a delayed translocation of the 5-LOX to the nuclear membrane, so that no more 5-LOX products are formed. However, through the interaction with 5-lipoxygenase activating protein (FLAP) in cellular assays, this function is compensated and partially restored⁴². The smaller N-terminal regulatory domain mainly consists of β -barrels and navigates the activity of 5-LOX. By binding of calcium (Ca²⁺) 5-LOX can be activated and translocate to the nuclear membrane, where phosphatidylcholine can bind at Trp13, Trp75 and Trp102 to anchor the protein to the nuclear membrane^{43,44}. In addition, the phosphorylation of

5-LOX can also regulate the activity of LT biosynthesis in a Ca^{2+} independent manner. Mitogen-activated protein kinase-activated protein kinase (MAPKAPK)-2 and the extracellular-signal regulated kinase (ERK) can upregulate the enzyme activity by phosphorylation at Ser271 and Ser663, respectively⁴⁵. In contrast the cyclic adenosine monophosphate (cAMP) dependent activity from protein kinase A (PKA) phosphorylates 5-LOX at Ser523 leading to decreased LT biosynthesis⁴⁶.

5-LOX is activated by the oxidation of the inactive ferrous (Fe^{2+}) to the active ferric (Fe^{3+}) by lipid hydroperoxides^{47,48}, which enables the coordination to a hydroxide ion instead of water and opens the cavity for the entrance of fatty acids^{41,43}. In case of AA, it catalyzes the stereospecific abstraction of a hydrogen at carbon (C)-7 to form a radical that rearranges to insert an oxygen at C-5 to produce 5-(S)-hydroperoxyeicosatetraenoic acid (5-(S)-HpETE). This hydroperoxide is reduced by peroxidases to the corresponding alcohol or further processed by the synthase activity of 5-LOX to LTA_4 . The instable intermediate is formed by the abstraction of the C-10 R-hydrogen with radical migration to C-6 to form a $\Delta^{7,9,11}$ -triene structure, where the C-5 hydroperoxide reacts instead of another oxygen by dehydration to an epoxide⁴⁹⁻⁵¹. Beside the synthase activity of 5-LOX another unique characteristic is the self-inactivation mechanism that tempers the pro-inflammatory response⁵². Inactivation can either take place via non-turnover-dependent structure instability due to the naturally instable structure of the activated enzyme or turnover-based suicide that involves the irredeemable inactivation of the enzyme⁵³⁻⁵⁵.

LTA_4 is immediately metabolized by two different enzymes synthesizing LTB_4 or cysteinyl LTs (cys-LTs). The most prominent products from the 5-LOX pathway are LTB_4 , which is formed by LTA_4 hydrolase (LTA_4H), and LTC_4 as product of the LTC_4 synthase (LTC_4S). The LTA_4H is a soluble, zinc-dependent epoxide hydrolase and aminopeptidase, widely distributed among mammalian cells⁵⁶. In contrast to LTA_4H the LTC_4S is a membrane-bound protein that is activated by Mg^{2+} as well as phosphatidylcholine and requires reduced glutathione (GSH) for its stability^{57,58}. Like the 5-lipoxygenase-activating protein (FLAP) and the microsomal prostaglandin E_2 synthase-1 (mPGES-1) the LTC_4S is a membrane-associated protein in eicosanoid and glutathione metabolism (MAPEG)⁵⁹. While neutrophils and M1 macrophages mostly produce LTB_4 , due to their relevant expression of LTA_4H , eosinophils, basophils and mast cells tend to synthesize cys-LTs in favor⁶⁰.

LTs act in local inflammation processes as paracrine mediators on G protein-coupled receptors (GPCRs) and induce intracellular signaling cascades^{60,61}. LTB_4 binds to the leukotriene B_4 receptor-1 and -2 (BLT1, BLT2)⁶⁰. The BLT-1 receptor is expressed on inflammatory cells and shows very high affinity ($K_d = 0.15\text{-}1\text{ nM}$) to LTB_4 mediating chemotaxis, Ca^{2+} influx and the expression of adhesion molecules for leukocyte infiltration⁶². The later discovered BLT2 receptor has a lower affinity to LTB_4 ($K_d = 61\text{ nM}$) and is also a seven transmembrane spanning

GPCR that mediates chemotaxis and causes Ca²⁺ influx⁶³. The chemotactic response can be inhibited by *Bordetella pertussis* toxin (PTX) suggesting that both receptors use Gα_{i/0} subunit signaling, while Ca²⁺ influx was only partially blocked^{62,64}. In neutrophils LTB₄ can also induce the production of LTB₄ and interleukin-8 (IL-8) and primes the cells for N-formyl-methionyl-leucyl-phenylalanine (fMLP) while enhancing C3b receptor expression⁶⁵. In monocytes and macrophages, the production of IL-1, IL-6, TNFα, IL-2 receptor expression and ROS formation is induced^{63,65}. In addition, LTB₄ produced in the cytosol also binds to the nuclear factor peroxisome proliferator-activated receptor-α (PPARα) that downregulates further production of LTB₄ and functions as a self-regulating mechanism⁶⁶. The cys-LTs bind to two different cys-LT receptors, which are also GPCRs mediating inflammatory response. Expressed on eosinophils, lung smooth muscle cells and tissue resident macrophages the cys LT₁-receptor signals cause bronchoconstriction, mucus release and bronchial edema from venules, that play important role in the pathophysiology of asthma⁶⁷.

The pro-inflammatory activity of LTs was intensively investigated since their discovery and now can be related to many inflammatory diseases like asthma, atherosclerosis, rheumatoid arthritis, atopic dermatitis, cystic fibrosis, psoriasis, diabetes, Alzheimer disease, multiples sclerosis and cancer. Due to the self-amplifying mechanism, LTs contribute to the progression of such diseases and prolong the recovery time. Despite being very helpful in acute infections and tissue injuries dysregulated production of leukotrienes is rather unhealthy and needs to be addressed in the therapy of excessive inflammation^{2,43,60,61,65}.

Table 1 Prominent lipid mediators and their biologic activity

Lipid mediators and their bioactivities via G-protein coupled receptors adapted from Dennis et al. 2015³⁵. BLT – LTB₄ receptor, COX – cyclooxygenase, CYP – cytochrome P450, ChemR23 – Chemerin receptor, CysLT – cysteinyl leukotriene receptor, DP – PGD₂ receptor, EP – PGE₂ receptor, FP – PGF_{2α} receptor, FPR2 – formyl peptide receptor 2, GPR – G-protein coupled receptor, IP – PGI₂ receptor, PPAR – peroxisome proliferator activated receptor, TP – thromboxane receptor.

Enzyme	Lipid mediator	Receptor	Biological activity
COX	PGE ₂	EP1, EP2, EP3, EP4	vasodilation, vascular permeability ↑, fever, hyperalgesia, IL-10 ↑, TNF-α ↓
	PGD ₂	DP1	vasodilation, neuro protection, mast cell maturation
		DP2	recruitment of eosinophils, allergic response
	PGF _{2α}	FP	smooth muscle contraction
	PGI ₂	IP	Vasodilation, thrombocyte aggregation ↓
	TXA ₂	TP	Vasoconstriction, thrombocyte aggregation ↑
5-LOX/ FLAP	LTB ₄	BLT1	Neutrophil recruitment, vascular permeability ↑
		BLT2	Epithelial barrier function ↑
	LTC ₄	CysLT1, CysLT2	Bronchoconstriction, vascular permeability ↑
15-LOX/5-	LXA ₄ , LXB ₄	ALX/FPR2	Neutrophil infiltration ↓, phagocytosis ↑

LOX, 12-LOX/5- LOX, Ac- COX/5- LOX	RvD1	ALX/FPR2, GRP32	Neutrophil infiltration ↓, phagocytosis ↑
	RvD1, RvD5, RvD3	GPR32	phagocytosis ↑
	RvD2	GPR18	Neutrophil infiltration ↓, phagocytosis ↑, efferocytosis ↑
CYP	EETs	PPAR α , PPAR γ	Vasodilation, pain sensitivity ↓, COX-2 expression ↓
CYP/5- LOX, Ac- COX/5- LOX	RvE1, RvE2	ChemR23, BLT1 _(antagonist)	Neutrophil infiltration ↓, phagocytosis ↑

1.3.2 5-Lipoxygenase-activating protein (FLAP)

Among the afore-mentioned MAPEG subfamily of proteins, FLAP is a very special member without enzymatic activity or the ability to bind GSH⁶⁸. It was identified via the activity of the indole-based compound MK-886, which potently decreased LT formation without effecting 5-LOX or cPLA₂, and first described as MK-886-binding protein by Dixon et al. in 1990⁶⁹. The structure of the 18 kDa enzyme was crystalized by binding of MK-591 with 4 Å resolution⁷⁰. FLAP is a homotrimer with four transmembrane α -helices (α 1- α 4) per monomer, that are linked via two cytosolic (C1, C2) and one luminal loop (L1)⁷⁰. Deep in the nuclear membrane between the α 1, α 2 and α 4 helices is the binding site for MK-591 forming van der Waals interactions with Val20, Val21, Gly24, Phe25, Ala27 from α 1 helix; Ala63 on helix α 2; Ile119, Lei120, Phe123 from helix α 4 and Tyr112 and Ile113 from the C2 loop. This inhibitor binding site is also considered as the AA binding site, which would fit to the location inside the nuclear membrane^{70,71}. After activation, 5-LOX translocates in close proximity to FLAP, where the interaction is believed to be dependent on the residues of the two cytosolic loops⁷⁰. This interaction can be prevented by FLAP inhibitors like MK-886 but not 5-LOX inhibitors like Zileuton^{4,72,73}. FLAP facilitates the AA to 5-LOX and favors the formation of 5-HpETE to LTA₄⁷⁴. Inhibition of FLAP as well as genetic knockout prevents LT formation in intact cells⁷⁵. The exogenous supply of AA restores the necessity of FLAP in LT biosynthesis⁷⁶.

1.3.3 Cyclooxygenase 1/2 and prostaglandins

The COXs are members of the myeloid-peroxidase superfamily and catalyze the metabolism of AA via PGG₂ by bisoxygenation and further reduces this intermediate product by peroxidase activity to PGH₂⁷⁷. The COX-1, back in the days of discovery just COX, was first isolated from sheep and bovine vesicles in 1976^{78,79}. For another 15 years COX-1 was believed to be the only COX in eukaryotic cells, until COX-2 was discovered in 1991^{80,81}. While COX-1 is constitutively expressed in many cells and tissues and regulates PG formation for

homeostatic activity like integrity of the gastric mucosa, mediating platelet function and regulating renal blood flow, COX-2 expression is induced by TNF α , IL-1 β or mitogenic factors such as lipopolysaccharide (LPS) and thus strongly related to inflammatory processes⁸²⁻⁸⁴. Both COX enzymes are built of homodimers and are around 65-74 kDa with similar tertiary structures. The primary difference between both subtypes is the first shell substitution from Ile434, His513 and Ile523 in COX-1 to Val434, Arg513 and Val523 in COX-2 which results in +25% increased volume in the binding pocket with Arg513 located at the base of the resulting side pocket^{85,86}. The final product of the two-step reaction PGH₂ is immediately metabolized by different PG-synthases, which products have numerous effects dependent on the tissue and activated receptors. PGE₂ is biosynthesized by PGE₂ synthase (PGES), PGD₂ by PGD synthase (PGDS), PGF_{2 α} by PGF synthase (PGFS), PGI₂ by PGI synthase (PGIS) and thromboxane (TX)A₂ by TX synthase^{87,88}. The prostanoids mediate their activity autocrine or paracrine via product specific GPCRs. PGE₂ is one of the most abundant synthesized prostanoids and can exert pro- and anti-inflammatory effects depending on the relevant receptor gene expression by the affected cells⁸⁹. The hyperalgesic effects of PGE₂ in early inflammation are for example mediated through EP1 and EP4 receptor signaling that acts on peripheral sensory neurons and the central sensory system to induce pain⁸⁹⁻⁹¹. PGE₂ is also involved in the induction of the other cardinal symptoms of inflammation via EP2 mediating vasodilatation and increases permeability and activation of EP3 inducing fever⁸⁹. Beside the involvement of PGE₂ in homeostatic mechanisms like the regulation of blood pressure, gastrointestinal integrity and fertility, the prostanoid can also exhibit anti-inflammatory effects^{7,89}. Especially in neuroinflammation PGE₂ blocks LPS- and ATP-induced cytokine release and mediates bradykinin-induced neuroprotection^{92,93}. Together with PGD₂ it also induces the formation of LXA₄ instead of LTB₄, which initiate the lipid mediator class switch and thus resolution^{19,20}. Another important prostanoid is PGD₂, which is associated with inflammatory, homeostatic and anti-inflammatory effects as well, mediated via D prostanoid receptor (DP) 1 and DP2 and low affinity to PPAR γ ⁷. PGI₂ and TXA₂, that is rapidly degraded to TXB₂, are mostly counterparts for their regulation of blood pressure on vascular smooth muscle cells and coagulation, while TXA₂ is formed mostly via platelet COX-1, PGI₂ formation is associated with COX-2^{94,95}. Although COX-2 is expressed upon activation of immune cells and appears to be more relevant for the acute inflammatory response, constitutively expressed COX-1 is also present in inflammatory cells and induced by LPS or cellular differentiation⁹⁶. It is known that both enzymes are involved in the initiation of the acute inflammation, but anti-inflammatory effects in later phases of the inflammatory process have also been proven^{7,77,97-99}. These diverse activities in homeostasis or different stages of inflammation within different tissues makes the use of NSAIDs or selective COX-2 inhibitors difficult. Even in diseases, where for example PGE₂ is clearly involved in the pathogenesis like arthritis, the

downregulation of other prostanoids by NSAIDs or COX-2 inhibitors makes the long-term usage problematic and is controversially discussed^{29,30,99,100}. This implies the necessity for more specific approaches to address downstream events related to specific PGs in relevant cells and tissues to modulate inflammatory response without interfering with homeostatic activities.

1.3.4 Microsomal prostaglandin E₂ synthase-1 (mPGES-1)

Around the 1970s and 1980s the existence of enzymes that catalyze the metabolization from PGH₂ to PGE₂ was recognized and first attempts to isolate the enzymes from seminal vesicles were reported^{101,102}. From 1999 to 2002 three PGES, namely, mPGES-1, cytosolic PGES (cPGES) and mPGES-2 were cloned and characterized⁸⁸. While cPGES and mPGES-2 are constitutively expressed and involved in homeostasis, mPGES-1 is inducible by LPS or IL-1 β exposure and is therefore relevant at sites of inflammation like COX-2¹⁰³. The mPGES-1 (16 kDa, 152 amino acids) belongs like FLAP to the MAPEG family and is a homotrimer, where each monomer consists of four transmembrane helices (TM1-4). The active site is a cone-shaped cavity located at the inner core of each monomer, where GSH is bound as cofactor by hydrogen bonds and π -interactions and the substrate enters the cavity by its peroxofuran with the two tails pointing to the lipid mediator membrane^{104,105}. The active site is separated from an inner core cavity by Arg73 and Asp49 on top of the active site functions as a proton acceptor due to its close proximity to Arg126, which increases the basicity. Additionally, Ser127 stabilizes the resulting thiolate of GSH with a hydrogen bridge^{104,106}. mPGES-1 is associated with inflammatory relevant PGE₂ production and the knockout of the enzyme has protective effects in different models of rheumatoid arthritis in mice, but the contradictory effects of PGE₂ cannot postulate the inflammatory profile of mPGES-1 for every inflammatory disease^{7,105,107,108}.

1.3.5. 15-Lipoxygenase and specialized pro-resolving mediators

The 15-LOX is like 5-LOX a lipid-peroxidizing enzyme that catalyze the metabolization of PUFAs by introduction of dioxygen at C-15 of AA¹⁰⁹. The first mammalian 15-LOX was found in 1975 in rabbit reticulocytes and 13 years later, in 1988, a similar enzyme was successfully purified from human eosinophils^{110,111}. In 1997 another subtype of 15-LOX, the 15-LOX-2, was cloned from human hair roots¹¹². The ALOX15 and ALOX15B genes are on chromosome 17 with similar structure around 75 kDa¹¹³. Like 5-LOX both 15-LOX subtypes consist of a C-terminal catalytic and an N-terminal regulatory membrane binding domain with a non-heme iron at the active site, which is bound by four His and one Ile. Another similarity to 5-LOX is the necessity of an oxidative activation from Fe²⁺ to Fe³⁺ by hydroperoxides^{114,115}. The entry of AA occurs tail-first which favors the insertion of oxygen at C-15 and produces 15-HpETE, while

12-HpETE can be formed as a side product to a lesser extent from 15-LOX-1 but not 15-LOX-2. While the metabolization of EPA to 12-hydroxyeicosapentaenoic acid (HEPE) is slightly more favored than the production of 12-hydroxyeicosatetraenoic acid (HETE) by 15-LOX-1, DHA is oxygenated to 17-hydroxydocosahexaenoic acid (HDHA) and 14-HDHA in approximately equal amounts. On the other hand, 15-LOX-2 still remains to synthesize 15-HEPE and 17-HDHA preferably¹¹⁶. Interestingly, methylation of the carboxyl group from the fatty acid substrates also allows substrate insertion head-first, which results in oxygenation on position C-5 for AA and EPA or C-7 for DHA, while bulky moieties revert these effects¹¹⁷. The expression of 15-LOX-2 is constitutive and the enzyme is mostly present in hair roots, the epidermal skin and the prostate but also in macrophages. 15-LOX-1 on the other hand is inducible by IL-4 or IL-13 in human macrophages eosinophils or the bronchial epithelial cells¹¹⁸⁻¹²². While the biological function of 15-LOX-2 is still mostly elusive, 15-LOX-1 together with acetylated COX, CYP450, 5-LOX and 12-LOX is known to be involved in the biosynthesis of SPMs, which actively promote resolution of inflammation and are in focus of recent research¹¹⁶. This group of lipid mediators is subdivided in LXs derived from AA, E-resolvins (Rvs) from EPA, D-Rvs from DHA as well as maresins (MaR) and protectins (PD) (Figure 3)¹²³. At the peak of the inflammatory response PGs are involved in the upregulation of 15-LOX-1 which induces the lipid mediator class switch and lead to the production of LXs¹²⁴. These mediators are mostly formed by transcellular biosynthetic pathways where LTA₄ is metabolized via 15-LOX-1 or the 15S-HpETE is oxygenated by 5-LOX to LXA₄¹²⁵. Additionally, acetylated COX-2 (ac-COX-2) by Aspirin[®] and CYP450 enzymes can convert AA to 15R-HpETE, which is a precursor for aspirin-triggered (AT) LXs¹²⁶. As a result of LX production, clearance of apoptotic neutrophils is induced, neutrophil migration is suppressed and ROS formation is reduced, additionally the production of anti-inflammatory cytokines is induced, which primes infiltrating monocytes and further initiate the resolution phase^{125,127}. Here E-Rvs are produced from EPA, which is catalyzed by acetylated COX-2 or CYP450 to 18-HEPE and is further processed by 5-LOX to RvE1 and RvE2 or by 15-LOX-1 or 12-LOX to RvE3, whereas RvE4 is biosynthesized by 5-LOX and 15-LOX-1^{123,128}. D-Rvs, MaRs and PDs are also produced via various enzymatic interactions from DHA. 15-LOX-1 can oxygenate DHA to 17-HDHA and 14-HDHA¹¹⁶. The D-Rvs are yielded from 17-HDHA by metabolization via 5-LOX to RvD1, RvD2, RvD3, RvD4 and RvD5. PD1 is also derived from 17-HDHA, which can isomerize to PDX¹²⁷. Both type of SPMs have also AT-isomers which are derived likewise to EPA from acetylated COX-2 and the resulting 17R-HDHA¹²⁹. MaRs are generated from 14-hydroperoxy-docosahexaenoic acid (HpDHA) and gets further converted to 13S, 14S-epoxy-MaR, which is an epoxide intermediate and gets rapidly converted to MaR1 and MaR2^{130,131}. The biological actions of these mediators are conducted via different GPCRs, namely N-formyl peptide 2/lipoxin A4 receptor (FPR2/ALX), GPR32, GPR18, GPR37, BLT1 and chemerin receptor 1 but also nuclear

receptors like PPAR γ and the estrogen receptor¹³².

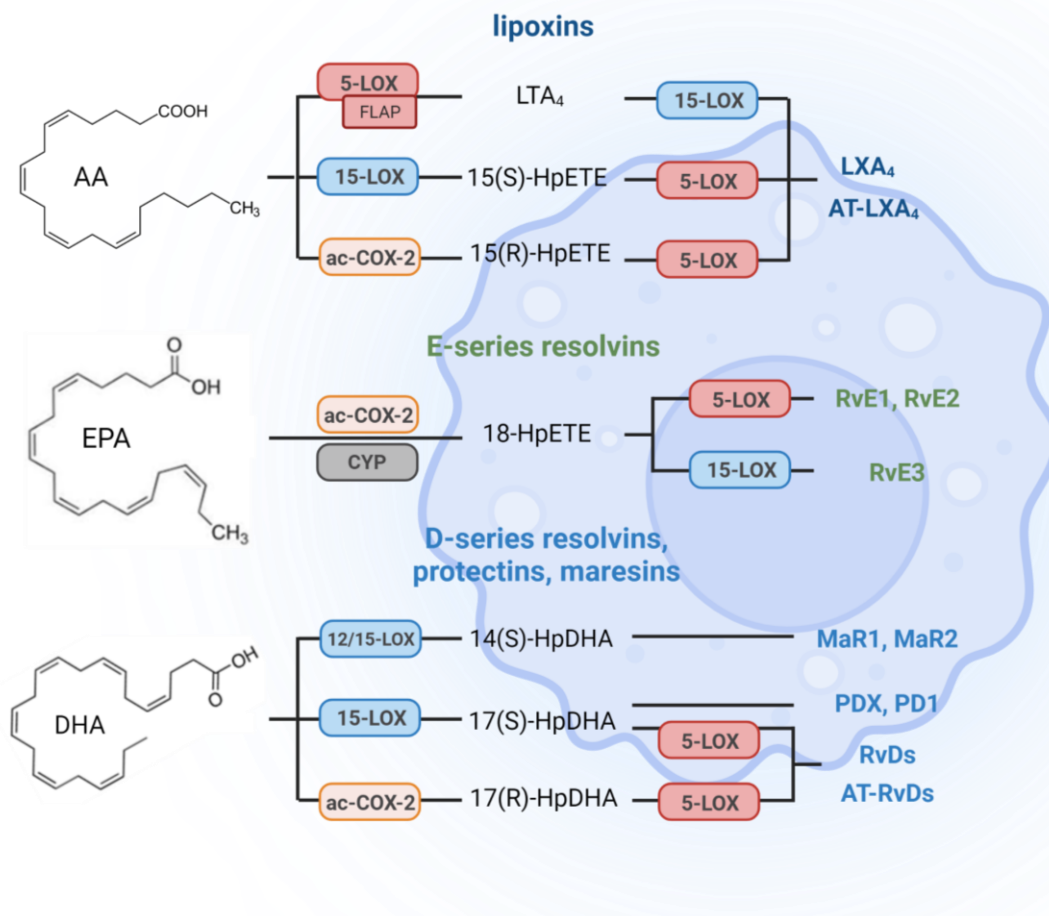


Figure 3 Biosynthetic pathways of SPMs according to N. Chiang et al. (2020)¹³³, C.N. Serhan et al. (2018)¹²³ and C.N. Serhan et al. (2011)¹²⁸. The metabolic pathway of AA to produce LX via 5-LOX/FLAP, 15-LOX and ac-COX-2 is shown as well as the production of E-resolvins from EPA via 18-HpETE by ac-COX-2 and CYP enzymes. D-Rvs, PDs and MaRs are synthesized from DHA via 12/15-LOX and ac-COX-2 together with cytosolic 5-LOX.

As PGE₂ induces the cardinal symptoms of inflammation, SPMs mediate the cardinal symptoms of resolution described by Basil et al., which are the removal of microbes, dead cells and cell debris, the restoration of vascular integrity and perfusion, regeneration of tissue, the remission of fever and connected to the afore-mentioned relief of pain¹³⁴. The investigation of these effects in the past years led to the question, how these effects can be used effectively to treat inflammatory diseases. SPMs are highly potent locally effective mediators that are produced at sites of inflammation. Due to unfavorable physicochemical properties and being prone to metabolic inactivation, the application of SPMs wouldn't be successful¹³². Finding an efficient way to modulate the inflammatory response by exploiting the effects of SPMs, is still a major challenge for recent research, which needs to be investigated.

1.4. Eicosanoid pathway Inhibitors

The usage of analgesic and antipyretic medicine is documented for more than 3500 years. Willow bark was used in different ways to treat pain and fever¹³⁵. Since the discovery of Aspirin[®] in 1897 many anti-inflammatory drugs were discovered interfering with the eicosanoid pathways. The most famous group of drugs are the NSAIDs including Aspirin[®], ibuprofen or diclofenac, which block the formation of PGs by unselectively inhibiting COX-1 and -2. But even before the target of the NSAIDs was found, the adverse side effects of long-term therapy were very well known¹³⁵. The link between gastric events and NSAIDs evolves around the maintenance of mucosal blood flow as well as the secretion of bicarbonate and mucus by constitutively COX-1-derived PGs especially PGE₂¹³⁶. This issue led to the development of selective COX-2 inhibitors like celecoxib and rofecoxib. But the predominant production of PGI₂ by COX-2 and the resulting dysbalance with elevated TXA₂, revealed the link between COX-2 inhibitor treatment and cardiovascular risk^{100,137}. Since all PGs mediate homeostatic relevant effects in certain tissues the specific downregulation of specific PGs at sites of inflammation is a major goal in the therapy of inflammatory diseases. The mPGES-1, known to be involved in the pathogenesis of rheumatoid arthritis, Alzheimer's disease, multiples sclerosis or arteriosclerosis, was identified as perfect target to accomplish this approach¹³⁸⁻¹⁴¹. Over the past two decades many mPGES-1 inhibitors were investigated. Due to the location of mPGES-1 in membranes and the necessity of inhibitors to act like AA-mimics, most drug candidates do not overcome unfavorable pharmacokinetic characteristics and lack efficacy in vivo and human whole blood¹⁴². Until now only 2 mPGES-1 inhibitors from Eli Lilly were tested in phase I clinical trials, but both were stopped due to the appearance of liver injuries, which were induced by toxic metabolites, according to a follow up study¹⁴³⁻¹⁴⁵.

The 5-lipoxygenase pathway implies like the aforementioned COX pathway promising targets to regulate inflammation. The investigation of direct 5-LOX inhibitors focusses on four classes. LT formation can be blocked by redox active 5-LOX inhibitors (1) that reduce the iron at the active site and thus impede the activation of the catalysis (2) compounds that act as iron-chelating drugs (zileuton) (3) drugs that act as AA-mimics and compete with the substrate for the binding site, and (4) allosteric modulators that act on the C2-like domain and antagonize the activation of 5-LOX^{146,147}. Despite enormous efforts to investigate 5-LOX inhibitors, only zileuton is approved on the market by the U.S. Food and Drug Administration (FDA) but not by the European Medicines Agency (EMA). Many drug candidates failed in clinical trials again due to pharmacokinetic issues, lack of efficiency in vivo and side effects in clinical trials¹⁴⁷. To reduce LT formation, the inhibition of FLAP is also a promising approach that has been investigated for two decades. MK-886, which was used for FLAP identification, was further investigated in clinical trials until phase II. But like MK591 and BAY-X1005, which were also tested in phase II clinical trials, none of the studies were continued for unclear reasons^{71,147}.

1.4.1. Dual inhibitors of the eicosanoid pathway

The biosynthetic networks of eicosanoids produce vastly different mediators that act in tightly regulated cascades. Inhibition of one pathway can lead to an overshooting production in other pathways, which could lead to more side effects. For example, a common side effect of Aspirin[®] upon long-term therapy is the development of AT-asthma, where increased biosynthesis of LTs induces bronchoconstriction and macrophage activity¹⁴⁸. The pharmacological strategy to inhibit the two main inflammatory eicosanoid pathways to circumvent the adverse effects emerged around 26 years ago. In 1994 a multi-target inhibitor called Licofelone was developed by Laufer et al. that inhibits FLAP, COX-1 and mPGES-1 and was later investigated in clinical trials^{146,149}. An alternative to dual COX/5-LOX inhibitors was given with the ongoing development of mPGES-1 as drug target, which could lead to a better cardiovascular compatibility¹⁵⁰.

1.4.2. BRP-187 as dual inhibitor of mPGES-1/FLAP

The investigation of new compounds to interfere with the eicosanoid pathway led to the development of a benzimidazole derivative BRP-7 in 2013 which potently suppresses LT formation by inhibiting FLAP but not 5-LOX. Additionally, it displayed no interaction with CYP3A4 or the human ether-a-go-go related gene (hERG), a potassium channel in the heart, where interaction is responsible for QT-time changes¹⁵¹. This structure as well as the isoxazole derivative 2-[4-(4-chlorophenyl)-3-methyl-1,2-oxazol-5-yl]-5-[(2-methylphenyl)methoxy]phenol that showed similar potency in the reduction of LTs^{152,153}, were used as lead compounds for the development for new multitarget inhibitors via a combined ligand- and structure-based screening approach. Here, 4-(4-chlorophenyl)-5-[4-(quinolin-2-ylmethoxy)phenyl]isoxazol-3-carboxylic acid (BRP-187/Figure 4) was identified as potent inhibitor of LT formation in intact polymorphonuclear leukocytes (PMNL)³. In docking studies and molecular dynamic (MD) simulations the potential binding site with FLAP was shown, where the carboxylic group interacts with B-Lys116 and C-His28, the quinoline group couples via π - π interaction with B-Tyr112 and has hydrophobic contact to B-Thr66³. In an intensive pharmacological characterization of BRP-187 the activity on eicosanoid formation was determined in various cell types with different stimuli. The IC₅₀ value of the compound in PMNL stimulated with A23187 (Ca²⁺-ionophore) was 60±10 nM. In intact monocytes stimulated with LPS/fMLP the potency even increased with an IC₅₀ of 7±1 nM, comparable to MK-886 in similar settings⁴. To study further the impact on other members of the MAPEG family, BRP-187 was tested against mPGES-1 and LTC₄-S. While LTC₄-S was not potently inhibited (IC₅₀= 6 μ M) the formation of PGE₂ by mPGES-1 was potently reduced with IC₅₀ around 0.2 μ M outperforming MK-886⁴. In a zymosan-induced mouse peritonitis model i.p. injected BRP-187 inhibited neutrophil infiltration and cys-LTs formation significantly at 10 mg/kg indicating activity in vivo⁴. Despite

very high activity in vitro and on the peritonitis model in mice, a calculated LogP value of 6.3035 (calculated by BIOVIA Draw 2019 x64) suggests low bioavailability and high plasma protein binding, as is often the case with acidic FLAP inhibitors⁷¹.

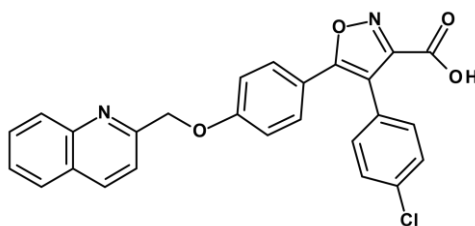


Figure 4 Chemical Structure of BRP-187 according to E. Banoglu et al.³. 4-(4-chlorophenyl)-5-[4-(quinolin-2-ylmethoxy)phenyl]isoxazol-3-carboxylic was identified as a new dual FLAP/mPGES-1 inhibitor

1.4.3. BRP-201 as new dual mPGES-1/FLAP inhibitor

The structural basis of BRP-7 was further tuned to develop new multitarget inhibitors. The substitution of a negatively charged group in position 4' or 5' promised a gain in effectiveness due to the interaction with His28, Lys116 and Arg117 of the FLAP binding pocket. The evaluation of the structure-activity relationship revealed 1,3,4-oxadiazol-5-thione as most beneficial substitution in position 5' of the benzimidazole ring⁵. The compound found in the screening, named BRP-201 ((5-{1-[(2-chlorophenyl)methyl]-2-[1-[4-(2-methylpropyl)phenyl]ethyl]-1H-benzimidazole-5-yl}-2,3-dihydro-1,3,4-oxadiazole-2-thione)/Figure 5), displayed high potency at inhibition of FLAP ($IC_{50} = 0.05 \pm 0.004 \mu M$) and mPGES-1 ($IC_{50} = 0.42 \pm 0.03 \mu M$), while LTC₄S was not affected as strong ($IC_{50} = 6.19 \pm 0.95 \mu M$). The isolated 5-LOX is also inhibited with an $IC_{50} = 0.6 \pm 0.4 \mu M$. In docking studies and molecular dynamic simulations, the binding sites of BRP-201 on FLAP, mPGES-1 and 5-LOX were calculated. For FLAP, the predicted cation- π interactions of acidic moieties on His28, Lys116 and Arg117 are important for compound binding⁵. The interaction with mPGES-1 is characterized by several polar interactions at the cytoplasmic part of the binding groove, because the 1,3,4-oxadiazol-5-thione group at 5' position of the benzimidazole ring interacts via water-mediated H-bonds and π - π interactions with Arg52 and His53. This interaction at the cytoplasmic entrance directs the hydrophobic rest of the molecule into the hydrophobic cavity for binding with additional π - π interactions and hydrophobic contacts⁵. Together, the modification of the initial hit BRP-7 led to a very potent multitarget inhibitor with new potential therapeutic usage that needs to be further investigated.

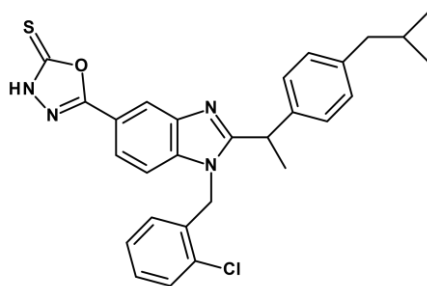


Figure 5 Chemical structure of BRP-201 according to Gür et al.⁵. Systemic structure activity relationship development on the 5-position of the benzimidazole ring led to (5-{1-[(2-chlorophenyl)methyl]-2-[1-[4-(2-methylpropyl)phenyl]ethyl]-1H-benzimidazole-5-yl}-2,3-dihydro-1,3,4-oxadiazole-2-thione) (BRP-201) as potent FLAP/mPGES-1 inhibitor.

1.4.4. Semisynthetic chalcone-based compounds as potential multitarget inhibitors

The development of new drugs with novel modes of action is a constant endeavor in pharmaceutical science and thus, the investigation of alternative drug targets in virtual screenings becomes more and more relevant¹⁵⁴. Natural products are very interesting molecules, because they often display several pharmacological effects on multiple targets. In a recent study such new target evaluation was performed for dihydrochalcones (DHCs), which were used in the development of sodium/glucose co-transporter 2 (SGLT2) inhibitors like dapagliflozin¹⁵⁵. Since the recognition of more therapeutic benefits by the usage of this drug e.g. in heart failure, DHCs returned in focus of research¹⁵⁶. From this study many of the selected compounds showed potent to moderate activity on COX-1 and 5-LOX. Isolated from *Melodorum fruticosum* the compound MF-14 and the semisynthetic oxidized derivative MF-15 displayed high potential as inhibitor of the aldol-keto reductase family 1 member C3 (AKR1C3) in enzalutamide-resistant metastatic castration resistant prostate cancer¹⁵⁷. Both compounds are 2-OH-benzylated derivatives of cardamonin (Figure 6), which by itself has strong anti-inflammatory effects during antitumoral treatment^{158,159}. Further studies revealed also bioactivity against mPGES-1 and therefore indicated a potential use in anti-inflammatory therapy¹⁶⁰.

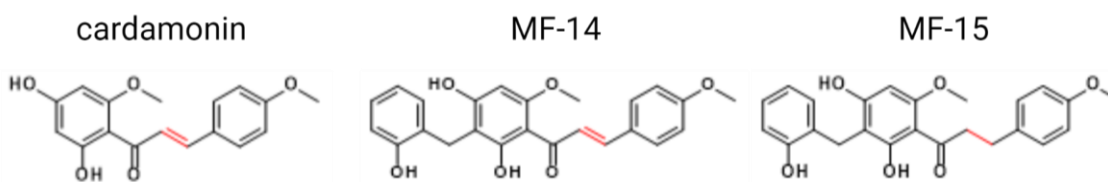


Figure 6 Chemical structure of cardamonin in comparison to MF-14 and MF-15 isolated from *Melodorum fruticosum* according to F. Mayr et al.¹⁵⁴. MF-14/15 are 2-OH-benzylated derivatives of cardamonin with potential anti-inflammatory properties.

1.5. Polymer-based nanoparticles

Nanomedicine is intensively investigated and moved in the focus of research over the past decade^{161,162}. Huge improvements in the field of diagnostics, drug delivery and therapeutic treatments are currently under development or have even already reached the market, using sophisticated biomaterials to cure or indicate certain diseases^{163,164}. The most recent breakthrough in the field of nanomedicine is the approval of the first vaccination against the severe acute respiratory syndrome coronavirus 2 (Sars-CoV-2) from BioNTech, where mRNA encoding the spike protein of the virus is encapsulated into liposomes that merge with the plasma membrane to effectively deliver the cargo¹⁶⁵. The utilization of nanomedicine as drug delivery systems is of high interest. Despite thousands of promising drug candidates are investigated, most of them fail to receive an approval due to unfavorable pharmacokinetics, physicochemical properties or systemic toxicity^{166,167}. Among different options, polymeric nanoparticles (NP) displayed high potential to improve bioavailability of formulated drugs by enhancing their solubility and circulation times, controlling the release profile and targeting specific cells or organs^{168,169}. The outstanding advantage of the use of polymers to formulate NPs is the high modifiability that allows to design hydrophilic or hydrophobic NPs with different shells or targeting/shielding units on the surface, to obtain a tailored delivery system for the encapsulated drug or patient specific needs^{170,171}. Natural polymers, which display high biocompatibility like dextran, albumin or hyaluronic acid are not suitable because of the multiple variations in the molecular weight (MW) and composition¹⁷². Therefore, synthetic polymers are used with controlled MW and/or chemical functionalization¹⁷³. One of the most investigated and highly biocompatible polymers is poly(lactide-co-glycolic acid) (PLGA) that is degraded to lactate and glycolate upon enzymatic degradation¹⁷⁴. On top of these advantages, PLGA can be easily formulated and the monomer composition can be altered to obtain different release kinetics¹⁷⁵. Not surprisingly, there are already 14 FDA approved products on the market using PLGA-based nano- or microparticles¹⁷⁶. A well established and equally biocompatible alternative to PLGA is acetalated dextran (AcDex). In contrast to dextran the functionalized derivative with acetal or ethoxy acetal (AceDex) groups is not water-soluble and therefore suitable for NP formulation and the encapsulation of hydrophobic drugs¹⁷⁷. Additionally, Ac(e)Dex degrades depending on the pH value, which could imply the usage of a passive targeting, since the body shows lower pH values in inflammatory tissues or after the uptake of infectious invaders or cell debris in the endolysosome^{178,179}.

The usage of nanoparticles is a great opportunity for modern medicine. Since most drug candidates fail to succeed because of unfavorable pharmacokinetics, the smart formulation into small containers with tailor-made properties to have high specificity is a promising strategy to circumvent these detrimental characteristics and give highly potent therapeutics a chance to get approved for clinical use¹⁸⁰.

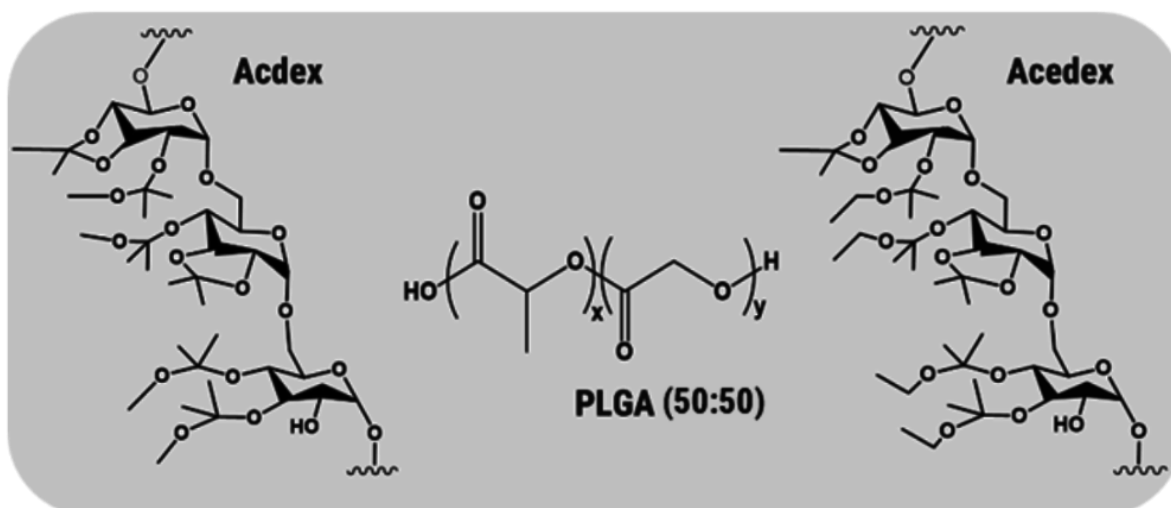


Figure 7 Chemical structure of the main polymers used in this study to form nanoparticles incorporated with anti-inflammatory compounds. Acetalated dextran (left), poly(lactide-co-glycolic acid) (middle) and ethoxy-acetalated dextran (right).

2. Aim of the thesis

The variety of therapeutic options for anti-inflammatory therapy we do have nowadays goes along with meticulous deliberations, if the treatment is worth the risk of side effects²⁹. Especially in chronic inflammatory diseases, where a long-term therapy is necessary, the therapeutic options are rare or their activity is decaying over the progression of the affliction^{29,30}. Therefore, the need of new approaches to fight the self-destructive and dysregulated immune response in inflammation is still compelling.

The various LMs are strongly involved in the onset, progression but also the resolution of inflammation^{36,60}. Many commonly used drugs on the market interfere with the LM-biosynthetic network by influencing mainly one pathway, especially the COX pathway - this fact led to the first initial objective of this thesis.

I The elucidation of commonly used therapeutics that interfere with the LM networks to better understand the risks and benefits of these drugs.

Beside the well-established COX inhibitors there are a variety of options to fight inflammation by more specific targeting. The dual inhibition of the COX and LT biosynthetic pathway arose over the past two decades with already promising drugs (licofelone) that were evaluated in clinical studies^{146,149}. Associated with a better safety profile the inhibition of mPGES-1 instead of COX-2 was further investigated in research and the similarity to FLAP, which is also an interesting drug target for LT inhibition, led to the development of dual mPGES-1 and FLAP inhibitors that were investigated lately^{3-5,150}. But like for the commonly available NSAIDs, the deeper understanding of the impact of BRP-187, BRP-201 and MF-14/15 on the entire LM network needs to be revealed. As a result, the next objective of this thesis was formed.

II The profound investigation of the anti-inflammatory impact and modulation of the LM profile by the multitarget inhibitors BRP-187, BRP-201 and MF-14/15.

Many recently investigated FLAP and mPGES-1 inhibitors are highly active in experimental in vitro settings but lack efficacy in complex bioassays or in vivo^{71,142}. Because of the location of the targeted proteins in bio-membranes and competition with AA in the active sites, the respective inhibitors share the same physicochemical characteristics, resulting in unfavorable kinetics, low solubility, low bioavailability, strong plasma protein binding and accumulation in hydrophobic tissues like membranes^{71,142}. The chemical adjustments of these disadvantages result mostly in loss of effectiveness^{3,5}. Thus, the investigation of the suitability of drug delivery systems is urgently needed. As prodigy in modern medicine, polymeric NPs could be an ideal

option to accomplishing the effectiveness of such potent inhibitors with unfavorable properties, which could save time and money in the development of new drugs¹⁸⁰. In an innovative cooperation, as part of a project in the SFB 1278 PolyTarget and in cooperation with the Institute of Organic and Macromolecular Chemistry at FSU Jena, the investigation of this approach was initiated. The encapsulation of BRP-187 and BRP-201 into polymeric NPs was analyzed, representing the third object of this study.

III In-depth investigation of the suitability of polymeric nanoparticles as drug delivery systems for the potent dual mPGES-1/FLAP inhibitors BRP-187 and BRP-201.

The impairment of pro-inflammatory lipid mediators can prevent the progression of inflammatory diseases². As counterpart in order to stop the inflammatory response the body produces SPMs to actively initiate the recovery of the affected tissue and help resolving inflammation¹⁹. Since the discovery of SPMs and the detection of their highly beneficial effects, new approaches to actively support inflammation resolution were discussed¹³². Since SPMs are instable hydrophobic fatty acid derivatives the treatment with these mediators would be rather ineffective, because of rapid metabolization or accumulation in bio-membranes¹³⁴. Another approach that is currently investigated is the development of SPM receptor agonists, for example, for the FPR2/ALX receptor, but until now no promising results from clinical studies were revealed¹⁸¹. Discovery of new strategies to promote inflammation resolution leaves room for deeper investigation and therefore builds the last objective of this thesis.

IV Identification of new approaches to actively promote the resolution of inflammation.

The investigation of these aims could provide great benefit for the development of inflammatory therapies and will contribute to big steps forward in anti-inflammatory (nano)medicine.

3. Manuscripts

Overview:

Manuscript I

Targeting biosynthetic networks of the proinflammatory and proresolving lipid metabolome

Werner, M., Jordan, P.M., Romp, E., Czapka, A., Rao, Z., Kretzer, C., Koeberle, A., Garscha, U., Pace, S., Claesson, H.-E., Serhan, C.N., Werz, O., Gerstmeier, J.

The FASEB Journal, 2019, 33(5): p. 6140-6153.

Anti-inflammatory drugs interfere with the metabolism of fatty acids via inhibition of cyclooxygenase (COX), 5-lipoxygenase (5-LOX) and 5-lipoxygenase activating protein (FLAP). According to the type of leukocyte these enzymes are also involved in the biosynthesis of specialized pro-resolving mediators (SPMs), which actively enhance resolution of inflammation. The influence of commonly used therapeutics regarding the production of SPMs is still elusive and will be intensively investigated in this study. With the obtained data clear disadvantages of approved drugs are pointed out and potential new strategies to favorably modulate the lipid mediator (LM) profile can be derived.

Manuscript II

Encapsulation of the dual FLAP/mPGES-1 inhibitor BRP-187 into acetalated dextran and PLGA nanoparticles improves its cellular bioactivity

Shkodra-Pula, B., Kretzer, C., Jordan, P.M., Klemm, P., Koeberle, A., Pretzel, D., Banoglu, E., Lorkowski, S., Wallert, M., Höppener, S., Stumpf, S., Vollrath, A., Schubert, S., Werz, O., Schubert, U.S.

Journal of Nanobiotechnology, 2020, 18(1):73

Dual inhibitors of 5-lipoxygenase activating protein (FLAP) and microsomal prostaglandin E₂ synthase-1 (mPGES-1) exert good anti-inflammatory efficacy at lower risk of side effects compared to non-steroidal anti-inflammatory drugs (NSAIDs) but despite these advantages the necessary lipophilic structure of these compounds is associated with low overall bioavailability. To improve the effectiveness of the well investigated dual FLAP/mPGES-1 inhibitor BRP-187 poly(lactic-co-glycolic acid) (PLGA) and acetalated dextran (Ac-Dex) were used forming nanoparticles (NPs) as carrier systems. This study shows how encapsulation of BRP-187 prolongs the effectiveness and enhances the potency to inhibit mPGES-1 in macrophages.

Manuscript III

Ethoxy acetalated dextran-based nanocarriers accomplish efficient inhibition of leukotriene formation by a novel FLAP antagonist in human leukocytes and blood

Kretzer, C., Shkodra-Pula, B., Klemm, P., Jordan, PM., Schröder, D., Cinar, G., Vollrath, A., Schubert, S., Nischang, I., Hoepfener, S., Stumpf, S., Banoglu, E., Gladigau, F., Bilancia, R., Rossi, A., Eggeling, C., Neugebauer, U., Schubert, US., Werz, O.

Cellular and Molecular Life Sciences, 2021 Dec 31;79(1):40.

The novel benzimidazole-based 5-lipoxygenase activating protein inhibitor (FLAP) BRP-201 potently inhibits leukotriene (LT) formation in isolated leukocytes but lacks efficacy in human whole blood due to unfavorable pharmacokinetic properties. Here, we described the encapsulation of BRP-201 into poly(lactic-co-glycolic acid) (PLGA) and ethoxy acetalated dextran (Ace-Dex), aiming to improve the bioavailability and develop a new therapeutic strategy to reduce inflammation. The data proves the suitability of Ace-Dex nanoparticles (NPs) to effectively transport BRP-201 to leukocytes in human whole blood and drastically reduced LT formation compared to free compound. The in-vitro effect was also confirmed in a sophisticated zymosan-induced peritonitis mouse model with i.v. application of the formulation, indicating the clear benefit of encapsulation.

Manuscript IV

Effect of Crystallinity on the Properties of Polycaprolactone Nanoparticles Containing the Dual FLAP/mPEGS-1 Inhibitor BRP-187

Vollrath, A., Kretzer, C., Beringer-Siemers, B., Shkodra, B., Czaplewska, J., Bandelli, D., Stumpf, S., Hoepfener, S., Weber, C., Werz, O., Schubert, US.

Polymers, 2021 Jul 31;13(15):2557.

Recently developed polycaprolactones (PCL) with constant hydrophobicity but a varying degree of crystallinity were prepared from ϵ -caprolactone (ϵ CL) and δ -caprolactone (δ -CL) isomers to formulate nanoparticles (NPs). With the encapsulated anti-inflammatory drug BRP-187 the polymers were tested on enzymatic degradation and their efficacy to reduce leukotriene (LT) formation in polymorphonuclear leukocytes (PMNL). The study showed that the crystallinity of the polymers influences the enzymatic degradation, which exerts different potential therapeutic options for the compound with immediate and delayed release settings. The aim of the study was to establish a base to develop a polymer library for tailor-made formulations in future inflammatory therapy.

Manuscript V

Shifting the Biosynthesis of Leukotrienes Toward Specialized Pro-Resolving Mediators by the 5-Lipoxygenase-Activating Protein (FLAP) Antagonist BRP-201

Kretzer, C., Jordan, PM., Bilancia, R., Rossi, A., Tuğçe Gür, M., Banoglu, E., U., Schubert, US., Werz, O.

Journal of Inflammation Research, 2022, Feb 9;15:911-925

Lipid mediators (LM) derived from fatty acids initiate and resolve inflammation depending on the synthetic pathways which include partially the same enzymes for both categories of products. In this complex network compound can interfere to favorably modulate the LM profile and prime the production of resolving specialized pro-resolving mediators (SPMs). Here, the benzimidazole-based 5-lipoxygenase activating protein (FLAP) inhibitor BRP-201 was studied regarding the modification of the lipid mediator profile. We showed strong evidence, that BRP-201 can shift the LM profile from LTs to the production of SPMs by inhibiting FLAP and enhancing the activity of 15- and 12-LOX, which leads to an active induction of resolution inflammation.

Manuscript VI

Natural chalcones elicit formation of specialized pro-resolving mediators and related 15-lipoxygenase products in human macrophages

Kretzer, C., Jordan, PM., Meyer, KPL., Hoff, D., Werner, M., Hofstetter R.K., Koeberle, A., Cala Peralta, A., Viault, G., Seraphin, D., Richomme, P., Helesbeux, JJ., Stuppner, H., Temml, V., Schuster, D., Werz, O.

Biochemical Pharmacology, 2022, Jan;195:114825.

Specialized pro-resolving mediators (SPMs) have anti-inflammatory properties that counteract the effect of leukotrienes (LT) and prostaglandins (PG) to resolve inflammation. Novel concepts of therapy try to find options that enhance the production of those SPMs rather than acting immunosuppressive by reducing LT and PG levels. In this study we present two dihydrochalcone-based compounds from *Melodrum fruticosum* that enhance the biosynthesis of SPMs and their precursors via activation of 15-lipoxygenase (LOX)-1. MF-14 and MF-15 strikingly evoked 12/15-LOX products along with translocation of 15-LOX-1 without additional stimulus while still exert inhibition of 5-LOX in exotoxin stimulated macrophages and ionophore stimulated HEK-cells, showing their ability to function as lipid mediator class switch inducer.

Manuscript I

Targeting biosynthetic networks of the proinflammatory and proresolving lipid metabolome

Werner, M., Jordan, P.M., Romp, E., Czapka, A., Rao, Z., Kretzer, C., Koeberle, A., Garscha, U., Pace, S., Claesson, H.-E., Serhan, C.N., Werz, O., Gerstmeier, J.

The FASEB Journal, 2019, 33(5): p. 6140-6153.

Der Kandidat / Die Kandidatin ist

Erstautor/-in, Ko-Erstautor/-in, Korresp. Autor/-in, Koautor/-in.

Anteile (in %) der Autoren / der Autorinnen an den vorgegebenen Kategorien der Publikation

Author	Conception	Data analysis	Experimental	Writing	Provision of Material
Werner M.	10 %	30 %	40 %	15 %	
Jordan P.M.	10 %	25 %	25 %	10 %	
Romp E.					
Czapka A.					
Rao Z.					
Kretzer C.	10 %	10 %	10 %		
Koeberle A.					
Garscha U.					
Pace S.					
Claesson H.-E.					
Serhan C.N.	10 %				
Werz O.	30 %			40 %	80 %
Gerstmeier J.	30 %	20 %		30 %	
Others		25 %	25 %	15 %	20%
Summe:	100 %	100 %	100 %	100 %	100 %

Unterschrift Kandidat/-in

Unterschrift Betreuer/-in (Mitglied der Fakultät)

Targeting biosynthetic networks of the proinflammatory and proresolving lipid metabolome

Markus Werner,* Paul M. Jordan,* Erik Romp,* Anna Czapka,* Zhigang Rao,* Christian Kretzer,* Andreas Koeberle,* Ulrike Garscha,* Simona Pace,* Hans-Erik Claesson,[†] Charles N. Serhan,[‡] Oliver Werz,^{*1} and Jana Gerstmeier^{*2}

*Department of Pharmaceutical/Medicinal Chemistry, Institute of Pharmacy, Friedrich Schiller University Jena, Jena, Germany; [†]Division of Hematology, Department of Medicine, Karolinska University Hospital Solna, Stockholm, Sweden; and [‡]Department of Anesthesia, Perioperative and Pain Medicine, Center for Experimental Therapeutics and Reperfusion Injury, Brigham and Women's Hospital-Harvard Medical School, Boston, Massachusetts, USA

ABSTRACT: Nonsteroidal anti-inflammatory drugs interfere with the metabolism of arachidonic acid to proinflammatory prostaglandins and leukotrienes by targeting cyclooxygenases (COXs), 5-lipoxygenase (LOX), or the 5-LOX-activating protein (FLAP). These and related enzymes act in conjunction with marked crosstalk within a complex lipid mediator (LM) network where also specialized proresolving LMs (SPMs) are formed. Here, we present how prominent LM pathways can be differentially modulated in human proinflammatory M1 and proresolving M2 macrophage phenotypes that, upon exposure to *Escherichia coli*, produce either abundant prostaglandins and leukotrienes (M1) or SPMs (M2). Targeted liquid chromatography–tandem mass spectrometry–based metabololipidomics was applied to analyze and quantify the specific LM profiles. Besides expected on-target actions, we found that: 1) COX or 15-LOX-1 inhibitors elevate inflammatory leukotriene levels, 2) FLAP and 5-LOX inhibitors reduce leukotrienes in M1 but less so in M2 macrophages, 3) zileuton blocks resolution-initiating SPM biosynthesis, whereas FLAP inhibition increases SPM levels, and 4) that the 15-LOX-1 inhibitor 3887 suppresses SPM formation in M2 macrophages. Conclusively, interference with discrete LM biosynthetic enzymes in different macrophage phenotypes considerably affects the LM metabolomes with potential consequences for inflammation-resolution pharmacotherapy. Our data may allow better appraisal of the therapeutic potential of these drugs to intervene with inflammatory disorders.—Werner, M., Jordan, P. M., Romp, E., Czapka, A., Rao, Z., Kretzer, C., Koeberle, A., Garscha, U., Pace, S., Claesson, H.-E., Serhan, C. N., Werz, O., Gerstmeier, J. Targeting biosynthetic networks of the proinflammatory and proresolving lipid metabolome. *FASEB J.* 33, 6140–6153 (2019). www.fasebj.org

KEY WORDS: resolution · macrophages · inflammation · leukotrienes · prostaglandins

Arachidonic acid (AA), eicosapentaenoic acid (EPA), and docosahexaenoic acid (DHA) are precursor substrates for lipoxygenases (LOXs) and cyclooxygenases (COXs) that

initiate the biosynthesis of potent bioactive lipid mediators (LMs) that regulate the initiation and resolution of inflammation (1, 2). Unresolved, chronic inflammation with elevated levels of proinflammatory prostaglandins (PGs) and leukotrienes (LTs) contributes to numerous widespread diseases, including arthritis, atherosclerosis and cardiovascular diseases, type 2 diabetes, asthma, and Alzheimer's disease that require therapeutic targeting of the inflammatory process and its resolution (3, 4). For pharmacological intervention with chronic inflammation, drugs that block the formation of PGs and LTs by inhibition of COX-1/2 and 5-LOX or 5-LOX-activating protein (FLAP), respectively, are commonly used (5, 6). Specifically, the so-called nonsteroidal anti-inflammatory drugs (NSAIDs, e.g., ibuprofen) that inhibit PG formation provoke their beneficial effects mainly by alleviating pain and by blocking acute inflammation (5) but are essentially inefficient at terminating inflammation or in promoting resolution and tissue repair.

A novel superfamily of LMs that are called specialized proresolving mediators (SPMs), including lipoxins (LXs),

ABBREVIATIONS: AA, arachidonic acid; COX, cyclooxygenase; cPLA₂, cytosolic phospholipase A₂; DHA, docosahexaenoic acid; EPA, eicosapentaenoic acid; FLAP, 5-LOX-activating protein; HDHA, hydroxy DHA; HEPE, hydroxyeicosapentaenoic acid; HETE, hydroxyeicosatetraenoic acid; LM, lipid mediator; LOX, lipoxygenase; LT, leukotriene; LX, lipoxin; MaR, maresin; MRM, multiple reaction monitoring; NSAID, nonsteroidal anti-inflammatory drug; PD, protectin; PG, prostaglandin; pg, picogram; Rv, resolvin; SPM, specialized proresolving mediator; UPLC-MS-MS, ultraperformance liquid chromatography–tandem mass spectrometry

¹ Correspondence: Department of Pharmaceutical/Medicinal Chemistry, Institute of Pharmacy, Friedrich Schiller University Jena, Philosophenweg 14, Jena 07743, Germany. E-mail: oliver.werz@uni-jena.de

² Correspondence: Department of Pharmaceutical/Medicinal Chemistry, Institute of Pharmacy, Friedrich Schiller University Jena, Philosophenweg 14, Jena 07743, Germany. E-mail: jana.gerstmeier@uni-jena.de

doi: 10.1096/fj.201802509P

This article includes supplemental data. Please visit <http://www.fasebj.org> to obtain this information.

resolvins (Rvs), maresins (MaRs), and protectins (PDs), that actively terminate inflammation and promote tissue regeneration are biosynthesized by COX and LOX pathways as well (Fig. 1A) (2, 7, 8). Thus, COX and 5-LOX pathway inhibitors may interfere with beneficial SPM formation too. Moreover, NSAIDs are frequently associated with adverse on-target side effects by suppressing homeostatic prostanoids (5) and by redirecting LM biosynthesis toward proinflammatory LTs (9). The 15-LOX-1 appears to be involved in inflammation in the respiratory tract (10, 11) but also in the formation of SPM, particularly in anti-inflammatory macrophage phenotypes (12).

LM biosynthesis inhibitors (including NSAIDs) have been evaluated in cell-based studies with limited read-out, mainly addressing inflammation-promoting PGs and LTs in proinflammatory immune cells (*i.e.*, neutrophils, monocytes, and M1-like macrophages), whereas SPMs have not yet been essentially studied because they are the newest mediators uncovered with novel proresolving functions (7, 13). Thus, modulation of SPM biosynthesis by COX and LOX inhibitors and other potential anti-inflammatory drugs on the cellular level is elusive. Moreover, because LM biosynthesis is organized within connected cascades that can crosstalk, pharmacological interference with one pathway may redirect toward other LM routes within competent cells (9, 14, 15).

Macrophages are innate immune cells that are crucial for initiation, maintenance, and resolution of inflammation depending on their phenotypes, namely, proinflammatory M1-like and proresolving, anti-inflammatory M2-like subtypes (16). Human M1 and M2 macrophages exposed to pathogenic bacteria produce differential LMs that distinguish their inflammatory or proresolving phenotypes: M1-like mainly generate 5-LOX- and COX-2-derived PGs and LTs, whereas M2-like produce predominantly 15-LOX-derived SPMs, including LX, Rv, PD, and MaR1 (12). Such bacteria-stimulated human macrophage phenotypes represent a pathophysiologically relevant, cell-based approach that enables the assessment of a broad spectrum of bioactive LMs by metabololipidomics. Therefore, we made use of this convenient experimental system for a comprehensive analysis of LM pathway inhibitors to reveal their ability to affect the complex network of proinflammatory and proresolving LMs.

MATERIALS AND METHODS

Cell isolation and polarization of macrophages

Leukocyte concentrates from freshly withdrawn peripheral blood of healthy adult human donors were provided by the Institute of Transfusion Medicine, Jena University Hospital (Jena, Germany). The experimental protocol was approved by the ethical committee of the Jena University Hospital. All methods were performed in accordance with the relevant guidelines and regulations. Peripheral blood mononuclear cells were isolated using dextran sedimentation and Ficoll-Histopaque 1077-1 (MilliporeSigma, Burlington, MA, USA) centrifugation. For differentiation and polarization toward M1 and M2 macrophages, criteria published by Werz *et al.* (12) were used. Thus, M1 macrophages were generated by incubating monocytes with 20 ng/ml granulocyte-macrophage colony-stimulating factor (Peprotech, Rocky Hill, NJ, USA) for 6 d in Roswell Park Memorial Institute

medium 1640 supplemented with 10% fetal calf serum, 2 mM *l*-glutamine (Merck, Kenilworth, NJ, USA), and penicillin-streptomycin (Merck), followed by 100 ng/ml LPS (MilliporeSigma) and 20 ng/ml INF- γ (Peprotech) treatment for another 48 h. M2 macrophages were incubated with 20 ng/ml M-CSF (Peprotech) for 6 d of differentiation plus 20 ng/ml IL-4 (Peprotech) for an additional 48 h of polarization.

Incubations of macrophages and LM metabololipidomics

Macrophages (2×10^6 /ml) were incubated in PBS containing 1 mM CaCl₂. Compounds or vehicle control (0.1% DMSO) were applied 15 min prior to stimulation with *E. coli* (serotype O6:K2: H1) at a ratio of 1:50 (M1/M2:*E. coli*) for 180 min at 37 °C. The 15-LOX-1 inhibitor 3887 was synthesized as described by Han *et al.* (17). Ibuprofen and celecoxib were purchased from MilliporeSigma, MK886 from Cayman Chemicals (Ann Arbor, MI, USA), zileuton from Sequoia Research Products (Pangbourne, United Kingdom), and RSC-3388 from Merck. Supernatants were transferred to 2 ml of ice-cold methanol containing 10 μ l of deuterium-labeled internal standards [200 nM d₅-5S-hydroxyicosatetraenoic acid (HETE), d₄-LTB₄, d₅-LXA₄, d₅-RvD₂, d₄-PGE₂ and 10 μ M d₅-AA] to facilitate quantification. Deuterated and nondeuterated LM standards were purchased from Cayman Chemicals. Sample preparation was conducted by adapting criteria published by Colas *et al.* (18). In brief, samples were kept at -20 °C for 60 min to allow protein precipitation. After centrifugation (1200 g, 4 °C, 10 min), 8 ml acidified H₂O (pH 3.5) was added and subjected to solid phase extraction (SPE). Solid phase cartridges (Sep-Pak Vac 6cc 500 mg/6 ml C18; Waters, Milford, MA, USA) were equilibrated with 6 ml methanol and 2 ml H₂O before samples were loaded onto columns. After washing with 6 ml H₂O and an additional 6 ml *n*-hexane, LMs were eluted with 6 ml methyl formate. Finally, the samples were brought to dryness using an evaporation system (TurboVap LV; Biotage, Uppsala, Sweden) and resuspended in 100 μ l methanol/water (50/50, v/v) for ultraperformance liquid chromatography-tandem mass spectrometry (UPLC-MS-MS) automated injections. LM profiling was analyzed with an Acquity UPLC system (Waters) and a QTrap 5500 Mass Spectrometer (Sciex, Framingham, MA, USA) equipped with a Turbo V Source and electrospray ionization. LMs were eluted using an Acquity UPLC BEH C18 column (1.7 μ m, 2.1 \times 100 mm; Waters) at 50 °C with a flow rate of 0.3 ml/min and a mobile phase consisting of methanol, water, and acetic acid at a ratio of 42:58:0.01 (v/v/v) that was ramped to 86:14:0.01 (v/v/v) over 12.5 min and then to 98:2:0.01 (v/v/v) for 3 min (Supplemental Table S1). The QTrap 5500 was operated in negative-ionization mode using scheduled multiple reaction monitoring (MRM) coupled with information-dependent acquisition. The scheduled MRM window was 60 s, optimized LM parameters (CE; Collision Energy, EP; Entrance Potential, DP; Declustering Potential, CXP; Collision Cell Exit Potential) were adopted (19), and the curtain gas pressure was set to 35 psi. The retention time and at least 6 diagnostic ions for each LM were confirmed by means of an external standard (Cayman Chemicals). Quantification was achieved by calibration curves for each LM. Linear calibration curves were obtained for each LM and gave *r*² values of 0.998 or higher (for fatty acids, 0.95 or higher). Additionally, the limit of detection for each targeted LM was determined (Supplemental Table S3).

LM coregulation network analysis

LM circular correlation network was generated with the Cytoscape 3.6.0. software. In brief, percentage changes *vs.* vehicle control (100%) for each LM obtained by treatment with ibuprofen, celecoxib, indomethacin, diflupolol [kind gift by Dr. Barbara

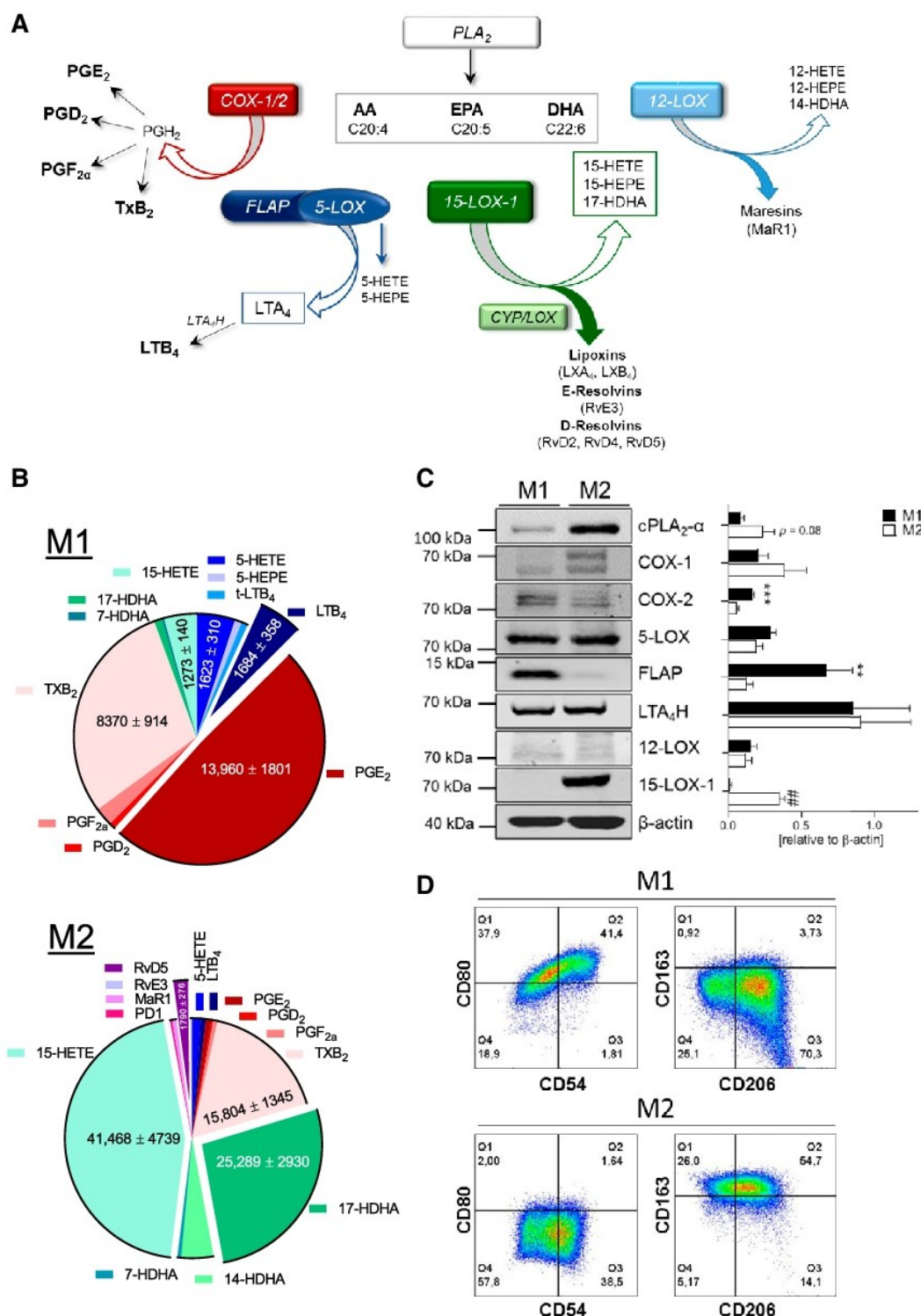


Figure 1. LM biosynthetic pathways in human M1 and M2 macrophages. *A*) Schematic overview on the bioactive eicosanoid and docosanoid pathways in inflammation and resolution. *B*) LM profiles of M1 and M2 macrophages upon exposure to pathogenic *E. coli*. Human monocyte-derived macrophages were polarized for 48 h to M1 and M2 (2×10^6 cells/ml) and incubated for 180 min with *E. coli* (O6:K2:H1; ratio = 1:50) at 37 °C. Formed LMs were isolated by SPE and analyzed by UPLC-MS-MS, shown as a pie chart. Values are means \pm SEM of $n = 24\text{--}34$ for M1 and $n = 33\text{--}39$ for M2. *C*) Protein expression of LM biosynthetic enzymes and β -actin by Western blot and densitometric analysis thereof; $n = 5$. Data were log-transformed for paired Student's *t* test; M1 vs. M2. ** $P=0.01$, *** $P=0.001$, $^{###}P=0.01$. *D*) Expression of surface polarization markers for M1 (CD54, CD80) and M2 (CD206, CD163), polarized for 48 h, was analyzed by flow cytometry, and representative histograms are shown from 3 independent experiments with separate donors.

Matuszczak (University of Innsbruck, Innsbruck, Austria), zileuton, MK886, 3887, and RSC-3388 were determined in M1 and M2 macrophages. With these values, a Bravais-Pearson correlation was performed to enlighten positively correlated LM species with a correlation coefficient of 0.7 or higher. Coregulated LM species appear in close proximity to each other, forming specific clusters where the distance and connection lines visualize their proximity. The size of nodes reflects the LM abundance (in picograms) of DMSO controls produced from 2×10^6 macrophages.

SDS-PAGE and Western blot

Cell lysates of macrophages (2×10^6 cells) were separated on 8% [cytosolic phospholipase A₂ (cPLA₂- α)], 10% (5-LOX, 12-LOX, 15-LOX-1, COX-1, COX-2, and LTA₄H), and 16% (FLAP) polyacrylamide gels and blotted onto nitrocellulose membranes (Amersham Protran Supported 0.45 μ m nitrocellulose; GE Healthcare, Chicago, IL, USA). The membranes were incubated with the following primary antibodies: polyclonal rabbit anti-cPLA₂ α , 1:200 (2832; Cell Signaling Technology, Danvers, MA, USA); rabbit polyclonal anti-5-LOX, 1:1000 (by Genscript, Piscataway, NJ, USA, to a peptide with the C-terminal 12 aa of 5-LOX: CSPDRIPNSVA; kindly provided by Dr. Marcia Newcomer, Louisiana State University, Baton Rouge, LA, USA); polyclonal rabbit anti-12-LOX, 1:200 (NBP2-29941; Novus Biologicals, Centennial, CO, USA); mouse monoclonal anti-15-LOX-1, 1:500 (ab119774; Abcam, Cambridge, United Kingdom); rabbit polyclonal anti-COX-1, 1:500 (4841; Cell Signaling Technology); rabbit polyclonal anti-COX-2, 1:500 (4842; Cell Signaling Technology); rabbit polyclonal anti-LTA₄H, 1:1000 (ab133512; Abcam); rabbit polyclonal anti-FLAP, 0.1 μ g/ml (ab85227; Abcam), and rabbit polyclonal anti- β -actin, 1:1000 (4967S; Cell Signaling Technology). Immunoreactive bands were stained with IRDye 800CW goat anti-mouse IgG (H+L), 1:10,000 (926-32210; Li-Cor Biosciences, Lincoln, NE, USA), IRDye 800CW goat anti-rabbit IgG (H+L), 1:15,000 (926-32211; Li-Cor Biosciences) and IRDye 680LT goat anti-mouse IgG (H+L), 1:40,000 (926-68020; Li-Cor Biosciences), and visualized by an Odyssey infrared imager (Li-Cor Biosciences). Data from densitometric analysis were background corrected.

Flow cytometry

Fluorescent staining for flow cytometric analysis of M1 or M2 macrophages after 48 h polarization was performed in flow cytometry buffer (PBS with 0.5% bovine serum albumin, 2 mM EDTA, and 0.1% sodium azide). Nonspecific antibody binding was blocked using mouse serum for 10 min at 4°C prior to antibody staining. Subsequently, macrophages were stained with fluorochrome-labeled antibody mixtures at 4°C for 30 min. The following antibodies were used: FITC anti-human CD14 (2 μ g/test, clone M5E2), PE anti-human CD54 (1 μ g/test, clone HA58), APC-H7 anti-human CD80 (0.25 μ g/test, clone L307.4; BD Biosciences, San Jose, CA, USA), PE-Cy7 anti-human CD163 (2 μ g/test, clone RM3/1; BioLegend, San Diego, CA, USA), PerCP-eFluor710 anti-human CD206 (0.06 μ g/test, clone 19.2; BD Biosciences, San Diego, CA, USA). Upon staining, M1 or M2 macrophages were analyzed using a Canto Plus flow cytometer (BD Biosciences), and data were analyzed using FlowJo X Software (BD Biosciences).

Statistical analysis

The sample size for experiments was chosen empirically based on previous studies (12, 20) to ensure adequate statistical power. Results are expressed as means \pm SEM of n observations, where n represents the number of experiments with cells from separate donors and performed on different days in triplicates, as

indicated. For the different treatments of cells with compounds, experiments were performed with $n \geq 5$ unless otherwise mentioned; for some experiments, $n < 5$ but ≥ 3 where highly consistent results were obtained. Analysis of data was conducted using Prism 7 software (GraphPad, La Jolla, CA, USA). Data were log-transformed to generate stronger Gaussian-distributed data sets amenable to parametric analysis. A paired Student's t test was used for comparison between 2 groups. The criterion for statistical significance is a value of $P < 0.05$. The Bravais-Pearson correlation was analyzed with Microsoft Excel 2016 (Redmond, WA, USA) and Cytoscape 3.6.0 software (<https://cytoscape.org/>).

RESULTS

Differential bioactive LM pathways in human M1 and M2 macrophage phenotypes

Proinflammatory M1-like macrophages were obtained by differentiation of human peripheral blood monocytes with granulocyte-macrophage colony-stimulating factor (6 d) and 48 h polarization with LPS plus INF- γ , whereas anti-inflammatory M2-like cells were made from monocytes by macrophage colony-stimulating factor-induced differentiation (6 d) followed by 48 h treatment with IL-4 (21). Metabololipidomics was applied to monitor broad-spectrum LM profiles of M1 and M2 macrophages. Adapting criteria published by Dalli and Serhan (19) for LM detection and quantitative analysis, we established a targeted lipidomics approach based on UPLC-MS-MS (Supplemental Tables S1–S3). This method allows simultaneous profiling and high-throughput (16 min) quantitative analysis of 33 LMs from M1 and M2 macrophages, identified based on published criteria (*e.g.*, matching fragmentation patterns and 6 characteristic diagnostic ions) by Colas *et al.* (18). UPLC-specific retention time and separation of each LM was validated by chemical standards (Supplemental Table S3), and signature ion pairs obtained *via* MRM were used for quantification (18).

The phenotype-specific LM profiles of *E. coli*-challenged M1 and M2 macrophages (ratio 1:50; M1/M2: *E. coli*, 180 min) is reported in Fig. 1B and Supplemental Table S4; a comprehensive overview of the investigated LM pathways is shown in Fig. 1A. In agreement with the overall superior fatty acid substrate release (Supplemental Table S4) in M2 macrophages, the protein level of cPLA₂- α was higher than that in M1 macrophages (Fig. 1C). The marked differences in the LM metabolome (Fig. 1B) is a consequence of the distinct expression pattern of LM biosynthetic enzymes in M1 *vs.* M2 macrophages (Fig. 1C). The M1 phenotype generated predominantly 5-LOX-related LTs and COX-related PGs as well as 11-HETE and 11-HEPE from AA and EPA, respectively, surpassing the respective capacities of M2 macrophages. Although 5-LOX and LTA₄H were equally expressed in both phenotypes, FLAP dominated in M1 macrophages (Fig. 1C), presumably accounting for higher LTB₄ levels. Consequent to higher COX-2 expression, PGE₂ biosynthesis was more than 20-fold higher in M1 *vs.* M2 cells, whereas the expression of COX-1 and formation of TXB₂ was superior in M2 macrophages. Control experiments without *E. coli* revealed marginal LM formation in either M1 or M2 macrophages that were below the detection limit in these

incubations (Supplemental Table S4) but are still relevant during several pathophysiological chronic diseases (18). Correct macrophage polarization was assured by flow cytometry analysis of surface markers CD54 and -80 for M1 and CD163 and -206 for M2 (Fig. 1D). Alterations of the phenotype during 180 min incubations of M1 and M2 with *E. coli* (*i.e.*, CD54, -80 for M1 and CD163, -206 for M2) were not observed, and *E. coli* incubation without cells failed to produce appreciable amounts of LM (unpublished results, see ref. 12).

Challenge of M1 macrophages by *E. coli* failed to produce abundant SPM below the detection limit of our analytical method (Supplemental Table S4), and the production of monohydroxylated SPM precursors was also minute as compared with M2 macrophages that generated substantial amounts of bioactive SPM including LXA₄, RvD2, -D4, -D5, Mar1, PD1, AT-PD1, and RvE3 as well as respective precursors (Fig. 1B and Supplemental Table S4). Accordingly, and in agreement with our previous study (12), protein expression of human 15-LOX-1, one of the key enzymes for SPM formation (22, 23), was not detectable in polarized M1 cells but abundantly expressed in the M2 phenotype (Fig. 1C). However, human 15-LOX-2 was reported by Snodgrass *et al.* (24) to be equally expressed in both macrophage phenotypes and to be capable of producing 15-HETE and 15-HEPE as well as DHA-derived 17-hydroxy DHA (HDHA). Note that isolated human 15-LOX-2 lacks the dual reaction specificity that is unique for human 15-LOX-1 that also generates 12-HETE, 12-HEPE, and 14-HDHA (in an ~10:1 ratio, at least for 15-HETE:12-HETE) (25). The dual reaction specificity of human 15-LOX-1 might be advantageous for SPM biosynthesis in M2 and may explain why all detectable 12-LOX products, including MaR1, were much higher in M2 *vs.* M1 macrophages, although 12-LOX levels did not differ between the phenotypes, suggesting that 15-LOX-1 can contribute to the biosynthesis of these LMs as well.

To evaluate how blockade of COX-1 or COX-2 affects the LM profiles in bacteria-challenged macrophages, the clinically used COX-1/2 inhibitor ibuprofen and the COX-2-selective celecoxib were studied. Pretreatment with both drugs for 15 min at 37 °C efficiently suppressed the formation of PGD₂, PGE₂, PGF₂, and TXB₂ in M1 and M2 phenotypes to a similar degree (Fig. 2A), even though the absolute capacities to biosynthesize PGE₂ were strikingly higher in M1 over M2 cells (Fig. 2B). Moreover, formation of the COX products 11-HETE and 11-HEPE (26) was effectively reduced by ibuprofen or celecoxib in M1 and to a minor extent also in M2 macrophages. Interestingly, both COX inhibitors significantly reduced 15-HETE biosynthesis in M1 (by ~70%) but not in M2 cells (Fig. 2).

In both macrophage phenotypes, particularly in M1, the biosynthesis of the 5-LOX products LTB₄ and its *trans*-isomers, 5-HETE, 5-HEPE, and 5S,6R-diHETE was strongly increased by celecoxib and, to a minor degree, by ibuprofen (at least in M1, Fig. 2), probably as a result of AA substrate shunting from the COX toward the 5-LOX and FLAP pathway as reported by Mazaleuskaya *et al.* (26). Notably, also 7-HDHA levels were increased by celecoxib in M1 (Fig. 2A) but not in M2 macrophages, which suggests an involvement of the 5-LOX pathway in M1 as well. SPM biosynthesis in the M2 phenotype was not suppressed by

the two COX inhibitors and rather slightly increased by ibuprofen. The levels of AA and EPA were strongly elevated by ibuprofen in M1 with minor impact on DHA, whereas in M2 macrophages such alterations were not observed (Fig. 2). Conclusively, the prominent blockade of both COX isoforms results in elevated free AA and EPA levels in M1 macrophages because AA and EPA cannot be converted to the respective COX products that actually dominate the LM profile of M1 and in shunting of LM formation toward proinflammatory 5-LOX products as observed by Mazaleuskaya *et al.* (26), whereas in M2 macrophages, the COX isoforms are less expressed with consequent little elevation for SPM levels.

Differential effects of 5-LOX and FLAP inhibitors on LM biosynthesis

Because inhibitors of 5-LOX and of FLAP are uniformly used to suppress the biosynthesis of LT and of other 5-LOX products (6), we next studied the clinically validated 5-LOX inhibitor zileuton (27) and the well-recognized FLAP inhibitor MK886 (28) in *E. coli*-induced LM biosynthesis in M1 and M2 macrophages side by side. In M1, low concentrations of zileuton (300 nM) and MK886 (30 nM) efficiently blocked the formation of LTB₄ and its *trans*-isomers by >50% with similar or somewhat minor efficiency for 5-HETE and 5-HEPE; at 3 μM, both inhibitors suppressed 5-LOX products by >85% in M1 macrophages (Fig. 3A, B). This is in sharp contrast to the M2 phenotype, in which 300 nM zileuton and 30 nM MK886 failed to significantly inhibit 5-LOX product formation; LTB₄ and 5-HETE levels remained >80%. Intriguingly, even at high inhibitor concentrations (3 μM), inhibition of 5-LOX product biosynthesis was much less pronounced in M2 macrophages with only 30–40% inhibition (Fig. 3A, B). In contrast, when the classic 5-LOX stimulus Ca²⁺-ionophore A23187 was used instead of *E. coli*, the 5-LOX inhibitory potencies of zileuton and MK886 were not different between M1 and M2 macrophages (Fig. 3C), with IC₅₀ values in the low nM range. Because A23187 failed to induce appreciable amounts of SPM and 15-LOX-1 products in both cell types (unpublished results), it was not further used in this study.

COX product formation was essentially not affected by zileuton or MK886, neither in M1 nor in M2 macrophages after *E. coli* stimulation. However, striking differential effects of zileuton and MK886 were obvious for the modulation of SPM biosynthesis and their precursors, particularly in M2 cells, which is in line with our previous study (12): 1) zileuton (3 μM), but not MK886, consistently suppressed (30–40%) the formation of 12-LOX- and 15-LOX-derived monohydroxylated products (*i.e.*, DHA-derived 17-HDHA and 14-HDHA, AA-derived 15-HETE and 12-HETE, and EPA-derived 15-HEPE and 12-HEPE); 2) zileuton (3 μM) blocked the formation of DHA-derived RvD2, RvD5, and Mar1 as well as the SPM derivatives 5,15-diHETE and 10S,17S-diHDHA, which were all elevated by low-dose MK886 (30 nM) and even more pronounced upon 3 μM MK886 treatment; 3) formation of EPA-derived RvE3 and its precursor 18-HEPE was inhibited by zileuton but not by MK886 (3 μM each, Fig. 3A, B). In contrast, AA-derived LXA₄ formation in M2 macrophages was reduced by both inhibitors, similar to

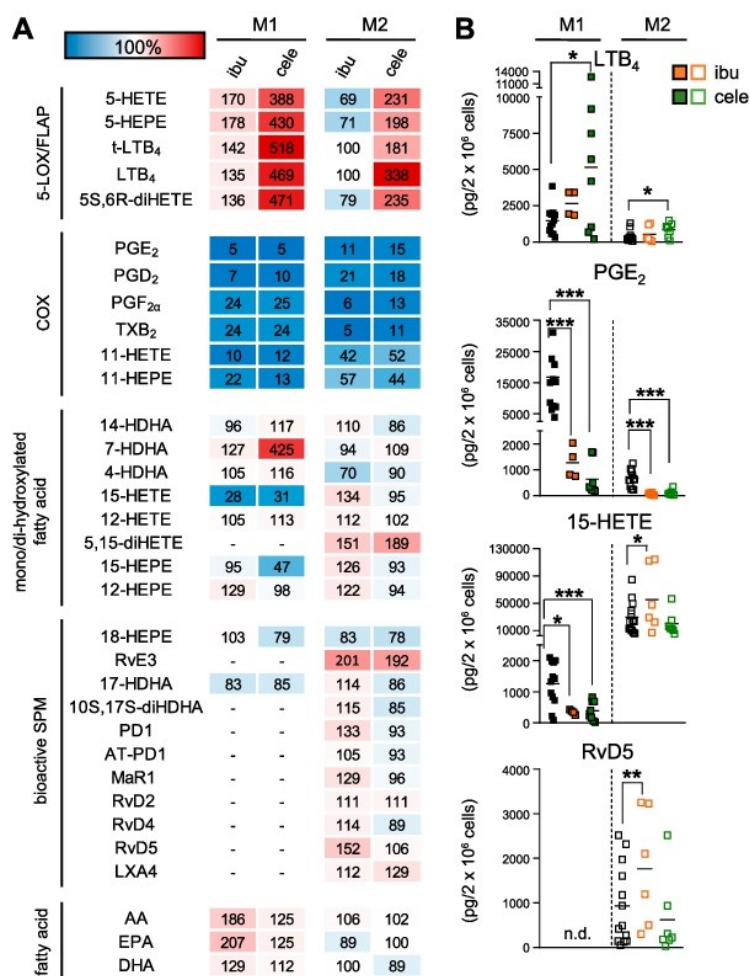


Figure 2. Effects of the COX inhibitors ibuprofen and celecoxib on LM biosynthesis in M1 and M2 macrophages. **A)** Human M1 or M2 (2×10^6 cells/ml) were preincubated with 30 μ M ibuprofen (ibu), 3 μ M celecoxib (cele), or vehicle (0.1% DMSO) for 15 min at 37 °C before incubation with *E. coli* (O6:K2:H1; ratio 1:50) for another 180 min. Formed LMs were extracted by SPE and analyzed by UPLC-MS-MS; means are shown in a heat map as percentage of vehicle-treated cells (= 100% control, white). For ibu, $n = 4$ in M1 ($n = 3$ for 17-HDHA), and $n = 6$ in M2 ($n = 4$ for RvD2; $n = 5$ for RvD4 and LXA₄). For cele, $n = 8$ in M1 ($n = 5$ for 14-HDHA, 15-HEPE, 12-HEPE, and 17-HDHA; $n = 7$ for 12-HETE) and $n = 7$ in M2 ($n = 6$ for RvE3, MaR1, RvD4). **B)** Effects of ibu (orange) and cele (green) on LTB₄, PGE₂, 15-HETE, and RvD5 biosynthesis in M1 and M2 cells, shown as picogram (pg)/ 2×10^6 cells. N.d., not detectable. Data were log-transformed for Student's paired *t* test. Ibu *vs.* vehicle in M1: LTB₄, $P = 0.1675$; PGE₂, $***P = 0.00016$; 15-HETE, $*P = 0.0118$, and in M2: LTB₄, $P = 0.8733$; PGE₂, $***P = 0.00011$; 15-HETE, $*P = 0.0360$; RvD5, $**P = 0.0089$. Cele *vs.* vehicle in M1: LTB₄, $*P = 0.0242$; PGE₂, $***P = 0.000001$; 15-HETE, $***P = 0.000002$, and in M2: LTB₄, $*P = 0.0139$; PGE₂, $***P = 0.000119$; 15-HETE, $P = 0.4608$; RvD5, $P = 0.6133$.

LTB₄ formation. Moreover, whereas zileuton and MK886 strongly (>80%) blocked 7-HDHA formation in M1 macrophages, both inhibitors failed in this respect in the M2 phenotype, suggesting that 7-HDHA in M2 macrophages is formed independent of 5-LOX or FLAP. The product 4-HDHA and the PDs PD1 and AT-PD1 were hardly affected by 5-LOX and FLAP inhibition. Alterations of AA, EPA, and DHA levels that were due to the inhibitors were moderate without conclusive tendencies. Together, both zileuton and MK886 strongly inhibit LT biosynthesis primarily in M1 macrophages, whereas only the 5-LOX inhibitor zileuton suppresses also 12-LOX- and 15-LOX-derived products (including SPM) in M2 cells, in which the FLAP inhibitor MK886 elevates formation of SPMs and their precursors, especially those that are derived from DHA.

Targeting 15-LOX-1 activity in M2 macrophages suppresses SPM formation and increases proinflammatory 5-LOX product biosynthesis

To study the role of 15-LOX-1 in LM formation in *E. coli*-activated M1 and M2 macrophages, the 15-LOX-1-selective inhibitor 3887 (17, 29) (Supplemental Fig. S2A)

was used. In line with the moderate protein expression of 15-LOX-1 in M1, LM formation was essentially unaffected by 300 nM 3887 in this macrophage subtype (alterations <25%), regardless of the biosynthetic LM pathway (*i.e.*, COX, 5-LOX, 12-LOX, and 15-LOX-1; Fig. 4A, C). In M2, however, the formation of 15-LOX-1-related monohydroxylated products, such as 12- and 15-HETE, 12- and 15-HEPE, as well as 14- and 17-HDHA, was concentration-dependently inhibited with consistent IC₅₀ \approx 200–300 nM (Fig. 4B and Supplemental Fig. S2B). We confirmed the dual reaction specificity of human 15-LOX-1 at position C15 and C12 for AA and EPA and C17 and C14 for DHA in a ratio of 10:1 (Supplemental Fig. S2C). Inhibitory effects of 3887 against 5-LOX (Supplemental Fig. S2D) or against 15-LOX-2 (29) were not evident. The formation of the 15-LOX-derived SPM—that is, LXA₄, RvD2, -D4, -D5, PD1, and AT-PD1, their derivatives 5,15-diHETE and 10S,17S-diHDHA, as well as MaR1—were efficiently suppressed by 3887 (IC₅₀ \approx 100–200 nM, Fig. 4B and Supplemental Fig. S2B). In parallel, 5-LOX-derived LTB₄, 5-HETE, and 5-HEPE concentration-dependently increased up to about 4-fold, presumably because of substrate redirection from the 15-LOX-1 to the 5-LOX pathway. Although 15-LOX-1 was shown to be involved

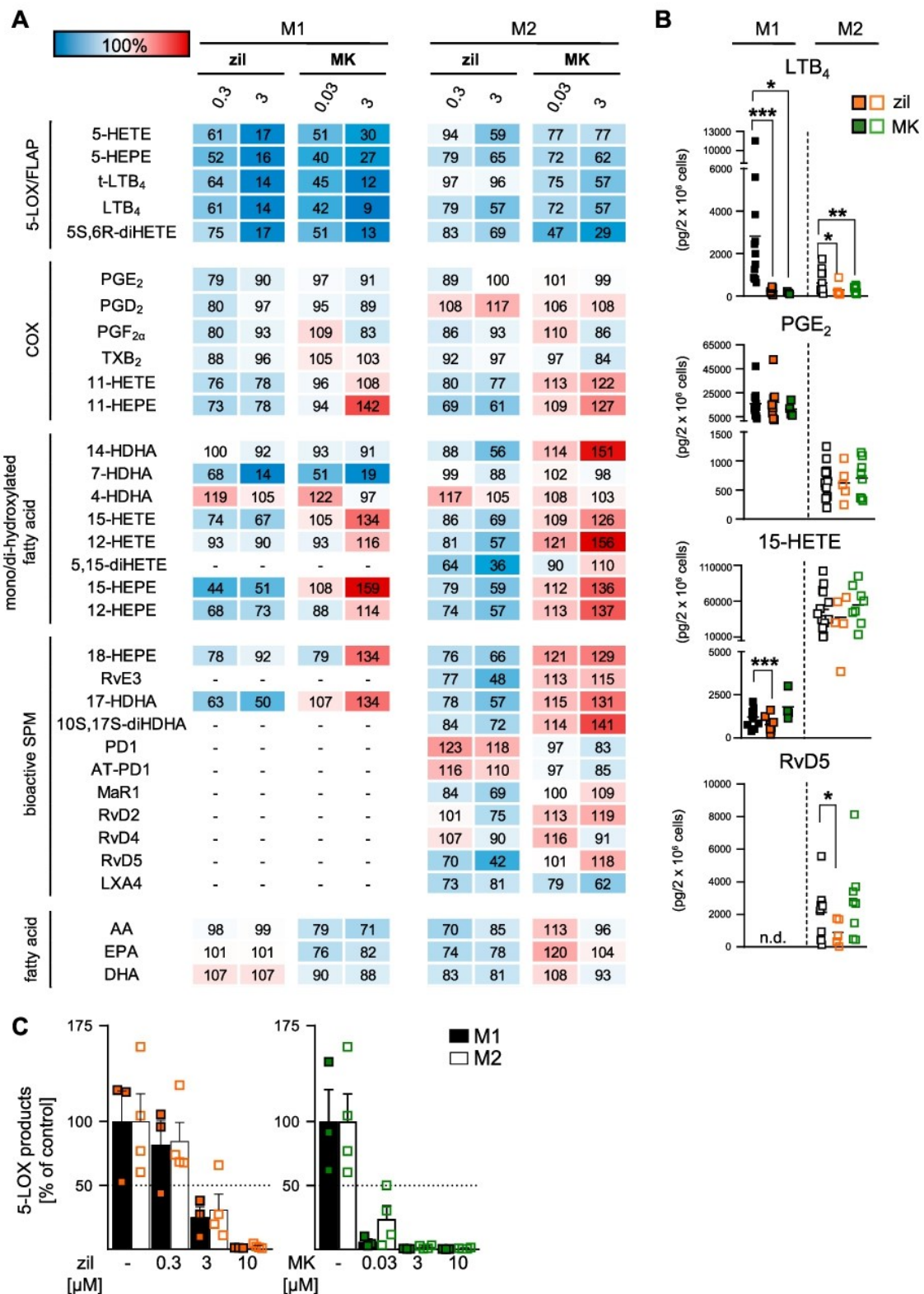


Figure 3. Effects of the 5-LOX inhibitor zileuton (zil) and the FLAP inhibitor MK886 (MK) on LM biosynthesis in M1 and M2. *A*) Human M1 and M2 (2×10^6 cells/ml) were preincubated with 0.3 or 3 μ M zileuton, 0.03 or 3 μ M MK886, or vehicle (0.1% DMSO) for 15 min at 37 °C and then incubated with *E. coli* (O6:K2:H1; ratio 1:50) for another 180 min. Formed LMs were extracted by SPE and analyzed by UPLC-MS-MS, and means are shown in a heat map as percentage of vehicle-treated cells (continued on next page)

in EPA-derived RvE3 biosynthesis in eosinophils (30), exposure of M2 cells to 3887 had only minor effects of EPA-derived LM, such as 18-HEPE and RvE3 (Fig. 4 and Supplemental Fig. S2B), whereas 15-HEPE levels were strongly suppressed, as expected. In general, LMs derived from EPA were less produced compared with AA or DHA products (Supplemental Fig. S2B). Interestingly, 3887 inhibited the formation of 7-HDHA in M2 (Fig. 4A, B) but not in M1 macrophages (Fig. 4A, C); 4-HDHA was not reduced but increased (Fig. 4B), and COX product formation as well as fatty acid substrate release was hardly affected by 3887 (Fig. 4A). Together, 3887 effectively suppresses 15-LOX-1-derived product formation including AA- and DHA-derived SPMs while increasing 5-LOX-related LM biosynthesis.

The cPLA₂ inhibitor RSC-3388 blocks the release of AA and EPA but not of DHA

To investigate how cPLA₂ inhibition affects the release of fatty acid substrates and in turn LM formation, we analyzed the LM profile of *E. coli*-stimulated M1 and M2 macrophages that were pretreated with RSC-3388, a commonly used cPLA₂ reference inhibitor (31). Although AA and EPA levels were significantly lowered by RSC-3388 (10 μM), particularly in the M2 subtype, the amounts of free DHA were rather increased (Fig. 5A, C). Along these lines, the substantial formation of AA- and EPA-derived LMs (PG and LT in M1 cells and 15-LOX-derived LM in M2 cells) was effectively decreased, but DHA-derived LMs (including D-series of SPM and their precursors) were elevated by RSC-3388 (Fig. 5A, B). These data suggest that cPLA₂ contributes to AA and EPA release and respective LM biosynthesis, but the enzyme is dispensable for DHA liberation and DHA-derived SPM generation.

M1 and M2 phenotype-specific network of coregulated LM

Given the broad diversity in LMs produced from bacteria-activated M1 and M2 macrophages, we analyzed the coregulation of specific LMs to enzyme-specific LM pathways in the two phenotypes under pharmacological modulation (for overview, see Supplemental Table S4). Unbiased analysis confirmed PG and LT clusters for the M1 phenotype (Fig. 6A), whereas SPMs and their 12-LOX- and 15-LOX-derived precursors associated with M2 macrophages (Fig. 6B). Thus, positively correlated LMs

clustered in close proximity to each other, whereas distant LMs and their clusters are not coregulated. For M1, 11- and 15-HETE and 15-HEPE positively correlated with prostanooids, reflecting their proximity to the COX pathway (Fig. 6A). Another prominent cluster in M1 cells grouped the typical 5-LOX and FLAP products, and 7-HDHA represents a 5-LOX- and FLAP-derived product in M1. For M2, however, 7-HDHA was associated with the 15-LOX-1 cluster (Fig. 6B), suggesting that 7-HDHA is biosynthesized by 5-LOX in M1 macrophages but mainly by 15-LOX-1 in M2 cells. As a result of abundant 15-LOX-1 expression in M2 macrophages, 7 SPMs and 6 SPM precursors grouped together (Fig. 6B), a cluster that is absent in the M1 phenotype. The 15-HETE and 17-HDHA biosynthesis clearly dominated the M2 phenotype. Of note, solely DHA-derived SPMs coregulated in a 15-LOX-1-dependent expression manner. AA-derived 5,15-diHETE, LXA₄, and EPA-derived RvE3 grouped together in a separate cluster distinct from the prominent 15-LOX-1 and 5-LOX and FLAP cluster.

DISCUSSION

Here we present how clinically relevant anti-inflammatory drugs and prominent LM biosynthesis inhibitors modulate the formation of proinflammatory and proresolving LMs in bacteria-stimulated human M1 and M2 macrophages (for an overview, see Fig. 7). Earlier studies on such agents almost exclusively assessed their potential to suppress proinflammatory PGs or LTs, applying test systems, such as stimulated whole blood or isolated neutrophils and monocytes, that reflect solely inflammatory conditions (26, 32, 33). We present here a new experimental, cell-based approach exploiting LM lipidomics profiling with UPLC-MS-MS to comprehensively evaluate these inhibitors for their impact on the biosynthesis of various LMs that determine not only the promotion of inflammation (*i.e.*, PG and LT) but also its resolution (*i.e.*, SPM). Our results broaden the knowledge about the pharmacological profile of different LM biosynthesis inhibitors and disclose for the first time their ability to manipulate SPM biosynthesis—insights that can allow better appraisal of their therapeutic potential to intervene with inflammatory disorders.

The motivation to conduct this study originated from various reasoning. First, the discovery of differential bacteria-induced formation of proinflammatory and proresolving LMs in human macrophage phenotypes (12) enables us for the first time to assess the effects of LM

(= 100% control, white). For zil, *n* = 8 in M1 (*n* = 4 for 14-HDHA, 7-HDHA, 12-HETE, and 17-HDHA; *n* = 6 for 15-HEPE and 12-HEPE; *n* = 7 for 4-HDHA, 18-HEPE, and DHA) and *n* = 5 in M2 (*n* = 4 for LXA₄). For MK, *n* = 4 in M1 and *n* = 8 in M2 (*n* = 6 for RvD2; *n* = 7 for MaR1; *n* = 4 for LXA₄). B) Effects of 3 μM zileuton (zil, orange) and 3 μM MK886 (MK, green) on LTB₄, PGE₂, 15-HETE, and RvD5 biosynthesis in M1 and M2, shown as pg/2 × 10⁶ cells. Data were log-transformed for paired Student's *t* test. N.d., not detectable. Zil *vs.* vehicle in M1: LTB₄, ****P* = 0.000006; PGE₂, *P* = 0.274; 15-HETE, ****P* = 0.00016, and in M2: LTB₄, **P* = 0.0475; PGE₂, *P* = 0.896; 15-HETE, *P* = 0.0797; RvD5, **P* = 0.0125. MK *vs.* vehicle in M1: LTB₄, **P* = 0.0234; PGE₂, *P* = 0.329; 15-HETE, *P* = 0.1324, and in M2: LTB₄, ***P* = 0.0083; PGE₂, *P* = 0.706; 15-HETE, *P* = 0.0719; RvD5, *P* = 0.2800. C) M1 and M2 (2 × 10⁶ cells/ml) were preincubated with zileuton, MK886, or vehicle (0.1% DMSO) for 15 min at 37 °C and then incubated with A23187 (2.5 μM) for another 10 min. Formed 5-LOX products (LTB₄, its isomers, 5-HETE, 5S,6R-diHETE, and 5-HEPE) were extracted by SPE and analyzed by UPLC-MS-MS. Data are given as means + SEM, *n* = 4 independent experiments, shown as percentage of vehicle control (= 100%).

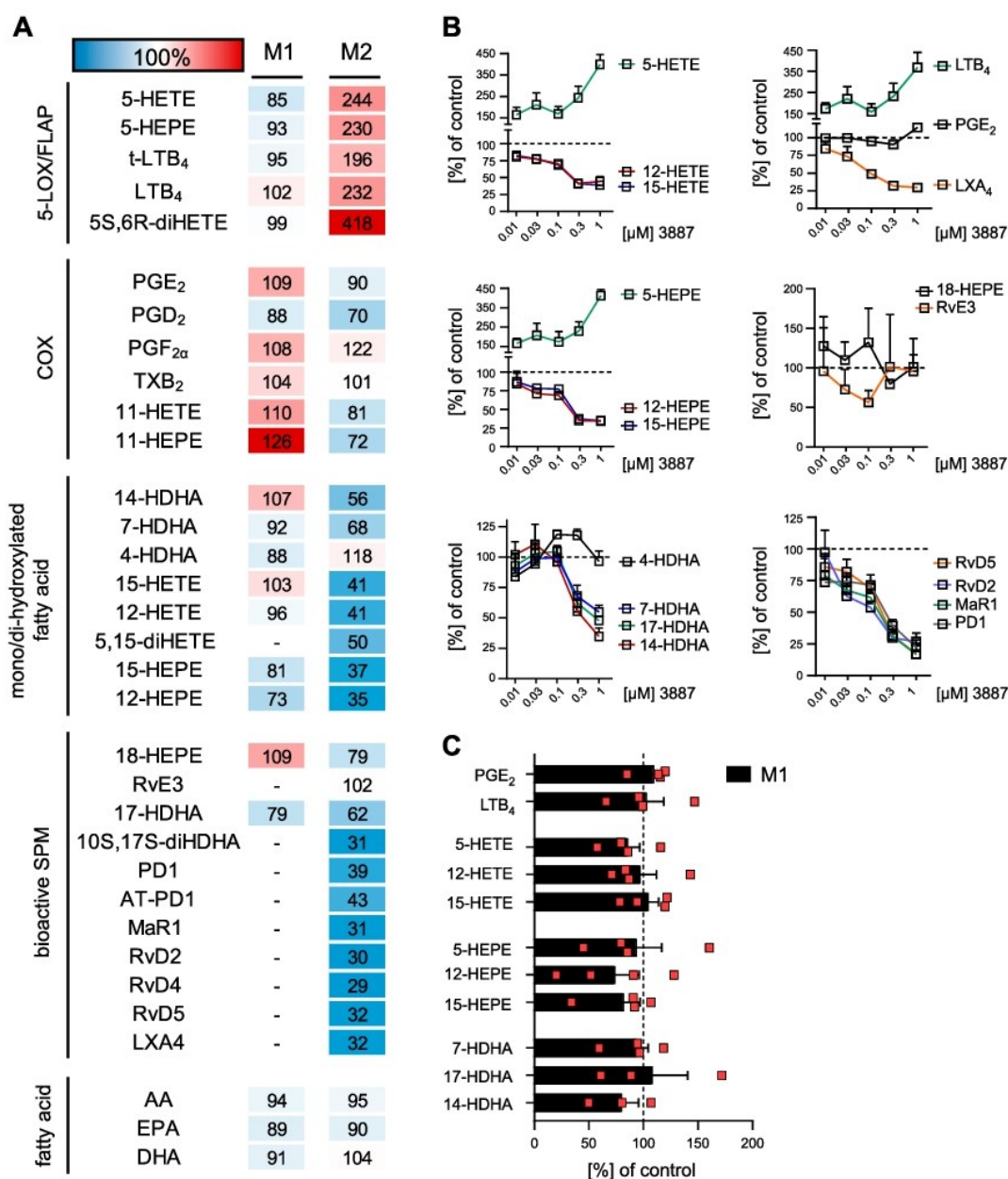


Figure 4. Effects of the 15-LOX-1 inhibitor 3887 on LM biosynthesis in M1 and M2. *A*) Human M1 and M2 (2×10^6 cells/ml) were preincubated with 300 nM 3887 or vehicle (0.1% DMSO) for 15 min at 37 °C before incubation with *E. coli* (O6:K2:H1; ratio 1:50) for another 180 min. Formed LMs were extracted by SPE and analyzed by UPLC-MS-MS, and results are given as percentages of vehicle-treated cells (= 100% control, white) shown as means in a heat map. *B*) Concentration-dependent inhibition of LM formation derived from AA (top), EPA (middle), and DHA (bottom) by 3887 in M2. *C*) Effects of 300 nM 3887 on LM formation in M1. Data are expressed as means + SEM of $n = 4$ in M1 ($n = 3$ for 14-HDHA and 17-HDHA) and $n = 3$ in M2, independent experiments, shown as percentage of uninhibited control (= 100%).

biosynthesis inhibitors under pathophysiologically relevant conditions that reflect either inflammation-promoting (M1-like) or inflammation-resolving (M2-like) potential. Second, COX and 5-LOX or FLAP inhibitors are considered beneficial in inflammation therapy because of the blockade of the formation of proinflammatory PGs and LTs (34), but how these drugs influence SPM biosynthesis, and thus resolution of inflammation is elusive (35, 36). Third, the

biosynthetic pathways of LMs are organized within connected cascades that can crosstalk within a complex network (14, 15), and therefore, pharmacological interference with one pathway may redirect toward other LM routes. In fact, COX inhibitors and the 15-LOX-1 inhibitor 3887 each increased formation of proinflammatory 5-LOX products. Fourth, proinflammatory and proresolving LMs might be partially biosynthesized by common enzymes, such as

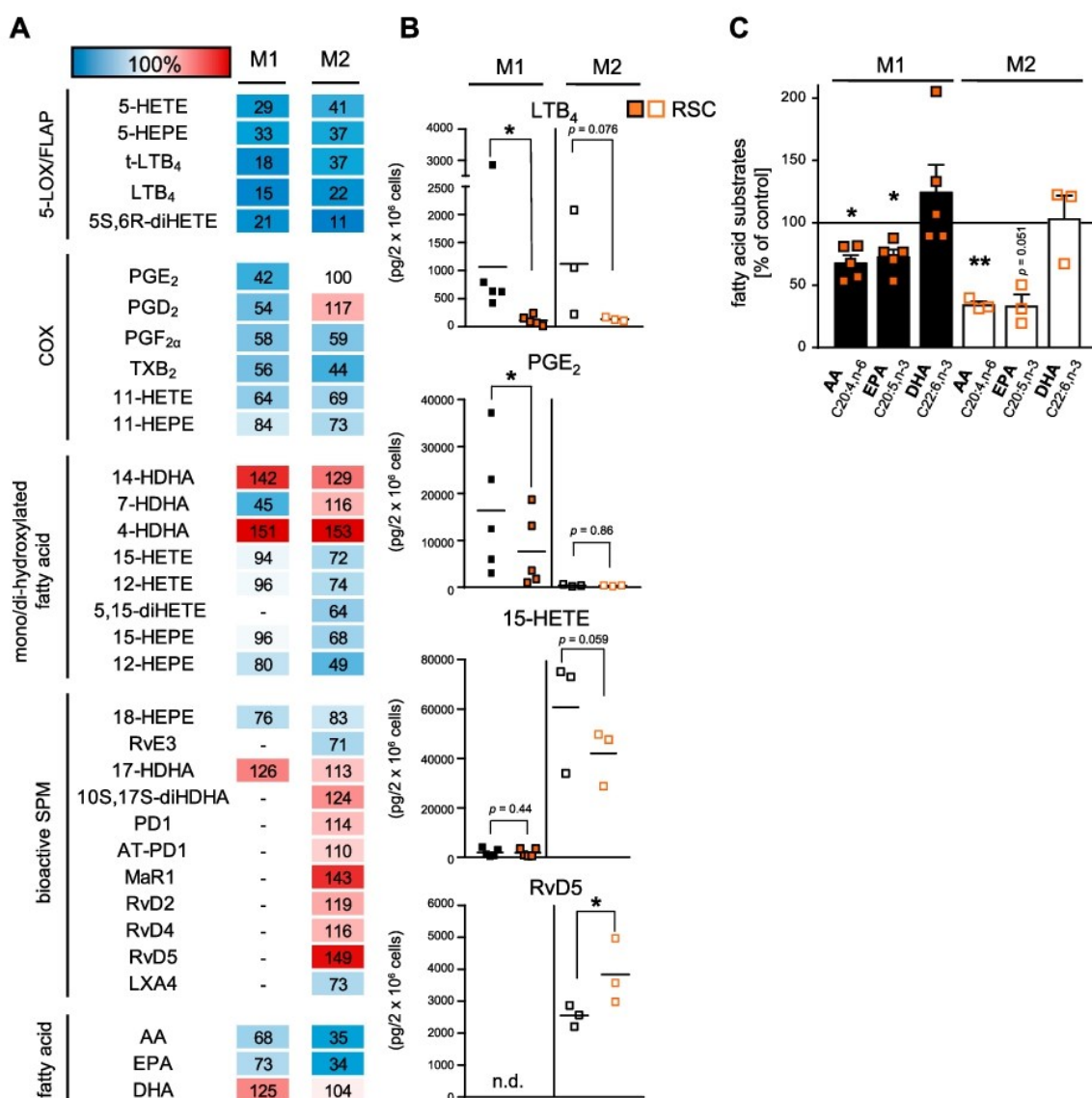


Figure 5. Effects of the cPLA₂ inhibitor RSC-3388 on LM biosynthesis in M1 and M2. *A*) Human M1 and M2 (2×10^6 cells/ml) were preincubated with 10 μ M RSC-3388 or vehicle (0.1% DMSO) for 15 min at 37 °C before incubation with *E. coli* (O6:K2:H1; ratio 1:50) for another 180 min. Formed LMs were extracted by SPE and analyzed by UPLC-MS-MS, and means are shown in a heat map as percentages of vehicle-treated cells (= 100% control, white) of $n = 5$ in M1 ($n = 2$ for 14-HDHA; $n = 3$ for 7-HDHA, 12-HETE, and 17-HDHA; $n = 4$ for 15-HEPE and 12-HEPE) and $n = 3$ in M2. *B*) Effects of RSC-3388 on LTB₄, PGE₂, 15-HETE, and RvD5 biosynthesis in M1 and M2 shown as pg/2 $\times 10^6$ cells. *C*) Effects of 10 μ M RSC-3388 on free AA, EPA, and DHA levels in M1 and M2 shown as percentage of vehicle control. N.d., not detectable. Data were log-transformed for statistical analysis, paired Student's *t* test; RSC vs. vehicle in M1: LTB₄, * $P = 0.0105$; PGE₂, * $P = 0.0161$; 15-HETE, $P = 0.4427$; AA, * $P = 0.0102$; EPA, * $P = 0.0165$; DHA, $P = 0.3332$ and in M2: LTB₄, $P = 0.0764$; PGE₂, $P = 0.8617$; 15-HETE, $P = 0.0590$; RvD5, * $P = 0.0377$; AA, ** $P = 0.0047$; EPA, $P = 0.0507$; DHA, $P = 0.9974$.

5-LOX or FLAP, that mediate formation of LTs but possibly also of LXs and Rvs (37). This implies that 5-LOX and FLAP inhibitors block inflammation but also may hamper resolution. Indeed, zileuton suppressed SPM formation, whereas FLAP inhibition failed in this respect and instead elevated SPM levels. Together, our data highlight the contribution of key enzymes in LM biosynthesis under pathophysiologically relevant conditions, and they suggest that drugs that act on these key enzymes may affect the overall

LM network with potential consequences for the pharmacotherapy of inflammation.

LMs produced *via* the COX-1/2 pathway display proinflammatory but also protective actions depending on stimulus, cell type, and status that program the ability to resolve inflammation (5, 38). Although beneficial effects of NSAIDs are well established for alleviating acute inflammation and pain (26, 39), they cause severe on-target side effects and may negatively impact inflammation

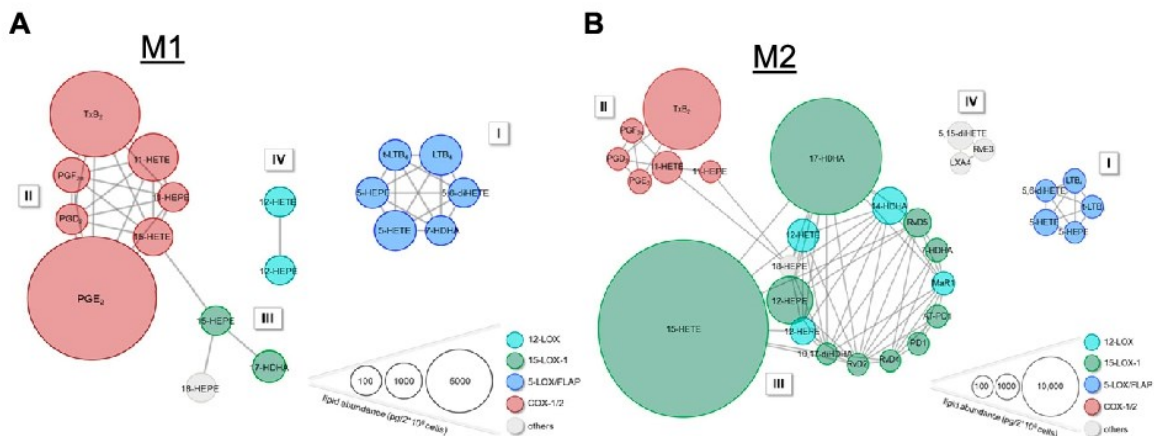


Figure 6. Network of coregulated eicosanoids and docosanoids in M1 and M2 macrophages. M1 (A) and M2 cells (B), corresponding to 2×10^6 cells/ml, were treated with vehicle (0.1% DMSO) or test compounds 15 min before challenge with *E. coli* (O6:K2:H1; ratio 1:50) for 180 min at 37 °C. LMs were isolated by SPE and analyzed by UPLC-MS-MS. Visualization of positive LM/LM correlations as circular network with $r \geq 0.7$. Nodes visualize the LM; for color and size meanings see legend.

resolution (35, 40). Thus, COX-2-deficient mice failed to resolve from inflammation, and the COX inhibitor indomethacin exacerbated inflammation because of reduced proresolving PGD₂ levels (41). Also, COX-2-derived PGD₂ ameliorated colonic inflammation in rats (42). In our study, both COX inhibitors efficiently reduced all prostanoids and caused a strong shift to the 5-LOX- and FLAP-mediated LT biosynthesis pathway in M1 and M2 macrophages but, interestingly, not to the 15-LOX and DHA pathway and SPM formation in the M2 phenotype. Elevated LT levels that were due to COX-1/2 inhibition are well known and are seemingly causative for increased risk for asthma, and more frequent gastrointestinal lesions might be due to LTB₄-elicited neutrophil infiltration (9, 43).

The proinflammatory functions of LTs are reflected by LTB₄ as potent chemo-attractant for neutrophils (44) and by cysteinyl-LTs that increase microvascular permeability and immune cell recruitment (45). Suppression of LT formation by targeting the 5-LOX pathway is a therapeutic

strategy to treat inflammatory disorders, neglecting, however, the role of 5-LOX in the biosynthesis of proresolving mediators, such as LXA₄ (46, 47). 5-LOX and FLAP are essential for LT biosynthesis (45) and apparently also for LX and Rv formation (12, 37, 48). However, our data with the 5-LOX inhibitor zileuton (27) and the FLAP inhibitor MK886 (28) in M1 and M2 macrophages reveal differential and more complex functions for 5-LOX and FLAP. Thus, zileuton blocked the formation of LT and SPM (LXA₄ and Rv), that supports the role of 5-LOX in LT and in LX and Rv formation. This suggests that zileuton and other 5-LOX inhibitors could interfere with inflammation resolution by inhibiting SPM biosynthesis. We also observed suppression of 15-LOX products by zileuton in M2 cells that were possibly due to direct interference with 15-LOX-1 that shares structural features with 5-LOX in the active site (49). In contrast, MK886 selectively suppressed LT biosynthesis, whereas, in agreement with our previous report (12), 15-LOX-1 products are increased in

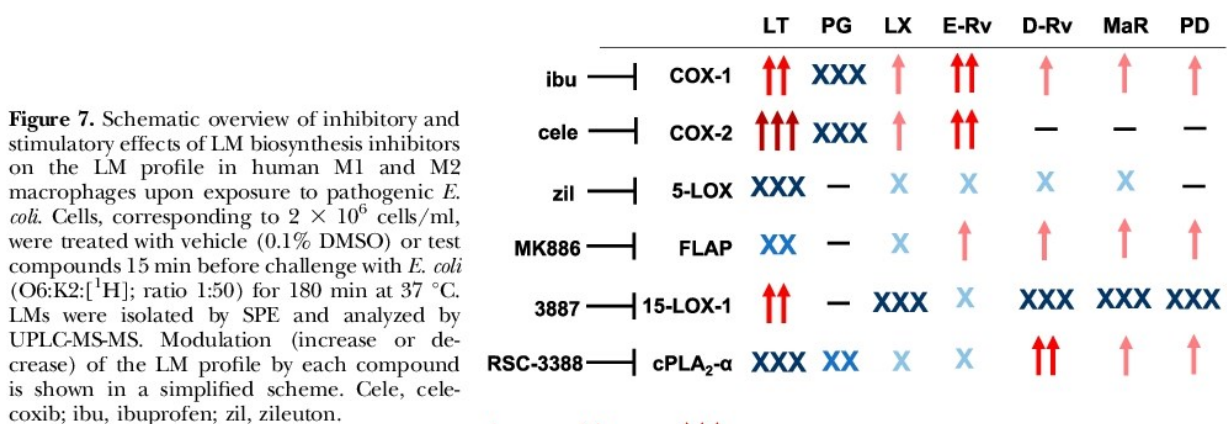


Figure 7. Schematic overview of inhibitory and stimulatory effects of LM biosynthesis inhibitors on the LM profile in human M1 and M2 macrophages upon exposure to pathogenic *E. coli*. Cells, corresponding to 2×10^6 cells/ml, were treated with vehicle (0.1% DMSO) or test compounds 15 min before challenge with *E. coli* (O6:K2:[¹H]; ratio 1:50) for 180 min at 37 °C. LMs were isolated by SPE and analyzed by UPLC-MS-MS. Modulation (increase or decrease) of the LM profile by each compound is shown in a simplified scheme. Cele, celecoxib; ibu, ibuprofen; zil, zileuton.

↑ > 110% ↑↑ > 140% ↑↑↑ > 200%
 X < 80% XX < 50% XXX < 20%

M2 macrophages, especially D-series Rv and MaR1. Obviously, zileuton and MK886 were much less efficient to inhibit *E. coli*-induced LT formation in M2 than in M1 cells, which is not readily understood. In control experiments with A23187, however, this bias was abolished, excluding unequal inhibitor availability in M1 and M2 macrophages or differential 5-LOX and FLAP expression as reasons. Possibly, the potency of zileuton and MK886 may depend on the signaling pathways that lead to activation of 5-LOX (e.g., phosphorylation and oxidative tone), which may differ for activation by A23187 and by pathogenic *E. coli* in M1 and M2 subtypes. Indeed, differential potencies for other 5-LOX inhibitors depending on kinase signaling and oxidative tone were observed before (50, 51).

We propose that 5-LOX subcellular localization and differential access to AA vs. DHA determines whether LTs or DHA-derived SPMs are preferably formed by 5-LOX, depending on the interaction with FLAP. Experimental evidence suggests that when activated 5-LOX interacts with FLAP at the nuclear membrane, AA is presented by FLAP and 5-LOX converts it to LT (52). But when 5-LOX is activated in a nonnuclear compartment and distant from FLAP [e.g., if 5-LOX phosphorylation at Ser271 is blocked (53) or FLAP inhibitors like MK886 prevent the interaction with FLAP (12)] then 5-LOX may preferably access DHA-derived intermediates to biosynthesize specific SPMs. In fact, in MK886-treated M2 cells, formation of the AA-derived SPM LXA₄ is reduced as LTB₄, but DHA-derived SPMs are still produced (Fig. 3A). We showed before that targeting of FLAP by MK886 in M2 macrophages precludes the interaction with 5-LOX at the nuclear membrane (12), supporting the hypothesis by other researchers (53) about a differentially regulated nonnuclear 5-LOX favoring the biosynthesis of proresolving LMs. In murine liver injury, the FLAP inhibitor BAY X-1005 reduced cysteinyl-LT formation but elevated SPM levels (54). Therefore, FLAP might be negligible for the biosynthesis of D-series Rv in M2 macrophages, and hence FLAP inhibitors may be more beneficial as anti-inflammatory drugs than direct 5-LOX inhibitors because they suppress proinflammatory LTs but might maintain SPM biosynthesis to enable resolution of inflammation, such as PDs and MaRs that do not rely on 5-LOX for their biosynthesis (55, 56).

Expression of 15-LOX-1 is characteristic for the M2 phenotype, as well as its high capacity to biosynthesize SPM compared with the M1 subset (12). However, 15-LOX-1 is a versatile enzyme that plays a role in both the onset and the termination of immune responses (10, 11, 57, 58). Recently, an anti-inflammatory role of 15-LOX and a related SPM in mouse skin was reported with implications for the maintenance of dermal integrity (59). In fact, current developments focus on small molecule 15-LOX activators to foster SPM formation and abrogate LT and PG production (60). On the other hand, 3887 inhibited dendrite and podosome formation in human dendritic cells, indicating an anti-inflammatory effect of 15-LOX-1 inhibitors (17). Targeting 15-LOX-1 by the selective inhibitor 3887 (17, 29) in M2 macrophages blocked the formation of all detectable SPMs. The inhibitor 3887, like COX inhibitors, redirected AA toward the 5-LOX pathway in the M2 phenotype with increased LTB₄ and 5-HETE levels,

indicating that both 15-LOX-1 and COX inhibitors have a complex effect mechanism of action and influence both inflammation and resolution. This suggests careful consideration of application and use of these inhibitors as potential therapeutics where LTs promote the disease and SPMs beneficially contribute to resolution and tissue regeneration (48).

cPLA₂ provides fatty acid substrates for COX and LOX to generate LMs (61). Results with the cPLA₂ inhibitor RSC-3388 support an involvement of cPLA₂ in AA and EPA release, particularly in M2 cells, in which cPLA₂ protein levels were higher than in M1 macrophages, accompanied by reduced levels of AA- and EPA-derived 5-LOX and 15-LOX products. Remarkably, RSC-3388 increased DHA levels and promoted the formation of DHA-derived SPMs as well as the respective precursors. Discrimination of DHA from AA release was reported earlier by Shikano *et al.* (62), and it was suggested that DHA supply in macrophages for SPM biosynthesis is mediated by secreted PLA₂ group IID (63).

Together, metabololipidomics of broad-spectrum LMs produced in bacteria-challenged human proinflammatory M1 and anti-inflammatory M2 macrophages led to important, partially unexpected insights into the pharmacological manipulation of bioactive LMs that determine initiation or resolution of inflammation. The pharmacological profiles of these drugs and agents that act on discrete LM biosynthetic enzymes can impact the overall LM network with potential consequences for inflammation pharmacotherapy. In search of more efficient and safer anti-inflammatory drugs, our data prompt for better consideration of the effects of such agents on SPM formation that may translate into resolution-based pharmacology as alternative strategies to resolve chronic inflammation. **[F]**

ACKNOWLEDGMENTS

This work was supported by the Deutsche Forschungsgemeinschaft (SFB1127, ChemBioSys, and SFB1278, Polytarget). J.G. received a Carl-Zeiss stipend, and C.N.S. was supported by U.S. National Institutes of Health, National Institute of General Medical Sciences Grant P01GM095467. The authors declare no conflicts of interest.

AUTHOR CONTRIBUTIONS

M. Werner performed the ibuprofen, celecoxib, zileuton, RSC-3388 experiments and performed the network analysis; P. M. Jordan performed the 3887 experiments, flow cytometry analysis, and A23187 studies; E. Romp performed MK886 experiments; A. Czapka, Z. Rao, and C. Kretzer performed Western blots; M. Werner, P. M. Jordan, A. Czapka, S. Pace, and J. Gerstmeier performed data analysis and prepared graphs; M. Werner, A. Koeberle, and J. Gerstmeier developed the ultraperformance liquid chromatography method; H.-E. Claesson supplied 3887; C. N. Serhan, O. Werz, and J. Gerstmeier designed the study; O. Werz and J. Gerstmeier wrote the manuscript; and all authors contributed to manuscript preparation.

REFERENCES

- Chiang, N., Fredman, G., Bäckhed, F., Oh, S. F., Vickery, T., Schmidt, B. A., and Serhan, C. N. (2012) Infection regulates pro-resolving mediators that lower antibiotic requirements. *Nature* **484**, 524–528
- Serhan, C. N. (2014) Pro-resolving lipid mediators are leads for resolution physiology. *Nature* **510**, 92–101
- Spite, M., Clària, J., and Serhan, C. N. (2014) Resolvins, specialized proresolving lipid mediators, and their potential roles in metabolic diseases. *Cell Metab.* **19**, 21–36
- Tabas, I., and Glass, C. K. (2013) Anti-inflammatory therapy in chronic disease: challenges and opportunities. *Science* **339**, 166–172
- Rainsford, K. D. (2007) Anti-inflammatory drugs in the 21st century. *Subcell. Biochem.* **42**, 3–27
- Wertz, O., Gerstmeier, J., and Garscha, U. (2017) Novel leukotriene biosynthesis inhibitors (2012–2016) as anti-inflammatory agents. *Expert Opin. Ther. Pat.* **27**, 607–620
- Serhan, C. N., and Petasis, N. A. (2011) Resolvins and protectins in inflammation resolution. *Chem. Rev.* **111**, 5922–5943
- Conte, M. S., Desai, T. A., Wu, B., Schaller, M., and Werlin, E. (2018) Pro-resolving lipid mediators in vascular disease. *J. Clin. Invest.* **128**, 3727–3735
- Rainsford, K. D. (1993) Leukotrienes in the pathogenesis of NSAID-induced gastric and intestinal mucosal damage. *Agents Actions* **39**, C24–C26
- Andersson, C. K., Claesson, H. E., Rydell-Törmänen, K., Swedmark, S., Hällgren, A., and Erjefält, J. S. (2008) Mice lacking 12/15-lipoxygenase have attenuated airway allergic inflammation and remodeling. *Am. J. Respir. Cell Mol. Biol.* **39**, 648–656
- Claesson, H. E. (2009) On the biosynthesis and biological role of eoxins and 15-lipoxygenase-1 in airway inflammation and Hodgkin lymphoma. *Prostaglandins Other Lipid Mediat.* **89**, 120–125
- Wertz, O., Gerstmeier, J., Libreros, S., De la Rosa, X., Werner, M., Norris, P. C., Chiang, N., and Serhan, C. N. (2018) Human macrophages differentially produce specific resolvin or leukotriene signals that depend on bacterial pathogenicity. *Nat. Commun.* **9**, 59
- Dalli, J., Colas, R. A., and Serhan, C. N. (2013) Novel n-3 immunoregulators: structures and actions. *Sci. Rep.* **3**, 1940; erratum: 4, 6726
- Yang, K., Ma, W., Liang, H., Ouyang, Q., Tang, C., and Lai, L. (2007) Dynamic simulations on the arachidonic acid metabolic network. *PLoS Comput. Biol.* **3**, e55
- He, C., Wu, Y., Lai, Y., Cai, Z., Liu, Y., and Lai, L. (2012) Dynamic eicosanoid responses upon different inhibitor and combination treatments on the arachidonic acid metabolic network. *Mol. Biosyst.* **8**, 1585–1594
- Motwani, M. P., and Gilroy, D. W. (2015) Macrophage development and polarization in chronic inflammation. *Semin. Immunol.* **27**, 257–266
- Han, H., Liang, X., Ekberg, M., Kritikou, J. S., Brunnström, Å., Pelcman, B., Matl, M., Miao, X., Andersson, M., Yuan, X., Schain, F., Parvin, S., Melin, E., Sjöberg, J., Xu, D., Westerberg, L. S., Björkholm, M., and Claesson, H. E. (2017) Human 15-lipoxygenase-1 is a regulator of dendritic-cell spreading and podosome formation. *FASEB J.* **31**, 491–504
- Colas, R. A., Shinohara, M., Dalli, J., Chiang, N., and Serhan, C. N. (2014) Identification and signature profiles for pro-resolving and inflammatory lipid mediators in human tissue. *Am. J. Physiol. Cell Physiol.* **307**, C39–C54
- Dalli, J., and Serhan, C. N. (2012) Specific lipid mediator signatures of human phagocytes: microparticles stimulate macrophage efferocytosis and pro-resolving mediators. *Blood* **120**, e60–e72
- Pace, S., Pergola, C., Dehm, F., Rossi, A., Gerstmeier, J., Troisi, F., Pein, H., Schaible, A. M., Weinigel, C., Rummeler, S., Northoff, H., Laufer, S., Maier, T. J., Rådmark, O., Samuelsson, B., Koeberle, A., Sautebin, L., and Wertz, O. (2017) Androgen-mediated sex bias impairs efficiency of leukotriene biosynthesis inhibitors in males. *J. Clin. Invest.* **127**, 3167–3176
- Murray, P. J., Allen, J. E., Biswas, S. K., Fisher, E. A., Gilroy, D. W., Goerdt, S., Gordon, S., Hamilton, J. A., Ivashkiv, L. B., Lawrence, T., Locati, M., Mantovani, A., Martinez, F. O., Mege, J. L., Mosser, D. M., Natoli, G., Saeij, J. P., Schultze, J. L., Shirey, K. A., Sica, A., Suttles, J., Udalova, I., van Ginderachter, J. A., Vogel, S. N., and Wynn, T. A. (2014) Macrophage activation and polarization: nomenclature and experimental guidelines. *Immunity* **41**, 14–20
- Aursnes, M., Tungen, J. E., Colas, R. A., Vlasakov, I., Dalli, J., Serhan, C. N., and Hansen, T. V. (2015) Synthesis of the 16S,17S-epoxyprotectin intermediate in the biosynthesis of protectins by human macrophages. *J. Nat. Prod.* **78**, 2924–2931
- Primdahl, K. G., Tungen, J. E., De Souza, P. R. S., Colas, R. A., Dalli, J., Hansen, T. V., and Vik, A. (2017) Stereocontrolled synthesis and investigation of the biosynthetic transformations of 16(S),17(S)-epoxy-PD_{n-3}DPA. *Org. Biomol. Chem.* **15**, 8606–8613
- Snodgrass, R. G., Zezina, E., Namgaladze, D., Gupta, S., Angioni, C., Geisslinger, G., Lütjohann, D., and Brüne, B. (2018) A novel function for 15-lipoxygenases in cholesterol homeostasis and CCL17 production in human macrophages. *Front. Immunol.* **9**, 1906
- Kutzner, L., Goloshchapova, K., Heydeck, D., Stehling, S., Kuhn, H., and Schebb, N. H. (2017) Mammalian ALOX15 orthologs exhibit pronounced dual positional specificity with docosahexaenoic acid. *Biochim Biophys Acta Mol Cell Biol Lipids* **1862**, 666–675
- Mazaleuskaya, L. L., Lawson, J. A., Li, X., Grant, G., Mesaros, C., Grosser, T., Blair, I. A., Ricciotti, E., and FitzGerald, G. A. (2016) A broad-spectrum lipidomics screen of antiinflammatory drug combinations in human blood. *JCI Insight* **1**, e87031
- Carter, G. W., Young, P. R., Albert, D. H., Bouska, J., Dyer, R., Bell, R. L., Summers, J. B., and Brooks, D. W. (1991) 5-lipoxygenase inhibitory activity of zileuton. *J. Pharmacol. Exp. Ther.* **256**, 929–937
- Gillard, J., Ford-Hutchinson, A. W., Chan, C., Charleson, S., Denis, D., Foster, A., Fortin, R., Leger, S., McFarlane, C. S., Morton, H., Piechuta, H., Riendeau, D., Rouzer, C. A., Rokach, J., Young, R., MacIntyre, D. E., Peterson, L., Bach, T., Eiemann, G., Hopple, S., Humes, J., Hupe, L., Luell, S., Metzger, J., Meurer, R., Miller, D. K., Opas, E., and Pacholok, S. (1989) L-663,536 (MK-886) (3-[1-(4-chlorobenzyl)-3-butylthio-5-isopropylindol-2-yl]-2,2-dimethylpropanoic acid), a novel, orally active leukotriene biosynthesis inhibitor. *Can. J. Physiol. Pharmacol.* **67**, 456–464
- Archambault, A. S., Turcotte, C., Martin, C., Provost, V., Larose, M. C., Laprise, C., Chakir, J., Bissonnette, É., Laviolette, M., Bossé, Y., and Flamand, N. (2018) Comparison of eight 15-lipoxygenase (LO) inhibitors on the biosynthesis of 15-LO metabolites by human neutrophils and eosinophils. *PLoS One* **13**, e0202424
- Isobe, Y., Arita, M., Matsueda, S., Iwamoto, R., Fujihara, T., Nakanishi, H., Taguchi, R., Masuda, K., Sasaki, K., Urabe, D., Inoue, M., and Arai, H. (2012) Identification and structure determination of novel anti-inflammatory mediator resolvin E3, 17,18-dihydroxyeicosapentaenoic acid. *J. Biol. Chem.* **287**, 10525–10534
- Seno, K., Okuno, T., Nishi, K., Murakami, Y., Watanabe, F., Matsuura, T., Wada, M., Fujii, Y., Yamada, M., Ogawa, T., Okada, T., Hashizume, H., Kii, M., Hara, S., Hagishita, S., Nakamoto, S., Yamada, K., Chikazawa, Y., Ueno, M., Teshirogi, I., Ono, T., and Ohtani, M. (2000) Pyrrolidine inhibitors of human cytosolic phospholipase A(2). *J. Med. Chem.* **43**, 1041–1044
- Khanapure, S. P., Garvey, D. S., Janero, D. R., and Letts, L. G. (2007) Eicosanoids in inflammation: biosynthesis, pharmacology, and therapeutic frontiers. *Curr. Top. Med. Chem.* **7**, 311–340
- Wertz, O., and Steinhilber, D. (2005) Development of 5-lipoxygenase inhibitors—lessons from cellular enzyme regulation. *Biochem. Pharmacol.* **70**, 327–333
- Funk, C. D. (2001) Prostaglandins and leukotrienes: advances in eicosanoid biology. *Science* **294**, 1871–1875
- Fukunaga, K., Kohli, P., Bonnans, C., Fredenburgh, L. E., and Levy, B. D. (2005) Cyclooxygenase 2 plays a pivotal role in the resolution of acute lung injury. *J. Immunol.* **174**, 5033–5039
- Sugimoto, M. A., Sousa, L. P., Pinho, V., Perretti, M., and Teixeira, M. M. (2016) Resolution of inflammation: what controls its onset? *Front. Immunol.* **7**, 160
- Lehmann, C., Homann, J., Ball, A. K., Blöcher, R., Kleinschmidt, T. K., Basavarajappa, D., Angioni, C., Ferreirós, N., Häfner, A. K., Rådmark, O., Proschak, E., Haeggström, J. Z., Geisslinger, G., Parnham, M. J., Steinhilber, D., and Kahnt, A. S. (2015) Lipoxin and resolvin biosynthesis is dependent on 5-lipoxygenase activating protein. *FASEB J.* **29**, 5029–5043
- Levy, B. D., Clish, C. B., Schmidt, B., Gronert, K., and Serhan, C. N. (2001) Lipid mediator class switching during acute inflammation: signals in resolution. *Nat. Immunol.* **2**, 612–619
- Dubois, R. N., Abramson, S. B., Crofford, L., Gupta, R. A., Simon, L. S., Van De Putte, L. B., and Lipsky, P. E. (1998) Cyclooxygenase in biology and disease. *FASEB J.* **12**, 1063–1073
- Gilroy, D. W., Colville-Nash, P. R., Willis, D., Chivers, J., Paul-Clark, M. J., and Willoughby, D. A. (1999) Inducible cyclooxygenase may have anti-inflammatory properties. *Nat. Med.* **5**, 698–701
- Wallace, J. L., McKnight, W., Reuter, B. K., and Vergnolle, N. (2000) NSAID-induced gastric damage in rats: requirement for inhibition of both cyclooxygenase 1 and 2. *Gastroenterology* **119**, 706–714
- Ajuebor, M. N., Singh, A., and Wallace, J. L. (2000) Cyclooxygenase-2-derived prostaglandin D(2) is an early anti-inflammatory signal in

- experimental colitis. *Am. J. Physiol. Gastrointest. Liver Physiol.* **279**, G238–G244
43. Burnett, B. P., and Levy, R. M. (2012) 5-Lipoxygenase metabolic contributions to NSAID-induced organ toxicity. *Adv. Ther.* **29**, 79–98
 44. Lämmermann, T., Afonso, P. V., Angermann, B. R., Wang, J. M., Kastenmüller, W., Parent, C. A., and Germain, R. N. (2013) Neutrophil swarms require LTB4 and integrins at sites of cell death in vivo. *Nature* **498**, 371–375
 45. Rådmark, O., Werz, O., Steinhilber, D., and Samuelsson, B. (2015) 5-Lipoxygenase, a key enzyme for leukotriene biosynthesis in health and disease. *Biochim. Biophys. Acta* **1851**, 331–339
 46. Levy, B. D., De Sanctis, G. T., Devchand, P. R., Kim, E., Ackerman, K., Schmidt, B. A., Szczeklik, W., Drazen, J. M., and Serhan, C. N. (2002) Multi-pronged inhibition of airway hyper-responsiveness and inflammation by lipoxin A(4). *Nat. Med.* **8**, 1018–1023
 47. Bhavsar, P. K., Levy, B. D., Hew, M. J., Pfeffer, M. A., Kazani, S., Israel, E., and Chung, K. F. (2010) Corticosteroid suppression of lipoxin A4 and leukotriene B4 from alveolar macrophages in severe asthma. *Respir. Res.* **11**, 71
 48. Serhan, C. N., and Savill, J. (2005) Resolution of inflammation: the beginning programs the end. *Nat. Immunol.* **6**, 1191–1197
 49. Gilbert, N. C., Bartlett, S. G., Waight, M. T., Neau, D. B., Boeglin, W. E., Brash, A. R., and Newcomer, M. E. (2011) The structure of human 5-lipoxygenase. *Science* **331**, 217–219
 50. Fischer, L., Steinhilber, D., and Werz, O. (2004) Molecular pharmacological profile of the nonredox-type 5-lipoxygenase inhibitor CJ-13,610. *Br. J. Pharmacol.* **142**, 861–868
 51. Fischer, L., Szellas, D., Rådmark, O., Steinhilber, D., and Werz, O. (2003) Phosphorylation- and stimulus-dependent inhibition of cellular 5-lipoxygenase activity by nonredox-type inhibitors. *FASEB J.* **17**, 949–951
 52. Gerstmeier, J., Weinigel, C., Rummler, S., Rådmark, O., Werz, O., and Garscha, U. (2016) Time-resolved in situ assembly of the leukotriene-synthetic 5-lipoxygenase/5-lipoxygenase-activating protein complex in blood leukocytes. *FASEB J.* **30**, 276–285
 53. Fredman, G., Ozcan, L., Spolitu, S., Hellmann, J., Spite, M., Backs, J., and Tabas, I. (2014) Resolvin D1 limits 5-lipoxygenase nuclear localization and leukotriene B4 synthesis by inhibiting a calcium-activated kinase pathway. *Proc. Natl. Acad. Sci. USA* **111**, 14530–14535
 54. Titos, E., Clària, J., Planagumà, A., López-Parra, M., González-Pérez, A., Gaya, J., Miquel, R., Arroyo, V., and Rodés, J. (2005) Inhibition of 5-lipoxygenase-activating protein abrogates experimental liver injury: role of Kupffer cells. *J. Leukoc. Biol.* **78**, 871–878
 55. Serhan, C. N., Dalli, J., Colas, R. A., Winkler, J. W., and Chiang, N. (2015) Protectins and maresins: new pro-resolving families of mediators in acute inflammation and resolution bioactive metabolome. *Biochim. Biophys. Acta* **1851**, 397–413
 56. Serhan, C. N., Yang, R., Martinod, K., Kasuga, K., Pillai, P. S., Porter, T. F., Oh, S. F., and Spite, M. (2009) Maresins: novel macrophage mediators with potent antiinflammatory and proresolving actions. *J. Exp. Med.* **206**, 15–23
 57. Feltenmark, S., Gautam, N., Brunström, A., Griffiths, W., Backman, L., Edenius, C., Lindbom, L., Björkholm, M., and Claesson, H. E. (2008) Eoxins are proinflammatory arachidonic acid metabolites produced via the 15-lipoxygenase-1 pathway in human eosinophils and mast cells. *Proc. Natl. Acad. Sci. USA* **105**, 680–685
 58. Serhan, C. N., Chiang, N., and Van Dyke, T. E. (2008) Resolving inflammation: dual anti-inflammatory and pro-resolution lipid mediators. *Nat. Rev. Immunol.* **8**, 349–361
 59. Kim, S. N., Akindehin, S., Kwon, H. J., Son, Y. H., Saha, A., Jung, Y. S., Seong, J. K., Lim, K. M., Sung, J. H., Maddipati, K. R., and Lee, Y. H. (2018) Anti-inflammatory role of 15-lipoxygenase contributes to the maintenance of skin integrity in mice. *Sci. Rep.* **8**, 8856
 60. Meng, H., McClendon, C. L., Dai, Z., Li, K., Zhang, X., He, S., Shang, E., Liu, Y., and Lai, L. (2016) Discovery of novel 15-lipoxygenase activators to shift the human arachidonic acid metabolic network toward inflammation resolution. *J. Med. Chem.* **59**, 4202–4209
 61. Leslie, C. C. (2015) Cytosolic phospholipase A₂: physiological function and role in disease. *J. Lipid Res.* **56**, 1386–1402
 62. Shikano, M., Masuzawa, Y., Yazawa, K., Takayama, K., Kudo, I., and Inoue, K. (1994) Complete discrimination of docosahexaenoate from arachidonate by 85 kDa cytosolic phospholipase A₂ during the hydrolysis of diacyl- and alkenylacylglycerophosphoethanolamine. *Biochim. Biophys. Acta* **1212**, 211–216
 63. Miki, Y., Yamamoto, K., Taketomi, Y., Sato, H., Shimo, K., Kobayashi, T., Ishikawa, Y., Ishii, T., Nakanishi, H., Ikeda, K., Taguchi, R., Kabashima, K., Arita, M., Arai, H., Lambeau, G., Bollinger, J. M., Hara, S., Gelb, M. H., and Murakami, M. (2013) Lymphoid tissue phospholipase A₂ group IID resolves contact hypersensitivity by driving antiinflammatory lipid mediators. *J. Exp. Med.* **210**, 1217–1234

Received for publication November 22, 2018.

Accepted for publication January 15, 2019.

Supplementary Materials

Supplemental Data

Targeting biosynthetic networks of the pro-inflammatory and pro-resolving lipid metabolome

Markus Werner, Paul M. Jordan, Erik Romp, Anna Czapka, Zhigang Rao, Christian Kretzer, Andreas Koeberle, Ulrike Garscha, Simona Pace, Hans-Erik Claesson, Charles N. Serhan, Oliver Werz and Jana Gerstmeier

Content: Supplemental Tables 1-4
Supplemental Figure 1-2

Supplemental Table 1. Ultra Performance Liquid Chromatography (UPLC) settings

Acquity™ UPLC system settings

Solvent A	H ₂ O (0.01% acetic acid)	
Solvent B	Methanol (0.01% acetic acid)	
Flow rate	0.3 ml/min	
Column	Acquity UPLC BEH C18 1.7 μM; 2.1 × 100 mm	
Column heater temperature	50 °C	
Gradient	Time (min)	Solvent % B
	0.0	42
	12.5	86
	12.5	98
	15.5	98
	15.5	42
	16	42

Supplemental Table 2. Mass spectrometer settings for multiple reaction monitoring

AB Sciex 5500 QTRAP MS settings for multiple reaction monitoring

Curtain gas	35
Collision gas	Medium
Ion spray voltage	-4000 eV
Temperature	500 °C
Ion source gas 1	40
Ion source gas 2	40

Supplemental Table 3. MRM transitions of lipid mediators used for quantitation and their retention times

diagnostic ion	Q1	Q3	DP	EP	CE	CXP	RT [min]	y = m · x [pg] [m · 10 ⁵ =]	r ²	LOD [pg / 10 µl]
5-LOX										
5-HETE	319.2	115.1	-80	-10	-21	-12	12.1	4.451	0.9994	1.560
5-HEPE	317.2	115.1	-80	-10	-18	-12	11.2	4.877	0.9992	1.560
t-LTB ₄	335.2	195.1	-80	-10	-22	-13	8.7	4.057	0.9992	1.560
LTB ₄	335.2	195.1	-80	-10	-22	-13	9.2	4.202	0.9998	0.780
5S,6R-diHETE	335.2	115.1	-80	-10	-20	-13	10.6	5.246	0.9990	0.390
COX										
PGE ₂	351.3	189.1	-80	-10	-25	-14	6.1	10.10	0.9990	0.195
PGD ₂	351.3	233.1	-80	-10	-16	-15	6.3	5.004	0.9993	0.195
PGF _{2a}	353.3	193.1	-80	-10	-34	-11	6.5	8.900	0.9991	0.390
TXB ₂	369.3	169.1	-80	-10	-22	-15	5.8	2.930	0.9996	0.390
11-HETE	319.2	167.1	-80	-10	-21	-12	11.6	1.713	0.9997	0.390
11-HEPE	317.2	167.1	-80	-10	-19	-12	10.7	3.984	0.9994	1.560
SPM precursor										
14-HDHA	343.2	205.1	-80	-10	-17	-14	11.7	13.32	0.9999	1.560
7-HDHA	343.2	141.1	-80	-10	-18	-15	11.9	8.024	0.9997	1.560
4-HDHA	343.2	101.1	-80	-10	-17	-15	12.4	6.159	0.9998	3.125
15-HETE	319.2	219.1	-80	-10	-19	-12	11.4	11.39	0.9996	1.560
12-HETE	319.2	179.1	-80	-10	-21	-12	11.7	4.846	0.9994	1.560
5,15-diHETE	335.2	201	-50	-10	-30	-13	8.8	12.74	0.9991	3.125
15-HEPE	317.2	219.1	-80	-10	-18	-12	10.7	6.065	0.9992	1.560
12-HEPE	317.2	179.1	-80	-10	-19	-12	10.8	4.897	0.9994	1.560
SPM										
18-HEPE	317.2	259.1	-80	-10	-16	-23	10.5	8.482	0.9993	1.560
RvE3	333.3	201.2	-80	-10	-20	-12	8.9	–	–	–
17-HDHA	343.2	245.1	-80	-10	-17	-14	11.5	23.86	0.9999	6.250
10S,17S-diHDHA	359.2	153.1	-80	-10	-21	-9	8.8	3.670	0.9994	0.195
PD1	359.2	153.1	-80	-10	-21	-9	8.8	3.670	0.9994	0.195
AT-PD1	359.2	153.1	-80	-10	-21	-9	8.8	3.670	0.9994	0.195
MaR1	359.2	250.1	-80	-10	-20	-16	9.1	30.58	0.9997	0.780
RvD2	375.2	175.1	-80	-10	-30	-13	6.4	15.72	0.9989	1.560
RvD4	375.2	101.1	-80	-10	-22	-10	7.8	11.63	0.9993	0.195
RvD5	359.2	199.1	-80	-10	-21	-13	8.9	8.138	0.9996	0.390
LXA ₄	351.2	115.1	-80	-10	-20	-13	6.9	5.702	0.9987	0.195
FA										
AA	303.3	259.1	-100	-10	-16	-18	13.8	71.55	0.9993	62.5
EPA	301.3	257.1	-100	-10	-16	-18	13.6	36.02	0.9996	31.25
DHA	327.3	283.1	-100	-10	-16	-18	13.8	64.02	0.9502	125

DP=Declustering Potential, EP=Entrance Potential, CE=Collision Energy, CXP=Collision Cell Exit Potential, RT=Retention Time, linear equation, coefficient of determination (r²) and limit of detection (LOD). LOD represents the lowest concentration of the standard curves showing a peak with more than five data points and signal to noise ratio higher than three (Means ± SEM, n=3).

Supplemental Table 4. LM biosynthesis in M1 and M2 macrophages upon exposure to pathogenic *E. coli*

	M1			M2		
	veh.	+ <i>E. Coli</i>		veh.	+ <i>E. Coli</i>	
5-HETE	-	1623	± 310	-	1157	± 166
5-HEPE	-	299	± 73	-	175	± 36
t-LTB ₄	-	256	± 65	-	296	± 34
LTB ₄	-	1684	± 358	-	643	± 129
5S,6R-diHETE	-	83	± 16	-	55	± 10
PGE ₂	804 ± 188	13,960	± 1801	31 ± 17	689	± 51
PGD ₂	14 ± 3.1	221	± 37	8.8 ± 4.0	237	± 28
PGF _{2α}	48 ± 13	811	± 94	8.2 ± 1.5	541	± 91
TXB ₂	762 ± 152	8370	± 914	280 ± 77	15,804	± 1345
11-HETE	-	2742	± 323	-	2695	± 267
11-HEPE	-	54	± 5.4	-	94	± 11
14-HDHA	-	61	± 10	-	4031	± 441
7-HDHA	-	98	± 20	-	453	± 42
4-HDHA	-	67	± 7.6	-	115	± 9.4
15-HETE	21 ± 4.3	1273	± 140	29 ± 14	41,468	± 4739
12-HETE	-	129	± 23	-	2965	± 341
5,15-diHETE	-	-	-	-	1712	± 235
15-HEPE	-	54	± 7.8	-	6952	± 1011
12-HEPE	-	27	± 7.5	-	1441	± 296
18-HEPE	-	41	± 4.6	-	140	± 14
RvE3	-	-	-	-	218	± 38
17-HDHA	-	414	± 53	-	25,289	± 2930
10S,17S-diHDHA	-	-	-	-	42	± 5.4
PD1	-	-	-	-	253	± 30
AT-PD1	-	-	-	-	306	± 38
MaR1	-	-	-	-	548	± 106
RvD2	-	-	-	-	177	± 27
RvD4	-	-	-	-	28	± 3.8
RvD5	-	-	-	-	1790	± 276
LXA ₄	-	-	-	-	54	± 15
AA	1650 ± 193	520,540	± 129,749	2341 ± 489	695,267	± 157,048
EPA	397 ± 61	165,472	± 28,706	548 ± 124	292,667	± 34,385
DHA	1604 ± 208	261,669	± 29,475	3256 ± 362	357,654	± 36,136

Human monocyte-derived macrophages were polarized for 48 hrs to M1 and M2 (2×10^6 cells/ml) and incubated for 180 min with vehicle or *E. coli* (O6:K2:H1; ratio = 1:50) at 37 °C. Formed LM were isolated by SPE and analyzed by UPLC-MS/MS, LOD according to Suppl Table 3. Data are given as means ± S.E.M. as pg/ 2×10^6 cells, n=4 for vehicle control in M1/M2 and for *E.coli* challenge in M1: n = 24-34 and in M2: n = 33-39.

Supplemental Figure 1

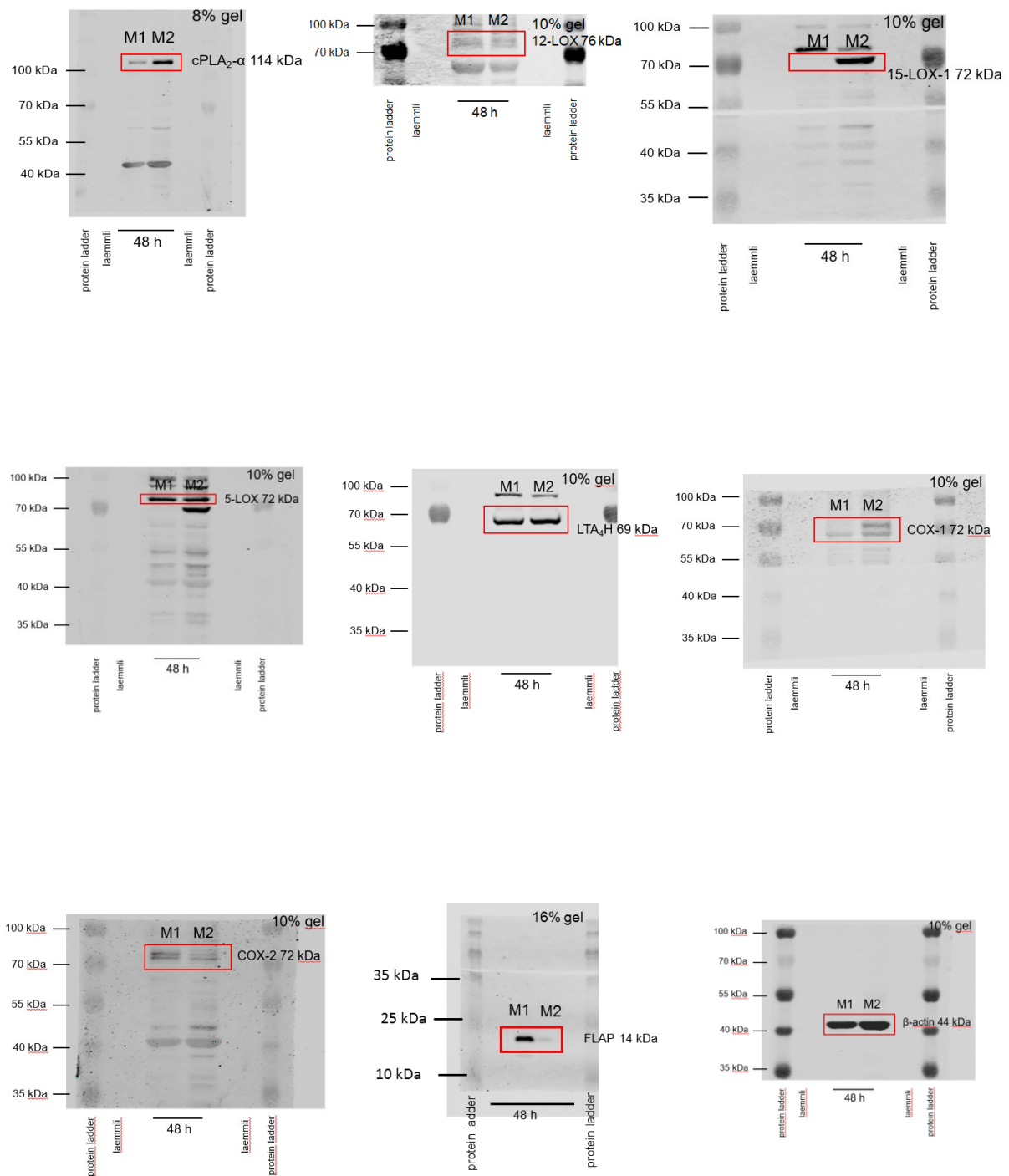


Figure S1. Representative full scan of Western blots shown in Figure 1C. Molecular weight markers are indicated on the left. Red boxes highlight the lanes that are displayed in the corresponding figures.

Supplemental Figure 2

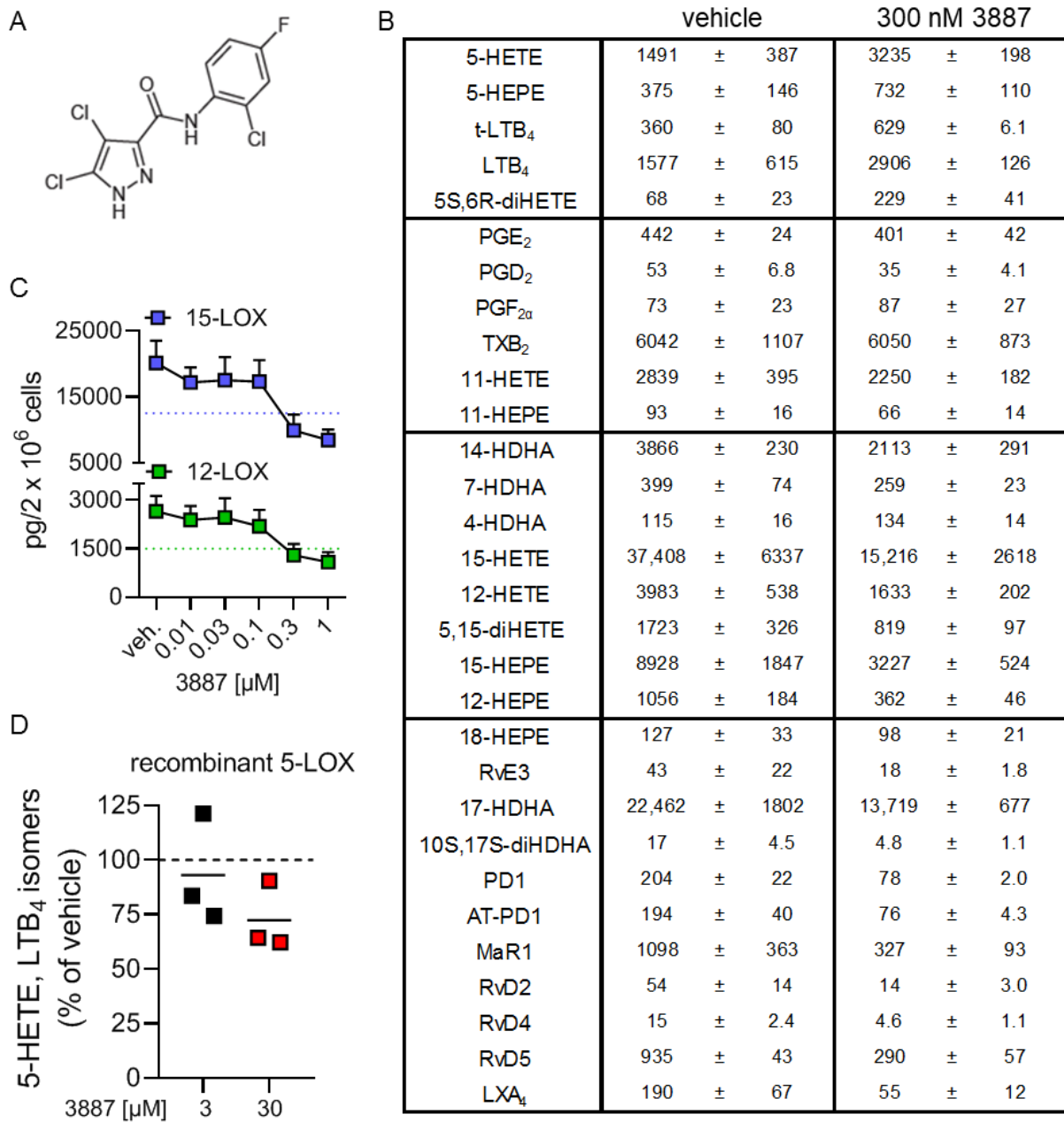


Figure S2. Effect of the 15-LOX-1 inhibitor 3887 on the lipid mediator profil. (A) Chemical structure of 3887. (B) LM profile in M2 macrophages, shown as $\text{pg}/2 \times 10^6$ cells of $n = 3$, corresponding to the heatmap in Figure 4A as mean + S.E.M.. (C) Concentration-dependent inhibition of mono-hydroxylated 15-LOX products (15-HETE, 15-HEPE and 17-HDHA) and 12-LOX products (12-HETE, 12-HEPE and 14-HDHA) in M2 macrophages. Data are given as mean + S.E.M. of $n = 3$ independent experiments, shown as $\text{pg}/2 \times 10^6$ M2. (D) Purified 5-LOX enzyme was preincubated with 3 and 30 μM 3887 before stimulation with 20 μM exogenous AA for 5-LOX product formation, analyzed by HPLC. Data are given as mean + single values of $n = 3$ independent experiments, shown as percentage of vehicle control (= 100%)

Manuscript II

Encapsulation of the dual FLAP/mPEGS-1 inhibitor BRP-187 into acetalated dextran and PLGA nanoparticles improves its cellular bioactivity

Shkodra-Pula, B., Kretzer, C., Jordan, P.M., Klemm, P., Koeberle, A., Pretzel, D., Banoglu, E., Lorkowski, S., Wallert, M., Höppener, S., Stumpf, S., Vollrath, A., Schubert, S., Werz, O., Schubert, U.S.

Journal of Nanobiotechnology, 2020, 18(1):73

Der Kandidat / Die Kandidatin ist

Erstautor/-in, Ko-Erstautor/-in, Korresp. Autor/-in, Koautor/-in.

Anteile (in %) der Autoren / der Autorinnen an den vorgegebenen Kategorien der Publikation

Author	Conception	Data analysis	Experimental	Writing	Provision of Material
Shkodra-Pula, B	20 %	40 %	40 %	20 %	
Kretzer C.	20 %	40 %	40 %	20 %	
Jordan P.M.					
Klemm P.					
Koeberle A.					
Pretzel D.					
Banoglu E.					20 %
Lorkowski S.					
Wallert M.					
Höppener S.					
Stumpf S.					
Vollrath A.				10 %	
Schubert S.	10 %			10 %	
Werz O.	20 %			20 %	30 %
Schubert US.	20 %			20 %	30 %
Others	10 %	20 %	20 %		20 %
Summe:	100 %	100 %	100 %	100 %	100 %

Unterschrift Kandidat/-in

Unterschrift Betreuer/-in (Mitglied der Fakultät)

RESEARCH

Open Access



Encapsulation of the dual FLAP/mPGES-1 inhibitor BRP-187 into acetalated dextran and PLGA nanoparticles improves its cellular bioactivity

Blerina Shkodra-Pula^{1†}, Christian Kretzer^{3†}, Paul M. Jordan³, Paul Klemm¹, Andreas Koeberle^{3,7}, David Pretzel¹, Erden Banoglu⁴, Stefan Lorkowski^{2,5}, Maria Wallert⁵, Stephanie Höppener^{1,2}, Steffi Stumpf¹, Antje Vollrath¹, Stephanie Schubert^{2,6}, Oliver Werz^{2,3*} and Ulrich S. Schubert^{1,2*} 

Abstract

Background: Dual inhibitors of the 5-lipoxygenase-activating protein (FLAP) and the microsomal prostaglandin E₂ synthase-1 (mPGES-1) may exert better anti-inflammatory efficacy and lower risks of adverse effects versus non-steroidal anti-inflammatory drugs. Despite these advantages, many dual FLAP/mPGES-1 inhibitors are acidic lipophilic molecules with low solubility and strong tendency for plasma protein binding that limit their bioavailability and bioactivity. Here, we present the encapsulation of the dual FLAP/mPGES-1 inhibitor BRP-187 into the biocompatible polymers acetalated dextran (Acdex) and poly(lactic-co-glycolic acid) (PLGA) via nanoprecipitation.

Results: The nanoparticles containing BRP-187 were prepared by the nanoprecipitation method and analyzed by dynamic light scattering regarding their hydrodynamic diameter, by scanning electron microscopy for morphology properties, and by UV–VIS spectroscopy for determination of the encapsulation efficiency of the drug. Moreover, we designed fluorescent BRP-187 particles, which showed high cellular uptake by leukocytes, as analyzed by flow cytometry. Finally, BRP-187 nanoparticles were tested in human polymorphonuclear leukocytes and macrophages to determine drug uptake, cytotoxicity, and efficiency to inhibit FLAP and mPGES-1.

Conclusion: Our results demonstrate that encapsulation of BRP-187 into Acdex and PLGA is feasible, and both PLGA- and Acdex-based particles loaded with BRP-187 are more efficient in suppressing 5-lipoxygenase product formation and prostaglandin E₂ biosynthesis in intact cells as compared to the free compound, particularly after prolonged preincubation periods.

Keywords: Acetalated dextran, PLGA, Nanoparticles, Leukotriene biosynthesis, FLAP inhibitor, MPGES-1, Dual inhibitor, BRP-187

Background

Inflammation is a physiological reaction of the body to fight harmful invaders and to restore damaged tissue. However, if inflammation persists and the body cannot return to homeostasis, chronic inflammatory diseases such as arthritis, Alzheimer's disease or arteriosclerosis can evolve [1]. Inflammation is initialized and maintained

*Correspondence: oliver.werz@uni-jena.de; ulrich.schubert@uni-jena.de

[†]Blerina Shkodra-Pula and Christian Kretzer contributed equally to the study

¹Laboratory of Organic and Macromolecular Chemistry (IOMC), Friedrich Schiller University Jena, Humboldtstraße 10, 07743 Jena, Germany

²Jena Center for Soft Matter (JCSM), Friedrich Schiller University Jena, Philosophenweg 7, 07743 Jena, Germany

Full list of author information is available at the end of the article



© The Author(s) 2020. This article is licensed under a Creative Commons Attribution 4.0 International License, which permits use, sharing, adaptation, distribution and reproduction in any medium or format, as long as you give appropriate credit to the original author(s) and the source, provide a link to the Creative Commons licence, and indicate if changes were made. The images or other third party material in this article are included in the article's Creative Commons licence, unless indicated otherwise in a credit line to the material. If material is not included in the article's Creative Commons licence and your intended use is not permitted by statutory regulation or exceeds the permitted use, you will need to obtain permission directly from the copyright holder. To view a copy of this licence, visit <http://creativecommons.org/licenses/by/4.0/>. The Creative Commons Public Domain Dedication waiver (<http://creativecommons.org/publicdomain/zero/1.0/>) applies to the data made available in this article, unless otherwise stated in a credit line to the data.

by prostaglandins (PG) and leukotrienes (LT) that are biosynthesized from arachidonic acid (AA) [2]. For PG formation, AA is first converted by cyclooxygenase-1 and -2 (COX-1/2) to the intermediate prostaglandin H_2 (PGH₂), which is subsequently metabolized by specific PG synthases into different bioactive prostanoids. Among them, prostaglandin E₂ (PGE₂) is massively produced by microsomal prostaglandin E₂ synthase-1 (mPGES-1) and is most relevant for inflammation, while other prostanoids (e.g. prostaglandin I₂, thromboxane A₂) are of importance for homeostatic processes, e.g., regulation of blood pressure and platelet aggregation [3]. Current anti-inflammatory therapies include non-steroidal anti-inflammatory drugs (NSAIDs) that prevent inflammation by blocking PG biosynthesis via inhibition of COX-1/2. However, inhibition of COX enzymes is associated with side effects since the formation of all prostanoids is blocked and AA is preferably metabolized to pro-inflammatory LT [4]. The formation of LT from AA is initialized by 5-lipoxygenase (5-LO) together with 5-LO-activating protein (FLAP), with the latter facilitating access of 5-LO to AA [5]; both proteins are pursued as molecular targets in the development of anti-inflammatory drugs [6].

BRP-187 (4-(4-chlorophenyl)-5-[4-(quinoline-2-yl-methoxy)phenyl] isoxazol-3-carboxylic acid) is a dual inhibitor of mPGES-1 and FLAP suppressing the formation of pro-inflammatory PGE₂ and LTs [7]. This pharmacological approach is proposed to be more efficacious and associated with fewer adverse effects than inhibition of the COX pathway [8]. However, BRP-187 is an acidic lipophilic molecule with low water solubility and a strong tendency for plasma protein binding, implying the need for new technological approaches to overcome these disadvantages. Encapsulation of small molecule drugs that exhibit a low solubility into biodegradable polymers (polyesters or polyketals) can improve their bioavailability [9, 10]. Here, we attempted to encapsulate BRP-187 into polymer-based nanoparticles (NPs) using poly(lactic-co-glycolic acid) (PLGA) and acetalated dextran (Acdex). These polymers were selected because they are biocompatible materials able to successfully encapsulate hydrophobic drugs, and as such, they could facilitate an increase in the retention time of the drug in the plasma [11]. As a polyester, PLGA is enzymatically hydrolyzed into physiological metabolites—lactate and glycolate [12], hence, it is used and widely investigated as a biomaterial for drug delivery [13–15]. The properties of PLGA are influenced by the ratio of lactic to glycolic acid units, with a 50:50 composition showing the fastest degradation [16]. An alternative to PLGA is Acdex, a recently developed dextran derivative offering favorable properties as carrier for drugs with low solubility [17]. Acdex is composed of acyclic and cyclic acetal groups, with the acyclic acetals

degrading faster than the cyclic acetal groups [17]. As a consequence, the degradation behavior of Acdex can be fine-tuned by varying the degree of substitution of the cyclic vs. acyclic acetal groups on the dextran backbone [18]. Most importantly, under slightly acidic conditions (e.g. pH 5.5), the acetal groups are cleaved, resulting in biocompatible, water-soluble dextran while instantly releasing the cargo [19]. In brief, the main advantage of Acdex lies in its facile synthesis (i), in the possibility to design formulations with a desired release profile by varying the cyclic vs. acyclic acetal groups in the dextran backbone (ii), and in its sensitivity to low pH levels—typical conditions of inflamed tissues and endosomal compartments [20]. In this view, both polymer formulations are intended for parenteral administration, with Acdex being suitable as an instant-release formulation, whereas PLGA might be suitable for extended-release formulations. In addition, based on the longer degradation time of the PLGA NPs in tissue (>40 days), depot formulations for local administration routes (e.g. intra-muscular or intra-articular for rheumatoid arthritis) could also be considered.

In this study, formulations of BRP-187-containing NPs of 130 to 230 nm using Acdex and PLGA as biodegradable encapsulating materials were prepared. The properties of these NPs were analyzed including the degradation behavior, and the FLAP/mPGES-1-inhibitory efficiency of BRP-187-containing NPs was evaluated in comparison to the free compound in different human primary leukocytes.

Results and discussion

The formulation parameters were designed to produce stable monodisperse particles of 100 to 200 nm and with high drug loading. The excipients used in the formulation were selected after careful consideration based on previous data from our lab, literature, and most importantly based on the technical requirements of the International Council for Harmonization (ICH) guidelines for pharmaceuticals for human use. Acetone was used as organic phase for the following reasons: It is a good solvent for both polymers (i); it is miscible with water, which is a pre-requisite for solvents used in nanoprecipitation (ii) [21]; it can be easily removed from the formulation by evaporation at room temperature (iii); and according to the ICH, acetone is a Class 3 solvent with a low toxicity [22]. Next, for the solubilization of the drug, due to the high lipophilicity of BRP-187, the choice of the solvent was limited only to dimethylsulfoxide (DMSO) and dimethylformamide (DMF). Thus, considering that DMF is more toxic than DMSO (residual concentration limit 880 ppm vs. 5000 ppm, respectively), the latter was selected for the formulation [22]. Meanwhile, the residual

amount of DMSO in our NP formulations was <250 ppm. Furthermore, the volumetric ratio of organic-to-aqueous phase was kept at 1:8 to produce particles <200 nm with an encapsulation efficiency $EE > 50\%$, higher volumetric ratios produce NPs >200 nm [23]. Partially-hydrolyzed poly(vinyl alcohol) (PVA) was used as surfactant and cryoprotectant to prevent aggregation during purification and lyophilization, respectively. We have previously demonstrated that PVA provided a superior stability of PLGA NPs than poloxamers and polysorbates at concentrations <0.5%, and no toxicity was evident even at 100-fold higher concentrations [10].

Characterization of NPs

Initial experiments revealed that NPs prepared by the nanoprecipitation method had a higher EE than NPs prepared by the emulsion-evaporation method. In addition, the nanoprecipitation method is favored because it is a low-energy method with an easy operation that can be easily adapted to large-scale production batches [24]. The size and polydispersity (PDI) of BRP-187-loaded NPs as well as unloaded control NPs were analyzed after purification and after lyophilization, and the zeta potential (ζ) was measured after lyophilization (Table 1). The average hydrodynamic diameter (d_H) of the final NPs was between 130 to 211 nm with PDI values of 0.09 to 0.28. PLGA NPs were in average up to 50 nm smaller than Acdex NPs.

Scanning electron microscopy (SEM) imaging showed a spherical morphology of the NPs and smaller NP sizes compared to the results acquired by DLS, a common phenomenon when using orthogonal characterization techniques (Fig. 1) [25]. The size of the NPs measured by SEM was as follows: Acdex 95 ± 11 nm, Acdex[BRP-187] 73 ± 8 nm, PLGA 96 ± 11 nm, and PLGA[BRP-187] 84 ± 6 nm. Furthermore, EE of all NPs is given in Table 1 and was roughly 60% for Acdex

particles and 80% for PLGA particles. Based on previous experiments, a drug-to-polymer content >3% (w/w) fed in the formulation resulted in problems with the stability of the suspension (data not shown), a phenomenon that was also reported by others [26–28]. Meanwhile, the conditions used in this protocol (3%, w/w) were effective to encapsulate more than 60% of the drug without compromising the stability of the NPs. In addition, BRP-187 is a highly potent drug ($IC_{50(FLAP)} = 8$ nM and $IC_{50(mPGES-1)} = 200$ nM) [7], and a loading capacity of 1.7 to 2.5% corresponded to 37 to 55 μ M of BRP-187 in 1 mg mL⁻¹ NP suspension. Here, it was observed that Acdex formed larger particles but encapsulated less drug compared to PLGA, which is probably due to different drug-polymer interactions [26].

Degradation profile of the nanoparticles

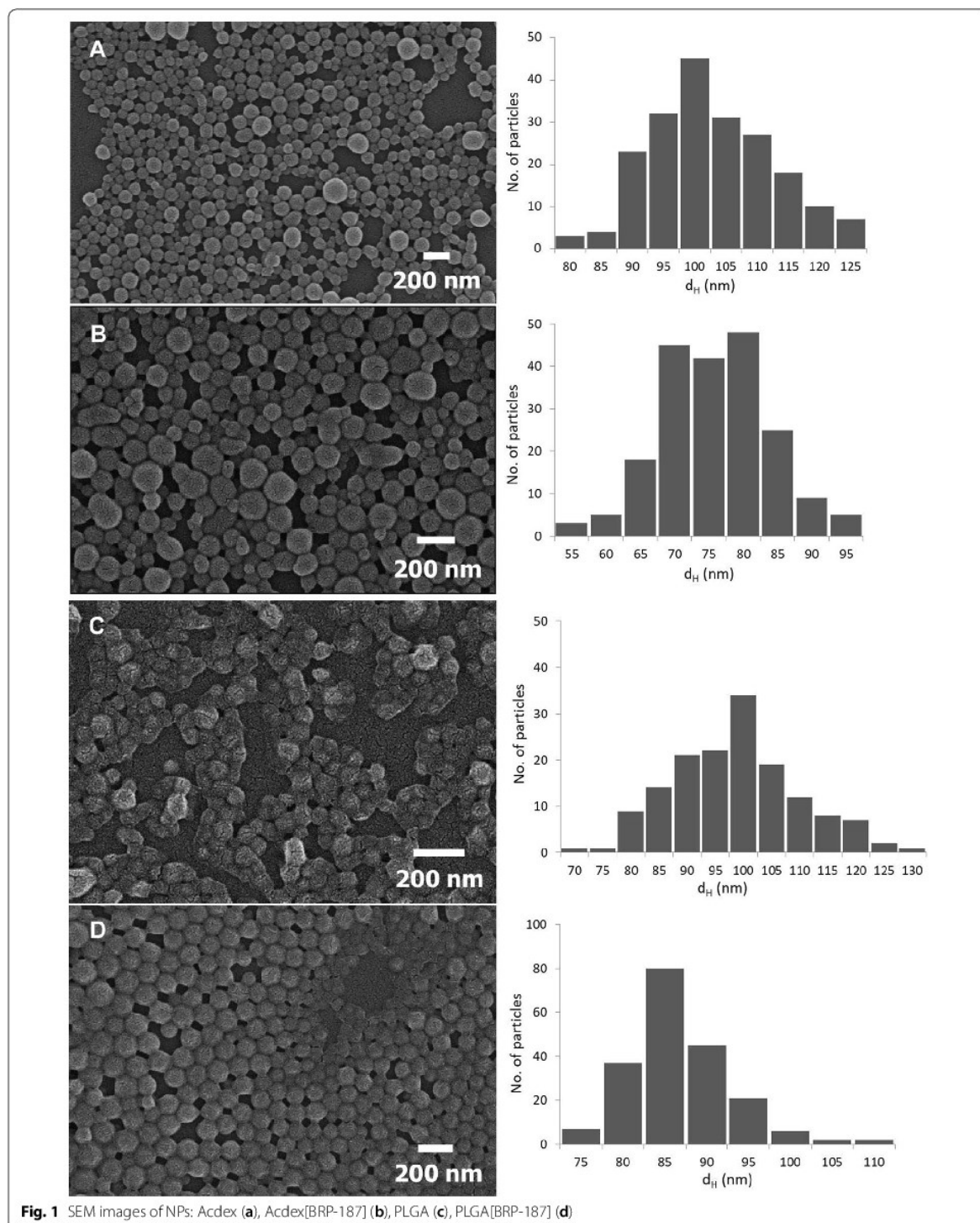
In DLS, the count rate corresponds to the number of the light photons detected in kilo-count per seconds (kcps), which is a good indicator of the quality of the measured sample [29]. A decreasing count rate indicates that less photons are detected (i.e. less light is scattered) [29] and, thus, less particles are present in a sample. In such a measurement, the NPs should show stable size and PDI values (100% intact NPs) at time point 0 of NPs incubated with buffer (Fig. 2a, c). As the NPs start to degrade, they steadily increase in size and polydispersity, which is a result of the degraded products dissolved in water (Fig. 2b, d). However, there is a chance that the aggregation of the NPs during the measurement might potentially take place based on the fact that the degradation products (dextran, acetone and methanol) might influence the conditions within the cuvette. This, in turn, might disturb the still intact NPs leading to a transient aggregation before they are completely degraded and solubilized in water. Aggregation that is only caused by

Table 1 Overview of the NP properties

NP formulation	After purification		After lyophilization			EE (%)	LC (%)	PVA (%)
	d_H (nm)	PDI	d_H (nm)	PDI	ζ (mV)			
Acdex	210 ± 26	0.17 ± 0.07	211 ± 35	0.26 ± 0.09	-12 ± 2	-	-	0.01 ± 0.000
Acdex[BRP-187]	196 ± 51	0.16 ± 0.11	178 ± 26	0.13 ± 0.07	-13 ± 8	59 ± 23	1.7 ± 0.6	0.01 ± 0.000
Acdex-Rhodb[BRP-187]	163 ± 15	0.20 ± 0.06	189 ± 37	0.28 ± 0.11	-24 ± 2	67 ± 10	2.0 ± 0.3	n.m.
PLGA	124 ± 6	0.06 ± 0.03	130 ± 2	0.09 ± 0.03	-20 ± 2	-	-	0.02 ± 0.002
PLGA[BRP-187]	153 ± 41	0.17 ± 0.14	158 ± 35	0.12 ± 0.06	-15 ± 3	76 ± 22	2.2 ± 0.6	0.03 ± 0.002
PLGA-DY635	143 ± 3	0.08 ± 0.03	154 ± 5	0.15 ± 0.02	-20 ± 1	-	-	0.02 ± 0.006
PLGA-DY635[BRP-187]	153 ± 2	0.12 ± 0.01	168 ± 9	0.19 ± 0.05	-19 ± 1	87 ± 6	2.5 ± 0.2	0.02 ± 0.002

Concentration of NPs used for the PVA assay was 3 mg mL⁻¹. SD for all measurements $n \geq 3$. n.m.—not measured

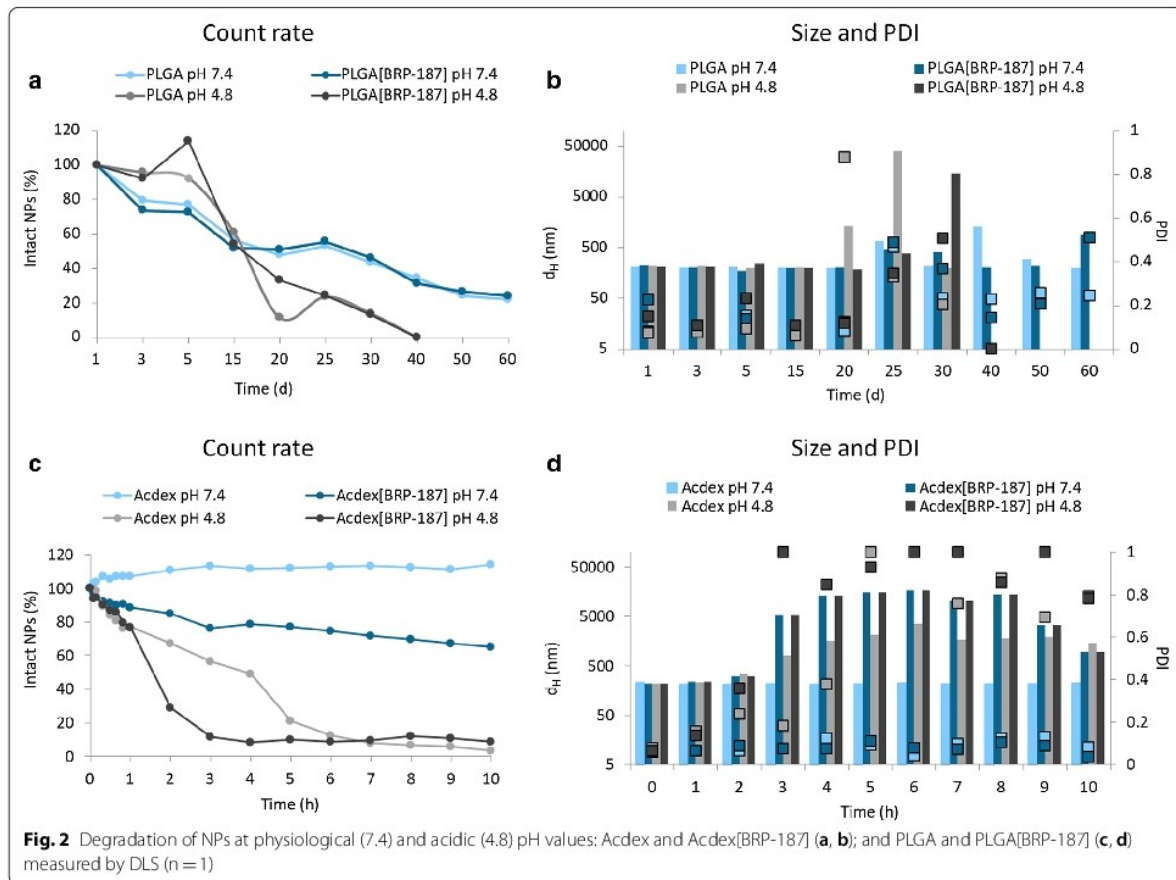
d_H , Hydrodynamic diameter obtained by DLS measurements. EE encapsulation efficiency. LC loading capacity



ionic strength of the buffer solution can be neglected since experiments with the same buffer concentration but higher pH values do not show aggregation (Fig. 2d). Consequently, the count rate decreases over time as the degradation of the NPs proceeds.

The release of a molecule from a NP polymer matrix depends on several factors, i.e. the structure-property relationship between the drug and the polymer, hydrophobicity of the drug and the polymer, as well as the degradation rate, melting point and crystallinity of the polymer [30]. The degradation rate of the polymeric NPs in a cell-free environment was studied since it directly influences the release kinetics of the drug from the NP core. According to the literature, Acdex is an acid-labile polymer with a considerably higher pH sensitivity compared to the PLGA polymer [17, 31]. Our results revealed that after 10 h of incubation Acdex NPs exhibit good stability at pH 7.4 showing only swelling of the NPs, whereas at the same pH value the Acdex[BRP-187] NPs degraded to a degree of about 25%. Furthermore, at pH 4.8 after 2 h, the Acdex NPs degraded by only about 30%, whereas the Acdex[BRP-187]

NPs degraded by 75% (Fig. 2c). This degradation behavior is suitable since NPs maintain 75% stability at physiological conditions. However, once internalized by the cells, the acidic environment of the endolysosome would trigger the degradation of Acdex, thereby releasing the drug. In case of PLGA, a complete degradation of NPs was observed at pH 4.8 within 40 days, whereas at pH 7.4, an 80% degradation was observed after 60 days (Fig. 2a), which is in line with previous studies [32–34]. Considering the degradation profile of the polymers in an acidic medium, the release of BRP-187 from Acdex NPs is expected to be fast due to the rapid degradation of the polymer, whereas the drug release from PLGA NPs is expected to be slower due to the diffusion of drug from the polymer matrix, since degradation of this polymer is very slow [35]. The degradation studies of the NPs at different pH values were investigated to obtain a first impression on the release of the drug from the NPs. However, it should be noted that such degradation profiles differ from the more complex environment of the endolysosomes [36].



Residual amount of PVA

Previously, we described effects of surfactants on the stability of drug-loaded NPs, where we demonstrated that concentrations of $\leq 1\%$ (w/v) PVA are desirable to formulate stable particles [10]. Here, we formulated NPs using 0.3% (w/v) PVA to obtain both suspension- and cryo-stability. The amount of residual PVA in the final NPs is listed in Table 1. The enzymatic- and pH-dependent degradation of the NPs relies not only on the properties of the polymer itself but is also strongly influenced by the digestibility of the surfactant. PVA coating can protect from enzymatic hydrolysis of the NPs by decreasing the wettability of the NPs [37], thus influencing the rate of degradation and drug release.

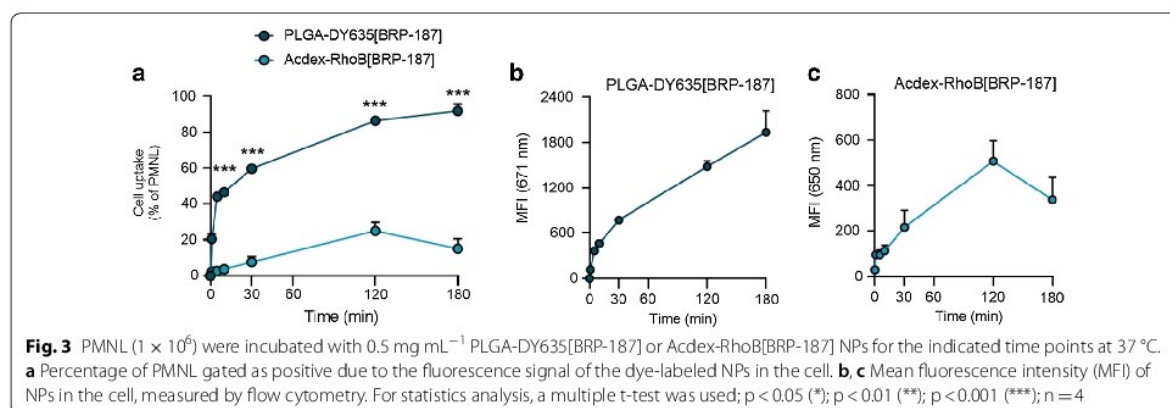
Fluorescence dye-labeled nanoparticle uptake in PMNL

PMNL (polymorphonuclear leukocytes) are pro-inflammatory innate immune cells that are abundant in the blood and produce substantial amounts of LTs and also PGE₂ as targets for BRP-187 [7, 38]. Therefore, we used human PMNL as relevant cells to study the uptake of BRP-187-loaded NPs that were covalently labeled with fluorescent dyes (i.e., PLGA-DY635, Acdex-RhodB) for visualization in the cells. The dye-labeled NPs (loaded with BRP-187) were efficiently taken up by PMNL, which depends however on the nature of the polymer, being superior for PLGA over Acdex (Fig. 3). Within 10 min, 40% of the PMNL digested PLGA-DY635[BRP-187] NPs. After 180 min, approx. 85% of the PMNL took up these NPs along with a concomitant increase of the mean fluorescence intensity (MFI) per PMNL up to 1937 ± 283 . Thus, PLGA NPs display an excellent cellular uptake. In contrast, Acdex-RhoB[BRP-187] NPs were taken up by only 23% of the PMNL after 120 min, with an even slightly lower uptake after 180 min, correlating with the MFI per cell over the entire time course (Fig. 3). According to the

degradation profile of Acdex NPs (Fig. 2), the lower abundance might be a consequence of the concomitant degradation and elimination of the polymer inside the cell. After 2 h, approx. 70% of Acdex[BRP-187] NPs are degraded at the endolysosomal pH of 4.8. Therefore, the fluorescence signal may not increase further, even though NPs are still taken up, because the elimination of the labeled monomers from the cell is ongoing. However, both PLGA- and Acdex-based NPs are rapidly taken up by PMNL, even though PLGA NPs are ingested by a higher fraction of cells as compared to Acdex NPs, which might be also a consequence of the degradation. Additionally, we used confocal laser scanning microscopy to confirm the cellular internalization of NPs into PMNL (Fig. 4). PLGA-DY635[BRP-187] NPs show a time-dependent accumulation within the cells which appears as an increase of the intracellular fluorescence signal over time that is most prominent after 3 h. For Acdex-RhoB[BRP-187] NPs a comparable signal was already observed after 30 min. Remarkably, the NP-uptake after 30 min, as measured by the corresponding fluorescence intensity signal, does not further increase upon longer incubation up to 3 h.

Encapsulation of BRP-187 into PLGA or Acdex NPs is not detrimental for target cells

Next, we evaluated whether or not the NPs may cause detrimental effects upon long-term incubation (≥ 24 h) towards relevant target cells. Since PMNL are short-lived cells upon isolation being not suitable for long-term cytotoxicity tests, human monocyte-derived macrophages were used since they also possess the capability to produce PGE₂ and LT [39]. None of the NP formulations (nor free BRP-187) showed detrimental effects on the viability of macrophages (with M1 or M2 phenotype) in terms of damage of the cell membrane over 24 h as measured by the lactate dehydrogenase (LDH) assay (Fig. 5). In



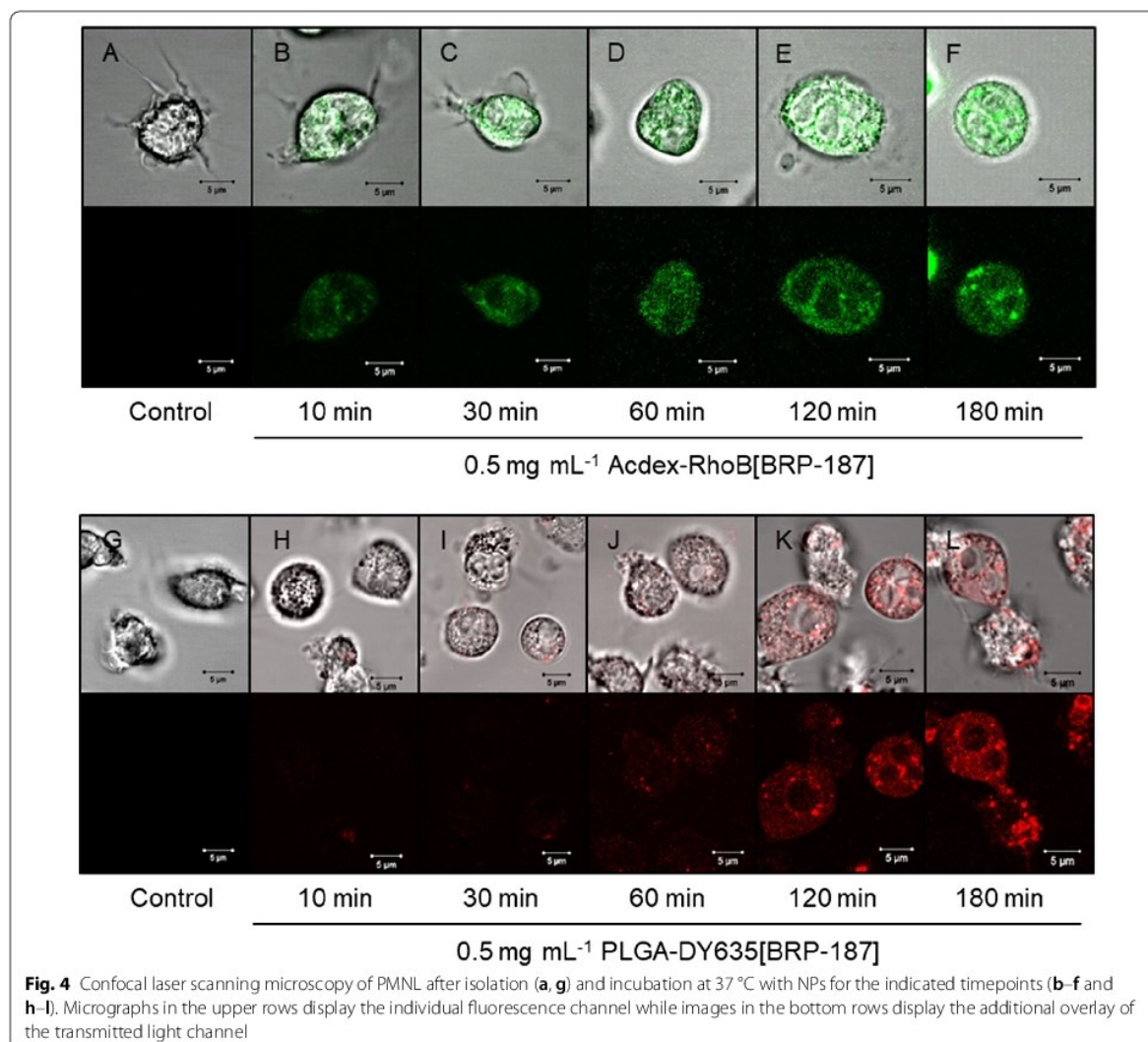


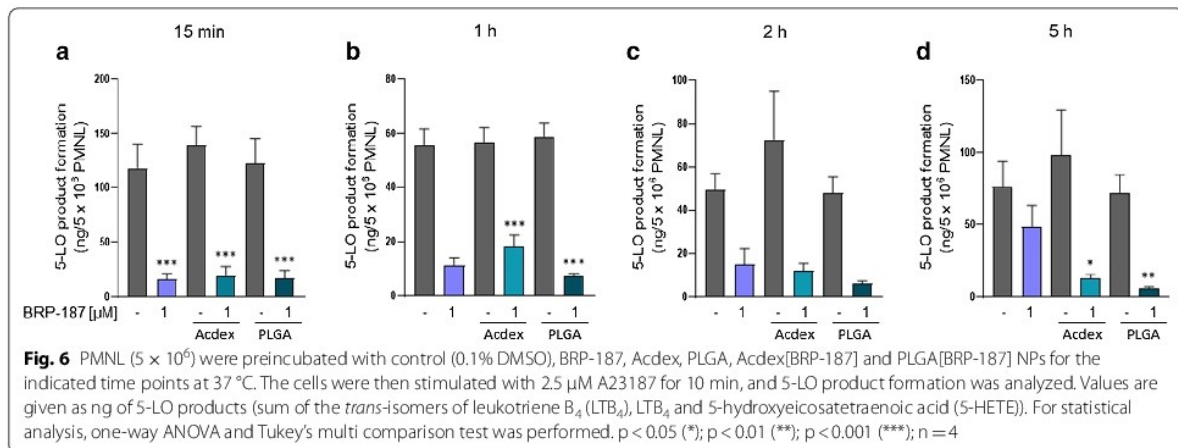
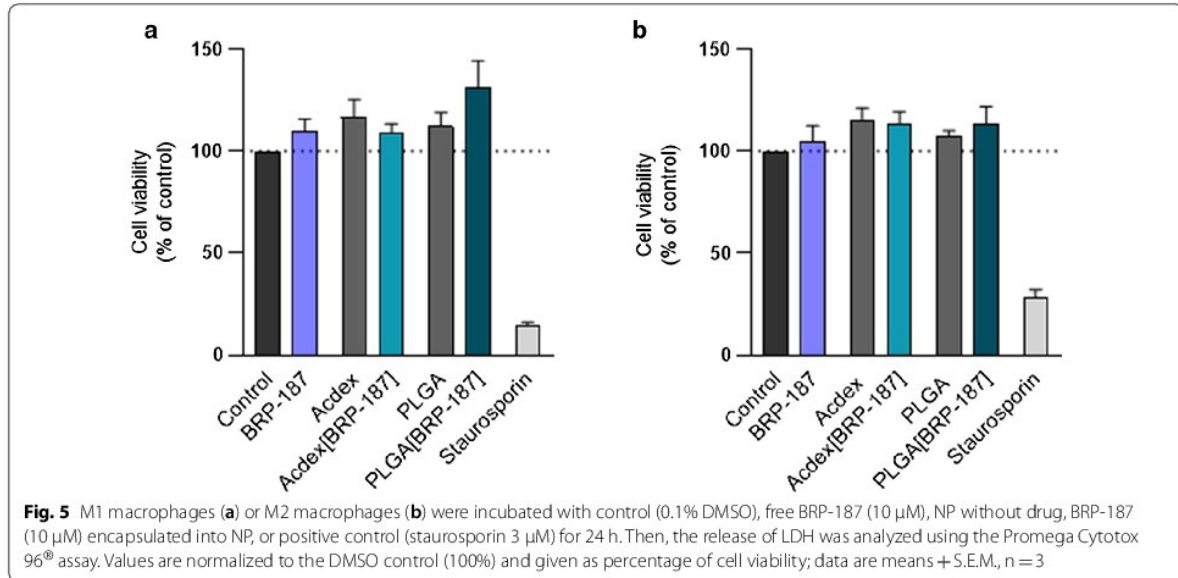
Fig. 4 Confocal laser scanning microscopy of PMNL after isolation (a, g) and incubation at 37 °C with NPs for the indicated timepoints (b–f and h–l). Micrographs in the upper rows display the individual fluorescence channel while images in the bottom rows display the additional overlay of the transmitted light channel

supportive experiments using a RAW264.7 macrophage cell line that was incubated for 72 h with the NPs, an MTT assay revealed also no significant cytotoxic effects (data not shown). Thus, the NPs exert no detrimental effects against relevant target cells at concentrations used in functional assays.

Effect of encapsulated BRP-187 on 5-LO product formation in PMNL

BRP-187 (1 μM) efficiently suppressed 5-LO product formation in isolated PMNL upon short preincubation periods ≤ 2 h (Fig. 6a–c), which is in agreement with our previous data [7]. However, after prolonged preincubation (5 h) with PMNL, the efficiency of BRP-187 (1 μM)

was clearly reduced and suppression of 5-LO product formation was only $37 \pm 5\%$ of the control (Fig. 6d). Of interest, BRP-187 encapsulated into PLGA or Acdex NPs (corresponding to 1 μM BRP-187 as well) potently and consistently inhibited 5-LO product formation in PMNL by 80 to 92%, even after a preincubation period of 5 h. Note that NPs devoid of BRP-187 did not suppress 5-LO activity in PMNL. Therefore, we conclude that encapsulation of BRP-187 into PLGA or Acdex NPs generally accomplishes efficient inhibition of 5-LO product formation in PMNL, and, moreover, allows to overcome the loss of potency of BRP-187 upon prolonged exposure (i.e. 5 h) of PMNL.

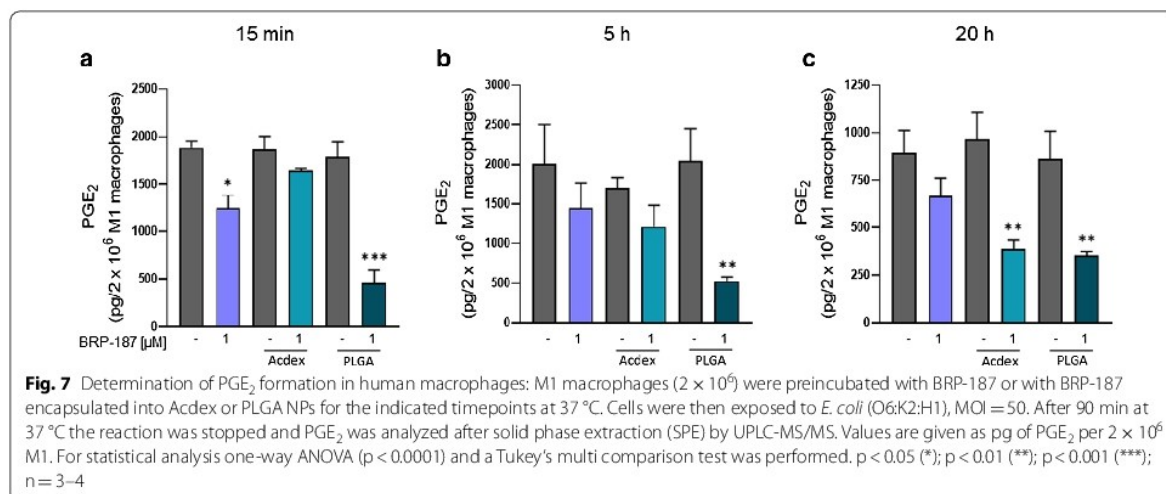


Effect of encapsulated BRP-187 on PGE₂ formation in human M1 macrophages

Human M1 macrophages express high levels of mPGES-1 [40] and, upon exposure to pathogenic *E. coli*, produce high amounts of pro-inflammatory PGE₂ [39]. Thus, *E. coli*-stimulated M1 macrophages are a suitable cell model to study the efficiency of mPGES-1 inhibitors. Note that many mPGES-1 inhibitors are highly potent in cell-free assays but markedly loose efficiency in cellular assays or in vivo [41], which necessitates technological approaches to overcome these hurdles. BRP-187 potently inhibited mPGES-1 in a cell-free assay (IC₅₀ = 0.2 μ M) [7], however, pretreatment of human M1 with 1 μ M BRP-187 caused only moderate inhibition (30–37%) of

E. coli-induced PGE₂ formation regardless of the preincubation period (15 min, 5 or 20 h). In our study, encapsulation of BRP-187 into PLGA NPs strongly suppressed PGE₂ levels at short (15 min) and prolonged (20 h) preincubation periods (Fig. 7). Also, Acdex[BRP-187] NPs caused strong reduction of PGE₂ formation when M1 were preincubated for 20 h, while 15 min pretreatment was not effective. These data are in line with the cellular uptake pattern of the NPs, where PLGA NPs surpassed the uptake efficiency of Acdex NPs. Note that again, as for 5-LO product formation in PMNL, the empty NPs did not suppress PGE₂ biosynthesis.

In summary, encapsulation of BRP-187 in PLGA and Acdex NPs overcomes the loss of effectiveness against



mPGES-1 in intact cells versus cell-free assay conditions and confers the drug marked potency, highlighting this technological approach for efficient interference with pro-inflammatory PGE₂ and LT formation in human cells. The beneficial effect of encapsulation of BRP-187 especially after prolonged incubations up to 20 h might be related to better stability and delayed release inside the cell. Intriguingly, encapsulation of BRP-187, particularly in PLGA-based NPs, accomplished efficient mPGES-1 inhibition in intact M1 macrophages, which was not the case for the free drug. It is conceivable that PLGA is cleaved in close proximity to the endoplasmic reticulum where mPGES-1 is located, thus, enabling unhindered access of BRP-187 to its target protein without being bound to other cellular membranes or cell compartments.

Conclusion

Encapsulation of BRP-187 into polymer-based NPs improves the potency and duration of bioactivity of the drug in relevant human primary leukocytes compared to the free drug. PLGA and Acdex were chosen as biocompatible matrix polymers. Both polymers enabled stable formulations of BRP-187-loaded NPs with a mono-disperse size distribution in the range of 200 nm and high EE according to a highly reproducible encapsulation method. It was shown that PLGA and Acdex NPs remained stable at physiological blood pH, whereas at pH 4.8, Acdex particles degraded very fast after 1 h, which indicates that they are biodegradable in the cellular endolysosome after they have been taken up via phagocytosis by PMNL or macrophages. According to the cellular uptake data, both kind of NPs are internalized by

PMNL and started to degrade, leading to the release of BRP-187 inside the cell, though the uptake of PLGA NPs is faster and more efficient than Acdex NPs. Most importantly, both PLGA- and Acdex-based NPs loaded with BRP-187 are more efficient in suppressing 5-LO product formation and PGE₂ biosynthesis in intact cells as compared to the free compound, particularly after prolonged preincubation periods. When isolated leukocytes were preincubated with BRP-187 for typical short-term periods, the compound was highly bioactive against FLAP [7], but prolonged exposure for more than 2 h markedly decreased the potency of BRP-187. Notably, encapsulation of BRP-187 in Acdex and PLGA particles accomplishes efficient mPGES-1 inhibition in M1 macrophages, which is a major step forward in the development of mPGES-1 inhibitors in general, since many mPGES-1 inhibitors fail in intact cells.

In view of the potential use of BRP-187 as drug for therapeutic treatment of chronic inflammatory diseases, the prolongation of its bioactivity is of utmost importance. An efficient encapsulation and release of BRP-187 is a promising approach to reach this aim. As a perspective, other biodegradable polymers for encapsulation of BRP-187 might be evaluated, and in addition to the properties reported here, further aspects of the nanoformulations (e.g. hydrophobicity, crystallinity and protein corona) might be assessed in more detail. It will also be challenging to study the effects of encapsulated BRP-187 in animal models of inflammation related to PGE₂ and LTs in the future. In such physiological environment, the various aspects of bioavailability including distribution in other tissues and influence of plasma proteins may be assessed.

Methods

Materials

Poly(*D,L*-lactic-*co*-glycolic) acid (Resomer RG 502 H, copolymer composition of 50:50, 7–17 kDa, acid terminated) was purchased from Evonik Industries (Germany). Partially hydrolyzed PVA (Mowiol 4–88), acetone (>99%) and dimethyl sulfoxide (DMSO >99%, spectroscopic grade) were all purchased from Sigma-Aldrich (Germany). The dye DY635 was purchased from Dyomics (Jena, Germany). The covalent coupling of PLGA polymer with the dye DY635 amine was performed according to a standard procedure with 1-ethyl-3-(3-dimethylaminopropyl)carbodiimide (EDC) and *N*-hydroxysuccinimide (NHS) and was provided by SmartDyeLivery (Jena, Germany). The acetalation of dextran was done according to an adapted procedure (Mw of parent dextran 60 kDa), degree of substitution (DS) 2.97 ($DS_{\text{cyclic acetal}} = 1.98$, $DS_{\text{acyclic acetal}} = 0.99$) [19]. BRP-187 was synthesized according to an established protocol [42]. Deuterated and non-deuterated lipid mediator standards for UPLC-MS–MS quantification were purchased from Cayman Chemical/Biomol (Germany). For further materials, see specific experimental section.

Acdex-rhodamine B synthesis

Rhodamine B was coupled to Acdex (Mw 9 to 11 kDa, Sigma Aldrich) according to an adapted procedure [43]: 1 g Acdex (6.17 mmol anhydroglucose unit, $DS_{\text{cyclic acetal}} = 0.56$, $DS_{\text{acyclic acetal}} = 2.14$) and 13 mg rhodamine B isothiocyanate were dissolved in 15 mL anhydrous pyridine and heated to 80 °C for 72 h under argon. The reaction mixture was precipitated in 150 mL distilled water, and centrifuged; the pellet was lyophilized. The resulting pink-colored powder was purified via gel permeation chromatography using BioBeads S-X1 in tetrahydrofuran (THF) to remove the free dye (yield 57%). Size-exclusion chromatography was performed in dimethylacetamide (DMAc) and 0.21% lithium chloride with a UV–VIS detector measuring at $\lambda = 562$ nm to prove the conjugation of the dye to the polymer.

Nanoparticle formulation

Particles were prepared by nanoprecipitation using a syringe pump (Aladdin AL1000-220, World Precision Instruments, Berlin, Germany) with a flow rate of 2 mL min⁻¹. First, 25 mg polymer (Acdex or PLGA) were dissolved in 5 mL acetone. For the drug solution, a 10 mg mL⁻¹ stock of BRP-187 in DMSO was prepared and sonicated in an ultrasound bath for 15 min at room temperature. Subsequently, 75 μ L of the drug solution were mixed with the polymer solution. For the aqueous phase, 40 mL of 0.3% (w/v) PVA solution were prepared. Further, the polymer (or polymer-drug) solution was injected into

the aqueous solution, while stirring at 800 rpm at room temperature. After nanoprecipitation, the samples were stirred for 24 h in a fume hood to evaporate the acetone. The particles were washed once, using a Rotina 380 R centrifuge (Hettich Lab Technology, Germany) at 12.851 $\times g$ for 60 min at 20 °C. After removing the supernatant, NPs were redispersed in 2.5 mL pure water, vortexed 5 to 10 s and then sonicated in an ultrasound bath for 30 min. For the Acdex NPs, 100 μ L of 0.01% triethylamine (TEA) of pH 9 were added to the suspension. The NPs were stored at 4 °C overnight to allow complete dispersion in water. The concentration of the particle dispersions was determined by freeze-drying up to six aliquots of 100 or 200 μ L NPs dispersion. The mass of the NPs was accurately weighed (Radwag Waagen, MYA 11.4Y, Germany) and an average was calculated for the NPs concentration.

Dynamic light scattering (DLS)

The size, polydispersity index and the zeta-potential of the particles was measured using a Zetasizer Nano ZS with a laser wavelength of $\lambda = 633$ nm (Malvern Instruments, Germany). The measurements were performed at 173° backscatter angle with the following settings: Five repeated measurements at 25 °C, each measurement with five runs of 30 s and a 30 s equilibration time. The zeta-potential of the lyophilized NPs was measured at 25 °C with three repeated measurements. The NPs were characterized after purification (10 μ L NP dispersion diluted in 1 mL pure water), and after lyophilization (100 μ L of NP dispersion were lyophilized and redispersed in 1 mL pure water). The intensity size distribution is reported as the hydrodynamic diameter (d_H) of the NPs.

The degradation behavior of Acdex and PLGA NPs was determined by monitoring the mean count rate (kcps). The NP samples were measured using fixed settings (37 °C, measurement position 4.65, and attenuator 7). The Acdex NPs were measured for 15 h: 180 measurements (delay between measurements 240 s), where each measurement consisted of three runs with 20 s run durations. The PLGA NPs were measured every day over a period of 60 days: Five measurements (with no delay between measurements), where each measurement consisted of one run with 30 s run duration.

UV–VIS spectroscopy

For the calculating the encapsulation efficiency (EE) and loading capacity (LC) of the drug in the NPs, aliquots of 200 μ L of the washed NP dispersion were lyophilized. The dry NP powder was dissolved in 200 μ L DMSO (spectroscopic grade). The polymer-drug solution was measured at $\lambda = 316$ nm with 3 \times 3 multiple reads per well and 2000 μ m well border using the Infinite M200 Pro platereader (Tecan Group, Switzerland). For all EE measurements, a Hellma

Quartz flat-transparent plate with 96 wells was used. A calibration curve of BRP-187 was obtained for each batch in the concentration range of 0.24 to $\mu\text{g mL}^{-1}$ with $R^2=0.9997$. Equations 1 and 2 were used to calculate EE and LC

$$LC = \frac{\text{mass of drug recovered}}{\text{mass of particle recovered}} \times 100 \quad (1)$$

$$EE = \frac{LC}{LC \text{ theoretical}} \times 100 \quad (2)$$

PVA assay

Determination of PVA in the NPs (% w/w) was performed using UV-VIS spectroscopy. PVA forms a complex with iodine, which absorbs light at $\lambda=650$ to 690 nm. In an adapted protocol, Lugol solution was used as iodine source [44]. Lyophilized NPs were redispersed in pure water (3 mg mL^{-1}) and 90 μL were pipetted into a 96-well plate. Then, 20 μL of 1 M sodium hydroxide was added to each NP-containing well, and the solutions were mixed for 15 min at 850 rpm at room temperature. Next, 20 μL 1 M hydrochloric acid, 60 μL 0.65 M boric acid and 10 μL of Lugol solution were added to each well. Measurements on the plate reader were done at $\lambda=650 \text{ nm}$ 15 min after the addition of the Lugol solution. The experiments were repeated three times for each NP formulation.

Scanning electron microscopy (SEM)

Electron microscopy imaging was performed with a Sigma VP Field Emission Scanning Electron Microscope (Carl-Zeiss, Jena, Germany) using an InLens detector with an accelerating voltage of 6 kV. The samples were coated with a thin layer of platinum (4 nm) via sputter coating (CCU-010 HV, Safematic, Switzerland) before the measurement. ImageJ was used to measure the particle sizes from the images acquired by the SEM, where a mean diameter was deduced by measuring 150 to 200 NPs/image.

Degradation study

The degradation behavior of loaded and unloaded NPs was tested at 37 °C in 0.05 M Tris-HCl buffer of pH 7.4 and 0.05 M acetate buffer of pH 4.8. Lyophilized NPs were dispersed in pure water (concentration of 3 to 7 mg mL^{-1}). Next, NPs were mixed with buffer solution incubated at 37 °C and analyzed by DLS. Acdex NPs were measured for 15 h, whereas PLGA NPs were measured over 60 days (see Sect. "Fluorescence dye-labeled nanoparticle uptake in PMNL"). The degradation of the NPs was analyzed by monitoring the change in the mean count rate, size and PDI in DLS.

Cell isolation and cell culture

Leukocyte concentrates were prepared from peripheral blood obtained from healthy human adult donors that received no anti-inflammatory treatment for the last 10 days (Institute of Transfusion Medicine, University Hospital Jena, Germany). The approval for the protocol was given by the ethical committee of the University Hospital Jena and all methods were performed in accordance with the relevant guidelines and regulations. To isolate PMNL and monocytes, the leukocyte concentrates were mixed with dextran (dextran from *Leuconostoc spp.* $M_w \sim 40,000 \text{ g mol}^{-1}$, Sigma Aldrich, Taufkirchen, Germany) for sedimentation of erythrocytes; the supernatant was centrifuged on lymphocyte separation medium (Histopaque®-1077, Sigma Aldrich). Contaminating erythrocytes in the pelleted PMNL were removed by hypotonic lysis using water. The pelleted PMNL were subsequently washed twice in ice-cold phosphate-buffered saline pH 7.4 (PBS) and finally resuspended in PBS. The peripheral blood mononuclear cell (PBMC) fraction on top of lymphocyte separation medium was washed with ice-cold PBS and seeded in cell culture flasks (Greiner Bio-one, Nuertingen, Germany) for 1.5 h (37 °C, 5% CO_2) in PBS with $\text{Ca}^{2+}/\text{Mg}^{2+}$ ($0.133 \text{ g L}^{-1}/0.1 \text{ g L}^{-1}$) to isolate monocytes by adherence. For differentiation and polarization of monocytes to M1 and M2 macrophages, we followed published procedures [39]. To obtain M1 macrophages, adherent monocytes were treated with 20 ng mL^{-1} granulocyte macrophage-colony stimulating factor (GM-CSF) Peprotech, Hamburg, Germany) for six days in RPMI 1640 supplemented with 10% fetal calf serum (FCS), 2 mmol L^{-1} L-glutamine, penicillin (100 U mL^{-1}) and streptomycin ($100 \mu\text{g mL}^{-1}$) for differentiation and were further incubated with 100 ng mL^{-1} lipopolysaccharide (LPS) and 20 ng mL^{-1} interferon- γ (Peprotech) for 48 h. M2 macrophages were obtained by treatment of monocytes with 20 ng mL^{-1} M-CSF (Peprotech) for 6 days, followed by 20 ng mL^{-1} IL-4 (Peprotech) for 48 h. Correct polarization and purity of macrophages was routinely checked by flow cytometry (FACS Canto Plus flow cytometer, BD Biosciences, Heidelberg, Germany) as reported [45] using the following antibodies: FITC anti-human CD14 (2 $\mu\text{g}/\text{test}$, clone M5E2, BD Biosciences), PE anti-human CD54 (1 $\mu\text{g}/\text{test}$, clone HA58, BD Biosciences), APC-H7 anti-human CD80 (0.25 $\mu\text{g}/\text{test}$, clone L307.4, BD Biosciences), PE-Cy7 anti-human CD163 (2 $\mu\text{g}/\text{test}$, clone RM3/1, Biolegend, San Diego, CA, USA), PerCP-eFluor710 anti-human CD206 (0.06 $\mu\text{g}/\text{test}$, clone 19.2, BD Biosciences, San Diego, CA, USA).

Determination of 5-LO product formation in PMNL

For evaluation of the effects on 5-LO product formation in human PMNL, cells ($5 \times 10^6 \text{ mL}^{-1}$) were

pre-incubated with BRP-187 or NPs (Acdex[blank], PLGA[blank], Acdex[BRP-187], PLGA[BRP-187]) for the indicated times (15 min up to 5 h) at 37 °C. Cells were then stimulated with 2.5 μM Ca^{2+} -ionophore A23187 (Cayman, Ann Arbor, USA) for 10 min, and then the incubation was stopped with 1 mL ice-cold methanol containing 200 ng mL^{-1} PGB_1 as internal standard. Samples were subjected to solid phase extraction and formed 5-LO products were separated and analyzed by RP-HPLC as described [46].

Determination of prostaglandin E_2 formation in human macrophages

Human monocyte-derived M1 macrophages (2×10^6 cells) were seeded in 6-well-plates and preincubated for 15 min, 5 or 20 h with BRP-187 or NPs (Acdex[blank], PLGA[blank], Acdex[BRP-187], PLGA[BRP-187]) at 37 °C. The macrophages were subsequently incubated with pathogenic *E. coli* [O6:K2:H1] for 90 min. The reaction was stopped with ice-cold methanol containing deuterium-labeled internal standards (d8-5S-HETE, d4-LTB₄, d5-LXA₄, d5-RvD2, and d4-PGE₂; 500 pg each). Samples were kept at -20 °C for one day to allow protein precipitation. After centrifugation ($2000 \times g$, 4 °C, 10 min), 8 mL acidified water was added (final pH = 3.5) and samples were subjected to solid phase extraction using RP-18 columns and PGE₂ was analyzed by UPLC-MS-MS exactly as described before [45].

Lactate dehydrogenase assay

The release of LDH from cells was analyzed using the CytoTox 96[®] Non-Radioactive Cytotoxicity Assay (Promega GmbH, Mannheim, Germany). Briefly, 1×10^6 M1 or M2 macrophages per well, suspended in RPMI-medium containing 10% FCS, penicillin/streptomycin and *L*-glutamine, were seeded in a 24-well plate. Lysis control and 0.2% triton X-100 were added to the cells and incubated for 45 min; compounds and control (0.1% DMSO) were added and incubated for 24 h at 37 °C. Stop solution was added, the plate was centrifuged ($250 \times g$, 4 min, room temperature) and 50 μL of supernatant from each well was transferred in a 96-well plate. Afterwards, 50 μL of substrate mixture was added and incubated for 30 min at room temperature in the dark. To finally stop the reaction, 50 μL of stop solution were added. The photometric measurement was performed at 490 nm using a Multiskan Spectrum plate reader (Thermo Fischer).

Fluorescence dye-labeled nanoparticle uptake in PMNL

Time-dependent uptake of fluorescence dye-labeled NPs by PMNL was analyzed by flow cytometry and confocal laser scanning microscopy. Adherent PMNL (2×10^6) were incubated for the indicated time points with

0.5 mg mL^{-1} labeled NPs (PLGA-DY635[BRP-187] or Acdex-RhoB[BRP-187]). For flow cytometry, cells were washed once with PBS containing 0.5% BSA and incubated with PBA-E (PBS with 0.5% BSA, 2 mM EDTA and 0.1% sodium azide) containing 0.4% lidocaine for detaching. PMNL containing fluorescently stained NPs were analyzed by flow cytometry using BD LSR Fortessa (BD Bioscience). The red laser (644 nm) in combination with 670/14 filters for DY635 labeled NPs and the violet laser (405 nm) in combination with 655/8 filters for rhodamine B labeled NPs were used for flow cytometric analysis. Data were analyzed using FlowJo X Software (BD Bioscience).

For confocal laser scanning microscopy, PMNL were (i) washed once with PBS after incubation with the respective NPs for the indicated time points as described above for flow cytometry, (ii) submerged with phenol red-free RPMI 1640 and (iii) subsequently subjected to microscopic analysis. CLSM images were acquired using a Zeiss LSM 880 (Carl Zeiss, Oberkochen, Germany) with following settings: PLGA NPs labeled with DY635: $\lambda_{\text{Ex}} = 633$ nm, $\lambda_{\text{Em}} = 638$ to 759 nm and transmission signal with PMT detector; Acdex NPs labeled with rhodamine B: $\lambda_{\text{Ex}} = 514$ nm, $\lambda_{\text{Em}} = 531$ to 703 nm and transmission signal with PMT detector. Images were captured with an iLCI Plan-Neofluar 63 \times objective using identical settings for image acquisition within experimental groups.

Abbreviations

5-LO: 5-Lipoxygenase; 5S-HETE: 5-Hydroxyicosatetraenoic acid; AA: Arachidonic acid; Acdex: Acetalated dextran; Acdex-RhoB: Acetalated dextran coupled to Rhodamine B; BSA: Bovine serum albumin; CLSM: Confocal laser scanning microscopy; COX: Cyclooxygenase; d_i : Hydrodynamic diameter; DL: Dynamic light scattering; DMAc: Dimethylacetamide; DMF: Dimethylformamide; DMSO: Dimethylsulfoxide; EDC: 1-Ethyl-3-(3-dimethylaminopropyl) carbodiimide; EDTA: Ethylenediaminetetraacetic acid; EE: Encapsulation efficiency; FCS: Fetal calf serum; FLAP: 5-Lipoxygenase-activating protein; GM-CSF: Granulocyte macrophage-colony stimulating factor; IC_{50} : Half maximal inhibitory concentration; ICH: International council for harmonization of technical requirements for pharmaceuticals for human use; IL-4: Interleukin 4; LC: Loading capacity; LDH: Lactate dehydrogenase; LT: Leukotrienes; LTB₄: Leukotriene B₄; LXA₄: Lipoxin A₄; MFI: Mean fluorescence intensity; mPGE₂-1: Microsomal prostaglandin E_2 synthase-1; MTT: 3-(4,5-Dimethylthiazol-2-yl)-2,5-diphenyltetrazolium bromide; NHs: *N*-Hydroxysuccinimide; NPs: Nanoparticles; NSAIDs: Nonsteroidal anti-inflammatory drugs; PBA-E: PBS with 0.5% BSA, 2 mM EDTA and 0.1% sodium azide; PBMC: Peripheral blood mononuclear cell; PBS: Phosphate buffer saline; PDI: Polydispersity index; PG: Prostaglandins; PGB_1 : Prostaglandin B₁; PGE₂: Prostaglandin E_2 ; PGH₂: Prostaglandin H₂; PLGA: Poly(lactic-co-glycolic) acid; PMNL: Polymorphonuclear leukocytes; PVA: Poly(vinyl alcohol); RP-HPLC: Reverse phase-high performance liquid chromatography; RvD2: Resolvin D2; SEM: Scanning electron microscope; SPE: Solid phase extraction; TEA: Triethylamine; THF: Tetrahydrofuran; UPLC-MS/MS: Ultra performance liquid chromatography tandem mass spectrometry.

Acknowledgements

The authors want to thank PD Dr. Christoph Enzensperger from SmartDye-Livery GmbH for the preparation of PLGA-DY635 polymer, as well as Bärbel Beringer-Siemers and Benjamin Schenz for technical support.

Authors' contributions

BSP, CK, PMJ, DP, MW and SS performed the experiments. BSP and CK wrote the manuscript. PK synthesized Acdex. EB synthesized BRP-187. BSP produced the nanoparticles. MW and SL did further characterization of NPs. SH supervised the electron microscopy. AK supervised the UPLC MS/MS analysis. AV, SS and OW made critical revision and corrected the manuscript. AV, SS, OW and USS designed the research and supervised the work. All authors read and approved the final manuscript.

Funding

This work was supported by the Deutsche Forschungsgemeinschaft (DFG), Collaborative Research Center SFB 1278 "PolyTarget", (project number 316213987 projects A04, C01 and Z01). The SEM facilities of the Jena Center for Soft Matter (JCSM) were also established with a grant from the DFG. The LSM880 ELYRA PS.1 was funded with a grant from the DFG.

Availability of data and materials

Not applicable.

Ethics approval and consent to participate

The experimental protocol was approved by the ethical committee of the University Hospital Jena (No. 5050-01/17). All methods were performed in accordance with the relevant guidelines and regulations.

Consent for publication

Not applicable.

Competing interests

The authors declare that they have no competing interests.

Author details

¹Laboratory of Organic and Macromolecular Chemistry (IOMC), Friedrich Schiller University Jena, Humboldtstraße 10, 07743 Jena, Germany. ²Jena Center for Soft Matter (JCSM), Friedrich Schiller University Jena, Philosophenweg 7, 07743 Jena, Germany. ³Department of Pharmaceutical/Medicinal Chemistry, Institute of Pharmacy, Friedrich Schiller University Jena, Philosophenweg 14, 07743 Jena, Germany. ⁴Department of Pharmaceutical Chemistry, Faculty of Pharmacy, Gazi University, Etiler, Yenimahalle, 06330 Ankara, Turkey. ⁵Institute of Nutritional Sciences, Friedrich Schiller University Jena, Dornburger Straße 25, 07743 Jena, Germany. ⁶Department of Pharmaceutical Technology and Biopharmacy, Institute of Pharmacy, Friedrich Schiller University Jena, Lessingstraße 8, 07743 Jena, Germany. ⁷Michael Popp Research Institute, University of Innsbruck, Mitterweg 24, 6020 Innsbruck, Austria.

Received: 26 February 2020 Accepted: 19 April 2020

Published online: 14 May 2020

References

- Medzhitov R. Inflammation 2010: New adventures of an old flame. *Cell*. 2010;140:771–6.
- Funk CD. Prostaglandins and leukotrienes: advances in eicosanoid biology. *Science*. 2001;294:1871–5.
- Samuelsson B, Morgenstern R, Jakobsson P. Membrane prostaglandin E synthase-1: a novel therapeutic target. *Pharmacol Rev*. 2007;59:207–24.
- Grosser T, Fries S, Fitzgerald GA. Biological basis for the cardiovascular consequences of COX-2 inhibition: therapeutic challenges and opportunities. *J Clin Invest*. 2006;116:4–15.
- Rådmark O, Werz O, Steinhilber D, Samuelsson B. 5-Lipoxygenase, a key enzyme for leukotriene biosynthesis in health and disease. *Biochim Biophys Acta Mol Cell Biol Lipids*. 2015;1851:331–9.
- Werz O, Gerstmeier J, Garscha U. Novel leukotriene biosynthesis inhibitors (2012–2016) as anti-inflammatory agents. *Expert Opin Ther Pat*. 2017;27:607–20.
- Garscha U, Voelker S, Pace S, Gerstmeier J, Emini B, Liening S, et al. BRP-187: a potent inhibitor of leukotriene biosynthesis that acts through impeding the dynamic 5-lipoxygenase/5-lipoxygenase-activating protein (FLAP) complex assembly. *Biochem Pharmacol*. 2016;119:17–26.
- Koerberle A, Werz O. Natural products as inhibitors of prostaglandin E2 and pro-inflammatory 5-lipoxygenase-derived lipid mediator biosynthesis. *Biotechnol Adv*. 2018;36:1709–23.
- Suarez S, Grover GN, Braden RL, Christman KL, Almutairi A. Tunable protein release from acetalated dextran microparticles: a platform for delivery of protein therapeutics to the heart post-MI. *Biomacromolecules*. 2013;14:3927–35.
- Shkodra-Pula B, Grune C, Traeger A, Vollrath A, Schubert S, Fischer D, et al. Effect of surfactant on the size and stability of PLGA nanoparticles encapsulating a protein kinase C inhibitor. *Int J Pharm*. 2019;566:756–64.
- Choi YH, Han HK. Nanomedicines: current status and future perspectives in aspect of drug delivery and pharmacokinetics. *J Pharm Invest*. 2018;48:43–60.
- Avgoustakis K. Polylactic-co-glycolic acid (PLGA). In: Wnek GE, Bowlin GL, editors. *Encycl Biomater Biomed Eng*. Taylor & Francis: Milton; 2008. p. 2259–69.
- Wang Y, Wen Q, Choi S. FDA's regulatory science program for generic PLA/PLGA-based drug products. *Am Pharm Rev*. 2016. <https://www.americapharmaceuticalreview.com/Featured-Articles/188841-FDA-s-Regulatory-Science-Program-for-Generic-PLA-PLGA-Based-Drug-Products/>. Accessed 26 Apr 2020.
- Danhier F, Ansorena E, Silva JM, Coco R, Le Breton A, Pr at V. PLGA-based nanoparticles: an overview of biomedical applications. *J Control Release*. 2012;161:505–22.
- Swider E, Koshkina O, Tel J, Cruz LJ, de Vries IJM, Srinivas M. Customizing poly(lactic-co-glycolic acid) particles for biomedical applications. *Acta Biomater*. 2018;73:38–51.
- Gentile P, Chiono V, Carmagnola I, Hatton PV. An overview of poly(lactic-co-glycolic acid) (PLGA)-based biomaterials for bone tissue engineering. *Int J Mol Sci*. 2014;15:3640–59.
- Bachelder EM, Pino EN, Ainslie KM. Acetalated dextran: a tunable and acid-labile biopolymer with facile synthesis and a range of applications. *Chem Rev*. 2017;117:1915–26.
- Wang Z, Gupta SK, Meenach SA. Development and physicochemical characterization of acetalated dextran aerosol particle systems for deep lung delivery. *Int J Pharm*. 2017;525:264–74.
- Bachelder EM, Beaudette TT, Broaders KE, Dashe J, Fr chet JMJ. Acetal-derivatized dextran: an acid-responsive biodegradable material for therapeutic applications. *J Am Chem Soc*. 2008;130:10494–5.
- Braga CB, Perli G, Becher TB, Ornelas C. Biodegradable and pH-responsive acetalated dextran (Ac-Dex) nanoparticles for NIR imaging and controlled delivery of a platinum-based prodrug into cancer cells. *Mol Pharm*. 2019;16:2083–94.
- Schubert S, Delaney JT Jr, Schubert US. Nanoprecipitation and nanoformulation of polymers: from history to powerful possibilities beyond poly(lactic acid). *Soft Matter*. 2011;7:1581–8.
- European Medicines Agency. ICH guideline Q3C (R6) on impurities: Guideline for residual solvents. 2019. https://www.ema.europa.eu/en/documents/scientific-guideline/international-conference-harmonisation-technical-requirements-registration-pharmaceuticals-human-use_en-33.pdf. Accessed 26 Feb 2020.
- Yu Y, Tan S, Zhao S, Zhuang X, Song Q, Wang Y, et al. Antitumor activity of docetaxel-loaded polymeric nanoparticles fabricated by Shirasu porous glass membrane-emulsification technique. *Int J Nanomedicine*. 2013;8:2641–52.
- Wang Y, Li P, Truong-Dinh Tran T, Zhang J, Kong L. Manufacturing techniques and surface engineering of polymer based nanoparticles for targeted drug delivery to cancer. *Nanomaterials*. 2016;6:26.
- Perevyazko I, Vollrath A, Hornig S, Pavlov GM, Schubert US. Characterization of poly(methyl methacrylate) nanoparticles prepared by nanoprecipitation using analytical ultracentrifugation, dynamic light scattering, and scanning electron microscopy. *J Polym Sci Part A Polym Chem*. 2010;48:3924–31.
- Dhakar RC, Maurya SD, Sagar BPS, Bhagat S, Kumar PS, Jain CP. Variables influencing the drug entrapment efficiency of microspheres: a pharmaceutical review. *Der Pharm Lett*. 2010;2:102–16.
- Singh R, Lillard JW. Nanoparticle-based targeted drug delivery. *Exp Mol Pathol*. 2009;86:215–23.
- Cheng J, Teply BA, Sherifi I, Sung J, Luther G, Gu FX, et al. Formulation of functionalized PLGA-PEG nanoparticles for in vivo targeted drug delivery. *Biomaterials*. 2007;28:869–76.

29. Manual: Zetasizer Nano User Manual (Man0485-1.1). <https://documents.in/document/manual-zetasizer-nano-user-manual-man0485-1.1.html>. Accessed 26 Feb 2020.
30. Karavelidis V, Karavas E, Giliopoulos D, Papadimitriou S, Bikiaris D. Evaluating the effects of crystallinity in new biocompatible polyester nanocarriers on drug release behavior. *Int J Nanomedicine*. 2011;6:3021–32.
31. Holy CE, Dang SM, Davies JE, Shoichet MS. In vitro degradation of a novel poly(lactide-co-glycolide) 75/25 foam. *Biomaterials*. 1999;20:1177–85.
32. Martins C, Sousa F, Araújo F, Sarmiento B. Functionalizing PLGA and PLGA derivatives for drug delivery and tissue regeneration applications. *Adv Healthc Mater*. 2018;7:1701035.
33. Engineer C, Parikh J, Raval A. Hydrolytic degradation behavior of 50/50 poly lactide-co-glycolide from drug eluting stents. *Trends Biomater Artif Organs*. 2010;24:131–8.
34. Evonik. RESOMER® controlled release polymers. 2019. <https://healthcare.evonik.com/product/health-care/en/products/biomaterials/resomer/pages/controlled-release.aspx>. Accessed 15 Aug 2019.
35. Karavelidis V, Giliopoulos D, Karavas E, Bikiaris D. Nanoencapsulation of a water soluble drug in biocompatible polyesters. Effect of polyesters melting point and glass transition temperature on drug release behavior. *Eur J Pharm Sci*. 2010;41:636–43.
36. Englert C, Brendel JC, Majdanski TC, Yildirim T, Schubert S, Gottschaldt M, et al. Pharmapolymer in the 21st century: synthetic polymers in drug delivery applications. *Prog Polym Sci*. 2018;87:107–64.
37. Lee SC, Oh JT, Jang MH, Chung SI. Quantitative analysis of polyvinyl alcohol on the surface of poly(D, L-lactide-co-glycolide) microparticles prepared by solvent evaporation method: effect of particle size and PVA concentration. *J Control Release*. 1999;59:123–32.
38. Surette ME. Lipopolysaccharides prime whole human blood and isolated neutrophils for the increased synthesis of 5-lipoxygenase products by enhancing arachidonic acid availability: involvement of the CD14 antigen. *J Exp Med*. 1993;178:1347–55.
39. Werz O, Gerstmeier J, Libreros S, De La Rosa X, Werner M, Norris PC, et al. Human macrophages differentially produce specific resolvin or leukotriene signals that depend on bacterial pathogenicity. *Nat Commun*. 2018;9:1–12.
40. Mosca M, Polentarutti N, Mangano G, Apicella C, Doni A, Mancini F, et al. Regulation of the microsomal prostaglandin E synthase-1 in polarized mononuclear phagocytes and its constitutive expression in neutrophils. *J Leukoc Biol*. 2007;82:320–6.
41. Koeberle A, Werz O. Perspective of microsomal prostaglandin E2 synthase-1 as drug target in inflammation-related disorders. *Biochem Pharmacol*. 2015;98:1–15.
42. Banoglu E, Çelikoğlu E, Völker S, Olgaç A, Gerstmeier J, Garscha U, et al. 4,5-Diarylisoaxazol-3-carboxylic acids: a new class of leukotriene biosynthesis inhibitors potentially targeting 5-lipoxygenase-activating protein (FLAP). *Eur J Med Chem*. 2016;113:1–10.
43. Hennig D, Schubert S, Dargatz H, Kostenis E, Fahr A, Schubert US, et al. Novel insights into appropriate encapsulation methods for bioactive compounds into polymers: a study with peptides and HDAC inhibitors. *Macromol Biosci*. 2014;14:69–80.
44. Spek S, Haeuser M, Schaefer MM, Langer K. Characterisation of PEGylated PLGA nanoparticles comparing the nanoparticle bulk to the particle surface using UV-VIS spectroscopy, SEC, 1H-NMR spectroscopy, and X-ray photoelectron spectroscopy. *Appl Surf Sci*. 2015;347:378–85.
45. Werner M, Jordan PM, Romp E, Czapka A, Rao Z, Kretzer C, et al. Targeting biosynthetic networks of the proinflammatory and proresolving lipid metabolome. *FASEB J*. 2019;33:6140–53.
46. Werz O, Bürkert E, Samuelsson B, Rådmark O, Steinhilber D. Activation of 5-lipoxygenase by cell stress is calcium independent in human polymorphonuclear leukocytes. *Blood*. 2002;99:1044–52.

Publisher's Note

Springer Nature remains neutral with regard to jurisdictional claims in published maps and institutional affiliations.

Ready to submit your research? Choose BMC and benefit from:

- fast, convenient online submission
- thorough peer review by experienced researchers in your field
- rapid publication on acceptance
- support for research data, including large and complex data types
- gold Open Access which fosters wider collaboration and increased citations
- maximum visibility for your research: over 100M website views per year

At BMC, research is always in progress.

Learn more biomedcentral.com/submissions



Manuscript III

Ethoxy acetalated dextran-based nanocarriers accomplish efficient inhibition of leukotriene formation by a novel FLAP antagonist in human leukocytes and blood

Kretzer, C., Shkodra-Pula, B., Klemm, P., Jordan, PM., Schröder, D., Cinar, G., Vollrath, A., Schubert, S., Nischang, I., Hoepfener, S., Stumpf, S., Banoglu, E., Gladigau, F., Bilancia, R., Rossi, A., Eggeling, C., Neugebauer, U., Schubert, US., Werz, O.

Cellular and Molecular Life Sciences, 2021 Dec 31;79(1):40.

Der Kandidat / Die Kandidatin ist

Erstautor/-in, Ko-Erstautor/-in, Korresp. Autor/-in, Koautor/-in.

Anteile (in %) der Autoren / der Autorinnen an den vorgegebenen Kategorien der Publikation

Author	Conception	Data analysis	Experimental	Writing	Provision of Material
Kretzer C.	20 %	50 %	50 %	30 %	
Shkodra-Pula B.	20 %	40 %	40 %	20 %	
Klemm P.					
Jordan PM.					
Schröder D.					
Cinar G.					
Vollrath A.					
Schubert S.					
Nischang I.					
Hoepfener S.					
Stumpf S.					
Banoglu E.					20 %
Gladigau F.					
Bilancia R.					
Rossi A.					
Eggeling C.					
Neugebauer U.					
Schubert US.	20 %			10 %	
Werz O.	20%			30 %	
Others	10%	10 %	10 %	10 %	80 %
Summe:	100 %	100 %	100 %	100 %	100 %

Unterschrift Kandidat/-in

Unterschrift Betreuer/-in (Mitglied der Fakultät)



Ethoxy acetalated dextran-based nanocarriers accomplish efficient inhibition of leukotriene formation by a novel FLAP antagonist in human leukocytes and blood

Christian Kretzer¹ · Blerina Shkodra^{2,3} · Paul Klemm^{2,3} · Paul M. Jordan¹ · Daniel Schröder⁴ · Gizem Cinar^{2,3} · Antje Vollrath^{2,3} · Stephanie Schubert^{3,5} · Ivo Nischang^{2,3} · Stephanie Hoepfener^{2,3} · Steffi Stumpf^{2,3} · Erden Banoglu⁶ · Frederike Gladigau^{7,8,9} · Rossella Bilancia¹⁰ · Antonietta Rossi¹⁰ · Christian Eggeling^{3,4,7,11} · Ute Neugebauer^{3,7,8,9} · Ulrich S. Schubert^{2,3} · Oliver Werz^{1,3}

Received: 20 September 2021 / Revised: 8 November 2021 / Accepted: 12 November 2021 / Published online: 31 December 2021
© The Author(s) 2021

Abstract

Leukotrienes are pro-inflammatory lipid mediators generated by 5-lipoxygenase aided by the 5-lipoxygenase-activating protein (FLAP). BRP-201, a novel benzimidazole-based FLAP antagonist, inhibits leukotriene biosynthesis in isolated leukocytes. However, like other FLAP antagonists, BRP-201 fails to effectively suppress leukotriene formation in blood, which limits its therapeutic value. Here, we describe the encapsulation of BRP-201 into poly(lactide-co-glycolide) (PLGA) and ethoxy acetalated dextran (Ace-DEX) nanoparticles (NPs), aiming to overcome these detrimental pharmacokinetic limitations and to enhance the bioactivity of BRP-201. NPs loaded with BRP-201 were produced via nanoprecipitation and the physicochemical properties of the NPs were analyzed in-depth using dynamic light scattering (size, dispersity, degradation), electrophoretic light scattering (effective charge), NP tracking analysis (size, dispersity), scanning electron microscopy (size and morphology), UV–VIS spectroscopy (drug loading), an analytical ultracentrifuge (drug release, degradation kinetics), and Raman spectroscopy (chemical attributes). Biological assays were performed to study cytotoxicity, cellular uptake, and efficiency of BRP-201-loaded NPs *versus* free BRP-201 to suppress leukotriene formation in primary human leukocytes and whole blood. Both PLGA- and Ace-DEX-based NPs were significantly more efficient to inhibit leukotriene formation in neutrophils *versus* free drug. Whole blood experiments revealed that encapsulation of BRP-201 into Ace-DEX NPs strongly increases its potency, especially upon pro-longed (≥ 5 h) incubations and upon lipopolysaccharide-challenge of blood. Finally, intravenous injection of BRP-201-loaded NPs significantly suppressed leukotriene levels in blood of mice *in vivo*. These results reveal the feasibility of our pharmacological approach using a novel FLAP antagonist encapsulated into Ace-DEX-based NPs with improved efficiency in blood to suppress leukotriene biosynthesis.

Keywords Anti-inflammatory therapy · 5-Lipoxygenase-activating protein · Poly(lactide-co-glycolide) (PLGA) · Acetalated dextran · Polymer nanoparticles (NPs) · Drug delivery

Abbreviations

5-LO 5-Lipoxygenase
5S-HETE 5-Hydroxyeicosatetraenoic acid
AA Arachidonic acid

Ace-DEX Ethoxy acetalated dextran
AUC Analytical ultracentrifuge
BSA Bovine serum albumin
 d_H Hydrodynamic diameter
DLS Dynamic light scattering
DMAc Dimethyl acetamide
DMSO Dimethyl sulfoxide
ELS Electrophoretic light scattering
EDTA Ethylenediaminetetraacetic acid
EE Encapsulation efficiency
FCS Fetal calf serum
FLAP 5-Lipoxygenase-activating protein
IC50 Half maximal inhibitory concentration

Christian Kretzer and Blerina Shkodra have contributed equally to this work.

✉ Ulrich S. Schubert
ulrich.schubert@uni-jena.de

✉ Oliver Werz
oliver.werz@uni-jena.de

Extended author information available on the last page of the article

LC	Loading capacity
LDH	Lactate dehydrogenase
LM	Lipid mediator
LPS	Lipopolysaccharide
LT	Leukotriene
MADLS	Multi-angle dynamic light scattering
MDM	Monocyte-derived macrophages
MFI	Mean fluorescence intensity
mPGES-1	Microsomal prostaglandin E2 synthase-1
MTT	3-(4,5-Dimethylthiazol-2-yl)-2,5-diphenyltetrazolium bromide
NPs	Nanoparticles
NTA	Nanoparticle tracking analysis
PBA-E	PBS with 0.5% BSA, 2 mM EDTA and 0.1% sodium azide
PBMC	Peripheral blood mononuclear cell
PBS	Phosphate-buffered saline
PDI	Polydispersity index
PG	Prostaglandin
PLGA	Poly(lactide- <i>co</i> -glycolide)
PVA	Poly (vinyl alcohol)
RP-HPLC	Reversed phase-high performance liquid chromatography
RvD2	Resolvin D2
SACM	<i>S. aureus</i> -conditioned medium
SEM	Scanning electron microscope
SPE	Solid phase extraction
TEA	Triethylamine
THF	Tetrahydrofuran
UPLC-MS/MS	Ultra performance liquid chromatography tandem mass spectrometry

Introduction

5-Lipoxygenase-activating protein (FLAP) and microsomal prostaglandin E₂ synthase-1 (mPGES-1) are considered as innovative drug targets [1] that accomplish the biosynthesis of the formation of pro-inflammatory lipid mediators from arachidonic acid (AA) involved in inflammation. Thus, FLAP assists 5-lipoxygenase (5-LO) in the generation of leukotrienes (LTs) that display potent chemotactic effects, activate pro-inflammatory leukocytes and constrict small vessels, while mPGES-1 catalyzes the transformation of cyclooxygenase-derived prostaglandin (PG)H₂ to PGE₂ that mediates pain and fever, and increases the vascular permeability [2, 3]. Our previous structure–activity relationship studies on benzimidazole-based dual inhibitors of FLAP and mPGES-1 revealed BRP-201 (5-{1-[(2-chlorophenyl)methyl]-2-[1-[4-(2-methylpropyl)phenyl]ethyl]-1H-benzimidazole-5-yl]-2,3-dihydro-1,3,4-oxadiazole-2-thione) as the most potent derivative [4]. However, BRP-201 and many other structurally different dual mPGES-1/FLAP inhibitors

or FLAP antagonists suffer from loss of efficiency in biological/pharmacological relevant environments apparently due to strong unspecific protein binding based on their acidic and lipophilic structures [1, 5]. Moreover, these compounds are afflicted with low water solubility that may further hinder their bioactivity and bioavailability.

Employing bioavailability enhancement techniques, such as encapsulation of drugs into polymer-based nanoparticles (NPs), could improve the drug pharmacokinetics, thus increasing their bioactivity [6]. Numerous studies have documented the great potential of poly(lactide-*co*-glycolide) (PLGA) as drug delivery tool, however, only very few approaches have exploited the benefits of acetalated dextran as a promising alternative [7–9]. Dextran is an established biomaterial that has been used in medicine for various applications [10–12]. Besides its biocompatibility, the advantages of acetalated dextran are mainly its facile synthesis and the opportunity to tailor its degradation kinetics based on the degree of acetal functionalization. Thus, the main advantage of acetalated dextran is that it can be tailored with faster degradation rates compared to PLGA. Moreover, acetalated dextran can be processed into NPs in the same manner as polyesters to encapsulate hydrophobic drugs [7, 8]. Ethoxy acetalated dextran (Ace-DEX) is a dextran derivative with a safe toxicity profile, which degrades into dextran, ethanol, and acetone—all non-harmful metabolites. In addition, the Ace-DEX metabolites should not cause an acidic microenvironment, which is an undesirable effect often associated with the acidic metabolites of PLGA degradation [13]. Nevertheless, both polymers offer application opportunities, for example, the long-lasting PLGA is generally advantageous for developing sustained-release formulations (parenteral, subcutaneous, or intra-articular/muscular), whereas Ace-DEX can be developed into parenteral formulations with varying drug release profiles. Therefore, in this study, we document the formulation and characterization of Ace-DEX and PLGA NPs loaded with BRP-201, and further compare the efficiency of the NPs with that of the free BRP-201.

Materials and methods

Materials

Poly(*D,L*-lactide-*co*-glycolide) (PLGA) (Resomer RG502 H, M_w 7000 to 17.000 g mol⁻¹, 50:50 co-polymer composition with carboxylic acid end groups), poly(vinyl alcohol) (PVA) (Mowiol 4–88, M_w 31.000 g mol⁻¹), dimethyl sulfoxide (DMSO, anhydrous ≥ 99.9%), acetone, triethylamine (TEA), Rhodamine B isothiocyanate (mixed isomers), anhydrous pyridine (99.8%), and all other materials were purchased from Sigma Aldrich unless otherwise stated. Methanol and *N,N*-dimethyl acetamide (DMAc) were

purchased from standard suppliers and were used without any further purification. THF was dried in a solvent purification system prior to use (SPS, Pure solv. EN, Innovative Technology). Lithium chloride (LiCl, 99%) was purchased from Acros Organics. Ethoxy acetalated dextran (Ace-DEX) was synthesized based on an established protocol where the hydroxyl groups of dextran were modified using 2-ethoxyprop-1-ene (95%, Fluorochem) (instead of 2-methoxypropene) [14]. Two batches of Ace-DEX were synthesized with the following properties: (#1) M_n 12,400 g mol⁻¹, dispersity (\bar{D}) of 1.68, and degree of substitution (DS) of acetal groups $DS_{cyclic} = 1.81$ and $DS_{acyclic} = 0.49$ and (#2) M_n 12,200 g mol⁻¹, $\bar{D} = 1.73$, $DS_{cyclic} = 1.17$, $DS_{acyclic} = 0.96$. The covalent coupling of Rhodamine B to Ace-DEX was achieved according to a previously published protocol [15]; M_n 22,400 g mol⁻¹, $\bar{D} = 1.38$, $DS_{cyclic} = 1.82$, $DS_{acyclic} = 0.04$, $DS_{Rho} = 0.374$ mg g⁻¹. PLGA-Rhodamine B was synthesized according to the procedure described in Sect. 2.2; $M_n = 10,900$ g mol⁻¹, $\bar{D} = 1.47$, $DS_{Rho} = 0.098$ μ g g⁻¹. Pure water was used in all experiments for the NP preparation.

PLGA-rhodamine B synthesis

In a Schlenk flask, PLGA (2 g, 0.29 mmol) and Rhodamine B isothiocyanate (27 mg, 0.05 mmol, 0.18 eq) were dissolved in anhydrous pyridine (20 mL) under Schlenk conditions. The dark red colored reaction solution was stirred at room temperature for 18 h, followed by stirring at 55 °C for 24 h. After cooling to room temperature, the reaction mixture was precipitated in a large excess of diethyl ether to get rid of the pyridine. The solid was collected by centrifugation and dissolved in THF. The resulting solution was precipitated in a large excess of methanol. The second precipitation step was repeated as often as necessary until the free dye was completely removed. The presence of free dye was checked between the precipitation steps by size exclusion chromatography measurements in DMAc and 0.21% LiCl with a UV-VIS detector at 555 nm. The obtained pellet from centrifugation was dried under vacuum, resulting in a pink colored powder (yield 58.2%).

Nanoparticle formulation

Particles were formulated by nanoprecipitation using a syringe pump (Aladdin AL1000-220, World Precision Instruments) with a flow rate of 2 mL min⁻¹. The organic solution was prepared by dissolving 25 mg of polymer (PLGA or Ace-DEX) in 5 mL acetone at 5 mg mL⁻¹ polymer concentration. To load the NPs with the drug, 75 μ L of 10 mg mL⁻¹ BRP-201 solution (initially dissolved in DMSO) was added to the polymer solution and vortexed. The organic solution was infused into 36 mL of pure water (+ 100 μ L of 0.01% TEA of pH = 10 for Ace-DEX NPs),

while stirring at 800 rpm at room temperature. After the organic solution had been completely transferred into pure water, 4 mL of PVA 3% (w/v) solution was added to the NP dispersion. The NP dispersions were stirred at 800 rpm for 12–24 h for acetone to evaporate. To purify the NPs, the dispersions were centrifuged at 16.639 \times g for 60 min at 20 °C (Centrifuge 5804 R, Eppendorf). The NP pellets were then redispersed into 2.5 mL pure water (+ 100 μ L of 0.01% TEA pH = 10 for Ace-DEX NPs). The NP dispersions were first vortexed for 10 s, sonicated in an ultrasound water-bath for 30 min, and stored overnight at 4 °C to allow for complete resuspension. The next day, NPs were lyophilized and the dried particles were stored at 4 °C. Rhodamine B-labeled Ace-DEX NPs were formulated according to the same protocol, except that the labeled Ace-DEX was mixed with pure Ace-DEX polymer in a 1:10 ratio. Ace-DEX NPs for in vivo application were prepared using a higher polymer and drug concentration, i.e., 15 mg mL⁻¹ and 10% (w w⁻¹) BRP-201 in relation to the polymer mass, respectively. The yield of the NPs was calculated according to the following formula:

$$\text{Yield}(\%) = \frac{(\text{mass of NPs recovered} - \text{mass of found PVA})}{(\text{mass of polymer} + \text{mass of drug}) \text{ fed in the formulation}} \times 100$$

Dynamic light scattering (DLS) and electrophoretic light scattering (ELS)

DLS and ELS were used to estimate the hydrodynamic diameter (d_H), polydispersity index (PDI), and zeta-potential (ζ -potential) of the NPs (Zetasizer Nano ZS, Malvern Instruments). The laser wavelength of the Zetasizer was $\lambda = 633$ nm and all measurements were performed at 25 °C and a 173° backscattering angle. The d_H and PDI of NPs were measured after evaporation of acetone, after centrifugation of NPs, and after lyophilization, while the ζ -potential was measured only after lyophilization of the NPs. The concentration of the measured NPs after purification and after lyophilization was 4 mg mL⁻¹ for Ace-DEX-based NPs and 7 mg mL⁻¹ for PLGA-based NPs. The DLS procedure for d_H and PDI estimations consisted of five measurements each consisting of 5 runs of 30 s, with an equilibration time of 30 s before and between measurements. The ELS procedure for the ζ -potential consisted of three measurements with 3 runs with 30 s equilibration time before and between measurements.

Nanoparticle tracking analysis (NTA)

A NanoSight NS500 (Malvern Panalytical) was used to determine the NP sizes in terms of HD. The lyophilized NPs

were redispersed in pure water and measured at the following concentrations:

50 $\mu\text{g mL}^{-1}$ for PLGA-based NPs, 10 $\mu\text{g mL}^{-1}$ for Ace-DEX-based NPs, 1 $\mu\text{g mL}^{-1}$ for BRP-201 drug precipitates. For each NP sample, five videos of 60 s acquisition time were captured at room temperature with instrument settings adjusted as reported in Table S1 (SI).

Scanning electron microscopy (SEM)

A Sigma VP field emission scanning electron microscope (Carl-Zeiss AG) was used to obtain the particle images. The microscope was operated with the InLens detector at a 6 kV acceleration voltage. 5 μL of NP dispersions were pipetted on mica substrates and air-dried. Before the measurement, samples were coated with a thin layer of platinum (4 nm) via sputter coating (CCU-010 HV, Safematic). ImageJ was used to estimate the NP size from 300 and 500 particles per image, for Ace-DEX and PLGA NPs, respectively.

UV-VIS spectroscopy

Encapsulation efficiency (EE) and loading capacity (LC) of the BRP-201-loaded particles were determined using a UV-VIS plate reader (Infinite M200 Pro Platereader, Tecan Group Ltd.). The samples were prepared as follows: three aliquots of 200 μL NP dispersion were lyophilized; the NP powder was accurately weighed and then redissolved in 200 μL of UV-grade DMSO. The solutions were pipetted on a Hellma Quartz 96-well plate and measured at $\lambda=316$ nm, with 3×3 multiple reads per well and a 2000 μm well border. A calibration curve of BRP-201 was obtained in a concentration range of 0.48–250 $\mu\text{g mL}^{-1}$, and the following formulas were used to calculate LC and EE, respectively.

$$LC = \frac{\text{mass of drug recovered}}{\text{mass of particle recovered}} \times 100$$

$$EE = \frac{LC}{LC_{\text{theoretical}}} \times 100$$

UV-VIS spectroscopy was also used to determine the content of the surfactant (% w⁻¹) in the lyophilized NPs according to a previously published protocol [16]. The concentration of the redispersed NPs was 3 mg mL^{-1} for the unlabeled NPs and approx. 0.5 mg mL^{-1} for the labeled NPs.

Degradation of NPs

Particle degradation was measured by DLS according to a previously described protocol [15]. The normalized value of

the measured count rate (in percentage) was used to plot the apparent degradation profile of the NPs against time.

Raman spectroscopy

Samples were placed on CaF₂ slides (Crystal GmbH, Germany) for Raman characterization, either as solid samples or drop coated (2 \times 5 μL and allowed to dry at ambient conditions). Raman spectra were recorded on an upright Raman microscope ($\alpha 300$, Witec) with a 600 l/mm grating. The Raman excitation laser (488 nm, Witec) was focused with a Nikon 100 \times NA 0.8 objective onto the sample resulting in 1 mW in the sample plane. Under these conditions, the best spatial resolution was around 300 nm. Single Raman spectra were recorded from bulk polymeric samples with an integration time of 1 s per spectrum. Raman maps were recorded with a step size of 125 nm utilizing the same conditions. Statistical analysis was performed using GNU R. Spectral pre-processing involved spike removal, baseline correction (polynomial baseline fitting) and normalization (area normalization). False color Raman images were generated by plotting the intensity ratio of the Raman bands at 1620 cm^{-1} (C=N vibration in BRP-201) and 1450 cm^{-1} (C-H deformation band for Ace-DEX NPs) and to the C=O stretching band at 1760 cm^{-1} (for PLGA NPs), respectively.

Drug release from the NPs

NPs were incubated in 0.05 mM acetate (pH=4.5) or 0.05 mM phosphate buffer (pH=7.4) at 37 °C for the following times: Ace-DEX NPs for 0.5, 1, 2, 5, 20, and 144 h; PLGA NPs for 0, 1, 7, 20, and 30 days. Additionally, control samples consisting of NPs in pure water were studied with the same experimental settings but without incubating the samples at 37 °C. All NP formulations were investigated at a concentration of 0.5 mg mL^{-1} .

Sedimentation velocity experiments were conducted using an Optima Analytical Ultracentrifuge (AUC) (Beckmann Coulter Instruments, Brea, CA) with an An-50 Ti eight-hole rotor. Rotor position eight was used as the counterbalance, enabling the optical module calibration. All ultracentrifuge cells contained double sector Epon centerpieces with a 12 mm solution optical path length and sapphire windows. The corresponding sectors were filled with approx. 440 μL pure solvent as a reference and approx. 420 μL of sample solution. Scans were acquired in four-minute intervals by using the interference optics and absorbance optical detection in terms of optical density (OD) at a wavelength of 316 nm, *i.e.* being representative of the encapsulated drug BRP-201. In total, 480 scans with a four-minute time interval (32 h) were recorded at a rotor speed of 1500 rpm. After that, the rotor speed was subsequently accelerated to 42,000 rpm for the investigation of

potentially present smaller species in the supernatant for a further 24 h (or 18 h for Ace-DEX NPs with 0.5–20 h incubation in acetate buffer and the respective control sample), also providing 480 scans (or 360 scans) with a 3 min time interval. All measurements were performed at 22 °C. Every fourth scan was considered for data evaluation. The recorded sedimentation velocity data were numerically analyzed with SEDFIT and the ls-g*(s) model considering non-diffusing species [17].

Cell isolation and cell culture

Leukocyte concentrates were prepared from peripheral blood obtained from healthy adult male and female donors that received no anti-inflammatory treatment for the last 10 days (Institute of Transfusion Medicine, Jena University Hospital). The approval for the protocol was given by the ethical committee of the Jena University Hospital and all methods were performed in accordance with the relevant guidelines and regulations. For isolation of neutrophils and monocytes, the leukocyte concentrates were mixed with dextran (from *leuconostoc spp.* $M_w \sim 40,000$, Sigma Aldrich) for sedimentation of erythrocytes and the supernatant was centrifuged on lymphocyte separation medium (Histopaque[®]-1077, Sigma Aldrich). Contaminating erythrocytes in the pelleted neutrophils were removed by hypotonic lysis (using water). Neutrophils were then washed twice in ice-cold phosphate-buffered saline (PBS) pH 7.4 and finally resuspended in PBS pH 7.4. The peripheral blood mononuclear cell (PBMC) fraction on top of the lymphocyte separation medium was washed with ice-cold PBS pH 7.4 and seeded in cell culture flasks (Greiner Bio-one) for 1.5 h (37 °C, 5% CO₂) in PBS pH 7.4 with Ca²⁺/Mg²⁺ to isolate monocytes by adherence. For differentiation and polarization of monocytes to M1 macrophages, we followed published procedures [18]. Thus, adherent monocytes were treated with 20 ng mL⁻¹ granulocyte macrophage-colony stimulating factor (Peprotech) for 6 days in RPMI 1640 supplemented with 10% fetal calf serum (FCS), 2 mmol L⁻¹ L-glutamine, penicillin (100 U mL⁻¹) and streptomycin (100 µg mL⁻¹), and further incubated with 100 ng mL⁻¹ LPS and 20 ng mL⁻¹ interferon-γ (Peprotech) for 48 h to obtain M1 macrophages. Correct polarization and purity of macrophages was routinely checked by flow cytometry (BD LSR Fortessa, BD Biosciences, Heidelberg, Germany) as reported [19] using the following antibodies: FITC anti-human CD14 (2 µg/test, clone M5E2, BD Biosciences), PE anti-human CD54 (1 µg/test, clone HA58, BD Biosciences), APC-H7 anti-human CD80 (0.25 µg/test, clone L307.4, BD Biosciences), PE-Cy7 anti-human CD163 (2 µg/test, clone RM3/1, Biolegend,

San Diego, CA, USA), PerCP-eFluor710 anti-human CD206 (0.06 µg/test, clone 19.2, BD Biosciences).

Fluorescence dye-labeled nanoparticle uptake in neutrophils

Time-dependent uptake of fluorescence dye-labeled NPs by neutrophils was analyzed by flow cytometry and confocal fluorescence microscopy. Adherent neutrophils (2×10^6) were incubated for 30 min or 3 h with LPS (1 µg mL⁻¹) or vehicle, and then with 0.5 mg mL⁻¹ labeled NPs (PLGA-Rho[BRP-201] or Ace-DEX-Rho[BRP-201]) for indicated time points. Cells were washed once with PBS pH 7.4 containing 0.5% BSA and incubated with PBA-E (PBS pH 7.4 with 0.5% BSA, 2 mM EDTA and 0.1% sodium azide). Neutrophils containing fluorescently stained NPs were analyzed by flow cytometry using BD LSR Fortessa (BD Biosciences). The violet laser (405 nm) in combination with 610/20 filters for Rhodamine B-labeled NPs were used for flow cytometric analysis. Data were analyzed using FlowJo X Software (BD Biosciences). For confocal imaging, 25 mm glass coverslips were first sonicated in double-distilled water for 20 min, and subsequently dried with pressured air and plasma-cleaned for 30 s. Neutrophils were diluted to 650,000 cells mL⁻¹ in PBS, and NP solution in PBS was added 3 min before imaging to a final concentration of 25 µg mL⁻¹. Images were taken on a Zeiss LSM 980 confocal microscope with ZEN 3.0 blue software suite at 37 °C and on a Zeiss LSM 880 microscope at 37 °C and 5% CO₂. On both setups, a Plan-Apochromat 63x/1.40 Oil-objective was used. For image analysis, ImageJ / Fiji were used [20, 21]. Figures were composed using FigureJ [22]. Time-line imaging was specifically realized by taking transmission brightfield images identifying the cell borders using the transmission T-PMT detector, and confocal fluorescence images of the NPs were recorded with a 561 nm laser source and detected between 570 and 680 nm with a GaAsP-PMT (pinhole size 1 airy unit). One three-dimensional image stack was taken every 5 min.

Evaluation of 5-lipoxygenase product formation in human neutrophils

For evaluation of the effects of test items on 5-LO product formation in human neutrophils, cells (5×10^6 mL⁻¹) were pre-incubated with BRP-201 NPs (Ace-DEX[BRP-201], PLGA[BRP-201]) and non-loaded NPs (Ace-DEX, PLGA) for different periods at 37 °C. Cells were then stimulated with 2.5 µM Ca²⁺-ionophore A23187 (Cayman) for 10 min, and the incubation was stopped with 1 mL ice-cold methanol containing 200 ng mL⁻¹ PGB₁ as internal standard. Samples were subjected to solid phase extraction

and formed 5-LO products (LTB₄, trans-isomers of LTB₄, 5-hydroperoxyeicosatetraenoic acid (5-HETE)) were separated and analyzed by RP-HPLC as previously described [23].

Determination of lipid mediator signature profiles in human monocyte-derived macrophages

Human monocyte-derived M1 macrophages (M1-MDM; 2×10^6 cells) were seeded in 6-well-plates and pre-incubated for 15 min, 5 h or 20 h with BRP-201 or NPs (Ace-DEX, PLGA, Ace-DEX[BRP-201], PLGA[BRP-201]) at 37 °C. The cells were subsequently incubated with *Staphylococcus aureus*-conditioned medium (SACM, *S. aureus* strain “6850”, 24 h culture, OD = 0.05) for 180 min. The reaction was stopped with ice-cold methanol containing deuterium-labeled internal standards (d8-5S-HETE, d4-LTB₄, d5-LXA₄, d5-RvD2, and d4-PGE₂; 500 pg each). Samples were kept at –20 °C for one day to allow protein precipitation. After centrifugation (2000×g, 4 °C, 10 min), 8 mL acidified water was added (final pH = 3.5) and samples were subjected to solid phase extraction using RP-18 columns and the lipid mediators (LMs) were analyzed by ultra-performance liquid chromatography-tandem mass spectrometry (UPLC-MS-MS) using an Acquity UPLC system (Waters) and a QTrap 5500 Mass Spectrometer (Sciex) equipped with an electrospray ionization source exactly as described before [18].

Determination of lipid mediator profiles in human whole blood

Freshly withdrawn whole blood in Li-heparin Monovettes (Sarstedt) from healthy adult donors that had not received any anti-inflammatory treatment the last 10 days was provided by the Institute of Transfusion Medicine, Jena University Hospital. The blood was incubated for different periods with either BRP-201 or NPs (Ace-DEX, Ace-DEX[BRP-201], PLGA, PLGA[BRP-201]) and stimulated with pathogenic *E. coli* (O6:K2:H1; 1×10^9 cells per mL blood) for 180 min. The reaction was stopped with ice-cold methanol containing the deuterium-labeled internal standards d8-5S-HETE, d4-LTB₄, d5-LXA₄, d5-RvD2, and d4-PGE₂ (500 pg, each). Samples were kept at –20 °C for 1 day to allow protein precipitation. After centrifugation (2000×g, 4 °C, 10 min) 8 mL acidified water was added (final pH = 3.5). The samples were subjected to solid phase extraction and analyzed by UPLC-MS-MS as described previously [18], see above (Sect. [Determination of lipid mediator signature profiles in human monocyte-derived macrophages](#)).

Inhibition of LTB₄ formation in murine blood in vivo

Adult (6–8 weeks) male CD1 mice (Charles River, Calco, Italy) were housed at the animal care facility of the Department of Pharmacy of the University of Naples “Federico II” and kept under controlled environment (i.e., temperature 21 ± 2 °C and humidity $60 \pm 10\%$) and provided with normal chow ad water ad libitum. Mice were allowed to acclimate for 4 days prior to experiments and were subjected to 12 h light/dark schedule. Treatments were conducted during the light phase. The experimental procedures were approved by the Italian Ministry and carried out in accordance with the EU Directive 2010/63/EU and the Italian DL 26/2014 for animal experiments and in compliance with the ARRIVE guidelines and Basel declaration including the 3R concept. Mice ($n = 6/\text{group}$) received an injection of 200 µL consisting of 7 mg mL^{-1} (46 mg kg^{-1}) Ace-DEX[BRP-201] NPs containing 4.6 mg kg^{-1} BRP-201 or the respective amount of Ace-DEX NPs in saline intravenously (i.v.) into the tail vein. After 3 h, zymosan (1 mg per mouse in 0.5 mL saline) was injected intraperitoneally (i.p.) to induce inflammation [24]. After another 4 h, mice were euthanized in a saturated CO₂ atmosphere, and blood (0.7–0.9 mL) was collected by intracardiac puncture through insertion of a 1 mL syringe with a needle of 22 gauge (Carl Roth GmbH & Co. KG, Karlsruhe, Germany) using citrate as anticoagulant (3.8%, w v⁻¹), immediately after euthanization. Plasma was obtained by centrifugation of the blood at 800×g at 4 °C for 10 min and immediately frozen for further analysis of LTB₄ via UPLC-MS-MS as described above.

Statistics

Results are expressed as mean \pm standard error of the mean (S.E.M) of n observations, where n represents the number of experiments with cells from separate donors, performed on different days. The sample size was chosen empirically based on previous studies to ensure statistical power [15, 18, 19]. Datasets were analyzed by GraphPad Prism 9.2.0 (GraphPad, La Jolla, CA, USA). One-way ANOVA and Tukey’s multiple comparisons test were used for statistical analysis in case of one different independent variable influences one continuous dependent variable. Multiple t-test was used for comparison of different concentrations of two groups. Two-way ANOVA was used for statistical analysis in case of two different categorical independent variables influence one continuous dependent variable, as indicated. The criterion for statistical significance is * $P < 0.05$; ** $P < 0.01$; *** $P < 0.001$.

Results and discussion

Nanoparticle formulation and characterization

For the encapsulation of BRP-201, we used two polymer materials with different degradation kinetics, i.e. PLGA and Ace-DEX that can be processed into NPs via nanoprecipitation applying the same formulation parameters (solvent, drug load, concentration, water-organic ratio, surfactant concentration) [15]. Previously, we used methoxy acetalated dextran (Ac-DEX) for the encapsulation of BRP-187, another mPGES-1/FLAP inhibitor and demonstrated the advantage of the encapsulating material [15]. However, upon degradation, Ac-DEX decomposes into dextran, acetone and methanol [25]. To omit the formation of methanol—although demonstrated to be non-toxic at concentrations usually applied for drug delivery—an ethoxy acetal derivative of dextran was used for encapsulation in this study. The ethoxy acetal derivative releases the less toxic ethanol instead of methanol upon degradation (SI, Fig. S1). This can be an advantage in case of higher doses of NPs are administered or in case of prolonged treatment times required during chronic treatments [14].

NPs with 3% (w w⁻¹) BRP-201 were first analyzed by DLS, which revealed that particles feature a size of around 150 to 200 nm with narrow size distribution (PDI < 0.2) (with the exception of Ace-DEX-Rho). All NPs had a negative ζ -potential of -20 to -30 mV, indicating stable NP formulations (Table 1). Similar insights were obtained from NTA measurements, where PLGA[BRP-201] showed a mixture of differently sized species in the formulation and a higher concentration of species larger than 200 nm (SI, Fig. S3B). A control experiment of precipitating the free drug without polymer into water showed that BRP-201 formed non-spherical particle-like precipitates of around 250 to

300 nm in hydrodynamic size. The size of the NPs as well as the formation of the drug precipitates were also confirmed by SEM (Fig. 1, and Fig. S2 in SI). The drug-formed precipitates were slightly larger in size and PDI than the polymeric NPs (SI Table S2, Fig. 1, Fig. S2 in SI). According to the SEM, the PLGA[BRP-201] formulation showed a mixture of uniformly distributed spherical NPs and particle-like structures of the drug (SI, Fig. S2B and C). Similar results were obtained from NTA measurements, where PLGA[BRP-201] showed a mixture of differently sized species in the formulation and a higher concentration of species larger than 200 nm (SI Fig. S3B, Table S2). NPs prepared with 3% (w w⁻¹) BRP-201 revealed optimal properties regarding size distribution and encapsulation efficiency (EE). However, to reach satisfactory doses in vivo, the preparation protocol for Ace-DEX NPs was optimized in order to further increase the drug loading. Both polymer and drug concentration fed in the formulation were increased to 15 mg mL⁻¹ and 10% (w w⁻¹), respectively. The resulting NPs remained within the desired size range of 150–270 nm, with a similar yield but with an EE of 100% (SI Table S3). Although the drug loading was considerably higher (92 $\mu\text{g mg}^{-1}$ NPs) when 10% (w w⁻¹) BRP-201 was fed in the formulation, drug precipitates were clearly present (Fig. 1C). Nevertheless, investigations of the particles via MADLS revealed that when NP dispersions were mixed with 0.9% NaCl, only 20% of the particle population was around 3 μm (SI Table S4, Fig. S13). In this case, Ace-DEX-based NPs were within a size range that pose a low risk of irritation at the injection site, [26] and are below the suggested limits of 5 μm for the upper particle size for injectable dispersions (SI Table S4) [27, 28]. Also, drug-loaded NPs measured after 28 days (stored at 4 °C) revealed that the particle size remained below the suggested limit of 5 μm (SI Table S5).

In general, the formulation parameters were efficient since the EE for all NPs was > 70% (Table 1). Based on the

Table 1 Summary of the physicochemical properties of NPs loaded with 3% (w/w) BRP-201

Formulations with 3% BRP-201	Purified NP suspension		Lyophilized NPs			Yield (%)	PVA (% w/w)	EE (%)	LC (% w/w)
	d _H (nm)	PDI	d _H (nm)	PDI	ζ (mV)				
PLGA	158 ± 5	0.11 ± 0.02	166 ± 12	0.07 ± 0.02	-24 ± 4	67	2 ± 0	—	—
PLGA[BRP-201] 3%	174 ± 5	0.15 ± 0.02	182 ± 7	0.13 ± 0.02	-22 ± 3	71	1 ± 0	75 ± 11	2.2 ± 0.3
PLGA-Rho	177 ± 11	0.13 ± 0.00	168 ± 11	0.09 ± 0.01	-25 ± 1	59	18 ± 1	—	—
PLGA-Rho[BRP-201] 3%	201 ± 6	0.14 ± 0.01	191 ± 7	0.12 ± 0.03	-23 ± 2	51	15 ± 1	79 ± 5	2.3 ± 0.2
Ace-DEX	140 ± 20	0.10 ± 0.05	172 ± 17	0.23 ± 0.08	-19 ± 6	41	3 ± 1	—	—
Ace-DEX[BRP-201] 3%	154 ± 27	0.08 ± 0.02	128 ± 32	0.09 ± 0.03	-24 ± 6	39	1 ± 0	69 ± 16	2.0 ± 0.5
Ace-DEX-Rho	185 ± 21	0.10 ± 0.02	391 ± 49	0.43 ± 0.05	-16 ± 1	58	10 ± 1	—	—
Ace-DEX-Rho[BRP-201] 3%	214 ± 11	0.08 ± 0.01	182 ± 7	0.08 ± 0.01	-27 ± 1	56	6 ± 0	70 ± 1	2.1 ± 0.1
BRP-201 precipitates	336 ± 79	0.23 ± 0.15	317 ± 44	0.18 ± 0.09	-23 ± 2	—	—	—	—

d_H (Z-average), PDI and zeta-potential (ζ) measured by DLS and ELS, where *n* represents number of batches (PLGA and Ace-DEX *n* = 8; Rho-labeled NPs *n* = 3; BRP-201 precipitates *n* = 5); EE and LC determined by UV–VIS spectroscopy (*n* = 9)

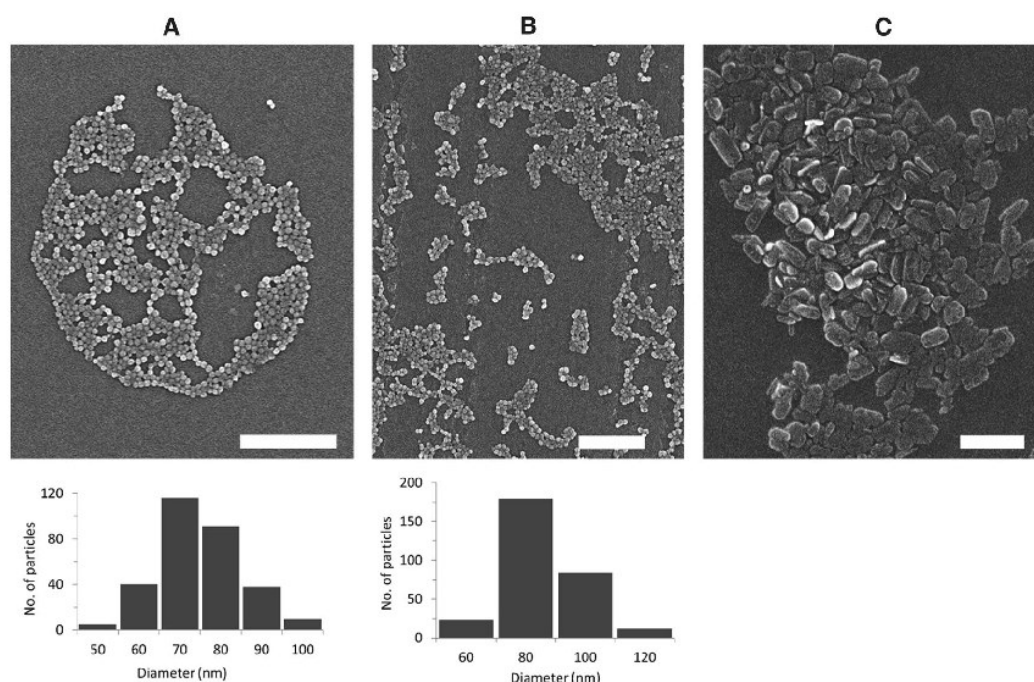


Fig. 1 Scanning electron micrographs of the NPs: Ace-DEX (A), Ace-DEX[BRP-201] (B), and BRP-201 precipitates (C). Histograms were generated from ImageJ measurements ($n=300$). The scale bars are 1 μm

spectroscopic quantification, the amount of BRP-201 in 1 mL of NPs dissolved in DMSO was around 318 μM for PLGA[BRP-201] and 139 μM for Ace-DEX[BRP-201] for NPs prepared with 3% ($w w^{-1}$) drug. Meanwhile, NPs prepared with 10% ($w w^{-1}$) drug contained on average 1.3 mM BRP-201 in 1 mL of NPs dissolved in DMSO. Considering that the IC_{50} of BRP-201 for inhibition of FLAP and mPGES-1 are 0.04 and 0.42 μM , respectively, stable NP dispersions with drug concentration of several hundred- to thousand-folds higher compared to the drugs' IC_{50} values were achieved. This is important for the biodistribution of the NPs in vivo since in general less than 15% of the injected dose of NPs reaches the intended target [29–31]. In addition, administering high doses of NPs reduces liver clearance and prolongs the circulation of NPs, since high doses of NPs overwhelm the receptors of Kupffer cells in the liver [32].

The amount of residual PVA was found to be on average 10% ($w w^{-1}$) in all NP dispersions, with the exception of the dye-labeled PLGA NPs, which retained 15 to 18% ($w w^{-1}$) of residual surfactant (Table 1). A higher amount of residual PVA was observed for NPs with 10% ($w w^{-1}$) BRP-201 (SI Table S3), since here the initial polymer concentration fed in the formulation was threefold higher when compared to the NPs with 3% ($w w^{-1}$) BRP-201 (Table 1). Note that surfactants are necessary to preserve the stability of the NPs, however, excess amounts should be removed

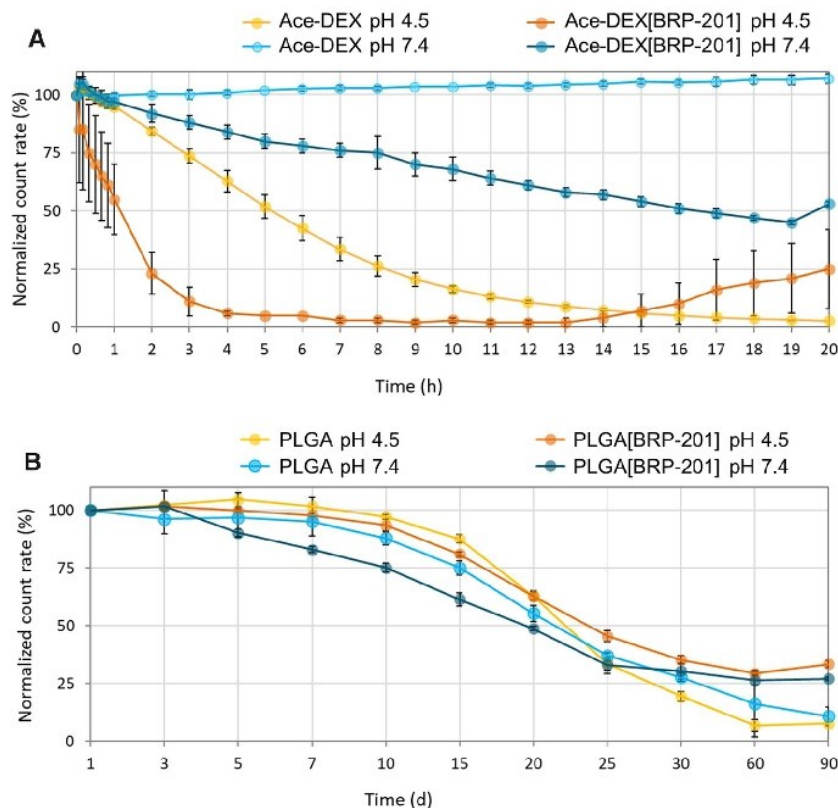
from the dispersion to diminish their influence on the NP cellular uptake processes [33].

Degradation of nanoparticles

The NP degradation behavior was studied in acetate (pH 4.5) and phosphate buffer (pH 7.4), both at 37 $^{\circ}\text{C}$. The count rate in DLS corresponds to the size and number of particles scattering the laser beam, i.e. a high count rate indicates numerous NPs scattering that light [34]. A decreasing count rate over time at fixed scattering detector conditions indicates the degradation of the NPs due to a decreasing size and/or their number [15].

Figure 2A shows that for Ace-DEX[BRP-201] NPs the count-rate decreased by about 50% after 50 min when incubated at pH 4.5, whereas at pH 7.4, the count-rate decreased by 50% of the NPs after approx. 20 h. Furthermore, the drug-loaded Ace-DEX NPs apparently degraded faster than their unloaded counterparts, regardless of the medium pH value, suggesting that BRP-201 may accelerate erosion of the NPs. The results further imply that at low pH, Ace-DEX NPs presumably show higher apparent erosion, which is observed first with an immediate increase in the size and PDI of the NPs (SI, Fig. S4, A and B). This could indicate aggregation of the NPs, occurring due to the fast hydrolysis of the acyclic

Fig. 2 Apparent decrease in count rates of PLGA and Ace-DEX NPs at 37 °C incubated in 0.05 mM acetate buffer (pH 4.5) and 0.05 mM phosphate buffer (pH 7.4), as measured by DLS at fixed scattering detector settings ($n=3$). The derived count rate on DLS was measured at pre-determined times, and plotted as normalized value against the derived count rate at timepoint 0 of incubation with buffer solution



acetals at their surfaces, followed by a further degradation towards the interior of NPs proceeding mainly from the slower hydrolysis of the cyclic acetals. The relatively fast degradation initiated by the cleavage of acetal groups is similar to polyketal-based polymers [14, 35]. In addition, the apparent erosion of the Ace-DEX NPs is faster under acidic conditions than at neutral pH value, indicated by a progressive decrease in the size of NPs (SI, Fig. S4, A), where after 20 h the size of the NPs decreased by about 40 nm for Ace-DEX[BRP-201].

On the other side, PLGA NPs followed a sigmoidal progression of count-rate decreases, typical for polyester-based polymers (Fig. 2B) [36, 37]. A 50% decrease in the count rate of the PLGA[BRP-201] NPs was observed between day 20 and 25 of incubations at both pH 4.5 and 7.4 (Fig. 2B). However, it should be noted that endogenous enzymes (esterases) or other solution components *in vitro* and *in vivo* could accelerate the degradation of PLGA, and hence its degradation rate could be faster than that observed in a buffer-only medium [38]. NPs labeled with Rhodamine B showed similar apparent degradation profiles as the non-labeled particles (SI, Figs. S5 and S6).

Drug release from the NPs

Ace-DEX[BRP-201] and PLGA[BRP-201] NPs were investigated via sedimentation velocity experiments with an AUC, using multi-detection for the observation of the apparent NP erosion processes and drug behavior (via RI detection and absorbance detection) [39, 40]. Ace-DEX[BRP-201] NPs were studied on a timescale between 0.5 and 144 h (Fig. 3, Figs. S9 and S10 in the SI). The sedimentation velocity experiments enable analytical tracking of sedimenting material according to its size in the centrifugal field. Thereby, material successively moves from the meniscus to the cell bottom at increased timescales captured with every scan by the detection modules (Fig. 3A). From these time- and radially-resolved sedimentation profiles, the differential distributions of sedimentation coefficients can be obtained, representative of the population of sedimenting material and its amount. The differential distribution of sedimentation coefficients, $ls-g^*(s)$, of the Ace-DEX[BRP-201] NPs in water (control) displayed the highest signal intensity in both detection mode (Fig. 3B and Fig. S9 (top)). The samples investigated at pH 4.5 and pH 7.4 showed differential distributions of sedimentation coefficients with lower intensities at increased timescales. Ace-DEX[BRP-201] NPs incubated for 144 h at pH 4.5

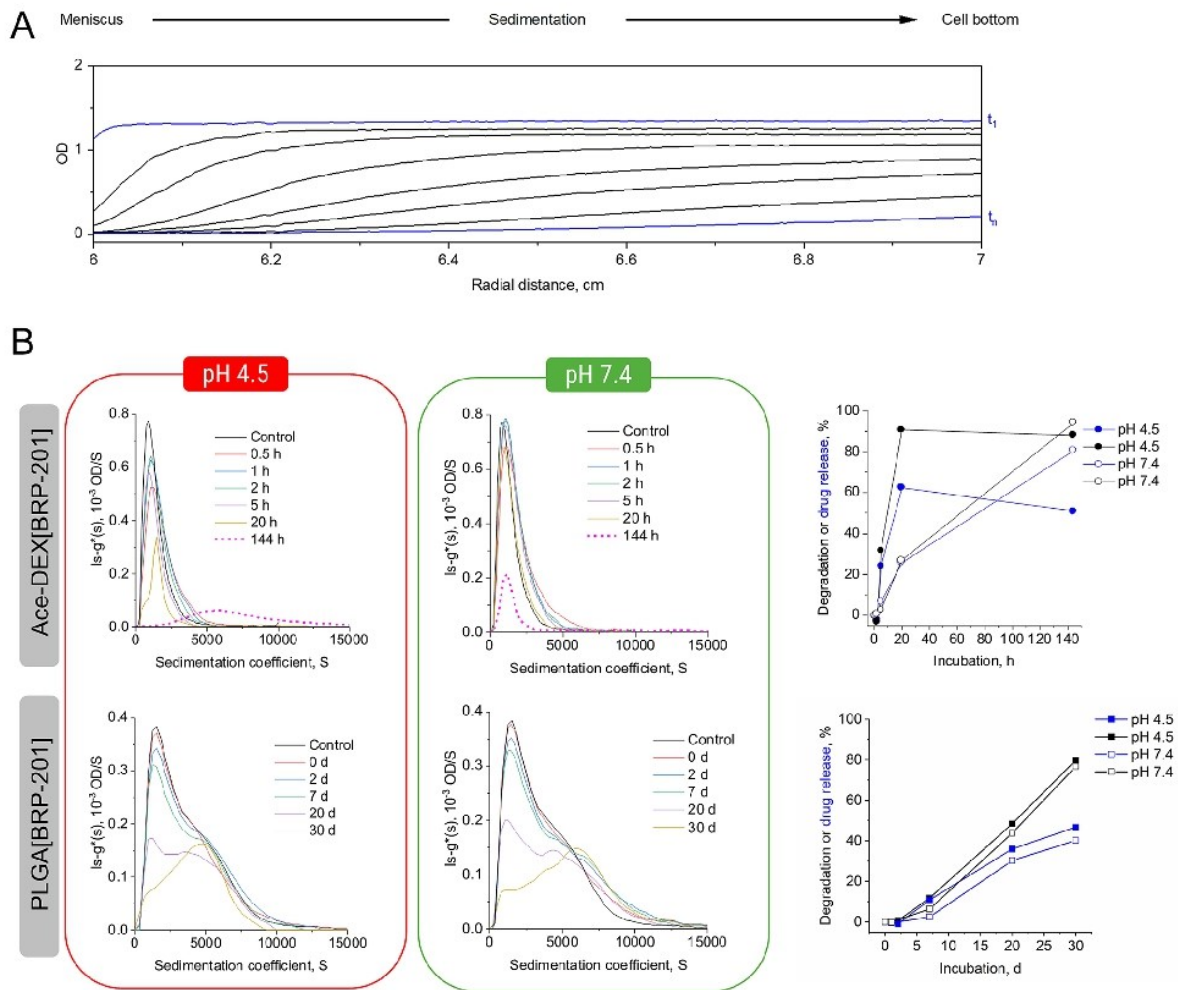


Fig. 3 **A** Selected sedimentation velocity profiles observed via absorbance detection at $\lambda=316$ nm (in terms of OD) of Ace-DEX[BRP-201] NPs incubated for 0.5 h at pH 4.5 and 37 °C with an early scan, t_1 , and a late scan, t_n , highlighted in blue. **B** Differential distributions of sedimentation coefficients, $ls-g^*(s)$, from sedimentation analysis of sedimentation velocity experiments at a rotor speed of 1500 rpm, observed via absorbance detection at $\lambda=316$ nm (in terms of OD) of the NPs after incubation in 0.05 mM acetate buffer (pH 4.5) (left), and 0.05 mM phosphate buffer (pH 7.4) (mid-

dle) at 37 °C; the control refers to drug-loaded NPs in water stored at 4 °C prior to the measurement. (Right) Apparent NP degradation and/or drug release was determined from the RI and UV signal intensities (in terms of integrated areas under the differential distribution curves), respectively, at pH 4.5 and pH 7.4. The values were calculated by normalization of areas under the curve from each time at measurement against the recorded areas under the curves from the NPs incubated for 0.5 h only

showed a distinct distribution of higher sedimentation coefficients, which indicates the presence of a distinct population of species (Fig. 3B, left), apparently absent at pH 7.4 (Fig. 3B, right). However, this distinct population at higher sedimentation coefficients was not seen that significant with the RI detection (SI, Fig. S9). Thus, the larger population of species that were only observed with the absorbance detection hint toward the formation of nanoprecipitates of poorly soluble BRP-201 after the complete NP erosion at pH 4.5.

Based on areas calculated from the differential distributions of sedimentation coefficients obtained from the absorbance detection in terms of OD, a time-dependent drug release from Ace-DEX[BRP-201] NPs at both pH values was clearly evident (Fig. 3B, right). Ace-DEX[BRP-201] NPs incubated at pH 4.5 released the encapsulated drug faster than at pH 7.4. After 5 h, the NPs released more than 20% of drug at pH 4.5, and less than 10% at pH 7.4. After 20 h, the NPs released about 60% of the drug at pH 4.5,

whereas at pH 7.4 only about 25% of the drug was released (Fig. 3B, right).

Investigations of PLGA[BRP-201] NPs revealed similar features of the differential distributions of sedimentation coefficients, $ls-g^*(s)$, from the absorbance detection (in terms of OD) and RI detection for samples mixed with buffer of pH 4.5 and pH 7.4 (solutions were primarily heated to 37 °C) immediately before the measurement (Fig. 3B left and middle (bottom); SI Fig. S9 (bottom)). The differential distributions of sedimentation coefficients based on absorbance detection clearly exposed a shoulder toward higher sedimentation coefficients becoming more evident and ultimately dominating the distribution after 30 days of incubation at both pH values (Fig. 3B, left and middle (bottom)). This shoulder indicates an abundance of larger species unveiled by active separation of the species in the AUC. In comparison to the results from the absorbance detection, the RI detection revealed a similar decrease of the signal intensity with increased incubation times regardless of the pH values, with a barely visible shoulder toward larger sedimentation coefficients, even after 30 days of incubation (SI, Fig. S19, left and middle (bottom)). This could be explained by the less sensitive RI detection when compared to the absorbance detection when considering the drug nanoprecipitates. The same BRP-201 nanoprecipitates were also observed in the SEM and indicated by the NTA as well (vide supra). Apparently, the drug tends to form nanosized objects in solution that are not encapsulated within the polymeric matrix (particularly forming during erosion). Those species have a distribution of sedimentation coefficients exceeding those of the NPs as seen by the other analytical techniques as well. The degradation, as well as the drug release appeared slightly faster for NPs incubated at pH 4.5, as was similarly observed for Ace-DEX[BRP-201] NPs (Fig. 3B, right). However, here the degradation and drug release started after approx. 7 days of incubation and reached approx. 50% apparent degradation and 30% drug release after 20 days of incubation at both pH values.

The derived apparent degradation data obtained from the AUC where also in accordance with the count-rate DLS data (representative of apparent degradation) at the same chosen timescales for both types of NPs (SI, Fig. S10). Nicely, the vastly different timescales (hours and days) for a decrease of count rates is mirrored with the sedimentation velocity AUC data (Fig. 3B, right). Further investigations performed at higher centrifugal speeds revealed the presence of smaller species in the supernatant that corresponded to the PVA surfactant (used in the formulation process), also showing a response faster for acetate buffer at pH 4.5 than for phosphate buffer at pH 7.4 for the Ace-DEX[BRP-201] NPs (SI, Fig. S11 (top)) while appearing less pronounced for the PLGA[BRP-201] NPs (SI, Fig. S11 (bottom)). After 144 h of incubation, the signal intensity of PVA increased

by approx. threefold for Ace-DEX[BRP-201] at both pH conditions, while simultaneously, the RI intensities of the NPs decreased by approx. tenfold at pH 4.5 and 18-fold at pH 7.4 (SI, Fig. S12, A). Similar trends were observed for PLGA-based NPs (SI, Fig. S12, B), and also for other medical NPs [40].

Chemical elucidation of nanoparticles via Raman spectroscopy

Raman spectroscopy was employed to investigate the chemical properties of individual formulations, and in particular, to investigate if free drug is present as precipitates in the Ace-DEX[BRP-201] and PLGA[BRP-201] formulations. The Raman mean spectra of the two polymers and the drug (Fig. 4) revealed characteristic structural features of the substances. For BRP-201, the most prominent Raman band was at 1620 cm^{-1} , which can be assigned to the C=N vibration in the benzimidazole ring, and was not overlapping with Ace-DEX (C-H deformation band around 1450 cm^{-1}) and PLGA (C=O stretching vibration at 1760 cm^{-1}) bands. Thus, it was used to visualize the relative abundance of the drug in the NPs. The false color Raman image of the PLGA[BRP-201] formulation (Fig. 4D) showed a non-homogeneous distribution of PLGA and BRP-201, where distinct regions with high abundance of BRP-201 were observed (green regions in Fig. 4D, and light grey Raman spectrum in 4E). The size of the regions in the false color Raman image was in the range of the spatial resolution limit, which means that indicated features must be 300 nm or smaller. Other regions were rich in PLGA and showed only a low BRP-201 content (blue regions in Fig. 4D, and dark grey Raman spectrum in 4E). For Ace-DEX[BRP-201] formulations, no such inhomogeneities were observed (Fig. 4B). Here, the drug and polymer were relatively equally distributed as noted from the small range in the false color intensity scale (Fig. 4B), and from the Raman spectra (Fig. 4C).

Furthermore, suspensions of Ace-DEX[BRP-201] NPs were incubated for 48 h at either pH 4.5 or pH 7.4, and subsequently samples were prepared by drop coating and analyzed. Only few larger accumulations of solid particles were found in the dried samples (bright field images, SI Fig. S7). Raman spectra of the dried NP samples (SI, Fig. S8) showed almost exclusively spectral contributions from BRP-201 at different concentrations. Spectral signals from Ace-DEX were not visible in the analyzed sample region. These results confirm that after 48 h, Ace-DEX[BRP-201] NPs were completely degraded, leaving only BRP-201 as detectable material in the Raman spectra.

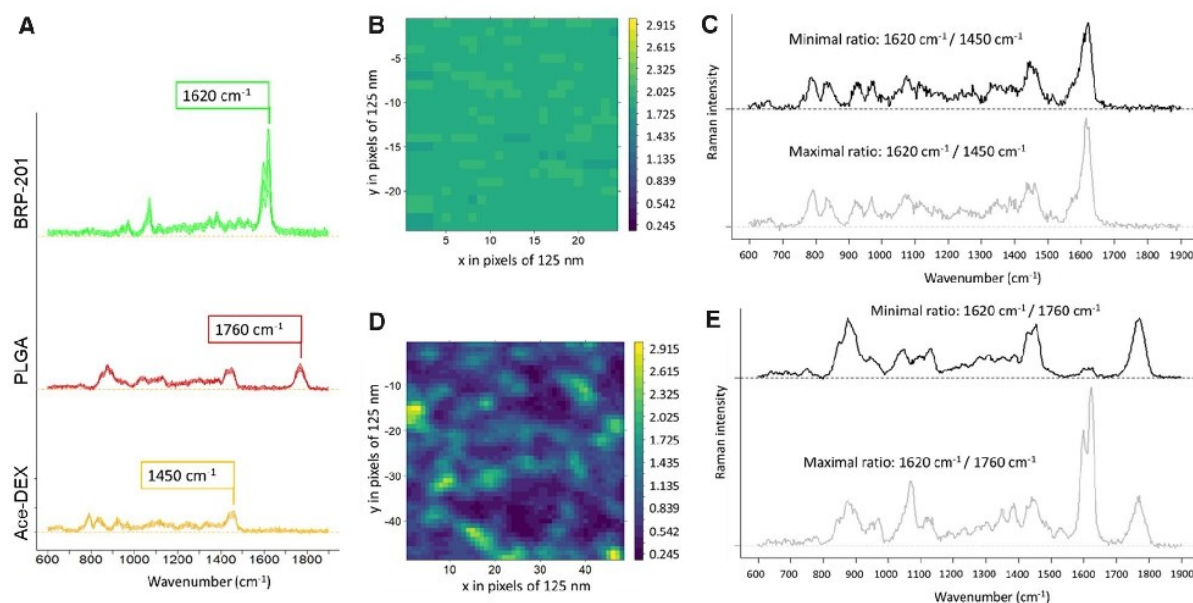


Fig. 4 **A** Mean Raman spectra with standard deviation of pure nano-material: BRP-201 precipitates (green), PLGA NPs (red) and Ace-DEX NPs (yellow); spectra were shifted on the y-axis for clarity; **B**, **D** false color Raman images calculated from the ratio of the Raman intensities at 1620 cm^{-1} (BRP-201) and **B** 1450 cm^{-1} (Ace-DEX)

or **D** 1760 cm^{-1} (PLGA), respectively; the color codes the intensity ratio; axis (x,y) are labeled in pixels that have dimensions of 125 \times 125 nm^2 each; **C**, **E** depict individual Raman spectra representing the extreme ratios from the false color Raman maps in **B** and **D**, respectively

NP uptake in neutrophils

Neutrophils are a major source for inflammatory lipid mediator (LM) production in the blood stream and were evaluated for NP uptake. We monitored the uptake of Rhodamine B-labeled NPs over 120 min for MFI measurement (Fig. 5A) and 45 min for imaging using transmission brightfield and confocal fluorescence microscopy (Fig. 5B) for identifying cells and NPs, respectively. Both types of NPs were sufficiently taken up by neutrophils with PLGA NPs being superior to Ace-DEX NPs (Fig. 5). However, the lower MFI of Ace-DEX NPs could also be a result of the faster decomposition inside the cell since the polymer is rapidly degraded at lower pH values. This hypothesis fits to the identical uptake until 60 min, where Ace-DEX NPs start to decompose (Fig. 2A).

Evaluation of free and encapsulated BRP-201 on cell viability in human primary leukocytes

We next analyzed free BRP-201, empty NP, and NPs loaded with BRP-201 for potential cytotoxic effects in human neutrophils and M1-MDM. After 5 h incubation of neutrophils, BRP-201 (1 μM) slightly but not significantly reduced cell viability (trypan blue staining) to 85%, while no detrimental effects on cell viability were detectable for the NPs

(Fig. 6A). Although neutrophils are a suitable cell model to study inhibition of 5-LO product formation, their short half-life hampers the suitability for long term (> 6 h) studies. Therefore, we also used M1-MDM that also generate substantial amounts of 5-LO products, representing relevant target cells with a pro-inflammatory phenotype, with the advantage of being suitable for prolonged incubations (up to 48 h). Using two cell viability assays that address mitochondrial functionality (MTT assay, Fig. 6B) and membrane integrity (LDH-assay, Fig. 6C) we found that in M1-MDM incubated for longer periods (24 h), cytotoxic effects of BRP-201 at 30 μM were obvious, a concentration that is 60- to 80-fold higher than the effective concentration to inhibit LM formation in these cells [4]. When BRP-201 was encapsulated in NPs, this detrimental effect was abolished, implying that the encapsulation of BRP-201 in Ace-DEX and PLGA NPs increases the compatibility of BRP-201.

Inhibition of 5-LO product formation by free and encapsulated BRP-201 in human primary leukocytes

To evaluate the efficiency of BRP-201 as free drug and encapsulated into NPs for inhibition of cellular 5-LO product formation, we first used human neutrophils as primary innate immune cells with high capacities to generate 5-LO

Fig. 5 Uptake of Rhodamine B-labeled NPs in human neutrophils. Neutrophils (2×10^6) were pre-incubated with $1 \mu\text{g mL}^{-1}$ LPS for 30 min or vehicle and then incubated with 0.5 mg mL^{-1} (PLGA-RhoB[BRP-201] or Ace-DEX-RhoB[BRP-201]) NPs for the indicated time points at 37°C . (A) Mean fluorescence intensity (MFI) of NPs in the cell, measured by flow cytometry. (B) Neutrophils (3×10^5) were seeded on coated coverslips. Images were taken on a Zeiss LSM 880 and a Zeiss LSM 980 microscope at 37°C and 5% CO_2 . A nanoparticle-solution was added to a final solution of $25 \mu\text{g mL}^{-1}$ before imaging. The top row represents the z-projected brightfield images of neutrophils, bottom row the single slide confocal fluorescence images of Rhodamine B emission of NPs, highlighting cellular NP uptake. Scale bars = $10 \mu\text{m}$.

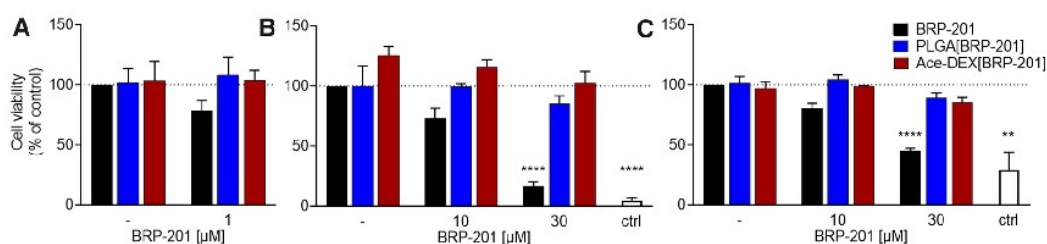
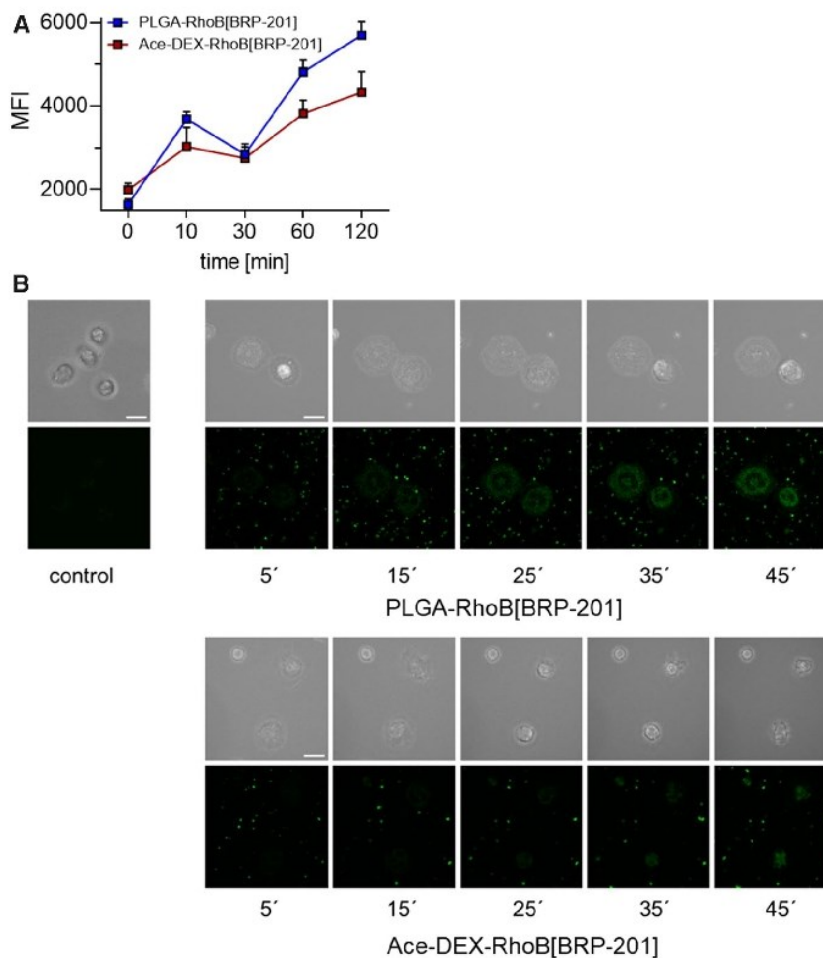


Fig. 6 Cytotoxicity analysis. (A) Neutrophils resuspended in PBS pH 7.4 containing 0.1% glucose were incubated with vehicle (“-”), BRP-201, empty NPs (“-”) or NPs loaded with BRP-201 for 5 h at 37°C . Then, cell viability was assessed by trypan blue staining with a ViCell XR device (Beckman Coulter). (B, C) M1-MDM in RPMI 1640 medium were incubated with vehicle, control ($3 \mu\text{M}$ staurosporine),

BRP-201, empty NPs or NPs loaded with BRP-201 for 24 h at 37°C and cell viability was assessed using MTT assay (B) or LDH release assay (C). Values are given as percentage of control (DMSO), data are means \pm S.E.M., $n=3$. For Statistics a one-way ANOVA and Tukey’s multiple comparisons test were performed

products involving FLAP [41]. Freshly isolated neutrophils were pre-incubated with the test items for various periods (i.e., 15 min, 1 h, 2 h, and 5 h) and then stimulated for FLAP-dependent 5-LO product formation using $2.5 \mu\text{M}$

A23187 for 10 min. When BRP-201 as well as drug-loaded NPs (PLGA and Ace-DEX) were pre-incubated for short periods (i.e., 15 min up to 2 h), the potency of free and of encapsulated BRP-201 was comparable with $> 80\%$

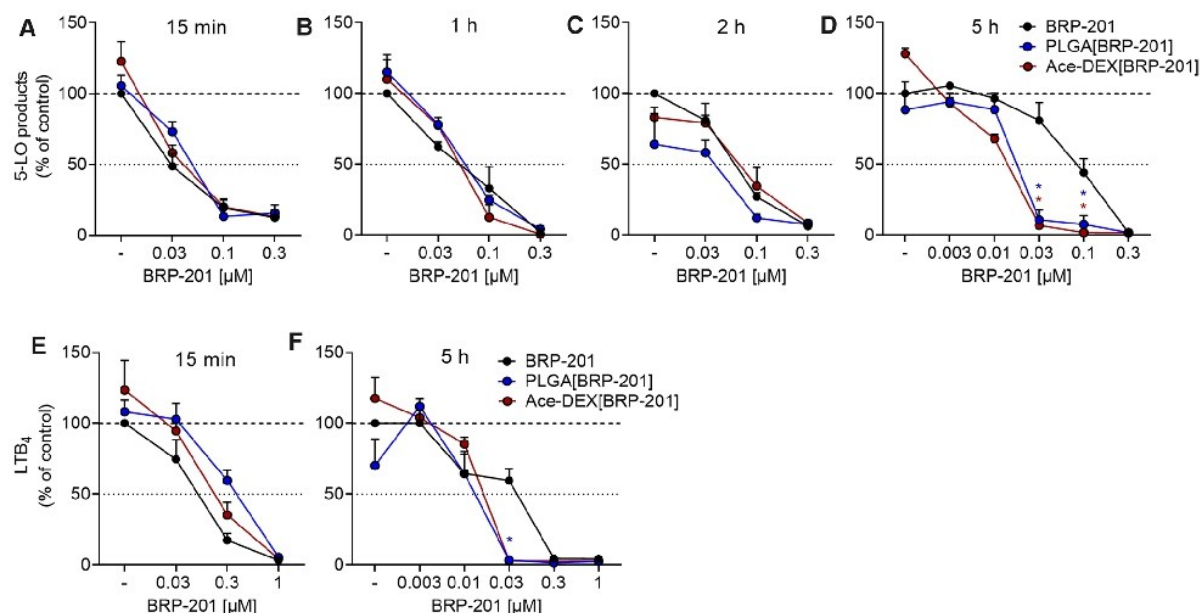


Fig. 7 Inhibition of 5-LO product formation by free and encapsulated BRP-201 in isolated leukocytes. **A–D** Neutrophils were pre-incubated with vehicle, BRP-201 or BRP-201-loaded NP made from PLGA or Ace-DEX for 15 min (**A**), 1 h (**B**), 2 h (**C**) or 5 h (**D**) at 37 °C and then stimulated with 2.5 μM A23187. After 10 min, the reaction was stopped, and 5-LO products were extracted via solid phase extraction (SPE) and analyzed with HPLC. Values are given as 5-LO products (LTB₄, trans-LTB₄ and 5-HETE) in percentage of control (vehicle,

DMSO=100%). **E, F** M1-MDM were pre-incubated with vehicle, BRP-201 or BRP-201-loaded NP made from PLGA or Ace-DEX for 15 min **E** or 5 h **F** at 37 °C and then stimulated with 0.1% *S. aureus*-conditioned medium (SACM). After 3 h at 37 °C, the reaction was stopped and LTB₄ was analyzed by UPLC–MS–MS. Values are given as percentage of the vehicle control. Data are means ± S.E.M., *n* = 3. For statistical analysis, two-way ANOVA and multiple *t* tests were performed

inhibition of 5-LO product formation at 0.1 μM and IC₅₀ values of approx. 30 nM (Fig. 7A–C). However, after 5 h preincubation, encapsulated BRP-201 in NPs was more efficient versus the free drug. Thus, at 30 nM, corresponding to the IC₅₀ of free BRP-201 under standard assay conditions in neutrophils [4], 5-LO product formation is potently reduced by Ace-DEX[BRP-201] or PLGA[BRP-201] down to 6 ± 4% and 11 ± 7% remaining activity, while free BRP-201 was much less potent and 81 ± 21% 5-LO product formation still remained (Fig. 7D); the IC₅₀ values for free BRP-201, Ace-DEX[BRP-201] and PLGA[BRP-201] after 5 h preincubation were 86, 13, and 18 nM. These data indicate that BRP-201 loses potency during prolonged (> 2 h) preincubation of neutrophils. However, potent inhibition of 5-LO product formation by BRP-201 is achieved and maintained in neutrophils over time due to encapsulation of the drug in Ace-DEX- and PLGA-based NPs.

Next, we performed experiments with pro-inflammatory M1-MDM stimulated with 0.1% *S. aureus*-conditioned medium (SACM) to induce 5-LO product formation within 3 h, according to [42]. In analogy to A23187-activated neutrophils, the results with M1-MDM confirmed the beneficial effect of BRP-201 encapsulation in NPs versus free drug

on 5-LO product formation after long-term incubation. Thus, after 5 h of preincubation, the amount of LTB₄ was reduced by 30 nM encapsulated BRP-201 down to 4 ± 0.8% for Ace-DEX[BRP-201] and 3 ± 0.7% for PLGA[BRP-201] NPs while free BRP-201 impaired LTB₄ formation only to 59 ± 8.3% (Fig. 7F). In contrast, preincubation of M1-MDM with Ace-DEX[BRP-201] or PLGA[BRP-201] NPs for only 15 min was slightly less efficient to inhibit 5-LO product formation versus the free drug (Fig. 7E), possibly due to retarded supply of BRP-201 from NPs into the cells.

Inhibition of 5-LO product formation by BRP-201 and NPs in human whole blood

One critical issue of FLAP as target for anti-inflammatory therapy is the need of rather lipophilic antagonists that compete with AA for binding to FLAP [43–45]. Due to these structural requirements most FLAP inhibitors display strong unspecific protein and membrane binding with overall poor bioavailability in more complex experimental settings such as whole blood, where excess of plasma protein as well as non-targeted cells (e.g. platelets, erythrocytes) are present and impair the efficiency of the compound. Thus, we tested the potency of free and encapsulated BRP-201 under

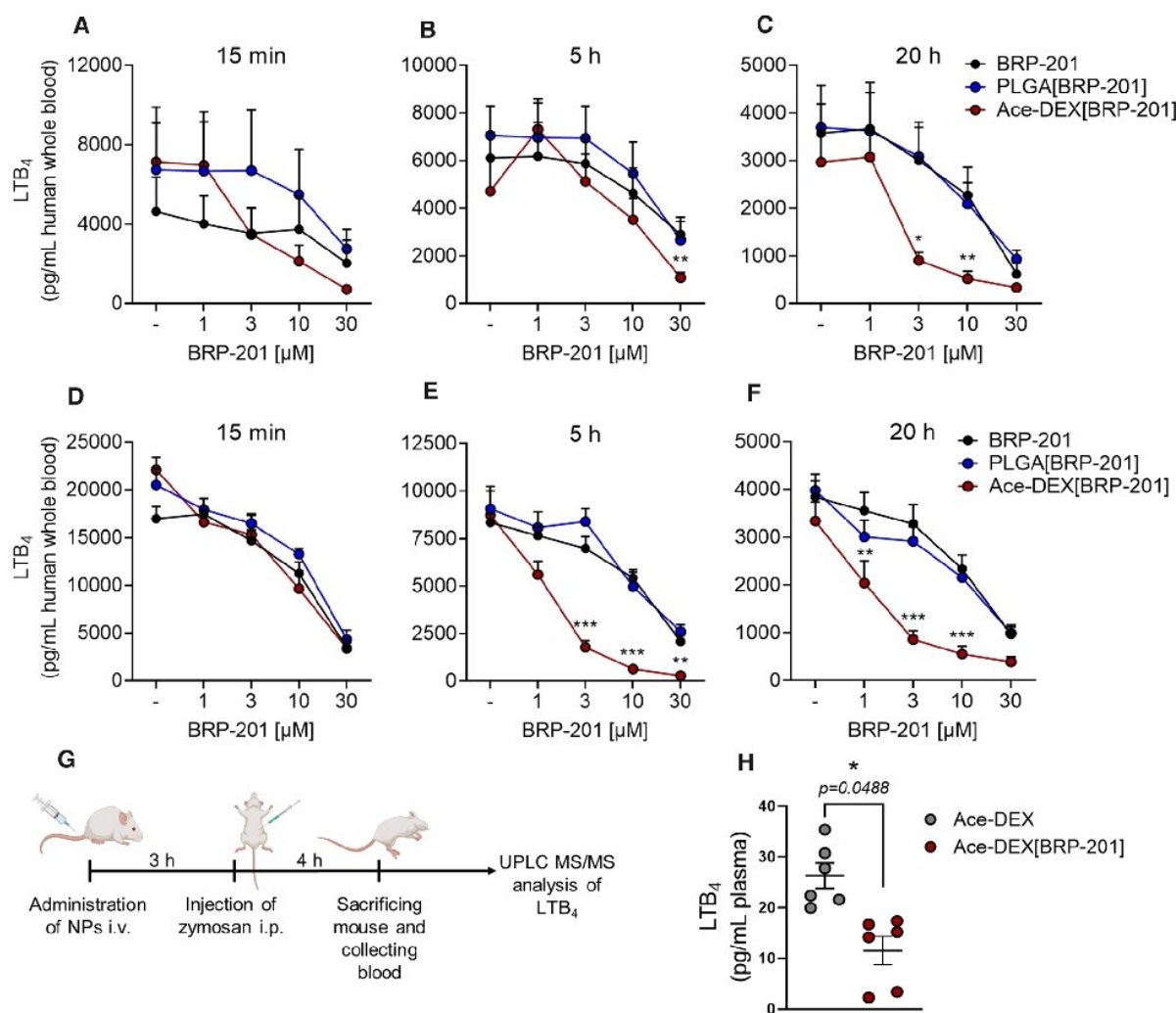


Fig. 8 Efficient inhibition of LTB₄ production by encapsulated BRP-201 in human whole blood and in blood of mice in vivo. **A–C** Freshly withdrawn blood was pre-incubated with vehicle, BRP-201, empty NPs or NPs loaded with BRP-201 for **A** 15 min, **B** 5 h or **C** 20 h prior to stimulation with *E. coli* (O6:K2:H1; 10⁹ bacteria per 1 mL blood) for 3 h at 37 °C. **D–F** Freshly withdrawn blood was first pre-treated with 100 ng mL⁻¹ LPS for 24 h and then pre-incubated with vehicle, BRP-201, empty NPs or NPs loaded with BRP-201 for **D** 15 min, **E** 5 h or **F** 20 h prior to stimulation with *E. coli* (O6:K2:H1; 10⁹ bacteria per 1 mL blood) for 3 h at 37 °C. The incubations were terminated

by addition of 2 mL ice-cold methanol and samples were analyzed for LTB₄ by UPLC–MS–MS as described. Data are means \pm S.E.M., $n=6$. **G** Timeline of mouse experiments. **H** Mice ($n=6$) received empty NPs or NPs loaded with BRP-201 by i.v. injection into the tail vein, 3 h prior zymosan administration (i.p.). After another 4 h, blood was collected by intracardiac puncture and plasma was prepared. LTB₄ was extracted from plasma by SPE and analyzed via UPLC MS–MS. For statistics, a two-way ANOVA, multiple t-tests and a ratio paired t-test were performed, $n=6$

varying preincubation periods (15 min, 5 h and 20 h) in *E. coli*-exposed human whole blood, where neutrophils and monocytes are the major sources for LT formation. Compared to the high potency of BRP-201 in isolated neutrophils resuspended in PBS pH 7.4 ($IC_{50}=0.03 \pm 0.013 \mu$ M), the compound significantly lost efficiency in whole blood with $IC_{50}=14.7 \pm 3.8 \mu$ M at 15 min and $10.4 \pm 2.1 \mu$ M at 20 h pre-incubation (Fig. 8). However, when encapsulated

into Ace-DEX, the potency of BRP-201 was improved about fivefold with an $IC_{50}=2.8 \pm 0.5 \mu$ M, in particular after prolonged (20 h) preincubation periods (Fig. 8C), while pre-treatment for 15 min (Fig. 8A) or 5 h (Fig. 8B) was less effective ($IC_{50}=4.2 \pm 0.9$ and $8.2 \pm 2.1 \mu$ M). In contrast, encapsulation of BRP-201 into PLGA did not significantly enhance its potency (Fig. 8A–C).

Next, we aimed at creating a pro-inflammatory environment within the whole blood incubations by pre-treatment of the blood with LPS for 24 h prior to addition of the free drug or drug-loaded NPs for various pre-incubation periods (15 min, 5 h and 20 h) and subsequent stimulation by addition of *E. coli* for another 3 h. Under these experimental conditions the LT-producing neutrophils and monocytes become activated by LPS similarly like at inflammatory sites. Again, free BRP-201 moderately suppressed LT formation, comparable as in the absence of LPS and independent of the preincubation period, with IC_{50} values in the range of 10–18 μM (Fig. 8D). But when the LPS-treated blood was pre-preincubated with Ace-DEX[BRP-201] NPs for 5 or 20 h, the efficiency of BRP-201 to inhibit LT formation strongly improved by about a factor of 10 ($IC_{50} = 1.6 \pm 0.3$ and 1.9 ± 0.4 μM , respectively), and was even superior as compared to blood devoid of LPS exposure (Fig. 8E and F). For example, while 20 h preincubation with 1 μM reduced LTB_4 formation down to $86 \pm 9\%$ in the absence of LPS, in LPS-treated blood the LTB_4 production was lowered down to $51 \pm 9\%$ (Fig. 8F).

Finally, we injected Ace-DEX[BRP-201] NPs *i.v.* via the tail vein of mice to test if encapsulated BRP-201 could suppress LTB_4 production in blood *in vivo*. Mice received a suspension of 46 mg kg^{-1} Ace-DEX[BRP-201] NPs, which corresponds to a dose of 4.6 mg kg^{-1} BRP-201, or 46 mg kg^{-1} empty Ace-DEX NPs without BRP-201. After 3 h, zymosan was injected (*i.p.*) in order to induce an inflammatory condition with increased LTB_4 formation in the blood, which was analyzed after another 4 h by UPLC-MS-MS (Fig. 8G). As can be seen from Fig. 8H, Ace-DEX[BRP-201] NPs significantly impaired the levels of LTB_4 as compared to empty Ace-DEX NPs devoid of drug, supporting the *in vivo* delivery performance of the formulation following *i.v.* injection.

Conclusion

This study was designed to improve the bioactivity of BRP-201, a potent FLAP antagonist that, however, loses potency in human blood when compared to isolated leukocytes—a common feature of almost all FLAP antagonists [43–45]. Such loss of efficiency of BRP-201 and other FLAP inhibitors in blood have been attributed to unspecific but strong plasma protein or cell membrane binding with consequently low efficacy in *in vivo* experiments and subsequent clinical trials [44, 45]. To tackle this problem, we used PLGA and Ace-DEX as biocompatible polymers to encapsulate BRP-201 into biodegradable NPs to mitigate plasma protein binding, and thus, to improve drug delivery to FLAP in the target cells within the blood. We optimized the NPs and comprehensively characterized their physicochemical properties, thus supporting the beneficial features of the

final formulations. In general, we found that the encapsulation of BRP-201 was more promising in Ace-DEX NPs than PLGA NPs, which was due to the formation of drug precipitates in PLGA NPs as indicated by SEM, AUC, and Raman mapping. Thus, Ace-DEX NPs present a more homogenous formulation than PLGA NPs with the desirable feature of achieving a fast release of BRP-201. The design of the NP carriers has also implications for inflammatory cell models, *i.e.*, BRP-201 loaded in Ace-DEX but not in PLGA was able to potently suppress LT formation in human whole blood, although both Ace-DEX[BRP-201] NPs and PLGA[BRP-201] NPs caused more potent inhibition of 5-LO product formation in isolated neutrophils and M1-MDM after prolonged pre-incubation *versus* the free drug, without any significant differences between the two polymers. Of interest, in addition to enhancing the LT-inhibitory potency, encapsulation of BRP-201 lowers cytotoxic effects after prolonged incubations with MDM. Under conditions where monocytes and neutrophils are activated by LPS to mimic an inflammatory environment, such as at sites of inflammation, the potency of Ace-DEX[BRP-201] NPs in blood is even further improved. In fact, when given *i.v.* to mice that were challenged with zymosan to induce an inflammatory reaction, Ace-DEX[BRP-201] NPs significantly lowered the LTB_4 levels in blood *in vivo*, supporting the feasibility of our approach and its benefit in anti-inflammatory therapy. In summary, we designed polymer-based nanoformulations of BRP-201, which have been characterized in detail for their physicochemical properties, drug loading and release, cytotoxicity, cellular uptake and desired bioactivity, eventually overcoming the detrimental challenges in the development of FLAP antagonists. Further optimization for scaling-up the batches beyond the laboratory bench may provide sufficient material for more advanced studies related to drug testing in preclinical and clinical settings.

Supplementary Information The online version contains supplementary material available at <https://doi.org/10.1007/s00018-021-04039-7>.

Acknowledgements The authors also acknowledge Johannes Max, Yves Carstensen and Friederike Richter for their support with preliminary screening of the NPs with SAXS, WAXS, and CLSM. Bärbel Beringer-Siemers is acknowledged for support with additional PVA measurements, Yasaman Pourdakheli for support with DLS measurements, and the veterinarian Dr. Antonio Baiano for animal care assistance.

Author contributions CK, BS, PMJ, DS, GC, SS, FG and RB performed the experiments. CK and BS wrote the manuscript. PK synthesized Ace-Dex. EB synthesized and investigated BRP-201. IN, SH, and UN supervised NP characterization. CE supervised imaging. RB and AR performed animal experiments. AV, SS, IN, and OW made critical revision and corrected the manuscript. AV, SS, CE, USS and OW designed the research and supervised the work. All authors read and approved the final manuscript.

Funding Open Access funding enabled and organized by Projekt DEAL. This work was supported by the Deutsche Forschungsgemeinschaft (DFG), Collaborative Research Center SFB 1278 “PolyTarget” (project number 316213987, projects A04, C01, C05, and Z01). The SEM facilities of the Jena Center for Soft Matter (JCSM) were also established with a grant from the German Science Foundation. This work was as well supported by the “Thüringer Aufbaubank (TAB)” and the “Europäischer Fonds für regionale Entwicklung (EFRE)” (2018FGI0025) for funding analytical ultracentrifugation facilities at the JCSM. The LSM880 ELYRA PS.1 was funded with a grant from the DFG. G.C. acknowledges support from the Free State of Thuringia and the European Social Fund (2019SD0129).

Availability of data and materials The datasets used and/or analyzed during the current study are available from the corresponding authors on reasonable request.

Code availability Not applicable.

Declarations

Conflict of interest The authors declare that they have no conflicts of interest and/or competing interests.

Ethical approval The experimental protocol for blood isolation and whole blood experiments were approved by the ethical committee of the University Hospital Jena (No. 5050-01/17). All methods were performed in accordance with the relevant guidelines and regulations.

Consent to participate The participants provided written informed consent and agreed on publication of the data. The experimental procedures of animal experiments were approved by the Italian Ministry and carried out in accordance with the EU Directive 2010/63/EU and the Italian DL 26/2014 for animal experiments and in compliance with the ARRIVE guidelines and Basel declaration including the 3R concept.

Open Access This article is licensed under a Creative Commons Attribution 4.0 International License, which permits use, sharing, adaptation, distribution and reproduction in any medium or format, as long as you give appropriate credit to the original author(s) and the source, provide a link to the Creative Commons licence, and indicate if changes were made. The images or other third party material in this article are included in the article's Creative Commons licence, unless indicated otherwise in a credit line to the material. If material is not included in the article's Creative Commons licence and your intended use is not permitted by statutory regulation or exceeds the permitted use, you will need to obtain permission directly from the copyright holder. To view a copy of this licence, visit <http://creativecommons.org/licenses/by/4.0/>.

References

- Koerberle A, Werz O (2018) Natural products as inhibitors of prostaglandin E2 and pro-inflammatory 5-lipoxygenase-derived lipid mediator biosynthesis. *Biotechnol Adv Elsevier* 36:1709–1723
- Rådmark O, Werz O, Steinhilber D, Samuelsson B (2015) 5-Lipoxygenase, a key enzyme for leukotriene biosynthesis in health and disease. *Biochim Biophys Acta Mol Cell Biol Lipids* 1851:331–9
- Samuelsson B, Morgenstern R, Jakobsson P (2007) Membrane prostaglandin E synthase-1: A Novel. *Pharmacol Rev* 59:207–224
- Gür ZT, Çalışkan B, Garscha UI, Olgaç A, Schubert US, Gerstmeier J et al (2018) Identification of multi-target inhibitors of leukotriene and prostaglandin E2 biosynthesis by structural tuning of the FLAP inhibitor BRP-7. *Eur J Med Chem* 150:876–99
- Riendeau D, Aspiotis R, Ethier D, Gareau Y, Grimm EL, Guay J et al (2005) Inhibitors of the inducible microsomal prostaglandin E2 synthase (mPGES-1) derived from MK-886. *Bioorganic Med Chem Lett* 15:3352–3355
- Shkodra-Pula B, Vollrath A, Schubert US, Schubert S (2020) Polymer-based nanoparticles for biomedical applications. In: Wolfgang JP, Feliu N (eds) *Colloids nanobiotechnology Synth Charact potential*, 16th edn. Elsevier, pp 233–252
- Bachelder EM, Pino EN, Ainslie KM (2017) Acetalated dextran: a tunable and acid-labile biopolymer with facile synthesis and a range of applications. *Chem Rev* 117:1915–1926
- Wannasarit S, Wang S, Figueiredo P, Trujillo C, Eburnea F, Simón-Gracia L et al (2019) Antitumor therapeutics: a virus-mimicking pH-responsive acetalated dextran-based membrane-active polymeric nanoparticle for intracellular delivery of antitumor therapeutics. *Adv Funct Mater* 29:1970351
- Volpatti LR, Matranga MA, Cortinas AB, Delcassian D, Daniel KB, Langer R et al (2020) Glucose-responsive nanoparticles for rapid and extended self-regulated insulin delivery. *ACS Nano* 14:488–197
- Lewis SM, Dirksen SR, Heitkemper MM, Bucher L, Harding MM (2014) Pathophysiologic mechanisms of disease. In: Lewis SM, Dirksen SR, Heitkemper MM, Bucher L, Harding MM (eds) *Medical-surgical Nurs Assess Manag Clin Probl*, 9th edn. Elsevier, pp 308–309
- World Health Organization (2019) World health organization model list of essential medicines. *Ment Holist Heal Some Int Perspect* 21:119–134
- Sun G, Mao JJ (2012) Engineering dextran-based scaffolds for drug delivery and tissue repair. *Nanomedicine* 7:1771–84
- Liu Y, Ghassemi AH, Hennink WE, Schwendeman SP (2012) The microclimate pH in poly(D, L-lactide-co-hydroxymethyl glycolide) microspheres during biodegradation. *Biomaterials* 33:7584–7593
- Kauffman KJ, Do C, Sharma S, Gallovic MD, Bachelder EM, Ainslie KM (2012) Synthesis and characterization of acetalated dextran polymer and microparticles with ethanol as a degradation product. *ACS Appl Mater Interfaces* 4:4149–4155
- Shkodra-Pula B, Kretzer C, Jordan PM, Klemm P, Koerberle A, Pretzel D et al (2020) Encapsulation of the dual FLAP/mPGES-1 inhibitor BRP-187 into acetalated dextran and PLGA nanoparticles improves its cellular bioactivity. *J Nanobiotechnology* 18:73
- Spek S, Haeuser M, Schaefer MM, Langer K (2015) Characterisation of PEGylated PLGA nanoparticles comparing the nanoparticle bulk to the particle surface using UV-VIS spectroscopy, SEC, 1H-NMR spectroscopy, and X-ray photoelectron spectroscopy. *Appl Surf Sci* 347:378–385
- Schuck P, Rossmannith P (2000) Determination of the sedimentation coefficient distribution by least-squares boundary modeling. *Biopolymers* 54:328–341
- Werz O, Gerstmeier J, Libreros S, De La Rosa X, Werner M, Norris PC et al (2018) Human macrophages differentially produce specific resolvins or leukotriene signals that depend on bacterial pathogenicity. *Nat Commun* 9:1–12
- Werner M, Jordan PM, Romp E, Czapka A, Rao Z, Kretzer C et al (2019) Targeting biosynthetic networks of the proinflammatory and proresolving lipid metabolome. *FASEB J* 33:6140–6153
- Schindelin J, Arganda-Carreras I, Frise E, Kaynig V, Longair M, Pietzsch T et al (2012) Fiji: an open-source platform for biological-image analysis. *Nat Methods* 9:676–682

21. Rueden CT, Schindelin J, Hiner MC, DeZonia BE, Walter AE, Arena ET et al (2017) ImageJ2: imageJ for the next generation of scientific image data. *BMC Bioinf* 18:1–26
22. Mutterer J, Zinck E (2013) Quick-and-clean article figures with FigureJ. *J Microsc* 252:89–91
23. Werz O, Bürkert E, Samuelsson B, Rådmark O, Steinhilber D (2002) Activation of 5-lipoxygenase by cell stress is calcium independent in human polymorphonuclear leukocytes. *Blood* 99:1044–1052
24. Rossi A, Pergola C, Pace S, Rådmark O, Werz O, Sautebin L (2014) In vivo sex differences in leukotriene biosynthesis in zymosan-induced peritonitis. *Pharmacol Res* 87:1–7
25. Broaders KE, Cohen JA, Beaudette TT, Bachelder EM, Fréchet JMJ (2009) Acetalated dextran is a chemically and biologically tunable material for particulate immunotherapy. *Proc Natl Acad Sci USA* 106:5497–502
26. Brazeau G, Sauberman SL, Gatlin L, Wisniecki P, Shah J (2011) Effect of particle size of parenteral suspensions on in vitro muscle damage. *Pharm Dev Technol* 16:591–598
27. Wong J, Brugger A, Khare A, Chaubal M, Papadopoulos P, Rabinow B et al (2008) Suspensions for intravenous (IV) injection: a review of development, preclinical and clinical aspects. *Adv Drug Deliv Rev* 60:939–54
28. Driscoll DF (2006) Lipid injectable emulsions: pharmacopeial and safety issues. *Pharm Res* 23:1959–1969
29. Wilhelm S, Tavares AJ, Dai Q, Ohta S, Audet J, Dvorak HF et al (2016) Analysis of nanoparticle delivery to tumours. *Nat Rev Mater* 26:1–12
30. Mitchell MJ, Billingsley MM, Haley RM, Wechsler ME, Peppas NA, Langer R (2020) Engineering precision nanoparticles for drug delivery. *Nat Rev Drug Discov* 20:101–24
31. (2019) Targeting for delivery. *Nat Biomed Eng* 3:671–672. <https://doi.org/10.1038/s41551-019-0457-5>
32. Ouyang B, Poon W, Zhang YN, Lin ZP, Kingston BR, Tavares AJ et al (2020) The dose threshold for nanoparticle tumour delivery. *Nat Mater* 19:1362–1371
33. Sahoo SK, Panyam J, Prabha S, Labhasetwar V (2002) Residual polyvinyl alcohol associated with poly (D, L-lactide-co-glycolide) nanoparticles affects their physical properties and cellular uptake. *J Control Release* 82:105–114
34. Malvern Panalytical: Zetasizer Nano User Manual (Man0485-1.1). 2013. p 94
35. Alameda BM, Palmer TC, Sisemore JD, Pierini NG, Patton DL (2019) Hydrolytically degradable poly(β -thioether ester ketal) thermosets: via radical-mediated thiol-ene photopolymerization. *Polym Chem R S Chem* 10:5635–5644
36. Brannigan RP, Dove AP (2017) Synthesis, properties and biomedical applications of hydrolytically degradable materials based on aliphatic polyesters and polycarbonates. *Biomater Sci* 5:9–21
37. Engineer C, Parikh J, Raval A (2010) Hydrolytic degradation behavior of 50/50 poly lactide-co-glycolide from drug eluting stents. *Trends Biomater Artif Organs* 24:131–138
38. Escudero A, Carregal-Romero S, Miguel-Coello AB, Rufz-Cabello J (2020) Engineered polymeric nanovehicles for drug delivery. In: Parak WJ, Feliu N (eds) *Colloids for nanobiotechnology*. Elsevier, pp 201–232
39. Cinar G, Englert C, Schubert US, Nischang I (2020) Salient features of medical nanoparticles in biological fluids from an analytical ultracentrifuge. *Nanoscale* 12:22462
40. Cinar G, Englert C, Lehmann M, Nischang I (2020) In situ, quantitative assessment of multifunctional nanoscale drug delivery systems in human serum. *Anal Chem*. 92:7932
41. Gerstmeier J, Weinigel C, Rummeler S, Rådmark O, Werz O, Garscha U (2016) Time-resolved in situ assembly of the leukotriene-synthetic 5-lipoxygenase/5-lipoxygenase-activating protein complex in blood leukocytes. *FASEB J* 30:276–285
42. Jordan PM, Gerstmeier J, Pace S, Bilancia R, Rao Z, Börner F et al (2020) *Staphylococcus aureus*-derived α -hemolysin evokes generation of specialized pro-resolving mediators promoting inflammation resolution. *Cell Rep*. 33:108247
43. Evans JF, Ferguson AD, Mosley RT, Hutchinson JH (2008) What's all the FLAP about?: 5-lipoxygenase-activating protein inhibitors for inflammatory diseases. *Trends Pharmacol Sci* 29:72–78
44. Gür ZT, Çalıřkan B, Banoglu E (2018) Drug discovery approaches targeting 5-lipoxygenase-activating protein (FLAP) for inhibition of cellular leukotriene biosynthesis. *Eur J Med Chem* 153:34–48
45. Pettersen D, Davidsson Ö, Whatling C (2015) Recent advances for FLAP inhibitors. *Bioorganic Med Chem Lett* 25:2607–2612

Publisher's Note Springer Nature remains neutral with regard to jurisdictional claims in published maps and institutional affiliations.

Authors and Affiliations

Christian Kretzer¹ · Blerina Shkodra^{2,3} · Paul Klemm^{2,3} · Paul M. Jordan¹ · Daniel Schröder⁴ · Gizem Cinar^{2,3} · Antje Vollrath^{2,3} · Stephanie Schubert^{3,5} · Ivo Nischang^{2,3} · Stephanie Hoepfner^{2,3} · Steffi Stumpf^{2,3} · Erden Banoglu⁶ · Frederike Gladigau^{7,8,9} · Rossella Bilancia¹⁰ · Antonietta Rossi¹⁰ · Christian Eggeling^{3,4,7,11} · Ute Neugebauer^{3,7,8,9} · Ulrich S. Schubert^{2,3} · Oliver Werz^{1,3}

¹ Department of Pharmaceutical/Medicinal Chemistry, Institute of Pharmacy, Friedrich Schiller University Jena, Philosophenweg 14, 07743 Jena, Germany

² Laboratory of Organic and Macromolecular Chemistry (IOMC), Friedrich Schiller University Jena, Humboldtstraße 10, 07743 Jena, Germany

³ Jena Center for Soft Matter (JCSM), Friedrich Schiller University Jena, Philosophenweg 7, 07743 Jena, Germany

⁴ Institute of Applied Optics and Biophysics, Friedrich Schiller University Jena, Max-Wien Platz 1, 07743 Jena, Germany

⁵ Department of Pharmaceutical Technology and Biopharmacy, Institute of Pharmacy, Friedrich Schiller University Jena, Lessingstraße 8, 07743 Jena, Germany

⁶ Department of Pharmaceutical Chemistry, Faculty of Pharmacy, Gazi University, Etiler, Yenimahalle, Ankara 06330, Turkey

⁷ Leibniz Institute of Photonic Technology, Albert-Einstein-Straße 9, 07745 Jena, Germany

⁸ Center for Sepsis Control and Care, Jena University Hospital, 07747 Jena, Germany

⁹ Institute of Physical Chemistry and Abbe Center of Photonics, Helmholtzweg 4, 07743 Jena, Germany

¹⁰ Department of Pharmacy, School of Medicine and Surgery, University of Naples Federico II, Via D. Montesano 49, 80131 Naples, Italy

¹¹ MRC Human Immunology Unit, Weatherall Institute of Molecular Medicine, University of Oxford, Headley Way, Oxford OX39DS, UK

Supplementary Materials

Ethoxy acetalated dextran-based nanocarriers accomplish efficient inhibition of leukotriene formation by a novel FLAP antagonist in human leukocytes and blood

Christian Kretzer ^{a,§}, Blerina Shkodra ^{b,c,§}, Paul Klemm ^{b,c}, Paul M. Jordan ^a, Daniel Schröder ^d, Gizem Cinar ^{b,c}, Antje Vollrath ^{b,c}, Stephanie Schubert ^{c,e}, Ivo Nischang ^{b,c}, Stephanie Hoepfner ^{b,c}, Steffi Stumpf ^{b,c}, Erden Banoglu ^f, Frederike Gladigau ^{g,h,i}, Rossella Bilancia ^j, Antonietta Rossi ^j, Christian Eggeling ^{c,d,g,k}, Ute Neugebauer ^{c,g,h,i}, Ulrich S. Schubert ^{b,c,*}, Oliver Werz ^{a,c,*}

§ authors contributed equally

^aDepartment of Pharmaceutical/Medicinal Chemistry, Institute of Pharmacy, Friedrich Schiller University Jena, Philosophenweg 14, 07743 Jena, Germany

^bLaboratory of Organic and Macromolecular Chemistry (IOMC), Friedrich Schiller University Jena, Humboldtstraße 10, 07743 Jena, Germany

^cJena Center for Soft Matter (JCSM), Friedrich Schiller University Jena, Philosophenweg 7, 07743 Jena, Germany

^dInstitute for Applied Optics and Biophysics, Friedrich Schiller University Jena, Max-Wien Platz 1, 07743 Jena, Germany

^eDepartment of Pharmaceutical Technology and Biopharmacy, Institute of Pharmacy, Friedrich Schiller University Jena, Lessingstraße 8, 07743 Jena, Germany

^fDepartment of Pharmaceutical Chemistry, Faculty of Pharmacy, Gazi University, Etiler, 06330 Yenimahalle, Ankara, Turkey

^gLeibniz Institute of Photonic Technology, Albert-Einstein-Straße 9, 07745 Jena, Germany

^hCenter for Sepsis Control and Care, Jena University Hospital, 07747 Jena, Germany

ⁱInstitute of Physical Chemistry and Abbe Center of Photonics, Helmholtzweg 4, 07743 Jena, Germany

^jDepartment of Pharmacy, School of Medicine and Surgery, University of Naples Federico II, Via D. Montesano 49, I-80131 Naples, Italy.

^kMRC Human Immunology Unit, Weatherall Institute of Molecular Medicine, University of Oxford, Headley Way, OX39DS Oxford, UK

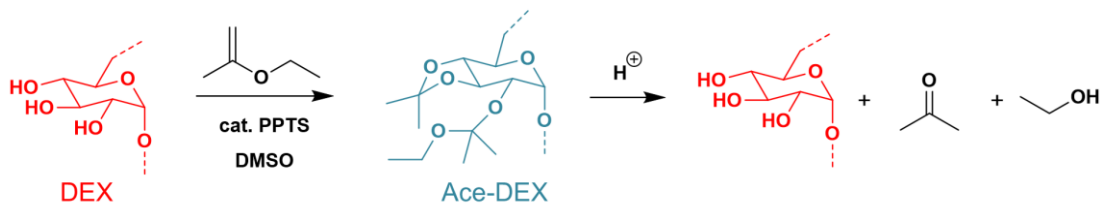


Figure S1. Synthesis of ethoxy acetalated dextran (Ace-DEX) and its degradation products upon hydrolysis.

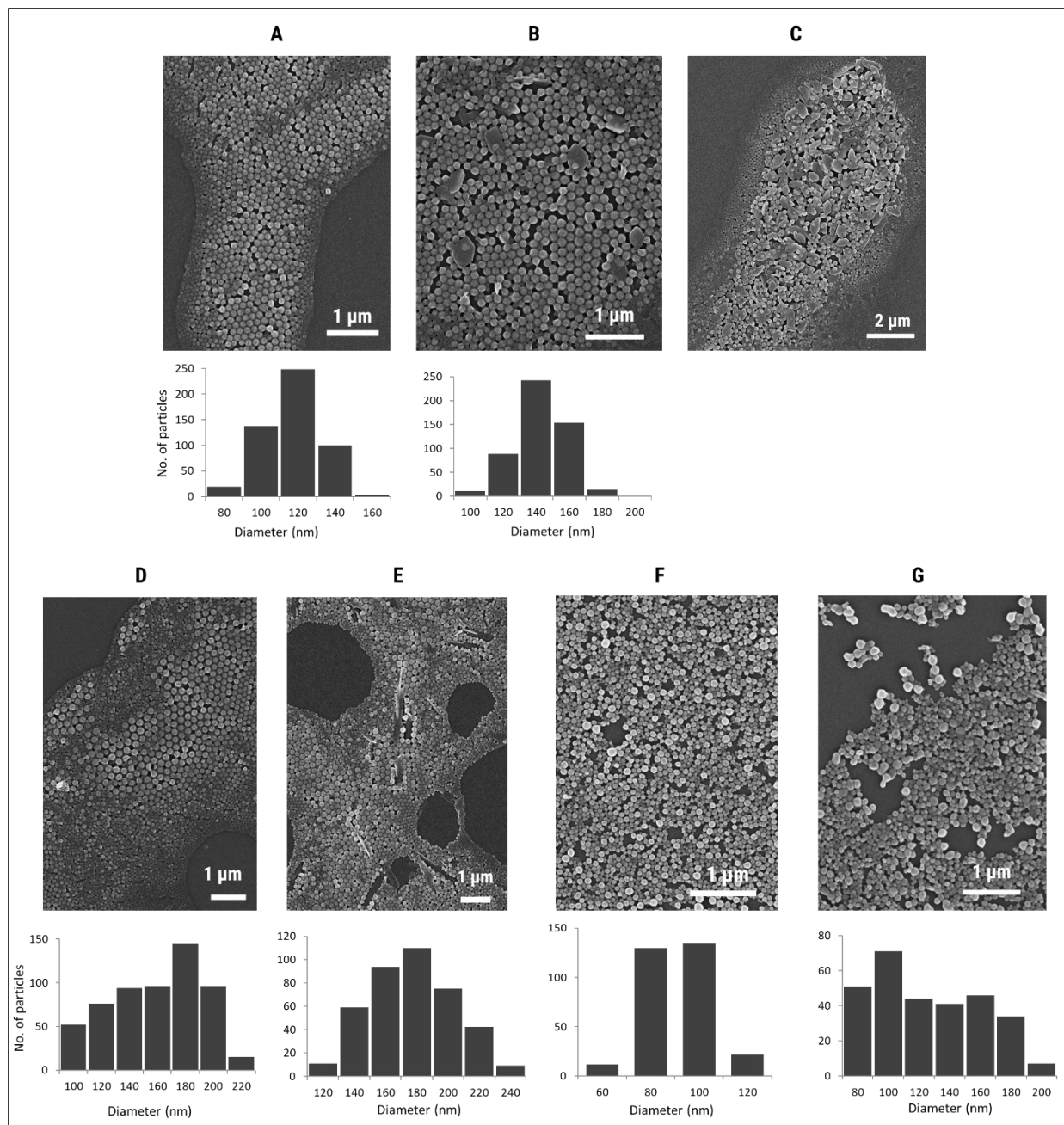


Figure S2. Scanning electron micrographs of the NPs: PLGA (A), PLGA[BRP-201] (B and C), PLGA-Rho (D), PLGA-Rho[BRP-201] (E), Ace-DEX-Rho (F), Ace-DEX-Rho[BRP-201] (G). Histograms were generated from ImageJ measurements ($n = 300$ to 500).

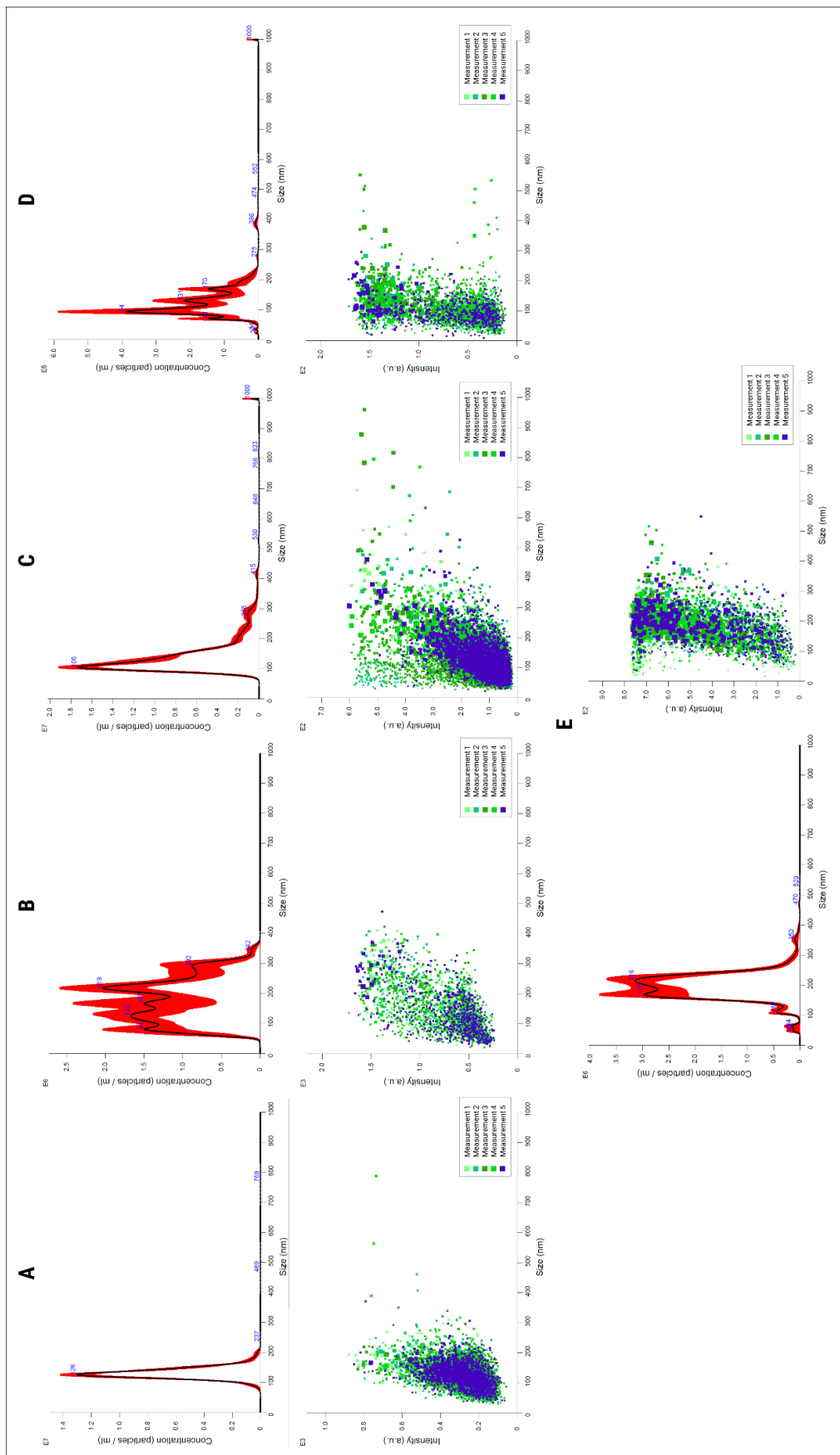


Figure S3. NTA measurements of the particle size (top row) and intensity distribution (bottom row): PLGA (A), PLGA[BRP-201] (B), Ace-DEX (C), Ace-DEX[BRP-201] (D), and BRP-201 precipitates (E).

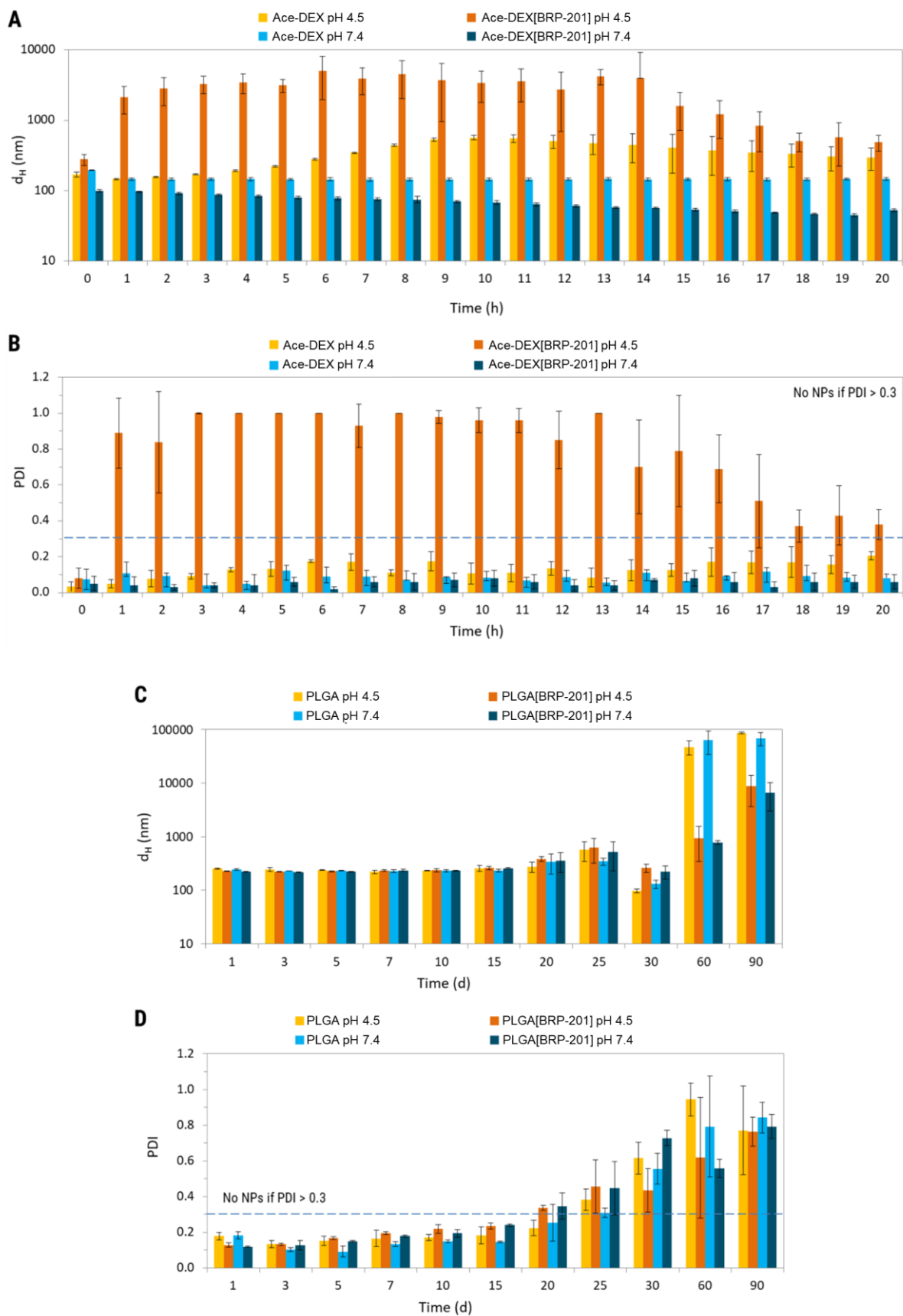


Figure S4. Size (A and C) and PDI (B and D) of the NPs over the 20 h measurements at 37 °C determined by DLS; NPs were incubated with 0.05 mM acetate buffer (pH 4.5) and 0.05 mM phosphate buffer (pH 7.4).

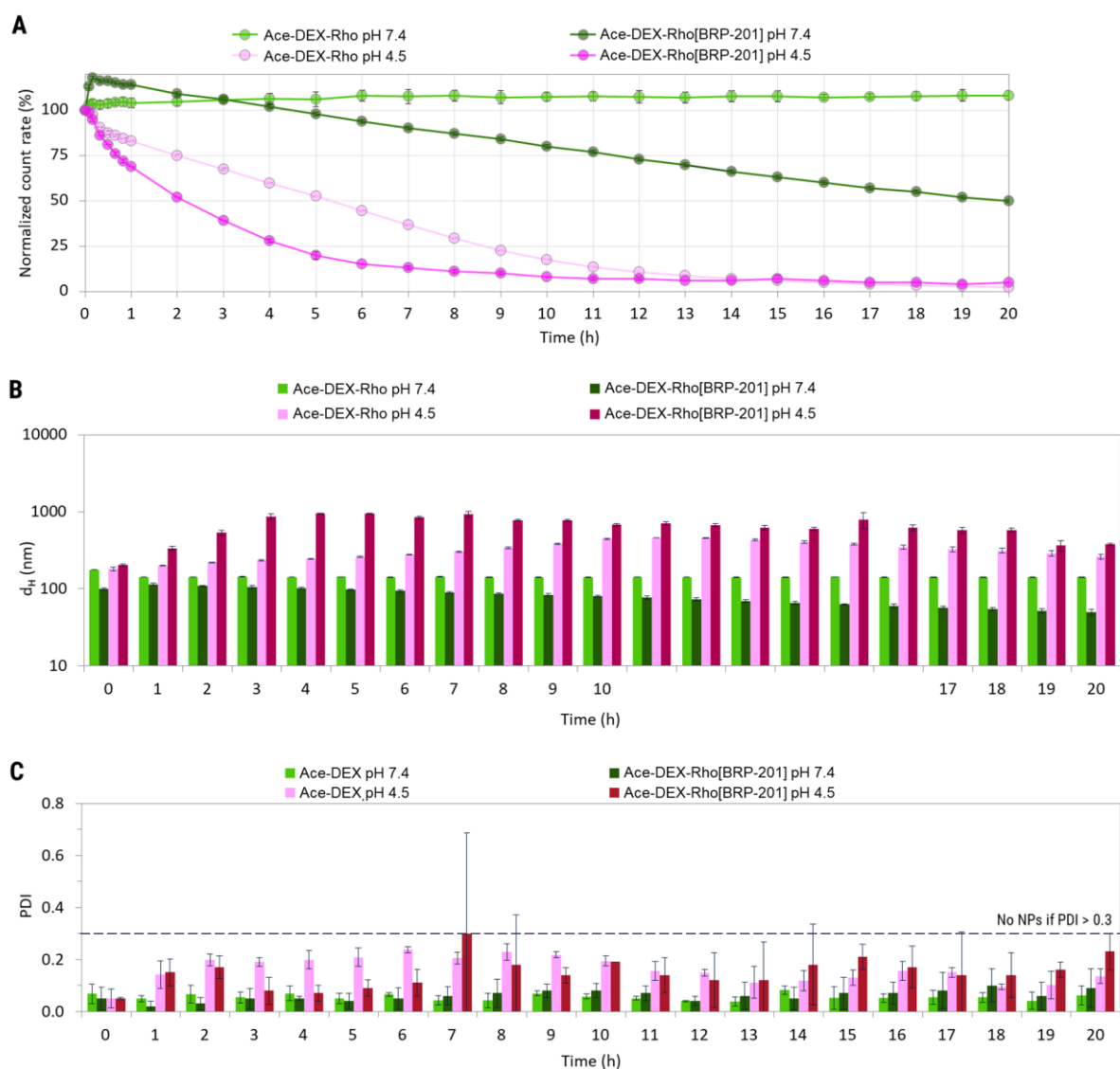


Figure S5. Degradation of Ace-DEX-Rho NPs at 37 °C incubated with 0.05 mM acetate buffer (pH 4.5) and 0.05 mM phosphate buffer (pH 7.4), as measured by DLS (n = 3) (A); the derived count rate on DLS was measured over predetermined time points, and plotted as normalized value against the derived count rate at timepoint 0 of incubation with buffer solution; concomitant size (B) and PDI (C) of the NPs over the 20 h measurements at 37 °C.

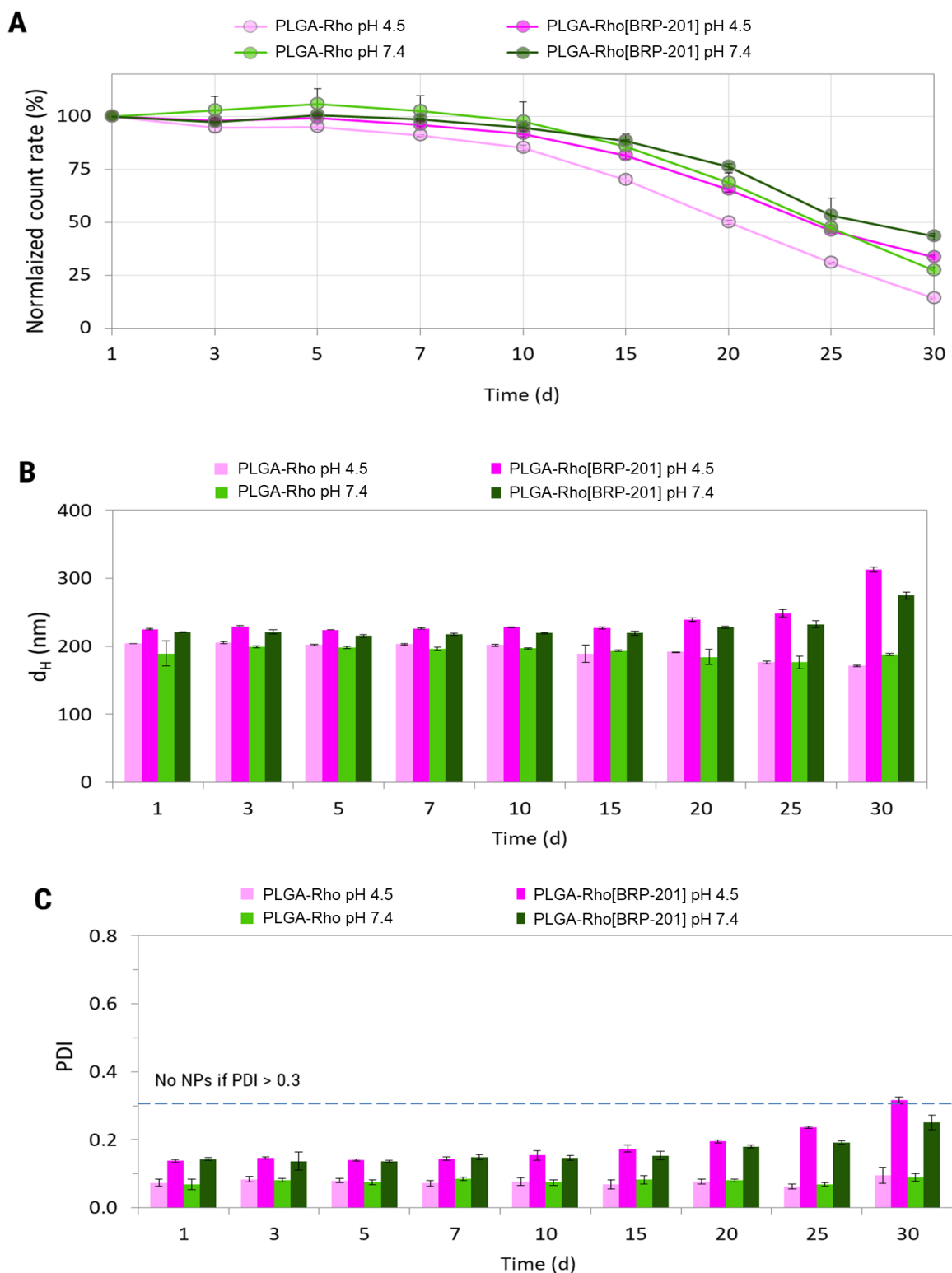


Figure S6. Degradation of Ace-DEX-Rho NPs at 37 °C incubated with 0.05 mM acetate buffer (pH 4.5) and 0.05 mM phosphate buffer (pH 7.4), as measured by DLS (n = 3) (A); the derived count rate on DLS was measured over predetermined time points, and plotted as normalized value against the derived count rate at timepoint 0 of incubation with buffer solution; concomitant size (B) and PDI (C) of the NPs over the 20 h measurements at 37 °C.

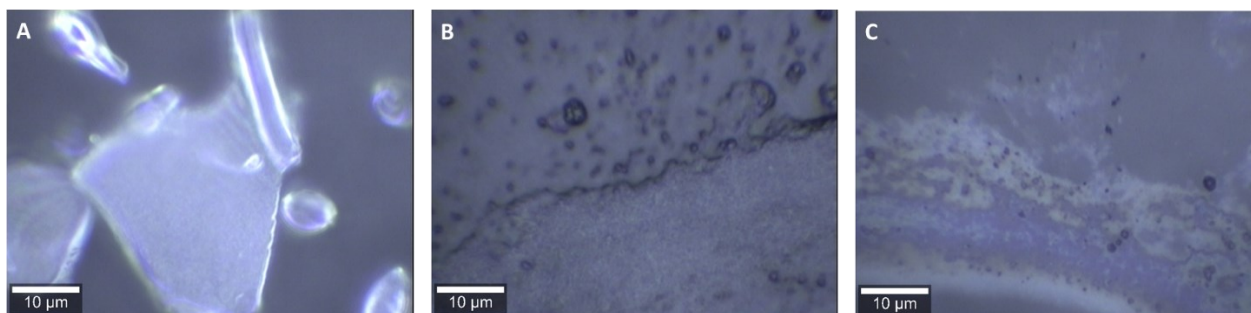


Figure S7. White light images of the drop coated sample of suspension of Ace-DEX[BRP-201]: (A) untreated Ace-DEX[BRP-201], (B) Ace-DEX[BRP-201] after 48h incubation at pH 4.5, (C) Ace-DEX[BRP-201] after 48h incubation at pH 7.4. It can be seen, that while initially large aggregations are present in the sample, after 48h incubation hardly any material is found on the slide. Raman spectra of the dried samples B and C are shown in Figure S8.

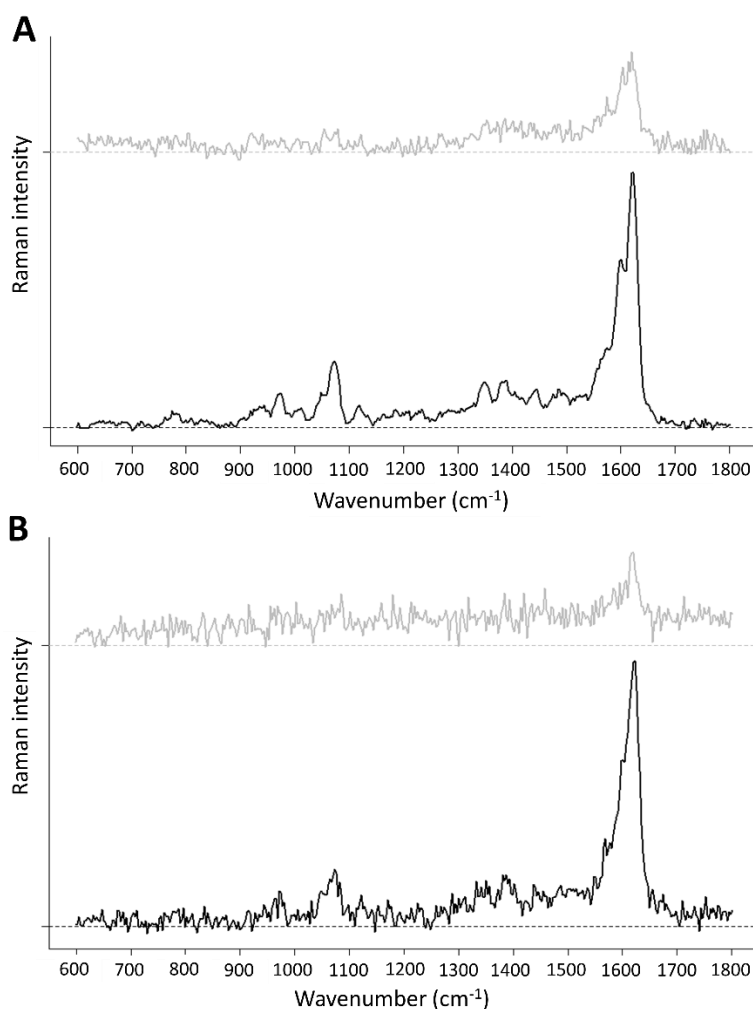


Figure S8. Spectra of the dried sample of Ace-DEX with BRP-201 after 48 h at pH 4.5 (A) and pH 7.4 (B). The upper (grey) spectra show the lowest intensity of the peak at 1620 cm^{-1} compared to the background, while the lower (black) spectra show the highest intensity. Peaks specific for Ace-DEX cannot be found in the spectra.

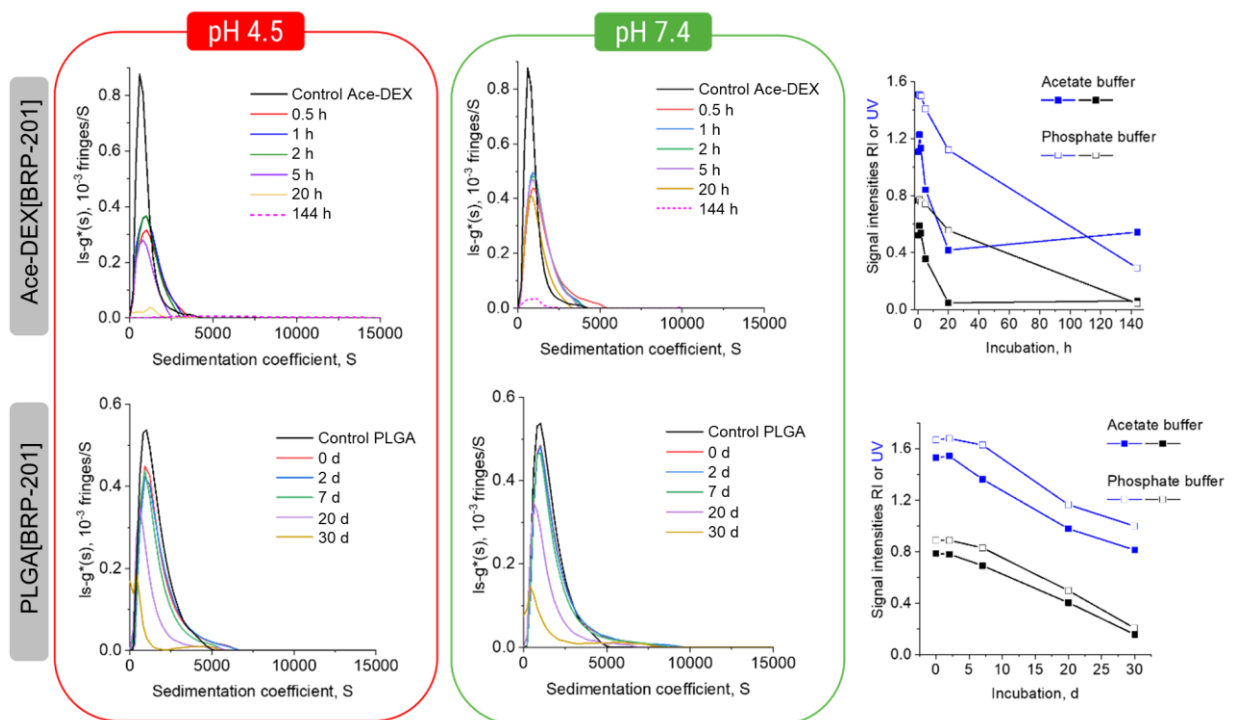


Figure S9. AUC investigation *via* refractive index (RI) detection of BRP-201-loaded NPs, incubated with buffers at 37 °C. Differential distribution of sedimentation coefficients, $Is - g^*(s)$, of Ace-DEX[BRP-201] NPs (top row) and PLGA[BRP-201] NPs (bottom row) incubated at 37 °C at different times and from experiments at a rotor speed of 1,500 rpm in acetate buffer (pH 4.5) (left) and phosphate buffer (pH 7.4) (middle). RI and UV (in terms of OD) signal received by integration of differential distributions of sedimentation coefficients, $Is - g^*(s)$, of particles against the incubation time at pH 4.5 and pH 7.4 (right). The control refers to NPs in water stored at 4 °C prior to the measurement.

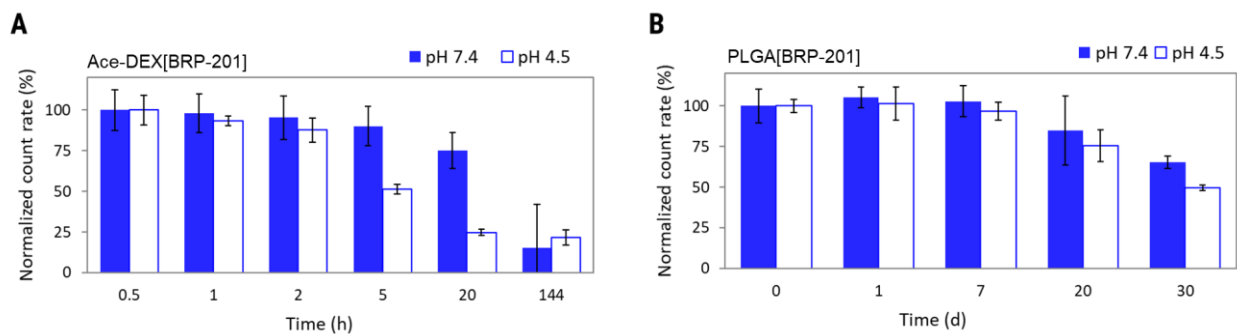


Figure S10. Degradation of NPs measured by DLS at the timepoints chosen for the degradation and/or the drug release measurements conducted on the AUC.

The RI signal intensity increased with longer incubation time at both pH values, probably due to the raise of the PVA amount in the supernatant as the NPs degraded [34] (Figure S12 and S13). For PLGA[BRP-201] NPs (Figure S13) the signal intensity of PVA in the supernatant was more pronounced for the NPs incubated at pH 4.5, even for the shortest incubation time, compared to pH 7.4. This may be a hint toward more pronounced degradation under acidic conditions.

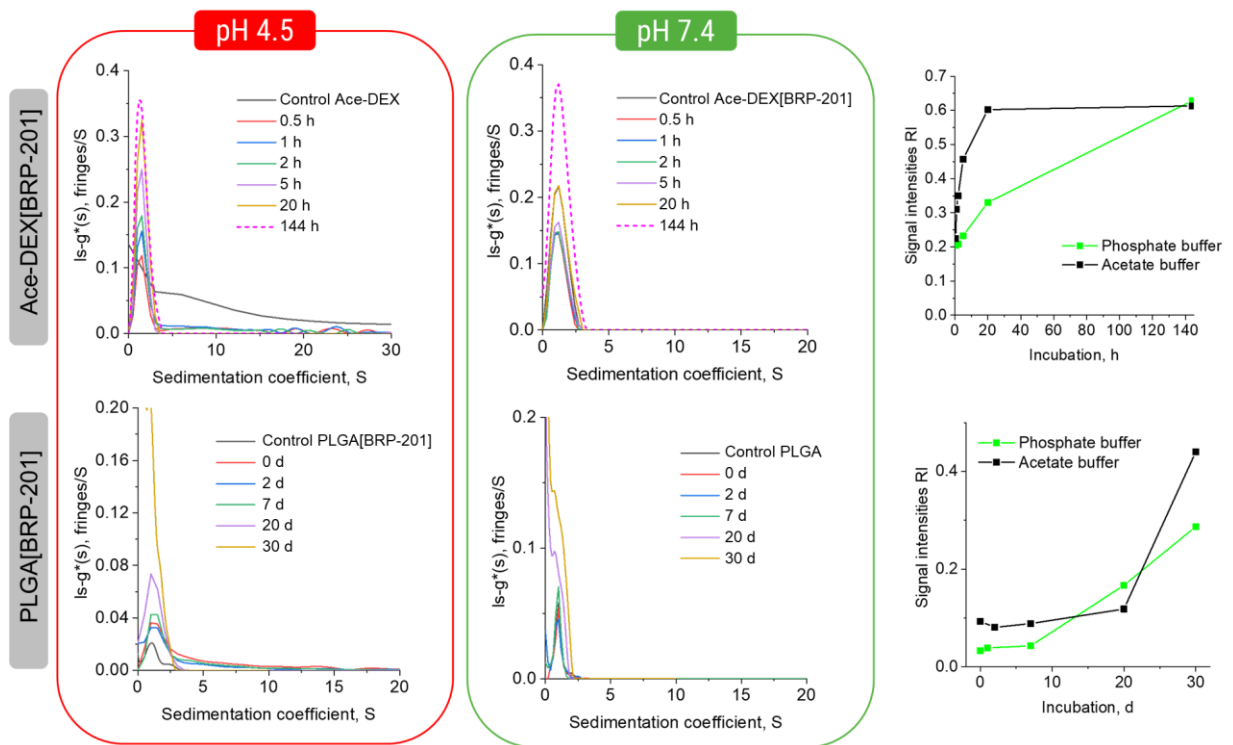


Figure S11. Differential distribution of sedimentation coefficients, $I_s - g^*(s)$, of Ace-DEX[BRP-201] (top row) and PLGA[BRP-201] NPs (bottom row) incubated at 37 °C, at pH 4.5 (left) and pH 7.4 (middle) measured at a rotor speed of 42,000 rpm after an overall 32 h of centrifugation at lower speed of 1500 rpm in order to observe the remaining supernatant. RI signal intensities received by integration of differential distributions of sedimentation coefficients, $I_s - g^*(s)$, of PVA in the supernatant against the incubation time (right).

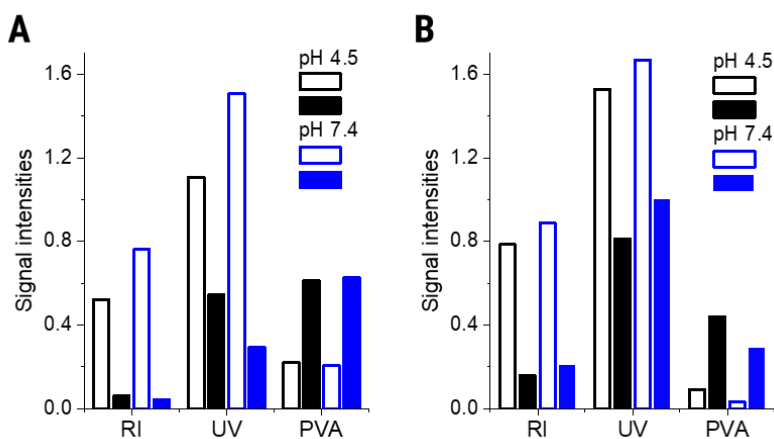


Figure S12. Signal intensities received by integration of differential distributions of sedimentation coefficients, $I_s - g^*(s)$, representative of solution composition of Ace-DEX[BRP-201] NPs incubated for 0.5 h (empty bars) and of the NPs incubated for 144 h (filled bars) (A), and of PLGA[BRP-201] NPs incubated for 0 d (empty bars) and of the NPs incubated for 30 d (filled bars) (B).

Table S1. NTA measurement settings for individual NP-samples.

Formulation	C ($\mu\text{g mL}^{-1}$)	Screen gain	Camera level	Focus	Detection threshold	Particles/frame
PLGA	50	10	8	26	4	27
PLGA[BRP-201]	50	11	5	26	4	32
Ace-DEX	10	10	11	19	7	71
Ace-DEX[BRP-201]	10	3	15	16	29	70
BRP-201 precipitates	10	3	8	14	14	78

Table S2. Overview of the size of the particles analyzed by different analytical methods.

Formulation	DLS intensity (nm)	DLS number (nm)	NTA mean (nm)	NTA mode (nm)	SEM (nm)
PLGA	165 \pm 13	136 \pm 9	131 \pm 19	123 \pm 19	108 \pm 15
PLGA[BRP-201]	185 \pm 5	139 \pm 7	179 \pm 70	218 \pm 70	133 \pm 15
Ace-DEX	180 \pm 13	104 \pm 6	148 \pm 76	105 \pm 76	70 \pm 10
Ace-DEX[BRP-201]	111 \pm 13	79 \pm 16	129 \pm 66	94 \pm 66	76 \pm 13
BRP-201 precipitates	317 \pm 44	252 \pm 38	198 \pm 45	215 \pm 45	/

Table S3. Summary of the physicochemical properties of the pooled NP-formulation loaded with 10% (w/w) BRP-201.

Pooled NPs with 10% BRP-201	Purified NP suspension			NP suspension + 0.9% NaCl			Yield (%)	PVA (% w/w)	EE (%)	LC (% w/w)
	d_H (nm)	PDI	ζ (mV)	d_H (nm)	PDI	ζ (mV)				
Ace-DEX	158	0.10	-8	152	0.03	-2	58	8.3 \pm 0.2	/	/
Ace-DEX[BRP-201]	237	0.24	-16	231	0.23	-1	66	5.5 \pm 0.3	108 \pm 11	98 \pm 12

Table S4. Particle size distribution of the NP suspensions for *in vivo* evaluation as measured *via* multi-angle light scattering (MADLS) with Zetasizer Ultra.

Formulations for <i>i.v.</i> injection	MADLS Angle	Purified NP suspension				NP suspension + 0.9% NaCl			
		Peak 1 d_H (nm)	Peak 1 (%)	Peak 2 d_H (nm)	Peak 2 (%)	Peak 1 d_H (nm)	Peak 1 (%)	Peak 2 d_H (nm)	Peak 2 (%)
Ace-DEX	173°	167	100	0	0	162	100	/	0
	90°	182	100	/	0	166	100	/	0
	13°	138	95	2	5	162	100	/	0
Ace-DEX[BRP-201]	173°	243	100	/	0	268	100	/	0
	90°	320	89	57	11	338	90	61	11
	13°	150	68	648	32	157	79	3344	21

Table S5. Particle size distribution of the NP suspensions for *in vivo* evaluation measured *via* multi-angle light scattering (MADLS) with Zetasizer Ultra after 28 days storage at 4 °C.

Formulations for <i>i.v.</i> injection	MADL S Angl e	Peak 1 d _H (nm)	Peak 1 (%)	Peak 2 d _H (nm)	Peak 2 (%)
Ace-DEX	173°	158	100	/	0
	90°	165	100	/	0
	13°	134	96	5161	3
Ace-DEX[BRP-201]	173°	638	95	57	5
	90°	1064	57	391	43
	13°	287	100	0	0

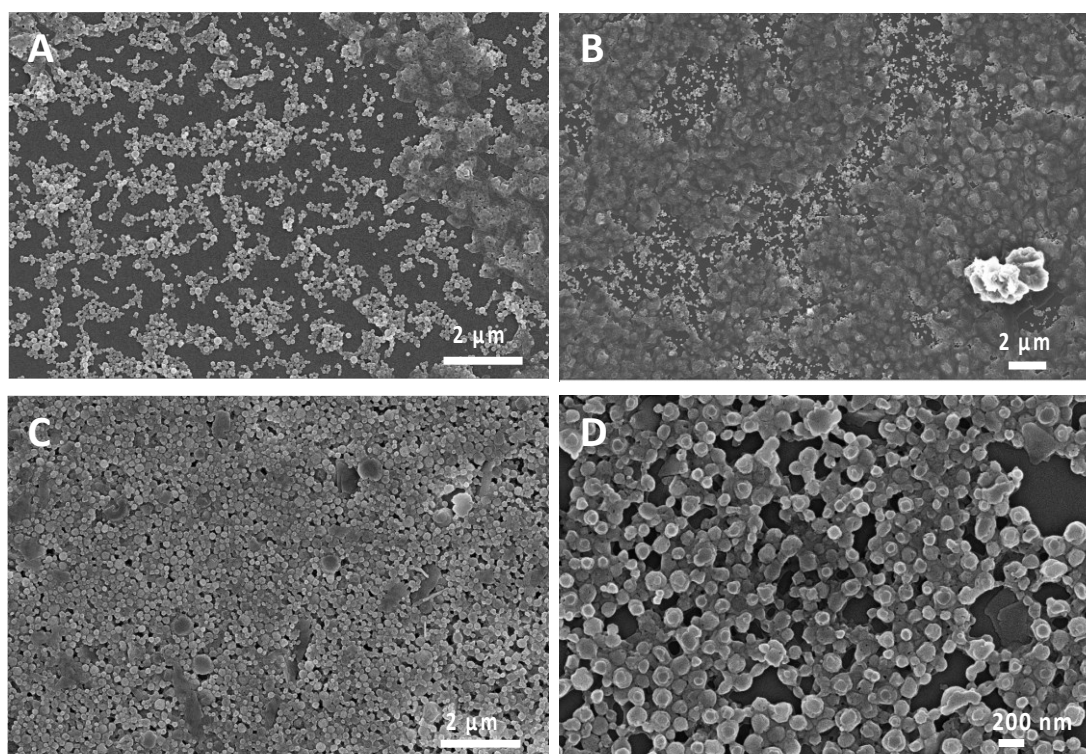


Figure S13. SEM micrographs of Ace-DEX NPs (A and B) and Ace-DEX[BRP-201] NPs (C and D) with 0.9% NaCl.

Manuscript IV

Effect of Crystallinity on the Properties of Polycaprolactone Nanoparticles Containing the Dual FLAP/mPEGS-1 Inhibitor BRP-187

Vollrath, A., Kretzer, C., Beringer-Siemers, B., Shkodra, B., Czaplewska, J., Bandelli, D., Stumpf, S., Hoepfener, S., Weber, C., Werz, O., Schubert, US.

Polymers, 2021 Jul 31;13(15):2557.

Der Kandidat / Die Kandidatin ist

Erstautor/-in, Ko-Erstautor/-in, Korresp. Autor/-in, Koautor/-in.

Anteile (in %) der Autoren / der Autorinnen an den vorgegebenen Kategorien der Publikation





Author	Conception	Data analysis	Experimental	Writing	Provision of Material
Vollrath A.	30 %	40 %		40 %	
Kretzer C.	20 %	30 %	30 %	20 %	
Beringer-Siemens B.			30 %		
Shkodra B.		10 %	10 %		
Czaplewska J.					
Bandelli D	10 %		10 %		
Stumpf S.			10 %		
Hoepfener S.			10 %		20 %
Weber C.					20 %
Werz O.	15 %			20 %	30 %
Schubert US.	15 %			20 %	30 %
Others		20 %			
Summe:	100 %	100 %	100 %	100 %	100 %

Unterschrift Kandidat/-in

Unterschrift Betreuer/-in (Mitglied der Fakultät)

Article

Effect of Crystallinity on the Properties of Polycaprolactone Nanoparticles Containing the Dual FLAP/mPEGS-1 Inhibitor BRP-187

Antje Vollrath ^{1,2}, Christian Kretzer ³, Baerbel Beringer-Siemers ¹, Blerina Shkodra ^{1,2} , Justyna A. Czaplowska ^{1,2}, Damiano Bandelli ^{1,2}, Steffi Stumpf ^{1,2}, Stephanie Hoepfener ^{1,2} , Christine Weber ^{1,2} , Oliver Werz ^{2,3}  and Ulrich S. Schubert ^{1,2,*}

- ¹ Laboratory of Organic Chemistry and Macromolecular Chemistry (IOMC), Friedrich Schiller University, Humboldtstraße 10, 07743 Jena, Germany; antje.vollrath@uni-jena.de (A.V.); baerbel.beringer-siemers@uni-jena.de (B.B.-S.); Blerina.Shkodra-pula@uni-jena.de (B.S.); justyna.czaplowska@uni-jena.de (J.A.C.); damianobandelli@gmail.com (D.B.); steffi-stumpf@uni-jena.de (S.S.); s.hoepfener@uni-jena.de (S.H.); christine.weber@uni-jena.de (C.W.)
- ² Jena Center for Soft Matter (JCSM), Friedrich Schiller University, Philosophenweg 7, 07743 Jena, Germany; oliver.werz@uni-jena.de
- ³ Department of Pharmaceutical/Medicinal Chemistry, Institute of Pharmacy, Friedrich Schiller University, Philosophenweg 14, 07743 Jena, Germany; christian.kretzer@uni-jena.de
- * Correspondence: ulrich.schubert@uni-jena.de



Citation: Vollrath, A.; Kretzer, C.; Beringer-Siemers, B.; Shkodra, B.; Czaplowska, J.A.; Bandelli, D.; Stumpf, S.; Hoepfener, S.; Weber, C.; Werz, O.; et al. Effect of Crystallinity on the Properties of Polycaprolactone Nanoparticles Containing the Dual FLAP/mPEGS-1 Inhibitor BRP-187. *Polymers* **2021**, *13*, 2557. <https://doi.org/10.3390/polym13152557>

Academic Editors: José Miguel Ferri, Vicent Fombuena Borràs and Miguel Fernando Aldás Carrasco

Received: 29 June 2021
Accepted: 29 July 2021
Published: 31 July 2021

Publisher's Note: MDPI stays neutral with regard to jurisdictional claims in published maps and institutional affiliations.



Copyright: © 2021 by the authors. Licensee MDPI, Basel, Switzerland. This article is an open access article distributed under the terms and conditions of the Creative Commons Attribution (CC BY) license (<https://creativecommons.org/licenses/by/4.0/>).

Abstract: Seven polycaprolactones (PCL) with constant hydrophobicity but a varying degree of crystallinity prepared from the constitutional isomers ϵ -caprolactone (ϵ CL) and δ -caprolactone (δ CL) were utilized to formulate nanoparticles (NPs). The aim was to investigate the effect of the crystallinity of the bulk polymers on the enzymatic degradation of the particles. Furthermore, their efficiency to encapsulate the hydrophobic anti-inflammatory drug BRP-187 and the final in vitro performance of the resulting NPs were evaluated. Initially, high-throughput nanoprecipitation was employed for the ϵ CL and δ CL homopolymers to screen and establish important formulation parameters (organic solvent, polymer and surfactant concentration). Next, BRP-187-loaded PCL nanoparticles were prepared by batch nanoprecipitation and characterized using dynamic light scattering, scanning electron microscopy and UV-Vis spectroscopy to determine and to compare particle size, polydispersity, zeta potential, drug loading as well as the apparent enzymatic degradation as a function of the copolymer composition. Ultimately, NPs were examined for their potency in vitro in human polymorphonuclear leukocytes to inhibit the BRP-187 target 5-lipoxygenase-activating protein (FLAP). It was evident by Tukey's multi-comparison test that the degree of crystallinity of copolymers directly influenced their apparent enzymatic degradation and consequently their efficiency to inhibit the drug target.

Keywords: polycaprolactone (PCL); polyesters; hydrophobic-hydrophilic balance (HHB); nanoparticle formulation; nanoparticle crystallinity; FLAP antagonist; BRP-187

1. Introduction

With the first clinical approval of a polymer-based nano-drug in 1995 [1], interest in developing polymers as nanocarriers of (bio)pharmaceutical drugs has been steadily growing [2,3]. Due to their favorable characteristics, e.g., adjustable physical and mechanical properties, it is not surprising that polymer-based nanomaterials are now established in many areas of bionanotechnology. Polymers are widely used in delivery systems for therapeutics, in matrices for tissue engineering and, among others, in polymer-based composites for biomedical purposes [4–6].

The main criteria in designing polymers for therapeutic use have been based mainly on the biocompatibility and the biodegradability of the polymer backbone as well as the suitability of the polymer to be processed into a stable pharmaceutical formulation [7].

However, there are other parameters of equal importance to be considered to optimize a polymer for its application as a delivery vehicle. In fact, parameters such as molar mass, functional end-groups, hydrophobic-hydrophilic balance (HHB), melting temperature (T_m) and crystallinity strongly influence the drug loading and the drug release kinetics from the polymer matrix [8].

Independent investigations of the influence of the polymer crystallinity on the resulting particle characteristics (e.g., particle formation and degradation) while keeping the key properties of the system constant are rare or only provide partial conclusions typically due to influences of a third variable [9]. In particular, alterations of HHB are frequently accompanied by changes in crystallinity [10]. It is hence currently not fully understood if degradation or general performance of hydrophobic pharmapolymers in aqueous media are, in fact, strongly influenced by polymer crystallinity or if the hydrophobicity is the dominating factor.

Today, the most commonly used polymers for biomedical applications are polyesters, such as polylactide (PLA), poly(lactide-*co*-glycolide) (PLGA) and polycaprolactone (PCL) [11]. They are easy to access and offer a range of interesting advantages; i.e., (i) a complete hydrolytic and/or enzymatic biodegradation, (ii) a facile and controlled synthesis to obtain defined molar masses, (iii) various modification possibilities of the polymer structure, and (iv) commercial availability [12]. The advantages of PCL compared to other aliphatic polyesters include interesting thermal properties, higher durability and manufacturability, and a good compatibility with other polymers [13,14]. Thus, PCL represents a promising candidate to design materials with tailor-made properties [13,15,16]. Bandelli et al. recently demonstrated that copolymerization of the constitutional isomers ϵ -caprolactone (ϵ CL) and δ -caprolactone (δ CL) with a varying ratio of ϵ CL and δ CL can generate a library of five copolyesters featuring a constant HHB and similar molar masses in the range of 7 to 10 kDa, but the copolymers showed a varying crystallinity [17]. They are hence suitable materials to study the sole influence of crystallinity on the particle properties and performance. In this study, we utilized this library of poly(ϵ CL-*ran*- δ CL) to formulate drug-loaded nanoparticles (NPs). The aim was to investigate, firstly, whether such polymers provide suitable properties (particle size and polydispersity) to form an NP-based drug delivery system, and secondly, to study the effect of the crystallinity of the bulk polymers on the enzymatic degradation and the *in vitro* performance of the resulting NPs.

The anti-inflammatory drug BRP-187 (4-(4-chlorophenyl)-5-[4-(quinoline-2-ylmethoxy)phenyl] isoxazol-3-carboxylic acid) is a dual inhibitor of the 5-lipoxygenase-activating protein (FLAP) and microsomal prostaglandin E2 synthase-1 (mPGES-1), which are crucial proteins within arachidonic acid (AA) metabolism. Inhibition of mPGES-1 and FLAP prevents the biosynthesis of pro-inflammatory prostaglandin (PG) E_2 and leukotrienes (LTs), respectively [18]. Several *in vitro* and *in vivo* studies with inhibitors of FLAP and/or mPGES-1 have demonstrated their efficient anti-inflammatory activity while exhibiting fewer adverse effects compared to the conventional non-steroidal anti-inflammatory drugs (NSAIDs) [19,20]. These observations suggest that dual inhibition of FLAP and/or mPGES-1, rather than blocking cyclooxygenase-1 or -2 pathways, might be a better strategy for intervention with inflammation. However, BRP-187 is a fatty acid-like molecule with poor water solubility and a strong tendency to bind plasma proteins [18]. Molecules exhibiting such properties typically cause challenges in reaching a sufficient bioavailability *in vivo* and require technological solutions to improve their pharmacokinetic drawbacks. We have previously demonstrated that encapsulating BRP-187 into PLGA NPs and acetalated dextran NPs enhanced its enzyme inhibition efficacy *in vitro* [21].

In the present study, we initially performed a high-throughput (HT) nanoprecipitation approach for the homopolymers P ϵ CL and P δ CL to screen a range of polymer and surfactant concentrations for the preparation of empty (unloaded) PCL particles. Once optimal formulation conditions were established, and drug-loaded NPs were prepared by batch nanoprecipitation of the P ϵ CL and P δ CL homopolymers as well as of the poly(ϵ CL-*ran*- δ CL) copolymers with BRP-187. PCL NPs with and without BRP-187 were characterized

for their critical quality attributes, namely their particle size, polydispersity index (PDI), surface charge and drug loading. Other particle properties i.e., nanodispersion stability and NP degradation behavior were also investigated. Ultimately, BRP-187-NPs were studied in vitro in human polymorphonuclear leukocytes (PMNL) for their efficiency to inhibit the drug target FLAP, in comparison to the free BRP-187.

2. Methods

2.1. Materials

The PCL homopolymers and P(ϵ CL-*ran*- δ CL) copolymers were synthesized as previously reported [17]. Key characterization data are listed in Table S1 in the Supplementary Information (SI). For further details on their synthesis, the reader is referred to literature reports [17]. Polyvinylalcohol (PVA) (Mowiol 4-88), tetrahydrofuran (THF), dimethylsulfoxide (DMSO) and lipase from the yeast *Candida rugosa* were purchased from Sigma-Aldrich (Germany). BRP-187 was synthesized according to a published protocol [18]. Further materials are described in the specific experimental sections.

2.2. Automated High-Throughput Nanoprecipitation

Automated high-throughput nanoprecipitation was performed in a 96-well plate (Greiner Bio-One GmbH, Frickenhausen, Germany) utilizing a FasTrans liquid handling robot (Analytik Jena GmbH, Jena, Germany). Starting with a polymer stock solution of 10 mg mL⁻¹ in THF, a dilution series with varying concentrations (0.25, 0.5, 1, 2, 3, 4, 5, 6, 7, 8, 9 and 10 mg mL⁻¹) was prepared. The polymer solutions (40 μ L) were then automatically pipetted into 200 μ L of either purified water (GenPure ultrapure water system, Thermo Scientific, Waltham, MA, USA) or PVA surfactant-containing aqueous solutions with a concentration of 0.25%, 0.5% or 1.0% (*w/v*). The resulting NP dispersions were mixed by pipetting up and down three times and then left for two hours for solvent evaporation. Each formulation was prepared twice. After solvent evaporation, the samples were diluted with pure water (1:2 ratio for a polymer concentration up to 4 mg mL⁻¹ and 1:10 ratio for all NPs prepared with a polymer concentration above 4 mg mL⁻¹) and investigated via dynamic light scattering (as described in Section 2.4) [22].

2.3. Batch Nanoprecipitation

Polymer solutions with 5 mg mL⁻¹ or 2.5 mg mL⁻¹ were prepared in THF via batch nanoprecipitation. For the drug-loaded particles, 10 mg mL⁻¹ of BRP-187 dissolved in DMSO were mixed with the polymer solution prior to formulation, which corresponded to 3% (*w/w*) of the drug to polymer mass. The drug stock solution was sonicated in an ultrasound water bath for 15 min at room temperature to ensure good dissolution. Particle formulation was carried out by injecting the polymer/drug solution into an aqueous phase containing 0.3% (*w/v*) PVA using a syringe pump (Aladdin AL1000-220, World Precision Instruments, Berlin, Germany) with a flow rate of 2 mL min⁻¹ while stirring at 800 rpm. The solvent/non-solvent ratio was set to 1:8. The resulting particle suspensions were stirred for 24 h at room temperature for solvent evaporation and then centrifuged at 12.851 \times g for 60 min at 20 °C using a Rotina 380 R centrifuge (Hettich Lab Technology, Tuttlingen, Germany). The supernatant was removed, and the NPs were re-dispersed in 2.5 mL pure water, vortexed and sonicated in an ultrasonic water bath for 30 min. The NPs were stored overnight at 4 °C and lyophilized in aliquots of 200 μ L. After lyophilization, the mass of the NPs was determined using a precise analytical balance (MYA 11.4Y, Radwag Waagen, Hilden, Germany). The yield was calculated as follows: (mass of NPs recovered – mass of found PVA)/(mass of polymer + mass of drug) in the formulation \times 100. To check reproducibility, five individual batches of the drug-loaded PCL particles were prepared and analyzed individually. The data provided represent the average values and the standard deviation of these five batches.

2.4. Dynamic Light Scattering (DLS) and Electrophoretic Light Scattering (ELS)

DLS measurements were performed utilizing a Nano ZS (Malvern Panalytical, Malvern, United Kingdom) with a laser wavelength of $\lambda = 633$ nm with non-invasive back-scatter (NIBS) technology [22]. The particle size is reported as the hydrodynamic diameter (d_H). The particle size distribution (PDI) was measured using pure water as a dispersant with a refractive index RI of 1330 and a viscosity of 0.8872 cP at 25 °C. Samples obtained from the automated HT-nanoprecipitation were measured at 25 °C in a micro cuvette (Brand GmbH, Wertheim, Germany) without any filtering step with the following settings: measurements of each sample were repeated three times for 10 sec at 25 °C. The samples obtained from batch nanoprecipitation were measured at a dilution of 1:10 up to 1:100 utilizing the following settings: five repeated measurements, each with five runs of 30 s. The zeta-potential of the lyophilized NPs was investigated by ELS using the same instrument at 25 °C with three repeated measurements.

The apparent degradation behavior of the NPs was analyzed by DLS by monitoring changes in the mean count rate at fixed measurement settings: measuring position at 4.65, attenuator factor 7 at 37 °C [21]. Before investigating, NPs were mixed with the enzyme solution (a lipase from *Candida rugosa*) in a 1:4 mass ratio of polymer to enzyme and incubated at 37 °C for pre-determined timepoints.

2.5. UV-Vis Spectroscopy Measurements

UV-Vis spectroscopy measurements were performed with the Infinite M200 Pro plate reader (Tecan Group, Männedorf, Switzerland). For determination of the encapsulation efficiency (EE) and the loading capacity (LC) of the BRP-187 in the PCL particles, lyophilized NPs were dissolved in DMSO, and the solutions were investigated in a flat-transparent 96-well quartz plate (Hellma, Jena, Germany) at $\lambda = 316$ nm with 3×3 multiple reads per well and a 2000 μm well border. A calibration curve of BRP-187 was obtained for each batch in the concentration range of 1.2 to 312.5 $\mu\text{g mL}^{-1}$ with $R^2 = 0.9997$. The LC was calculated as follows: $\text{LC} = (\text{mass of drug recovered})/(\text{mass of particle recovered}) \times 100$. The EE was calculated as follows: $\text{EE} = \text{LC found}/(\text{mass of drug used}) \times 100$. The determination of PVA in the NPs (% *w/w*) was performed according to the published protocol [23].

2.6. Scanning Electron Microscopy (SEM)

A Sigma VP Field Emission Scanning Electron Microscope (Carl-Zeiss, Jena, Germany) equipped with an InLens detector with an accelerating voltage of 6 kV was used for electron microscopy imaging. Before the measurement, the samples were coated with a thin layer of platinum (4 nm) via sputter coating (CCU-010 HV, Safematic, Zizers, Switzerland).

2.7. Cell Isolation

The leukocytes isolation was performed according to a published protocol [21]. Leukocyte concentrates were prepared from peripheral blood obtained from healthy human adult donors that received no anti-inflammatory treatment for the last ten days (Institute of Transfusion Medicine, University Hospital Jena). The approval for the protocol was given by the ethical committee of the University Hospital Jena, and all methods were performed in accordance with the relevant guidelines and regulations. To isolate PMNL, the leukocyte concentrates were mixed with dextran (*Leuconostoc* spp. MW ~40,000, Sigma Aldrich, Taufkirchen, Germany) for sedimentation of erythrocytes and the supernatant was centrifuged on lymphocyte separation medium (Histopaque®-1077, Sigma Aldrich, Taufkirchen, Germany). Contaminating erythrocytes in the pelleted neutrophils were removed by hypotonic lysis (water). PMNL were then washed twice in ice-cold phosphate-buffered saline (PBS) and finally resuspended in PBS plus 0.1% of glucose and 1 mM CaCl_2 .

2.8. Determination of FLAP-Dependent 5-LO Product Formation in PMNL

The evaluation of the effects on FLAP was performed according to our established protocol [21]. We assessed FLAP-dependent 5-LO product formation in human PMNL,

cells ($5 \times 10^6 \text{ mL}^{-1}$) were pre-incubated with BRP-187 or NPs for indicated timepoints at 37°C . The cells were stimulated with $2.5 \mu\text{M Ca}^{2+}$ -ionophore A23187 (Cayman, Ann Arbor, USA) for 10 min, and the incubation was stopped with 1 mL ice-cold methanol containing 200 ng mL^{-1} PGB₁ as an internal standard. Samples were subjected to solid phase extraction, and the formed lipid mediators (leukotriene B₄ (LTB₄), trans-isomers of LTB₄, 5-hydroxyeicosatetraenoic acid (5-HETE)) were separated and analyzed by reverse-phase high-performance liquid chromatography (RP-HPLC) as previously described [24]. Statistical analysis was performed with log-transformed values to obtain Gaussian-distributed data sets. Experiments were analyzed via one-way ANOVA and Tukey's multicomparison test with GraphPad Prism 9.1.2 (GraphPad, La Jolla, CA, USA).

2.9. Cell Viability

Freshly isolated PMNL were incubated with a control sample with 0.1% DMSO, BRP-187 ($10 \mu\text{M}$) or NPs containing the respective amount of BRP-187 ($10 \mu\text{M}$) at 37°C in PBS containing 0.1% of glucose. After 5 h the cell suspension was subjected to a Vi-CELL XR cell counter (Beckman Coulter, Lahntal, Germany), for determination of cell viability by trypan blue staining.

3. Results and Discussion

In our previous study, five poly($\epsilon\text{CL-ran-}\delta\text{CL}$) copolymers, herein named $\epsilon 87\text{-}\delta 13$, $\epsilon 81\text{-}\delta 19$, $\epsilon 75\text{-}\delta 25$, $\epsilon 61\text{-}\delta 39$ and $\epsilon 45\text{-}\delta 55$, and the two respective homopolymers P ϵCL and P δCL , herein referred to as $\epsilon 100\text{-}\delta 0$ and $\epsilon 0\text{-}\delta 100$, were synthesized exhibiting a constant HHB [17]. It was demonstrated that the HHB of the bulk polymers correlated with the HHB of the corresponding NPs when particles were prepared in THF using a polymer concentration of 1 mg mL^{-1} [17]. In the present study, the particle formation of the $\epsilon 100\text{-}\delta 0$ and $\epsilon 0\text{-}\delta 100$ was investigated over a wider range of polymer concentrations in THF ranging from 0.25 to 10 mg mL^{-1} using an automated pipetting robot that was adapted for the HT-nanoprecipitation [25]. Particles were formulated without surfactant as well as with PVA of different concentrations (0.25 to 1% (w/v)). Previous studies revealed that PVA of less than 0.5% (w/v) generated stable drug-loaded PLGA NPs, and it could be demonstrated that even concentrations of up to 5% (w/v) were generally non-toxic in vitro [26]. $\epsilon 100\text{-}\delta 0$ and $\epsilon 0\text{-}\delta 100$ homopolymers both formed NPs up to the highest tested polymer concentration of 10 mg mL^{-1} when PVA was used as a surfactant (SI, Figure S1). Even the lowest tested PVA concentration of 0.25% (w/v) was sufficient to obtain stable particle dispersions and $\epsilon 100\text{-}\delta 0$ NPs with a size of 150 to 300 nm and $\epsilon 0\text{-}\delta 100$ NPs with a particle size of 120 to 280 nm with $\text{PDI} < 0.3$. However, $\epsilon 0\text{-}\delta 100$ NPs prepared without surfactant failed to produce stable NP dispersions above concentrations of 0.5 mg mL^{-1} as indicated by a strong aggregation of the particles. This is not surprising since $\epsilon 0\text{-}\delta 100$ is above its glass transition temperature at room temperature, which could disturb the particle formation in the absence of a stabilizer. It is well-known that several factors influence the final NP properties, including the polymer concentration, the solvent used to dissolve the polymer and the type and the concentration of the surfactant [26–28]. THF was demonstrated to be a suitable solvent in the HT-screening, resulting in stable particle formation within a broad polymer concentration range when PVA was used as a surfactant. Hence, it was selected as solvent for the subsequently performed BRP-187 encapsulation experiments. All other formulation parameters for the preparation of PCL[BRP-187] NP were adapted from our previous study that described the encapsulation of BRP-187 into PLGA NPs [21]. The first batch nanoprecipitation with the drug and a polymer concentration of 5 mg mL^{-1} in THF yielded large particles with a diameter (d_H) of 400 to 600 nm with high LC values (SI, Table S2). However, the particles revealed significant aggregation after centrifugation and lyophilization, as indicated by the higher PDI values of 0.3 to 0.6 . Hence, the initial polymer concentration was reduced to 2.5 mg mL^{-1} to optimize the dispersion stability and to decrease the particle size [28]. Particles within a size range of 200 to 260 nm and PDI values below 0.3 were obtained for all PCLs using a polymer concentration of 2.5 mg mL^{-1}

(Table 1, SI Table S4). It was further observed that empty NPs were approximately 30 to 50 nm smaller compared to the BRP-187-loaded NPs (SI, Table S3). The particle size of the empty NPs increased by approximately 40 to 80 nm when NPs were lyophilized and subsequently reconstituted in water (SI, Table S3). Similar tendencies were also observed for the PCL[BRP-187] NPs, although here the difference in size was on average only about 30 to 50 nm (Table 1), presumably caused by the strong affinity of the hydrophobic drug with the polymer matrix [29]. The particles were also investigated via SEM (Figure 1), which revealed individual or clustered particle populations within the particle size range as indicated by DLS measurements.

Table 1. Overview of PCL[BRP-187] NP properties prepared in THF using a polymer concentration of 2.5 mg mL⁻¹.

ϵ CL/ δ CL (mol %)	T _m (°C)	X _c ^a (%)	d _H ^b (nm)	PDI ^b	ZP ^c (mV)	d _H ^c (nm)	PDI ^c	PVA % (w/w)	Yield ^d (%)	LC ^e (%)
ϵ 100- δ 0	69	73	229 ± 13	0.08 ± 0.02	-50 ± 1	268 ± 21	0.27 ± 0.09	4.5	87	1.5 ± 0.1
ϵ 87- δ 13	54	44	211 ± 5	0.08 ± 0.02	-38 ± 2	251 ± 13	0.30 ± 0.14	4.5	76	1.4 ± 0.5
ϵ 81- δ 19	52	38	218 ± 13	0.08 ± 0.02	-41 ± 1	267 ± 24	0.37 ± 0.27	4.7	81	1.4 ± 0.2
ϵ 75- δ 25	42	28	225 ± 13	0.16 ± 0.11	-34 ± 1	260 ± 23	0.42 ± 0.20	5.0	67	1.9 ± 0.6
ϵ 61- δ 39	24	4	209 ± 13	0.06 ± 0.12	-40 ± 1	223 ± 16	0.16 ± 0.10	8.2	61	1.7 ± 0.1
ϵ 45- δ 55	/ [*]	0	200 ± 13	0.10 ± 0.12	-32 ± 1	237 ± 61	0.18 ± 0.08	6.7	52	1.4 ± 0.2
ϵ 0- δ 100	/ [*]	8	259 ± 32	0.28 ± 0.14	-45 ± 2	262 ± 20	0.26 ± 0.26	5.5	54	3.2 ± 1.2

d_H represents the intensity-weighted distribution (n ≥ 4 batches) and zeta-potential (ZP) (n = 3 ELS measurements) * Amorphous or near amorphous polymers with glass transition temperature T_g below 37 °C [17]. ^a Bulk degree of crystallinity as determined by wide-angle X-ray scattering (WAXS) at room temperature. ^b NPs measured after purification. ^c NPs measured after lyophilization and subsequent resuspension in water. ^d Yield = (mass of NPs recovered - mass of found PVA)/(mass of polymer + mass of drug) in the formulation × 100. ^e Determined by UV-VIS spectroscopy at λ = 316 nm (n = 4) and calculated using LC = (mass of drug recovered)/(mass of particle recovered) × 100.

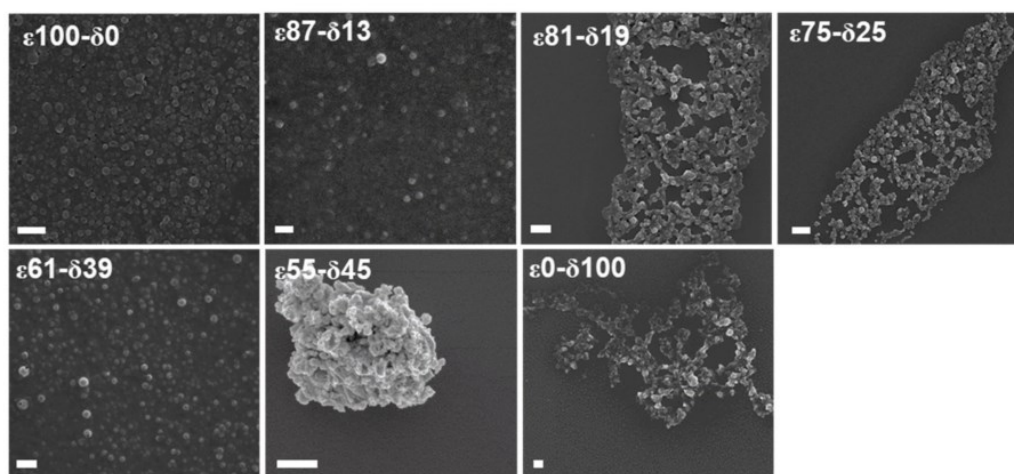


Figure 1. SEM micrographs of PCL[BRP-187] particles consisting of the homo- or copolymers with a varying composition. Scale bar = 1 μ m.

The average LC of the PCL[BRP-187] NPs was between 1.4 and 1.9% for ϵ 100- δ 0 and the poly(ϵ CL-*ran*- δ CL) copolymers (Table 1) and similar to the LC values of PLGA NPs encapsulating the same drug [21]. The only exception was the ϵ 0- δ 100 homopolymer with an LC of 3.2%, probably due to its almost liquified state at room temperature. This resulted in a viscous dispersion with emulsion-like properties in which the drug was apparently entrapped during the purification process.

In general, the yield of both empty and drug-loaded PCL NPs decreased with increasing molar fraction of δ CL (Figure 2A). In other words, NP yield increased with the degree of crystallinity of the polyester materials. Amorphous materials are frequently utilized as excipients in pharmaceutical formulations since they are known to increase the dissolution

rate of insoluble drugs and to enhance their bioavailability [30]. However, their major disadvantage is seen in the fact that they exhibit high energy states at a molecular level and thus are prone to physical instabilities. In particular, such tendencies were observed with the NPs of the amorphous P δ CL homopolymer, which displayed a higher polydispersity and the lowest yield. In technical terms, the low yield of the copolymers with a higher fraction of δ CL could have resulted from their near-molten state at room temperature causing them to sediment at a lower rate due to their lower density. Thus, after 60 min of centrifugation, a lower amount of the NPs was recovered.

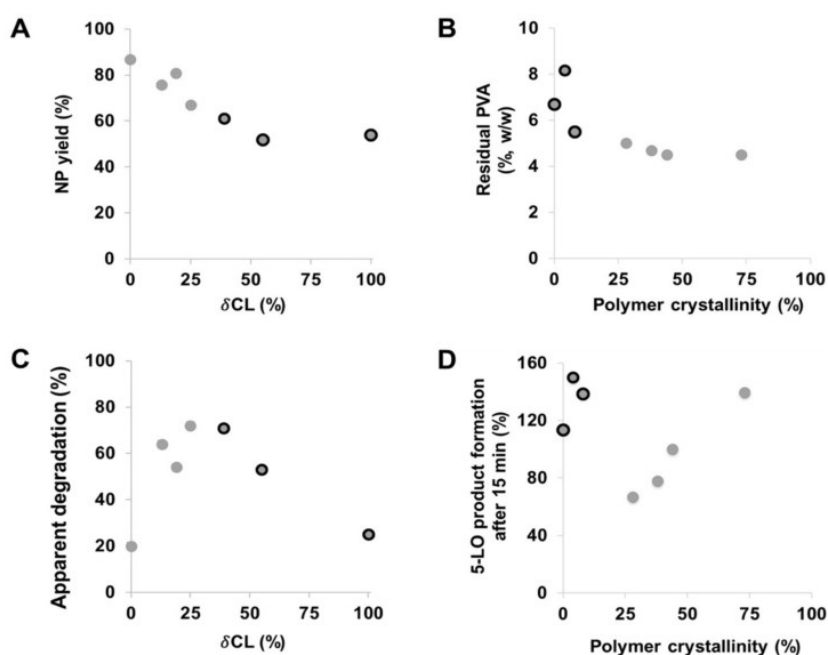


Figure 2. Influence of the δ CL fraction on the yield of drug-loaded PCL NPs (A), influence of the polymer crystallinity on the residual PVA content of drug-loaded PCL NPs (B), apparent degradation represented by the normalized relative count rate (%) after 20 h plotted against the δ CL fraction of the copolymers (C) and influence of polymer crystallinity on the efficiency of drug-loaded PCL NPs to inhibit 5-LO product formation (D). Black-circled data points represent PCL polymers with a degree of crystallinity below 10% and a $T_g < 37^\circ\text{C}$.

Furthermore, it was observed that the residual amount of PVA in the drug-loaded NPs was higher compared to the empty NPs for all PCL copolymers (Table 1 and SI, Table S3). As mentioned before, such differences are typically a result of strong drug–polymer interactions [31], and in this case, the interactions of the BRP-187 with the chains of PVA polymer. Moreover, the residual PVA content was noticeably higher for less crystalline copolymers with a higher δ CL fraction and highest for the particles consisting of the P δ CL homopolymer (Figure 2B). Apparently, the surfactant molecules tended to stick to the surface or were even incorporated into the particles formed from amorphous polyesters that are above their glass transition temperature during formulation. As soon as the materials were semicrystalline and below T_m , the degree of crystallinity did not influence the amount of residual PVA anymore. Besides providing dispersion stability, surfactants also influence the degradation rate of NPs since they adsorb at the surface of the particles forming a layer that protects from enzymatic hydrolysis to some degree [32]. Additional characterization experiments of the PCL[BRP-187] NPs were performed to investigate the degradation kinetics as well as the biological evaluation of the NP efficiency to inhibit the drug targets in vitro.

3.1. Degradation Studies

Among the aliphatic polyesters that are most commonly investigated for drug delivery applications, PCL has a superior thermal stability, with a decomposition temperature of 100 °C higher above that of the typical PLA- and PGA-based polymers [15]. Due to its high durability, P ϵ CL has found a wide range of applications mainly for implantable medical devices [33,34], in which degradation occurs over two to four years [13]. However, to tailor their application for drug delivery purposes, faster degradation kinetics of the P ϵ CL are desirable and can be achieved by copolymerization of ϵ CL with its isomer δ CL [9]. Introducing δ CL repeating units to the P ϵ CL polymer decreases its degree of crystallinity [17], and as such, it increases its rate of degradation as confirmed by investigations of films [35]. Figure 3 shows the enzymatic degradation of the PCL[BRP-187] particles incubated for 24 h at 37 °C as monitored by DLS. The apparent NPs degradation was inferred by monitoring changes in the sample concentration over time, as indicated by the count rate on the DLS under constant measurement settings [21]. In agreement with literature reports regarding film degradation, Figure 3 reveals that the degradation of the most crystalline ϵ 100- δ 0 was the slowest in the nanoparticulate state. ϵ 100- δ 0 is predominantly a semicrystalline material with a melting point considerably higher than the experimental temperature of 37 °C. It was noticed that except for the ϵ 0- δ 100 homopolymer, which degraded only about 25% after 24 h, the NP degradation rate generally increased with the amount of the δ CL (Figure 3A). This was expected since the long-range order and the compact structure of crystalline materials requires higher levels of energy for degradation compared to the less organized molecular arrangement of amorphous materials [29,36].

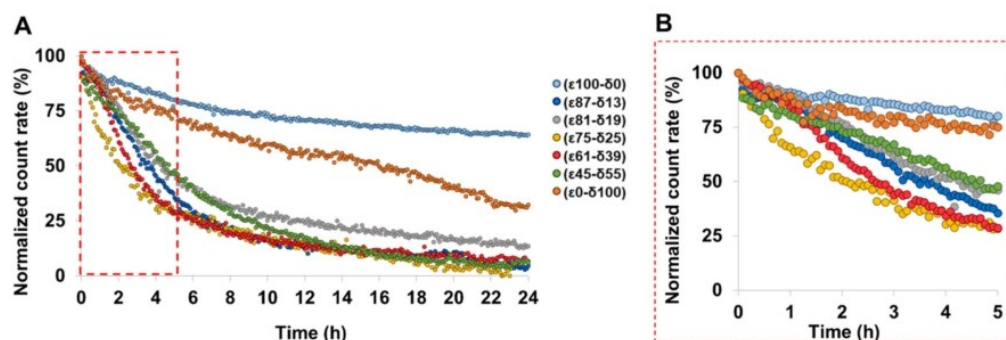


Figure 3. Normalized count rate of BRP-187-loaded PCL NPs incubated with *Candida rugosa* as measured by DLS for 24 h (A). (B) depicts a zoomed-in area into the data until 5 h.

This observation is further confirmed by other studies that have also demonstrated that the amorphous regions within bulk and/or films of P ϵ CL polymer degraded faster compared to the crystalline regions [35,37,38]. Another study with similar observations argued that polyesters with higher crystallinity exhibit a slower degradation because in a densely packed crystal, it is more difficult for the enzymes to reach the cleavable bonds [39]. In general, our results revealed that all copolymer NPs featured an apparent degradability above 50% within 5 h (Figure 3B). A faster initial degradation was particularly observed for the ϵ 75- δ 25 and ϵ 61- δ 39 copolymers since they exhibit melting points (42 °C and 24 °C, respectively [17]) that are closer to the experimental temperature of 37 °C, which was chosen to simulate the conditions of the human body (Figures 2C and 3B) [8].

3.2. In vitro Performance of NPs

Although clear influences of the polymer crystallinity and physical state on NP formulation and enzymatic degradation were found, other effects might come into play in the more complex environment of a cell. The PCL[BRP-187] particles were hence tested in human PMNL for bioactivity. PMNL are the most abundant leukocytes in the blood and

are a major source for FLAP-dependent 5-LO product biosynthesis, thus they are suitable cells for evaluation of various anti-LT agents. Note that FLAP as helper-protein of 5-LO has no enzyme activity that can be experimentally assessed, but instead assists 5-LO in LT formation by facilitating the access towards the substrate for the 5-LO enzyme. At first, the PCL[BRP-187] NPs were compared to the free drug for their influence on the cell viability of PMNL (cytotoxicity). No cytotoxic effects of the particles were found within a 5 h incubation as shown in the SI (Figure S2). These results were in agreement with previous studies that demonstrated PCL NPs to be biocompatible [40,41]. Considering their good biocompatibility, all PCL[BRP-187] particles as well as the free drug were studied for their efficiency to inhibit the drug target FLAP in PMNL and, thus, to prevent 5-LO product formation [42]. Therefore, a drug concentration of 0.3 μM was chosen for free and encapsulated BRP-187, which were investigated at different preincubation times (15 min, 1 h, 2 h and 5 h, respectively). As shown in Figure 4A, 5-LO product formation was clearly suppressed after 15 min of incubation with the PCL[BRP-187] particles to variant degrees, but essentially the particles performed as efficiently as the free drug. Apart from this, there was no significant difference between the different PCL[BRP-187] polymers at longer incubation time points (i.e., 1–5 h; Figure 4B and SI, Figure S3). More specifically, the NPs prepared with $\epsilon 75\text{-}\delta 25$ prevented the 5-LO product formation most after 15 min of incubation (Figure 4A). This observation also correlated with the fastest apparent degradation of the $\epsilon 75\text{-}\delta 25$ copolymer (Figure 3B), which might be promoted by its melting point of 42 $^{\circ}\text{C}$, which is around the temperature of cell incubation (i.e., 37 $^{\circ}\text{C}$). Karavelidis et al. reported that other polyesters with melting points around 37 $^{\circ}\text{C}$ exhibited a faster drug release [8]. It can be inferred that the rapid degradation of $\epsilon 75\text{-}\delta 25$ led to an accelerated release of the BRP-187, thereby considerably preventing the 5-LO product formation at early time points (Figure 2C,D). NPs formed from PCL with higher ϵCL fraction and hence higher T_m , as well as a higher degree of crystallinity, were less effective. As shown in Figure 2D, the 5-LO product formation was almost linearly dependent on the polymer crystallinity if only the semicrystalline materials are considered. The better performance of the NPs with lower crystallinity could be explained by two effects based on two different release mechanisms. Firstly, less crystalline materials with a larger fraction of amorphous domains enable a faster diffusion of the drug through the polymer matrix without barriers formed by crystalline domains [11,43]. Secondly, if the drug release is promoted through polymer degradation, these amorphous domains would most likely be more accessible for enzymes catalyzing the polyester hydrolysis [11].

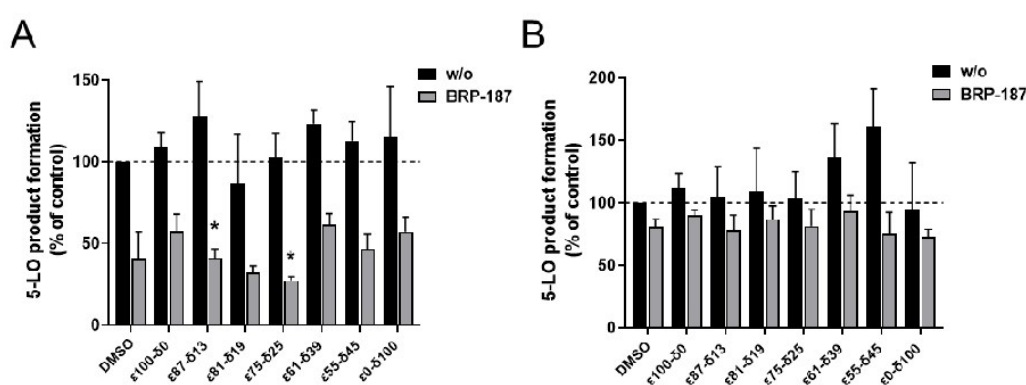


Figure 4. Measurement of 5-LO product formation as an indicator for the inhibition of the drug target FLAP by BRP-187 [36]. PMNL preincubated with DMSO, BRP-187 (0.3 μM), empty PCL particles (labeled as w/o) or PCL particles with BRP-187 (labeled with BRP-187; 0.3 μM respective BRP-187) for 15 min (A) or 5 h (B) at 37 $^{\circ}\text{C}$. Values are given as 5-LO products as a percentage of control (DMSO) ($n = 3$). Statistical analysis was performed via one-way ANOVA and Tukeys multi comparison test with logarithmic trans-formed data (* $p < 0.05$).

Based on the apparent enzymatic degradation of the PCL NPs, a burst release of the drug is conceivable considering the immediate decrease in the count rate of at least 5 to 10% of all PCL NPs (Figure 3B). The slightly higher efficiency of the NPs to inhibit 5-LO product formation in PMNL within 15 min supports this idea (Figure 4A). For the polymers with a degree of crystallinity below 10% and $T_g < 37^\circ\text{C}$, namely $\epsilon 61\text{-}\delta 39$, $\epsilon 55\text{-}\delta 45$ and $\epsilon 00\text{-}\delta 100$, inhibition of 5-LO product formation is less apparent after 15 min of incubation (Figure 2D, black-circled data points). This is presumably because these polymers are molten and more viscous at 37°C . As a consequence, they could delay the release of the drug and therefore hamper the drug action in the cells.

Furthermore, the coating effect of PVA might reduce the influence of the crystallinity of NPs or their intracellular drug release. It is reported that increasing amounts of residual surfactant decrease the cellular uptake of the NPs [44,45]. This could explain why the PCL copolymers with a higher fraction of δCL containing more residual PVA (Figure 2B) were less efficient to inhibit 5-LO product formation after 15 min of incubation (Figure 2C, Figure 4A) when compared to the PCL copolymers with a higher ϵCL fraction containing less residual PVA. However, no correlation was observed between suppression of 5-LO product formation and the PVA content in the formulation, showing that the trend cannot be generalized (SI, Figure S4).

4. Conclusions

A library of poly($\epsilon\text{CL-ran-}\delta\text{CL}$) copolymers with a constant HHB but different degrees of crystallinity were used to encapsulate BRP-187 into polymer NPs. PCL[BRP-187] particles with a diameter of 200 to 300 nm were successfully produced, whereby a comparable drug-loading was observed with LC between 1.4% and 1.9%, with the exception of the P δCL homopolymer, which revealed a higher LC. It was evident that the degree of crystallinity directly influenced the enzymatic degradation rate of the PCL copolymer, whereby the degradation increased with an increasing fraction of δCL repeating units. In addition, increasing the amount of δCL in the polymer increased the amount of residual surfactant in the NP formulation but decreased the final NP yield. The release of bioactive BRP-187 from the PCL NPs was demonstrated in vitro in PMNL by inhibiting FLAP-dependent 5-LO product formation, whereby the inhibition efficiency was dependent on the degree of crystallinity of the copolymers used for the particle formulation. The NPs of $\epsilon 75\text{-}\delta 25$ revealed the fastest degradation and inhibited the 5-LO product formation more than the other copolymers after 15 min of incubation in PMNL; longer preincubation times (1 to 5 h) reduced the potency. In conclusion, although all PCL copolymers were suited to produce NPs, the $\epsilon 75\text{-}\delta 25$ copolymer can be considered as a more promising candidate to be further investigated for both its physicochemical properties and its performance in more complex biological models. When designing superior materials for NP-mediated drug delivery, it hence seems promising to rely on polymers that are in a solid state of matter at 37°C but feature a low degree of crystallinity. However, it is not yet clear if these observations can be applied to other systems. Thus, our future research will concentrate on the encapsulation of other anti-inflammatory drugs in the polymer library with constant HHB to determine if the effect of polymer crystallinity of the present PCL systems can be transferred to other actives. In addition, we are currently establishing similar libraries mimicking the HHB of PLA to understand if our findings can be generalized in the field of polyester-based drug carrier materials.

Supplementary Materials: The following are available online at <https://www.mdpi.com/article/10.3390/polym13152557/s1>, Figure S1: Hydrodynamic diameter (intensity-weighted distribution, circles) and PDI (bars) of the homopolymer $\epsilon 100\text{-}\delta 0$ and $\epsilon 0\text{-}\delta 100$ NPs over a range of PVA concentration used in the formulation, Figure S2: Cell viability measured with a Beckman ViCell XR cell counter by trypan blue staining. A total of 1×10^7 PMNL were diluted in PBS plus 0.1% of glucose and incubated with DMSO, BRP-187 (10 μM), empty PCL particles (labeled as w/o) or PCL particles with BRP-187 (labeled with BRP-187; respective amount to 10 μM BRP-187) for 5 h at 37°C . Values are given as 5-LO products as a percentage of control (DMSO) ($n = 3$), Figure S3: Measurement of 5-LO product

formation as indicator for the inhibition of the drug target 5-lipoxygenase-activating protein (FLAP) by BRP-187.[37] A total of 5×10^6 polymorphonuclear leukocytes (PMNL) diluted in PBS containing 0.1% glucose and 1mM CaCl_2 were preincubated with DMSO, BRP-187 (0.3 μM), empty PCL particles (labeled as w/o) or PCL particles with BRP-187 (labeled as BRP-187; 0.3 μM respective BRP-187) for 1 h (A) and 2 h (B) at 37 °C and further stimulated with 2.5 μM A23187 for 10 min. The reaction was stopped with 1 mL ice-cold methanol containing 200 ng mL⁻¹ PGB1 as internal standard. Lipid mediators were extracted via solid-phase extraction (SPE) and analyzed with HPLC. Values are given as 5-LO products (LTB4, its trans-isomers 4 and 5-HETE) as a percentage of control (DMSO) (n = 3), Figure S4: Influence of the residual PVA on the efficiency of drug-loaded PCL NPs on 5-LO inhibition. Black-circled data points represent PCL polymers with bulk degree of crystallinity below 10% and glass transition temperature $T_g < 37$ °C. Table S1: Molar mass and composition of the (co)polyesters. Details are described in a previous publication, Table S2: Properties of PCL[BRP-187] NPs formulated from THF utilizing polymer concentration of 5 mg mL⁻¹ (n = 1 batch), Table S3: Particle properties of empty PCL NPs prepared in THF with c = 2.5 mg mL⁻¹ (n = 2 batches) obtained by DLS and ELS measurements after purification and after lyophilization and subsequent resuspension (n = 2 for purified NPs, n = 1 for lyophilized NPs), Table S4: DLS intensity-weighted size distribution of PCL[BRP-187] NPs of one formulation round after purification, as well as after lyophilization and resuspension in water.

Author Contributions: Performance of experiments, A.V., C.K., B.B.-S., S.S.; writing—review and editing, A.V., C.K., B.S., C.W.; polymer synthesis, D.B.; synthesis of BRP-187, J.A.C.; supervision, S.H., C.W., O.W., U.S.S.; project administration, A.V. All authors have read and agreed to the published version of the manuscript.

Funding: This work was supported by the Deutsche Forschungsgemeinschaft (DFG), Collaborative Research Center SFB 1278 “PolyTarget”, (project number 316213987, projects A04, A06 and Z01). The SEM facilities of the Jena Center for Soft Matter (JCSM) were established with a grant from the DFG (INST 275/307-1 FUGG).

Institutional Review Board Statement: Not applicable.

Informed Consent Statement: Not applicable.

Data Availability Statement: The data presented in this study are available on request from the corresponding author.

Conflicts of Interest: The authors declare no conflict of interest.

References

- Barenholz, Y. Doxil[®]—the first fda-approved nano-drug: Lessons learned. *J. Control. Release* **2012**, *160*, 117–134. [CrossRef]
- Mitragotri, S.; Burke, P.A.; Langer, R. Overcoming the challenges in administering biopharmaceuticals: Formulation and delivery strategies. *Nat. Rev. Drug Discov.* **2014**, *13*, 655–672. [CrossRef]
- Murthy, S.K. Nanoparticles in modern medicine: State of the art and future challenges. *Int. J. Nanomed.* **2007**, *2*, 129–141.
- Guo, Z.C.; Poot, A.A.; Grijpma, D.W. Advanced polymer-based composites and structures for biomedical applications. *Eur. Polym. J.* **2021**, *149*, 110388. [CrossRef]
- Keshvardoostchokami, M.; Majidi, S.S.; Huo, P.P.; Ramachandran, R.; Chen, M.L.; Liu, B. Electrospun nanofibers of natural and synthetic polymers as artificial extracellular matrix for tissue engineering. *Nanomaterials* **2021**, *11*, 21. [CrossRef]
- Shkodra, B.; Vollrath, A.; Schubert, U.S.; Schubert, S. Polymer-based nanoparticles for biomedical applications. In *Colloids for Nanobiotechnology—Synthesis, Characterization and Potential Applications*, 1st ed.; Parak, W., Feliu, N., Eds.; Elsevier: Amsterdam, The Netherlands, 2020; Volume 16, pp. 233–252.
- Englert, C.; Brendel, J.C.; Majdanski, T.C.; Yildirim, T.; Schubert, S.; Gottschaldt, M.; Windhab, N.; Schubert, U.S. Pharmapolymers in the 21st century: Synthetic polymers in drug delivery applications. *Prog. Polym. Sci.* **2018**, *87*, 107–164. [CrossRef]
- Karavelidis, V.; Karavas, E.; Giliopoulos, D.; Papadimitriou, S.; Bikiaris, D. Evaluating the effects of crystallinity in new biocompatible polyester nanocarriers on drug release behavior. *Int. J. Nanomed.* **2011**, *6*, 3021–3032.
- Song, Q.L.; Xia, Y.N.; Hu, S.Y.; Zhao, J.P.; Zhang, G.Z. Tuning the crystallinity and degradability of PCL by organocatalytic copolymerization with delta-hexalactone. *Polymer* **2016**, *102*, 248–255. [CrossRef]
- Schneiderman, D.K.; Hillmyer, M.A. Aliphatic polyester block polymer design. *Macromolecules* **2016**, *49*, 2419–2428. [CrossRef]
- Kamaly, N.; Yameen, B.; Wu, J.; Farokhzad, O.C. Degradable controlled-release polymers and polymeric nanoparticles: Mechanisms of controlling drug release. *Chem. Rev.* **2016**, *116*, 2602–2663. [CrossRef]
- Danhier, F.; Ansorena, E.; Silva, J.M.; Coco, R.; Le Breton, A.; Preat, V. PLGA-based nanoparticles: An overview of biomedical applications. *J. Control. Release* **2012**, *161*, 505–522. [CrossRef]

13. Woodruff, M.A.; Hutmacher, D.W. The return of a forgotten polymer-polycaprolactone in the 21st century. *Prog. Polym. Sci.* **2010**, *35*, 1217–1256. [CrossRef]
14. Hakkarainen, M.; Hoglund, A.; Odellius, K.; Albertsson, A.C. Tuning the release rate of acidic degradation products through macromolecular design of caprolactone-based copolymers. *J. Am. Chem. Soc.* **2007**, *129*, 6308–6312. [CrossRef] [PubMed]
15. Engelberg, I.; Kohn, J. Physicomechanical properties of degradable polymers used in medical applications—A comparative-study. *Biomaterials* **1991**, *12*, 292–304. [CrossRef]
16. Lee, I.H.; Palombo, M.S.; Zhang, X.P.; Szekely, Z.; Sinko, P.J. Design and evaluation of a cxcr4 targeting peptide 4dv3 as an hiv entry inhibitor and a ligand for targeted drug delivery. *Eur. J. Pharm. Biopharm.* **2019**, *138*, 11–22.
17. Bandelli, D.; Muljajew, I.; Scheuer, K.; Max, J.B.; Weber, C.; Schacher, F.H.; Jandt, K.D.; Schubert, U.S. Copolymerization of caprolactone isomers to obtain nanoparticles with constant hydrophobicity and tunable crystallinity. *Macromolecules* **2020**, *53*, 5208–5217. [CrossRef]
18. Garscha, U.; Voelker, S.; Pace, S.; Gerstmeier, J.; Emini, B.; Liening, S.; Rossi, A.; Weinigel, C.; Rummeler, S.; Schubert, U.S.; et al. BRP-187: A potent inhibitor of leukotriene biosynthesis that acts through impeding the dynamic 5-lipoxygenase/5-lipoxygenase-activating protein (FLAP) complex assembly. *Biochem. Pharmacol.* **2016**, *119*, 17–26. [CrossRef]
19. Koeberle, A.; Werz, O. Natural products as inhibitors of prostaglandin e-2 and pro-inflammatory 5-lipoxygenase-derived lipid mediator biosynthesis. *Biotechnol. Adv.* **2018**, *36*, 1709–1723. [CrossRef]
20. Koeberle, A.; Zettl, H.; Greiner, C.; Wurglics, M.; Schubert-Zsilavecz, M.; Werz, O. Pirinixic acid derivatives as novel dual inhibitors of microsomal prostaglandin e-2 synthase-1 and 5-lipoxygenase. *J. Med. Chem.* **2008**, *51*, 8068–8076. [CrossRef]
21. Shkodra-Pula, B.; Kretzer, C.; Jordan, P.M.; Klemm, P.; Koeberle, A.; Pretzel, D.; Banoglu, E.; Lorkowski, S.; Wallert, M.; Hoppener, S.; et al. Encapsulation of the dual FLAP/mPEGs-1 inhibitor brp-187 into acetalated dextran and plga nanoparticles improves its cellular bioactivity. *J. Nanobiotechnol.* **2020**, *18*, 73. [CrossRef] [PubMed]
22. Malvern Panalytical; Zetasizer Nano User Manual man0485. Available online: <https://www.Malvernpanalytical.Com/de/learn/knowledge-center/user-manuals/man0485en> (accessed on 8 July 2021).
23. Spek, S.; Haeuser, M.; Schaefer, M.M.; Langer, K. Characterisation of pegylated PLGA nanoparticles comparing the nanoparticle bulk to the particle surface using UV/Vis spectroscopy, SEC, H-1 nmr spectroscopy, and x-ray photoelectron spectroscopy. *Appl. Surf. Sci.* **2015**, *347*, 378–385. [CrossRef]
24. Werz, O.; Burkert, E.; Samuelsson, B.; Radmark, O.; Steinhilber, D. Activation of 5-lipoxygenase by cell stress is calcium independent in human polymorphonuclear leukocytes. *Blood* **2002**, *99*, 1044–1052. [CrossRef] [PubMed]
25. Perevyazko, I.Y.; Vollrath, A.; Pietsch, C.; Schubert, S.; Pavlov, G.M.; Schubert, U.S. Nanoprecipitation of poly(methyl methacrylate)-based nanoparticles: Effect of the molar mass and polymer behavior. *J. Polym. Sci. Pol. Chem.* **2012**, *50*, 2906–2913. [CrossRef]
26. Shkodra-Pula, B.; Grune, C.; Traege, A.; Vollrath, A.; Schuber, S.; Fischer, D.; Schubert, U.S. Effect of surfactant on the size and stability of plga nanoparticles encapsulating a protein kinase c inhibitor. *Int. J. Pharm.* **2019**, *566*, 756–764. [CrossRef] [PubMed]
27. Beck-Broichsitter, M.; Nicolas, J.; Couvreur, P. Solvent selection causes remarkable shifts of the “ouzo region” for poly(lactide-co-glycolide) nanoparticles prepared by nanoprecipitation. *Nanoscale* **2015**, *7*, 9215–9221. [CrossRef]
28. Homs, M.; Caldero, G.; Monge, M.; Morales, D.; Solans, C. Influence of polymer concentration on the properties of nano-emulsions and nanoparticles obtained by a low-energy method. *Colloids Surf. A Physicochem. Eng. Asp.* **2018**, *536*, 204–212. [CrossRef]
29. Sanchez, A.; Mejia, S.P.; Orozco, J. Recent advances in polymeric nanoparticle-encapsulated drugs against intracellular infections. *Molecules* **2020**, *25*, 3760. [CrossRef]
30. Newman, A.; Hastedt, J.E.; Yazdani, M. New directions in pharmaceutical amorphous materials and amorphous solid dispersions. *AAPS Open* **2017**, *3*, 7. [CrossRef]
31. Du, S.; Li, W.S.; Wu, Y.R.; Fu, Y.; Yang, C.Q.; Wang, J. Comparison of the physical and thermodynamic stability of amorphous azelnidipine and its coamorphous phase with piperazine. *RSC Adv.* **2018**, *8*, 32756–32764. [CrossRef]
32. Lee, S.C.; Oh, J.T.; Jang, M.H.; Chung, S.I. Quantitative analysis of polyvinyl alcohol on the surface of poly(d,l-lactide-co-glycolide) microparticles prepared by solvent evaporation method: Effect of particle size and PVA concentration. *J. Control. Release* **1999**, *59*, 123–132. [CrossRef]
33. Hollander, J.; Genina, N.; Jukarainen, H.; Khajeheian, M.; Rosling, A.; Makila, E.; Sandler, N. Three-dimensional printed PCL-based implantable prototypes of medical devices for controlled drug delivery. *J. Pharm. Sci.* **2016**, *105*, 2665–2676. [CrossRef] [PubMed]
34. Manoukian, O.S.; Arul, M.R.; Sardashti, N.; Stedman, T.; James, R.; Rudraiah, S.; Kumbar, S.G. Biodegradable polymeric injectable implants for long-term delivery of contraceptive drugs. *J. Appl. Polym. Sci.* **2018**, *135*, 46068. [CrossRef]
35. Eldsater, C.; Erlandsson, B.; Renstad, R.; Albertsson, A.C.; Karlsson, S. The biodegradation of amorphous and crystalline regions in film-blown poly(epsilon-caprolactone). *Polymer* **2000**, *41*, 1297–1304. [CrossRef]
36. Pitt, G.G.; Gratzl, M.M.; Kimmel, G.L.; Surles, J.; Sohndler, A. Aliphatic polyesters ii. The degradation of poly (dl-lactide), poly (epsilon-caprolactone), and their copolymers in vivo. *Biomaterials* **1981**, *2*, 215–220. [CrossRef]
37. Cook, W.J.; Cameron, J.A.; Bell, J.P.; Huang, S.J. Scanning electron-microscopic visualization of biodegradation of polycaprolactones by fungi. *J. Polym. Sci. Pol. Lett.* **1981**, *19*, 159–165. [CrossRef]
38. Tilstra, L.; Johnsonbaugh, D. The biodegradation of blends of polycaprolactone and polyethylene exposed to a defined consortium of fungi. *J. Environ. Polym. Degrad.* **1993**, *1*, 10. [CrossRef]

39. Bandelli, D.; Helbing, C.; Weber, C.; Seifer, M.; Muljajew, I.; Jandt, K.D.; Schubert, U.S. Maintaining the hydrophilic hydrophobic balance of polyesters with adjustable crystallinity for tailor-made nanoparticles. *Macromolecules* **2018**, *51*, 5567–5576. [[CrossRef](#)]
40. Lukaszewicz, S.; Mikolajczyk, A.; Blasiak, E.; Fic, E.; Dziedzicka-Wasylewska, M. Polycaprolactone nanoparticles as promising candidates for nanocarriers in novel nanomedicines. *Pharmaceutics* **2021**, *13*, 191. [[CrossRef](#)]
41. Ortiz, R.; Prados, J.; Melguizo, C.; Arias, J.L.; Ruiz, M.A.; Alvarez, P.J.; Caba, O.; Luque, R.; Segura, A.; Aranega, A. 5-fluorouracil-loaded poly(epsilon-caprolactone) nanoparticles combined with phage e gene therapy as a new strategy against colon cancer. *Int. J. Nanomed.* **2012**, *7*, 95–107.
42. Radmark, O.; Werz, O.; Steinhilber, D.; Samuelsson, B. 5-lipoxygenase, a key enzyme for leukotriene biosynthesis in health and disease. *Biochim. Biophys. Acta* **2015**, *1851*, 9. [[CrossRef](#)] [[PubMed](#)]
43. Tallury, P.; Alimohammadi, N.; Kalachandra, S. Poly(ethylene-co-vinyl acetate) copolymer matrix for delivery of chlorhexidine and acyclovir drugs for use in the oral environment: Effect of drug combination, copolymer composition and coating on the drug release rate. *Dent. Mater.* **2007**, *23*, 404–409. [[CrossRef](#)] [[PubMed](#)]
44. Prabha, S.; Labhasetwar, V. Effect of residual polyvinyl alcohol on nanoparticle-mediated gene transfection in breast cancer cells. *Mol. Ther.* **2003**, *7*, S67.
45. Sahoo, S.K.; Panyam, J.; Prabha, S.; Labhasetwar, V. Residual polyvinyl alcohol associated with poly (d,l-lactide-co-glycolide) nanoparticles affects their physical properties and cellular uptake. *J. Control. Release* **2002**, *82*, 105–114. [[CrossRef](#)]

Supplementary Materials

Supporting information

Effect of crystallinity on the properties of polycaprolactone nanoparticles containing the dual FLAP/mPEGS-1 inhibitor BRP-187-187

Antje Vollrath ^{a,b}, Christian Kretzer ^c, Bärbel Beringer-Siemers ^a, Blerina Shkodra ^{a,b}, Justyna A. Czaplowska ^a, Damiano Bandelli ^{a,b}, Steffi Stumpf ^{a,b}, Stephanie Hoepfner ^{a,b}, Christine Weber ^{a,b}, Oliver Werz ^{b,c}, Ulrich S. Schubert ^{a,b}*

* Corresponding author

^aLaboratory of Organic Chemistry and Macromolecular Chemistry (IOMC)
Friedrich Schiller University, Humboldtstraße 10, 07743 Jena, Germany

^bJena Center for Soft Matter (JCSM)
Friedrich Schiller University, Philosophenweg 7, 07743 Jena, Germany

^cDepartment of Pharmaceutical/Medicinal Chemistry, Institute of Pharmacy
Friedrich Schiller University, Philosophenweg 14, 07743 Jena, Germany

Table S1. Molar mass and composition of the (co)polyesters. Details are described in a previous publication.^[1]

$\epsilon\text{CL}/\delta\text{CL}^{\text{a}}$ (mol %)	$M_{\text{n, theo}}^{\text{b}}$ (kg mol ⁻¹)	$M_{\text{n, NMR}}^{\text{a}}$ (kg mol ⁻¹)	$M_{\text{n, SEC}}^{\text{c}}$ (kg mol ⁻¹)	$D_{\text{SEC}}^{\text{c}}$
100/0	11	13	19	1.17
87/13	9	13	21	1.57
81/19	9	10	19	1.41
75/25	8	10	19	1.30
61/39	7	9	16	1.26
45/55	7	7	15	1.21
0/100	10	9	6	1.09

(a) Determined by ¹H-NMR spectroscopy of the purified polymers.

(b) Molar mass expected from monomer conversions and the feed ratio.

(c) Determined by size exclusion chromatography (eluent CHCl₃, refractive index detection, polystyrene calibration).

Supporting information

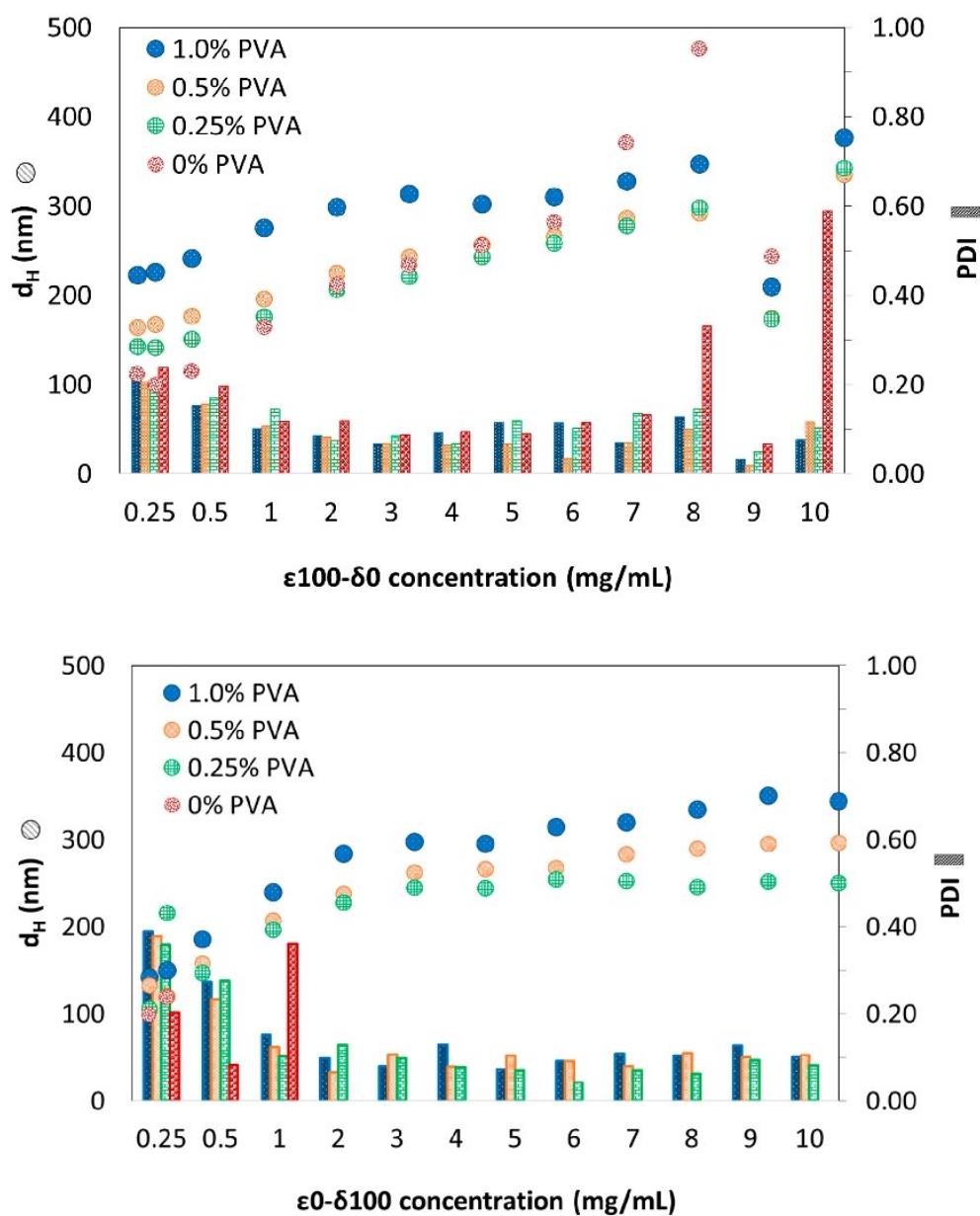


Figure S1. Hydrodynamic diameter (intensity-weighted distribution, circles) and PDI (bars) of the homopolymer $\epsilon 100\text{-}\delta 0$ and $\epsilon 0\text{-}\delta 100$ NPs over a range of PVA concentration used in the formulation.

Supporting information

Table S2. Properties of PCL[BRP-187] NPs formulated from THF utilizing polymer concentration of 5 mg mL⁻¹ (n = 1 batch).

ϵ CL/ δ CL (mol %)	Purified NPs ^a		Lyophilized NPs ^b		PVA ^d (%, w/w)	Yield ^e (%)
	d_H (nm)	PDI	d_H (nm)	PDI		
ϵ 100- δ 0	593	0.52	461	0.40	2.00	97
ϵ 87- δ 13	427	0.23	349	0.30	2.01	86
ϵ 81- δ 19	445	0.24	465	0.33	1.82	99
ϵ 75- δ 25	421	0.28	651	0.62	1.88	95
ϵ 61- δ 39	407	0.19	443	0.40	1.63	76
ϵ 45- δ 55	397	0.26	414	0.36	2.26	60
ϵ 0- δ 100	403	0.49	436	0.49	1.66	53

d_H represents the intensity-weighted distribution.

(a) NPs measured after purification.

(b) NPs measured after lyophilization and subsequent resuspension in water.

(c) Determined by UV-VIS spectroscopy at $\lambda = 316$ nm (n = 4) and calculated using $LC = (\text{mass of drug recovered}) / (\text{mass of particle recovered}) \times 100$.

(d) The determination of PVA in the NPs (% w/w) was performed according to the published protocol.^[15](e)

Yield = (mass of NPs recovered including PVA residue) / (mass of polymer + mass of drug) in the formulation $\times 100$.

Table S3. Particle properties of empty PCL NPs prepared in THF with c = 2.5 mg mL⁻¹ (n = 2 batches) obtained by DLS and ELS measurements after purification and after lyophilization and subsequent resuspension (n = 2 for purified NPs, n = 1 for lyophilized NPs).

ϵ CL/ δ CL (mol %)	Purified NPs ^a		Lyophilized NPs ^b		ZP ^b (mV)	PVA ^c (%, w/w)	Yield ^d (%)
	d_H (nm)	PDI	d_H (nm)	PDI			
ϵ 100- δ 0	250	0.08	250	0.21	-33	2.0	93
ϵ 87- δ 13	177	0.05	253	0.27	-23	2.0	68
ϵ 81- δ 19	193	0.06	268	0.28	-38	1.8	70
ϵ 75- δ 25	196	0.05	279	0.33	-32	1.9	76
ϵ 61- δ 39	170	0.08	220	0.21	-13	1.6	54
ϵ 45- δ 55	163	0.06	205	0.23	-33	2.3	51
ϵ 0- δ 100	212	0.08	285	0.30	-40	1.7	67

d_H represents the intensity-weighted distribution (five measurements) and zeta-potential (ZP) (three measurements).

(a) NPs measured after purification.

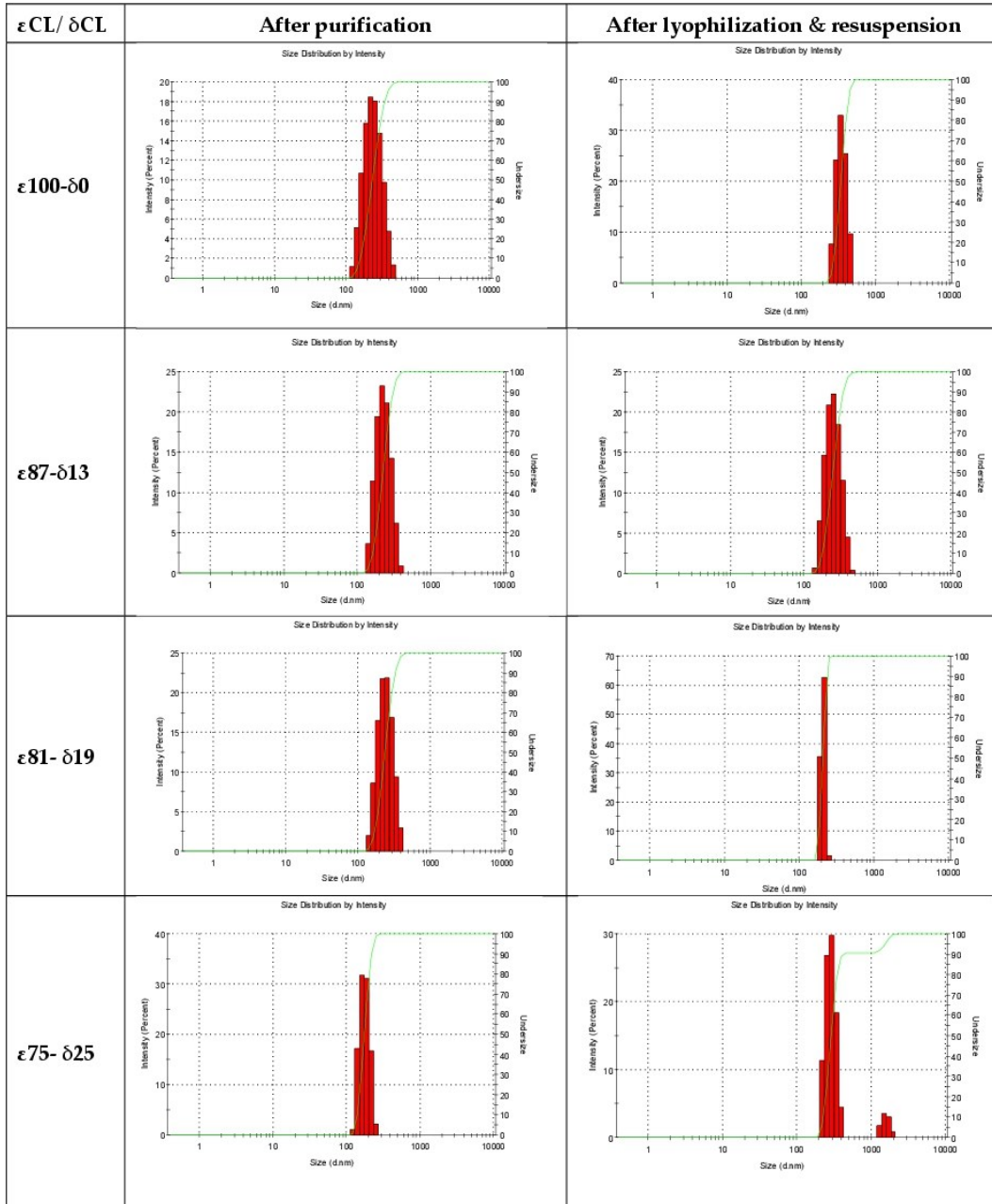
(b) NPs measured after lyophilization and subsequent resuspension in water.

(c) The determination of PVA in the NPs (% w/w) was performed according to the published protocol.^[15]

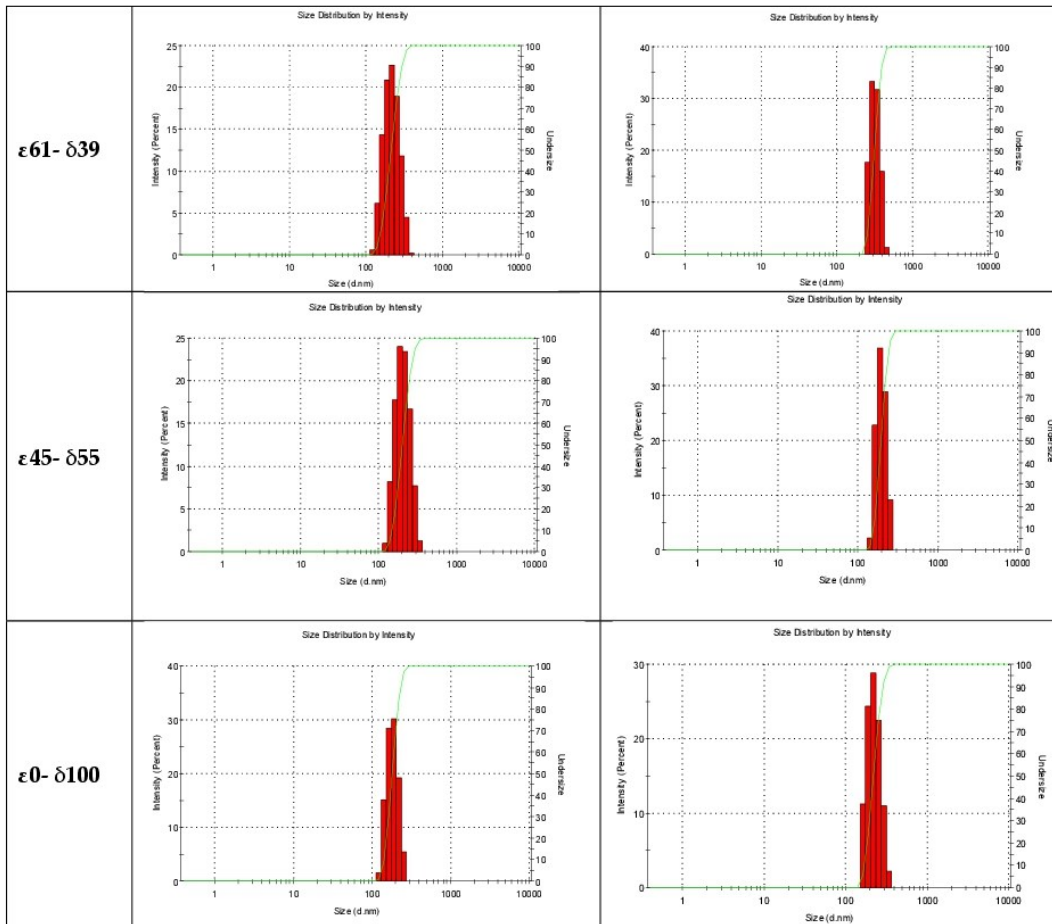
(d) Yield = (mass of NPs recovered – mass of found PVA) / (mass of polymer + mass of drug) in the formulation $\times 100$.

Supporting information

Table S4. DLS intensity-weighted size distribution of PCL[BRP-187] NPs of one formulation round after purification, as well as after lyophilization and resuspension in water.



Supporting information



Supporting information

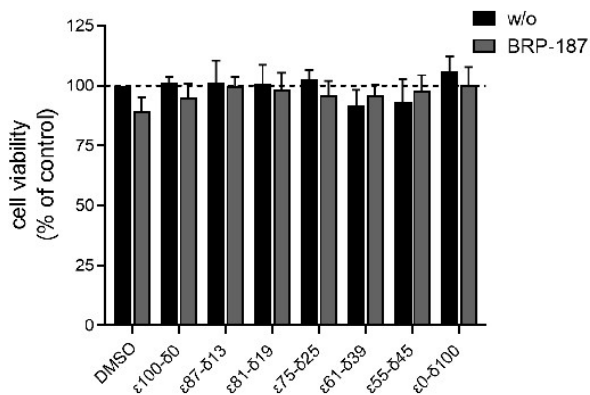


Figure S2. Cell viability measured with a Beckman ViCell XR cell counter by trypan blue staining. A total of 1×10^7 PMNL were diluted in PBS plus 0.1% of glucose and incubated with DMSO, BRP-187 (10 μ M), empty PCL particles (labeled as w/o) or PCL particles with BRP-187 (labeled with BRP-187; respective amount to 10 μ M BRP-187) for 5 h at 37 °C. Values are given as 5-LO products as a percentage of control (DMSO) (n = 3).

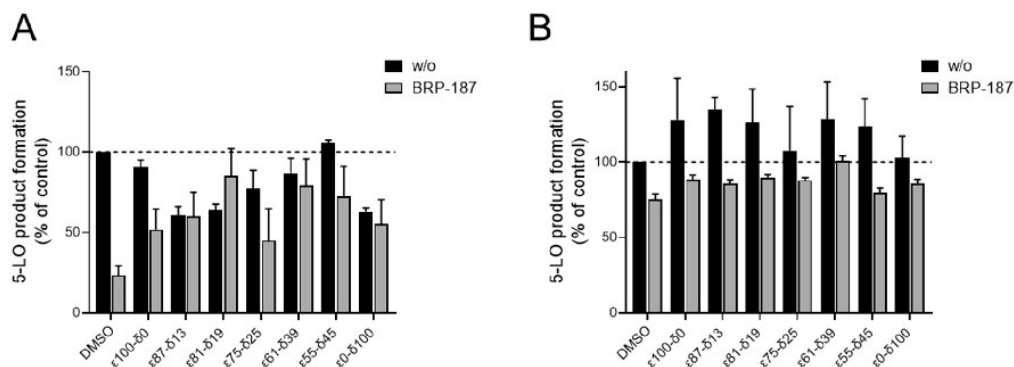


Figure S3. Measurement of 5-LO product formation as indicator for the inhibition of the drug target 5-lipoxygenase-activating protein (FLAP) by BRP-187.^[37] A total of 5×10^6 polymorphonuclear leukocytes (PMNL) diluted in PBS containing 0.1% glucose and 1mM CaCl_2 were preincubated with DMSO, BRP-187 (0.3 μ M), empty PCL particles (labeled as w/o) or PCL particles with BRP-187 (labeled as BRP-187; 0.3 μ M respective BRP-187) for 1 h (A) and 2 h (B) at 37 °C and further stimulated with 2.5 μ M A23187 for 10 min. The reaction was stopped with 1 mL ice-cold methanol containing 200 ng mL^{-1} PGB1 as internal standard. Lipid mediators were extracted via solid-phase extraction (SPE) and analyzed with HPLC. Values are given as 5-LO products (LTB_4 , its trans-isomers $_4$ and 5-HETE) as a percentage of control (DMSO) (n = 3).

Supporting information

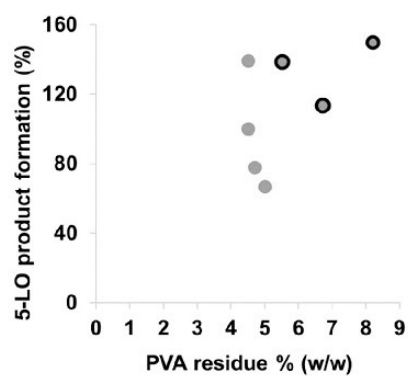


Figure S4. Influence of the residual PVA on the efficiency of drug-loaded PCL NPs on 5-LO inhibition. Black-circled data points represent PCL polymers with bulk degree of crystallinity below 10% and glass transition temperature $T_g < 37$ °C.

Manuscript V

Shifting the Biosynthesis of Leukotrienes Toward Specialized Pro-Resolving Mediators by the 5-Lipoxygenase-Activating Protein (FLAP) Antagonist BRP-201

Kretzer, C., Jordan, PM., Bilancia, R., Rossi, A., Tuğçe Gür, M., Banoglu, E., Schubert, US., Werz, O.

Journal of Inflammation Research, 2022, Feb 9;15:911-925

Der Kandidat / Die Kandidatin ist

Erstautor/-in, Ko-Erstautor/-in, Korresp. Autor/-in, Koautor/-in.

Anteile (in %) der Autoren / der Autorinnen an den vorgegebenen Kategorien der Publikation

Author	Conception	Data analysis	Experimental	Writing	Provision of Material
Kretzer C.	40 %	70 %	60 %	40 %	
Jordan P.M.		10 %	10 %	10 %	
Bilancia R			10 %		
Rossi A.					
Tuğçe Gür M.					
Banoglu E.	10 %				30 %
Schubert US.					
Werz O.	40 %			40 %	70 %
Others	10 %	20 %	20 %	10 %	
Summe:	100 %	100 %	100 %	100 %	100 %

Unterschrift Kandidat/-in

Unterschrift Betreuer/-in (Mitglied der Fakultät)

Shifting the Biosynthesis of Leukotrienes Toward Specialized Pro-Resolving Mediators by the 5-Lipoxygenase-Activating Protein (FLAP) Antagonist BRP-201

Christian Kretzer¹, Paul M Jordan¹, Rossella Bilancia², Antonietta Rossi², Tuğçe Gür Maz³, Erden Banoglu³, Ulrich S Schubert^{4,5}, Oliver Werz^{1,5}

¹Department of Pharmaceutical/Medicinal Chemistry, Institute of Pharmacy, Friedrich Schiller University Jena, Jena, 07743, Germany; ²Department of Pharmacy, School of Medicine and Surgery, University of Naples Federico II, Naples, I-80131, Italy; ³Department of Pharmaceutical Chemistry, Faculty of Pharmacy, Gazi University, Yenimahalle, 06560, Ankara, Turkey; ⁴Laboratory of Organic and Macromolecular Chemistry (IOMC), Friedrich Schiller University Jena, Jena, 07743, Germany; ⁵Jena Center for Soft Matter (JCSM) Friedrich Schiller University Jena, Jena, 07743, Germany

Correspondence: Oliver Werz, Email oliver.werz@uni-jena.de

Background and Purpose: Lipid mediators (LM) play crucial roles in the complex inflammation process with respect to initiation, maintenance, and resolution. Proinflammatory leukotrienes (LTs), generated by 5-lipoxygenase (LOX) and the 5-LOX-activating protein (FLAP), initiate and maintain inflammation while specialized pro-resolving mediators (SPMs) formed by various LOXs as key enzymes promote inflammation resolution and the return to homeostasis. Since 5-LOX also contributes to SPM biosynthesis, smart pharmacological manipulation of the 5-LOX pathway and accompanied activation of 12-/15-LOXs may accomplish suppression of LT formation but maintain or even elevate SPM formation. Here, we demonstrated that the FLAP antagonist BRP-201 possesses such pharmacological profile and causes a switch from LT toward SPM formation.

Methods and Results: Comprehensive LM metabololipidomics with activated human monocyte-derived macrophages (MDM) of M1 or M2 phenotype showed that BRP-201 strongly inhibits LT formation induced by bacterial exotoxins. In parallel, SPM levels and 12/15-LOX-derived products were markedly elevated, in particular in M2-MDM. Intriguingly, in unstimulated MDM, BRP-201 induced formation of 12/15-LOX products including SPM and caused 15-LOX-1 subcellular redistribution without affecting 5-LOX. Experiments with HEK293 cells stably expressing either 5-LOX with or without FLAP, 15-LOX-1 or 15-LOX-2 confirmed suppression of 5-LOX product formation due to FLAP antagonism by BRP-201 but activated 15-LOX-1 in the absence of FLAP. Finally, in zymosan-induced murine peritonitis, BRP-201 (2 mg/kg, ip) lowered LT levels but elevated 12/15-LOX products including SPMs.

Conclusion: BRP-201 acts as FLAP antagonist but also as 12/15-LOX activator switching formation of pro-inflammatory LTs toward inflammation-resolving SPM, which reflects a beneficial pharmacological profile for intervention in inflammation.

Keywords: lipoxygenase, specialized pro-resolving mediators, leukotrienes, lipid mediators

Introduction

Lipid mediators (LM) orchestrate inflammatory responses by modulation of the innate immune system and thereby determine the body's reaction to harmful stimuli like microbial infections or tissue damage.^{1,2} Upon cell activation during inflammation, phospholipase (PL)A₂ enzymes release polyunsaturated fatty acids (PUFA) like arachidonic acid (AA), eicosapentanoic acid (EPA), and docosahexaenoic acid (DHA) that are transformed into LM in complex interconnected networks.^{3–5} Within these complex LM networks (Figure 1), enzymatic pathways leading to leukotriene (LT) and prostaglandin (PG) formation from AA predominate at the onset of inflammation.^{2,6} In contrast, the specialized pro-resolving mediators (SPM) that encompass lipoxins (LX), resolvins (RV), protectins (PD), and maresins (MaR) are

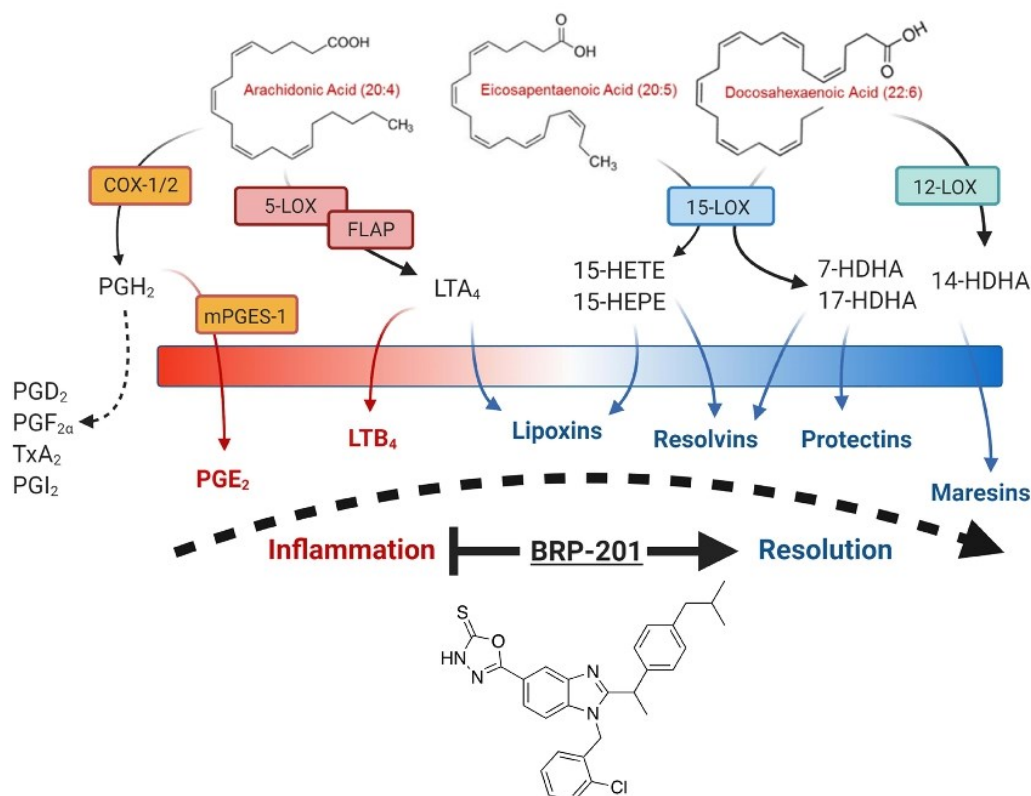


Figure 1 Biochemical pathways of lipid mediator formation and the influence of BRP-201. Schematic overview of LM-biosynthetic pathways during the acute phase of inflammation (red) and the inflammation resolution phase (blue). COX-1/2 and 5-LOX/FLAP generate PGE₂ and LTB₄, respectively, which are the major pro-inflammatory LM, while 12- and 15-LOX, partially in conjunction with 5-LOX, biosynthesize the SPMs namely lipoxins, E- and D-series resolvins, protectins and maresins. The FLAP antagonist BRP-201 suppresses LTB₄ formation but elevates generation of SPM, and may thereby promote inflammation resolution.

produced from these PUFAs in a delayed manner in order to terminate and resolve inflammation leading to tissue repair and regeneration.^{2,4}

For PG formation, cyclooxygenase (COX)-1 and -2 produce the intermediate PGH₂ from AA, which is further metabolized by different synthases to PG and thromboxane (TX), where PGE₂ is massively formed in inflammation by microsomal prostaglandin E₂ synthase-1 (mPGES-1) with vasodilatory, tissue permeabilizing, pain sensitizing, and fever inducing effects.⁷ The formation of LT is accomplished by conversion of AA by 5-lipoxygenase (5-LOX) aided by the nuclear membrane-bound 5-LOX-activating protein (FLAP) to 5(*S*)-hydroperoxyeicosatetraenoic acid (5-HPETE) that is further dehydrated to the epoxide LTA₄ or reduced to 5(*S*)-hydroxyeicosatetraenoic acid (5-HETE).⁸ Conversion of LTA₄ by LTA₄ hydrolase (LTA₄H) yields LTB₄ that exacerbates inflammation and recruits neutrophils while LTC₄ synthase converts LTA₄ to LTC₄, D₄ and E₄ that increase vasopermeability and constrict small vessels and bronchi.^{9,10} For FLAP, no enzymatic activity has yet been shown and it is believed that FLAP facilitates the access of 5-LOX to AA that is provided by cPLA₂ at the nuclear membrane.⁸ FLAP is mandatory for LT formation *in vivo* and in intact cells from endogenously provided AA, and genetic or pharmacological interference with FLAP efficiently blocks LT formation, conferring FLAP as promising drug target for LT-related disorders.^{11,12} In contrast, transformations of PUFAs by the 12/15-LOXs are apparently independent of FLAP.^{13,14}

The biosynthesis of SPMs is mainly driven by 12/15-LOXs, partially in conjunction with 5-LOX at least for LX and RV biosynthesis, while MaR and PD formation is 5-LOX-independent.⁴ Furthermore, CYP enzymes or acetylated COX-2 (by aspirin) may act together with 5-LOX to generate EPA-derived RVs via 18-HEPE, and epimers of LX and RV via

15*R*-HETE or 17*R*-HDHA, respectively. 12/15-LOX, CYP and Ac-COX-2 confer the first step in the conversion of PUFAs and then 5-LOX acts on the de-novo-biosynthesized precursors 15-HETE, 15-HEPE, 18-HEPE and 17-HDHA as substrates for SPM formation. Whether FLAP assists 5-LOX in the production of SPM from those mono-hydroxylated precursors is still a matter of debate¹⁵ but accumulating evidence indicates that SPM formation is FLAP-independent.^{13,14,16}

Anti-inflammatory drugs like COX or 5-LOX inhibitors suppress formation of all PG or LT, respectively, but are essentially inefficient to resolve inflammation and cause adverse side effects in clinical therapy.^{17–19} Novel smart inhibitors that promote the switch from pro-inflammatory to pro-resolving LM might have potential as new pharmacological strategy not only to dampen inflammation but also to push its resolution, tissue regeneration and return to homeostasis.²⁰ Here, we studied the pharmacological profile of the recently identified FLAP antagonist BRP-201 (5-{1-[(2-chlorophenyl)methyl]-2-[1-[4-(2-methylpropyl)phenyl]ethyl]-1H-benzimidazole-5-yl]-2,3-dihydro-1,3,4-oxadiazole-2-thione)²¹ for modulation of broad LM networks (Figure 1) in human pro-inflammatory M1 and anti-inflammatory M2 monocyte-derived macrophages (MDM) and in the peritoneum of zymosan-challenged mice *in vivo*. Our data show that in both experimental models BRP-201 efficiently blocked LT formation but elevated concomitant generation of SPM and their 12/15-LOX-derived precursors.

Materials and Methods

Materials

BRP-201 was synthesized as reported by us before.²¹ Deuterium-labeled and non-labeled LM standards for ultra-performance liquid chromatography-tandem mass spectrometry (UPLC-MS-MS) quantification were obtained from Cayman Chemical/Biomol (Hamburg, Germany). All other chemicals were obtained at Sigma-Aldrich (Taufkirchen, Germany) unless stated otherwise.

Cell Isolation and Cell Culture

Leukocyte concentrates obtained from the Institute of Transfusion Medicine of the University Hospital Jena were prepared from peripheral blood from healthy human adult donors that had not taken any anti-inflammatory drugs for the last 10 days prior to blood donation. Informed consent was provided by the donors. The ethical committee of the University Hospital approved the protocol, and all performed methods were in accordance with the relevant regulations and guidelines. To isolate monocytes, the erythrocytes were sedimented by mixing the leukocyte concentrates with dextran (from *leuconostoc* spp. MW ~40,000, Sigma Aldrich, Taufkirchen, Germany). The supernatant was covered with lymphocyte separation medium (Histopaque[®]-1077, Sigma Aldrich, Taufkirchen, Germany) and centrifuged (2000 *g*, 10 min, 4°C). The peripheral blood mononuclear cells (PBMC) on the top of the lymphocyte separation medium were washed twice with ice-cold PBS and seeded in cell culture flasks for 1 h (37°C, 5% CO₂) in PBS with Ca²⁺/Mg²⁺ to isolate the adherent monocytes. Differentiation and polarization into M1 and M2 macrophages was performed as described.¹⁴ In brief, to obtain M1 macrophages, adherent monocytes were treated with 20 ng mL⁻¹ granulocyte macrophage-colony stimulating factor (GM-CSF, Peprotech, Hamburg, Germany) for six days in RPMI 1640 supplemented with 10% fetal calf serum (FCS), 2 mmol L⁻¹ L-glutamine, penicillin (100 U mL⁻¹) and streptomycin (100 µg mL⁻¹) and subsequently incubated for another 48 h with 100 ng mL⁻¹ lipopolysaccharide (LPS) and 20 ng mL⁻¹ interferon- γ (IFN- γ , Peprotech). To obtain M2 macrophages, 20 ng mL⁻¹ M-CSF (Peprotech) was added to monocytes for six days, followed by 20 ng mL⁻¹ IL-4 (Peprotech) for 48 h. Correct polarization and purity of macrophages were routinely checked by flow cytometry (FACS Canto Plus flow cytometer, BD Biosciences, Heidelberg, Germany) as reported¹⁴ using the following antibodies: FITC anti-human CD14 (2 µg/test, clone M5E2, BD Biosciences), PE anti-human CD54 (1 µg/test, clone HA58, BD Biosciences), APC-H7 anti-human CD80 (0.25 µg/test, clone L307.4, BD Biosciences), PE-Cy7 anti-human CD163 (2 µg/test, clone RM3/1, Biolegend, San Diego, CA, USA), PerCP-eFluor710 anti-human CD206 (0.06 µg/test, clone 19.2, BD Biosciences, San Diego, CA, USA).

HEK293 cells (purchased commercially from ATCC) stably expressing human 5-LOX, 5-LOX plus FLAP, 15-LOX-1 and 15-LOX-2²² were cultured in monolayers (37°C, 5% CO₂) in DMEM containing 10% FCS, penicillin (100 U/mL)

and streptomycin (100 µg/mL). HEK293 cells expressing 5-LOX or 5-LOX/FLAP were selected by 200 µg mL⁻¹ hygromycin B and/or 400 µg mL⁻¹ geneticin, respectively; cells expressing 15-LOX-1 or 15-LOX-2 were obtained by using the plasmids pCMV6_15-LOX-1 (Origene, NM_001140) and pcDNA3.1/neom (+) 15-LOX-2 and selected with 400 µg mL⁻¹ geneticin.

Immunofluorescence Microscopy

M2-MDM (1×10^6 cells) were seeded onto glass coverslips in a 12-well plate and cultured for 48 h. BRP-201, vehicle (0.1% DMSO) or 1% Staphylococcus aureus 6850-conditioned medium (SACM) was added for 180 min at 37°C. The process was stopped by fixation with 4% paraformaldehyde solution. Acetone (3 min, 4°C) and 0.25% triton X-100 (10 min, RT) were used for permeabilization before blocking with normal goat serum 10% (50062Z, ThermoFisher). Coverslips were incubated with mouse monoclonal anti-15-LOX-1 antibody, 1:100 (ab119774, Abcam, Cambridge, UK) and rabbit anti-5-LOX antibody, 1:100 (1550 AK6, kindly provided by Dr. Olof Radmark, Karolinska Institutet, Stockholm, Sweden) at 4°C overnight. 15-LOX-1 was stained with the fluorophore-labeled secondary antibodies; Alexa Fluor 488 goat anti-rabbit IgG (H+L), 1:500 (A11034, ThermoFisher) and Alexa Fluor 555 goat anti-mouse IgG (H+L); 1:500 (A21424, ThermoFisher). Nuclear DNA was stained with ProLong Gold Antifade Mountant with DAPI (15395816, ThermoFisher). Samples were analyzed by a Zeiss Axiovert 200M microscope, and a Plan Neofluar $\times 40/1.30$ Oil (DIC III) objective (Carl Zeiss, Jena, Germany). An AxioCam MR camera (Carl Zeiss) was used for image acquisition.

Evaluation of Lipoxygenase Product Formation in HEK293 Cells

For evaluation of the effects on LOX product formation in stably transfected HEK293 cells, 2×10^6 cells per mL were preincubated with BRP-201 or vehicle (0.1% DMSO) in PBS pH 7.4 containing 0.1% glucose and 1 mM CaCl₂ for 15 min. LM biosynthesis was initiated by addition of 2.5 µM A23187 plus 1 µM AA at 37°C and terminated after 15 min. Alternatively, to determine the stimulatory effects of BRP-201, cells were incubated with BRP-201 or vehicle for 180 min at 37°C. The reactions were stopped by addition of 2 mL ice-cold methanol containing 10 µL of deuterium-labeled internal standards (200 nM d8-5S-HETE, d4-LTB₄, d5-LXA₄, d5-RvD2, d4-PGE₂ and 10 µM d8-AA) to facilitate LM quantification. Samples were kept at -20°C for one day to allow protein precipitation. After centrifugation (2000 g, 4°C, 10 min), the supernatants were subjected to solid phase extraction of formed LM that were then separated and analyzed by UPLC MS/MS as reported¹³ and described in the following sections.

Determination of Lipid Mediator Profile in Human Monocyte-Derived Macrophages

Human monocyte-derived M1 and M2 macrophages (2×10^6 cells) were seeded in 6-well-plates and incubated with BRP-201 or vehicle at 37°C with or without subsequent (after 10 min) addition of SACM, (from 24 h culture with OD = 0.05) for 180 min. The reaction was stopped with 2 mL ice-cold methanol containing deuterium-labeled internal standards (200 nM, d8-5S-HETE, d4-LTB₄, d5-LXA₄, d5-RvD2, d4-PGE₂ and 10 µM d8-AA). Samples were kept at -20°C for one day to allow protein precipitation. After centrifugation (2000 \times g, 4°C, 10 min), supernatants were subjected to solid phase extraction and LM analysis by UPLC-MS-MS exactly as reported before¹³ and described in the following paragraph.

Lipid Mediator Metabololipidomics by UPLC-MS-MS

Analysis of LM by UPLC-MS-MS was performed as reported by us before.¹³ In brief, to 2 mL aliquots of supernatants obtained from incubated HEK293 cells and MDM as described previously, 8 mL acidified H₂O (final pH = 3.5) was added and the samples were subjected to solid phase cartridges (Sep-Pak[®] Vac 6cc 500 mg/6 mL C18; Waters, Milford, MA). The columns had been equilibrated with 6 mL methanol and 2 mL H₂O prior to sample loading. After washing with 6 mL H₂O and subsequently with 6 mL *n*-hexane, LM were eluted with 6 mL methyl formate. The samples were dried using a TurboVap LV evaporation system (Biotage, Uppsala, Sweden) and resuspended in 100 µL methanol/water (50/50, v/v) for UPLC-MS-MS analysis. LM analysis was conducted with an Acquity[™] UPLC system (Waters, Milford, MA, USA) and a QTRAP 5500 Mass Spectrometer (ABSciex, Darmstadt, Germany) equipped with a Turbo V[™] Source

and electrospray ionization. The LM were separated on an ACQUITY UPLC® BEH C18 column (1.7 μm , 2.1 \times 100 mm; Waters, Eschborn, Germany) at 50°C at a flow rate of 0.3 mL/min and a mobile phase consisting of methanol-water-acetic acid of 42:58:0.01 (v/v/v) that was ramped to 86:14:0.01 (v/v/v) over 12.5 min and then to 98:2:0.01 (v/v/v) for 3 min. The QTRAP 5500 was operated in the negative ionization mode using scheduled multiple reaction monitoring (MRM) coupled with information-dependent acquisition. The scheduled MRM window was 60 sec, optimized LM parameters were adopted,¹³ and the curtain gas pressure was set to 35 psi. The retention time and at least six diagnostic ions for each LM were confirmed by means of an external standard (Cayman Chemical/Biomol GmbH, Hamburg, Germany). Quantification was achieved by calibration curves for each LM. Linear calibration curves were obtained for each LM and gave r^2 values of 0.998 or higher. Additionally, the limit of detection for each targeted LM was determined.¹³

Zymosan-Induced Peritonitis Mouse Model

Adult (8 weeks) male CD1 mice (Charles River, Calco, Italy) were housed at the animal care facility of the Department of Pharmacy of the University of Naples “Federico II” and kept under controlled environment (ie, temperature 21 \pm 2°C and humidity 60 \pm 10%) and provided with normal chow and water ad libitum. Mice were allowed to acclimatize for four days prior to experiments and were subjected to 12 h light/dark schedule. Experiments were conducted during the light phase. The experimental procedures were approved by the Italian Ministry and carried out in accordance with the EU Directive 2010/63/EU and the Italian DL 26/2014 for animal experiments and in compliance with the ARRIVE guidelines and Basel declaration including the 3R concept. Mice (n=6/group) received BRP-201 (2 mg/kg) or vehicle (2% DMSO in saline) by intraperitoneal (ip) injection of 0.5 mL/mouse, given 30 min prior to peritonitis induction by zymosan (1 mg/mouse in 0.5 mL saline, ip). After 2 h mice were euthanized in a saturated CO₂ atmosphere and peritoneal lavage was obtained by washing the peritoneal cavity with 3 mL ice-cold PBS and subsequent centrifugation (18,000 \times g, 5 min, 4°C). Samples were immediately frozen for further analysis of LMs via UPLC-MS-MS as described previously.

Statistics

Results are expressed as mean + S.E.M. of independent experiments, where n represents the indicated numbers from separate donors performed on different days which is given in the figure legends for each and every figure panel. For animal experiments n=6 mice in each group were examined. Statistical analysis and graphs were made using GraphPad Prism 8 software (San Diego, CA). Unpaired *t*-test was used to analyze experiments for comparison of two groups; while for multiple comparisons, ANOVA with Bonferroni or Dunnett multiple comparison tests were applied as indicated. *p*-value \leq 0.05 is a criterion for statistical significance.

Results

BRP-201 Suppresses Formation of Pro-Inflammatory 5-LOX Products and Elevates 12/15-LOX Products in Activated Macrophages

Previous results showed that BRP-201 is able to effectively suppress LT formation in human primary neutrophils²¹ but whether or not other branches of the LM network are affected by this compound remains unknown. To study the influence of BRP-201 on LM networks in a broader context, we employed human M1- and M2-MDM that generate multiple LM upon exposure to pathogenic bacteria¹⁴ due to cell activation by exotoxins like α -hemolysin.²³ M1- and M2-MDM were preincubated with BRP-201 (0.1 to 3 μM) and then LM biosynthesis was elicited by *Staphylococcus aureus*-conditioned medium (SACM, containing exotoxins) within 180 min, which are appropriate and biologically relevant experimental settings to induce LM biosynthesis in human MDM.²³

In M1-MDM, BRP-201 reduced the formation of the 5-LOX products LTB₄ and its trans-isomers, 5-HETE, 5-HEPE and 5S,6R-diHETE in a concentration-dependent manner, starting at 0.1 μM , where especially LTB₄ was significantly impaired by more than 50% (Figure 2A and B). PGE₂, another major pro-inflammatory LM typically derived from M1-MDM, as well as other PG were hardly reduced (approx 20% at 3 μM BRP-201) or not altered (Figure 2A), indicating

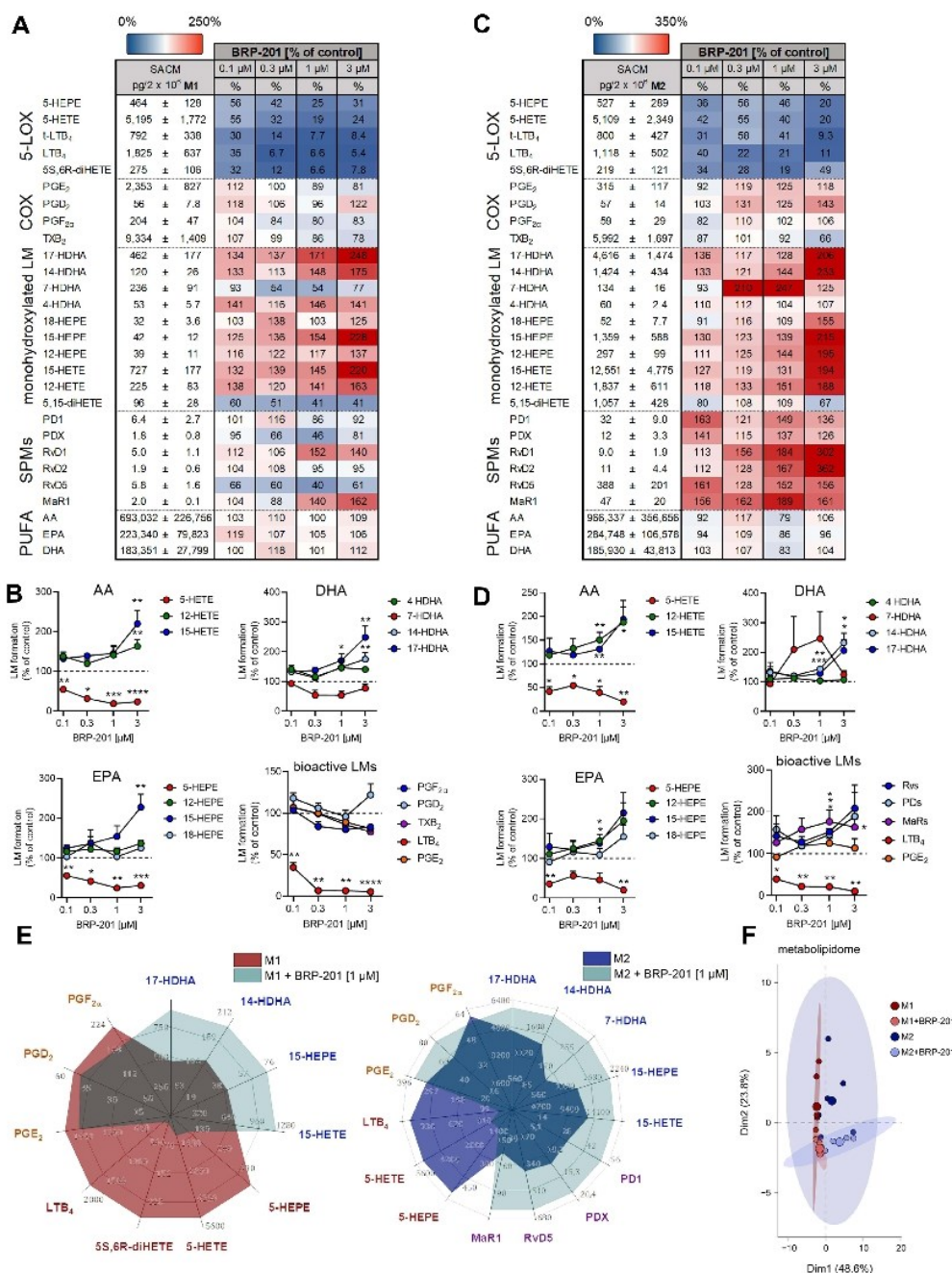


Figure 2 Modulation of exotoxin-induced LM formation in M1- and M2-MDM by BRP-201. M1- and M2-MDM (2×10^6) were resuspended in 1 mL PBS containing 1 mM CaCl₂, pre-incubated with BRP-201 (0.1, 0.3, 1 or 3 μM, as indicated) or vehicle (0.1% DMSO) for 10 min at 37°C, and stimulated with 1% SACM (from 6850 strain) for 180 min at 37°C. Then, the supernatants were collected, formed LMs were extracted by SPE and analyzed by UPLC-MS/MS. (A and C) Results are presented in pg/2 × 10⁶ M1-MDM (A) and M2-MDM (C) for vehicle control (100%) given as mean ± SEM, and as percentage ± SEM of BRP-201-treated cells versus vehicle control (100%) in a heatmap: n=3–6. (B and D) Effects of BRP-201 on the AA-, DHA-, and EPA-derived monohydroxylated products and bioactive PGs, LTB₄ and SPM produced in M1-MDM (B) or M2-MDM (D). Results are shown as percentage, given as mean ± SEM, of BRP-201-treated cells versus vehicle control (100%), n=3–6. (E) Amounts of formed LM in pg/2 × 10⁶ MDM are shown in a spider web graph indicating the impact of BRP-201 at 1 μM on LM signature profiles, n=3–6. (F) Principal component analysis of the LMs (PGD₂, PGE₂, PGF_{2α}, TXB₂, 18-HDHA, LTB₄, 5-HEPE, 5-HETE, 5S,6R-diHETE, PDX, RvD5, MaR1, 4-HDHA, 7-HDHA, 18-HEPE, 14-HDHA, 17-HDHA, 12-HEPE, 15-HEPE, 12-HETE, 15-HETE, 5,15-diHETE) organized by LM classes in vehicle- and BRP-201-treated M1- and M2-MDM (corresponding data in (A) and (C) at 1 μM BRP-201), n=3–6. Statistical analysis was performed via ratio-paired t-test, and principal component analysis was performed using R Studio (version 1.4) with implemented R packages FactoMineR and factextra. * p<0.05, ** p<0.01, *** p<0.001, **** p<0.0001.

that BRP-201 mainly acts as inhibitor of the 5-LOX pathway devoid of substrate shunting effects toward COX products observed for certain other 5-LOX inhibitors.^{14,24,25} Notably, 12/15-LOX-derived products formed from AA (12-HETE and 15-HETE), EPA (12-HEPE and 15-HEPE) and DHA (17-HDHA, 14-HDHA) were elevated after BRP-201 treatment, while 5,15-diHETE and 7-HDHA that are proposed to be partially produced by 5-LOX,¹⁴ were rather impaired (Figure 2A and B). Because in particular 15-lipoxygenation was elevated, this may hint to LM shunting toward 15-LOX-2 which in contrast to 15-LOX-1 is constitutively expressed in M1 macrophages²³ and specifically oxygenates C15 but not C12.²⁶ Note that formation of SPM is low in M1-MDM, as reported before,^{13,14} and even though some SPM such as RvD1 and MaR1 were somewhat increased, the other members were inconsistently modulated, and also the release of PUFAs was not markedly affected by BRP-201 (Figure 2A).

A similar pattern of modulation of LM biosynthesis by BRP-201 was evident in SACM-activated M2-MDM. Thus, BRP-201 at 0.1 μ M suppressed formation of 5-LOX products by approx. 60%, accompanied by slightly elevated levels of COX products at higher BRP-201 concentrations (Figure 2C and D). Of interest, BRP-201 markedly elevated formation of all detectable SPM, namely PD1, PDX, RvD1, RvD2, RvD5, and MaR1 with most pronounced effects at 3 μ M for RvD1 and RvD2 (> 3-fold increase) (Figure 2C and D). In line with these findings, the formation of 17-HDHA and 14-HDHA, the precursors of these SPM, as well as 18-HEPE and the 12/15-LOX-derived 12-HETE, 12-HEPE, 15-HETE and 15-HEPE were increased, while 4-HDHA was not altered. Like in M1-MDM, the release of PUFAs was not

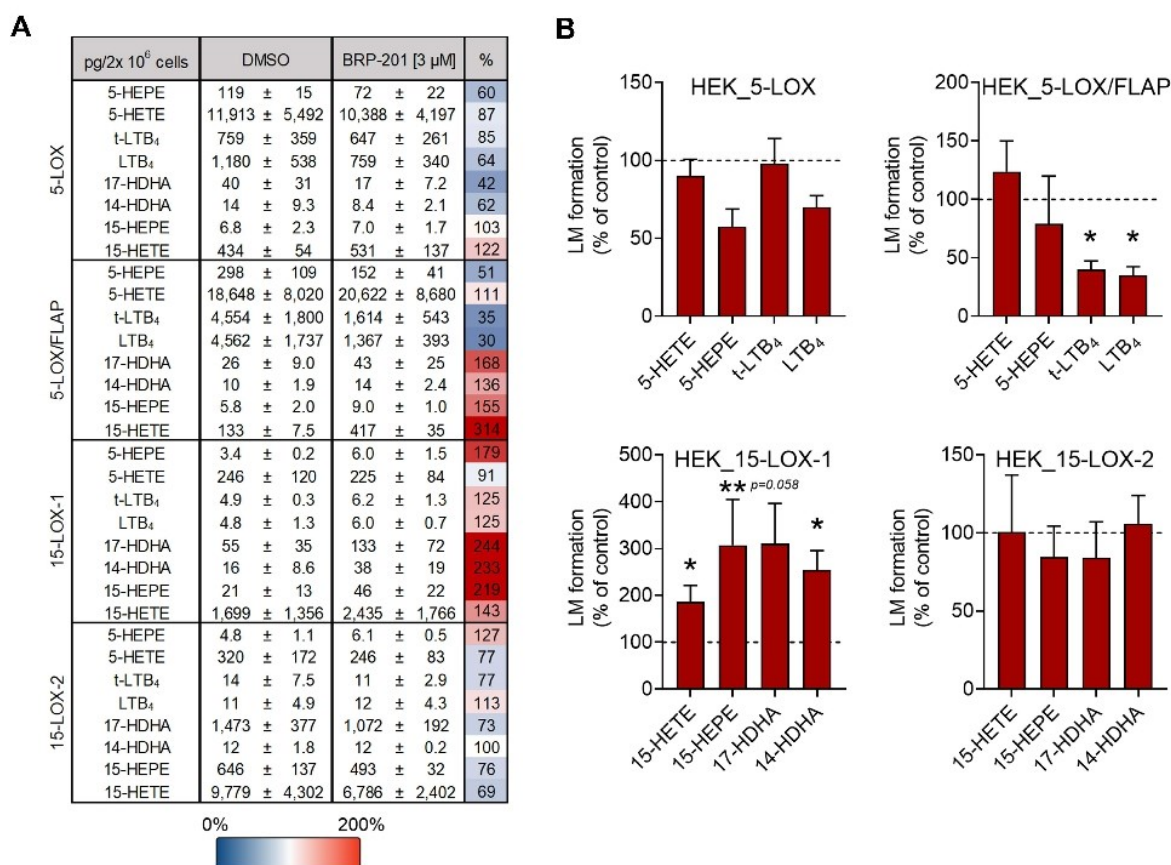


Figure 3 Modulation of LM biosynthesis in HEK293 cells transfected with LOX isoforms by BRP-201: impact of co-expression of FLAP with 5-LOX. HEK293 cells (2×10^6) transfected with human recombinant 5-LOX, 5-LOX and FLAP, 15-LOX-1 or 15-LOX-2 were resuspended in PBS containing 1 mM CaCl₂ and 0.1% glucose, incubated with vehicle (0.1% DMSO) or BRP-201 (3 μ M) for 15 min at 37°C and then stimulated with A23187 (2.5 μ M) plus AA (1 μ M) at 37°C for 15 min. Afterwards, the formed LMs were extracted from the supernatants using SPE and analyzed by UPLC-MS/MS. Data, given as mean \pm SEM, are shown as (A) absolute values in pg/2 \times 10⁶ cells, and (B) as percentage of BRP-201-treated cells versus vehicle control (100%), n=3. Statistical analysis was performed via logarithmic paired t-test. * p<0.05, ** p<0.01.

markedly affected by BRP-201 in the M2 phenotype (Figure 2C). In Figure 2E and D, LM class switch in M1- and M2-MDM due to BRP-201 is visualized by comparison of selected representative bioactive LM and their precursors. Principal component analysis of the LMs formed in vehicle- and BRP-201-treated M1- and M2-MDM revealed different clusters that are separated, especially for M2-MDM, supporting the LM class switch due to BRP-201 (Figure 2F).

Modulation of 5-LOX/FLAP and 15-LOX Pathways in Stably Transfected HEK293 Cells

To gain more insight into the modulation of different LOX pathways by BRP-201, we took advantage of HEK293 cells that neither express any LOX nor FLAP per se but are convenient cell-based LOX expression models for studying select LOX pathways.^{22,27} We employed stably transfected HEK293 cells with either 5-LOX alone, with 5-LOX and FLAP, with 15-LOX-1 or with 15-LOX-2, respectively, as described previously.²² The cells were pretreated with BRP-201 (3 μ M) for 15 min, stimulated with 2.5 μ M A23187 and 1 μ M AA for 15 min, and LOX products were analyzed by UPLC-MS-MS. As expected from our previous studies on FLAP and FLAP antagonists,²⁷ in HEK293 cells expressing only 5-LOX (no FLAP), the formation of 5-LOX products was low and not significantly suppressed by BRP-201. However, upon co-expression of 5-LOX with FLAP, BRP-201 efficiently inhibited the FLAP-dependent generation of LTA₄ hydrolysis products LTB₄ and trans-LTB₄ (Figure 3A and B). In parallel, BRP-201 strongly elevated 15-HETE formation but only in cells that express both 5-LOX and FLAP (Figure 3A). Of interest, in HEK293 cells expressing 15-LOX-1, BRP-201 markedly elevated (up to 3-fold) the formation of 15-HEPE and of 17-HDHA and 14-HDHA from endogenous EPA and DHA, respectively, but also 15-HETE biosynthesis from endogenous and/or exogenous AA was increased by about twofold (Figure 3). In contrast, BRP-201 failed to enhance product formation by 15-LOX-2 (Figure 3). Taken together, BRP-201 inhibits the biosynthesis of pro-inflammatory 5-LOX products in activated M1- and M2-MDM as well as in stimulated HEK293 cells, apparently by acting at FLAP, but stimulates SPM and 15-LOX product formation, especially in M2-MDM.

BRP-201 Activates Macrophages for Formation of SPM and Related 12/15-LOX Products

To assess whether active induction of 15-LOXs is the reason for elevated SPMs and related LM we exposed M1- and M2-MDM to BRP-201 (0.3, 1 or 3 μ M) without additional stimulus for 180 min and determined the LM profiles. Interestingly, BRP-201 concentration-dependently induced the formation of 12/15-LOX products in both M1- and M2-MDM, with comparable efficiencies (about 2.5- to 3-fold) for 12-lipoxygenated (12-HETE, 12-HEPE and 14-HDHA) and 15-lipoxygenated products (15-HETE, 15-HEPE, and 17-HDHA) (Figure 4A–D). Along these lines, BRP-201 elevated SPM levels, in particular PD1, RvD5 and MaR1 in M2-MDM (Figure 4B and D). In contrast, formation of COX- and 5-LOX-derived products were not or only marginally elevated by BRP-201 and also 4-HDHA and 7-HDHA were not or less increased. Moreover, BRP-201 failed to elevate the levels of free PUFAs in both MDM phenotypes (Figure 4A and B), implying that elevated 12/15-LOX product formation is not simply due to larger amounts of substrate.

Subcellular redistribution of 5-LOX and 15-LOX-1 from a soluble locale to a membrane compartment in (SACM- or bacteria-) activated human MDM is a determinant for their activation, access to substrate, and eventually for LM formation.^{14,23} We studied whether BRP-201 is able to induce such subcellular redistribution and, thus, activation of 5-LOX and 15-LOX-1 in M2-MDM by using immunofluorescence microscopy. In analogy to SACM, 1 μ M BRP-201 caused 15-LOX-1 translocation from the cytosol to a membrane compartment within 180 min (Figure 4E). However, in contrast to SACM that caused 5-LOX nuclear membrane translocation, BRP-201 failed in this respect with 5-LOX remaining in the nucleosol (Figure 4E), confirming that BRP-201 may not activate 5-LOX.

To further support activation of 15-LOXs by BRP-201, we exposed HEK293 cells expressing 15-LOX-1 or 15-LOX-2 to 3 μ M BRP-201 for 180 min and measured LM formation. For HEK cells expressing 15-LOX-1, an about 2- to 3-fold elevation of 15-HETE, 15-HEPE and 14-HDHA was observed (Figure 4F). Also, in HEK293 cells expressing the isoform 15-LOX-2, a moderate elevation of these LOX products in response to BRP-201 was evident. In conclusion, BRP-201 is able to activate 15-LOX-1 in MDM and in HEK293 cells to generate related LM.

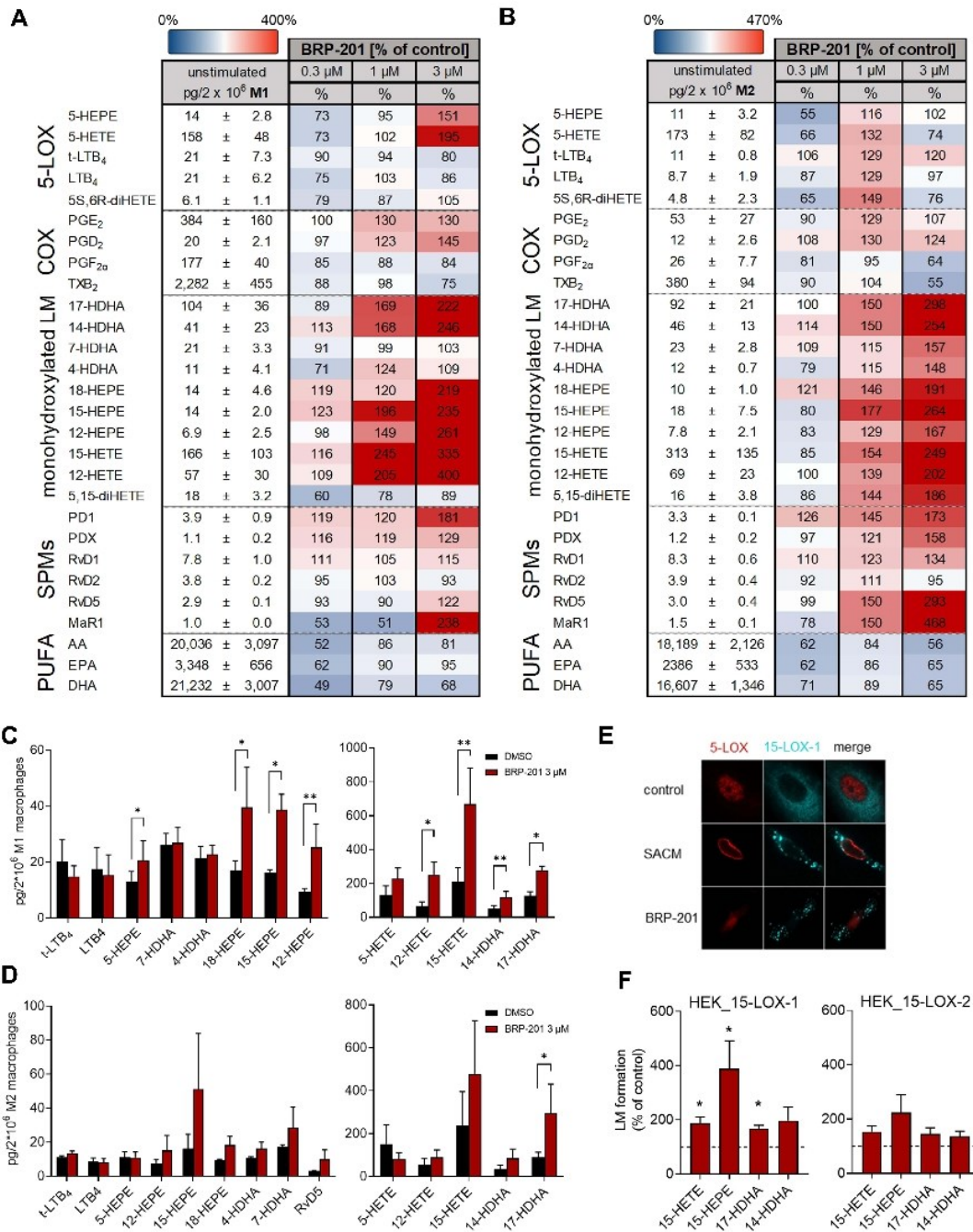


Figure 4 Induction of LM biosynthesis and 15-LOX-1 activation by BRP-201 in MDM and HEK293 cells. (A–D) Induction of LM biosynthesis by BRP-201 in MDM. M1- and M2-MDM (2×10^6) were resuspended in PBS containing 1 mM CaCl₂ and incubated with vehicle (0.1% DMSO) or BRP-201 (0.3, 1, or 3 μM as indicated) for 180 min at 37°C. Then, formed LMs were extracted from the supernatants using SPE and analyzed by UPLC-MS/MS. Results are presented in pg/2 × 10⁶ M1-MDM (A) and M2-MDM (B) for vehicle control (100%), given as mean ± SEM, and as percentage ± SEM of BRP-201-treated cells versus vehicle control (100%) in a heatmap; n=3–6. Induction of the most abundant LM in M1-MDM (C) and M2-MDM (D) by 3 μM BRP-201; results, given as mean ± SEM, are presented in pg/2 × 10⁶ cells; n=3–6. (E) Subcellular redistribution of 5-LOX and 15-LOX-1 in M2-MDM. Cells were resuspended in PBS containing 1 mM CaCl₂ and 5 mM MgCl₂ and incubated with 1 μM BRP-201, 1% SACM (from strain 6850) or vehicle (0.1% DMSO). After 180 min, cells were fixed, permeabilized, and incubated with antibodies against 5-LOX (red) and 15-LOX-1 (cyan-blue), and analyzed by immunofluorescence microscopy; scale bars = 10 μm. Results shown for one single cell are representative of approximately 100 individual cells analyzed in n=3 independent experiments with separate donors, each. (F) HEK293 cells (2×10^6) transfected with human recombinant 15-LOX-1 or 15-LOX-2 were resuspended in PBS containing 1 mM CaCl₂ and 0.1% glucose and incubated with vehicle (0.1% DMSO) or BRP-201 (3 μM) for 180 min at 37°C. Then, formed LMs were extracted from supernatants by SPE and analyzed by UPLC-MS/MS. Results, given as mean ± SEM, are presented as percentage of BRP-201-treated cells versus vehicle control (100%), n=3. Statistical analysis was performed with a ratio-paired t-test or logarithmic paired t-test. * p<0.05, ** p<0.01.

BRP-201 Suppresses Formation of 5-LOX Products and Elevates 12/15-LOX Products in Zymosan-Induced Murine Peritonitis in vivo

In order to study if BRP-201 induces an LM class switch also in vivo, we pre-treated CD1 mice ip with 2 mg/kg BRP-201 for 30 min before peritonitis induction; due to the poor solubility of BRP-201, application of higher doses was not feasible. We then injected zymosan (ip) into the peritoneum in order to elicit broad spectrum LM formation within 2 hrs²⁸ and analyzed the LM profile in the peritoneal lavage (exudates). As shown in Figure 5A and C, LTB₄ formation was lowered upon BRP-201 treatment from 337±37 to 224±75 pg/mL exudate, and also the 5-LOX products trans-LTB₄, 5S,6R-diHETE and 5-HETE were decreased by about 28 to 38%. In contrast, the sum of DHA- and EPA-derived 12/15-LOX products was significantly elevated (Figure 5B), with most pronounced effects for 12-HEPE and 14-HDHA (Figure 5A and C). Also, the sum of SPM was slightly increased (Figure 5B), in particular for PDX, but did not reach statistical significance (Figure 5A and C). AA-derived 12/15-LOX products (eg, 15-HETE), COX-derived prostanoids and LM formed by other pathways (eg, 4-HDHA and 7-HDHA), as well as PUFAs were not markedly changed by BRP-201 (Figure 5A and B). These data further support the hypothesis that BRP-201 induces a shift in the biosynthesis from pro-inflammatory 5-LOX- toward pro-resolving 12/15-LOX-derived LM.

Discussion

Current anti-inflammatory pharmacotherapy related to intervention with LM relies on the interference with single enzymatic pathways in a complex LM network, that is, inhibition of COX-1/2-dependent PG formation by NSAIDs like ibuprofen, diclofenac or celecoxib, or suppression of 5-LOX-dependent LT biosynthesis by zileuton.^{29,30} NSAID-mediated reduction of the levels of PGs with homeostatic functions is frequently afflicted with severe side effects in the gastrointestinal tract, the kidneys and the cardiovascular system.³¹ Moreover, inhibition of PG formation by NSAIDs favors elevated LT levels by substrate redirection and cross talk-mediated shunting phenomena further promoting unwanted effects.^{13,18,24} Novel alternative strategies for intervention with inflammatory disorders focus on the development of dual inhibitors that block formation of both pro-inflammatory PGs (ie PGE₂) and LTs, such as COX/5-LOX or mPGES-1/5-LOX inhibitors, aiming at circumventing these side effects.^{30,32} The discovery of SPMs and their favorable functions in inflammation resolution² shifted the paradigm from anti-inflammatory toward resolution pharmacology.³³ Thus, new concepts for inflammation pharmacotherapy were proposed that pursue the switch from pro-inflammatory eicosanoids toward inflammation-resolving SPMs, potentially accomplished by agents that dually block pro-inflammatory PGE₂ and LT formation but stimulate SPM biosynthesis.^{28,34–37} Such pharmacological LM class switch strategies may bear a significant potential to effectively relieve chronic inflammation devoid of side effects of classical anti-inflammatory drugs.

Here, we showed that the FLAP antagonist BRP-201 causes an LM class switch in human macrophages, and to a minor extent also in murine peritoneum in vivo, by shifting the biosynthesis of LTs toward SPMs. BRP-201 was recently revealed as FLAP antagonist²¹ that efficiently inhibited LT formation in a convenient and well-recognized screening assay based on ionophore-activated human neutrophils³⁸ with IC₅₀ in the two-digit nanomolar range. To better estimate its pharmacological profile and potential, we analyzed the effects of BRP-201 within more complex LM networks using a more biologically relevant cellular system that allows better analysis of modulation of other LM branches. Thus, we employed human MDM with M1- and M2-like phenotype that when stimulated with bacterial exotoxins, produce a broad range of different types of LM, including PGs, LTs and SPM that can be analyzed by UPLC-MS-MS.^{13,14,23}

The M1-phenotype generated substantial PG and LT but only moderate amounts of SPMs and their precursors upon exotoxin-challenge, which is in agreement with strong expression of COX-2 and FLAP but lack of 15-LOX-1, respectively.^{14,23} Accordingly, in M1-MDM, FLAP antagonism by BRP-201 caused potent suppression of 5-LOX products including LTB₄, while the detectable SPMs were hardly and inconsistently affected. But human M1-MDM express low levels of 15-LOX-2²³ that in contrast to the 12/15-lipoxygenating 15-LOX-1 isoform, selectively oxygenate solely carbon 15 and 17 in AA/EPA and DHA, respectively, but not carbon 12 and 14.³⁹ Indeed, BRP-201 elevated 15-HETE, 15-HEPE and 17-HDHA in M1-MDM but also 12-HETE, 12-HEPE and 14-HDHA. Shifts from 5- to 12/15-lipoxygenation in M1-MDM were observed also with 3-*O*-acetyl-11-keto-β-boswellic acid (AKBA) that alters the

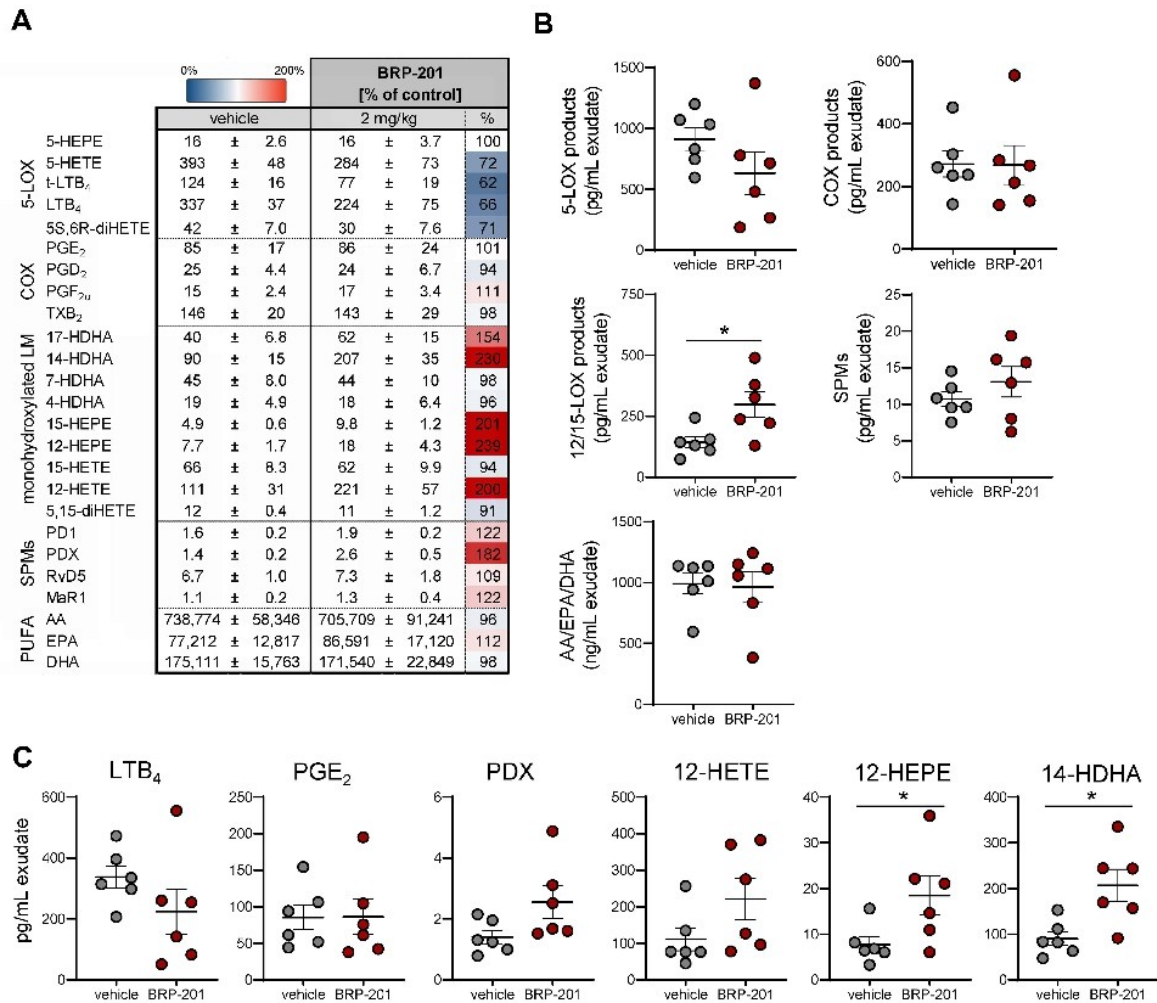


Figure 5 Effects of BRP-201 on LM biosynthesis during zymosan-induced murine peritonitis. Mice received BRP-201 (2 mg/kg) i.p. 30 min prior to i.p. injection of zymosan (1 mg/mouse). After 2 h, animals were sacrificed and peritoneal exudates were collected by lavage with 3 mL cold PBS. Formed LMs were extracted from the exudates using SPE and analyzed by UPLC-MS-MS. Results, given as means \pm SEM, are presented in pg/mL exudate and as percentage of BRP-201-treated mice versus vehicle-treated controls (100%) in a heatmap (A), and as scatter dot plots (B) for LM grouped in different classes such as 5-LOX products (sum of LTB₄, t-LTB₄, 5S,6R-diHETE, 5-HETE and 5-HEPE), COX products (sum of PGE₂, PGD₂, PGF_{2 α} , TXB₂), 12/15-LOX products (sum of 14-HDHA, 12-HEPE, 17-HDHA and 15-HEPE) and SPMs (sum of PD1, PDX, RvD5, and MaR1) in pg/mL exudate and PUFAs (sum of AA, EPA, DHA) in ng/mL exudate. Data are shown as single values (circles) and as means (black lines) \pm SEM. (C) Selected bioactive and predominantly produced LMs are presented; given in pg/mL exudate; n = 6. Statistical analysis was performed by unpaired t-test; * p < 0.05.

regiospecificity of 5-LOX via binding to an allosteric site of the enzyme.²² Whether BRP-201 acts in analogy to AKBA at this site of 5-LOX is unknown but conceivable, as discussed in the following paragraphs.

The pronounced abundance of 15-LOX-1 in M2-MDM enables formation of high amounts of SPMs and their precursors.¹⁴ In these cells, BRP-201 caused substantial elevation of SPM formation as well as the respective precursors 17-HDHA and 14-HDHA, suggesting that BRP-201 effectively redirects LM formation from 5-LOX/FLAP to 15-LOX-1. Among the mono-hydroxylated products in M2-MDM, only those generated by 15-LOX-1, namely 17-HDHA, 14-HDHA, 15-HEPE, 15-HETE, 12-HEPE and 12-HETE were concentration-dependently elevated by BRP-201 but not 7-HDHA, 4-HDHA, 18-HEPE and 5,15-diHETE that are formed independent of 15-LOX-1 or in conjunction with 5-LOX.¹³

The hypothesis that BRP-201 elevates 12/15-LOX product formation in two ways, that is, i) via a FLAP-dependent shift of the 5-LOX regiospecificity to a 12/15-lipoxygenating enzyme, and ii) by FLAP-independent activation of 15-LOX-1, is supported by our results obtained with LOX isoform-transfected HEK293 cells that are suitable as defined

model systems to study selective LOX isoforms²² and the role of FLAP.^{27,40} Thus, BRP-201 redirected ionophore-induced LM formation only in 5-LOX-expressing HEK293 when FLAP was co-expressed, where classical FLAP-dependent 5-LOX products (ie, LTB₄ and tr-LTB₄) were suppressed but 12/15-LOX products were increased. Intriguingly however, BRP-201 elevated 12/15-LOX product formation also in HEK293 cells expressing 15-LOX-1 that are devoid of 5-LOX and FLAP, but not so in cells expressing the 15-LOX-2 isoform.

5-LOX plays a dual role in the formation of pro-inflammatory LTs on one hand and of anti-inflammatory/pro-resolving SPM on the other, which raises the question how the biosynthesis of these disparate LM is orchestrated in the cellular context.²⁰ Moreover, it is questionable if pharmacological concepts can be pursued that allow favorable modulation of LM biosynthesis by interference with the 5-LOX pathway, that is, suppression of LTs without lowering SPM but rather stimulating the formation of the latter. As potential mechanisms, allosteric modulation/inhibition of 5-LOX leading to a shift of the regioselectivity toward a 12/15-lipoxygenating enzyme, but also antagonism of FLAP are both conceivable. The pentacyclic triterpene acids 3-*O*-acetyl-11-keto- β -boswellic acid (AKBA)²² and celastrol²⁸ promote SPM formation in human neutrophils and macrophages as well as in inflamed murine peritoneum, apparently by allosteric modulation of 5-LOX shifting the regioselectivity from 5- to 12/15-lipoxygenation. Although BRP-201 clearly differs in structure from AKBA and celastrol, modulation of the 5-LOX regioselectivity by BRP-201 at this allosteric site is conceivable and would explain the elevated formation of 12/15-LOX products in M1-MDM and 5-LOX/FLAP-expressing HEK293 cells that are both devoid of 15-LOX-1.

The balance of LTs and SPM in leukocytes might be achieved through differential subcellular localization of 5-LOX where nuclear 5-LOX in proximity to FLAP favors LT generation while cytoplasmic 5-LOX distant from FLAP favors LXA₄ formation.¹⁶ Thus, FLAP antagonists should prevent nuclear membrane-bound 5-LOX from generating LT but still permit activated cytosolic 5-LOX to oxygenate SPM precursors such as 15-HETE, 17-HDHA, and 18-HEPE to SPM. In fact, in human *E. coli*-activated M2-MDM, the FLAP antagonist MK886 blocked formation of classical 5-LOX-derived products while the SPM RvD5 and MaR1 and other 12/15-LOX products were elevated.^{13,14} Also, in murine peritonitis, MK886 markedly reduced the levels of LTB₄, tr-LTB₄ and 5-HETE in the peritoneal exudates while the amounts of LXA₄, PD1, RvD4 and RvD5 remained elevated.³⁵ Similarly, the FLAP antagonist BAY X-1005 blocked cysteinyl-LT formation but elevated SPM levels during murine liver injury.⁴¹ In agreement with these actions of FLAP antagonists in vivo, BRP-201 caused a trend toward lowered levels of LTB₄ and of other classical 5-LOX products in the exudates of zymosan-challenged mice, while the levels of all detectable SPM, their precursors and most other 12/15-LOX-derived products were rather increased. Due to the poor water solubility of BRP-201, we could apply only a low dose of 2 mg/kg by ip injection which might be suboptimal, explaining why statistical significance could not be reached for single LM, except for 12-HEPE and 14-HDHA. Moreover, since the biology of murine 15-LOX-1 differs from that of the human ortholog in various aspects, in particular in the reaction specificity,^{26,39} it is also plausible that BRP-201 might be more active toward the human than to the mouse enzyme. Note that COX-derived prostanoids and LM formed by other pathways (eg, 4-HDHA and 7-HDHA) were not markedly affected in these murine peritoneal exudates, again supporting a concrete LM switch toward 12/15-LOX products. These data also imply that simple substrate redirection²⁴ is unlikely as reason for elevated SPM and 12/15-LOX products. Rather, BRP-201, besides antagonizing FLAP, may cause stimulation of 15-LOX-1 activity in resident cells of the peritoneum thereby elevating formation of SPM and other 12/15-lipoxygenated products, supported by the induction of 12/15-LOX product formation in 15-LOX-1-expressing M2-MDM and HEK293 cells in the absence of a stimulus.

In general, the induction of cellular formation of LOX products requires the supply of free PUFA as substrates and the activation of LOXs that travel within the cell to access the substrate and to convert it.^{3,8,14,26} Our results suggest that elevation of 12/15-LOX products by BRP-201 in the absence of a stimulus (like A23187 or *S. aureus*) is primarily caused by stimulation of 15-LOX-1 and by facilitating the access of the LOX to its substrates, without marked increase of free PUFA supply. Thus, BRP-201 did not elevate PUFA levels in MDM but clearly induced 15-LOX-1 redistribution from the cytosol to a membrane compartment, along with 12/15-LOX product formation. Notably, BRP-201 failed to evoke translocation and product formation of 5-LOX in MDM, implying selectivity for modulation of LOX isoforms. Direct activators of 15-LOX in cell free-assays were reported⁴² and proposed to shift the AA metabolic network toward inflammation resolution. Allosteric activation of 15-LOX at a second AA binding site based on molecular dynamics simulations may be causative⁴³ but experimental data confirming such shift in cells or in vivo are still missing.

Interaction of BRP-201 with such allosteric AA binding site at 15-LOX-1 is conceivable, especially in view of the fact that BRP-201 acts as AA mimetic at FLAP competing with AA.²¹

Conclusion

Using human macrophages and mouse peritonitis as experimental models, we showed that BRP-201 induces a switch in the formation of pro-inflammatory 5-LOX-derived LT toward inflammation-resolving 12/15-LOX-derived SPM which reflects a beneficial pharmacological profile for intervention in inflammation. While the suppression of LT formation is obviously due to antagonism of FLAP, the stimulation of SPM and 12/15-LOX product formation by BRP-201 might be due to FLAP-dependent redirection of 5-LOX subcellular redistribution, allosteric modulation of 5-LOX, and by activation of 15-LOX-1. Therefore, BRP-201 is an interesting tool and lead for development of novel pharmacological strategies that pursue fostering of SPMs as immunoresolvents to promote inflammation resolution.

Data Sharing Statement

The datasets generated and analyzed in this study will be available from the corresponding author upon reasonable request.

Acknowledgments

The authors thank Heidi Traber, Petra Wiecha, Katrin Fischer and Alrun Schumann for expert technical assistance.

Author Contributions

All authors significantly contributed to the reported work related to the conception, study design, execution, acquisition of data, analysis and interpretation; took part in drafting, revising or critically reviewing the article; gave final approval of the manuscript; have agreed on the journal to which the article has been submitted; agree to be accountable for all aspects of the work.

Funding

This work was supported by the Deutsche Forschungsgemeinschaft (DFG), Collaborative Research Center SFB 1278 “PolyTarget” (project number 316213987, projects A04 and Z01). The study of the chemical development of BRP-201 was supported by The Scientific and Technological Research Council of Turkey (TÜBİTAK Grant No: 112S596).

Disclosure

Professor Erden Banoglu reports grants from TUBITAK, during the conduct of the study. The authors declare no conflicts of interest in this work.

References

1. Calder PC, Harwood J, Lloyd-Evans E. Eicosanoids. *Essays Biochem.* 2020;64(3):423–441. doi:10.1042/EBC20190083
2. Serhan CN. Pro-resolving lipid mediators are leads for resolution physiology. *Nature.* 2014;510(7503):92–101. doi:10.1038/nature13479
3. Astudillo AM, Balboa MA, Balsinde J. Selectivity of phospholipid hydrolysis by phospholipase A2 enzymes in activated cells leading to polyunsaturated fatty acid mobilization. *Biochim Biophys Acta Mol Cell Biol Lipids.* 2019;1864(6):772–783. doi:10.1016/j.bbalip.2018.07.002
4. Chiang N, Serhan CN, Harwood J, Lloyd-Evans E. Specialized pro-resolving mediator network: an update on production and actions. *Essays Biochem.* 2020;64(3):443–462. doi:10.1042/EBC20200018
5. Dennis EA, Norris PC. Eicosanoid storm in infection and inflammation. *Nat Rev Immunol.* 2015;15(8):511–523. doi:10.1038/nri3859
6. Funk CD. Prostaglandins and leukotrienes: advances in eicosanoid biology. *Science.* 2001;294(5548):1871–1875. doi:10.1126/science.294.5548.1871
7. Smith WL, Urade Y, Jakobsson PJ. Enzymes of the cyclooxygenase pathways of prostanoid biosynthesis. *Chem Rev.* 2011;111(10):5821–5865. doi:10.1021/cr2002992
8. Radmark O, Wertz O, Steinhilber D, Samuelsson B. 5-Lipoxygenase, a key enzyme for leukotriene biosynthesis in health and disease. *Biochim Biophys Acta.* 2015;1851(4):331–339. doi:10.1016/j.bbalip.2014.08.012
9. Haeggstrom JZ. Leukotriene biosynthetic enzymes as therapeutic targets. *J Clin Invest.* 2018;128(7):2680–2690. doi:10.1172/JCI97945
10. Peters-Golden M, Henderson WR Jr. Leukotrienes. *N Engl J Med.* 2007;357(18):1841–1854. doi:10.1056/NEJMra071371
11. Gur ZT, Caliskan B, Banoglu E. Drug discovery approaches targeting 5-lipoxygenase-activating protein (FLAP) for inhibition of cellular leukotriene biosynthesis. *Eur J Med Chem.* 2018;153:34–48. doi:10.1016/j.ejmech.2017.07.019

12. Pettersen D, Davidsson O, Whalling C. Recent advances for FLAP inhibitors. *Bioorg Med Chem Lett*. 2015;25(13):2607–2612. doi:10.1016/j.bmcl.2015.04.090
13. Werner M, Jordan PM, Romp E, et al. Targeting biosynthetic networks of the proinflammatory and proresolving lipid metabolome. *FASEB J*. 2019;33(5):6140–6153. doi: 10.1096/fj.201802509R
14. Werz O, Gerstmeier J, Libreros S, et al. Human macrophages differentially produce specific resolvins or leukotriene signals that depend on bacterial pathogenicity. *Nat Commun*. 2018;9(1):59. doi:10.1038/s41467-017-02538-5
15. Lehmann C, Homann J, Ball AK, et al. Lipoxin and resolvins biosynthesis is dependent on 5-lipoxygenase activating protein. *FASEB J*. 2015;29(12):5029–5043. doi:10.1096/fj.15-275487
16. Fredman G, Ozcan L, Spolitu S, et al. Resolvin D1 limits 5-lipoxygenase nuclear localization and leukotriene B4 synthesis by inhibiting a calcium-activated kinase pathway. *Proc Natl Acad Sci USA*. 2014;111(40):14530–14535. doi:10.1073/pnas.1410851111
17. Mahesh G, Anil Kumar K, Reddanna P. Overview on the discovery and development of anti-inflammatory drugs: should the focus be on synthesis or degradation of PGE2? *J Inflamm Res*. 2021;14:253–263. doi:10.2147/JIR.S278514
18. Rainsford KD. Anti-inflammatory drugs in the 21st century. *Subcell Biochem*. 2007;42:3–27.
19. Serhan CN, Levy BD. Resolvins in inflammation: emergence of the pro-resolving superfamily of mediators. *J Clin Invest*. 2018;128(7):2657–2669. doi:10.1172/JCI97943
20. Gilbert NC, Newcomer ME, Werz O. Untangling the web of 5-lipoxygenase-derived products from a molecular and structural perspective: the battle between pro- and anti-inflammatory lipid mediators. *Biochem Pharmacol*. 2021;193:114759. doi:10.1016/j.bcp.2021.114759
21. Gur ZT, Caliskan B, Garscha U, et al. Identification of multi-target inhibitors of leukotriene and prostaglandin E2 biosynthesis by structural tuning of the FLAP inhibitor BRP-7. *Eur J Med Chem*. 2018;150:876–899. doi:10.1016/j.ejmech.2018.03.045
22. Gilbert NC, Gerstmeier J, Schexnaydre EE, et al. Structural and mechanistic insights into 5-lipoxygenase inhibition by natural products. *Nat Chem Biol*. 2020;16(7):783–790. doi:10.1038/s41589-020-0544-7
23. Jordan PM, Gerstmeier J, Pace S, et al. Staphylococcus aureus-derived alpha-hemolysin evokes generation of specialized pro-resolving mediators promoting inflammation resolution. *Cell Rep*. 2020;33(2):108247. doi:10.1016/j.celrep.2020.108247
24. He C, Wu Y, Lai Y, Cai Z, Liu Y, Lai L. Dynamic eicosanoid responses upon different inhibitor and combination treatments on the arachidonic acid metabolic network. *Mol Biosyst*. 2012;8(5):1585–1594. doi:10.1039/c2mb05503a
25. Werz O, Gerstmeier J, Garscha U. Novel leukotriene biosynthesis inhibitors (2012–2016) as anti-inflammatory agents. *Expert Opin Ther Pat*. 2017;27(5):607–620. doi:10.1080/13543776.2017.1276568
26. Ivanov I, Kuhn H, Heydeck D. Structural and functional biology of arachidonic acid 15-lipoxygenase-1 (ALOX15). *Gene*. 2015;573(1):1–32. doi:10.1016/j.gene.2015.07.073
27. Gerstmeier J, Weinigel C, Barz D, Werz O, Garscha U. An experimental cell-based model for studying the cell biology and molecular pharmacology of 5-lipoxygenase-activating protein in leukotriene biosynthesis. *Biochim Biophys Acta*. 2014;1840(9):2961–2969. doi:10.1016/j.bbagen.2014.05.016
28. Pace S, Zhang K, Jordan PM, et al. Anti-inflammatory celestrol promotes a switch from leukotriene biosynthesis to formation of specialized pro-resolving lipid mediators. *Pharmacol Res*. 2021;167:105556. doi:10.1016/j.phrs.2021.105556
29. Patrono C, Baigent C. Coxibs, traditional NSAIDs, and cardiovascular safety post-PRECISION: what we thought we knew then and what we think we know now. *Clin Pharmacol Ther*. 2017;102(2):238–245. doi:10.1002/cpt.696
30. Sala A, Proschak E, Steinhilber D, Rovati GE. Two-pronged approach to anti-inflammatory therapy through the modulation of the arachidonic acid cascade. *Biochem Pharmacol*. 2018;158:161–173. doi:10.1016/j.bcp.2018.10.007
31. Patrignani P, Patrono C. Cyclooxygenase inhibitors: from pharmacology to clinical read-outs. *Biochim Biophys Acta*. 2015;1851(4):422–432. doi:10.1016/j.bbailp.2014.09.016
32. Koeberle A, Werz O. Natural products as inhibitors of prostaglandin E2 and pro-inflammatory 5-lipoxygenase-derived lipid mediator biosynthesis. *Biotechnol Adv*. 2018;36(6):1709–1723. doi:10.1016/j.biotechadv.2018.02.010
33. Dalli J. Does promoting resolution instead of inhibiting inflammation represent the new paradigm in treating infections? *Mol Aspects Med*. 2017;58:12–20. doi:10.1016/j.mam.2017.03.007
34. Cheung SY, Werner M, Esposito L, et al. Discovery of a benzenesulfonamide-based dual inhibitor of microsomal prostaglandin E2 synthase-1 and 5-lipoxygenase that favorably modulates lipid mediator biosynthesis in inflammation. *Eur J Med Chem*. 2018;156:815–830. doi:10.1016/j.ejmech.2018.07.031
35. Gerstmeier J, Kretzer C, Di Micco S, et al. Novel benzoxanthene lignans that favorably modulate lipid mediator biosynthesis: a promising pharmacological strategy for anti-inflammatory therapy. *Biochem Pharmacol*. 2019;165:263–274. doi:10.1016/j.bcp.2019.03.003
36. Van Anh TT, Mostafa A, Rao Z, et al. From Vietnamese plants to a biflavonoid that relieves inflammation by triggering the lipid mediator class switch to resolution. *Acta Pharm Sin B*. 2021;11(6):1629–1647. doi:10.1016/j.apsb.2021.04.011
37. Zhang K, Pace S, Jordan PM, et al. Beneficial modulation of lipid mediator biosynthesis in innate immune cells by antirheumatic Tripterygium wilfordii glycosides. *Biomolecules*. 2021;11(5):746. doi:10.3390/biom11050746
38. Werz O, Steinhilber D. Development of 5-lipoxygenase inhibitors—lessons from cellular enzyme regulation. *Biochem Pharmacol*. 2005;70(3):327–333. doi:10.1016/j.bcp.2005.04.018
39. Kuhn H, Humeniuk L, Kozlov N, Roigas S, Adel S, Heydeck D. The evolutionary hypothesis of reaction specificity of mammalian ALOX15 orthologs. *Prog Lipid Res*. 2018;72:55–74. doi:10.1016/j.plipres.2018.09.002
40. Gerstmeier J, Weinigel C, Rummeler S, Radmark O, Werz O, Garscha U. Time-resolved in situ assembly of the leukotriene-synthetic 5-lipoxygenase/5-lipoxygenase-activating protein complex in blood leukocytes. *FASEB J*. 2016;30(1):276–285. doi:10.1096/fj.15-278010
41. Titos E, Claria J, Planaguma A, et al. Inhibition of 5-lipoxygenase-activating protein abrogates experimental liver injury: role of Kupffer cells. *J Leukoc Biol*. 2005;78(4):871–878. doi:10.1189/jlb.1204747
42. Meng H, McClendon CL, Dai Z, et al. Discovery of novel 15-Lipoxygenase activators to shift the human arachidonic acid metabolic network toward inflammation resolution. *J Med Chem*. 2016;59(9):4202–4209. doi:10.1021/acs.jmedchem.5b01011
43. Meng H, Dai Z, Zhang W, Liu Y, Lai L. Molecular mechanism of 15-lipoxygenase allosteric activation and inhibition. *Phys Chem Chem Phys*. 2018;20(21):14785–14795. doi:10.1039/C7CP08586A

Journal of Inflammation Research

Dovepress

Publish your work in this journal

The Journal of Inflammation Research is an international, peer-reviewed open-access journal that welcomes laboratory and clinical findings on the molecular basis, cell biology and pharmacology of inflammation including original research, reviews, symposium reports, hypothesis formation and commentaries on: acute/chronic inflammation; mediators of inflammation; cellular processes; molecular mechanisms; pharmacology and novel anti-inflammatory drugs; clinical conditions involving inflammation. The manuscript management system is completely online and includes a very quick and fair peer-review system. Visit <http://www.dovepress.com/testimonials.php> to read real quotes from published authors.

Submit your manuscript here: <https://www.dovepress.com/journal-of-inflammation-research-journal>

Manuscript VI

Natural chalcones elicit formation of specialized pro-resolving mediators and related 15-lipoxygenase products in human macrophages

Kretzer, C., Jordan, PM., Meyer, KPL., Hoff, D., Werner, M., Hofstetter R.K., Koeberle, A., Cala Peralta, A., Viault, G., Seraphin, D., Richomme, P., Helesbeux, JJ., Stuppner, H., Temml, V., Schuster, D., Werz, O.

Biochemical Pharmacology, 2022, Jan;195:114825.

Der Kandidat / Die Kandidatin ist

Erstautor/-in, Ko-Erstautor/-in, Korresp. Autor/-in, Koautor/-in.

Anteile (in %) der Autoren / der Autorinnen an den vorgegebenen Kategorien der Publikation

Author	Conception	Data analysis	Experimental	Writing	Provision of Material
Kretzer C.	30 %	60 %	40 %	30 %	
Jordan PM.		10 %	10 %	10 %	
Meyer KPL.		10 %	10 %		
Hoff D.		10 %	20 %		
Werner M.					
Hofstetter RK.					
Koeberle A.					
Cala Peralta A.					
Viault G.					
Seraphin D.					
Richomme P.					10 %
Helesbeux JJ.					10 %
Stuppner H.					20 %
Temml V.					
Schuster D.	10 %				20 %
Werz O.	40 %			40 %	40 %
Others	20 %	10 %	20 %	20 %	
Summe:	100 %	100 %	100 %	100 %	100 %

Unterschrift Kandidat/-in

Unterschrift Betreuer/-in (Mitglied der Fakultät)



Contents lists available at ScienceDirect

Biochemical Pharmacology

journal homepage: www.elsevier.com/locate/biochempharm

Natural chalcones elicit formation of specialized pro-resolving mediators and related 15-lipoxygenase products in human macrophages

Christian Kretzer^a, Paul M. Jordan^a, Katharina P.L. Meyer^a, Daniel Hoff^a, Markus Werner^a, Robert Klaus Hofstetter^a, Andreas Koeberle^{a,b}, Antonio Cala Peralta^c, Guillaume Viault^c, Denis Seraphin^c, Pascal Richomme^c, Jean-Jacques Helesbeux^c, Hermann Stuppner^d, Veronika Temml^e, Daniela Schuster^e, Oliver Werz^{a,*}

^a Department of Pharmaceutical/Medicinal Chemistry, Institute of Pharmacy, Friedrich Schiller University Jena, Philosophenweg 14, Jena 07743, Germany

^b Michael Popp Institute and Center for Molecular Biosciences Innsbruck (GMBI), University of Innsbruck, Innsbruck 6020, Austria

^c Univ Angers, SONAS, SFR QUASAV, Angers F-49000, France

^d Institute of Pharmacy/Pharmacognosy, Center for Molecular Biosciences Innsbruck (GMBI), University of Innsbruck, Innrain 80/82, Innsbruck 6020, Austria

^e Department of Pharmaceutical and Medicinal Chemistry, Paracelsus Medical University Salzburg, Salzburg 5020, Austria

ARTICLE INFO

Keywords:

Chalcones
15-lipoxygenase
Lipid mediators
Specialized pro-resolving mediators
Macrophages
Inflammation resolution

ABSTRACT

Specialized pro-resolving mediators (SPMs) comprise lipid mediators (LMs) produced from polyunsaturated fatty acids (PUFAs) via stereoselective oxygenation particularly involving 12/15-lipoxygenases (LOXs). In contrast to pro-inflammatory LMs such as leukotrienes formed by 5-LOX and prostaglandins formed by cyclooxygenases, the SPMs have anti-inflammatory and inflammation-resolving properties. Although glucocorticoids and non-steroidal anti-inflammatory drugs (NSAIDs) that block prostaglandin production are still prime therapeutics for inflammation-related diseases despite severe side effects, novel concepts focus on SPMs as immunoresolvents for anti-inflammatory pharmacotherapy. Here, we studied the natural chalcone MF-14 and the corresponding dihydrochalcone MF-15 from *Melodorum fruticosum*, for modulating the biosynthesis of LM including leukotrienes, prostaglandins, SPM and their 12/15-LOX-derived precursors in human monocyte-derived macrophage (MDM) M1- and M2-like phenotypes. In MDM challenged with *Staphylococcus aureus*-derived exotoxins both compounds (10 μ M) significantly suppressed 5-LOX product formation but increased the biosynthesis of 12/15-LOX products, especially in M2-MDM. Intriguingly, in resting M2-MDM, MF-14 and MF-15 strikingly evoked generation of 12/15-LOX products and of SPMs from liberated PUFAs, along with translocation of 15-LOX-1 to membranous compartments. Enhanced 12/15-LOX product formation by the chalcones was evident also when exogenous PUFAs were supplied, excluding increased substrate supply as sole underlying mechanism. Rather, MF-14 and MF-15 stimulate the activity of 15-LOX-1, supported by experiments with HEK293 cells transfected with either 5-LOX, 15-LOX-1 or 15-LOX-2. Together, the natural chalcone MF-14 and the dihydrochalcone MF-15 favorably modulate LM biosynthesis in human macrophages by suppressing pro-inflammatory leukotrienes but stimulating formation of SPMs by differential interference with 5-LOX and 15-LOX-1.

Abbreviations: AA, arachidonic acid; AKR1C3, aldo-keto reductase family 1 member C3; COX, cyclooxygenase; cPLA₂, cytosolic phospholipase A₂; DHA, docosahexaenoic acid; EtOAc, ethyl acetate; EPA, eicosapentaenoic acid; FCS, fetal calf serum; GM-CSF, granulocyte macrophage-colony stimulating factor; IFN, interferon; HDHA, hydroxydocosahexaenoic acid; HETE, hydroxyeicosatetraenoic acid; HEPE, hydroxyeicosapentaenoic acid; IL, interleukin; LDH, lactate dehydrogenase; LM, lipid mediator; LPS, lipopolysaccharide; LOX, lipoxygenase; LT, leukotriene; LX, lipoxin; MaR, maresin; M-CSF, macrophage-colony stimulating factor; MDM, monocyte-derived macrophages; mPGES, microsomal prostaglandin E₂ synthase; MTT, 3-(4,5-dimethyl-2-thiazolyl)-2,5-diphenyl-2H-tetrazolium bromide; NSAIDs, non-steroidal anti-inflammatory drugs; PBMC, peripheral blood mononuclear cells; PD, protectin; PG, prostaglandin; PMNL, polymorphonuclear leukocytes; PUFAs, polyunsaturated fatty acids; RV, resolvin; SACM, *Staphylococcus (S.) aureus* 6850-conditioned medium; SPE, solid phase extraction; SPM, specialized pro-resolving mediators; THF, tetrahydrofuran; TX, thromboxane; UPLC-MS-MS, ultra-performance liquid chromatography-tandem mass spectrometry.

* Corresponding author.

E-mail address: oliver.werz@uni-jena.de (O. Werz).

<https://doi.org/10.1016/j.bcp.2021.114825>

Received 28 September 2021; Received in revised form 1 November 2021; Accepted 2 November 2021

Available online 8 November 2021

0006-2952/© 2021 Elsevier Inc. All rights reserved.

1. Introduction

Initiation, maintenance and resolution of acute inflammation are well-orchestrated processes regulated by lipid mediators (LMs) that are biosynthesized from free polyunsaturated fatty acids (PUFAs) [1]. Among these PUFAs, arachidonic acid (AA, ω -6) is metabolized at the onset of inflammation to prostaglandins (PGs) and leukotrienes (LTs), generated by cyclooxygenases (COX) and by the 5-lipoxygenase (5-LOX) pathway, respectively, which promote the maintenance of inflammatory processes and contribute to related diseases like rheumatoid arthritis, atherosclerosis, respiratory disorders, Alzheimer's disease and cancer [2–4]. In contrast, resolution of inflammation is promoted by another superfamily of LMs that are specialized pro-resolving mediators (SPMs) encompassing resolvins (RVs), protectins (PDs) and maresins (MaRs) mainly produced by 12/15-LOXs from the ω -3 PUFAs eicosapentaenoic acid (EPA) or docosahexaenoic acid (DHA) [5]. These SPMs are highly potent signaling molecules blocking excessive neutrophil infiltration and pro-inflammatory cytokine secretion, increase the phagocytic and efferocytotic capacities of macrophages, and stimulate tissue repair and regeneration [6]. Common anti-inflammatory therapies such as the use of glucocorticoids and non-steroidal anti-inflammatory drugs (NSAIDs)

suppress PG formation within this complex LM network, causing side effects due to substrate shunting into other non-targeted biosynthetic LM branches [7,8]. A novel concept pursues the support of inflammation resolution using application of SPMs and their precursors as well as elevation of endogenous SPM biosynthesis by supplementation of EPA and DHA [9]. Quite recently, manipulation of LM formation by natural products was reported that resulted in a shift from LTs and PGs to SPMs in the complex LM network by smart interference with 5-LOX at an allosteric site [10,11]. Here, we report on a chalcone and its corresponding dihydrochalcone that, apart from inhibiting 5-LOX and related LT formation, are able to stimulate human monocyte-derived macrophages (MDM) for generation of SPM, apparently by cellular translocation and activation of 15-LOX-1.

Among natural products, flavonoids including chalcones have been in the focus of anti-inflammatory research for many years. Chalcones are ring-opened flavone-like structures and are widely distributed in daily consumables like vegetables, spices or various plants [12]. The structure of these types of compounds allows many different interactions with inflammation-related proteins [13]. In the analysis of new therapeutic options, natural and synthetic chalcones have been identified as anti-inflammatory agents that inhibit COX-2-derived PG formation and LT

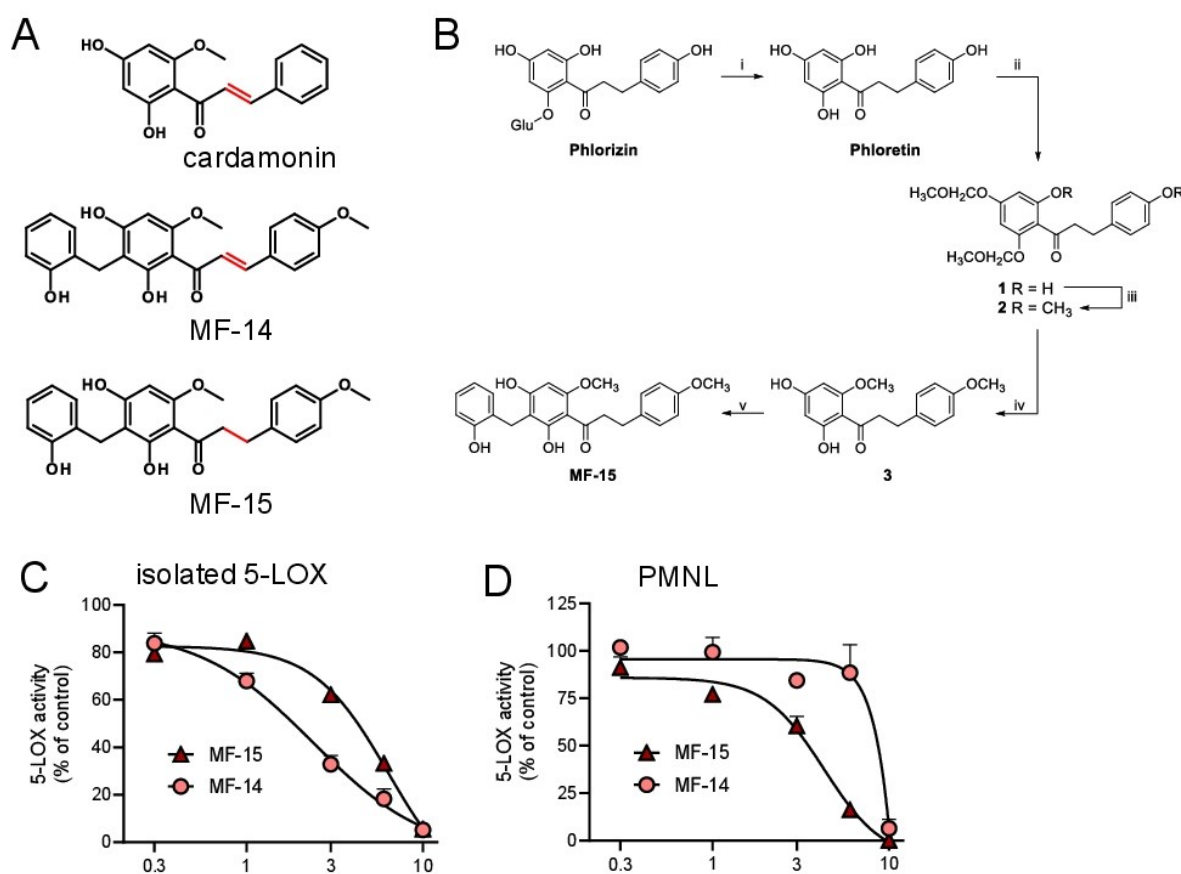


Fig. 1. The natural chalcone MF-14 and the dihydrochalcone MF-15 are cardamonin derivatives that inhibit human 5-lipoxygenase. (A) Chemical structures of MF-14 and MF-15 derived from cardamonin. (B) Semi-synthesis of MF-15. i: HCl 1.25 N, MeOH, 90 °C, 3 h, 85%; ii: MOM-Br, diisopropylamine, dry THF, RT, 20 min, 54%; iii: methyl iodide, NaH 60%, THF, 0 °C, 1.5 h, 69%; iv: *p*TSA, DCM/EtOH 1/7, 60 °C, 1 h, 75%; v: 2-hydroxybenzyl alcohol, ZnCl₂, dioxane, MW 130 °C, 30 min, 60%. (C,D) Inhibition of 5-LOX activity by MF-14 and MF-15. (C) Isolated human recombinant 5-LOX was diluted in PBS containing EDTA (1 mM) and incubated with MF-14 or MF-15 at the indicated concentrations (in μM) or vehicle (0.1% DMSO) for 10 min on ice. The samples were placed at 37 °C for 30 sec and then stimulated with 20 μM AA plus 2 mM CaCl₂ for 10 min at 37 °C. (D) Freshly isolated human PMNL (10⁷ cells per mL) were diluted in PBS containing 1 mM CaCl₂ and 0.1% glucose and incubated with MF-14 or MF-15 at the indicated concentrations (in μM) or vehicle (0.1% DMSO) for 10 min at 37 °C and then stimulated with 2.5 μM A23187 for 10 min at 37 °C. After termination of the incubations, the formed lipid mediators were extracted by SPE and 5-LOX products were analyzed via RP-HPLC. Values are means ± SEM, given as percentage of vehicle control (=100%), n = 3.

production involving 5-LOX [13–15]. In addition to the anti-inflammatory activities chalcones are also examined as antidepressant, analgesic and anticarcinogenic drugs [16,17]. Here, we investigated the natural chalcone MF-14 ((*E*)-1-[2,4-dihydroxy-3-[(2-hydroxyphenyl)methyl]-6-methoxy-phenyl]-3-(4-methoxyphenyl)prop-2-en-1-one) and the corresponding dihydrochalcone MF-15 (1-[2,4-dihydroxy-3-[(2-hydroxyphenyl)methyl]-6-methoxy-phenyl]-3-(4-methoxyphenyl)propan-1-one) that are structurally derived from cardamonin (Fig. 1A), and contained in the leaves of *Melodorum fruticosum*. Previous studies showed that especially MF-15 facilitates strong antineoplastic effects as well as inhibition of androgen receptor signaling pathways and decreased aldo-keto reductase family 1 member C3 (AKR1C3) expression to treat enzalutamide-resistant prostate cancer *in vitro* [18]. Our data demonstrate that in addition to their LT-suppressing actions via blocking 5-LOX, these chalcones act as elicitors of SPM biosynthesis in human macrophages implying potential as therapeutics for the treatment of inflammatory diseases.

2. Materials and methods

2.1. Materials

Isolation of MF-14 from *Melodorum fruticosum* was performed as previously described [18]. To obtain sufficient quantities for experimentation, MF-15 was semi-synthesized as described below from phlorizin that was efficiently extracted and purified from apple tree leaves. ¹H and ¹³C NMR along with 2D NMR data were obtained on a JEOL JNM-ECZS 400 MHz spectrometer (400 and 100 MHz, respectively) in deuterated acetone and calibrated using the residual non-deuterated solvent resonance as internal reference. Chemical shifts (δ) are reported in ppm with (br) s used for (broad) singlet, d for doublet and t for triplet. Deuterium-labelled and non-labelled LM standards for ultra-performance liquid chromatography-tandem mass spectrometry (UPLC-MS-MS) quantification were obtained from Cayman Chemical/Biomol (Hamburg, Germany). All other chemicals were obtained at Sigma-Aldrich (Taufkirchen, Germany) unless stated otherwise.

2.2. Semi-synthesis of MF-15

(*E*)-1-[2,4-Bis(methoxymethoxy)-6-hydroxyphenyl]-3-(4-hydroxyphenyl)prop-2-en-1-one (di-MOM-phloretin, **compound 1**): To a solution of phloretin (92 mg, 0.34 mmol) in dry tetrahydrofuran (THF) (5 mL) MOM-Br (0.07 mL, 2.2 eq.) and diisopropylamine (0.15 mL, 2.5 eq.) were successively added at 0 °C. The reaction mixture was stirred at room temperature (RT) for 20 min. Then, it was diluted with 10 mL of water, neutralized with 1 M aqueous HCl and extracted with 3 × 15 mL of EtOAc. Combined organic layers were dried over Na₂SO₄, filtered and evaporated under reduced pressure. The crude was purified by silica-gel column chromatography eluted with a mixture of petroleum ether/acetone (gradient from 9:1 to 7:3) leading to 66 mg of **compound 1** (54% yield). ¹H NMR (δ ppm, (CD₃)₂CO, 400 MHz): 13.72 (br s, 1H), 8.13 (br s, 1H), 7.10 (d, *J* = 8.4 Hz, 2H), 6.75 (d, *J* = 8.4 Hz, 2H), 6.30 (d, *J* = 2.3 Hz, 1H), 6.21 (d, *J* = 2.3 Hz, 1H), 5.35 (s, 2H), 5.24 (s, 2H), 3.48 (s, 3H), 3.44 (s, 3H), 3.37 (t, *J* = 7.7 Hz, 2H), 2.90 (t, *J* = 7.7 Hz, 2H). ¹³C NMR (δ ppm, (CD₃)₂CO, 100 MHz): 206.0, 167.7, 164.4, 161.3, 156.4, 133.1, 130.2, 116.0, 107.3, 97.6, 95.6, 95.0, 94.8, 57.0, 56.5, 46.9, 30.4.

(*E*)-1-[2,4-Bis(methoxymethoxy)-6-methoxyphenyl]-3-(4-methoxyphenyl)prop-2-en-1-one (**compound 2**): NaH (195 mg, 3 eq.) and methyl iodide (0.71 mL, 5.9 eq.) were successively added to a solution of di-MOM-phloretin 1 (700 mg, 1.93 mmol) in 27 mL of dry THF at 0 °C. The resulting reaction mixture was stirred at the same temperature for 1.5 h. Then, 10 mL of ice-cold water were added and the mixture was extracted with 3 × 30 mL of EtOAc. Combined organic layers were dried over Na₂SO₄, filtered and evaporated under reduced pressure. The crude was purified by silica-gel column chromatography eluted with a mixture of petroleum ether/acetone (9:1) leading to 520 mg of **compound 2**

(69% yield). ¹H NMR (δ ppm, (CD₃)₂CO, 400 MHz): 7.15 (d, *J* = 8.4 Hz, 2H), 6.83 (d, *J* = 8.4 Hz, 2H), 6.47 (d, *J* = 2.0 Hz, 1H), 6.40 (d, *J* = 2.0 Hz, 1H), 5.20 (s, 2H), 5.12 (s, 2H), 3.76 (s, 3H), 3.75 (s, 3H), 3.44 (s, 3H), 3.38 (s, 3H), 2.98 (t, *J* = 7.4 Hz, 2H), 2.88 (t, *J* = 7.4 Hz, 2H). ¹³C NMR (δ ppm, (CD₃)₂CO, 100 MHz): 202.3, 160.5, 158.9, 158.6, 156.0, 134.3, 130.1, 116.5, 114.5, 96.7, 95.4, 95.2, 94.7, 56.4, 56.3, 56.2, 55.4, 47.1, 29.4.

(*E*)-1-[2,4-Bis(hydroxy)-6-methoxyphenyl]-3-(4-methoxyphenyl)prop-2-en-1-one (**compound 3**): **Compound 2** (345 mg, 0.88 mmol) was dissolved in 16 mL of a 7:1 mixture EtOH/CH₂Cl₂. An excess of pTSA (2.05 g, 13.6 eq.) was added. The reaction mixture was stirred at 60 °C for 1 h. Then, approximately half of the solvents were evaporated under reduced pressure. The resulting solution was diluted with water (20 mL) and saturated aqueous NaHCO₃ solution up to pH 6, extracted with 3 × 30 mL of EtOAc. Combined organic layers were dried over Na₂SO₄, filtered and evaporated under reduced pressure. The crude was purified by silica-gel column chromatography eluted with a mixture of petroleum ether/acetone (9:1) leading to 201 mg of **3** (75% yield). All spectroscopic data were in accordance with the ones reported for the corresponding natural derivative [19].

(*E*)-1-[2,4-Bis(hydroxy)-3-(2-hydroxybenzyl)-6-methoxyphenyl]-3-(4-methoxyphenyl)prop-2-en-1-one (MF-15): 2',4'-dihydroxy-4,6'-dimethoxydihydrochalcone **3** (83.6 mg, 0.277 mmol), 2 mL dry dioxane, 2-hydroxybenzyl alcohol (34.4 mg, 1 eq.) and ZnCl₂ (35 mg, 1 eq.) were transferred into a microwave reactor. Then, the reaction mixture was irradiated at 130 °C for 0.5 h. It was quenched by adding 10 mL H₂O, extracted with 3 × 10 mL EtOAc. Combined organic layers were dried over Na₂SO₄, filtered and evaporated under reduced pressure. The crude was purified by silica-gel column chromatography eluted with a mixture of petroleum ether/acetone (from 3:1 to 3:2 ratio) leading to 68 mg of MF-15 as a colorless solid (60% yield). All spectroscopic data were in accordance with the ones reported for the corresponding natural derivative [20].

2.3. Cell isolation and cell culture

Leukocyte concentrates were prepared from peripheral blood obtained from healthy human adult donors that received no anti-inflammatory treatment for the last 10 days (Institute of Transfusion Medicine, University Hospital Jena). The approval for the protocol was given by the ethical committee of the University Hospital Jena and all methods were performed in accordance with the relevant guidelines and regulations. To isolate polymorphonuclear leukocytes (PMNL) and monocytes, the leukocyte concentrates were mixed with dextran (dextran from *Leuconostoc* spp. MW ~40,000) for sedimentation of erythrocytes; the supernatant was centrifuged on lymphocyte separation medium (Histopaque®-1077). Contaminating erythrocytes in the pelleted neutrophils were removed by hypotonic lysis using water. PMNL were then washed twice in ice-cold phosphate buffer saline (PBS) and finally resuspended in PBS. The peripheral blood mononuclear cell (PBMC) fraction on top of the lymphocyte separation medium was washed with ice-cold PBS and seeded in cell culture flasks (Greiner Bio-one, Nuertingen, Germany) for 1.5 h (37 °C, 5% CO₂) in PBS with Ca²⁺/Mg²⁺ to isolate monocytes by adherence. For differentiation and polarization of monocytes to M1- and M2-like macrophages, we followed published procedures [21]. Thus, adherent monocytes were treated with 20 ng mL⁻¹ granulocyte macrophage-colony stimulating factor (GM-CSF) (Peprotech, Hamburg, Germany) for 6 days in RPMI 1640 supplemented with 10% fetal calf serum (FCS), 2 mmol L⁻¹ L-glutamine, penicillin (100 U mL⁻¹) and streptomycin (100 µg mL⁻¹) for differentiation and further incubated with 100 ng mL⁻¹ lipopolysaccharide (LPS) and 20 ng mL⁻¹ interferon- γ (Peprotech) for 48 h to get M1-MDM. To obtain M2-MDM, monocytes were treated with 20 ng mL⁻¹ M-CSF (Peprotech) for 6 days, followed by 20 ng mL⁻¹ interleukin (IL)-4 (Peprotech) for 48 h. Unpolarized M0-MDM were obtained by differentiation with M-CSF and GM-CSF (10 ng mL⁻¹, each) for 6 days

[21,22]. Correct polarization and purity of MDM was routinely checked by flow cytometry (LSRFortessa™ cell analyzer, BD Biosciences, Heidelberg, Germany) as reported [8] using the following antibodies: FITC anti-human CD14 (clone M5E2, BD Biosciences), APC-H7 anti-human CD80 (clone L307.4, BD Biosciences), PE-Cy7 anti-human CD54 (clone HA58, Biolegend, Koblenz, Germany), PE anti-human CD163 (clone GHI/61, BD Biosciences), and APC anti-human CD206 (clone 19.2, BD Biosciences). HEK293 cells were cultured in monolayers (37 °C, 5% CO₂) in DMEM containing FCS (10%), penicillin (100 U mL⁻¹) and streptomycin (100 µg mL⁻¹). HEK293 cell lines stably expressing 5-LOX, 15-LOX-1 or 15-LOX-2 were selected using geneticin (400 µg) as reported [10]. Transfection of HEK293 cells was performed by using pcDNA3.1 plasmids and lipofectamine according to the manufacturer's protocol (Invitrogen, Darmstadt, Germany) and as reported before [23].

2.4. Expression, purification and activity assay of human recombinant 5-LOX

E. coli BL21 was transformed with pT3-5-LO plasmid at 30 °C overnight to express recombinant 5-LOX as described before [24]. The bacteria were treated with lysis buffer containing triethanolamine (50 mM, pH 8.0), EDTA (5 mM), phenylmethanesulfonyl fluoride (1 mM), soybean trypsin inhibitor (60 µg mL⁻¹), dithiothreitol (2 mM) and lysozyme (1 mg mL⁻¹) before sonification (3×15 s) to obtain cell lysates. 5-LOX was purified from supernatants after centrifugation of the lysates (40,000×g; 20 min, 4 °C) by using an ATP-agarose column and diluted with PBS buffer containing 1 mM EDTA. For evaluation of 5-LOX product formation, 0.5 µg purified 5-LOX was diluted in 1 mL PBS containing 1 mM EDTA and pre-incubated with vehicle (0.1% DMSO) or test compounds for 15 min on ice and then stimulated with 20 µM AA and 2 mM CaCl₂ for 10 min at 37 °C. The reaction was stopped by addition of 1 mL ice-cold methanol containing PGB₁ (200 ng) as internal standard, and 5-LOX products (i.e., *trans*-isomers of LTB₄ and 5-H(P)ETE) were analyzed by RP-HPLC as described previously [25]. Briefly, 530 µL acidified PBS and 200 ng of internal PGB₁ standard were added and solid phase extraction (SPE) using C18 RP-columns (100 mg, UCT, Bristol, PA, USA) was performed. After elution with methanol, samples were analyzed by RP-HPLC using a C-18 Radial-PAK column (Waters, Eschborn, Germany).

2.5. Cytotoxicity assays in human MDM

Cytotoxicity was studied by analysis of lactate dehydrogenase (LDH) release (cell integrity) and by 3-(4,5-dimethyl-2-thiazolyl)-2,5-diphenyl-2H-tetrazolium bromide (MTT) assay (cell viability) in M0-MDM. The release of LDH from the cells was analyzed using the CytoTox 96® Non-Radioactive Cytotoxicity Assay (Promega GmbH, Mannheim, Germany). In brief, 10⁶ M0-MDM per well were suspended in RPMI-medium containing 10% FCS, penicillin/streptomycin and L-glutamine, and seeded in a 24-well plate. Lysis control and 0.2% triton X-100 were added to the cells and incubated for 45 min; compounds and control (0.1% DMSO) were added and incubated for another 24 h at 37 °C. Stop solution was added, the plate was centrifuged (250×g, 4 min, RT) and 50 µL of supernatant from each well was transferred in a 96-well plate. Afterwards, 50 µL of substrate mixture was added and incubated for 30 min at RT in the dark. To finally stop the reaction, 50 µL of stop solution were added. The photometric measurement was performed at 490 nm using a Multiskan Spectrum plate reader (Thermo Fischer Scientific, Scientific, Darmstadt, Germany) as reported before [26].

For analysis of cytotoxic effects by MTT assay [27], 10⁵ M0-MDM per well were seeded in a 96 well plate (triplicates). Briefly, test compounds or controls (DMSO as vehicle control; staurosporine (1 µM) as positive control) were added and incubated for 48 h (37 °C, 5% CO₂). Next, the MTT solution was added and cells were incubated for another 2 h under the aforementioned conditions. Then, 100 µL SDS lysis buffer was added under gently shaking for 20 h at 175 rpm in the dark. VIS detection was

used to measure the corresponding reaction at 570 nm.

2.6. Evaluation of 5-LOX product formation in human PMNL

For evaluation of 5-LOX product formation in human PMNL, 10⁷ cells per mL PBS plus 1 mM CaCl₂ and 0.1% glucose were incubated with test compounds for 15 min at 37 °C and then stimulated with 2.5 µM Ca²⁺-ionophore A23187 (Cayman, Ann Arbor, USA) for 10 min. The incubation was stopped with 1 mL ice-cold methanol containing 200 ng mL⁻¹ PGB₁ as internal standard. Samples were subjected to SPE and formed LM were separated and analyzed by RP-HPLC as described [28].

2.7. Determination of the lipid mediator profile in human MDM and in HEK293 cells

Human MDM (2×10⁶ cells in 1 mL PBS plus 1 mM CaCl₂) were seeded in 6-well-plates and preincubated for 15 min with test compounds at 37 °C. The macrophages were subsequently incubated with 1% (v/v) *Staphylococcus (S.) aureus* 6850-conditioned medium (SACM, 24 h culture from OD = 0.05) for 3 h to induce LM formation, as reported recently [29]. Alternatively, MDM (2×10⁶ cells in 1 mL PBS plus 1 mM CaCl₂) were incubated with the test compounds with or without AA, EPA, DHA (1 µM each) at 37 °C for 3 h.

HEK293 cells (2×10⁶ cells in 1 mL PBS plus 1 mM CaCl₂ and 0.1% glucose) were preincubated with test compounds or vehicle (0.1% DMSO) for 10 min at 37 °C, and LM biosynthesis was initiated by addition of 2.5 µM A23187 plus 1 µM AA for another 15 min at 37 °C. Alternatively, HEK293 cells were incubated with test compounds or vehicle (0.1% DMSO) together with AA, EPA, DHA (1 µM each) for 3 h at 37 °C.

Incubation of either MDM or HEK293 cells was stopped with 2 mL ice-cold methanol containing deuterium-labeled internal standards (d8-5S-HETE, d4-LTB₄, d5-LXA₄, d5-RvD2, and d4-PGE₂; 500 pg each). Samples were kept at -20 °C for one day to allow protein precipitation. After centrifugation (2000×g, 4 °C, 10 min), 8 mL acidified water was added (final pH = 3.5) and samples were subjected to solid phase extraction using RP-18 columns. LMs were analyzed by UPLC-MS/MS [21].

2.8. SDS-PAGE and Western blot

Cell lysates of MDM (2×10⁶ cells) were separated on 10% polyacrylamide gels and blotted onto nitrocellulose membranes (Amersham Protran Supported 0.45 µm nitrocellulose; GE Healthcare, Chicago, IL, USA). The membranes were incubated with the following primary antibodies: rabbit polyclonal anti-5-LOX, 1:1000 (Genscript, Piscataway, NJ, USA, to a peptide with the C-terminal 12 aa of 5-LOX: CSPDRIPNSVAL; kindly provided by Dr. Marcia Newcomer, Louisiana State University, Baton Rouge, LA, USA); mouse monoclonal anti-15-LOX-1, 1:500 (ab119774; Abcam, Cambridge, United Kingdom); rabbit polyclonal anti-COX-2, 1:500 (4842; Cell Signaling Technology); rabbit polyclonal anti-15-LOX-2, 1:500 (ab23691; Abcam), and rabbit polyclonal anti-β-actin, 1:1000 (4967S; Cell Signaling Technology). Immunoreactive bands were stained with IRDye 800CW goat anti-mouse IgG (H + L), 1:10,000 (926-32210; Li-Cor Biosciences, Lincoln, NE, USA), IRDye 800CW goat anti-rabbit IgG (H + L), 1:15,000 (926 32211; Li-Cor Biosciences) and IRDye 680LT goat anti-mouse IgG (H + L), 1:40,000 (926-68020; Li-Cor Biosciences), and visualized by an Odyssey infrared imager (Li-Cor Biosciences). Data from densitometric analysis were background corrected.

2.9. Flow cytometry

Cells were stained in PBS pH 7.4 containing 0.5% BSA, 2 mM EDTA and 0.1% sodium azide by Zombie Aqua™ Fixable Viability Kit (Biolegend, San Diego, CA, USA) for 5 min at 4 °C to determine cell viability.

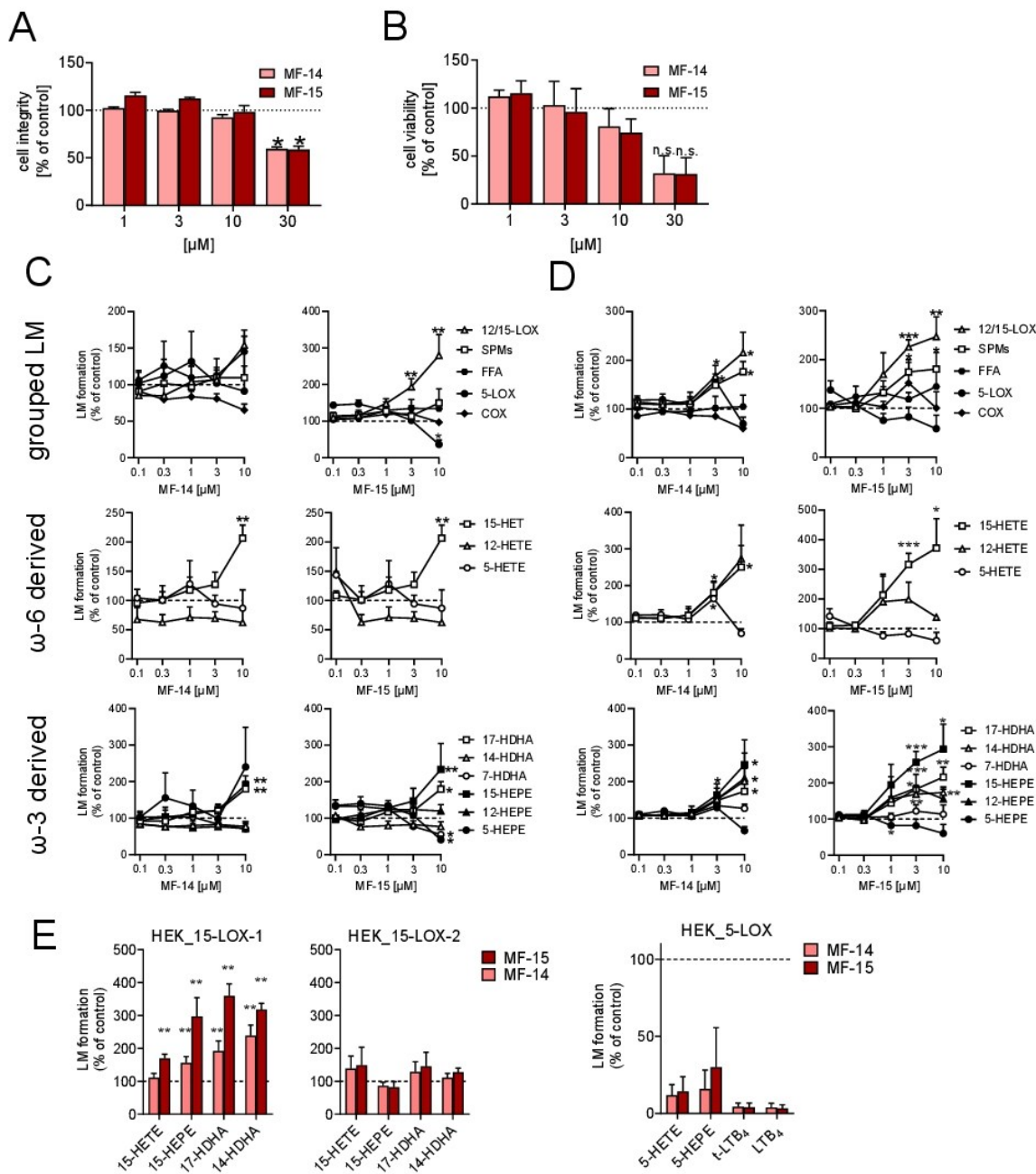


Fig. 2. Effects of MF-14 and MF-15 on LM profiles of exotoxin-stimulated M1- and M2-MDM and of LOX-transfected HEK293 cells. (A,B) Human unpolarized MDM were kept in RPMI 1640 medium and incubated with MF-14 or MF-15 at the indicated concentrations or vehicle (0.1% DMSO) for 24 h at 37 °C and cell integrity and viability was assessed using (A) LDH release assay and (B) MTT assay, respectively. Values are means \pm SEM, given as percentage of vehicle control (=100% integrity or viability), $n = 3$. Statistics was performed via matched one-way ANOVA and Dunnett's multiple comparisons test against the DMSO control, * $p < 0.05$. (C) M1-MDM and (D) M2-MDM (2×10^6 , each) were diluted in PBS containing 1 mM CaCl₂, incubated with vehicle (0.1% DMSO), MF-14 or MF-15 (10 μ M, each) for 10 min at 37 °C and stimulated with SAGM (1%) for 180 min at 37 °C. Then, formed LM were extracted from the supernatants by SPE and analyzed by UPLC-MS/MS. Results are given as mean \pm SEM, presented as percentage of SAGM-stimulated vehicle control (=100%), $n = 5$. Upper panels: grouped LM produced by 12/15-LOX, SPM, PUFA, 5-LOX and COX (according to Table 1); middle panels: sum of ω -6-derived LM as indicated; lower panels: sum of ω -3-derived LM as indicated. (E) Stably LOX-transfected HEK293 cells (2×10^6 cells in 1 mL PBS containing 1 mM CaCl₂ and 0.1% glucose), were pre-incubated with vehicle (0.1% DMSO), MF-14 or MF-15 (10 μ M, each) for 15 min at 37 °C and then stimulated with 2.5 μ M ionophore A23187 plus 1 μ M AA at 37 °C. Afterwards the reaction was stopped with ice-cold methanol and formed LMs were extracted by SPE and analyzed by UPLC-MS/MS. Results are given as mean \pm S.E.M in percentage versus vehicle control (=100%) for 5-LOX, 15-LOX-1-, and 15-LOX-2-transfected cells, $n = 3$. Statistical analysis was performed via ratio-paired t -test, * $p < 0.05$, ** $p < 0.01$, *** $p < 0.001$, **** $p < 0.0001$.

Table 1

MF-14 and MF-15 modulate LM profiles of exotoxin-stimulated M1- and M2-MDM. M1- and M2-MDM (2×10^6 cells, each) were preincubated in PBS containing 1 mM CaCl_2 with vehicle (0.1% DMSO), MF-14 or MF-15 (10 μM , each) for 10 min at 37°C and then stimulated with SACM (1%) for 180 min at 37°C . Formed LM in the supernatants were analyzed by UPLC-MS/MS. Results are given in pg/ 2×10^6 cells as means \pm SEM and as -fold change versus SACM-stimulated vehicle control (ctrl. = 1), n = 5. Results below the limit of quantification are indicated as non-quantifiable (n.q.).

	M1 ctrl	MF-14	-fold	M1 ctrl	MF-15 [10 μM]	-fold	M2 ctrl	MF-14 [10 μM]	-fold	M2 ctrl	MF-15 [10 μM]	-fold
5-LOX												
5-HEPE	416 \pm 148	240 \pm 183	0.6	289 \pm 74	110 \pm 33	0.4	247 \pm 36	169 \pm 43	0.7	445 \pm 98	182 \pm 60	0.4
5-HETE	3590 \pm 1757	1325 \pm 380	0.4	2710 \pm 1244	1183 \pm 580	0.4	2759 \pm 462	1704 \pm 274	0.6	6452 \pm 2550	2364 \pm 648	0.4
1-LTB ₄	283 \pm 111	142 \pm 111	0.5	244 \pm 65	77 \pm 32	0.3	332 \pm 26	186 \pm 36	0.6	731 \pm 272	222 \pm 70	0.3
LTB ₄	1387 \pm 572	867 \pm 943	0.6	1310 \pm 470	267 \pm 129	0.2	609 \pm 101	461 \pm 108	0.8	1655 \pm 737	391 \pm 108	0.2
5S,6R-dihETE	145 \pm 72	70 \pm 51	0.5	119 \pm 54	42 \pm 23	0.3	121 \pm 8	90 \pm 18	0.7	357 \pm 152	104 \pm 32	0.3
COX												
PGE ₂	6251 \pm 4286	5543 \pm 6450	0.9	1962 \pm 506	2627 \pm 578	1.3	354 \pm 91	601 \pm 213	1.7	249 \pm 36	337 \pm 54	1.4
PGD ₂	85 \pm 25	107 \pm 33	1.3	38 \pm 3	73 \pm 15	1.9	75 \pm 27	110 \pm 46	1.5	46 \pm 8	63 \pm 17	1.4
PGF _{2α}	822 \pm 280	765 \pm 564	0.9	474 \pm 105	522 \pm 79	1.1	220 \pm 109	325 \pm 208	1.5	100 \pm 23	130 \pm 32	1.3
TXB ₂	17936 \pm 6018	12400 \pm 10781	0.7	10165 \pm 1203	8963 \pm 1219	0.9	10668 \pm 4323	7162 \pm 4038	0.7	5301 \pm 1354	4984 \pm 1779	0.9
SPM precursors												
17-HDHA	926 \pm 237	1697 \pm 264	1.8	510 \pm 171	1276 \pm 384	2.5	5986 \pm 2970	11486 \pm 6004	1.9	2906 \pm 1255	5075 \pm 1151	1.7
14-HDHA	168 \pm 38	118 \pm 19	0.7	140 \pm 26	107 \pm 34	0.8	1467 \pm 521	2846 \pm 1710	1.9	719 \pm 146	1208 \pm 238	1.7
7-HDHA	116 \pm 22	75 \pm 47	0.6	86 \pm 20	42 \pm 3	0.5	286 \pm 112	397 \pm 181	1.4	184 \pm 29	202 \pm 45	1.1
4-HDHA	89 \pm 16	90 \pm 10	1.0	63 \pm 11	72 \pm 14	1.1	88 \pm 19	95 \pm 26	1.1	94 \pm 13	90 \pm 11	1.0
15-HEPE	91 \pm 19	174 \pm 32	1.9	61 \pm 17	124 \pm 30	2.0	816 \pm 405	2553 \pm 1448	3.1	351 \pm 155	801 \pm 198	2.3
12-HEPE	51 \pm 12	34 \pm 14	0.7	54 \pm 13	71 \pm 25	1.3	207 \pm 74	475 \pm 251	2.3	116 \pm 16	178 \pm 35	1.5
15-HETE	1552 \pm 134	3276 \pm 706	2.1	930 \pm 162	3088 \pm 678	3.3	9654 \pm 4569	21506 \pm 8179	2.2	3979 \pm 1132	12835 \pm 3561	3.2
12-HETE	857 \pm 359	282 \pm 250	0.3	449 \pm 207	1028 \pm 377	2.3	1679 \pm 484	4188 \pm 1967	2.5	1703 \pm 609	2236 \pm 745	1.3
5,15-dihETE	105 \pm 46	61 \pm 65	0.6	52 \pm 6	28 \pm 4	0.5	900 \pm 570	1781 \pm 1211	2.0	384 \pm 143	619 \pm 290	1.6
FFA SPMs												
PD1	3.0 \pm 0.7	4.7 \pm 0.4	1.5	2.0 \pm 0.6	4.1 \pm 2.3	2.0	17 \pm 7	32 \pm 16	1.9	10 \pm 2	18 \pm 7	1.8
PDX	8.0 \pm 3.3	15.9 \pm 1.8	2.0	5.5 \pm 2.7	13.7 \pm 8.0	2.5	31 \pm 9	55 \pm 17	1.8	31 \pm 9	60 \pm 25	1.9
RvD5	8.9 \pm 3.1	5.6 \pm 3.7	0.6	5.8 \pm 1.8	2.8 \pm 0.4	0.5	368 \pm 252	733 \pm 490	2.0	106 \pm 62	190 \pm 93	1.8
MaR1	5.9 \pm 2.4	2.7 \pm 2.9	0.5	2.5 \pm 1.6	3.4 \pm 2.2	1.3	33 \pm 9	46 \pm 11	1.4	23 \pm 10	34 \pm 15	1.5
AA	632322 \pm 294318	813832 \pm 585167	1.3	486287 \pm 215813	722736 \pm 355550	1.5	708077 \pm 325600	881911 \pm 480958	1.2	592316 \pm 302582	736718 \pm 381686	1.2
EPA	229764 \pm 101624	315238 \pm 213017	1.4	174013 \pm 82639	291918 \pm 148084	1.7	240368 \pm 121104	309628 \pm 172859	1.3	227858 \pm 124036	266763 \pm 154736	1.2
DHA	174632 \pm 34609	231448 \pm 68947	1.3	160498 \pm 32851	176109 \pm 44458	1.1	183458 \pm 43893	184596 \pm 59792	1.0	151096 \pm 44656	173852 \pm 53984	1.2

Non-specific antibody binding was blocked by using mouse serum (10 min at 4°C) prior to staining by the following fluorochrome-labelled antibodies (20 min, 4°C): FITC anti-human CD14 (clone M5E2, BD Biosciences), APC-H7 anti-human CD80 (clone L307.4, BD Biosciences), PE-Cy7 anti-human CD54 (clone HA58, Biolegend), PE anti-human CD163 (clone GHI/61, BD Biosciences), and APC anti-human CD206 (clone 19.2, BD Biosciences) to determine M1 and M2 surface marker expression using a LSRFortessaTM cell analyzer (BD Biosciences), and data were analyzed using FlowJo X Software (BD Biosciences).

2.10. Immunofluorescence microscopy

MDM (10^6 cells) were seeded onto glass coverslips in a 12-well plate and cultured for 48 h. SACM, test compounds or DMSO (0.1% as vehicle) were added at 37°C and stopped after the indicated times by fixation with 4% paraformaldehyde solution. Acetone (3 min, 4°C) followed by 0.25% Triton X-100 for 10 min at RT was used for permeabilization prior to blocking with normal goat serum 10% (50062Z, Thermo Fisher Scientific). Coverslips were incubated with mouse monoclonal anti-15-LOX-1 antibody, 1:100 (ab119774, Abcam, Cambridge, UK) and rabbit anti-5-LOX antibody, 1:100 (1550 AK6, kindly provided by Dr. Olof Radmark, Karolinska Institutet, Stockholm, Sweden) at 4°C overnight. 5-LOX and 15-LOX-1 were stained with the fluorophore-labeled secondary antibodies; Alexa Fluor 555 goat anti-mouse IgG (H + L); 1:500 (A21424, Thermo Fisher Scientific) and Alexa Fluor 488 goat anti-rabbit IgG (H + L); 1:500 (A11034, Thermo Fisher Scientific). Samples were analyzed by a Zeiss Axiovert 200 M microscope, and a Plan Neofluar $\times 40/1.30$ Oil (DIC III) objective (Carl Zeiss, Jena, Germany). An AxioCam MR camera (Carl Zeiss) was used for image acquisition.

2.11. Statistical analysis

The sample size for experiments with MDM and PMNL was chosen empirically based on previous studies [21] to ensure adequate statistical power. The results are expressed as mean \pm standard error of the mean (SEM) of n observations, where n represents the number of experiments with cells from separate donors, performed on different days, as indicated. Datasets were analyzed by GraphPad Prism 9.1.2 (GraphPad, La Jolla, CA, USA) using one-way ANOVA and ratio-paired *t*-test to overcome interindividual differences of human donors.

3. Results

3.1. The chalcones MF-14 and MF-15 inhibit 5-LOX product formation

Our previous *in silico* target prediction approach identified human 5-LOX as potential target of a variety of natural chalcones [15]. Here, we assessed the efficiency of the natural chalcone MF-14 and its corresponding dihydrochalcone MF-15 (Fig. 1A) to interfere with the activity of human 5-LOX in cell-free and cell-based assays. While MF-14 was isolated from *Melodorum fruticosum* as previously described [18], to obtain MF-15 in sufficient quantities, a semi-synthetic approach was used. Thus, hydrolysis of phlorizin yielded its aglycone, phloretin (Pt), as previously described [30]. Pt was then protected in positions 2' and 4' using MOMBr as alkylating agent in the presence of a base with an optimized yield of 54% for **compound 1** (Fig. 1B). The two remaining phenol functions of **1** were alkylated with methyl iodide leading to **2** (69%). Removal of the acetal protecting groups yielded **3**, already known as a secondary metabolite isolated from the trunk wood of *Iranthera laevis* Markgr [19]. Monobenzylation of **3** using modified conditions from Urgaonkar et al. [31] allowed the synthesis of MF-15 with 60% yield for this step and an overall yield of 14% (5 steps) from phlorizin.

We studied inhibition of the enzymatic activity of isolated human 5-LOX and 5-LOX product formation in Ca^{2+} -ionophore A23187-activated human neutrophils, which both are well-established and convenient test systems for initial and routine studies of 5-LOX inhibitors, where respective mediators are analyzed by RP-HPLC (UV detection at 235 and 280 nm) [27]. The chalcone MF-14 with an $\text{IC}_{50} = 2.4 \pm 0.3 \mu\text{M}$ was more potent against isolated 5-LOX (Fig. 1C) than in neutrophils ($\text{IC}_{50} = 7.7 \pm 1 \mu\text{M}$; Fig. 1D), while the corresponding dihydrochalcone MF-15 showed similar potency in both experimental settings ($\text{IC}_{50} = 3.5 \pm 0.2 \mu\text{M}$ for isolated 5-LOX; $\text{IC}_{50} = 3.1 \pm 0.3 \mu\text{M}$ in neutrophils; Fig. 1C and D), thus, being somewhat superior over MF-14 in intact cells.

3.2. Modulation of LM profiles by MF-14 and MF-15 in exotoxin-stimulated human MDM

For more comprehensive analysis of the effects of the chalcones on broad and complex LM networks under pathophysiological relevant conditions, we used polarized human MDM with either pro-inflammatory (M1-) or anti-inflammatory (M2-like) phenotype that

were stimulated by bacterial exotoxins for 3 h [8,21,29]. M1-MDM express abundant 5-LOX and 5-LOX-activating protein (FLAP) but hardly 15-LOX-1, whereas M2-MDM express both 5-LOX/FLAP and substantial amounts of 15-LOX-1 [21]. First, we investigated whether the chalcones are cytotoxic, displaying detrimental effects on the viability and integrity of MDM, using MTT assay and LDH release analysis. Neither MF-14 nor MF-15 up to 10 μ M significantly affected cellular viability of MDM in these assays over 24 h (Fig. 2A and B). At higher concentrations, i.e., 30 μ M, both compounds caused detrimental effects on the cell integrity (LDH assay) and a tendency towards loss of cell viability (MTT assay), prompting us to limit the concentrations for further investigations to \leq 10 μ M.

As reported before, upon exposure to bacterial exotoxins, M1-MDM produce mainly pro-inflammatory COX-derived PGs/TX and 5-LOX-derived LTs, while M2-MDM generate substantial amounts of SPM and their 15-LOX-1-derived monohydroxylated precursors [8,21,29]. We studied the LM profiles of M1- and M2-MDM by targeted LM metabolomics using UPLC-MS/MS [8]. M1-MDM produced higher amounts of various COX-derived LM (PGD₂ α , PGE₂, PGF₂ α and TXB₂) as compared to M2-MDM, without strong differences related to 5-LOX product (5-HEPE, 5-HETE, t-LTB₄, LTB₄ and 5S,6R-di-HETE) formation between the two phenotypes (Table 1). In contrast, formation of SPM (PD1, PDX, RvD5 and MaR1) and of other 12/15-LOX products (17-HDHA, 14-HDHA, 15-HEPE, 15-HETE, 12-HEPE, 12-HETE) was much higher in M2-MDM. Preincubation of the MDM with MF-14 and MF-15 at 10 μ M, each, clearly inhibited the biosynthesis of SACM-induced 5-LOX products in both phenotypes (Table 1), where MF-15 appeared to be somewhat more efficient than MF-14, especially for inhibition of LTB₄. Among COX products, TXB₂ formation was reduced by MF-14 but less pronounced by MF-15 in both MDM subtypes, while PGs were hardly affected or rather elevated, in particular in M2-MDM (Table 1). Of interest, both chalcones enhanced the formation of 12/15-LOX products including SPMs, more consistently in M2- versus M1-MDM. Note that among these mono/di-hydroxylated PUFAs, MF-14 and MF-15 failed to elevate 4-HDHA, 7-HDHA and 5,15-diHETE that are not or not exclusively formed by 12/15-LOXs; the amounts of liberated PUFAs were all moderately increased by MF-14 and MF-15 in both MDM phenotypes (Table 1).

Table 2

MF-14 and MF-15 modulate ionophore A23187-induced LM formation in LOX-transfected HEK293 cells. Stably LOX-transfected HEK293 cells (2×10^6 cells in 1 mL PBS containing 1 mM CaCl₂ and 0.1% glucose), were pre-incubated with vehicle (0.1% DMSO), MF-14 or MF-15 (10 μ M, each) for 15 min at 37 °C and then stimulated with 2.5 μ M ionophore A23187 plus 1 μ M AA at 37 °C. Afterwards, the reaction was stopped with ice-cold methanol and formed LMs were extracted by SPE and analyzed by UPLC-MS/MS. Results are given in pg/ 2×10^6 cells as means \pm S.E.M and as -fold change versus ionophore-stimulated vehicle control (ctrl. = 1), n = 3.

	LM	DMSO	MF-14 pg/ 2×10^6 cells	-fold	MF-15 pg/ 2×10^6 cells	-fold	
5-LOX	5-HEPE	119 \pm 15	16 \pm 11	0.1	30 \pm 24	0.2	
	5-HETE	11,913 \pm 5492	712 \pm 59	0.1	754 \pm 72	0.1	
	t-LTB ₄	759 \pm 359	15 \pm 5	0.0	11 \pm 1	0.0	
	LTB ₄	1180 \pm 538	16 \pm 3	0.0	14 \pm 3	0.0	
	17-HDHA	40 \pm 31	49 \pm 24	1.2	92 \pm 75	2.3	
	14-HDHA	13.6 \pm 9.3	14.3 \pm 9.1	1.1	18.9 \pm 13.5	1.4	
	15-HEPE	6.8 \pm 2.3	9.6 \pm 3.7	1.4	9.3 \pm 4.5	1.4	
	15-HETE	434 \pm 54	589 \pm 219	1.4	501 \pm 92	1.2	
	15-LOX-1	5-HEPE	3.4 \pm 0.2	3.8 \pm 0.3	1.1	3.5 \pm 0.4	1.0
		5-HETE	246 \pm 120	202 \pm 67	0.8	273 \pm 102	1.1
t-LTB ₄		4.9 \pm 0.3	6.9 \pm 2.5	1.4	12.2 \pm 3.6	2.5	
LTB ₄		4.8 \pm 1.3	5.5 \pm 1.4	1.2	10.9 \pm 4.0	2.3	
17-HDHA		55 \pm 35	116 \pm 85	2.1	181 \pm 111	3.3	
14-HDHA		16 \pm 9	40 \pm 21	2.5	55 \pm 32	3.4	
15-HEPE		21 \pm 13	34 \pm 24	1.6	54 \pm 33	2.6	
15-HETE		1699 \pm 1356	1539 \pm 1124	0.9	2542 \pm 1911	1.5	
15-LOX-2		5-HEPE	4.8 \pm 1.1	3.4 \pm 0.7	0.7	3.3 \pm 0.5	0.7
		5-HETE	320 \pm 172	136 \pm 35	0.4	167 \pm 29	0.5
	t-LTB ₄	14.2 \pm 7.5	3.9 \pm 1.2	0.3	5.9 \pm 1.7	0.4	
	LTB ₄	10.9 \pm 4.9	2.2 \pm 0.9	0.2	4.5 \pm 2.1	0.4	
	17-HDHA	1473 \pm 377	1708 \pm 377	1.2	1865 \pm 485	1.3	
	14-HDHA	12 \pm 2	13 \pm 2	1.1	15 \pm 2	1.3	
	15-HEPE	646 \pm 137	549 \pm 113	0.9	504 \pm 113	0.8	
	15-HETE	9779 \pm 4302	10,407 \pm 3092	1.1	10,566 \pm 4593	1.1	

Next, the potency of MF-14 and MF-15 was studied in more detail in concentrations-response experiments (0.1 to 10 μ M) using SACM-activated MDM. In M1-MDM, formation of COX products and SPM as well as PUFA release were hardly affected by either chalcone, but again mono/di-hydroxylated 12/15-LOX metabolites were significantly increased, more pronounced by MF-15 versus MF-14, starting at 3 μ M MF-15 (Fig. 2C). 5-LOX products were suppressed only by MF-15 at 10 μ M. A comparable pattern of LM modulation was found in M2-MDM, where mono/di-hydroxylated 12/15-LOX products and SPM were most strikingly elevated with significant effects at 3 and 10 μ M for both chalcones, with some superiority for MF-15 (Fig. 2D). To estimate if the stimulatory effects of chalcones on LOX product formation depends on the type of substrate, we differentially analyzed the modulation of mono/di-hydroxylated products derived from either ω -6-PUFA (AA) or ω -3-PUFA (EPA and DHA). Obviously, those LOX products that require a C15- or C17-lipoxygenation such as 15-HETE and 15-HEPE or 17-HDHA, made from AA and EPA or DHA, respectively, were most prominently affected (Fig. 2C and D). This suggests that the chalcones preferably stimulate C15-lipoxygenation in MDM irrespective of the type of PUFA substrate.

3.3. MF-14 and MF-15 preferably stimulate 15-LOX-1 activity in HEK cells

In humans, two isoforms 15-LOX-1 and 15-LOX-2 exist that not only differ in the cell type-dependent expression but also in the regioselectivity of PUFA oxygenation: while 15-LOX-2 (equally present at low amounts in human M1- and M2-MDM [29]; Fig. 5B) selectively catalyzes oxygenation of C15 in AA and EPA and C17 in DHA, 15-LOX-1 (abundant in human M2-MDM) also oxygenates C12 in AA and EPA and C14 in DHA, although to a minor degree versus C15 and C17 [32]. To further dissect if and which 15-LOX isoform confers the stimulatory effects of the chalcones, we took advantage of HEK293 cells stably transfected with either human 15-LOX-1 or 15-LOX-2; cells expressing human 5-LOX were studied as additional control. Preincubation of HEK293 cells with chalcones and subsequent stimulation with 2.5 μ M ionophore A23187 plus 1 μ M AA, according to previous studies [10,23], showed that both chalcones (10 μ M), again preferably MF-15, strongly elevated

Table 3

MF-14 and MF-15 induce LM formation in M1- and M2-MDM. M1- and M2-MDM (2×10^6 cells in 1 mL PBS containing 1 mM CaCl₂) were incubated with vehicle (0.1 % DMSO) or with MF-14 or MF-15 (10 μM) for 180 min at 37 °C. Formed LM in the supernatants were analyzed by UPLC-MS/MS. Results are given in pg/ 2×10^6 cells as means \pm S.E.M and as -fold change versus unstimulated vehicle control (ctrl. = 1), n = 5.

0	1	60	M1 MDM						M2 MDM					
			DMSO	MF-14	-fold	DMSO	MF-15	-fold	DMSO	MF-14	-fold	DMSO	MF-15	-fold
5-LOX	5-HEPE	8.1 \pm 1.3	19.4 \pm 2.3	2.4	5.3 \pm 0.5	15.1 \pm 2.8	2.8	5.4 \pm 0.9	23.1 \pm 3.2	4.2	8.3 \pm 3.3	22.4 \pm 3.9	2.7	
	5-HETE	61.7 \pm 23.3	122 \pm 37	2.0	35.1 \pm 9.5	120 \pm 32	3.4	25.3 \pm 5.8	140 \pm 36	5.5	36.7 \pm 12.7	189 \pm 53	5.1	
	1-LTB ₄	17.1 \pm 6.9	14.9 \pm 5.8	0.9	6.8 \pm 2.2	9.9 \pm 1.1	1.4	6.4 \pm 3.7	13.0 \pm 3.3	2.0	5.8 \pm 3.0	20.7 \pm 7.7	3.5	
	LTB ₄	11.5 \pm 4.2	24.5 \pm 6.7	2.1	4.6 \pm 1.1	11.1 \pm 3.6	2.4	5.6 \pm 2.1	13.8 \pm 3.8	2.5	4.8 \pm 1.8	25.5 \pm 10.9	5.3	
	5S,6R-dihETE	1.8 \pm 0.3	3.9 \pm 1.1	2.2	1.3 \pm 0.4	3.3 \pm 0.2	2.5	0.5 \pm 0.3	2.1 \pm 0.5	3.8	0.6 \pm 0.2	3.1 \pm 1.5	5.0	
	PGE ₂	1505 \pm 610	752 \pm 202	0.5	546 \pm 168	561 \pm 212	1.0	34.9 \pm 7.2	60 \pm 16	1.7	36.9 \pm 6.4	72 \pm 12	1.9	
COX	PGD ₂	23.8 \pm 8.6	25.6 \pm 8.1	1.1	11.3 \pm 2.7	16.8 \pm 6.0	1.5	6.8 \pm 1.6	9.7 \pm 1.6	1.4	9.8 \pm 1.6	13 \pm 0	1.3	
	PGF _{2α}	560 \pm 239	349 \pm 176	0.6	205 \pm 50	158 \pm 52	0.8	19.0 \pm 3.1	21.4 \pm 6.3	1.1	20.4 \pm 4.7	38 \pm 16	1.9	
	TXB ₂	6731 \pm 1720	3789 \pm 808	0.6	3168 \pm 617	2354 \pm 703	0.7	378 \pm 82	304 \pm 71	0.8	533 \pm 129	1166 \pm 693	2.2	
	17-HDHA	76.1 \pm 20.8	581 \pm 420	7.6	37.9 \pm 5.5	195 \pm 73	5.1	33.7 \pm 8.0	967 \pm 455	28.7	46.0 \pm 10.2	696 \pm 195	15.1	
14-HDHA	41.6 \pm 13.7	159.1 \pm 73.5	3.8	6.3 \pm 0.7	37.5 \pm 9.8	5.9	9.4 \pm 1.5	329 \pm 157	34.8	14.4 \pm 3.5	244 \pm 86	17.0		
12/15-LOX	7-HDHA	18.0 \pm 3.5	15.9 \pm 3.0	0.9	10.5 \pm 1.8	14.7 \pm 2.5	1.4	12.0 \pm 4.1	55.1 \pm 23.7	4.6	9.8 \pm 2.6	38.4 \pm 8.3	3.9	
	4-HDHA	13.7 \pm 3.4	31.9 \pm 4.5	2.3	9.0 \pm 1.6	27.1 \pm 8.0	3.0	10.6 \pm 2.3	47.7 \pm 10.0	4.5	15.0 \pm 4.6	60.8 \pm 10.9	4.1	
	15-HEPE	13.7 \pm 3.1	59.2 \pm 38.6	4.3	5.9 \pm 0.9	19.3 \pm 4.6	3.3	6.2 \pm 0.8	123 \pm 55	19.9	7.6 \pm 1.7	74.0 \pm 19.7	9.7	
	12-HEPE	8.9 \pm 4.0	33.4 \pm 6.4	3.8	3.4 \pm 0.4	16.6 \pm 3.9	4.8	3.6 \pm 0.8	63.7 \pm 28.2	17.6	5.0 \pm 1.4	107 \pm 63	21.4	
	15-HETE	94.8 \pm 31.2	1167 \pm 907	12.3	51.5 \pm 12.6	385 \pm 152	7.5	20.9 \pm 2.9	1934 \pm 906	36.6	35.7 \pm 13.9	1467 \pm 486	41.1	
	12-HETE	241 \pm 212	557 \pm 263	2.3	27 \pm 4	194 \pm 66	7.3	19.9 \pm 2.6	713 \pm 374	35.8	28.5 \pm 11.0	1783 \pm 903	36.6	
5,15-dihETE	38.6 \pm 12.6	11.7 \pm 1.8	0.3	12.5 \pm 4.1	10.4 \pm 1.6	0.8	10.1 \pm 4.4	47.1 \pm 30.5	4.6	6.0 \pm 2.3	25.1 \pm 12.9	4.2		
SPMs	PD1	0.8 \pm 0.3	1.3 \pm 0.3	1.5	1.0 \pm 0.2	0.9 \pm 0.2	1.0	0.9 \pm 0.1	2.3 \pm 0.7	2.6	0.8 \pm 0.1	1.4 \pm 0.3	1.8	
	PDX	2.1 \pm 0.4	4.1 \pm 0.8	1.9	1.9 \pm 0.1	2.6 \pm 0.3	1.4	2.2 \pm 0.4	4.3 \pm 1.0	2.0	2.3 \pm 0.4	4.6 \pm 1.1	2.0	
	PMO5	2.0 \pm 0.8	2.1 \pm 0.7	1.0	1.4 \pm 0.5	1.5 \pm 0.3	1.1	1.8 \pm 0.9	35.8 \pm 21.0	19.9	1.9 \pm 0.5	15.6 \pm 8.9	8.2	
	MaR1	2.9 \pm 2.2	1.7 \pm 1.1	0.6	3.1 \pm 1.8	1.7 \pm 1.4	0.6	2.2 \pm 1.7	8.7 \pm 5.4	3.9	2.2 \pm 1.8	3.6 \pm 2.2	1.7	
	AA	36894 \pm 17530	362368 \pm 295912	9.8	24292 \pm 12653	254992 \pm 205073	10.5	22004 \pm 7943	284347 \pm 174831	12.9	29361 \pm 8529	310294 \pm 192949	10.6	
PUFA	EPA	6181 \pm 3342	113524 \pm 99337	18.4	3827 \pm 1789	43073 \pm 32916	11.3	2577 \pm 751	55025 \pm 31217	21.4	4518 \pm 1624	62506 \pm 34402	13.8	
	DHA	28662 \pm 8325	81260 \pm 37528	2.8	14467 \pm 2608	51858 \pm 23877	3.6	16391 \pm 2923	93140 \pm 22434	5.7	25228 \pm 5947	102093 \pm 25346	4.0	

product formation (15-HETE, 15-HEPE, 17-HDHA and 14-HDHA) in cells expressing 15-LOX-1 but not so in cells expressing the 15-LOX-2 isoform (Table 2, Fig. 2E). In HEK293 cells expressing 5-LOX, strong suppression of 5-LOX products was obvious by MF-14 and MF-15 without significant elevation of 12/15-LOX products (Table 2, Fig. 2E), as expected. Conclusively, MF-14 and MF-15 inhibit 5-LOX product formation in PMNL and MDM but increase 12/15-LOX products and SPM formation in MDM.

3.4. MF-14 and MF-15 elicit formation of 12/15-LOX products and SPMs by stimulating 15-LOX-1

To gain further insights in whether MF-14 and MF-15 could induce 15-LOX-1 activation and thus elicit SPM formation in MDM without the need of an additional stimulus (such as SACM or ionophore), we simply exposed M1- and M2-MDM to the chalcones for 3 h and analyzed the LM formed by UPLC-MS/MS. In both MDM phenotypes, the chalcones induced LOX product formation versus vehicle control with similar effectiveness for MF-14 and MF-15 and without affecting COX products (Table 3, Fig. 3A and B). Along these lines, the chalcones strongly elevated the liberation of PUFAs, a general prerequisite for enabling LM biosynthesis in intact cells. The stimulatory effects of the chalcones were most prominent for 12/15-LOX products in M2-MDM, especially for 15-HETE and 12-HETE with up to 68- and 74-fold increases, respectively, and also SPM were elevated up to 19-fold (Table 3, Fig. 3A and B). Note that also 5-LOX products were elevated by the chalcones but to a lower degree (max. up to 6-fold). The magnitude of 12/15-LOX product formation induced by the chalcones in M2-MDM is approx. 30–44% of that obtained with SACM, while 5-LOX products are only 2–5% (compare absolute quantities shown in Table 3 with those in Table 1). Concentration-response studies showed that in M2-MDM significant induction of 12/15-LOX products was achieved also at 3 μM of either MF-14 or MF-15, whereas 5-LOX product formation was unaffected at this concentration (Fig. 3A and B). As observed for SACM-stimulated MDM, the chalcones consistently stimulated lipoxygenation irrespective of the type of substrate (ω 3- or ω 6-PUFA).

Activation of 15-LOX-1 and of 5-LOX and respective product formation in stimulated M2 macrophages is associated with subcellular redistribution of the enzymes from a soluble to a membranous

compartment, where enzymatic transformation of the liberated PUFAs takes place [21,29]. Therefore, we studied the subcellular localization of 15-LOX-1, and for comparison of 5-LOX, in M2-MDM and how this is affected by the chalcones in a temporal manner (15, 30, 180 min) using immunofluorescence microscopy; SACM was used a positive control [29]. In resting vehicle-treated cells, 5-LOX and 15-LOX-1 were diffusely distributed within the nucleus and cytosol, respectively, while addition of SACM caused 5-LOX enrichment at the nuclear envelope and 15-LOX-1 accumulation at yet undefined particulate structures after 30 min, as observed before [21,29]. The same 5-LOX and 15-LOX-1 subcellular redistribution pattern as for SACM was evident also for MF-14 and MF-15 (10 μM) with even more rapid induction by MF-15 starting already at 15 min (Fig. 3C).

To exclude that simply the elevation of PUFA liberation accounts for elevated LOX product formation, we supplemented M2-MDM with substantial amounts of exogenous DHA, EPA and AA (1 μM, each) to circumvent the requirement of endogenous substrate supply. As shown in Table 4, formation of 12/15-LOX products including SPM in response to MF-14 and MF-15 was still markedly elevated, up to 56-fold for 15-HETE, with a similar pattern for the overall LM profile as in the absence of exogenous substrate (Table 3). Finally, we studied if human LOXs in transfected HEK293 cells could be activated by the chalcones without additional stimulus but in the presence of DHA, EPA and AA (1 μM, each). Again, MF-14 and even more efficiently MF-15 enhanced the formation of typical 12/15-LOX products in HEK293 cells expressing 15-LOX-1 but hardly in cells expressing the 15-LOX-2 isoform and less efficiently also in 5-LOX-transfected cells (Fig. 4). Together, MF-14 and MF-15 are able to substantially elicit 12/15-LOX products including SPM in intact cells by two mechanisms: (i) induction of endogenous PUFA substrate release and (ii) selective and strong stimulation of the 15-LOX-1 isoform.

3.5. MF-14 and MF-15 do not affect MDM polarization and LM-biosynthetic enzyme expression

In addition to these short-term effects of the chalcones observed within approx. 3 h, we explored if MF-14 and MF-15 could also affect the polarization of MDM towards the M1 and M2 phenotype as well as expression of LM-biosynthetic key enzymes during 48 h of MDM

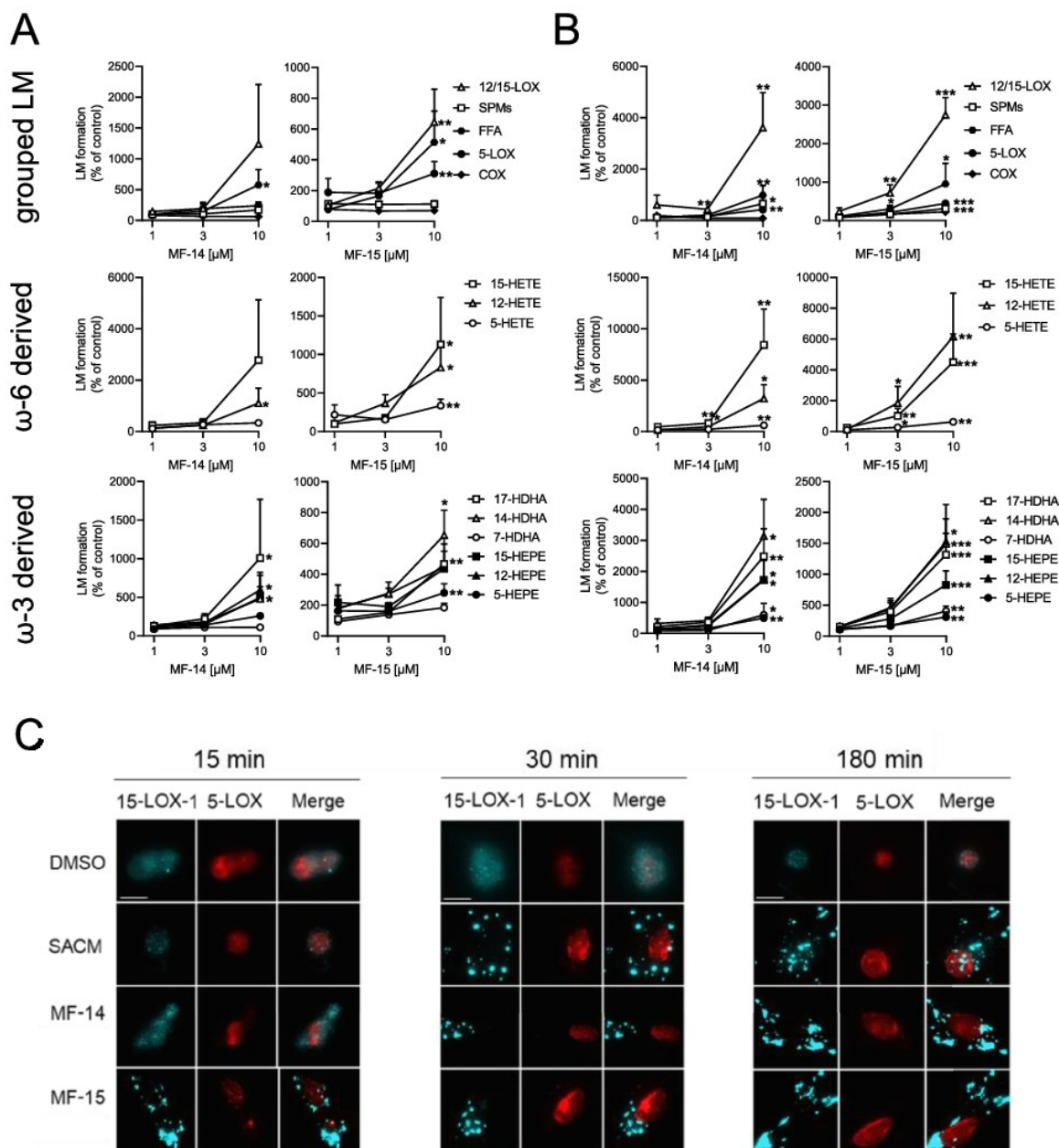


Fig. 3. MF-14 and MF-15 induce SPM biosynthesis and activate 15-LOX-1 in MDM. (A) M1-MDM and (B) M2-MDM (2×10^6 , each) were diluted in PBS containing 1 mM CaCl_2 , incubated with vehicle (0.1% DMSO), MF-14 or MF-15 (10 μM , each) for 180 min at 37 °C. Then, formed LM were extracted from the supernatants by SPE and analyzed by UPLC-MS/MS. Results are given as mean \pm S.E.M., presented as percentage of vehicle-treated control (=100%, $n = 5$). Upper panels: grouped LM produced by 12/15-LOX, SPM, PUFA, 5-LOX and COX (according to Table1); middle panels: sum of ω -6-derived LM as indicated; lower panels: sum of ω -3-derived LM as indicated. Statistical analysis was performed via ratio-paired *t*-test, * $p < 0.05$, ** $p < 0.01$, *** $p < 0.001$, **** $p < 0.0001$. (C) M2-MDM (10^6 cells in PBS plus 1 mM CaCl_2 and 5 mM MgCl_2) were incubated with MF-14 or MF-15 (10 μM , each), SACM (1%) or vehicle (0.1% DMSO) for 180 min. Then, the cells were fixed, permeabilized, and incubated with antibodies against 5-LOX (red) and 15-LOX-1 (cyan blue). Immunofluorescence detection was determined via Zeiss Axiolab microscope; scale bars = 10 μm . Results shown for one single cell are representative for approximately 100 individual cells analyzed in $n = 3$ independent experiments with separate donors, each.

polarization where the cells acquire these proteins in a phenotype-specific manner, i.e., COX-2 for M1- and 15-LOX-1 for M2-MDM. Flow cytometry analysis of CD54 and CD80 (markers for M1) as well as CD163 and CD206 (markers for M2) revealed no significant changes upon treatment of unpolarized MDM for 48 h in the presence of 10 μM MF-15, but interestingly, treatment with 10 μM MF-14 strongly reduced

the expression of the M2 marker CD206, without any effects on CD54, CD80 or CD163 (Fig. 5A). Western blot analysis of COX-2, 5-LOX and 15-LOX-1 protein levels showed no significant modulation of their expression by the chalcones at 10 μM during polarization to M1- or M2-MDM (Fig. 5B). These data indicate the chalcones MF-14 and MF-15 affect LM networks in polarized macrophages at the level of enzymatic

Table 4

MF-14 and MF-15 induce LM formation in M1- and M2-MDM in the presence of exogenous PUFA. M1- and M2-MDM (2×10^6 cells in 1 mL PBS containing 1 mM CaCl_2) were incubated with vehicle (0.1 % DMSO) or with MF-14 or MF-15 (10 μM); all samples received AA, EPA and DHA (1 μM , each). After 180 min at 37 °C, formed LM in the supernatants were analyzed by UPLC-MS/MS. Results are given in $\text{pg}/2 \times 10^6$ cells as means \pm S.E.M and as -fold change versus unstimulated vehicle control (ctrl. = 1) that received only the PUFAs, n = 3.

		M2-MDM							
		DMSO		MF-14		-fold	MF-15		-fold
5-LOX	5-HEPE	345	\pm 190	1245	\pm 74	3.6	1025	\pm 77	3.0
	5-HETE	122	\pm 59	664	\pm 97	5.5	782	\pm 84	6.4
	t-LTB ₄	4.6	\pm 1.2	13.5	\pm 4.6	3.0	21.9	\pm 7.0	4.8
	LTB ₄	1.7	\pm 0.3	26.2	\pm 8.5	15.9	31.2	\pm 10.7	18.9
	5S,6R-diHETE	1.9	\pm 1.0	5.8	\pm 1.7	3.0	8.3	\pm 2.7	4.3
COX	PGE ₂	90	\pm 10	92	\pm 18	1.0	110	\pm 18	1.2
	PGD ₂	72	\pm 23	72	\pm 19	1.0	86	\pm 16	1.2
	PGF _{2α}	41	\pm 11	48	\pm 13	1.2	58	\pm 17	1.4
	TXB ₂	315	\pm 65	169	\pm 27	0.5	240	\pm 44	0.8
12/15-LOX	17-HDHA	222	\pm 74	2784	\pm 111	12.5	2213	\pm 62	10.0
	14-HDHA	40	\pm 15	361	\pm 55	9.1	316	\pm 69	7.9
	7-HDHA	100	\pm 29	332	\pm 36	3.3	302	\pm 25	3.0
	4-HDHA	172	\pm 65	688	\pm 106	4.0	689	\pm 85	4.0
	15-HEPE	77.2	\pm 33.4	3043	\pm 507	39.4	2630	\pm 226	34.1
	12-HEPE	48.0	\pm 27.4	748	\pm 71	15.6	800	\pm 113	16.7
	15-HETE	80.4	\pm 33.2	4493	\pm 324	55.9	4353	\pm 505	54.1
	12-HETE	33.7	\pm 10.5	391	\pm 24	11.6	475	\pm 75	14.1
	5,15-diHETE	168	\pm 37	92	\pm 17	0.5	83	\pm 4	0.5
	SPMs	PD1	7.7	\pm 1.0	12.2	\pm 2.2	1.6	17.6	\pm 1.0
	PDX	7.8	\pm 1.0	35.3	\pm 1.9	4.5	33.5	\pm 1.5	4.3
	RvD5	3.7	\pm 1.0	41.3	\pm 11.0	11.1	49.1	\pm 8.7	13.3
	MaR1	0.7	\pm 0.1	6.6	\pm 1.1	9.1	7.1	\pm 0.3	9.8
PUFA	AA	283,014	\pm 75,653	1,260,910	\pm 140,332	4.5	1,183,611	\pm 41,237	4.2
	EPA	322,106	\pm 54,447	750,468	\pm 72,546	2.3	681,909	\pm 8675	2.1
	DHA	143,001	\pm 40,219	471,581	\pm 39,321	3.3	434,404	\pm 8555	3.0

biosynthesis of the LM but not primarily by modulation of MDM polarization or of LM-biosynthetic enzyme expression.

4. Discussion

Here we showed that the natural chalcone MF-14 and its corresponding dihydrochalcone MF-15 from *Melodorum fruticosum* leaves [18], suppress pro-inflammatory LT formation by inhibiting 5-LOX but elevate the generation of inflammation-resolving SPMs by stimulating cellular 15-LOX-1. Of note these SPM/15-LOX-1-stimulatory effects were evident not only in exotoxin-activated MDM but also when resting MDM, especially M2-MDM, were exposed to the chalcones. Both chalcones caused liberation of free PUFAs as LM substrates and induced 15-LOX-1 subcellular redistribution in M2-MDM, which are major prerequisites for LM formation in intact cells [21,29,32]. Inhibition of 5-LOX and stimulation of 15-LOX-1 in intact cells, with minor effects on the 15-LOX-2 isoform, was confirmed in activated as well as in resting HEK293 cells transfected with the respective LOX. Together, these chalcones are effective inhibitors of 5-LOX but also act as agonists for macrophages and non-immunocompetent (HEK293) cells to stimulate 15-LOX-1 activity which culminates in elevated SPM levels. Small molecules with such LM-modulatory ability, shifting the biosynthesis from pro-inflammatory to pro-resolving LM, are of great interest for innovative inflammation pharmacotherapy [6,9,33].

The major drugs applied for the clinical treatment of inflammatory diseases are glucocorticoids and NSAIDs that both push back inflammation by suppressing the biosynthesis of pro-inflammatory mediators such as cytokines, chemokines, and PGs [7,34,35]. But these mediators are crucial regulators of the normal immune response and/or play important roles in the homeostasis of the body, explaining why their suppression by drugs is afflicted with severe on-target side effects [7,36]. Moreover, the unwanted actions of NSAIDs are also due to substrate shunting to other LM routes, resulting in elevated LT levels due to redirection of AA for conversion by 5-LOX [8,37,38]. The discovery of the superfamily of SPM as LM that terminate inflammation and stimulate its resolution, along with tissue repair and regeneration without

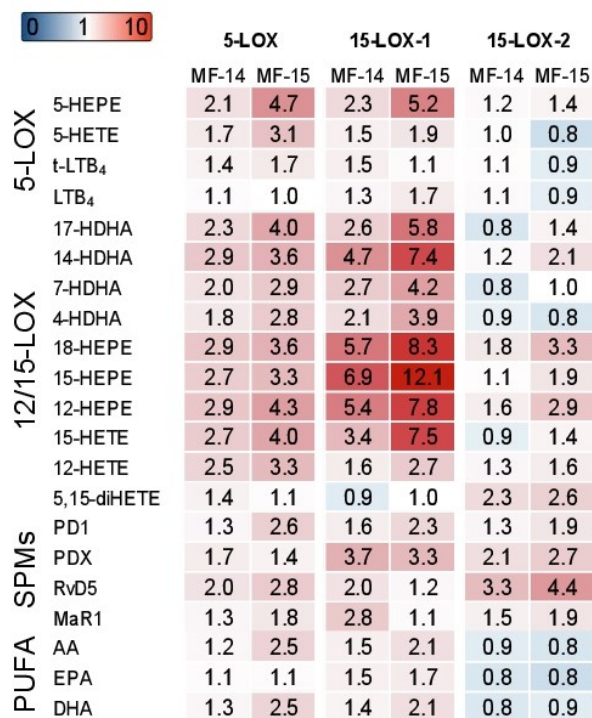


Fig. 4. MF-14 and MF-15 induce 15-LOX-1-related LM formation in HEK293 cells. HEK293 cells (2×10^6 cells in 1 mL PBS containing 1 mM CaCl_2 plus 0.1% glucose) were incubated with AA, EPA, and DHA (1 μM , each) plus vehicle (0.1 % DMSO) or MF-14 or MF-15 (10 μM , each) for 180 min at 37 °C. Then, formed LMs were extracted by SPE and analyzed by UPLC-MS/MS. Results (mean of n = 3 experiments) are given as -fold increase versus vehicle-treated control cells (=100%) in a heatmap.

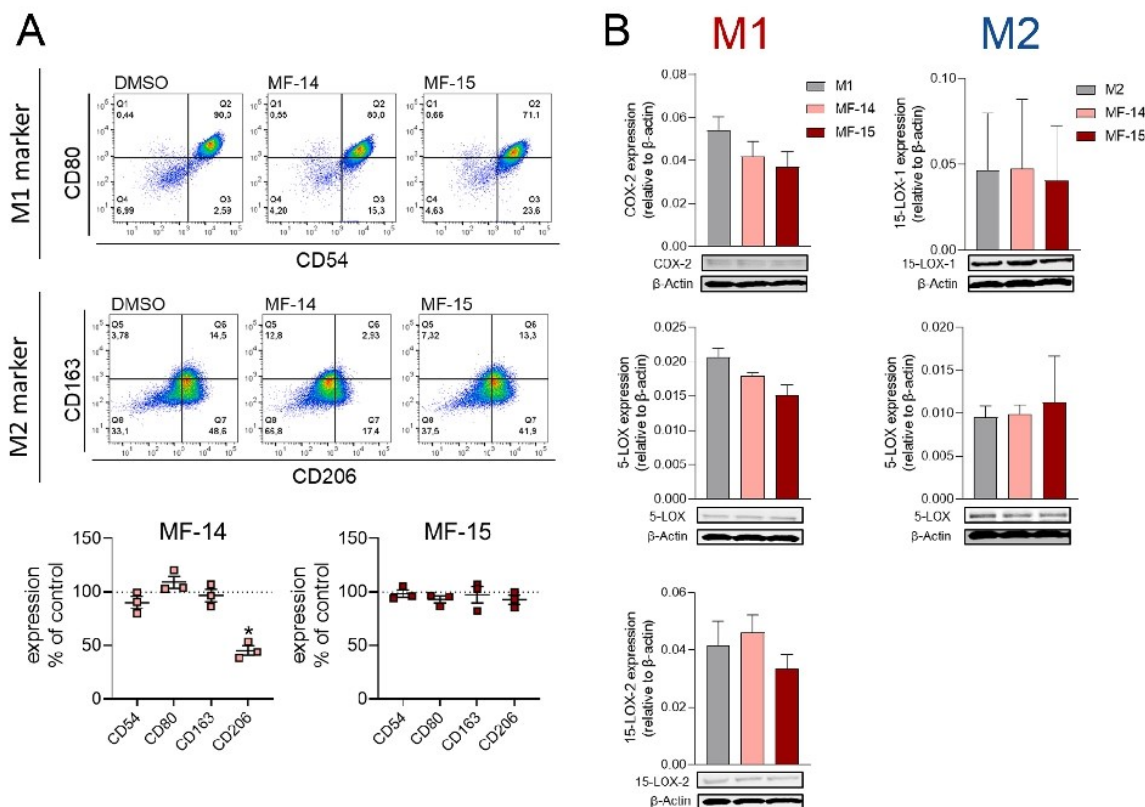


Fig. 5. Effects of MF-14 and MF-15 on macrophage surface markers and the protein level of LM-biosynthetic enzymes during MDM polarization. (A) Unpolarized MDM were treated with MF-14 or MF-15 (3 μ M, each) or 0.1% DMSO as vehicle. After 48 h, expression of the surface markers CD54 and CD80 (M1-like) as well as CD163 and CD206 (M2-like) among living CD14⁺ cells was analyzed by flow cytometry. Upper panel: shown are representative pseudocolor dot plots of the surface markers. Mean fluorescence intensity (MFI) of each marker was determined. Lower panel: the change of the MFI from MF-14- and MF-15-treated MDM against the MFI of DMSO-treated cells (control) was calculated and is given in % of control in scatter dot plots as single values and means \pm S.E.M., $n = 3$. Statistics are calculated with raw data (MFI), * $p < 0.05$ MF-14 vs. control group, ratio paired t -test. (B) Unpolarized MDM were incubated with MF-14 or MF-15 (10 μ M, each) for 48 h during the polarization process to M1- or M2-MDM. Cell lysates were prepared and immunoblotted for expression of 5-LOX, 15-LOX-2 and COX-2 in M1-MDM and of 5-LOX and 15-LOX-1 in M2-MDM, followed by densitometric analysis against β -actin (for normalization). Data are shown as mean \pm S.E.M., $n = 3-5$. Statistical analysis was performed via ratio-paired t -test.

being immunosuppressive, have prompted a paradigm shift in the view of inflammation pharmacotherapy [9,39]. There is accumulating evidence that many inflammation-related diseases might be connected to low SPM levels while elevating SPM in tissues, for example by exogenous application of SPM or supplementation of DHA and EPA, limits inflammation without immunosuppression and typical side effects of classical anti-inflammatory drugs [33,40]. In this respect, the chalcones MF-14 and MF-15 are able to elevate SPM levels as well as their precursors in human macrophages and could be of interest as potential candidates for further development as novel agents that promote the resolution of persistent and excessive inflammation.

Chalcones are polyphenolic compounds of the flavonoid family displaying antioxidant, oxygen scavenging, anti-inflammatory and anti-cancer activities [13,41,42]. Various natural and synthetic chalcones have been reported to reduce LT or PGE₂ levels [13], and their ability to inhibit 5-LOX activity was demonstrated for various structural derivatives using experimental models [14,43–47] supported also by *in silico* approaches [48,49]. However, stimulatory effects on SPM formation or on 12/15-LOX product formation have not been shown yet to the best of our knowledge, rather, inhibition of 15-LOX was reported for some hydroxychalcone-triazole hybrids [50]. Our previous unbiased *in silico* target prediction approach identified human 5-LOX as potential target of natural chalcones, where we confirmed 5-LOX inhibition for phloretin and 3-OH-phloretin [15]. In the present study, we investigated

MF-14 and MF-15 that are 2-OH-benzylated derivatives derived from cardamomin, which were identified as inhibitors of the androgen-synthesizing enzyme AKR1C3 [18]. Interestingly, in line with the inhibition of AKR1C3 [18], the dihydrochalcone MF-15 was consistently somewhat more effective versus the corresponding chalcone MF-14 for modulation of cellular LM biosynthesis. Both compounds inhibited the activity of isolated human recombinant 5-LOX in a cell-free assay in the one-digit micromolar range with comparable potency in A23187-activated human neutrophils that are known to substantially generate 5-LOX products including LTs under inflammatory conditions [51]. Inhibition of 5-LOX and suppression of LT formation by the chalcones was also evident in exotoxin-stimulated human MDM with either M1 or M2 phenotype, which are considered as adequate, biological relevant *in vitro* test systems for LM modulators [8]. The potency of the chalcones to inhibit 5-LOX activity in MDM was less pronounced as compared to PMNL and HEK293 cells, which might be due to potential differences in 5-LOX activation in the two cell types (e.g., Ca²⁺ and phosphorylation) under the distinct experimental conditions (e.g., different stimuli and incubation periods), as observed for other 5-LOX inhibitors before [24,52]. Moreover, when resting MDM were exposed to chalcones, 5-LOX product formation was even modestly induced rather than inhibited, possibly due to the accompanied elevated levels of free AA; an effect that is potentially caused by cPLA₂ activation when 5-LOX is non-activated and has a low catalytic turnover. Along these lines, the

chalcones did not reduce the stimulus-induced release of AA or other PUFAs, excluding diminished substrate supply as reason for suppressed LT formation. In a definite experimental cell-based system, that is, A23187-activated HEK293 cells transfected with human recombinant 5-LOX [23], the chalcones were unequivocally identified as efficient 5-LOX inhibitors, regardless of the absence or presence of exogenous AA as substrate. Note that the inhibition of 5-LOX by the chalcones did not redirect AA to the COX pathway. Hence, the elevation of 12/15-LOX products by the chalcones is unlikely due to the well-known substrate shunting of 5-LOX inhibitors [52]. This is further supported by results with MF-15-treated M2-MDM that had been supplemented with exogenous PUFA, where the dihydrochalcone still enhanced SPM and 12/15-LOX product formation, despite ample supply of substrate.

It is intriguing that MF-14 and MF-15 failed to inhibit other LOXs but instead increased or even induced the activities of endogenous 15-LOX-1 in M2-MDM and of human recombinant 15-LOX-1 in HEK293 cells. Many other phenolic compounds that inhibit 5-LOX such as NDGA also interfere with 12/15-LOXs [10,53,54]. But some small molecule 5-LOX inhibitors including benzenesulfonamide-derivatives [55], ginkgolic acid [56], 3-O-acetyl-11-keto boswellic acid (AKBA) [10], the biflavonoid 8-methylsotrocin-4'-ol [57] and celastrol [11] were shown to enhance or to trigger the formation of 12-/15-LOX products including SPM in human neutrophils or macrophages or in inflamed murine peritoneal exudates. Among those compounds, only celastrol was found to induce 12/15-LOX product formation, albeit only up to approx. 5- or 2-fold in M2-MDM in absence or presence of exogenous PUFA, respectively [11], while the chalcones caused 70- or 50-fold elevations in this respect. Thus, the chalcones are considered effective activators of 15-LOX-1. Pronounced activation of 15-LOX-1 in M2-MDM without marked stimulation of 5-LOX and COX enzymes was observed also for the *S. aureus*-derived exotoxin α -hemolysin that mediates 15-LOX activation via its surface receptor ADAM10 [29]. In contrast to exotoxins [29], the ADAM10 inhibitor GL254023X (40 μ M) did not affect MF-15-induced LM formation (data not shown), excluding the involvement of ADAM10, as expected. Our experiments with HEK293 cells showed that 15-LOX-2 was less efficiently stimulated by MF-14 and MF-15, suggesting a certain degree of preference for the 15-LOX-1 isoform. Human M2-MDM strongly express 15-LOX-1 but hardly 15-LOX-2 [29], and 15-LOX-1 translocates to membranous structures in M2-MDM upon challenge with MF-14/MF-15, in analogy to treatment with α -hemolysin [29] or celastrol [11]. In fact, 12/15-LOX product formation in M1-MDM that express only the 15-LOX-2 but not the 15-LOX-1 isoform, was only moderately increased by MF-14 and MF-15. It should be noted that only the 15-LOX-1 isoform catalyzes oxygenation of AA and EPA at C12 or DHA at C14 position [32,58], yielding 12-HETE and 12-HEPE or 14-HDHA, respectively, which were strongly elevated by the chalcones. Finally, prolonged exposure of MDM to the chalcones at concentrations that activated 15-LOX-1 (i.e., 3 to 10 μ M) for 24 or 48 h did neither affect cell viability nor MDM polarization and phenotype-selective expression of the LM-biosynthetic enzymes 5-LOX, 15-LOX-1 or COX-2, respectively.

In conclusion, the natural chalcones MF-14 and MF-15 efficiently stimulate 15-LOX-1 activity in M2-MDM and HEK293 cells for substantial LM formation. In biologically relevant cellular settings using human M2-MDM, the chalcones caused a favorable LM class shift related to inflammation: impaired formation of LT but elevated levels of SPM, which may reduce pro-inflammatory reactions but may govern resolution of inflammation and tissue regeneration. More comprehensive investigations in experimental and disease-relevant animal models may reveal the pharmacological potential of these compounds for anti-inflammatory pharmacotherapy.

Declaration of Competing Interest

The authors declare that they have no known competing financial interests or personal relationships that could have appeared to influence

the work reported in this paper.

Acknowledgments

This work was supported by the Deutsche Forschungsgemeinschaft (DFG), Collaborative Research Center SFB 1278 "PolyTarget", projects A04, C01, C05 and Z01. The SEM facilities of the Jena Center for Soft Matter (JCSM) were also established with a grant from the German Science Foundation. V.T. is funded by the FWF Hertha Firnberg project T942. A.C.P. is funded by the RFI Objectif Végétal (Région Pays de la Loire) and FEDER. H.S. was funded by GECT Euregio Tirolo-Südtirol-Trentino (IPN55). Apple tree leaves were provided to SONAS thanks to a collaboration with INRAE Angers (Marie-Noëlle BRISSET, Matthieu GAUCHER and Laurence Feugy).

References

- [1] C.N. Serhan, J. Savill, Resolution of inflammation: The beginning programs the end, *Nat. Immunol.* 6 (12) (2005) 1191–1197, <https://doi.org/10.1038/ni1276>.
- [2] C.D. Funk, Prostaglandins and leukotrienes: Advances in eicosanoid biology, *Science*. 294 (5548) (2001) 1871–1875, <https://doi.org/10.1126/science.294.5548.1871>.
- [3] R.A. Whittington, E. Planel, N. Terrando, Impaired resolution of inflammation in Alzheimer's disease: A review, *Front. Immunol.* 8 (2017), <https://doi.org/10.3389/fimmu.2017.01464>.
- [4] R. Medzhitov, Inflammation New Adventures of an Old Flame, *Cell*. 140 (2010) 771–776, <https://doi.org/10.1016/j.cell.2010.03.006>.
- [5] Christopher D. Buckley, Derek W. Gilroy, Charles N. Serhan, Proresolving lipid mediators and mechanisms in the resolution of acute inflammation, *Immunity*. 40 (3) (2014) 315–327, <https://doi.org/10.1016/j.immuni.2014.02.009>.
- [6] Charles N. Serhan, Pro-resolving lipid mediators are leads for resolution physiology, *Nature*. 510 (7503) (2014) 92–101, <https://doi.org/10.1038/nature13479>.
- [7] K.D. Rainsford, Anti-inflammatory drugs in the 21st century, *Sub-Cell. Biochem.* 42 (2007) 3–27, https://doi.org/10.1007/1-4020-5688-5_1.
- [8] Markus Werner, Paul M. Jordan, Erik Romp, Anna Czapka, Zhigang Rao, Christian Kretzer, Andreas Koeberle, Ulrike Garscha, Simona Pace, Hans-Erik Claesson, Charles N. Serhan, Oliver Werz, Jana Gerstmeier, Targeting biosynthetic networks of the proinflammatory and proresolving lipid metabolome, *FASEB J* 33 (5) (2019) 6140–6153, <https://doi.org/10.1096/fsb2.v33.5.10.1096/fj.201802509R>.
- [9] C.N. Serhan, B.D. Levy, Resolvins in inflammation: Emergence of the pro-resolving superfamily of mediators, *J. Clin. Invest.* 128 (2018) 2657–2669, <https://doi.org/10.1172/JCI97943>.
- [10] Nathaniel C. Gilbert, Jana Gerstmeier, Erin E. Schexnaydre, Friedemann Böner, Ulrike Garscha, David B. Neau, Oliver Werz, Marcia E. Newcomer, Structural and mechanistic insights into 5-lipoxygenase inhibition by natural products, *Nat. Chem. Biol.* 16 (7) (2020) 783–790, <https://doi.org/10.1038/s41589-020-0544-7>.
- [11] Simona Pace, Kehong Zhang, Paul M. Jordan, Rossella Bilancia, Wenfei Wang, Friedemann Böner, Robert K. Hofstetter, Marianna Potenza, Christian Kretzer, Jana Gerstmeier, Dagnar Fischer, Stefan Lorkowski, Nathaniel C. Gilbert, Marcia E. Newcomer, Antonietta Rossi, Xinchun Chen, Oliver Werz, Anti-inflammatory celastrol promotes a switch from leukotriene biosynthesis to formation of specialized pro-resolving lipid mediators, *Pharmacol. Res.* 167 (2021) 105556, <https://doi.org/10.1016/j.phrs.2021.105556>.
- [12] Giulia Di Carlo, Nicola Mascolo, Angelo A. Izzo, Francesco Capasso, Flavonoids: Old and new aspects of a class of natural therapeutic drugs, *Life Sci.* 65 (4) (1999) 337–353, [https://doi.org/10.1016/S0024-3205\(99\)00120-4](https://doi.org/10.1016/S0024-3205(99)00120-4).
- [13] Debarshi Kar Mahapatra, Sanjay Kumar Bharti, Vivek Asati, Chalcone Derivatives: Anti-inflammatory Potential and Molecular Targets Perspectives, *Curr Top Med Chem.* 17 (28) (2017) 3146–3169, <https://doi.org/10.2174/1568026617666170914160446>.
- [14] Felipe Herencia, M.Luisa Ferrándiz, Amalia Ubeda, JoséN. Domínguez, Jaime E. Charis, Gracela M. Lobo, M.José Alcaraz, Synthesis and anti-inflammatory activity of chalcone derivatives, *Bioorg. Med. Chem. Lett.* 8 (10) (1998) 1169–1174, [https://doi.org/10.1016/S0960-894X\(98\)00179-6](https://doi.org/10.1016/S0960-894X(98)00179-6).
- [15] F. Mayr, G. Möller, U. Garscha, J. Fischer, P.R. Castaño, S.G. Inderbilen, V. Temml, B. Waltenberger, S. Schwaiger, R.W. Hartmann, C. Gege, S. Martens, A. Odermatt, A.V. Pandey, O. Werz, J. Adamski, H. Stuppner, D. Schuster, Finding new molecular targets of familiar natural products using in silico target prediction, *Int. J. Mol. Sci.* 21 (2020) 1–18, <https://doi.org/10.3390/ijms21197102>.
- [16] Zhe-Hao Huang, Li-Quan Yin, Li-Ping Guan, Zhao-Hui Li, Cheng Tan, Screening of chalcone analogs with anti-depressant, anti-inflammatory, analgesic, and COX-2-inhibiting effects, *Bioorg. Med. Chem. Lett.* 30 (11) (2020) 127173, <https://doi.org/10.1016/j.bmcl.2020.127173>.
- [17] Sarah E. Kovar, Cody Fourman, Christine Kinstedt, Brandon Williams, Christopher Morris, Kwang-jin Cho, Daniel M. Ketcha, Chalcones bearing a 3,4,5-trimethoxyphenyl motif are capable of selectively inhibiting oncogenic K-Ras signaling, *Bioorg. Med. Chem. Lett.* 30 (11) (2020) 127144, <https://doi.org/10.1016/j.bmcl.2020.127144>.

- [18] M. Kafka, F. Mayr, V. Temml, G. Möller, J. Adamski, J. Höfer, S. Schwaiger, I. Heidegger, B. Matuszczak, D. Schuster, H. Klocker, J. Bektic, H. Stuppner, I. E. Eder, Dual inhibitory action of a novel *akt1c3* inhibitor on both full-length ar and the variant AR-V7 in enzalutamide resistant metastatic castration resistant prostate cancer, *Cancers*. 12 (2020) 1–18, <https://doi.org/10.3390/cancers12082092>.
- [19] Raimundo Braz Filho, Marcelo S. Da Silva, Otto R. Gottlieb, Flavonoids from *Iryanthera laevis*, *Phytochemistry*. 19 (6) (1980) 1195–1197, [https://doi.org/10.1016/0031-9422\(80\)83082-2](https://doi.org/10.1016/0031-9422(80)83082-2).
- [20] Uma Prawat, Orapan Chairerk, Unreuthai Phupornprasert, Abdul-Wahab Salae, Pittaya Tuntiwachwuttikul, Two New C-benzylated Dihydrochalcone Derivatives from the Leaves of *Melodorum siamensis*, *Planta Med.* 79 (01) (2012) 83–86, <https://doi.org/10.1055/s-0000005810.1055/s-002-2428910.1055/s-0032-1327950>.
- [21] O. Werz, J. Gerstmeier, S. Libreros, X. de la Rosa, M. Werner, P.C. Norris, N. Chiang, C.N. Serhan, Human macrophages differentially produce specific resolvins or leukotriene signals that depend on bacterial pathogenicity, *Nat. Commun.* 9 (2018) 1–12, <https://doi.org/10.1038/s41467-017-02538-5>.
- [22] J. Dalli, C.N. Serhan, Specific lipid mediator signatures of human phagocytes: microparticles stimulate macrophage efferocytosis and pro-resolving mediators, *Blood*. 120 (2012), <https://doi.org/10.1182/blood-2012-04-423525>.
- [23] Jana Gerstmeier, Christina Weinigel, Dagmar Barz, Oliver Werz, Ulrike Garscha, An experimental cell-based model for studying the cell biology and molecular pharmacology of 5-lipoxygenase-activating protein in leukotriene biosynthesis, *Biochim. Biophys. Acta – Gen. Subj.* 1840 (9) (2014) 2961–2969, <https://doi.org/10.1016/j.bbagen.2014.05.016>.
- [24] Lutz Fischer, Dagmar Szellas, Olof Rådmark, Dieter Steinhilber, Oliver Werz, Phosphorylation- and stimulus-dependent inhibition of cellular 5-lipoxygenase activity by nonredox-type inhibitors, *FASEB J.* 17 (8) (2003) 1–24, <https://doi.org/10.1096/fsb2.v17.810.1096.fj.02-0815je>.
- [25] D. Steinhilber, T. Herrmann, H.J. Roth, Separation of lipoxins and leukotrienes from human granulocytes by high-performance liquid chromatography with a Radial-Pak cartridge after extraction with an octadecyl reversed-phase column, *J. Chromatography B*. 493 (1989) 361–366, [https://doi.org/10.1016/S0378-4347\(00\)82742-5](https://doi.org/10.1016/S0378-4347(00)82742-5).
- [26] B. Shkodra-Pula, C. Kretzer, P.M. Jordan, P. Klemm, A. Koeberle, D. Pretzel, E. Banoglu, S. Lorkowski, M. Wallert, S. Höppener, S. Stumpf, A. Vollrath, S. Schubert, O. Werz, U.S. Schubert, Encapsulation of the dual FLAP/mPEGS-1 inhibitor BRP-187 into acetylated dextran and PLGA nanoparticles improves its cellular bioactivity, *J. Nanobiotechnol.* 18 (2020) 73, <https://doi.org/10.1186/s12951-020-00620-7>.
- [27] L. Thomas, Z. Rao, J. Gerstmeier, M. Raasch, C. Weinigel, S. Rummeler, D. Menche, R. Müller, C. Pergola, A. Mosig, O. Werz, Selective upregulation of TNF α expression in classically-activated human monocyte-derived macrophages (M1) through pharmacological interference with V-ATPase, *Biochem. Pharmacol.* 130 (2017) 71–82, <https://doi.org/10.1016/j.bcp.2017.02.004>.
- [28] O. Werz, E. Bürkert, B. Samuelsson, O. Rådmark, D. Steinhilber, Activation of 5-lipoxygenase by cell stress is calcium independent in human polymorphonuclear leukocytes, *Blood*. 99 (2002) 1044–1052, <https://doi.org/10.1182/blood.V99.3.1044>.
- [29] Paul M. Jordan, Jana Gerstmeier, Simona Pace, Rossella Bilancia, Zhigang Rao, Friedemann Börner, Laura Miek, Óscar Gutiérrez-Gutiérrez, Vandana Arakandy, Antonietta Rossi, Armando Ialenti, Cristina González-Estévez, Bettina Löffler, Lorena Tuchscherer, Charles N. Serhan, Oliver Werz, *Staphylococcus aureus*-Derived α -Hemolysin Evokes Generation of Specialized Pro-resolving Mediators Promoting Inflammation Resolution, *Cell Rep.* 33 (2) (2020) 108247, <https://doi.org/10.1016/j.celrep.2020.108247>.
- [30] Amol Gupte, John K. Buolamwini, Synthesis and biological evaluation of phloridzin analogs as human concentrative nucleoside transporter 3 (hCNT3) inhibitors, *Bioorg. Med. Chem. Lett.* 19 (3) (2009) 917–921, <https://doi.org/10.1016/j.bmcl.2008.11.112>.
- [31] S. Urganekar, H.S. la Pierre, I. Meir, H. Lund, D. Raychaudhuri, J.T. Shaw, Synthesis of Antimicrobial Natural Products Targeting FtsZ: (\pm)-Dichamanetin and (\pm)-2'-Hydroxy-5'-benzylisovaranol-B, *Org. Lett.* 7 (2005), <https://doi.org/10.1021/ol052269z>.
- [32] Igor Ivanov, Hartmut Kuhn, Dagmar Heydeck, Structural and functional biology of arachidonic acid 15-lipoxygenase-1 (ALOX15), *Gene*. 573 (1) (2015) 1–32, <https://doi.org/10.1016/j.gene.2015.07.073>.
- [33] Jesmond Dalli, Charles N Serhan, Identification and structure elucidation of the pro-resolving mediators provides novel leads for resolution pharmacology, *Br. J. Pharmacol.* 176 (8) (2019) 1024–1037, <https://doi.org/10.1111/bph.v176.810.1111/bph.14336>.
- [34] Charles A. Dinarello, Anti-inflammatory Agents: Present and Future, *Cell*. 140 (6) (2010) 935–950, <https://doi.org/10.1016/j.cell.2010.02.043>.
- [35] T. Hanke, D. Merk, D. Steinhilber, G. Geisslinger, M. Schubert-Zsilavecz, Small molecules with anti-inflammatory properties in clinical development, *Pharmacol. Ther.* 157 (2016) 163–187, <https://doi.org/10.1016/j.pharmthera.2015.11.011>.
- [36] P.J. Barnes, Glucocorticosteroids, *Handbook Exp. Pharmacol.* 237 (2017) 93–115, https://doi.org/10.1007/164_2016_62.
- [37] Kun Yang, Wenzhe Ma, Huanhuan Liang, Qi Ouyang, Chao Tang, Lihua Lai, Robert B Russell, Dynamic simulations on the arachidonic acid metabolic network, *PLoS Comput. Biol.* 3 (3) (2007) e55, <https://doi.org/10.1371/journal.pcbi.0030055>.
- [38] C. He, Y. Wu, Y. Lai, Z. Cai, Y. Liu, L. Lai, Dynamic eicosanoid responses upon different inhibitor and combination treatments on the arachidonic acid metabolic network, *Mol. BioSystems*. 8 (2012) 1585–1594, <https://doi.org/10.1039/c2mb05503a>.
- [39] J. Dalli, Does promoting resolution instead of inhibiting inflammation represent the new paradigm in treating infections? *Mol. Aspects Med.* 58 (2017) 12–20, <https://doi.org/10.1016/j.mam.2017.03.007>.
- [40] Victor Fattori, Tiago H. Zaninelli, Fernanda S. Rasquel-Oliveira, Rubia Casagrande, Waldiceu A. Verri, Specialized pro-resolving lipid mediators: A new class of non-immunosuppressive and non-opioid analgesic drugs, *Pharmacol. Res.* 151 (2020) 104549, <https://doi.org/10.1016/j.phrs.2019.104549>.
- [41] C. Kontogiorgis, M. Mantzanidou, D. Hadjipavlou-Litina, Chalcones and their potential role in inflammation, *Mini Rev. Med. Chem.* 8 (2008) 1224–42, <https://doi.org/10.2174/138955708786141034>.
- [42] Anna-Maria Katsori, Dinitra Hadjipavlou-Litina, Recent progress in therapeutic applications of chalcones, *Exp. Opin. Ther. Pat.* 21 (10) (2011) 1575–1596, <https://doi.org/10.1517/13543776.2011.596529>.
- [43] Satoshi Sogawa, Yasunori Nihiro, Hiroki Ueda, Akihiro Izumi, Tokutaro Miki, Hitoshi Matsmoto, Toshio Satoh, 3,4-Dihydroxychalcones as potent 5-lipoxygenase and cyclooxygenase inhibitors, *J. Med. Chem.* 36 (24) (1993) 3904–3909, <https://doi.org/10.1021/jm00076a019>.
- [44] Yasuko Koshihara, Yasuo Fujimoto, Hideo Inoue, A new 5-lipoxygenase selective inhibitor derived from *Artocarpus communis* strongly inhibits arachidonic acid-induced ear edema, *Biochem. Pharmacol.* 37 (11) (1988) 2161–2165, [https://doi.org/10.1016/0006-2952\(88\)90576-X](https://doi.org/10.1016/0006-2952(88)90576-X).
- [45] Chika Nakamura, Nobuhide Kawasaki, Hideki Miyataka, Ezhuthachan Jayachandran, In Ho Kim, Kenneth L Kirk, Takeo Taguchi, Yoshio Takeuchi, Hitoshi Hori, Toshio Satoh, Synthesis and biological activities of fluorinated chalcone derivatives, *Bioorg. Med. Chem.* 10 (3) (2002) 699–706, [https://doi.org/10.1016/S0968-0896\(01\)00319-4](https://doi.org/10.1016/S0968-0896(01)00319-4).
- [46] Martino Forino, Simona Pace, Giuseppina Chianese, Laura Santagostini, Markus Werner, Christina Weinigel, Silke Rummeler, Gelsomina Fico, Oliver Werz, Orazio Tagliatalata-Scafati, Humudifical and Bioactive Prenylated Polyphenols from Hops (*Humululus lupulus* cv. “Cascade”), *J. Nat. Prod.* 79 (3) (2016) 590–597, <https://doi.org/10.1021/acs.jnatprod.5b01052>.
- [47] Nimmanapalli P. Reddy, Polamarasetty Aparoy, T. Chandra Mohan Reddy, Chandrani Achari, P. Ramu Sridhar, Pallu Reddanna, Design, synthesis, and biological evaluation of prenylated chalcones as 5-LOX inhibitors, *Bioorg. Med. Chem.* 18 (16) (2010) 5807–5815, <https://doi.org/10.1016/j.bmc.2010.06.107>.
- [48] M Arockia Babu, Neeraj Shakya, Philip Prathipati, S.G Kaskhedikar, Anil K Saxena, Development of 3D-QSAR models for 5-lipoxygenase antagonists: chalcones, *Bioorg. Med. Chem.* 10 (12) (2002) 4035–4041, [https://doi.org/10.1016/S0968-0896\(02\)00313-9](https://doi.org/10.1016/S0968-0896(02)00313-9).
- [49] Shweta Sinha, S.L. Manju, Mukesh Doble, Chalcone-Thiazole Hybrids: Rational Design, Synthesis, and Lead Identification against 5-Lipoxygenase, *ACS Med. Chem. Lett.* 10 (10) (2019) 1415–1422, <https://doi.org/10.1021/acsmchemlett.9b00193i0.1021/acsmchemlett.9b00193.s001>.
- [50] Andrew N. Boshra, Hajjaj H.M. Abdu-Allah, Anber F. Mohammed, Alaa M. Hayallah, Click chemistry synthesis, biological evaluation and docking study of some novel 2'-hydroxychalcone-triazole hybrids as potent anti-inflammatory agents, *Bioorg. Chem.* 95 (2020) 103505, <https://doi.org/10.1016/j.bioorg.2019.103505>.
- [51] Pierre Borgeat, Biochemistry of the lipoxygenase pathways in neutrophils, *Can. J. Physiol. Pharmacol.* 67 (8) (1989) 936–942, <https://doi.org/10.1139/y89-147>.
- [52] Oliver Werz, Dieter Steinhilber, Development of 5-lipoxygenase inhibitors – Lessons from cellular enzyme regulation, *Biochem Pharmacol.* 70 (3) (2005) 327–333, <https://doi.org/10.1016/j.bcp.2005.04.018>.
- [53] Hamid Sadeghian, Atena Jabbari, 15-Lipoxygenase inhibitors: a patent review, *Exp Opin Ther Pat.* 26 (1) (2016) 65–88, <https://doi.org/10.1517/13543776.2016.1113259>.
- [54] Oliver Werz, Inhibition of 5-lipoxygenase product synthesis by natural compounds of plant origin, *Planta Med.* 73 (13) (2007) 1331–1357, <https://doi.org/10.1055/s-2007-990242>.
- [55] S.-Y. Cheung, M. Werner, L. Esposito, F. Troisi, V. Cantone, S. Liening, S. König, J. Gerstmeier, A. Koeberle, R. Bilancia, R. Rizza, A. Rossi, F. Roviezzo, V. Temml, D. Schuster, H. Stuppner, M. Schubert-Zsilavecz, O. Werz, T. Hanke, S. Pace, Discovery of a benzensulfonamide-based dual inhibitor of microsomal prostaglandin E2 synthase-1 and 5-lipoxygenase that favorably modulates lipid mediator biosynthesis in inflammation, *Eur. J. Med. Chem.* 156 (2018) 815–830, <https://doi.org/10.1016/j.ejmech.2018.07.031>.
- [56] J. Gerstmeier, J. Seegers, F. Witt, B. Waltenberger, V. Temml, J.M. Röllinger, H. Stuppner, A. Koeberle, D. Schuster, O. Werz, Ginkgolic Acid is a Multi-Target Inhibitor of Key Enzymes in Pro-Inflammatory Lipid Mediator Biosynthesis, *Front. Pharmacol.* 10 (2019) 797, <https://doi.org/10.3389/fphar.2019.00797>.
- [57] Tran Thi Van Anh, Alilou Mostafa, Zhigang Rao, Simona Pace, Stefan Schwaiger, Christian Kretzer, Veronika Temml, Carsten Giesel, Paul M. Jordan, Rossella Bilancia, Christina Weinigel, Silke Rummeler, Birgit Waltenberger, Tran Hung, Antonietta Rossi, Hermann Stuppner, Oliver Werz, Andreas Koeberle, From Vietnamese plants to a biflavonoid that relieves inflammation by triggering the lipid mediator class switch to resolution, *Acta Pharm Sin B*. 11 (6) (2021) 1629–1647, <https://doi.org/10.1016/j.apsb.2021.04.011>.
- [58] R.G. Snodgrass, B. Brüne, Regulation and Functions of 15-Lipoxygenases in Human Macrophages, *Front. Pharmacol.* 10 (2019) 1–12, <https://doi.org/10.3389/fphar.2019.00719>.

4. Discussion

The development of new approaches to combat inflammatory diseases is an ongoing process. A unique aspect in the research of LM evolves from the fact that they are responsible for the onset and the termination of inflammation^{2,19}. The usage of drugs, which interfere with the tightly regulated LM cascades, triggers a previously unexplored change of the LM profiles. This LM composition guides the inflammatory events of the surrounding, and positively affects the progression of healing or further harm. To favorably modulate the LM spectrum early investigations provided proof that inhibition of mPGES-1 and FLAP are interesting approaches to accomplish specific downregulation of detrimental pathways without affecting mediators that are urgently needed for the resolution of inflammation or the homeostasis of the body^{71,182}. But the best concepts of therapy and the most specific and potent compounds are worthless as long as their physicochemical properties would not allow them to meet their target in a physiological environment. With the awareness of these aspects, the present thesis was designed to characterize new compounds that can favorably modulate the LM profile and investigate the eligibility of polymeric NPs to increase the efficiency of these multitarget inhibitors. In the following sections, the results of the thesis are intensively discussed to connect the acquired knowledge of the different studies and clarify their contribution to the scientific progression of anti-inflammatory pharmacotherapy.

4.1. The influence of approved therapeutics on LM networks

NSAIDs are the most commonly used drugs in anti-inflammatory pharmacotherapy and since the discovery of PGs and the two COX isoforms the mode of action was thought to be identified^{82,183,184}. The uncovering of SPMs as highly beneficial lipid mediators added another segment to the picture and the influence of NSAIDs as well as COX-2 or 5-LOX inhibitors on the whole metabololipidome is still elusive. In different stages of inflammation, macrophages differentially produce different subsets of LM¹²². M1 macrophages produce predominantly PGs and LTs due to high expression of COX-2 and FLAP, which are induced by IFN γ and bacterial endotoxins like LPS. In the resolution phase the cytokine milieu changes and anti-inflammatory cytokines like IL-4 and IL-10 polarize the subtype of macrophages to M2, which express 15-LOX-1¹²². These subtypes can be challenged with human pathogenic *E. coli* to induce LM biosynthesis¹²². The incubation of the two macrophage subtypes with ibuprofen and celecoxib showed a significantly reduced biosynthesis of all detectable PGs (PGE₂, PGD₂, TXB₂, PGF_{2 α}) and corresponding precursors (11-HETE, 11-HEPE), as expected. A clear downside highlighted is the overshooting production of LTs in M1. Thus, the selective COX-2 inhibitor elevated LT production more than ibuprofen, which could occur due to the high concentration

(30 μ M) of ibuprofen, which may lead to pleiotropic effects. This activation of LT biosynthesis is reminiscent to the development of aspirin-induced asthma upon long term therapy¹⁴⁸. In M2 macrophages a similar picture is observable. PGs are reduced after celecoxib treatment with induced 5-LOX products. Interestingly in M1 macrophages, 15-HETE production is also reduced. The COX subtypes are able to synthesize 15(R)-HETE, which is measured here, since 15-LOX enzymes synthesize only 15(S)-HETE. As a result, the treatment of ibuprofen and celecoxib reduces the formation of an important precursor (15(R)-HETE) of AT-LXA₄ that could be produced by intercellular pathways with neutrophils to initiate resolution phase^{21,125,185}.

The only approved 5-LOX inhibitor zileuton was also tested in this experimental setup. Since zileuton binds as iron chelating agent the assumption that zileuton could also inhibit 15-LOX activity is strong¹⁴⁶. Indeed, zileuton reduced not only pro-inflammatory leukotrienes but also affected 15/12-LOX products in M1 and M2, which could actively delay the resolution phase and reveals the unspecific inhibition of LOXs. In contrast, inhibition of FLAP by MK-886 promoted SPMs and SPM precursor production, while LT synthesis was effectively reduced in M1 but not as effectively in M2, presumably due to minor expression of FLAP. The interference of MK-886 with the 5-LOX pathway did not upregulate PGs levels.

Beyond the analysis of the modulation of the LM profile by common therapeutics, this study, by using 3887, also confirmed that 15-LOX-1 but not 15-LOX-2 is responsible for SPM production, since 15-LOX-2 is expressed in M1 and M2^{116,122,186}. But what was not considered in any of these studies and might be important to investigate in the future, is the capability of 15-LOX-2 to produce precursors that can be further metabolized by intercellular crosstalk in companion with neutrophils, which could lead to the production of SPMs and an early induction of the resolution phase. Therefore, the ability to induce 15-LOX derived products in M1 should be considered important for future results and further studies.

Taken together, manuscript I indicated clear disadvantages of common anti-inflammatory drugs with respect to the overall LM profiles on the cellular level and pointed out their potential side effects upon long-term therapy. Only FLAP inhibition by MK-886 favorably modulated LM biosynthesis in M1 and M2. These findings highlighted the necessity of new anti-inflammatory drugs with a better LM safety profile.

4.2. LM profiling of new multitarget inhibitors

Latest research of new promising chemical structures that inhibit FLAP and mPGES-1 suggests potent anti-inflammatory drugs with better risk:benefit profile than established pharmaceuticals^{105,147}. Targeting the downstream enzymes of LT and PG biosynthesis (mPGES-1, LTA₄-H, LTC₄-S, FLAP) might be associated with fewer side effects and more beneficial LM profiles^{187,188}. To provide evidence, BRP-201, BRP-187 and MF-14/15 were tested in similar

experimental settings. As expected from the data sets with MK-886, the new FLAP antagonists BRP-201 and BRP-187 (Table 2) are potently reducing LT biosynthesis while AA is not shunted into PG biosynthetic pathways. At concentrations of 3 μ M both BRP-compounds inhibit PGE₂ formation more efficient than MK-886 to around 80% of the control. Non-published data from our lab points out that inhibition of PGE₂ formation in intact cells is not as potent as in isolated A549 microsomes overexpressing mPGES-1. Considering that potent inhibition of the 5-LOX pathway usually results in elevated COX products and vice versa¹⁸⁷, the moderate inhibitory potential of BRP-187 and BRP-201 against mPGES-1 should be rated higher. The diminished levels of LTB₄ and PGE₂ are desired in the treatment of asthma, rheumatoid arthritis, cardiovascular disease, arteriosclerosis or psoriasis, while no substrate shunting or decreased levels of PGD₂ lead to adverse effects^{2,148,187,189–191}. An interesting experiment yet to perform might be the evaluation of the inhibitory potential of these compounds against mPGES-2, which is responsible for gastrointestinal protective PGE₂ formation¹⁹².

MF-14 and -15 were identified as 5-LOX inhibitors, with potential action against COX and influence on mPGES-1 activity^{154,160}. The IC₅₀ values were first determined for isolated 5-LOX and for 5-LOX in PMNL. Interestingly, MF-14 displayed higher potency against isolated 5-LOX, while MF-15 is more effective in PMNL suggesting that the lack of the double bond in the chalcone-like structure awards more structural flexibility of the alkyl aryl ether, which could fit better in binding pockets maybe also within FLAP. In general, there is no information which type of 5-LOX inhibitor these chalcones could be. The overall lipophilic structure could act like a competitive antagonist of AA in the binding pocket. This could have been assessed via exogenous substrate addition or by wash-out experiments. Subsequent experiments with HEK-293 cells overexpressing 5-LOX indicated again very high potency of MF-14 and MF-15 even in the presence of exogenous AA. In contrast to zileuton both chalcones increased the formation of 15-LOX products in M1 and M2, which would exclude an iron-chelating mode of action, because this would affect all LOXs products, as pointed out in manuscript I. MF-14, which was less effective in LT inhibition, slightly reduced PGE₂ biosynthesis, while MF-15 elevated PGE₂ levels, maybe due to moderate substrate shunting effects. Despite potent LT inhibition and influence on PGE₂ production, BRP-201 and the chalcones but not BRP-187 strongly elevated 15-LOX products such as 15-HETE, 15-HEPE and 17-HDHA in M1 macrophages. In early stages of inflammation where mostly neutrophils with high 5-LOX activity and M1 macrophages with high amounts of 5-LOX and COX-2 products are in charge of the immune response, the elevated formation of 15-LOX products as precursors for transcellularly synthesized LXA₄ and Rvs could lead to an earlier initiation of the resolution phase^{9,127}. Recent studies revealed positive effects of LXs in acute renal failure in mice, the reduction of serum-amyloid-A expression in a COPD model in mice, and highly beneficial modulation of the cardiometabolic disease^{193–196}.

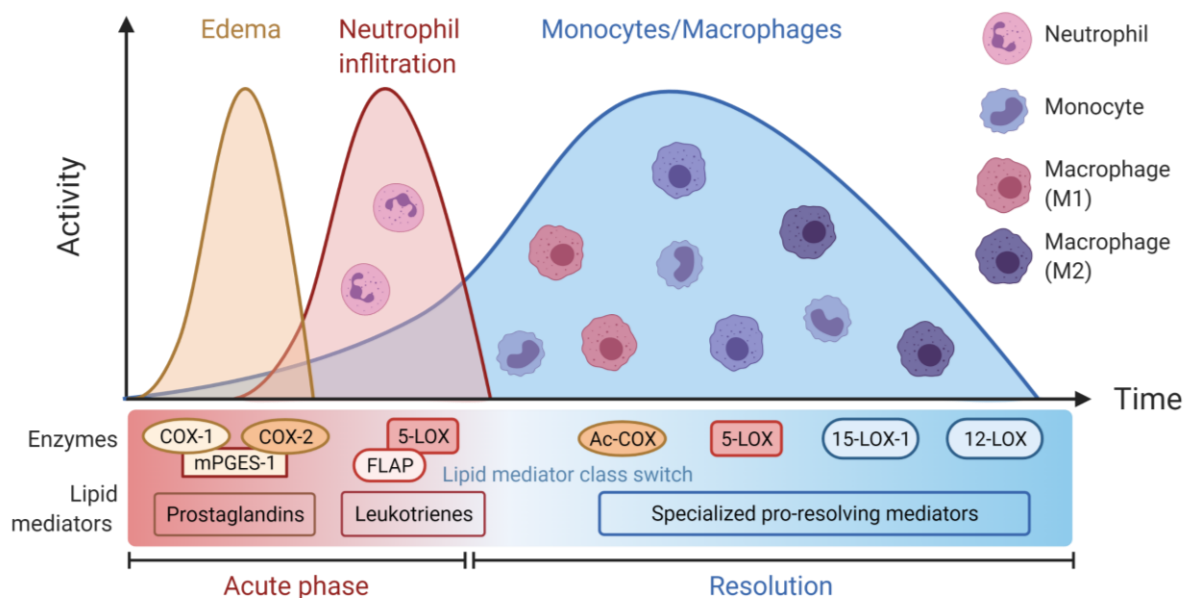


Figure 8 Course of inflammation from initiation to resolution according to J. Park et al. (2020)¹³². After activation by inflammatory stimuli PGE_2 is released causing edema and neutrophils infiltrate following the LTB_4 gradient. After the acute phase monocytes infiltrate into the tissue and LXs initiate a lipid mediator class switch. M2 macrophages mature to synthesize SPMs and regain homeostasis.

The LM profile in M2 macrophages, which represents the phenotype in the inflammation resolution phase, is also ameliorated by treatment with either of the BRP-187, BRP-201 and the dihydrochalcones. The amounts of proinflammatory leukotrienes in M2 are not reduced as much as in M1 macrophages because the expression of FLAP is lower in the latter cell type¹²². Slightly elevated levels of PGs might be beneficial in the resolution phase, as PGE_2 and PGD_2 are responsible for priming leukocytes to produce LXs over LTs^{19,20,89}. In some settings PGE_2 is even responsible for strong anti-inflammatory effects by activation of the EP4 receptor in the lung or neurons^{92,93,197}. Probably the most important effect of the chalcones and BRP-compounds in this experimental setting is the direct enhancement of SPMs and their precursors. The increase of 15-LOX products could beneficially affect the healing progression at sites of inflammation and help to resolve chronic inflammatory conditions, while relief pain and restore homeostasis (Figure 8)^{36,132,134}. BRP-187 did not elevate 12/15-LOX products in M1 macrophages unlike BRP-201 and the chalcones which remarkably increased SPM and SPM precursor biosynthesis in M2 macrophages. The effect on SPM precursors decays at higher concentrations than 3 μ M, while SPM levels remain elevated in contrast to BRP-201 and MF-14/15, which concentration dependently increased SPMs and 12/15-LOX products. Therefore, it can be suggested, that BRP-187 in comparison to BRP-201 and MF-14/15 utilizes another mode of action for stimulating 12/15-LOX product biosynthesis in macrophages, as discussed later in section 4.4.

The LM profiles induced by BRP-187, BRP-201, MF-14 and MF-15 showed highest similarity with MK-886 in manuscript I and with a previously studied benzsulfonamide-based dual

mPGES-1 and FLAP inhibitor¹⁹⁸. All investigated compounds (MF- and BRP-compounds) displayed higher potency than MK-886, which reached phase II clinical trials, but was not further developed for unknown reasons⁷¹. Structurally, BRP-201 and BRP-187 share certain similarities with MK-886. The chlorobenzyl moiety is present in all molecules and the planar indole ring in MK-886 has similar conformation like the benzimidazole of BRP-201. Hence, a similar pattern of LM modulation by these compounds was expected although BRP-201 induces 15-LOX products strongly in M1 and M2, while BRP-187 and MK-886 only elevate levels of SPM precursors in M2 by a minor degree. Possible reasons for this effect are discussed later in this thesis.

Besides the evaluation of the lipid mediator profile in human monocyte-derived macrophages (MDM) BRP-201 was tested in a zymosan-induced peritonitis mouse model *in vivo*. Here, BRP-201 displayed similar results, enhancing 12/15-LOX products, while LTs are reduced and PGs were not elevated at a low dose of 2 mg/kg. Notably, even though BRP-201 is more potent than MK-886 *in vitro*, MK-886 was more effective in the same setting at 1 mg/kg^{72,73}. The reasons for this difference can be low solubility (LogP 8.5855, calculated by BIOVIA Draw 2019 x64) and high metabolic rate of BRP-201, which would decrease the overall bioavailability of the compound. In fact, BRP-187, BRP-201 and MF compounds share unfavorable physicochemical features and the improvement of the structures or the smart delivery towards the targets is a very important point for future development. Conclusively, BRP-201, BRP-187 and MF-14/15 demonstrate favorable LM profile modulation in M1 and M2 macrophages as well as *in vivo* with potentially fewer risk of side effects than established therapeutics like ibuprofen and zileuton, which were discussed in the first section of the discussion. The LM profile indicates sufficient reduction of pro-inflammatory products, while the biosynthesis of anti-inflammatory mediators is even enhanced. The selective targeting of downstream proteins like mPGES-1 that is specifically upregulated upon inflammatory conditions circumvents the detrimental effects on gastrointestinal integrity as well as cardiovascular events^{136,191}. This leaves us with three compounds that outstandingly modulate activated leukocytes to produce favorable LM profile signatures for the reduction of inflammation and promotion of resolution. As indicated in the aims of this thesis, the delivery of these compounds to their targets is the next big hurdle to overcome within this study^{71,142}.

4.3. mPGES-1/FLAP inhibitors as anti-inflammatory payloads in polymeric NPs

Bioavailability, plasma protein binding, volume of distribution, metabolic stability and half-life elimination are routinely assessed in drug development and are one of the main reasons why promising drug candidates are not further progressed¹⁹⁹. Indicated by the structure of especially BRP-201 and BRP-187 the aforementioned properties would be major obstacles to continue the investigation. The acidic and lipophilic structures of both compounds cause high

plasma protein binding, the calculated logP values (BRP-201= 8.5855, BRP-187= 6.3035) suggest a large volume of distribution associated with a long half-life and a high metabolic rate²⁰⁰⁻²⁰². Despite the unfavorable physicochemical properties, the high potency of the substances and the beneficial modulation of the LM spectrum warrant the effort to develop new methods (Figure 9). Here, we present investigations on the suitability of polymeric NPs as drug delivery systems to improve the efficacy of mPGES-1 and FLAP inhibitors in leukocytes, human whole blood, and in vivo.

The examined NPs were stable monodisperse particles with a size range about 100-250 nm, a slightly negative ζ -potential and an encapsulation efficiency (EE) above 50%. A negative ζ -potential is required for NPs, which are intended to be injected into the blood stream, because positively charged NPs have strong affinity to negatively charged cell surfaces, which causes agglomeration of the cells and therefore cytotoxicity^{203,204}. Particles in the size range of 100-350 nm are internalized by leukocytes, especially macrophages, via clathrin-mediated endocytosis (a form of phagocytosis), which was also inhibited by cytochalasin D (data not shown) as an inhibitor of actin polymerization^{205,206}. The uptake of BRP-201 and BRP-187 NPs, shown in manuscript II and III, were assessed by fluorescent associated cell sorting (FACS) and confocal laser scanning microscopy (CLSM) to distinguish between uptake or adhesion of NPs. By using FACS the differential analysis between adherent and internalized NPs was not possible, even though several washing steps might have avoided this problem. Here, especially Ac(e)Dex as rather lipophilic polymers could accomplish stronger adherence to biomembranes²⁰⁷. In CLSM experiments we confirmed the cellular uptake of PLGA and Ac(e)Dex NPs loaded with BRP-201 and BRP-187, which is a highly valuable fact to grasp since we proved that drug-loaded NPs are able to be up taken inside the cells, where the cargo is released. In this context the strong phagocytotic activity of neutrophils and macrophages guarantees a passive targeting of the NPs to immune cells, as these cells also express abundant FLAP/mPGES-1 and are responsible for SPM biosynthesis^{2,122,205}. Once the NP is inside the cell, an important step to release the anti-inflammatory cargo is the degradation of the polymers. In both studies a degradation analysis for PLGA and Ac(e)Dex was performed, proving the pH-dependent biodegradability of Ac(e)Dex¹⁷⁷. PLGA, as already introduced, is enzymatically cleaved inside the cell and displayed a higher stability in physiological solution¹⁷⁴. As Ac(e)Dex dissolves rapidly at acidic pH the passive targeting is even enhanced, because endolysosomal pH dissolves the polymer inside the cells and releases the cargo²⁰⁸. Beside the well-established polymers Ac(e)Dex and PLGA, new polymers were developed to encapsulate anti-inflammatory drugs and to provide a library of polymers that can be used in different therapeutic settings depending on their characteristics and activity profile. An adequate carrier system is as important as the appropriate drug for the addressed disease. Individual needs on drug release profiles and passive/active targeting can be altered by the

polymer²⁰⁹. In manuscript IV we investigated poly- ϵ - and poly- δ -caprolactones (PCLs) with different polymer ratios, changing the crystallinity of the polymer and thus the activity profile of BRP-187 as anti-inflammatory payload. Polymers with a crystallinity of 25-50% and a melting point of 37 °C degraded faster and released the drug efficiently, resulting in the same bioactivity as free BRP-187. Hence, the polymers with ratios between 87:13; 81:19 and 75:25 P ϵ CL:P δ CL are suitable compositions for short term treatment, where the encapsulated drug should act rapidly like in systemic inflammatory response syndrome (SIRS)²¹⁰. This effect is explained by the higher amount of amorphous domains, which enable faster diffusion of the compound and increase the accessibility of water for hydrolysis and faster degradation^{173,211}. PCL-based NPs embedded in a fibrin glue-based gel system with methylprednisolone as cargo displayed effectiveness in a rat model of induced spinal cord injury, implying the suitability as delivery system for BRP-187 or BRP-201 in the future²¹².

The toxicological evaluation of the formed NPs was also a critical point to assess in all studies. None of the formulations in all our studies showed cytotoxic effects. In fact, free BRP-201 displayed moderate cytotoxicity in human MDM, which however was completely abolished upon encapsulation into NPs. This effect was already observed for PLGA-NPs and amphotericin B but not yet for Ac(e)Dex-NPs²¹³. The potent decrease of the cytotoxicity may avoid additional stress for non-targeted cells and tissues, lowering the expected adverse effects of BRP-201. This fact alone is an obvious benefit of the encapsulation of BRP-201 NPs. One of the most important aspects of our studies was the assurance of bioactivity (e.g. LT biosynthesis inhibition) of the compounds encapsulated into NPs. The drug-loaded formulations were tested in human PMNL and macrophages compared to the free drug. Of note, no additional barriers such as plasma protein binding or additional cells are present in this experimental setup. Hence, the free compounds may act efficiently on LT biosynthesis. To study short- and long-term effects, the preincubation time was varied from 15 min up to 5 h in PMNL and even up to 20 h in macrophages. Incredibly, BRP-187 and BRP-201 when incorporated into nanoparticles showed the same bioactivity in short-term experiments as the free drugs and the potency upon 5 h and 20 h treatments was even significantly enhanced. An equal activity after only 15 min of treatment was not expected, because the encapsulated drug had to cross additional barriers in this experimental setup e.g. the uptake of the NPs inside the cells, the degradation of the NPs as well as the diffusion outside the polymeric matrix. Interesting results were obtained in experiments with longer incubation times of 5 h. As shown in manuscript II, free BRP-187 lost its potency to inhibit 5-LOX product formation, while the encapsulated compound remained active. Recent stability studies indicated that BRP-187 is photosensitive and degraded upon long exposure (data not shown), which could explain the loss of bioactivity. On top of this, the metabolization through CYP enzymes and enzymatic hydrolysis are possible explanations for this effect. However, if incorporated into AcDex- and

PLGA-NPs the efficiency of the drugs remained. The higher efficiency after long-term incubations and the same potency with short-term treatments suggests that BRP-187 encapsulated into polymeric NPs is a promising approach for the management of inflammatory diseases surpassing the use of the drug itself.

On top of these results related to suppression of 5-LOX product formation, we found that PLGA NPs are able to efficiently carry BRP-187 to mPGES-1 granting a potent reduction of PGE₂ biosynthesis. As indicated before, targeting mPGES-1 in a cellular environment is difficult and often less efficient than in cell-free assays. BRP-187 at 3 μM reduced the PGE₂ formation in M1 MDM to around 78±3% of the DMSO control while 0.1 μM of BRP-187 encapsulated in PLGA NPs achieved the same effect (79±12 %), therefore enhancing the potency of BRP-187 by 30-fold (data not shown). 1 μM BRP-187 decreased PGE₂ formation to 27±11% of the control after 15 min preincubation. Interestingly, AcDex[BRP-187] had not initially the same effect, but displayed equipotent inhibition after 20 h. A possible reason for the strong tendency of PLGA[BRP-187] NPs to inhibit mPGES-1 could be the cleavage of PLGA in close proximity to the mPGES-1 enzyme at the ER.

Conclusively, the incorporation of BRP-187 as anti-inflammatory cargo in NPs certainly led to significant improvements in the bioactivity profile of the drug. Future assessment in complex animal models addressing chronic inflammatory states like the collagen induced arthritis or joint pain models in mice, where potent reduction of LTB₄ and PGE₂ are from utmost importance, could reveal further benefits of these formulations. Also important for future experiments is the performance of the BRP-187 NPs in human whole blood. Since abundant plasma proteins and different cell types that may impair the potency of BRP-187 are included in such test matrix, the results of whole blood experiments could give hints for potential future use in clinical studies.

In manuscript III, we investigated BRP-201 incorporated into PLGA and AceDex NPs. Similar to the previous study on BRP-187 the compound was tested in human PMNL and macrophages. Surprisingly, the effect of PLGA[BRP-187]-NPs on PGE₂ formation was not apparent upon PLGA[BRP-201] treatment. Despite the inconsistent distribution of BRP-201 in PLGA-NPs as revealed by Raman spectroscopy, the inhibition of LT formation in M1 MDM and PMNL showed similar results for BRP-187 and BRP-201 in both studies. Thus, a correlation between the bioactivity of drugs inside NPs and the interaction between polymer and compound can be deduced. Apparently, the interaction between polymer and drug can alter the overall physicochemical properties of the NP in a way that different degradation kinetics and affinities towards cellular components have a strong impact, where and when the drug is released inside the cell. In a future collaboration within the SFB PolyTarget, the microscopic analysis of labeled polymer and labeled compound will reveal the difference between both formulations and maybe explain the different activity profiles^{214,215}. BRP-201 in NPs (just like

BRP-187 NPs in the previous study) increased the potency on LT inhibition of the compound in PMNL after 5 h. But unlike the previous study, AceDex and PLGA even improved the potency of the drug upon long incubations. A possible reason could be the effective transport of BRP-201 to the target. Even free BRP-201, although no disruptive factors are in the medium, is not completely bound to FLAP under these assay conditions. Possible accumulations in membranes may decrease the potency of BRP-201, while after prolonged incubation with NPs the compound seem to be more efficiently delivered to the FLAP, hence decreasing the IC_{50} value of BRP-201.

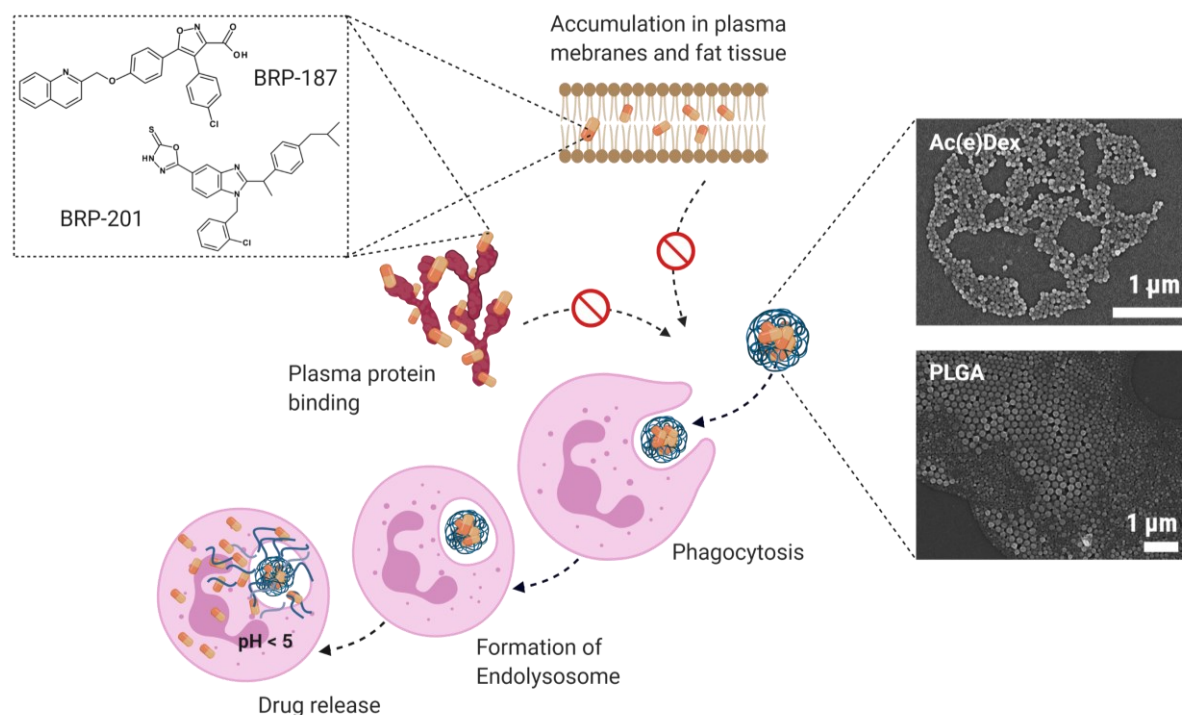


Figure 9 Effect and mode of action of NPs to prevent inactivation of active pharmaceutical ingredient (API). Polymeric NPs prevent lipophilic compounds from accumulation in plasma membranes and fat tissue and reduce their tendency to bind to plasma proteins. The NP is phagocytosed by leukocytes and degraded inside the cell where the drug is released.

A critical issue often pointed out during this thesis is the poor bioactivity of FLAP inhibitors in blood⁷¹. Since NPs as drug delivery systems are designed to prevent plasma protein binding and to transport BRP-201 without potential off-target binding to FLAP, we assessed the efficiency to inhibit LT formation of free drug and encapsulated into NPs using freshly withdrawn human whole blood. While PLGA NPs displayed no benefit over free BRP-201, NP formulations of with AceDex inhibited LTB_4 formation more potently after 15 min and 5 h versus free drug. After 20 h preincubation the NPs unfolded their full potential and decreased the IC_{50} -value of BRP-201 by 5-fold. In order to induce an inflammatory environment in the whole blood, we exposed the blood to LPS for 24 h prior to treatment with free drug or NPs. This experimental setting was designed to mimic the intervention with the drug after the inflammation was initiated. Here the benefit of AceDex[BRP-201] NPs further increased as the

formulation showed high potency compared to other treatments even after 5 h of preincubation by increasing the activity of BRP-201 by 10-fold. The reason for the increase of potency under these experimental conditions were studied. Firstly, we investigated the influence of LPS on PMNL phagocytotic activity. Even though literature indicated a higher phagocytotic activity after LPS exposure²¹⁶ our FACS analysis of PMNL primed with LPS for 1 h and incubated with NPs showed no effects compared to PMNL devoid of LPS priming. Possible reasons for these results could be that the incubation time to prime leukocytes is too short. However, since isolated PMNL are short-lived cells, an experimental setup with longer incubation periods was not possible. Higher phagocytotic activity may explain the increased activity of AceDex[BRP-201] NPs, but why are then PLGA NPs still not effective? Like mentioned earlier, Raman spectroscopy revealed that BRP-201 was not homogeneously distributed within PLGA NPs. Possibly, the degradation of PLGA is not as fast as that of AceDex and BRP-201 was not able to effectively diffuse outside of the NP inside the cell due to the inconsistent distribution. Another explanation for this effect, which would also explain why PLGA NPs are not effective, is the low intracellular pH value after LPS treatment. Experimental attempts to determine the intracellular pH of PMNL after LPS treatment were not successful in our laboratory but it was shown that the treatment of LPS activates the NLRP3 inflammasome and induces lysosomal acidification by v-ATPase activation^{217,218}. Such endolysosomal acidification may enhance the degradation of AceDex NPs, which leads to faster intracellular release of BRP-201¹⁷⁷. The improved uptake and the faster degradation under inflammatory conditions of AceDex[BRP-201] NPs implies a suitable usage for anti-inflammatory therapy. While the NPs remain stable in homeostatic tissues, the increased activity and low pH at inflammatory sites may lead to efficient NP uptake and rapid release of BRP-201 to effectively counteract inflammation via beneficial modulation of the LM profile.

Finally, in order to confirm the feasibility of our drug delivery system we used a zymosan-induced peritonitis mouse model with an i.v. injection of the NPs. The poor solubility of BRP-201 excluded the preparation of an injectable formulation with free BRP-201 for comparison, since thrombotic events were expected. Nevertheless, upon i.v. injection of AceDex[BRP-201] NPs we observed significantly reduced LTB₄ levels in plasma compared to the NP control, making BRP-201 the first dual mPGES-1 and FLAP inhibitor encapsulated into NPs that showed beneficial modulation of the LM profile *in vivo*²¹⁹. Future studies in animal models with systemic inflammation like the cecal ligation and puncture mouse model, where low to high grade septic conditions can be induced, may reveal further benefits of this formulation²²⁰. In a collaboration with the University Hospital Jena a project proposal for the testing of free BRP-201 injected i.p. in this model has been submitted to legal authorities and potential outcomes are further discussed in the last section of the discussion. However, such studies with an i.v. injection will be an important step for further evaluation of NP formulations with anti-

inflammatory drugs.

Together, our studies provided irrevocable proof for the suitability of polymeric NPs as delivery systems for drugs to be potentially applied in anti-inflammatory pharmacotherapy. The NPs were able to supply the hydrophobic cargo effectively inside the cells and furthermore increased the efficacy of the drugs upon long-term incubations. BRP-187 encapsulated into PLGA NPs showed high potency for specific suppression of PGE₂ in human M1 MDM. Finally, AceDex NPs carrying BRP-201 caused a strong increase of potency in human whole blood and reduced LTB₄ formation in mice *in vivo*, which is a significant step forward in the development of new options for anti-inflammatory treatments that circumvent the detrimental features of several (potential) drugs²⁹.

4.4. Promotion of SPM biosynthesis as new pharmacological approach

LTs and PGs are known since the 70s/80s and intensively studied over the past 50 years^{2,49,78}. Drugs that interfere with their production are known even longer, although the mode of action was only clarified after the discovery of the pro-inflammatory LMs²²¹. With the discovery of the pro-resolving actions of some oxidized lipids and the identification of a new class of LMs (namely the SPMs), the understanding of inflammation has changed. Resolution of inflammation is an active process, which needs to be “turned on”^{124,222}. Recent research provided evidence that inflammation related diseases are connected to low SPM levels, while the endogenous supply of SPMs or the SPM substrates DHA and EPA limits inflammation without suppression of the immune system or typical side-effects of established anti-inflammatory therapeutics^{6,223}. As a result, new strategies emerged that aim to enhance the resolution rather than to block the onset of inflammation^{22,127}. Since SPMs are mostly oxidized ω 3-PUFAs, the overall metabolic stability and therefore the bioavailability by oral as well as *i.v.* treatment is considered to be moderate, which lowers the effectiveness of supplying these mediators exogenously. The development of SPM receptor agonists is one possible approach to mimic the beneficial effects of SPMs. The investigated FRP2/ALX agonist ACT-389949 and 15(R/S)-methyl-LXA₄ displayed potential advantage in the treatment of asthmatic children with acute episodes and topical treatment of infantile eczema, but also recruited β -arrestin-mediated receptor internalization, which ultimately caused the ligands to act as functional “antagonists”^{132,224,225}.

SPMs are lipid mediators that act locally restricted at sites of their production in a paracrine and autocrine manner^{123,226}. Derived from this fact, another interesting approach is the enhancement of the local SPM and SPM precursor production, by modulation of the metabololipidome, the activation of 15-LOX-1 or the allosteric alteration of 5-LOX to favor 15-LOX product formation. In the section 4.2. of this discussion the effects of BRP-201 and MF-14/15 on the lipid mediator profile of MDM challenged with bacterial exotoxins was illustrated.

Further investigations presented in manuscript V and VI revealed additional benefits of these compounds that illustrates a new perspective of anti-inflammatory treatment and evokes the development of a new class of drugs – “lipid mediator class switch inducers”.

BRP-201 was developed as a multitarget inhibitor with potent activity on FLAP and mPGES-1, but a direct influence on SPM production of BRP-201 or any other balanced dual mPGES/FLAP inhibitor was never investigated⁵. In the studies presented in manuscript V, we incubated BRP-201 with unchallenged macrophages and observed an increase of 15-LOX products in M1 and M2 phenotypes. This effect was not observed by incubation of untreated MDM with BRP-187 (data not shown), which is a possible reason for the larger induction of 15-/12-LOX products as well as SPMs in MDM challenged with SACM compared to BRP-187. A direct activation of the 15-LOX-1 was confirmed via immunofluorescence microscopy (IF) and the incubation of unstimulated HEK-293 cells overexpressing 15-LOX-1. A potent induction of 12/15-LOX products was not only present in M2 but also in M1 macrophages, which express high amounts of FLAP and COX-2 but no 15-LOX-1. Hence, the activation of the constitutively expressed 15-LOX-2 was further investigated by a 15-LOX-2-transfected HEK cell system, where a direct influence of BRP-201 on this LOX was not confirmed. Additionally, the lipid mediator profile showed elevated 15-HETE, 15-HEPE and 17-HDHA, but also elevated levels of oxidized 12- and 14-PUFAs, which are not synthesized by 15-LOX-2. Notably, the amount of 5-HETE and 5-HEPE in unchallenged M1 macrophages after treatment with 3 μ M BRP-201 was elevated, while LTB₄ was even reduced, indicating that an activation of especially SPM biosynthetic pathways is initiated, rather than all LOXs pathways. The increase in 15-/12-LOX products due to BRP-201 is not associated with an elevated supply of PUFAs in contrast to MF-14/15, where the release of all PUFAs but especially EPA was increased significantly. MF-14/15 excessively increased 15-/12-LOX product formation in M1 and M2 macrophages, e.g. elevating 15-HETE to 92.5 -fold of baseline production as most pronounced effect. Immunofluorescence (IF) images revealed 15-LOX-1 activation after just 15 min upon MF-15 treatment, which appeared earlier than the control where cells were treated with SACM. Exogenous supply of AA, EPA and DHA to M2 MDM treated with MF-14/15 confirmed that the increase of 15-/12-LOX products was indeed due to enzyme activation and not just due to elevated fatty acid liberation. These effects observed in MDM were also confirmed in HEK cell systems overexpressing the indicated enzymes, with the highest influence on 15-LOX-1.

Triggering 15-/12-LOX product formation without additional stimulus was previously shown in human neutrophils, macrophages or in inflamed murine peritoneal exudates for 3-O-acetyl-11-keto boswellic acid (AKBA), the biflavanoid 8-methylsocotrin-4'-ol, and celastrol^{227–229}. A specific stimulation of 15-LOX-1 product formation in M2 macrophages was observed for the *S. aureus*-derived exotoxin α -hemolysin, which activates 15-LOX via the surface receptor a disintegrin and metalloproteinase domain-containing protein 10 (ADAM10)⁸. Due to equivalent

induction of 15-HETE and 17-HDHA, this mode of activation was tested for the MF14/15 but the ADAM10 inhibitor GI254023X did not affect MF-15-induced LM formation in contrast to α -hemolysin⁸. Interestingly, MF-14/15 seem to activate preferably 15-LOX-1, which is indicated by a much higher increase of 15-LOX products in M2 expressing 15-LOX-1 rather than in M1 expressing only moderate levels of 15-LOX-2. BRP-201 on the other hand induced e.g. 17-HDHA equally in unchallenged M1 and M2 MDM. Therefore, it can be assumed that the mode of activation of 15-LOX formation by both types of compounds is different. For BRP-201 it is conceivable that beside the substrate shunting effect and the direct activation of 15-LOX-1 in M2 the compound allosterically alters the preferred carbon for oxygen incorporation to carbon 12/15 while 5-LOX is interacting with FLAP. In experiments with non-immunocompetent transfected HEK293 cells 12/15-LOX products were increased with the influence of BRP-201 only in cells co-expressing 5-LOX and FLAP but not in cells expressing 5-LOX alone. The role of 5-LOX in SPM formation is intensively discussed over the past years. While 5-LOX, when interacting with FLAP at the nucleus membrane, favors production of LTB₄, activated 5-LOX in the cytoplasm favors production of LXA₄²³⁰. FLAP antagonists like MK-886 or as presented in this study BRP-187 are capable of inhibiting LT formation by membrane-bound 5-LOX but still enhance the progression of 15-HETE, 17-HDHA and 18-HEPE to SPMs in exotoxin-stimulated macrophages. This effect was also confirmed in vivo for MK-886 by zymosan-induced peritonitis or for BAY X-1005, which reduced cys-LTs and elevated SPM levels during a murine liver injury^{231,232}. But in contrast to conventional FLAP inhibitors, BRP-201 activates 15-LOX product formation also in M1 MDM, which is comparable to AKBA. The latter compound is able to alter the oxygenation of 5-LOX from carbon 5 to carbon 12/15, which leads to the production of 12-HETE and 15-HETE in neutrophils²²⁷. In case of BRP-201, taking into account that an increase of 15-HETE, 15-HEPE, 14-HDHA and 17-HDHA was only detectable in HEK cells expressing 5-LOX and FLAP, the compound acts as an AA mimic and could bind to FLAP thereby altering the process where the substrate is handed over to 5-LOX while LT formation. Thus, the position of oxygenation of AA, EPA or DHA in the cavity of 5-LOX seemingly changes due to the modulation of AA binding site of FLAP. While this mechanism is conceivable, supporting experiments are still missing. In fact, data on isolated neutrophils which express high amounts of 5-LOX and FLAP incubated with BRP-201 do not lead to sufficient 15-LOX product formation like AKBA.

Activation of 15-LOX-1 by BRP-201 was confirmed by IF microscopy indicating subcellular redistribution after 3 h of treatment in M2 MDM. In 2016 Meng et al. discovered activators of 15-LOX, that share structural elements with BRP-201 like the linked benzyl ring and the imidazole structure of the molecule²³³. These compounds are also found to shift the lipid mediator profile towards the resolution of inflammation. In molecular dynamics simulations the same authors proposed an allosteric activation of 15-LOX-1 at a second AA binding site, which

could also be applied to the activity of BRP-201²³⁴.

MF-14/15 as mentioned earlier are much stronger activators of 15-LOX-1 than BRP-201. While an allosteric modulation of LOXs is also conceivable by their structure, the chalcones have plenty of protein targets in human cells. A substantial difference versus BRP-201 is the strong antineoplastic effects of MF-14/15. The compounds are inhibitors of AKR1C3, which also has an influence on the lipidome by reducing PGD₂ and PGF_{2α}²³⁵. Therefore, PGD₂ is remarkably increased in SACM-challenged M1 and M2 MDM after chalcone treatment. Since PGD₂ is also responsible for the lipid mediator class switch, this could be of utmost importance for the initiation of the resolution phase¹⁹, although it should not have an effect on the short-term production on 15-LOX products in this experimental setup. Experiments with exogenous supply of PGD₂, where a change in the formation of 15-LOX products would give hints, may help to reveal if the autocrine effect of PGD₂ could cause such a response after just 180 min. Interestingly, in line with AKR1C3 inhibition, MF-15 appears to be superior to MF-14. Thus, the free rotation of the methyl-phenyl ring possible by sp³ conformation of the C-atoms of the link seem to have a major influence of the target binding.

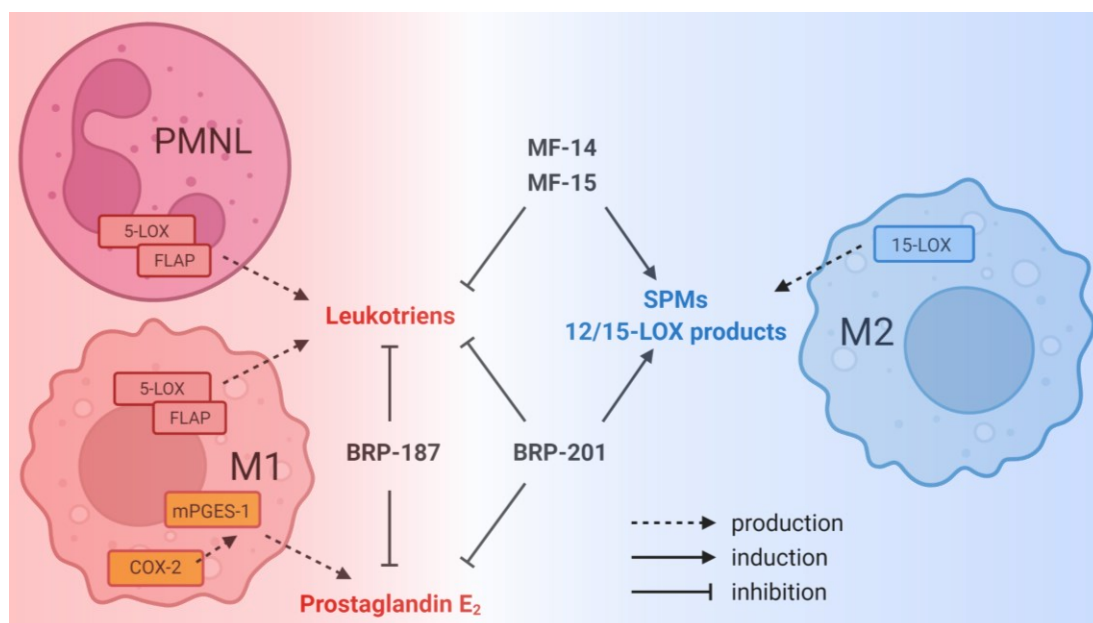


Figure 10 Schematic overview of the effects of BRP-187, BRP-201 and MF-14/15 in pro-inflammatory PMNL, M1 macrophages and anti-inflammatory M2 macrophages. BRP-187 and BRP-201 inhibit mPGES-1 derived PGE₂-formation and 5-LOX/FLAP derives LTB₄ formation, while BRP-201 also activates 15-LOX-1 derived SPM and SPM precursor production. MF-14/15 inhibit 5-LOX and rapidly induce 15-LOX product formation.

Conclusively, the chalcones and BRP-201 are strong activators of 15-LOX-1. They upregulate the formation of SPMs and their precursors that are crucial regulators of inflammation resolution²²². The data obtained in this study provides evidence to initiate the development of a new class of anti-inflammatory drugs – namely “lipid mediator class switch inducers”, which may have potential to revolutionize the therapy of many inflammation-related diseases with reduced side-effects.

4.5. Conclusion

The ever-rising threat of dysregulated inflammatory processes causes many different pathological disorders and can lead to harmful diseases like asthma, rheumatoid arthritis, Alzheimer disease, autoimmunity, arteriosclerosis, diabetes and even cancer¹⁷. Important for the regulation of the innate immune response are LMs derived from AA like PGE₂ and LTB₄², but available drugs for inhibition of these inflammation-driving mediators are often related to severe on-target side effects^{136,191}. To diminish the adverse effects of anti-inflammatory therapy, more specific inhibition of the downstream enzymes of LM biosynthesis are needed circumventing the interference with homeostatic mediators, and a deeper understanding of the influence of those drugs on the LM profile is mandatory. In this thesis, substantial knowledge on LM profile modulation was gathered by studying common and novel therapeutics on different types of macrophages. Here, the outstanding effects of dual inhibitors of mPGES-1 and FLAP were clearly pointed out. The investigated compounds were found to potently reduce formation of pro-inflammatory LT and PGE₂ in different cell types as well as in vivo, indicating a much safer profile for potential therapeutic usage against inflammatory diseases. In the course of the study, a polymeric-nanocarrier system was developed and investigated to efficiently transport the encapsulated compounds with unfavorable pharmacokinetic properties to the intracellular targets. The effectiveness of drug-loaded NPs was proven in different setups and the carrier system is able to enhance the effectiveness of BRP-187 against mPGES-1 and the potency of BRP-201 in human whole blood and in vivo. These findings are a major step forward in nanomedicine and might be milestone in the therapy of chronic inflammatory diseases related to LM.

In the past decades of research, the understanding of the inflammatory process changed with the discovery of SPMs. Therefore, the influence of the investigated drugs on SPM formation was examined in detail. The experiments with BRP-187, BRP-201 and MF-14/15 revealed highly beneficial effects on SPM and SPM precursor production. BRP-201 and MF-14/15 were found to activate the 15-LOX-1 and drastically enhance the production of SPMs. Alongside with few other compounds that are known yet, these potential drugs accomplish a favorable lipid mediator profile appropriate to cure inflammation with downregulated pro-inflammatory LMs and highly upregulated SPMs that will enhance the healing process. The data acquired in this study may contribute to change the future of anti-inflammatory therapy, where inflammation is not just inhibited but resolution is actively promoted by the help of small molecules and the introduction of a new class of drugs – the “lipid mediator class switch inducer” that fosters SPM formation.

5. References

1. Gilroy, D. W. & Bishop-Bailey, D. Lipid mediators in immune regulation and resolution. *British Journal of Pharmacology* vol. 176 (2019).
2. C. Funk. Prostaglandins and leukotrienes: Advances in eicosanoid biology. *Science (1979)* **294**, 1871–1875 (2001).
3. Banoglu, E. *et al.* 4,5-Diarylisoaxazol-3-carboxylic acids: A new class of leukotriene biosynthesis inhibitors potentially targeting 5-lipoxygenase-activating protein (FLAP). *European Journal of Medicinal Chemistry* **113**, 1–10 (2016).
4. Garscha, U. *et al.* BRP-187: A potent inhibitor of leukotriene biosynthesis that acts through impeding the dynamic 5-lipoxygenase/5-lipoxygenase-activating protein (FLAP) complex assembly. *Biochemical Pharmacology* **119**, 17–26 (2016).
5. Gür, Z. T. *et al.* Identification of multi-target inhibitors of leukotriene and prostaglandin E2 biosynthesis by structural tuning of the FLAP inhibitor BRP-7. *European Journal of Medicinal Chemistry* **150**, 876–899 (2018).
6. Fattori, V., Zaninelli, T. H., Rasquel-Oliveira, F. S., Casagrande, R. & Verri, W. A. Specialized pro-resolving lipid mediators: A new class of non-immunosuppressive and non-opioid analgesic drugs. *Pharmacological Research* **151**, 104549 (2020).
7. Ricciotti, E. & Fitzgerald, G. A. Prostaglandins and inflammation. *Arteriosclerosis, Thrombosis, and Vascular Biology* **31**, 986–1000 (2011).
8. Jordan, P. M. *et al.* Staphylococcus aureus-Derived α -Hemolysin Evokes Generation of Specialized Pro-resolving Mediators Promoting Inflammation Resolution. *Cell Reports* **33**, (2020).
9. Medzhitov, R. Origin and physiological roles of inflammation. *Nature* **454**, 428–435 (2008).
10. Ferrero-Miliani, L., Nielsen, O. H., Andersen, P. S. & Girardin, S. E. Chronic inflammation: Importance of NOD2 and NALP3 in interleukin-1 β generation. *Clinical and Experimental Immunology* **147**, 227–235 (2007).
11. Ley, K., Laudanna, C., Cybulsky, M. I. & Nourshargh, S. Getting to the site of inflammation: The leukocyte adhesion cascade updated. *Nature Reviews Immunology* **7**, 678–689 (2007).
12. Nathan, C. Points of control in inflammation. *Nature* **420**, 846–852 (2002).
13. Epstein, F. H. & Weiss, S. J. Tissue Destruction by Neutrophils. *New England Journal of Medicine* **320**, 365–376 (1989).
14. Robb, C. T., Dyrinda, E. A., Gray, R. D., Rossi, A. G. & Smith, V. J. Invertebrate extracellular phagocyte traps show that chromatin is an ancient defence weapon. *Nature Communications* **5**, (2014).
15. Unanue, E. R. *ANTIGEN-PRESENTING FUNCTION OF THE MACROPHAGE*. (1984).
16. den Haan, J. M. M., Arens, R. & van Zelm, M. C. The activation of the adaptive immune system: Cross-talk between antigen-presenting cells, T cells and B cells. *Immunology Letters* **162**, 103–112 (2014).
17. Medzhitov, R. Inflammation 2010: New Adventures of an Old Flame. *Cell* **140**, 771–776 (2010).
18. Headland, S. E. & Norling, L. v. The resolution of inflammation: Principles and challenges. *Seminars in Immunology* **27**, 149–160 (2015).
19. Serhan, C. N. & Savill, J. Resolution of inflammation: The beginning programs the end. *Nature Immunology* **6**, 1191–1197 (2005).
20. Feehan, K. T. & Gilroy, D. W. Is Resolution the End of Inflammation? *Trends in Molecular Medicine* **25**, 198–214 (2019).
21. Machado, F. S. & Aliberti, J. Role of lipoxin in the modulation of immune response during infection. *International Immunopharmacology* **8**, 1316–1319 (2008).
22. Serhan, C. N., Chiang, N. & Van Dyke, T. E. Resolving inflammation: Dual anti-inflammatory and pro-resolution lipid mediators. *Nature Reviews Immunology* **8**, 349–361 (2008).
23. Chen, J. *et al.* RvE1 Attenuates Polymicrobial Sepsis-Induced Cardiac Dysfunction and Enhances Bacterial Clearance. *Frontiers in Immunology* **11**, 1–15 (2020).
24. Ravichandran, K. S. Beginnings of a Good Apoptotic Meal: The Find-Me and Eat-Me Signaling Pathways. *Immunity* **35**, 445–455 (2011).
25. Perretti, M. The resolution of inflammation: New mechanisms in patho-physiology open opportunities for pharmacology. *Seminars in Immunology* **27**, 145–148 (2015).
26. Nathan, C. & Ding, A. Nonresolving Inflammation. *Cell* **140**, 871–882 (2010).
27. Uysal, H. *et al.* Structure and pathogenicity of antibodies specific for citrullinated collagen type II in experimental arthritis. *Journal of Experimental Medicine* **206**, 449–462 (2009).

28. Han, H. *et al.* Calcium-sensing soluble adenylyl cyclase mediates TNF signal transduction in human neutrophils. *Journal of Experimental Medicine* **202**, 353–361 (2005).
29. Tabas Ira & Christopher, G. Anti-Inflammatory Therapy in Chronic Disease: Challenges and Opportunities. *Science (1979)* **339**, 166–172 (2013).
30. Chistiakov, D. A., Melnichenko, A. A., Grechko, A. V., Myasoedova, V. A. & Orekhov, A. N. Potential of anti-inflammatory agents for treatment of atherosclerosis. *Experimental and Molecular Pathology* **104**, 114–124 (2018).
31. Richter, A. *et al.* Impact of treatment with biologic DMARDs on the risk of sepsis or mortality after serious infection in patients with rheumatoid arthritis. *Annals of the Rheumatic Diseases* **75**, 1667–1673 (2016).
32. Pawelec, G., Goldeck, D. & Derhovanessian, E. Inflammation, ageing and chronic disease. *Current Opinion in Immunology* **29**, 23–28 (2014).
33. Sousa, L. P., Alessandri, A. L., Pinho, V. & Teixeira, M. M. Pharmacological strategies to resolve acute inflammation. *Current Opinion in Pharmacology* **13**, 625–631 (2013).
34. Mouchlis, V. D. & Dennis, E. A. Phospholipase A 2 catalysis and lipid mediator lipidomics. *Biochimica et Biophysica Acta - Molecular and Cell Biology of Lipids* **1864**, 766–771 (2019).
35. Dennis, E. A. and P. C. N. Eicosanoid storm in infection and inflammation. *Nature Reviews Immunology* **11**, 511–523 (2015).
36. Serhan, C. N., Chiang, N., Dalli, J. & Levy, B. D. Lipid mediators in the resolution of inflammation. *Cold Spring Harbor Perspectives in Biology* **7**, (2015).
37. Borgeat, P., Hamberg, M. & Samuelsson, B. Transformation of arachidonic acid and homo γ linolenic acid by rabbit polymorphonuclear leukocytes. Monohydroxy acids from novel lipoxygenases. *Journal of Biological Chemistry* **251**, 7816–7820 (1976).
38. Samuelsson, B. Leukotrienes: a new class of mediators of immediate hypersensitivity reactions and inflammation. *Adv Prostaglandin Thromboxane Leukot Res* **11**, 1–13 (1983).
39. Borgeat, P. & Samuelsson, B. Arachidonic acid metabolism in polymorphonuclear leukocytes: Unstable intermediate in formation of dihydroxy acids. *Proc Natl Acad Sci U S A* **76**, 3213–3217 (1979).
40. Funk, C. D., Hoshiko, S., Matsumoto, T., Radmark, O. & Samuelsson, B. Characterization of the human 5-lipoxygenase gene. 2587–2591 (1989).
41. Gilbert, N. C. *et al.* The Structure of Human 5-Lipoxygenase. **331**, 217–220 (2011).
42. Gerstmeier, J. *et al.* 5-Lipoxygenase-activating protein rescues activity of 5-lipoxygenase mutations that delay nuclear membrane association and disrupt product formation. *FASEB Journal* **30**, 1892–1900 (2016).
43. Werz, O. & Steinhilber, D. Therapeutic options for 5-lipoxygenase inhibitors. *Pharmacology and Therapeutics* **112**, 701–718 (2006).
44. Kulkarni, S., Das, S., Funk, C. D., Murray, D. & Cho, W. Molecular Basis of the Specific Subcellular Localization of the C2-like Domain of 5-Lipoxygenase. *Journal of Biological Chemistry* **277**, 13167–13174 (2002).
45. Werz, O., Klemm, J., Samuelsson, B. & Rådmark, O. 5-Lipoxygenase is phosphorylated by p38 kinase-dependent MAPKAP kinases. *Proc Natl Acad Sci U S A* **97**, 5261–5266 (2000).
46. Luo, M. *et al.* Protein kinase A inhibits leukotriene synthesis by phosphorylation of 5-lipoxygenase on serine 523. *J Biol Chem* **279**, 41512–20 (2004).
47. Percival, M. D. Human 5-lipoxygenase contains an essential iron. *Journal of Biological Chemistry* **266**, 10058–10061 (1991).
48. Chasteen, N. D. *et al.* Characterization of the non-heme iron center of human 5-lipoxygenase by electron paramagnetic resonance, fluorescence, and ultraviolet-visible spectroscopy: redox cycling between ferrous and ferric states. *Biochemistry* **32**, 9763–71 (1993).
49. Panossian, A., Hamberg, M. & Samuelsson, B. On the mechanism of biosynthesis of leukotrienes and related compounds. *FEBS Letters* **150**, 511–513 (1982).
50. Maas, R. L., Ingram, C. D., Taber, D. F., Oates, J. A. & Brash, A. R. Stereospecific removal of the DR hydrogen atom at the 10-carbon of arachidonic acid in the biosynthesis of leukotriene A₄ by human leukocytes. *J Biol Chem* **257**, 13515–9 (1982).
51. Rådmark, O. & Samuelsson, B. 5-Lipoxygenase: Mechanisms of regulation. *Journal of Lipid Research* **50**, 40–45 (2009).
52. Häfner, A. K., Kahnt, A. S. & Steinhilber, D. Beyond leukotriene formation—The noncanonical functions of 5-lipoxygenase. *Prostaglandins and Other Lipid Mediators* **142**, 24–32 (2019).
53. Percival, M. D., Denis, D., Riendeau, D. & Gresser, M. J. Investigation of the mechanism of non-turnover-dependent inactivation of purified human 5-lipoxygenase. Inactivation by H₂O₂ and inhibition by metal ions. *Eur J Biochem* **210**, 109–17 (1992).
54. Aharony, D., Redkar-Brown, D. G., Hubbs, S. J. & Stein, R. L. Kinetic studies on the inactivation of 5-lipoxygenase by 5(S)-hydroperoxyeicosatetraenoic acid. *Prostaglandins* **33**,

- 85–100 (1987).
55. Lepley, R. A. & Fitzpatrick, F. A. Irreversible inactivation of 5-lipoxygenase by leukotriene A4. Characterization of product inactivation with purified enzyme and intact leukocytes. *J Biol Chem* **269**, 2627–31 (1994).
 56. Haeggström, J. Z. Leukotriene A4 hydrolase/aminopeptidase, the gatekeeper of chemotactic leukotriene B4 biosynthesis. *Journal of Biological Chemistry* **279**, 50639–50642 (2004).
 57. Lam, B. K., Penrose, J. F., Freeman, G. J. & Austen, K. F. Expression cloning of a cDNA for human leukotriene C4 synthase, an integral membrane protein conjugating reduced glutathione to leukotriene A4. *Proc Natl Acad Sci U S A* **91**, 7663–7 (1994).
 58. Welsch, D. J. *et al.* Molecular cloning and expression of human leukotriene-C4 synthase. *Proc Natl Acad Sci U S A* **91**, 9745–9 (1994).
 59. Jakobsson, P. J., Morgenstern, R., Mancini, J., Ford-Hutchinson, A. & Persson, B. Common structural features of MAPEG -- a widespread superfamily of membrane associated proteins with highly divergent functions in eicosanoid and glutathione metabolism. *Protein Sci* **8**, 689–92 (1999).
 60. Haeggström, J. Z. & Wetterholm, A. Enzymes and receptors in the leukotriene cascade. *Cellular and Molecular Life Sciences* **59**, 742–753 (2002).
 61. Sasaki, F. & Yokomizo, T. The leukotriene receptors as therapeutic targets of inflammatory diseases. *International Immunology* **31**, 607–615 (2019).
 62. Tager, A. M. & Luster, A. D. BLT1 and BLT2: The leukotriene B4 receptors. *Prostaglandins Leukotrienes and Essential Fatty Acids* **69**, 123–134 (2003).
 63. Yokomizo, T., Kato, K., Terawaki, K., Izumi, T. & Shimizu, T. A second leukotriene B(4) receptor, BLT2. A new therapeutic target in inflammation and immunological disorders. *J Exp Med* **192**, 421–32 (2000).
 64. Yokomizo, T., Izumi, T., Chang, K., Takuwa, Y. & Shimizu, T. A G-protein-coupled receptor for leukotriene B4 that mediates chemotaxis. *Nature* **387**, 620–4 (1997).
 65. Minigh, J. Leukotriene B4. *xPharm: The Comprehensive Pharmacology Reference* **30**, 1–4 (2007).
 66. Narala, V. R. *et al.* Leukotriene B4 is a physiologically relevant endogenous peroxisome proliferator-activated receptor- α agonist. *Journal of Biological Chemistry* **285**, 22067–22074 (2010).
 67. Lynch, K. R. *et al.* Characterization of the human cysteinyl leukotriene CysLT1 receptor. *Nature* **399**, 789–793 (1999).
 68. Häfner, A. K. *et al.* Characterization of the interaction of human 5-lipoxygenase with its activating protein FLAP. *Biochimica et Biophysica Acta - Molecular and Cell Biology of Lipids* **1851**, 1465–1472 (2015).
 69. Dixon, R. A. F., Diehl, R. E., Opast, E., Rands, E. & Millerll, D. K. Requirement of a 5-lipoxygenase-activating protein for leukotriene synthesis. **343**, 282–284 (1990).
 70. Ferguson, A. D. *et al.* Crystal Structure of 5-Lipoxygenase – Activating Protein. *Science* (1979) **1**, 510–512 (2007).
 71. Evans, J. F., Ferguson, A. D., Mosley, R. T. & Hutchinson, J. H. What's all the FLAP about?: 5-lipoxygenase-activating protein inhibitors for inflammatory diseases. *Trends in Pharmacological Sciences* **29**, 72–78 (2008).
 72. Pergola, C. *et al.* The novel benzimidazole derivative BRP-7 inhibits leukotriene biosynthesis in vitro and in vivo by targeting 5-lipoxygenase-activating protein (FLAP). *British Journal of Pharmacology* **171**, 3051–3064 (2014).
 73. Garscha, U. *et al.* Pharmacological profile and efficiency in vivo of diflapolin, the first dual inhibitor of 5-lipoxygenase-activating protein and soluble epoxide hydrolase. *Scientific Reports* **7**, 1–14 (2017).
 74. Abramovitz, M. *et al.* 5-Lipoxygenase-activating protein stimulates the utilization of arachidonic acid by 5-lipoxygenase. *European Journal of Biochemistry* **215**, 105–111 (1993).
 75. Byrum, R. S., Goulet, J. L., Griffiths, R. J. & Koller, B. H. Role of the 5-lipoxygenase-activating protein (FLAP) in murine acute inflammatory responses. *J Exp Med* **185**, 1065–75 (1997).
 76. Rouzer, C. A. *et al.* Characterization of cloned human leukocyte 5-lipoxygenase expressed in mammalian cells. *J Biol Chem* **263**, 10135–40 (1988).
 77. Chandrasekharan, N. V. & Simmons, D. L. The cyclooxygenases. *Genome Biology* **5**, 1–7 (2004).
 78. Hemler, M., Lands, W. E. M. & Smith, W. L. Purification of the cyclooxygenase that forms prostaglandins. Demonstration of two forms of iron in the holoenzyme. *Journal of Biological Chemistry* **251**, 5575–5579 (1976).
 79. Miyamoto, T., Ogino, N., Yamamoto, S. & Hayaishi, O. Purification of prostaglandin endoperoxide synthetase from bovine vesicular gland microsomes. *Journal of Biological*

- Chemistry* **251**, 2629–2636 (1976).
80. Kujubu, D. A., Fletcher, B. S., Varnum, B. C., Lim, R. W. & Herschman, H. R. TIS10, a phorbol ester tumor promoter-inducible mRNA from Swiss 3T3 cells, encodes a novel prostaglandin synthase/cyclooxygenase homologue. *J Biol Chem* **266**, 12866–72 (1991).
 81. Xie, W. L., Chipman, J. G., Robertson, D. L., Erikson, R. L. & Simmons, D. L. Expression of a mitogen-responsive gene encoding prostaglandin synthase is regulated by mRNA splicing. *Proc Natl Acad Sci U S A* **88**, 2692–6 (1991).
 82. Vane, J. R., Bakhle, Y. S. & Botting, R. M. Cyclooxygenases 1 and 2. *Annual Review of Pharmacology and Toxicology* **38**, 97–120 (1998).
 83. Kang, Y.-J., Mbonye, U. R., DeLong, C. J., Wada, M. & Smith, W. L. Regulation of intracellular cyclooxygenase levels by gene transcription and protein degradation. *Prog Lipid Res* **46**, 108–25 (2007).
 84. Tanabe, T. & Tohnai, N. Cyclooxygenase isozymes and their gene structures and expression. *Prostaglandins Other Lipid Mediat* **68–69**, 95–114 (2002).
 85. Orlando, B. J. & Malkowski, M. G. Crystal structure of rofecoxib bound to human cyclooxygenase-2. *Acta Crystallographica Section:F Structural Biology Communications* **72**, 772–776 (2016).
 86. Garavito, R. M., Malkowski, M. G. & DeWitt, D. L. The structures of prostaglandin endoperoxide H synthases-1 and -2. *Prostaglandins Other Lipid Mediat* **68–69**, 129–52 (2002).
 87. Smith, W. L., Dewitt, D. L. & Garavito, R. M. CYCLOOXYGENASES : Structural , Cellular , and. *Annu Rev Biochem* **69**, 145–182 (2000).
 88. Smith, W. L., Urade, Y. & Jakobsson, P. J. Enzymes of the cyclooxygenase pathways of prostanoid biosynthesis. *Chemical Reviews* **111**, 5821–5865 (2011).
 89. Sugimoto, Y. & Narumiya, S. Prostaglandin E receptors. *Journal of Biological Chemistry* **282**, 11613–11617 (2007).
 90. Moriyama, T. *et al.* Sensitization of TRPV1 by EP1 and IP reveals peripheral nociceptive mechanism of prostaglandins. *Mol Pain* **1**, 3 (2005).
 91. Konya, V., Marsche, G., Schuligoi, R. & Heinemann, A. E-type prostanoid receptor 4 (EP4) in disease and therapy. *Pharmacology and Therapeutics* **138**, 485–502 (2013).
 92. Caggiano, A. O. & Kraig, R. P. Prostaglandin E2 and 4-aminopyridine prevent the lipopolysaccharide-induced outwardly rectifying potassium current and interleukin-1beta production in cultured rat microglia. *J Neurochem* **70**, 2357–68 (1998).
 93. Noda, M. *et al.* Neuroprotective role of bradykinin because of the attenuation of pro-inflammatory cytokine release from activated microglia. *J Neurochem* **101**, 397–410 (2007).
 94. Kawabe, J., Ushikubi, F. & Hasebe, N. Prostacyclin in vascular diseases. - Recent insights and future perspectives -. *Circ J* **74**, 836–43 (2010).
 95. Félétou, M., Verbeuren, T. J. & Vanhoutte, P. M. Endothelium-dependent contractions in SHR: a tale of prostanoid TP and IP receptors. *Br J Pharmacol* **156**, 563–74 (2009).
 96. McAdam, B. F. *et al.* Effect of regulated expression of human cyclooxygenase isoforms on eicosanoid and isoeicosanoid production in inflammation. *J Clin Invest* **105**, 1473–82 (2000).
 97. Gilroy, D. W. *et al.* Inducible cyclooxygenase may have anti-inflammatory properties. *Nature Medicine* **5**, 698–701 (1999).
 98. Morteau, O. *et al.* Impaired mucosal defense to acute colonic injury in mice lacking cyclooxygenase-1 or cyclooxygenase-2. *J Clin Invest* **105**, 469–78 (2000).
 99. Aoki, T. & Narumiya, S. Prostaglandins and chronic inflammation. *Trends in Pharmacological Sciences* **33**, 304–311 (2012).
 100. Funk, C. D. & FitzGerald, G. A. COX-2 inhibitors and cardiovascular risk. *Journal of Cardiovascular Pharmacology* **50**, 470–479 (2007).
 101. Ogino, N., Miyamoto, T., Yamamoto, S. & Hayaishi, O. Prostaglandin endoperoxide E isomerase from bovine vesicular gland microsomes, a glutathione-requiring enzyme. *J Biol Chem* **252**, 890–5 (1977).
 102. Tanaka, Y., Ward, S. L. & Smith, W. L. Immunochemical and kinetic evidence for two different prostaglandin H-prostaglandin E isomerases in sheep vesicular gland microsomes. *J Biol Chem* **262**, 1374–81 (1987).
 103. Murakami, M. *et al.* Regulation of prostaglandin E2 biosynthesis by inducible membrane-associated prostaglandin E2 synthase that acts in concert with cyclooxygenase-2. *Journal of Biological Chemistry* **275**, 32783–32792 (2000).
 104. Sjögren, T. *et al.* Crystal structure of microsomal prostaglandin E2 synthase provides insight into diversity in the MAPEG superfamily. *Proc Natl Acad Sci U S A* **110**, 3806–3811 (2013).
 105. Koeberle, A. & Werz, O. Perspective of microsomal prostaglandin E2 synthase-1 as drug target in inflammation-related disorders. *Biochemical Pharmacology* **98**, 1–15 (2015).
 106. Hammarberg, T. *et al.* Mutation of a critical arginine in microsomal prostaglandin e synthase-1

- shifts the isomerase activity to a reductase activity that converts prostaglandin H2 into prostaglandin F2 α . *Journal of Biological Chemistry* **284**, 301–305 (2009).
107. Trebino, C. E. *et al.* Impaired inflammatory and pain responses in mice lacking an inducible prostaglandin E synthase. *Proc Natl Acad Sci U S A* **100**, 9044–9 (2003).
 108. Kamei, D. *et al.* Reduced pain hypersensitivity and inflammation in mice lacking microsomal prostaglandin E synthase-1. *Journal of Biological Chemistry* **279**, 33684–33695 (2004).
 109. Kuhn, H. & Thiele, B. J. The diversity of the lipoxygenase family. Many sequence data but little information on biological significance. *FEBS Letters* **449**, 7–11 (1999).
 110. Schewe, T., Halangk, W., Hiebsch, C. & Rapoport, S. M. A lipoxygenase in rabbit reticulocytes which attacks phospholipids and intact mitochondria. *FEBS Lett* **60**, 149–52 (1975).
 111. Sigal, E. *et al.* Arachidonate 15-lipoxygenase from human eosinophil-enriched leukocytes: partial purification and properties. *Biochem Biophys Res Commun* **150**, 376–83 (1988).
 112. Brash, A. R., Boeglin, W. E. & Chang, M. S. Discovery of a second 15S-lipoxygenase in humans. *Proc Natl Acad Sci U S A* **94**, 6148–52 (1997).
 113. Kuhn, H., Banthiya, S. & Van Leyen, K. Mammalian lipoxygenases and their biological relevance. *Biochimica et Biophysica Acta - Molecular and Cell Biology of Lipids* **1851**, 308–330 (2015).
 114. Rooks, M.G and Garrett, W.S, 2016. Structural and functional biology of arachidonic acid 15-lipoxygenase-1 (ALOX15). *Physiol Behav* **573**, 1–32 (2015).
 115. Kobe, M. J., Neau, D. B., Mitchell, C. E., Bartlett, S. G. & Newcomer, M. E. The structure of human 15-lipoxygenase-2 with a substrate mimic. *Journal of Biological Chemistry* **289**, 8562–8569 (2014).
 116. Snodgrass, R. G. & Brüne, B. Regulation and Functions of 15-Lipoxygenases in Human Macrophages. *Frontiers in Pharmacology* **10**, 1–12 (2019).
 117. Schwarz, K., Borngräber, S., Anton, M. & Kuhn, H. Probing the substrate alignment at the active site of 15-lipoxygenases by targeted substrate modification and site-directed mutagenesis. Evidence for an inverse substrate orientation. *Biochemistry* **37**, 15327–35 (1998).
 118. Conrad, D. J., Kuhn, H., Mulkins, M., Highland, E. & Sigal, E. Specific inflammatory cytokines regulate the expression of human monocyte 15-lipoxygenase. *Proc Natl Acad Sci U S A* **89**, 217–221 (1992).
 119. Jisaka, M., Kim, R. B., Boeglin, W. E., Nanney, L. B. & Brash, A. R. Molecular cloning and functional expression of a phorbol ester-inducible 8S-lipoxygenase from mouse skin. *Journal of Biological Chemistry* **272**, 24410–24416 (1997).
 120. Brash, A. R., Boeglin, W. E. & Chang, M. S. Discovery of a second 15S-lipoxygenase in humans. *Proc Natl Acad Sci U S A* **94**, 6148–52 (1997).
 121. Finkbeiner, E. & Highland, E. Cloning of human to the reticulocyte airway 154lipoxygenase : enzyme and expression identity in epithelium ditions using rabbit reticulocyte RNA as a standard (Fig . (2020).
 122. Werz, O. *et al.* Human macrophages differentially produce specific resolvin or leukotriene signals that depend on bacterial pathogenicity. *Nature Communications* **9**, 1–12 (2018).
 123. Serhan, C. N. & Levy, B. D. Resolvins in inflammation: Emergence of the pro-resolving superfamily of mediators. *Journal of Clinical Investigation* vol. 128 2657–2669 (2018).
 124. Levy, B. D., Clish, C. B., Schmidt, B., Gronert, K. & Serhan, C. N. Lipid mediator class switching during acute inflammation: Signals in resolution. *Nature Immunology* **2**, 612–619 (2001).
 125. Serhan, C. N. Lipoxins and aspirin-triggered 15-epi-lipoxins are the first lipid mediators of endogenous anti-inflammation and resolution. *Prostaglandins Leukotrienes and Essential Fatty Acids* **73**, 141–162 (2005).
 126. Clish, C. B. *et al.* Local and systemic delivery of a stable aspirin-triggered lipoxin prevents neutrophil recruitment in vivo. *Proc Natl Acad Sci U S A* **96**, 8247–8252 (1999).
 127. Serhan, C. N. Pro-resolving lipid mediators are leads for resolution physiology. *Nature* **510**, 92–101 (2014).
 128. Serhan, C. N. & Petasis, N. A. Resolvins and protectins in inflammation resolution. *Chemical Reviews* **111**, 5922–5943 (2011).
 129. Serhan, C. N. *et al.* Novel functional sets of lipid-derived mediators with antiinflammatory actions generated from omega-3 fatty acids via cyclooxygenase 2-nonsteroidal antiinflammatory drugs and transcellular processing. *Journal of Experimental Medicine* **192**, 1197–1204 (2000).
 130. Dalli, J. *et al.* The novel 13S,14S-epoxy-maresin is converted by human macrophages to maresin 1 (MaR1), inhibits leukotriene A4 hydrolase (LTA4H), and shifts macrophage phenotype. *FASEB J* **27**, 2573–83 (2013).
 131. Deng, B. *et al.* Maresin biosynthesis and identification of maresin 2, a new anti-inflammatory

- and pro-resolving mediator from human macrophages. *PLoS One* **9**, e102362 (2014).
132. Park, J., Langmead, C. J. & Riddey, D. M. New Advances in Targeting the Resolution of Inflammation: Implications for Specialized Pro-Resolving Mediator GPCR Drug Discovery. *ACS Pharmacology and Translational Science* **3**, 88–106 (2020).
 133. Chiang, N. & Serhan, C. N. Specialized pro-resolving mediator network: an update on production and actions. *Essays Biochem* **64**, 443–462 (2020).
 134. Basil, M. C. & Levy, B. D. Specialized pro-resolving mediators: Endogenous regulators of infection and inflammation. *Nature Reviews Immunology* vol. 16 (2016).
 135. Desborough, M. J. R. & Keeling, D. M. The aspirin story – from willow to wonder drug. *British Journal of Haematology* **177**, 674–683 (2017).
 136. Hawkey, C. J. COX-1 and COX-2 inhibitors. *Best Practice and Research: Clinical Gastroenterology* **15**, 801–820 (2001).
 137. Koeberle, A., Laufer, S. A. & Werz, O. Design and Development of Microsomal Prostaglandin E2 Synthase-1 Inhibitors: Challenges and Future Directions. *Journal of Medicinal Chemistry* **59**, 5970–5986 (2016).
 138. Westman, M. *et al.* Expression of microsomal prostaglandin E synthase 1 in rheumatoid arthritis synovium. *Arthritis Rheum* **50**, 1774–80 (2004).
 139. Chaudhry, U. A., Zhuang, H., Crain, B. J. & Doré, S. Elevated microsomal prostaglandin-E synthase-1 in Alzheimer's disease. *Alzheimers Dement* **4**, 6–13 (2008).
 140. Kihara, Y. *et al.* Targeted lipidomics reveals mPGES-1-PGE2 as a therapeutic target for multiple sclerosis. *Proc Natl Acad Sci U S A* **106**, 21807–12 (2009).
 141. Gómez-Hernández, A. *et al.* Overexpression of COX-2, Prostaglandin E synthase-1 and prostaglandin E receptors in blood mononuclear cells and plaque of patients with carotid atherosclerosis: regulation by nuclear factor-kappaB. *Atherosclerosis* **187**, 139–49 (2006).
 142. Bergqvist, F., Morgenstern, R. & Jakobsson, P.-J. A review on mPGES-1 inhibitors: From preclinical studies to clinical applications. *Prostaglandins & Other Lipid Mediators* **147**, 106383 (2020).
 143. Jin, Y. *et al.* Pharmacodynamic comparison of LY3023703, a novel microsomal prostaglandin e synthase 1 inhibitor, with celecoxib. *Clin Pharmacol Ther* **99**, 274–84 (2016).
 144. Jin, Y. *et al.* Dose-dependent acute liver injury with hypersensitivity features in humans due to a novel microsomal prostaglandin E synthase 1 inhibitor. *Br J Clin Pharmacol* **84**, 179–188 (2018).
 145. Norman, B. H. *et al.* Identification and Mitigation of Reactive Metabolites of 2-Aminoimidazole-Containing Microsomal Prostaglandin E Synthase-1 Inhibitors Terminated Due to Clinical Drug-Induced Liver Injury. *J Med Chem* **61**, 2041–2051 (2018).
 146. Pergola, C. & Werz, O. 5-Lipoxygenase inhibitors: A review of recent developments and patents. *Expert Opinion on Therapeutic Patents* **20**, 355–375 (2010).
 147. Werz, O.; Gerstmeier, J.; Garscha, U. Novel leukotriene biosynthesis inhibitors (2012-2016) as anti-inflammatory agents. *Expert Opinion on Therapeutic Patents* **27(5)**, 607–620 (2017).
 148. Hamad, A. M., Sutcliffe, A. M. & Knox, A. J. Aspirin-induced asthma: clinical aspects, pathogenesis and management. *Drugs* **64**, 2417–32 (2004).
 149. Laufer, S., Tries, S., Augustin, J. & Dannhardt, G. Pharmacological profile of a new pyrrolizine derivative inhibiting the enzymes cyclo-oxygenase and 5-lipoxygenase. *Arzneimittelforschung* **44**, 629–36 (1994).
 150. Koeberle, A. *et al.* Pirinixic acid derivatives as novel dual inhibitors of microsomal prostaglandin E2 synthase-1 and 5-lipoxygenase. *Journal of Medicinal Chemistry* **51**, 8068–8076 (2008).
 151. Zhou, P., Babcock, J., Liu, L., Li, M. & Gao, Z. Activation of human ether-a-go-go related gene (hERG) potassium channels by small molecules. *Acta Pharmacol Sin* **32**, 781–8 (2011).
 152. Banoglu, E. *et al.* Identification of novel benzimidazole derivatives as inhibitors of leukotriene biosynthesis by virtual screening targeting 5-lipoxygenase-activating protein (FLAP). *Bioorganic and Medicinal Chemistry* **20**, 3728–3741 (2012).
 153. Çalişkan, B., Luderer, S., Özkan, Y., Werz, O. & Banoglu, E. Pyrazol-3-propanoic acid derivatives as novel inhibitors of leukotriene biosynthesis in human neutrophils. *European Journal of Medicinal Chemistry* **46**, 5021–5033 (2011).
 154. Mayr, F. *et al.* Finding new molecular targets of familiar natural products using in silico target prediction. *International Journal of Molecular Sciences* **21**, 1–18 (2020).
 155. Meng, W. *et al.* Discovery of dapagliflozin: a potent, selective renal sodium-dependent glucose cotransporter 2 (SGLT2) inhibitor for the treatment of type 2 diabetes. *J Med Chem* **51**, 1145–9 (2008).
 156. Uthman, L. *et al.* Direct Cardiac Actions of Sodium Glucose Cotransporter 2 Inhibitors Target Pathogenic Mechanisms Underlying Heart Failure in Diabetic Patients. *Front Physiol* **9**, 1575 (2018).

157. Kafka, M. *et al.* Dual inhibitory action of a novel akr1c3 inhibitor on both full-length ar and the variant AR-V7 in enzalutamide resistant metastatic castration resistant prostate cancer. *Cancers (Basel)* **12**, 1–18 (2020).
158. Qi, W. *et al.* Cardamonin protects against doxorubicin-induced cardiotoxicity in mice by restraining oxidative stress and inflammation associated with Nrf2 signaling. *Biomedicine & Pharmacotherapy* **122**, 109547 (2020).
159. Hou, S. *et al.* Cardamonin attenuates chronic inflammation and tumorigenesis in colon. *Cell Cycle* **18**, 3275–3287 (2019).
160. Engels, N. S. H. Discovery of Novel Anti-inflammatory Natural Products Isolated from Plants Used in Traditional Vietnamese Medicine. *Ph.D. Dissertation Universität Innsbruck* (2019).
161. Limeres, M. J., Moretton, M. A., Bernabeu, E., Chiappetta, D. A. & Cuestas, M. L. Thinking small, doing big: Current success and future trends in drug delivery systems for improving cancer therapy with special focus on liver cancer. *Mater Sci Eng C Mater Biol Appl* **95**, 328–341 (2019).
162. Parveen, S., Misra, R. & Sahoo, S. K. Nanoparticles: a boon to drug delivery, therapeutics, diagnostics and imaging. *Nanomedicine* **8**, 147–66 (2012).
163. Webster, T. J. Nanomedicine: what's in a definition? *Int J Nanomedicine* **1**, 115–6 (2006).
164. Satalkar, P., Elger, B. S. & Shaw, D. M. Defining Nano, Nanotechnology and Nanomedicine: Why Should It Matter? *Sci Eng Ethics* **22**, 1255–1276 (2016).
165. Widger, A., Triano, C., Alatovic, J. & Sylke Maas, Ph. D. Pfizer and BioNTech Achieve First Authorization in the World for a Vaccine to Combat COVID-19. <https://investors.biontech.de/news-releases/news-release-details/pfizer-and-biontech-achieve-first-authorization-world-vaccine/>.
166. Flühmann, B., Ntai, I., Borchard, G., Simoens, S. & Mühlebach, S. Nanomedicines: The magic bullets reaching their target? *European Journal of Pharmaceutical Sciences* **128**, 73–80 (2019).
167. DiMasi, J. A., Grabowski, H. G. & Hansen, R. W. Innovation in the pharmaceutical industry: New estimates of R&D costs. *Journal of Health Economics* **47**, 20–33 (2016).
168. Choi, Y. H. & Han, H.-K. Nanomedicines: current status and future perspectives in aspect of drug delivery and pharmacokinetics. *J Pharm Investig* **48**, 43–60 (2018).
169. Ventola, C. L. Progress in Nanomedicine: Approved and Investigational Nanodrugs. *P T* **42**, 742–755 (2017).
170. Din, F. U. *et al.* Effective use of nanocarriers as drug delivery systems for the treatment of selected tumors. *Int J Nanomedicine* **12**, 7291–7309 (2017).
171. Fornaguera, C. & García-Celma, M. J. Personalized Nanomedicine: A Revolution at the Nanoscale. *J Pers Med* **7**, (2017).
172. El-Say, K. M. & El-Sawy, H. S. Polymeric nanoparticles: Promising platform for drug delivery. *Int J Pharm* **528**, 675–691 (2017).
173. Kamaly, N., Yameen, B., Wu, J. & Farokhzad, O. C. Degradable Controlled-Release Polymers and Polymeric Nanoparticles: Mechanisms of Controlling Drug Release. *Chem Rev* **116**, 2602–63 (2016).
174. Escudero, A., Carregal-Romero, S., Miguel-Coello, A. B. & Ruíz-Cabello, J. Engineered polymeric nanovehicles for drug delivery. in *Colloids for nanobiotechnology* (eds. Parak, W. J. & Feliu, N.) vol. 16 201–232 (Elsevier, 2020).
175. Gentile, P., Chiono, V., Carmagnola, I. & Hatton, P. V. An overview of poly(lactic-co-glycolic) acid (PLGA)-based biomaterials for bone tissue engineering. *Int J Mol Sci* **15**, 3640–59 (2014).
176. Wang, Y., Qin, B., Xia, G. & Choi, S. H. FDA's Poly (Lactic-Co-Glycolic Acid) Research Program and Regulatory Outcomes. *AAPS J* **23**, 92 (2021).
177. Bachelder, E. M., Pino, E. N. & Ainslie, K. M. Acetalated dextran: A tunable and acid-labile biopolymer with facile synthesis and a range of applications. *Chemical Reviews* **117**, 1915–1926 (2017).
178. Broaders, K. E., Cohen, J. A., Beaudette, T. T., Bachelder, E. M. & Fréchet, J. M. J. Acetalated dextran is a chemically and biologically tunable material for particulate immunotherapy. *Proc Natl Acad Sci U S A* **106**, 5497–502 (2009).
179. Bachelder, E. M., Beaudette, T. T., Broaders, K. E., Dashe, J. & Fréchet, J. M. J. Acetal-derivatized dextran: An acid-responsive biodegradable material for therapeutic applications. *J Am Chem Soc* **130**, 10494–10495 (2008).
180. Mitchell, M. J. *et al.* Engineering precision nanoparticles for drug delivery. *Nature Reviews Drug Discovery* vol. 20 101–124 (2020).
181. Perretti, M. & Godson, C. Formyl peptide receptor type 2 agonists to kick-start resolution pharmacology. *British Journal of Pharmacology* **177**, 4595–4600 (2020).
182. Koeberle, A. & Werz, O. Perspective of microsomal prostaglandin E2 synthase-1 as drug target in inflammation-related disorders. *Biochemical Pharmacology* **98**, 1–15 (2015).

183. Meirer, K., Steinhilber, D. & Proschak, E. Inhibitors of the arachidonic acid cascade: Interfering with multiple pathways. *Basic and Clinical Pharmacology and Toxicology* **114**, 83–91 (2014).
184. Varrassi, G., Pergolizzi, J. V, Dowling, P. & Paladini, A. Ibuprofen Safety at the Golden Anniversary: Are all NSAIDs the Same? A Narrative Review. *Adv Ther* **37**, 61–82 (2020).
185. Romano, M. Lipoxin and aspirin-triggered lipoxins. *ScientificWorldJournal* **10**, 1048–1064 (2010).
186. Wuest, S. J. A., Crucet, M., Gemperle, C., Loretz, C. & Hersberger, M. Expression and regulation of 12/15-lipoxygenases in human primary macrophages. *Atherosclerosis* **225**, 121–127 (2012).
187. He, C. *et al.* Dynamic eicosanoid responses upon different inhibitor and combination treatments on the arachidonic acid metabolic network. *Molecular BioSystems* **8**, 1585–1594 (2012).
188. Mazaleuskaya, L. L. *et al.* A broad-spectrum lipidomics screen of antiinflammatory drug combinations in human blood. *JCI Insight* **1**, (2016).
189. Tsuge, K., Inazumi, T., Shimamoto, A. & Sugimoto, Y. Molecular mechanisms underlying prostaglandin E₂-exacerbated inflammation and immune diseases. *International Immunology* **31**, 597–606 (2019).
190. Di Gennaro, A. & Haeggström, J. Z. Targeting leukotriene B₄ in inflammation. *Expert Opinion on Therapeutic Targets* **18**, 79–93 (2014).
191. Funk, C. D. & FitzGerald, G. A. COX-2 inhibitors and cardiovascular risk. *Journal of Cardiovascular Pharmacology* **50**, 470–479 (2007).
192. Gudis, K. *et al.* Microsomal prostaglandin E synthase (mPGES)-1, mPGES-2 and cytosolic PGES expression in human gastritis and gastric ulcer tissue. *Laboratory Investigation* **85**, 225–236 (2005).
193. Kieran, N. E. *et al.* Modification of the transcriptomic response to renal ischemia/reperfusion injury by lipoxin analog. *Kidney Int* **64**, 480–92 (2003).
194. Bozinovski, S. *et al.* Serum amyloid A opposes lipoxin A₄ to mediate glucocorticoid refractory lung inflammation in chronic obstructive pulmonary disease. *Proc Natl Acad Sci U S A* **109**, 935–40 (2012).
195. Ndisang, J. F. & Rastogi, S. Cardiometabolic diseases and related complications: current status and future perspective. *Biomed Res Int* **2013**, 467682 (2013).
196. Fu, T. *et al.* Therapeutic Potential of Lipoxin A₄ in Chronic Inflammation: Focus on Cardiometabolic Disease. *ACS Pharmacology and Translational Science* **3**, 43–55 (2020).
197. Birrell, M. A. *et al.* Anti-inflammatory effects of PGE₂ in the lung: role of the EP₄ receptor subtype. *Thorax* **70**, 740–7 (2015).
198. Cheung, S.-Y. *et al.* Discovery of a benzenesulfonamide-based dual inhibitor of microsomal prostaglandin E₂ synthase-1 and 5-lipoxygenase that favorably modulates lipid mediator biosynthesis in inflammation. *European Journal of Medicinal Chemistry* **156**, 815–830 (2018).
199. Brodniewicz, T. & Gryniewicz, G. Preclinical drug development. *Acta Poloniae Pharmaceutica - Drug Research* **67**, 578–585 (2010).
200. Gardiner, P., Cox, R. J. & Grime, K. Plasma protein binding as an optimizable parameter for acidic drugs. *Drug Metabolism and Disposition* **47**, 865–873 (2019).
201. Kratochwil, N. A., Huber, W., Müller, F., Kansy, M. & Gerber, P. R. Predicting plasma protein binding of drugs: A new approach. *Biochemical Pharmacology* **64**, 1355–1374 (2002).
202. Pereira De Sousa, I. & Bernkop-Schnürch, A. Pre-systemic metabolism of orally administered drugs and strategies to overcome it. *Journal of Controlled Release* **192**, 301–309 (2014).
203. Deryabin, D. G. *et al.* A zeta potential value determines the aggregate's size of penta-substituted [60] fullerene derivatives in aqueous suspension whereas positive charge is required for toxicity against bacterial cells. *Journal of Nanobiotechnology* **13**, 1–13 (2015).
204. Shao, X. R. *et al.* Independent effect of polymeric nanoparticle zeta potential/surface charge, on their cytotoxicity and affinity to cells. *Cell Proliferation* **48**, 465–474 (2015).
205. Gustafson, H. H., Holt-Casper, D., Grainger, D. W. & Ghandehari, H. Nanoparticle uptake: The phagocyte problem. *Nano Today* **10**, 487–510 (2015).
206. Kapellos, T. S. *et al.* A novel real time imaging platform to quantify macrophage phagocytosis. *Biochem Pharmacol* **116**, 107–19 (2016).
207. Braga, C. B., Perli, G., Becher, T. B. & Ornelas, C. Biodegradable and pH-Responsive Acetalated Dextran (Ac-Dex) Nanoparticles for NIR Imaging and Controlled Delivery of a Platinum-Based Prodrug into Cancer Cells. *Molecular Pharmaceutics* **16**, 2083–2094 (2019).
208. Schützmann, M. P. *et al.* Endo-lysosomal A β concentration and pH trigger formation of A β oligomers that potentially induce Tau missorting. *Nature Communications* **12**, 1–14 (2021).
209. Begines, B. *et al.* Polymeric nanoparticles for drug delivery: Recent developments and future prospects. *Nanomaterials* **10**, 1–41 (2020).

210. Kaukonen, K.-M., Bailey, M., Pilcher, D., Cooper, D. J. & Bellomo, R. Systemic inflammatory response syndrome criteria in defining severe sepsis. *N Engl J Med* **372**, 1629–38 (2015).
211. Tallury, P., Alimohammadi, N. & Kalachandra, S. Poly(ethylene-co-vinyl acetate) copolymer matrix for delivery of chlorhexidine and acyclovir drugs for use in the oral environment: effect of drug combination, copolymer composition and coating on the drug release rate. *Dent Mater* **23**, 404–9 (2007).
212. Karabey-Akyurek, Y. *et al.* Localized delivery of methylprednisolone sodium succinate with polymeric nanoparticles in experimental injured spinal cord model. *Pharmaceutical Development and Technology* **22**, 972–981 (2017).
213. Casa, D. M. *et al.* Poly(L-lactide) Nanoparticles Reduce Amphotericin B Cytotoxicity and Maintain Its In Vitro Antifungal Activity. *J Nanosci Nanotechnol* **15**, 848–54 (2015).
214. Kühne, M. *et al.* Biocompatible sulfated valproic acid-coupled polysaccharide-based nanocarriers with HDAC inhibitory activity. *J Control Release* **329**, 717–730 (2021).
215. Schermelleh, L. *et al.* Super-resolution microscopy demystified. *Nat Cell Biol* **21**, 72–84 (2019).
216. Surette, M. E. Lipopolysaccharides prime whole human blood and isolated neutrophils for the increased synthesis of 5-lipoxygenase products by enhancing arachidonic acid availability: involvement of the CD14 antigen. *Journal of Experimental Medicine* **178**, 1347–1355 (1993).
217. Tyrtysnaia, A. A. *et al.* Acute neuroinflammation provokes intracellular acidification in mouse hippocampus. *Journal of Neuroinflammation* **13**, 1–11 (2016).
218. Yu, S., Green, J., Wellens, R., Lopez-Castejon, G. & Brough, D. Bafilomycin A1 enhances NLRP3 inflammasome activation in human monocytes independent of lysosomal acidification. *FEBS Journal* **288**, 3186–3196 (2021).
219. Brusini, R., Varna, M. & Couvreur, P. Advanced nanomedicines for the treatment of inflammatory diseases. (2020).
220. Rademann, P. *et al.* Mitochondria-targeted antioxidants SkQ1 and MitoTEMPO failed to exert a long-term beneficial effect in murine polymicrobial sepsis. *Oxidative Medicine and Cellular Longevity* **2017**, (2017).
221. Dinarello, C. A. Anti-inflammatory Agents: Present and Future. *Cell* **140**, 935–50 (2010).
222. Serhan, C. N. Discovery of specialized pro-resolving mediators marks the dawn of resolution physiology and pharmacology. *Molecular Aspects of Medicine* **58**, 1–11 (2017).
223. Dalli, J. & Serhan, C. N. Identification and structure elucidation of the pro-resolving mediators provides novel leads for resolution pharmacology. *Br J Pharmacol* **176**, 1024–1037 (2019).
224. Wu, S. H., Chen, X. Q., Liu, B., Wu, H. J. & Dong, L. Efficacy and safety of 15(R/S)-methyl-lipoxin A4 in topical treatment of infantile eczema. *British Journal of Dermatology* **168**, 172–178 (2013).
225. Kong, X., Wu, S. H., Zhang, L. & Chen, X. Q. Pilot application of lipoxin A4 analog and lipoxin A4 receptor agonist in asthmatic children with acute episodes. *Experimental and Therapeutic Medicine* **14**, 2284–2290 (2017).
226. Leuti, A., Maccarrone, M. & Chiurchiù, V. Proresolving lipid mediators: Endogenous modulators of oxidative stress. *Oxidative Medicine and Cellular Longevity* **2019**, (2019).
227. Gilbert, N. C. *et al.* Structural and mechanistic insights into 5-lipoxygenase inhibition by natural products. *Nature Chemical Biology* **16**, 783–790 (2020).
228. Van Anh, T. T. *et al.* From Vietnamese plants to a biflavonoid that relieves inflammation by triggering the lipid mediator class switch to resolution. *Acta Pharmaceutica Sinica B* **11**, 1629–1647 (2021).
229. Pace, S. *et al.* Anti-inflammatory celastrol promotes a switch from leukotriene biosynthesis to formation of specialized pro-resolving lipid mediators. *Pharmacological Research* **167**, (2021).
230. Fredman, G. *et al.* Resolvin D1 limits 5-lipoxygenase nuclear localization and leukotriene B4 synthesis by inhibiting a calcium-activated kinase pathway. *Proc Natl Acad Sci U S A* **111**, 14530–5 (2014).
231. Titos, E. *et al.* Inhibition of 5-lipoxygenase-activating protein abrogates experimental liver injury: role of Kupffer cells. *J Leukoc Biol* **78**, 871–8 (2005).
232. Gerstmeier, J. *et al.* Novel benzoxanthene lignans that favorably modulate lipid mediator biosynthesis: A promising pharmacological strategy for anti-inflammatory therapy. *Biochemical Pharmacology* **165**, (2019).
233. Meng, H. *et al.* Discovery of Novel 15-Lipoxygenase Activators to Shift the Human Arachidonic Acid Metabolic Network toward Inflammation Resolution. *Journal of Medicinal Chemistry* **59**, 4202–4209 (2016).
234. Meng, H., Dai, Z., Zhang, W., Liu, Y. & Lai, L. Molecular mechanism of 15-lipoxygenase allosteric activation and inhibition. *Physical Chemistry Chemical Physics* **20**, 14785–14795 (2018).
235. Matsuura, K. *et al.* Identification of a principal mRNA species for human 3 α -hydroxysteroid

dehydrogenase isoform (AKR1C3) that exhibits high prostaglandin D2 11-ketoreductase activity. *Journal of Biochemistry* **124**, 940–946 (1998).

IV Acknowledgements

Abschließend möchte ich allen Personen danken, die mir den Abschluss dieser Arbeit ermöglicht haben und mich auf meinem Weg unterstützt haben.

Mein besonderer Dank gilt Prof. Dr. Oliver Werz, der mir einen reibungslosen und professionellen Einstieg in die Promotion ermöglichte. Seine einzigartige Fähigkeit wissenschaftlichen Diskurs anzuregen, bildete die Grundlage für meine sehr lehrreiche und produktive Zeit am Lehrstuhl für Pharmazeutisch/Medizinische Chemie. Die aus seiner herausragenden Kooperationsfähigkeit resultierende starke wissenschaftliche Vernetzung in unterschiedliche Themengebiete war ein weiteres Fundament meiner Arbeit und ermöglichte mir den Einblick in eine Vielzahl von Forschungsgebieten. Durch das entgegengebrachte Vertrauen hatte ich die Möglichkeit Projekte selbst zu betreuen und neuen Ansätzen nachzugehen, was mir in meiner weiteren Karriere sehr helfen wird. Vielen Dank für die überragende wissenschaftliche Ausbildung und die Möglichkeit zur Promotion an diesem Lehrstuhl!

Weiterhin gilt mein besonderer Dank Prof. Dr. Ulrich S. Schubert, der durch die Initiierung des SFB 1278 PolyTarget eine einzigartige Plattform für die Forschung im Bereich Nanomedizin geschaffen hat. Sein unvergleichliches Engagement Jena zu einer festen internationalen Größe in diesem Bereich zu formen ist sehr inspirierend gewesen. Danke für die Möglichkeit Teil dieses einzigartigen Projektes gewesen zu sein.

Ein großes Dankeschön auch an Prof. Dr. Ulrike Garscha, die mir zum Diplom die Grundlagen für das wissenschaftliche Arbeiten näherbrachte und stets mit Rat und Tat zur Seite stand.

Im gleichen Zuge möchte ich mich bei Prof. Dr. Andreas Koeberle für die sehr gute Zusammenarbeit in vielen gemeinsamen Projekten bedanken.

Außerdem danke ich Prof. Dr. Gerhard Scriba für die damalige Zweitbetreuung meiner Diplomarbeit und die netten Gespräche im Büro während der Corona Zeit.

Besonders hervorheben möchte ich die Freundschaft mit Paul M. Jordan, der mich durch unseren gesunden, freundschaftlichen Konkurrenzkampf stets forderte und mit dem ich unzählige witzige Stunden im Studium, beim Lernen, in der Freizeit, im Labor und später auch im Büro verbringen durfte. Meinen allerhöchsten Respekt vor deinen Leistungen und vor dem was du zweifelsohne noch erreichen wirst.

Vielen Dank auch an unseren weiteren Weggefährten und Mitglied der „Guys on Ph.Eur.“ (g.o.p.e) Konstantin Neukirch, mit dem das Studieren, Feiern, Arbeiten und vor allem Diskutieren stets eine Freude war. Ihr beide seid aus meinem Leben nicht mehr weg zu denken, auch wenn uns nun große Entfernungen trennen.

Weiterhin danke ich Blerina Shkodra für die einwandfreie Zusammenarbeit auf dem Projekt A04 des SFB PolyTarget.

Einen weiteren besonderen Dank möchte ich an Patrick Schädel, Anna Czapka und Andre Gollowitzer richten, die während der Arbeit am Institut zu sehr guten Freunden geworden sind, mit denen ich jederzeit gern Zeit verbrachte.

Ein großes Dankeschön auch an meine Kollegen Laura M., Erik R., Jana F., Markus W., Robert. K. H., Konstantin L., Helmut P., Katharina L.P.M., Daniel H., Friedemann B., Finja W., Stefanie K., Stefanie L., Rao Z. für die tolle Zusammenarbeit und die schönen Momente im Institut.

Einen weiteren Dank an alle Technikerinnen des Instituts für die tolle Zusammenarbeit und die tatkräftige Unterstützung in vielen Projekten.

Anschließend danke ich Carlo Kadgien für seine intensive Freundschaft der letzten Jahre und die Unterstützung in allen Lebenslagen. Du hast mir immer geholfen die vor mir liegende Arbeit durchzuziehen und ich freue mich auf viele weitere lustige Erlebnisse.

Unendlich vielen Dank an dieser Stelle auch an Uwe Merker, der in der Mensa stets eine Stärkung für den harten Laboralltag bereithielt und auch nach Feierabend für die richtige Abkühlung sorgte. Vielen Dank für alles was du für mich getan hast.

Zum Schluss möchte ich meiner Familie für die großartige Unterstützung in allen Lebenslagen danken. Ohne euch wäre nichts davon möglich gewesen. Ein besonderes Dankeschön geht an meinen verstorbenen Opa Hans Karl Möckel, dem diese Arbeit gewidmet ist. Er zog mich bei sich auf und glaubte immer an meine Fähigkeiten. Er wird für immer ein prägender Teil meines Lebens sein und aller Erfolg in meinem Leben gebührt ihm.

V Appendix

Appendix 1 – Contribution to figures in the manuscripts

Manuskript Nr. I

Kurzreferenz: Werner et al. (2019), The FASEB Journal

Beitrag des Doktoranden:

Abbildung(en) # 1	<input type="checkbox"/>	100 % (die in dieser Abbildung wiedergegebenen Daten entstammen vollständig experimentellen Arbeiten, die der Kandidat/die Kandidatin durchgeführt hat)
	<input type="checkbox"/>	0 % (die in dieser Abbildung wiedergegebenen Daten basieren ausschließlich auf Arbeiten anderer Koautoren)
	<input checked="" type="checkbox"/>	Etwaiger Beitrag des Doktoranden / der Doktorandin zur Abbildung: 15 % Kurzbeschreibung des Beitrages: <i>Datenerhebung und Aufnahme der Bilder zu Panel C Western Blot Daten von M1 und M2 Makrophagen</i>

Abbildung(en) # 2-7	<input type="checkbox"/>	100 % (die in dieser Abbildung wiedergegebenen Daten entstammen vollständig experimentellen Arbeiten, die der Kandidat/die Kandidatin durchgeführt hat)
	<input checked="" type="checkbox"/>	0 % (die in dieser Abbildung wiedergegebenen Daten basieren ausschließlich auf Arbeiten anderer Koautoren)
	<input type="checkbox"/>	Etwaiger Beitrag des Doktoranden / der Doktorandin zur Abbildung: _____ % Kurzbeschreibung des Beitrages:

Abbildung(en) # S1	<input type="checkbox"/>	100 % (die in dieser Abbildung wiedergegebenen Daten entstammen vollständig experimentellen Arbeiten, die der Kandidat/die Kandidatin durchgeführt hat)
	<input type="checkbox"/>	0 % (die in dieser Abbildung wiedergegebenen Daten basieren ausschließlich auf Arbeiten anderer Koautoren)
	<input checked="" type="checkbox"/>	Etwaiger Beitrag des Doktoranden / der Doktorandin zur Abbildung: 50 % Kurzbeschreibung des Beitrages: <i>Datenerhebung und Aufnahme der Western Blot Daten von M1 und M2 Makrophagen</i>

Abbildung(en) # S2	<input type="checkbox"/>	100 % (die in dieser Abbildung wiedergegebenen Daten entstammen vollständig experimentellen Arbeiten, die der Kandidat/die Kandidatin durchgeführt hat)
	<input checked="" type="checkbox"/>	0 % (die in dieser Abbildung wiedergegebenen Daten basieren ausschließlich auf Arbeiten anderer Koautoren)
	<input type="checkbox"/>	Etwaiger Beitrag des Doktoranden / der Doktorandin zur Abbildung: _____% Kurzbeschreibung des Beitrages:

Unterschrift Kandidat/-in
Fakultät)

Unterschrift Betreuer/-in (Mitglied der

Manuskript Nr. II

Kurzreferenz: Shkodra-Pula et al. (2020) J Nanobiotechnol

Beitrag des Doktoranden:

Abbildung(en) # 1-2	<input type="checkbox"/>	100 % (die in dieser Abbildung wiedergegebenen Daten entstammen vollständig experimentellen Arbeiten, die der Kandidat/die Kandidatin durchgeführt hat)
	<input checked="" type="checkbox"/>	0 % (die in dieser Abbildung wiedergegebenen Daten basieren ausschließlich auf Arbeiten anderer Koautoren)
	<input type="checkbox"/>	Etwaiger Beitrag des Doktoranden / der Doktorandin zur Abbildung: _____ % Kurzbeschreibung des Beitrages:

Abbildung(en) # 3	<input type="checkbox"/>	100 % (die in dieser Abbildung wiedergegebenen Daten entstammen vollständig experimentellen Arbeiten, die der Kandidat/die Kandidatin durchgeführt hat)
	<input type="checkbox"/>	0 % (die in dieser Abbildung wiedergegebenen Daten basieren ausschließlich auf Arbeiten anderer Koautoren)
	<input checked="" type="checkbox"/>	Etwaiger Beitrag des Doktoranden / der Doktorandin zur Abbildung: 50 % Kurzbeschreibung des Beitrages: <i>Vorbereitung Zellen, Datenerhebung, Datenanalyse, Statistik</i>

Abbildung(en) # 4	<input type="checkbox"/>	100 % (die in dieser Abbildung wiedergegebenen Daten entstammen vollständig experimentellen Arbeiten, die der Kandidat/die Kandidatin durchgeführt hat)
	<input type="checkbox"/>	0 % (die in dieser Abbildung wiedergegebenen Daten basieren ausschließlich auf Arbeiten anderer Koautoren)
	<input checked="" type="checkbox"/>	Etwaiger Beitrag des Doktoranden / der Doktorandin zur Abbildung: 80 % Kurzbeschreibung des Beitrages: <i>Vorbereitung Zellen, Datenerhebung, Datenanalyse, Bildbearbeitung</i>

Abbildung(en) # 5-7	<input checked="" type="checkbox"/>	100 % (die in dieser Abbildung wiedergegebenen Daten entstammen vollständig experimentellen Arbeiten, die der Kandidat/die Kandidatin durchgeführt hat)
	<input type="checkbox"/>	0 % (die in dieser Abbildung wiedergegebenen Daten basieren ausschließlich auf Arbeiten anderer Koautoren)
	<input type="checkbox"/>	Etwaiger Beitrag des Doktoranden / der Doktorandin zur Abbildung: _____ % Kurzbeschreibung des Beitrages:

Unterschrift Kandidat/-in

Unterschrift Betreuer/-in (Mitglied der Fakultät)

Manuskript Nr. III

Kurzreferenz: Kretzer et al. (2021) Cell Mol Life Sci.

Beitrag des Doktoranden:

Abbildung(en) # 1-4	<input type="checkbox"/>	100 % (die in dieser Abbildung wiedergegebenen Daten entstammen vollständig experimentellen Arbeiten, die der Kandidat/die Kandidatin durchgeführt hat)
	<input checked="" type="checkbox"/>	0 % (die in dieser Abbildung wiedergegebenen Daten basieren ausschließlich auf Arbeiten anderer Koautoren)
	<input type="checkbox"/>	Etwaiger Beitrag des Doktoranden / der Doktorandin zur Abbildung: _____% Kurzbeschreibung des Beitrages:

Abbildung(en) # 6	<input type="checkbox"/>	100 % (die in dieser Abbildung wiedergegebenen Daten entstammen vollständig experimentellen Arbeiten, die der Kandidat/die Kandidatin durchgeführt hat)
	<input type="checkbox"/>	0 % (die in dieser Abbildung wiedergegebenen Daten basieren ausschließlich auf Arbeiten anderer Koautoren)
	<input checked="" type="checkbox"/>	Etwaiger Beitrag des Doktoranden / der Doktorandin zur Abbildung: 60 % Kurzbeschreibung des Beitrages: <i>Zellaufbereitung, Zellinkubation, Vorbereitung Mikroskopie und FACS Analyse, Aufbereitung der Daten</i>

Abbildung(en) # 7-8	<input checked="" type="checkbox"/>	100 % (die in dieser Abbildung wiedergegebenen Daten entstammen vollständig experimentellen Arbeiten, die der Kandidat/die Kandidatin durchgeführt hat)
	<input type="checkbox"/>	0 % (die in dieser Abbildung wiedergegebenen Daten basieren ausschließlich auf Arbeiten anderer Koautoren)
	<input type="checkbox"/>	Etwaiger Beitrag des Doktoranden / der Doktorandin zur Abbildung: _____% Kurzbeschreibung des Beitrages:

Abbildung(en) # S1-S13	<input type="checkbox"/>	100 % (die in dieser Abbildung wiedergegebenen Daten entstammen vollständig experimentellen Arbeiten, die der Kandidat/die Kandidatin durchgeführt hat)
	<input checked="" type="checkbox"/>	0 % (die in dieser Abbildung wiedergegebenen Daten basieren ausschließlich auf Arbeiten anderer Koautoren)
	<input type="checkbox"/>	Etwaiger Beitrag des Doktoranden / der Doktorandin zur Abbildung: _____% Kurzbeschreibung des Beitrages:

Unterschrift Kandidat/-in

Unterschrift Betreuer/-in (Mitglied der Fakultät)

Manuskript Nr. IV

Kurzreferenz Vollrath et al. (2021) Polymers

Beitrag des Doktoranden:

Abbildung(en) # 1	<input type="checkbox"/>	100 % (die in dieser Abbildung wiedergegebenen Daten entstammen vollständig experimentellen Arbeiten, die der Kandidat/die Kandidatin durchgeführt hat)
	<input checked="" type="checkbox"/>	0 % (die in dieser Abbildung wiedergegebenen Daten basieren ausschließlich auf Arbeiten anderer Koautoren)
	<input type="checkbox"/>	Etwaiger Beitrag des Doktoranden / der Doktorandin zur Abbildung: _____ % Kurzbeschreibung des Beitrages: <i>(z. B. „Abbildungsteile a, d und f“ oder „Auswertung der Daten“ etc)</i>

Abbildung(en) # 2	<input type="checkbox"/>	100 % (die in dieser Abbildung wiedergegebenen Daten entstammen vollständig experimentellen Arbeiten, die der Kandidat/die Kandidatin durchgeführt hat)
	<input type="checkbox"/>	0 % (die in dieser Abbildung wiedergegebenen Daten basieren ausschließlich auf Arbeiten anderer Koautoren)
	<input checked="" type="checkbox"/>	Etwaiger Beitrag des Doktoranden / der Doktorandin zur Abbildung: 20 % Kurzbeschreibung des Beitrages: <i>Aufbereitung der Zellen, Durchführung Experiment, Aufbereitung der Daten</i>

Abbildung(en) # 3	<input type="checkbox"/>	100 % (die in dieser Abbildung wiedergegebenen Daten entstammen vollständig experimentellen Arbeiten, die der Kandidat/die Kandidatin durchgeführt hat)
	<input checked="" type="checkbox"/>	0 % (die in dieser Abbildung wiedergegebenen Daten basieren ausschließlich auf Arbeiten anderer Koautoren)
	<input type="checkbox"/>	Etwaiger Beitrag des Doktoranden / der Doktorandin zur Abbildung: 20 % Kurzbeschreibung des Beitrages: <i>Aufbereitung der Zellen, Durchführung Experiment, Aufbereitung der Daten</i>

Abbildung(en) # 4	<input checked="" type="checkbox"/>	100 % (die in dieser Abbildung wiedergegebenen Daten entstammen vollständig experimentellen Arbeiten, die der Kandidat/die Kandidatin durchgeführt hat)
	<input type="checkbox"/>	0 % (die in dieser Abbildung wiedergegebenen Daten basieren ausschließlich auf Arbeiten anderer Koautoren)
	<input type="checkbox"/>	Etwaiger Beitrag des Doktoranden / der Doktorandin zur Abbildung: 20 % Kurzbeschreibung des Beitrages: <i>Aufbereitung der Zellen, Durchführung Experiment, Aufbereitung der Daten</i>

Abbildung(en) # S1	<input type="checkbox"/>	100 % (die in dieser Abbildung wiedergegebenen Daten entstammen vollständig experimentellen Arbeiten, die der Kandidat/die Kandidatin durchgeführt hat)
	<input checked="" type="checkbox"/>	0 % (die in dieser Abbildung wiedergegebenen Daten basieren ausschließlich auf Arbeiten anderer Koautoren)
	<input type="checkbox"/>	Etwaiger Beitrag des Doktoranden / der Doktorandin zur Abbildung: 20 % Kurzbeschreibung des Beitrages: <i>Aufbereitung der Zellen, Durchführung Experiment, Aufbereitung der Daten</i>

Abbildung(en) # S2-S4	<input checked="" type="checkbox"/>	100 % (die in dieser Abbildung wiedergegebenen Daten entstammen vollständig experimentellen Arbeiten, die der Kandidat/die Kandidatin durchgeführt hat)
	<input type="checkbox"/>	0 % (die in dieser Abbildung wiedergegebenen Daten basieren ausschließlich auf Arbeiten anderer Koautoren)
	<input type="checkbox"/>	Etwaiger Beitrag des Doktoranden / der Doktorandin zur Abbildung: 20 % Kurzbeschreibung des Beitrages: <i>Aufbereitung der Zellen, Durchführung Experiment, Aufbereitung der Daten</i>

Unterschrift Kandidat/-in

Unterschrift Betreuer/-in (Mitglied der Fakultät)

Manuskript Nr. V

Kurzreferenz Kretzer et al. (2022) J Inflamm Res.

Beitrag des Doktoranden / der Doktorandin

Beitrag des Doktoranden / der Doktorandin zu Abbildungen, die experimentelle Daten wiedergeben (nur für Originalartikel):

Abbildung(en) # 1	<input checked="" type="checkbox"/>	100 % (die in dieser Abbildung wiedergegebenen Daten entstammen vollständig experimentellen Arbeiten, die der Kandidat/die Kandidatin durchgeführt hat)
	<input type="checkbox"/>	0 % (die in dieser Abbildung wiedergegebenen Daten basieren ausschließlich auf Arbeiten anderer Koautoren)
	<input type="checkbox"/>	Etwaiger Beitrag des Doktoranden / der Doktorandin zur Abbildung: _____ % Kurzbeschreibung des Beitrages: <i>(z. B. „Abbildungsteile a, d und f“ oder „Auswertung der Daten“ etc)</i>

Abbildung(en) # 2	<input type="checkbox"/>	100 % (die in dieser Abbildung wiedergegebenen Daten entstammen vollständig experimentellen Arbeiten, die der Kandidat/die Kandidatin durchgeführt hat)
	<input type="checkbox"/>	0 % (die in dieser Abbildung wiedergegebenen Daten basieren ausschließlich auf Arbeiten anderer Koautoren)
	<input checked="" type="checkbox"/>	Etwaiger Beitrag des Doktoranden / der Doktorandin zur Abbildung: 95% Kurzbeschreibung des Beitrages: <i>Zellaufbereitung, Durchführung der Experimente, Auswertung der Daten, Erstellen der Graphen</i>

Abbildung(en) # 3-4	<input checked="" type="checkbox"/>	100 % (die in dieser Abbildung wiedergegebenen Daten entstammen vollständig experimentellen Arbeiten, die der Kandidat/die Kandidatin durchgeführt hat)
	<input type="checkbox"/>	0 % (die in dieser Abbildung wiedergegebenen Daten basieren ausschließlich auf Arbeiten anderer Koautoren)
	<input type="checkbox"/>	Etwaiger Beitrag des Doktoranden / der Doktorandin zur Abbildung: 95% Kurzbeschreibung des Beitrages: <i>Zellaufbereitung, Durchführung der Experimente, Auswertung der Daten, Erstellen der Graphen</i>

Abbildung(en) # 5	<input type="checkbox"/>	100 % (die in dieser Abbildung wiedergegebenen Daten entstammen vollständig experimentellen Arbeiten, die der Kandidat/die Kandidatin durchgeführt hat)
	<input type="checkbox"/>	0 % (die in dieser Abbildung wiedergegebenen Daten basieren ausschließlich auf Arbeiten anderer Koautoren)
	<input checked="" type="checkbox"/>	Etwaiger Beitrag des Doktoranden / der Doktorandin zur Abbildung: 50% Kurzbeschreibung des Beitrages: <i>Probenaufbereitung, Auswertung der Daten, Erstellung der Graphen</i>

Unterschrift Kandidat/-in

Unterschrift Betreuer/-in (Mitglied der Fakultät)

Manuskript Nr. VI

Kurzreferenz Kretzer et al. (2022) Biochem Pharmacol.

Beitrag des Doktoranden:

Abbildung(en) #1	<input type="checkbox"/>	100 % (die in dieser Abbildung wiedergegebenen Daten entstammen vollständig experimentellen Arbeiten, die der Kandidat/die Kandidatin durchgeführt hat)
	<input type="checkbox"/>	0 % (die in dieser Abbildung wiedergegebenen Daten basieren ausschließlich auf Arbeiten anderer Koautoren)
	<input checked="" type="checkbox"/>	Etwaiger Beitrag des Doktoranden / der Doktorandin zur Abbildung: 80 % Kurzbeschreibung des Beitrages: <i>Durchführung Experimente, Auswertung der Daten, Erstellung der Graphen und Strukturformeln</i>

Abbildung(en) #2	<input type="checkbox"/>	100 % (die in dieser Abbildung wiedergegebenen Daten entstammen vollständig experimentellen Arbeiten, die der Kandidat/die Kandidatin durchgeführt hat)
	<input type="checkbox"/>	0 % (die in dieser Abbildung wiedergegebenen Daten basieren ausschließlich auf Arbeiten anderer Koautoren)
	<input checked="" type="checkbox"/>	Etwaiger Beitrag des Doktoranden / der Doktorandin zur Abbildung: 70 % Kurzbeschreibung des Beitrages: <i>Durchführung Experimente, Auswertung der Daten, Erstellung der Graphen</i>

Abbildung(en) #3	<input type="checkbox"/>	100 % (die in dieser Abbildung wiedergegebenen Daten entstammen vollständig experimentellen Arbeiten, die der Kandidat/die Kandidatin durchgeführt hat)
	<input type="checkbox"/>	0 % (die in dieser Abbildung wiedergegebenen Daten basieren ausschließlich auf Arbeiten anderer Koautoren)
	<input checked="" type="checkbox"/>	Etwaiger Beitrag des Doktoranden / der Doktorandin zur Abbildung: 80 % Kurzbeschreibung des Beitrages: <i>Durchführung Experimente, Auswertung der Daten, Erstellung der Graphen, Aufnahme und Auswertung Fluoreszenzbilder</i>

Abbildung(en) #4	<input checked="" type="checkbox"/>	100 % (die in dieser Abbildung wiedergegebenen Daten entstammen vollständig experimentellen Arbeiten, die der Kandidat/die Kandidatin durchgeführt hat)
	<input type="checkbox"/>	0 % (die in dieser Abbildung wiedergegebenen Daten basieren ausschließlich auf Arbeiten anderer Koautoren)
	<input type="checkbox"/>	Etwaiger Beitrag des Doktoranden / der Doktorandin zur Abbildung: _____ % Kurzbeschreibung des Beitrages: <i>Durchführung Experimente, Auswertung der Daten, Erstellung der Graphen, Aufnahme und Auswertung Fluoreszenzbilder</i>

Abbildung(en) #5	<input type="checkbox"/>	100 % (die in dieser Abbildung wiedergegebenen Daten entstammen vollständig experimentellen Arbeiten, die der Kandidat/die Kandidatin durchgeführt hat)
	<input type="checkbox"/>	0 % (die in dieser Abbildung wiedergegebenen Daten basieren ausschließlich auf Arbeiten anderer Koautoren)
	<input checked="" type="checkbox"/>	Etwaiger Beitrag des Doktoranden / der Doktorandin zur Abbildung: 20 % Kurzbeschreibung des Beitrages: <i>Aufbereitung Zellen, Auswertung der Daten, Erstellen der Graphen</i>

Unterschrift Kandidat/-in

Unterschrift Betreuer/-in (Mitglied der Fakultät)

Appendix 2 – List of Publications and conference contributions

List of publications

- 1. Synthesis, Biological Evaluation and Structure-Activity Relationships of Diflapolin Analogues as Dual sEH/FLAP Inhibitors**
L. Vieider, E. Romp, V. Temml, J. Fischer, **C. Kretzer**, M. Schoenthaler, A. Taha, V. Hernández-Olmos, S. Sturm, D. Schuster, O. Werz, U. Garscha, B. Matuszczak
ACS Med Chem Lett. 2018 Nov 29;10(1):62-66
- 2. Targeting biosynthetic networks of the proinflammatory and proresolving lipid metabolome**
M. Werner, P.M. Jordan, E. Romp, A. Czapka, Z. Rao, **C. Kretzer**, A. Koeberle, U. Garscha, S. Pace, H.-E. Claesson, C.N. Serhan, O. Werz, J. Gerstmeier
FASEB J. 2019 May;33(5):6140-6153.
- 3. Novel benzoxanthene lignans that favorably modulate lipid mediator biosynthesis: A promising pharmacological strategy for anti-inflammatory therapy**
J. Gerstmeier, **C. Kretzer**, S. Di Micco, L. Miek, H. Butschek, V. Cantone, R. Bilancia, R. Rizza, F. Troisi, N. Cardullo, C. Tringali, A. Ialenti, A. Rossi, G. Bifulco, O. Werz, S. Pace
Biochem Pharmacol. 2019 Jul;165:263-274.
- 4. Improved Bioactivity of the Natural Product 5-Lipoxygenase Inhibitor Hyperforin by Encapsulation into Polymeric Nanoparticles**
A. Traeger, S. Voelker, B. Shkodra-Pula, **C. Kretzer**, S. Schubert, M. Gottschaldt, U.S. Schubert, O. Werz
Mol Pharm. 2020 Mar 2;17(3):810-816.
- 5. Discovery of Novel 5-Lipoxygenase-Activating Protein (FLAP) Inhibitors by Exploiting a Multistep Virtual Screening Protocol**
A. Olgac, A. Carotti, **C. Kretzer**, S. Zergiebel, A. Seeling, U. Garscha, O. Werz, A. Macchiarulo, E. Banoglu
J Chem Inf Model. 2020 Mar 23;60(3):1737-1748.
- 6. Encapsulation of the dual FLAP/mPEGS-1 inhibitor BRP-187 into acetalated dextran and PLGA nanoparticles improves its cellular bioactivity**
B. Shkodra-Pula, **C. Kretzer**, P.M. Jordan, P. Klemm, A. Koeberle, D. Pretzel, E. Banoglu, S. Lorkowski, M. Wallert, S. Höppener, S. Stumpf, A. Vollrath, S. Schubert, O. Werz, U.S. Schubert
J Nanobiotechnology. 2020 May 14;18(1):73.
- 7. Anti-inflammatory celastrol promotes a switch from leukotriene biosynthesis to formation of specialized pro-resolving lipid mediators**
S. Pace, K.Zhang, P.M. Jordan, R. Bilancia, W. Wang, F. Börner, R.K. Hofstetter, M. Potenza, **C. Kretzer**, J. Gerstmeier, D. Fischer, S. Lorkowski, N.C. Gilbert, M.E. Newcomer, A. Rossi, X. Chen, O. Werz
Pharmacol Res. 2021 May;167:105556.

- 8. Biocompatible valproic acid-coupled nanoparticles attenuate lipopolysaccharide-induced inflammation**
M. Kühne, **C. Kretzer**, H. Lindemann, M. Godmann, T. Heinze, O. Werz, T. Heinzel
Int J Pharm. 2021 May 15;601:120567.
- 9. From Vietnamese plants to a biflavonoid that relieves inflammation by triggering the lipid mediator class switch to resolution**
T.T. Van Anh, A. Mostafa, Z. Rao, S. Pace, S. Schwaiger, **C. Kretzer**, V. Temml, C. Giesel, P.M. Jordan, R. Bilancia, C. Weinigel, S. Rummler, B. Waltenberger, T. Hung, A. Rossi, H. Stuppner, O. Werz, A. Koeberle
- 10. Effect of Crystallinity on the Properties of Polycaprolactone Nanoparticles Containing the Dual FLAP/mPEGS-1 Inhibitor BRP-187**
A. Vollrath, **C. Kretzer**, B. Beringer-Siemers, B. Shkodra, J.A. Czaplewska, D. Bandelli, S. Stumpf, S. Hoepfener, C. Weber, O. Werz, U.S. Schubert
Polymers (Basel). 2021 Jul 31;13(15):2557.
- 11. Encapsulation of the Anti-inflammatory Dual FLAP/sEH Inhibitor Diflapolin Improves the Efficiency in Human Whole Blood**
C. Grune, **C. Kretzer**, S. Zergiebel, S. Kattner, J. Thamm, S. Hoepfener, O. Werz, D. Fischer
J Pharm Sci. 2021 Oct 29;S0022-3549(21)00570-0.
- 12. Ethoxy acetalated dextran-based nanocarriers accomplish efficient inhibition of leukotriene formation by a novel FLAP antagonist in human leukocytes and blood**
C. Kretzer, B. Shkodra, P. Klemm, P.M. Jordan, D. Schröder, G. Cinar, A. Vollrath, S. Schubert, I. Nischang, S. Hoepfener, S. Stumpf, E. Banoglu, F. Gladigau, R. Bilancia, A. Rossi, C. Eggeling, U. Neugebauer, U.S. Schubert, O. Werz
Cell Mol Life Sci. 2021 Dec 31;79(1):40.
- 13. Natural chalcones elicit formation of specialized pro-resolving mediators and related 15-lipoxygenase products in human macrophages**
C. Kretzer, P.M. Jordan, K.P.L. Meyer, D. Hoff, M. Werner, R.K. Hofstetter, A. Koeberle, A. Cala Peralta, G. Viault, D. Seraphin, P. Richomme, J.-J. Helesbeux, H. Stuppner, V. Temml, D. Schuster, O. Werz
Biochem Pharmacol. 2022 Jan;195:114825.
- 14. Shifting the Biosynthesis of Leukotrienes Toward Specialized Pro-Resolving Mediators by the 5-Lipoxygenase-Activating Protein (FLAP) Antagonist BRP-201**
C. Kretzer, P.M. Jordan, R. Bilancia, A. Rossi, T. Gür Maz, E. Banoglu, U.S. Schubert, O. Werz
J Inflamm Res. 2022 Feb 9;15:911-925.
- 15. Novel potent benzimidazole-based microsomal prostaglandin E₂ synthase-1 (mPGES-1) inhibitors derived from BRP-201 that also inhibit leukotriene C₄ synthase**
A. G. Ergül, T. Gür Maz, **C. Kretzer**, A. Olğaç, P.M. Jordan, B. Çalıřkan, O. Werz, E. Banoglu
Eur J Med Chem. 2022 Mar 5;231:114167.

16. Discovery and Optimization of Piperazine Urea Derivatives as Soluble Epoxide Hydrolase (sEH) Inhibitors

İ. Çapan, P.M. Jordan, A. Olğaç, B. Çalışkan, **C. Kretzer**, O. Werz, E. Banoglu
ChemMedChem. 2022 Apr 24;e202200137.

17. Rotational constriction of curcuminoids impacts 5-lipoxygenase and mPGES-1 inhibition and evokes a lipid mediator class switch in macrophages.

Rao Z, Caprioglio D, Gollowitzer A, **Kretzer C**, Imperio D, Collado JA, Watl L, Lackner S, Appendino G, Muñoz E, Temml V, Werz O, Minassi A, Koeberle A.
Biochem Pharmacol. 2022 Aug 3;203:115202. doi: 10.1016/j.bcp.2022.115202.

Conference contributions

DPHG Annual Meeting 2019, Heidelberg Germany (01.09.2019 – 04.09.2019), Poster presentation:
Encapsulation of the dual FLAP/mPGES-1 inhibitor BRP187 in biodegradable polymers improves its bioavailability and efficacy

Appendix 3 – Eigenständigkeitserklärung

Hiermit bestätige ich, Christian Kretzer, dass mir die gültige Promotionsordnung der Fakultät für Biowissenschaften der Friedrich-Schiller-Universität Jena bekannt ist und ich diese Dissertation selbstständig angefertigt habe. Des Weiteren habe ich keine Textabschnitte eines Dritten oder eigene Prüfungsarbeiten ohne Kennzeichnung übernommen und alle verwendeten Hilfsmittel und Quellen in meiner Arbeit angegeben. Zur Erarbeitung dieser Dissertation und zur Auswahl und Auswertung der Materialien sowie zur Erstellung der Manuskripte wurde weiterhin nur die Hilfe von Prof. Dr. O. Werz und Prof. Dr. U. S. Schubert in Anspruch genommen. Dritten Parteien wurden weder unmittelbare noch mittelbare geldwerte Leistungen im Zusammenhang mit den Inhalten dieser Arbeit gezahlt. Darüber hinaus habe ich keine Hilfe einer kommerziellen Promotionsvermittlung in Anspruch genommen.

Ich versichere, dass die hier vorgelegte Dissertation zuvor weder für eine staatliche noch eine andere wissenschaftliche Prüfung eingereicht wurde. Zudem habe ich weder diese Arbeit, noch eine gleiche oder in wesentlichen Teilen ähnliche Version oder eine andere Abhandlung bei einer anderen Hochschule oder Fakultät vorgelegt.

Ort, Datum

Unterschrift

Appendix 4 – Supportive information

Table 2 LM profile of BRP-187 in 2×10^6 human monocyte-derived M1 and M2 macrophages. M1- and M2-MDM (2×10^6) were resuspended in 1 mL PBS containing 1 mM CaCl₂, pre-incubated with BRP-187 (0.1, 0.3, 1 or 3 μ M, as indicated) or vehicle (0.1% DMSO) for 10 min at 37 °C, and stimulated with 1% SACM (from 6850 strain) for 180 min at 37 °C. Then, the supernatants were collected, formed LMs were extracted by SPE and analyzed by UPLC-MS/MS. Results are presented in pg/2 $\times 10^6$ M1-MDM and M2-MDM for vehicle control (100%) given as mean \pm SEM, and as percentage \pm SEM of TG-201-treated cells versus vehicle control (100%) in a heatmap; n=3-6.

	SACM	BRP-187 [%-change]				SACM	BRP-187 [%-change]				
		pg/2 $\times 10^6$ M1					pg/2 $\times 10^6$ M2				
		0.1 μ M	0.3 μ M	1 μ M	3 μ M		0.1 μ M	0.3 μ M	1 μ M	3 μ M	
		% \pm SEM	% \pm SEM	% \pm SEM	% \pm SEM		% \pm SEM	% \pm SEM	% \pm SEM	% \pm SEM	
5-LOX	5-HEPE	371 \pm 83	90 \pm 9	70 \pm 4	48 \pm 6	26 \pm 6	523 \pm 165	36 \pm 7	78 \pm 5	123 \pm 38	21 \pm 3
	5-HETE	4113 \pm 1053	91 \pm 4	68 \pm 6	44 \pm 5	20 \pm 5	5653 \pm 1390	42 \pm 10	78 \pm 12	91 \pm 29	22 \pm 3
	t-LTB ₄	571 \pm 208	67 \pm 9	55 \pm 7	31 \pm 4	23 \pm 4	648 \pm 255	31 \pm 7	88 \pm 18	67 \pm 7	13 \pm 2
	LTB ₄	1321 \pm 413	79 \pm 9	53 \pm 6	25 \pm 3	11 \pm 5	1019 \pm 318	40 \pm 7	75 \pm 17	67 \pm 16	12 \pm 2
	5S,6R-diHETE	202 \pm 65	65 \pm 7	53 \pm 6	29 \pm 4	8 \pm 3	188 \pm 68	34 \pm 9	82 \pm 18	55 \pm 9	51 \pm 40
COX	PGE ₂	2070 \pm 574	181 \pm 80	95 \pm 3	85 \pm 5	78 \pm 3	336 \pm 80	92 \pm 4	95 \pm 10	153 \pm 37	110 \pm 20
	PGD ₂	57 \pm 7	129 \pm 25	91 \pm 7	84 \pm 6	85 \pm 4	61 \pm 10	103 \pm 4	100 \pm 11	131 \pm 32	93 \pm 13
	PGF _{2α}	253 \pm 65	106 \pm 18	82 \pm 1	77 \pm 3	76 \pm 1	96 \pm 26	82 \pm 12	94 \pm 9	163 \pm 46	103 \pm 14
	TXB ₂	7908 \pm 1477	116 \pm 23	95 \pm 2	92 \pm 2	82 \pm 1	6742 \pm 1589	87 \pm 9	99 \pm 10	184 \pm 81	99 \pm 10
12/15-LOX	17-HDHA	847 \pm 211	149 \pm 29	107 \pm 8	108 \pm 6	106 \pm 2	5073 \pm 1672	108 \pm 6	104 \pm 12	194 \pm 74	98 \pm 9
	14-HDHA	124 \pm 14	123 \pm 3	96 \pm 8	100 \pm 10	119 \pm 12	973 \pm 294	124 \pm 11	104 \pm 11	154 \pm 39	104 \pm 12
	7-HDHA	166 \pm 56	115 \pm 9	51 \pm 19	46 \pm 16	59 \pm 10	158 \pm 19	107 \pm 7	97 \pm 13	473 \pm 257	80 \pm 8
	4-HDHA	67 \pm 7	127 \pm 14	110 \pm 8	110 \pm 13	135 \pm 16	83 \pm 13	101 \pm 8	93 \pm 5	106 \pm 37	97 \pm 8
	18-HEPE	34 \pm 2	96 \pm 7	84 \pm 6	85 \pm 4	89 \pm 17	53 \pm 7	103 \pm 11	90 \pm 4	184 \pm 58	86 \pm 10
	15-HEPE	68 \pm 12	114 \pm 8	94 \pm 8	89 \pm 4	96 \pm 6	1199 \pm 431	129 \pm 24	111 \pm 15	274 \pm 94	128 \pm 31
	12-HEPE	38 \pm 6	100 \pm 13	98 \pm 6	97 \pm 4	98 \pm 8	231 \pm 76	127 \pm 21	110 \pm 17	220 \pm 56	122 \pm 24
	15-HETE	1165 \pm 236	137 \pm 20	100 \pm 4	98 \pm 2	102 \pm 3	12872 \pm 3927	130 \pm 21	106 \pm 14	220 \pm 69	127 \pm 26
	12-HETE	240 \pm 46	111 \pm 10	96 \pm 6	96 \pm 9	112 \pm 10	1550 \pm 443	128 \pm 14	117 \pm 18	161 \pm 32	121 \pm 18
	5,15-diHETE	124 \pm 34	92 \pm 7	62 \pm 3	39 \pm 8	31 \pm 4	973 \pm 297	136 \pm 22	124 \pm 31	187 \pm 64	40 \pm 10
SPMs	PD1	6.5 \pm 1.6	102 \pm 12	87 \pm 9	95 \pm 2	95 \pm 12	27.9 \pm 8.0	163 \pm 35	124 \pm 23	157 \pm 24	228 \pm 127
	PDX	5.4 \pm 4.2	127 \pm 38	133 \pm 138	145 \pm 112	88 \pm 23	10.9 \pm 2.5	141 \pm 28	125 \pm 20	122 \pm 19	75 \pm 20
	RvD1	5.2 \pm 0.9	118 \pm 9	137 \pm 68	102 \pm 40	117 \pm 6	7.3 \pm 1.5	113 \pm 8	131 \pm 22	187 \pm 30	196 \pm 91
	RvD2	2.9 \pm 0.7	185 \pm 74	94 \pm 13	97 \pm 4	95 \pm 13	6.6 \pm 2.7	112 \pm 6	113 \pm 21	125 \pm 13	225 \pm 124
	RvD5	6.3 \pm 0.9	102 \pm 10	83 \pm 11	57 \pm 13	103 \pm 14	221 \pm 118	161 \pm 48	120 \pm 18	204 \pm 62	191 \pm 98
	MaR1	7.8 \pm 6.1	154 \pm 40	95 \pm 20	100 \pm 34	92 \pm 3	30 \pm 12	156 \pm 34	149 \pm 31	220 \pm 61	137 \pm 74
PUFA	AA	501738 \pm 142378	99 \pm 12	107 \pm 8	99 \pm 6	85 \pm 14	656418 \pm 244819	92 \pm 11	86 \pm 7	108 \pm 9	95 \pm 6
	EPA	153439 \pm 50364	112 \pm 5	120 \pm 11	114 \pm 10	105 \pm 4	201621 \pm 76304	94 \pm 10	81 \pm 7	112 \pm 20	101 \pm 3
	DHA	176845 \pm 18822	100 \pm 16	105 \pm 11	97 \pm 7	86 \pm 19	164317 \pm 31553	103 \pm 12	86 \pm 7	98 \pm 21	98 \pm 4